

SAFIR2014 – The Finnish Research Programme on Nuclear Power Plant Safety 2011–2014

Final Report



SAFIR2014 – The Finnish Research Programme on Nuclear Power Plant Safety 2011–2014

Final Report

Jari Hämäläinen & Vesa Suolanen (eds.)



ISBN 978-951-38-8226-6 (Soft back ed.)

ISBN 978-951-38-8227-3 (URL: <http://www.vtt.fi/publications/index.jsp>)

VTT Technology 213

ISSN-L 2242-1211

ISSN 2242-1211 (Print)

ISSN 2242-122X (Online)

Copyright © VTT 2015

JULKAISIJA – UTGIVARE – PUBLISHER

Teknologian tutkimuskeskus VTT Oy

PL 1000 (Tekniikantie 4 A, Espoo)

02044 VTT

Puh. 020 722 111, faksi 020 722 7001

Teknologiska forskningscentralen VTT Ab

PB 1000 (Teknikvägen 4 A, Esbo)

FI-02044 VTT

Tfn +358 20 722 111, telefax +358 20 722 7001

VTT Technical Research Centre of Finland Ltd

P.O. Box 1000 (Tekniikantie 4 A, Espoo)

FI-02044 VTT, Finland

Tel. +358 20 722 111, fax +358 20 722 7001

Abstract

The Finnish Nuclear Power Plant Safety Research Programme 2011–2014, SAFIR2014, was a 4-year national technical and scientific research programme on the safety of nuclear power plants. The programme was funded by the Finnish State Nuclear Waste Management Fund (VYR), as well as other key organisations operating in the area of nuclear energy. The programme provided the necessary conditions for maintaining knowledge needed for ensuring the continuance of safe use of nuclear power, for developing new know-how and for participation in international co-operation. Major part of Finnish public research on nuclear power plant safety during the years 2011–2014 was carried out in the SAFIR2014 programme.

The SAFIR2014 Steering Group, responsible of the strategic alignments of the programme, consisted of representatives of the Radiation and Nuclear Safety Authority (STUK), Ministry of Employment and the Economy (MEE), Technical Research Centre of Finland Ltd (VTT), Teollisuuden Voima Oyj (TVO), Fortum, Fennovoima Oy, Lappeenranta University of Technology (LUT), Aalto University (Aalto), Finnish Funding Agency for Technology and Innovation (Tekes), Finnish Institute of Occupational Health (FIOH) and the Swedish Radiation Safety Authority (SSM).

The research programme was divided into nine areas: Man, organisation and society, Automation and control room, Fuel research and reactor analysis, Thermal hydraulics, Severe accidents, Structural safety of reactor circuits, Construction safety, Probabilistic risk analysis (PRA), and Development of research infrastructure. A reference group was assigned to each of these areas to respond for the scientific guidance and to supervise the projects in the area.

Research projects of the programme were chosen on the basis of annual call for proposals. The annual volume of the SAFIR2014-programme in 2011–2014 was approximately 10 M€ and 70 person years. Main funding organisations were the Finnish State Nuclear Waste Management Fund (VYR) with over 5 M€ and VTT with nearly 3 M€ annually. In 2014 research was carried out in 45 projects.

The research in the programme was carried out by VTT Technical Research Centre of Finland Ltd, Lappeenranta University of Technology, Aalto University, University of Jyväskylä, Finnish Meteorological Institute, Finnish Institute of Occupational Health, and Finnish Software Measurement Association FISMA. A few subcontractors also contributed to the work in some projects.

This report gives a summary of the technical results of the SAFIR2014 programme from the entire programme with emphasis on the results achieved during the years 2013–2014. The results obtained during the years 2011–2012 have been reported in detail in the Interim Seminar Report.

Keywords

nuclear safety, safety management, nuclear power plants, human factors, safety culture, automation systems, control room, nuclear fuels, reactor physics, core transient analysis, thermal hydraulics, modelling, severe accidents, structural safety, construction safety, risk assessment, research infrastructure

Preface

The Finnish Research Programme on Nuclear Power Plant Safety 2011–2014, SAFIR2014, continued a series of Finnish national research programmes in nuclear energy that started in 1989. The programmes were initially carried out separately in the fields of operational aspects of safety (YKÄ 1990–1994, RETU 1995–1998) and structural safety (RATU 1990–1994, RATU2 1995–1998), and then in combined programmes (FINNUS 1999–2002, SAFIR 2003–2006, SAFIR2010 2007–2010). Simultaneously research has been carried out in the national nuclear waste management programmes (KYT2014 in parallel with SAFIR2014).

SAFIR2014 research programme was divided into the following research areas: (1) Man, organisation and society; (2) Automation and control room; (3) Fuel research and reactor analysis; (4) Thermal hydraulics; (5) Severe accidents; (6) Structural safety of reactor circuits; (7) Construction safety; and (8) Probabilistic Risk Analysis (PRA). A special area has been (9) Development of research infrastructure. Each of these areas comprised of 2–8 research projects. The research results have been published in scientific journals, conference papers and research reports.

The programme management structure consists of the Steering Group, a Reference Group in each of the nine research areas, a number of ad hoc groups in various fields, and programme administration. The SAFIR2014 Steering Group had representatives of the Radiation and Nuclear Safety Authority (STUK), Ministry of Employment and the Economy (MEE), Technical Research Centre of Finland Ltd (VTT), Teollisuuden Voima Oyj (TVO), Fortum, Fennovoima Oy, Lappeenranta University of Technology (LUT), Aalto University (Aalto), Finnish Funding Agency for Technology and Innovation (Tekes), Finnish Institute of Occupational Health (FIOH) and the Swedish Radiation Safety Authority (SSM).

The research in the programme was carried out by VTT Technical Research Centre of Finland Ltd, Lappeenranta University of Technology, Aalto University, University of Jyväskylä, Finnish Meteorological Institute, Finnish Institute of Occupational Health, and Finnish Software Measurement Association FISMA. A few subcontractors also contributed to the work in some projects.

This report has been prepared by the programme management in cooperation with the project managers and researchers.

More information about SAFIR2014 can be found on <http://safir2014.vtt.fi>. Finnish national research on nuclear power plant safety continues in SAFIR2018 programme for the years 2015–2018, see <http://safir2018.vtt.fi>

Contents

Abstract	3
Preface	5
1. Introduction.....	13
1.1 Role of SAFIR2014 in Finnish nuclear safety research.....	13
1.2 Research areas and projects.....	16
1.3 Statistical information.....	25
1.4 Administration, seminars and international evaluation	30
1.5 Structure of the report	31
1.6 Acknowledgements.....	31
2. Managing safety culture throughout the lifecycle of nuclear plants (MANSCU)	33
2.1 MANSCU summary report.....	33
2.2 Supporting safe design in the nuclear industry by understanding cultural features of design organizations.....	45
3. Sustainable and future oriented expertise (SAFEX2014).....	54
3.1 SAFEX2014 summary report.....	54
4. Signalled and silenced aspects of nuclear safety (SISIANS)	62
4.1 SISIANS summary report.....	62
5. Coverage and rationality of the software I&C safety assurance (CORSICA).....	72
5.1 CORSICA summary report.....	72
6. Human-automation collaboration in incident and accident situations (HACAS)	82
6.1 HACAS summary report.....	82
6.2 Studying automation awareness in nuclear power plants.....	92

7. Safety evaluation and reliability analysis of nuclear automation (SARANA)	103
7.1 SARANA summary report	103
7.2 Formal verification of nuclear power plant I&C	113
8. Safety requirements specification and management in nuclear power plants (SAREMAN)	122
8.1 SAREMAN summary report.....	122
9. Identification of fault situations propagating between different systems and disciplines (IFAPROBE)	132
9.1 IFAPROBE summary report	132
10. Criticality safety and transport methods in reactor analysis (CRISTAL) ..	142
10.1 CRISTAL summary report	142
10.2 Adjoint-based uncertainty analysis of lattice-physics calculations with CASMO-4.....	152
11. Three-dimensional reactor analyses (KOURA)	161
11.1 KOURA summary report	161
12. Development of Finnish Monte Carlo reactor physics code (KÄÄRME) ...	172
12.1 KÄÄRME summary report	172
12.2 Group constant preparation with Serpent.....	180
13. Neutronics, nuclear fuel and burnup (NEPAL)	189
13.1 NEPAL summary report	189
14. Extensive fuel modelling (PALAMA)	198
14.1 PALAMA summary report.....	198
14.2 FINIX fuel behaviour module: development and applications	208
15. Enhancement of safety evaluation tools (ESA)	218
15.1 ESA summary report.....	218
16. Experimental studies on containment phenomena (EXCOP)	229
16.1 EXCOP summary report	229
16.2 PPOOLEX Experiments with a Sparger	239
17. OpenFOAM CFD-solver for nuclear safety related flow simulations (NUFOAM)	249
17.1 NUFOAM summary report.....	249
17.2 OpenFOAM and subcooled nucleate boiling in fuel rod bundles	259
18. Numerical modelling of condensation pool (NUMPOOL)	269
18.1 NUMPOOL summary report	269

19. PWR PACTEL experiments (PAX)	279
19.1 PAX summary report.....	279
19.2 Loop seal experiments and calculations	289
20. Modeling of steam generators of nuclear power plants (SGEN)	299
20.1 SGEN summary report.....	299
21. Uncertainty evaluation for best estimate analyses (UBEA)	309
21.1 UBEA summary report	309
21.2 The use of VEERA test results in uncertainty quantification.....	319
22. Thermal hydraulics and fuel integrity in spent fuel dry cask interim storage facility (SPEFU)	330
22.1 SPEFU summary report.....	330
23. Core debris coolability and environmental consequence analysis (COOLOCE-E)	339
23.1 COOLOCE-E summary report.....	339
23.2 Coolability of realistically shaped debris beds	349
24. Chemistry of fission products (FISKES)	359
24.1 FISKES summary report	359
25. Thermal hydraulics of severe accidents (TERMOSAN)	369
25.1 TERMOSAN summary report	369
25.2 Fukushima Accident Analysis.....	376
26. Transport and chemistry of fission products (TRAFI)	387
26.1 TRAFI summary report.....	387
26.2 Recent findings on iodine behaviour in a severe accident.....	397
27. Reactor vessel failures, vapour explosions and spent fuel pool accidents (VESPA)	407
27.1 VESPA summary report.....	407
28. Passive Containment Cooling System tests (PCCS)	417
28.1 PCCS summary report.....	417
29. Environmental influence on cracking susceptibility and ageing of nuclear materials (ENVIS)	427
29.1 ENVIS summary	427
29.2 Low Temperature Crack Propagation (LTCP) Susceptibility of Nickel-Based Alloy 182, 82, 152 and 52 Weld Metals.....	438
30. Fracture assessment of reactor circuit (FAR)	449
30.1 FAR summary report.....	449

31. Monitoring of the structural integrity of materials and components in reactor circuit (MAKOMON)	459
31.1 MAKOMON summary report	459
31.2 Comparison of Artificial flaws in Austenitic Steel Welds with NDE Methods.....	468
32. RI-ISI analyses and inspection reliability of piping systems (RAIPSYS)...	479
32.1 RAIPSYS summary report.....	479
32.2 Effect of initial flaw and load assumptions on risk estimate changes	493
33. Advanced surveillance technique and embrittlement modelling (SURVIVE)	508
33.1 SURVIVE summary report	508
34. Water chemistry and plant operating reliability (WAPA)	517
34.1 WAPA summary report	517
35. Fatigue affected by residual stresses, environmental and thermal fluctuations (FRESH).....	527
35.1 FRESH summary report.....	527
35.2 Welding stress analyses	537
36. Heavy fouling and corrosion risks in the cooling water systems of NPPs and methods for their mitigation (RICO).....	547
36.1 RICO summary report.....	547
37. Impact 2014 (IMPACT2014) and Structural mechanics analysis of soft and hard impacts (SMASH)	555
37.1 IMPACT2014 summary report.....	555
37.2 SMASH summary report	565
37.3 Testing and modelling of vibration propagation and damping in a 3D-structure impacted multiple times with a soft projectile (IMPACT2014 and SMASH)	575
38. Ageing management of concrete structures in nuclear power plants (MANAGE)	592
38.1 MANAGE summary report.....	592
39. Seismic safety of nuclear power plants: targets for research and education (SESA)	604
39.1 SESA summary report	604
40. Extreme weather and nuclear power plants (EXWE)	620
40.1 EXWE summary report	620
40.2 High specific enthalpy in the recent and projected future climate of Finland	630

41. Risk assessment of large fire loads (LARGO)	640
41.1 LARGO summary report	640
41.2 Predicting the heat release rate of liquid pool fires using CFD	650
42. PRA development and application (PRADA)	660
42.1 PRADA summary report.....	660
43. FinPSA knowledge transfer (FINPSA-TRANSFER)	674
43.1 FINPSA-TRANSFER summary report.....	674
44. Enhancement of Lappeenranta instrumentation of nuclear safety experiments (ELAINE)	684
44.1 ELAINE summary report	684
44.2 Experiences and conducted experimental work with PIV in the ELAINE project.....	693
45. Renewal of hot cell infrastructure (REHOT)	704
45.1 REHOT summary report	704
45.2 Mechanical testing of radioactive materials in a hot cell environment	713

1. Introduction

1.1 Role of SAFIR2014 in Finnish nuclear safety research

The Finnish Nuclear Power Plant Safety Research Programme 2011–2014, SAFIR2014, was a 4-year national technical and scientific research programme on the safety of nuclear power plants. The programme was funded by the Finnish State Nuclear Waste Management Fund (VYR), as well as other key organisations operating in the area of nuclear energy. The programme provided the necessary conditions for maintaining knowledge needed for ensuring the continuance of safe use of nuclear power, for developing new know-how and for participation in international co-operation. Major part of Finnish public research on nuclear power plant safety during the years 2011–2014 was carried out in the SAFIR2014 programme.

The mission of the research programme is derived from the stipulations of the Finnish Nuclear Energy Act concerning the ensuring and availability of expertise in nuclear safety. The objective of SAFIR2014 was to develop and maintain experimental research capability, as well as the safety assessment methods and nuclear safety expertise of Finnish nuclear power plants, in order that, should new issues related to nuclear safety arise, their significance can be assessed without delay. The objective has been realised in the research work. Besides producing top level scientific results SAFIR2014 has been also an increasingly important platform in the education of experts. SAFIR2014 has also been an important network in Finland on domestic and international level.

Research projects of SAFIR2014 were chosen on the basis of annual call for proposals. The annual volume of the programme in 2011–2014 was approximately 10 M€ and 70 person years. Main funding organisations were the VYR with over 5 M€ and VTT with nearly 3 M€ annually. In 2014 research was carried out in 45 projects. Compared with the previous programmes, the funding increased significantly due to the Government decisions-in-principle confirmed by the Parliament in 2010. The VYR funding is proportional to the nuclear power capacity where also planned capacity is included.



Figure 1. Organisations represented in the SAFIR2014 Steering Group.

The period 2011–2014 of SAFIR2014 involved licensing processes for power plants that are in use and under construction, as well as overall safety evaluations related to licence terms. Continuous technical updates took place in Loviisa 1 and 2 as well as in Olkiluoto 1 and 2 plant units. Particularly the Fukushima Daiichi accident made it necessary to plan safety improvements in both sites. The construction of Olkiluoto 3 unit has continued and also the planning of Hanhikivi 1 and Olkiluoto 4 for which the Parliament of Finland accepted the applications for a Decision-in-Principle (DiP) in 2010. A new decision related to the DiP of Hanhikivi 1 was made in 2014. The YVL guides were reformed by STUK both with respect to the structure and the way of presentation.

Research on nuclear safety requires profound training and commitment. The national research programmes have provided the backbone for this activity. During the period of SAFIR2014 several experts who have taken part in construction and use of the currently operating plants have retired. The licensing processes and the possibility to recruit new persons in research projects have given an opportunity to experts from different generations to work together and thus transfer knowledge to the younger generation. Globalisation and networking highlight the importance of national safety research. The national research programme is an important channel for information exchange, and provides a chance to direct limited national resources to the most useful international research programmes in a more focused manner.

International co-operation is an essential part of the SAFIR2014 programme. Participation in OECD/NEA experimental and database projects is one of the key inter-

national activities. Further, international contacts include Nordic co-operation within Nordic Nuclear Safety Research (NKS) and Nordic Thermal-Hydraulic Network (Northnet), and participation in other international experimental research programmes and various IAEA working groups. At European level, it is topical to establish modes of co-operation and joint programming in the area of Gen II and Gen III light water reactor safety, with the support of Horizon 2020 (EU Framework Programme for Research and Innovation).

Besides research activities, the SAFIR2014 programme supports the development of research infrastructure in Finland. The existing experimental nuclear technology facilities and equipment, especially hot cell research capabilities, require renovation. Further, the thermal hydraulics experimentation facility needs updated instrumentation for producing measurement results suitable for the validation of computational methods.

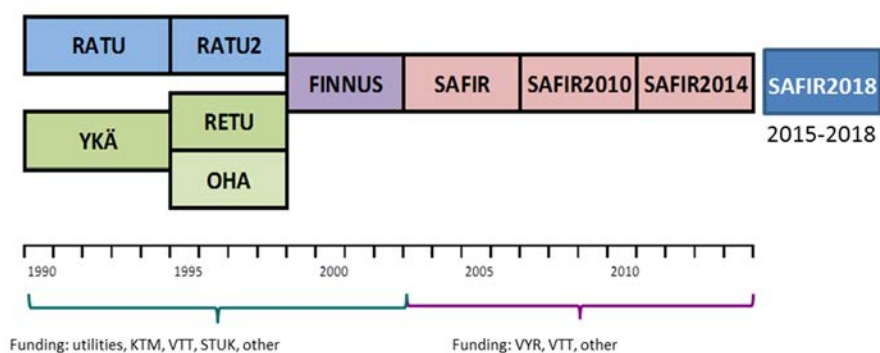


Figure 2. The history of Finnish research programmes on NPP safety.

The SAFIR2014 programme has taken advantage of the results obtained and lessons learned in the preceding national research programmes. The programmes in the area of nuclear safety (YKÄ & RATU 1990–1994, RETU&RATU2 1995–1998, FINNUS 1999–2002, SAFIR 2003–2006, SAFIR2010 2007–2010 and SAFIR2014 2011-2014) have had the total volume of 143 M€ and 1 165 person years. According to the final reports of the successive programmes they have produced 4 544 publications in various categories and 45 Doctor, 20 Licentiate and 119 Master level academic degrees. The extent of the various programmes is given in Table 1. The Finnish public nuclear safety research will continue in the SAFIR2018 programme during the years 2015–2018.

Table 1. Finnish national research programmes on NPP safety in 1990-2014.

Programme	Volume, M€	Volume, person years	Total number of publications	Academic degrees		
				Dr.	Lic.	M.Sc.
YKÄ 1990-1994	15,4	168	318	6	5	10
RATU 1990-1994	8,2	76	322	1	3	3
RETU 1995-1998	9,8	107	405	3	2	2
RATU2 1995-1998	7,5	60	280	3	4	11
FINNUS 1999-2002	14,4	130	564	6	2	18
SAFIR 2003-2006	19,7	148	545	6	1	17
SAFIR2010 2007-2010	27,5	197	866	8	1	31
SAFIR 2014 2011-2014	40,1	279	1244	12	2	27

1.2 Research areas and projects

Research in SAFIR2014 has been conducted according to the Framework Plan [1], the Annual Plans [2-5] and decisions of the Steering and Reference Groups. Additional guidance is given in the management handbook [6]. The research has been to a large extent continuation of the research themes in the preceding programme SAFIR2010 [7]. The research areas and research needs were defined in the Framework Plan. SAFIR2014 research programme was divided in nine research areas:

1. Man, organisation and society
2. Automation and control room
3. Fuel research and reactor analysis
4. Thermal hydraulics
5. Severe accidents
6. Structural safety of reactor circuits
7. Construction safety
8. Probabilistic risk analysis (PRA)
9. Development of research infrastructure.

These research areas included both research projects of the named topic and interdisciplinary co-operation projects. Each research area had a Reference Group that consisted of experts from all organisations involved in the Steering Group. The Reference Groups had the responsibility on scientific guidance and supervisory in their area. The aim of the research area nine was to ensure high level research facilities also in future in the nuclear safety research work.

In 2014 research was carried out in 45 projects. VTT was the responsible research organisation in 35 of the projects and was also responsible of the coordination of the programme. During SAFIR2014 there have been altogether 50 separate research projects. In some projects, researchers from 1-3 different organisations were

participating and co-operating. The summary of the volumes of the projects in 2011-2014 is given in Table 2. The realised figures for 2014 were not available at the time of this report and the figures are based on the plans.

The scientific results of the programme have been reported in the Annual Reports [8-11], in the Interim Seminar report [12] and in the publications. A complete set of the publications has been distributed to the organisations represented in the Steering Group.

Table 2. The research projects in SAFIR2014 in 2011-2014.

Group	Project and principal research organisation	Acronym	Funding (thousand Euro)					Volume (person-years)					Total		
			2011	2012	2013	2014	2014 plan	2011	2012	2013	2014				
1. Man, organisation and society															
	Managing safety culture throughout the lifecycle of nuclear plants VTT	MANSCU	353.3	338.4	308.4	250.0	250.0	2.5	2.19	2.43	1.62	8.74			
	Sustainable and future oriented expertise FIOH, Aalto	SAFEX2014	131.6	74.2	89.2	89.0	89.0	1.42	0.65	0.82	0.85	3.74			
	Signalled and silenced aspects of nuclear safety University of Jyväskylä	SISIANs	-	-	72.1	86.0	86.0	-	-	0.79	0.81	1.6			
2. Automation and control room															
	Coverage and rationality of the software I&C safety assurance VTT, FISMA Ry, Spinet	CORSICA	178.5	181.1	140.3	137.4	137.4	1.43	1.42	1.23	0.95	5.03			
	Human-automation collaboration in incident and accident situations VTT	HACAS	222.3	228.7	207.3	192.0	192.0	1.48	1.23	1.38	1.24	5.33			
	Safety evaluation and reliability analysis of nuclear automation VTT	SARANA	454.8	344.2	317.1	274.0	274.0	3.46	3.0	2.71	2.42	11.59			
	Safety requirements specification and management in nuclear power plants VTT	SAREMAN	194.9	155.6	174.6	192.5	192.5	1.6	1.3	1.55	1.48	5.93			

Group	Project and principal research organisation	Acronym	Funding (thousand Euro)				Volume (person-years)				Total
			2011	2012	2013	2014	2011	2012	2013	2014	
	Identification of fault situations propagating between different systems and disciplines <i>Aalto</i>	IFAPROBE	-	-	100.4	77.5	-	0.93	0.76	1.69	
3.	Fuel research and reactor analysis					plan					
	Criticality safety and transport methods in reactor analysis <i>VTT</i>	CRISTAL	293.9	228.0	202.8	204.0	2.34	1.7	1.61	7.56	
	Three-dimensional reactor analyses <i>VTT</i>	KOURA	398.8	278.2	287.9	234.0	2.9	1.91	1.54	8.35	
	Development of Finnish Monte Carlo reactor physics code <i>VTT</i>	KÄÄRME	221.7	191.0	200.1	210.0	1.65	1.84	1.79	6.58	
	Neutronics, nuclear fuel and burnup <i>Aalto</i>	NEPAL	125.3	131.0	127.7	134.0	1.83	1.61	1.37	6.85	
	Extensive fuel modelling <i>VTT</i>	PALAMA	407.2	338.1	357.0	353.0	3.12	2.9	2.81	11.6	
	Radionuclide source term analysis <i>VTT</i>	RASTA	-	61.0	-	-	-	-	-	0.55	
4.	Thermal hydraulics										
	Application of best estimate plus uncertainty evaluation method <i>VTT</i>	BEPUE	94.0	-	-	-	0.8	-	-	0.8	
	Enhancement of safety evaluation tools <i>VTT</i>	ESA	468.8	455.0	455.0	397.0	3.1	4.15	2.62	13.27	

Group	Project and principal research organisation	Acronym	Funding (thousand Euro)					Volume (person-years)					Total
			2011	2012	2013	2014	2014	2011	2012	2013	2014	2014	
	Experimental studies on containment phenomena <i>LUT</i>	EXCOP	258.8	294.3	253.0	207.1		2.0	2.3	2.0	1.76	8.06	
	OpenFOAM CFD-solver for nuclear safety related flow simulations <i>VTT</i>	NUFOAM	165.0	185.8	146.4	145.0		2.22	1.75	1.43	1.15	6.55	
	Numerical modelling of condensation pool <i>VTT</i>	NUMPOOL	119.4	116.1	117.4	119.0		0.86	0.84	0.82	0.75	3.27	
	Improvement of PACTEL facility simulation environment <i>LUT</i>	PACSIM	50.6	49.5	-	-		0.38	0.38	-	-	0.76	
	PWR PACTEL experiments <i>LUT</i>	PAX	386.2	276.4	340.9	258.0		2.8	2.7	3.1	1.99	10.59	
	Modeling of steam generators of nuclear power plants <i>VTT</i>	SGEN	70.0	82.1	101.2	101.0		0.55	0.73	0.77	0.7	2.75	
	Uncertainty evaluation for best estimate analyses <i>VTT</i>	UBEA	-	101.1	88.0	80.0		-	1.0	1.11	0.76	2.87	
	Thermal hydraulics and fuel integrity in spent fuel dry cask interim storage facility <i>VTT</i>	SPEFU	-	-	87.4	87.0		-	-	0.66	0.63	1.29	

Group	Project and principal research organisation	Acronym	Funding (thousand Euro)					Volume (person-years)					Total		
			2011	2012	2013	2014	2014 plan	2011	2012	2013	2014	2014 y			
5. Severe accidents															
	Core debris coolability VTT	COOLOCE	172.4	-	-	-	1.22	-	-	-	-	-	-	-	1.22
	Core debris coolability and environmental consequence analysis VTT	COOLOCE-E	-	190.5	170.1	183.0	-	-	1.48	1.32	1.24	1.24	1.24	4.04	
	Chemistry of fission products VTT	FISKE	182.1	137.9	-	-	1.4	-	1.2	-	-	-	-	2.6	
	Chemistry of fission products VTT	FISKES	-	-	121.3	148.0	-	-	-	0.86	1.05	1.05	1.05	1.91	
	Thermal hydraulics of severe accidents VTT	TERMOSAN	203.4	204.0	180.4	152.0	1.56	1.17	1.04	1.58	1.63	1.63	1.63	4.66	
	Transport and chemistry of fission products VTT	TRAFI	369.4	318.3	240.5	249.0	3.64	2.62	1.58	1.58	1.63	1.63	1.63	9.47	
	Reactor vessel failures, vapour explosions and spent fuel pool accidents VTT	VESPA	-	145.1	134.2	150.0	-	1.3	0.89	0.89	1.55	1.55	1.55	3.74	
	Passive Containment Cooling System tests LUT	PCCS	-	-	204.9	157.0	-	-	-	1.18	1.19	1.19	1.19	2.37	

Group	Project and principal research organisation	Acronym	Funding (thousand Euro)				Volume (person-years)				Total				
			2011	2012	2013	2014	2011	2012	2013	2014					
6.	Structural safety of reactor circuits														
	Environmental influence on cracking susceptibility and ageing of nuclear materials VTT	ENVIS	618.6	696.5	680.1	596.0	plan	4.67	5.9	4.57	4.29	19.43			
	Fracture assessment of reactor circuit VTT	FAR	255.1	250.2	238.1	215.0		1.7	1.5	1.47	1.14	5.81			
	Monitoring of the structural integrity of materials and components in reactor circuit VTT	MAKOMON	238.2	192.5	185.1	172.0		1.66	1.14	1.1	0.86	4.76			
	RI-ISI analyses and inspection reliability of piping systems VTT	RAIPSYS	155.1	152.0	130.0	117.0		1.05	1.0	1.07	0.79	3.91			
	Advanced surveillance technique and embrittlement modelling VTT	SURVIVE	118.3	165.0	158.0	167.0		0.67	0.8	1.03	1.14	3.64			
	Water chemistry and plant operating reliability VTT	WAPA	182.2	153.3	180.1	172.0		1.71	1.1	0.95	1.07	4.83			
	Fatigue affected by residual stresses, environment and thermal fluctuations VTT	FRESH	-	155.0	170.0	168.0		-	1.06	1.14	0.93	3.13			
	Heavy fouling and corrosion risks in the cooling water systems of NPPs and methods for their mitigation VTT	RICO	-	-	117.8	105.0		-	-	0.72	0.86	1.58			

Group	Project and principal research organisation	Acronym	Funding (thousand Euro)				Volume (person-years)				Total		
			2011	2012	2013	2014	2011	2012	2013	2014			
7. Construction safety													
	Impact 2014 VTT	IMPACT2014	460.6	547.5	444.6	710.0	plan	2.57	2.7	2.16	1.62	9.05	
	Ageing management of concrete structures in nuclear power plants VTT	MANAGE	227.1	186.6	159.7	140.8		1.2	0.81	1.35	0.76	4.12	
	Structural mechanics analyses of soft and hard impacts VTT	SMASH	250.5	225.0	204.1	177.0		1.8	1.58	1.09	1.1	5.57	
	Seismic safety of nuclear power plants. Targets for research and education. VTT	SESA	111.3	155.7	164.9	132.0		0.67	0.8	1.14	0.82	3.43	
8. Probabilistic risk analysis (PRA)													
	Extreme weather and nuclear power plants FMI	EXWE	169.0	196.5	173.9	109.0		1.77	2.15	1.73	1.05	6.7	
	Risk assessment of large fire loads VTT	LARGO	210.0	197.0	212.0	185.0		1.27	1.17	1.37	1.07	4.88	
	PRA development and application VTT	PRADA	237.4	213.3	235.0	189.0		1.78	1.89	1.87	1.62	7.16	
	FinPSA knowledge transfer VTT	FINPSA-TRANSFER	-	187.0	187.0	169.0		-	1.56	1.56	1.33	4.45	

		Funding (thousand Euro)					Volume (person-years)				
Group	Project and principal research organisation	Acronym	2011	2012	2013	2014	2011	2012	2013	2014	Total
9.	Development of research infrastructure					plan	y	y	y	y	
	Enhancement of Lappeenranta instrumentation of nuclear safety experiments <i>LUT</i>	ELAINE	387.8	317.5	423.0	270.0	1.4	1.5	2.5	1.71	7.11
	Renewal of hot cell infrastructure <i>VTT</i>	REHOT	154.0	624.8	818.1	1350.0	0.86	2.5	3.64	3.48	10.48
0.	Programme administration:										
	SAFIR2014 administration and information (2011-2014) (VAT included) <i>VTT</i>	ADMIRE	195.8	223.9	276.8	286.0	0.88	0.96	1.1	1.0	3.94
	TOTAL		9493.4	9944.9	10383.9	10296.3	69.92	71.35	74.27	63.8	279.34

1.3 Statistical information

The annual volume of the SAFIR2014 programme in 2011-2014 has been 9,5-10,4 M€ and approximately 70 person years. Main funding organisations in 2011-2014 were the Finnish State Waste Management Fund VYR with 5,2-5,6 M€ and VTT with 2,7-2,9 M€ annually. In 2014 the planned funding shares were 56% (VYR) and 27% (VTT) (Figure 7).

The Finnish power companies Teollisuuden Voima Oyj, Fortum and Fennovoima Oy funded substantially the research via VYR funding based on the Finnish Nuclear Energy Act, and also with additional separate funding portions to selected projects.

Lappeenranta University of Technology, the Aalto University in Espoo, and the University of Jyväskylä have also funded the projects in the programme. The Finnish Institute of Occupational Health has funded a project in the human research area. The Finnish Meteorological Institute has funded a project in the PRA research area. The funding of the research organisations is related to the self-financing portions in the research projects.

Nordic Nuclear Safety Research (NKS) and Swedish Radiation Safety Authority (SSM) have also funded research in the SAFIR2014 programme.

The total funding in the SAFIR2014 research areas in 2011-2014 is shown in Figure 3. The corresponding distribution of the VYR funding to the research areas is shown in Figure 4. Distribution of funding and person years in the nine research areas of SAFIR2014 in 2014 have been illustrated in Figures 5 and 6 respectively.

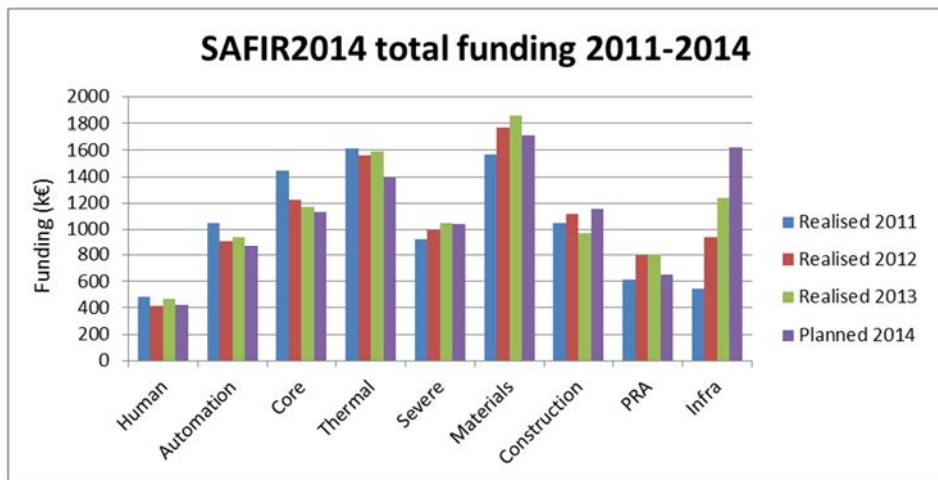


Figure 3. Total funding in the SAFIR2014 research areas in 2011-2014.

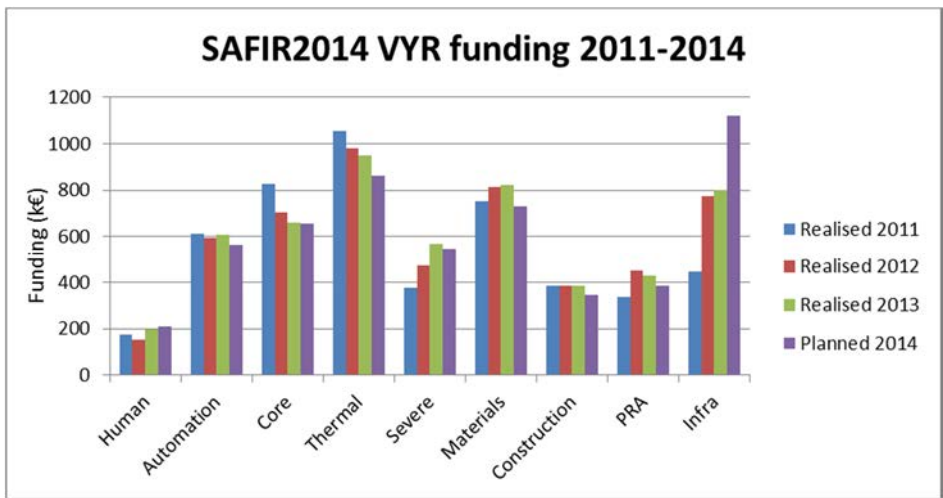


Figure 4. VYR funding in the SAFIR2014 research areas in 2011-2014.

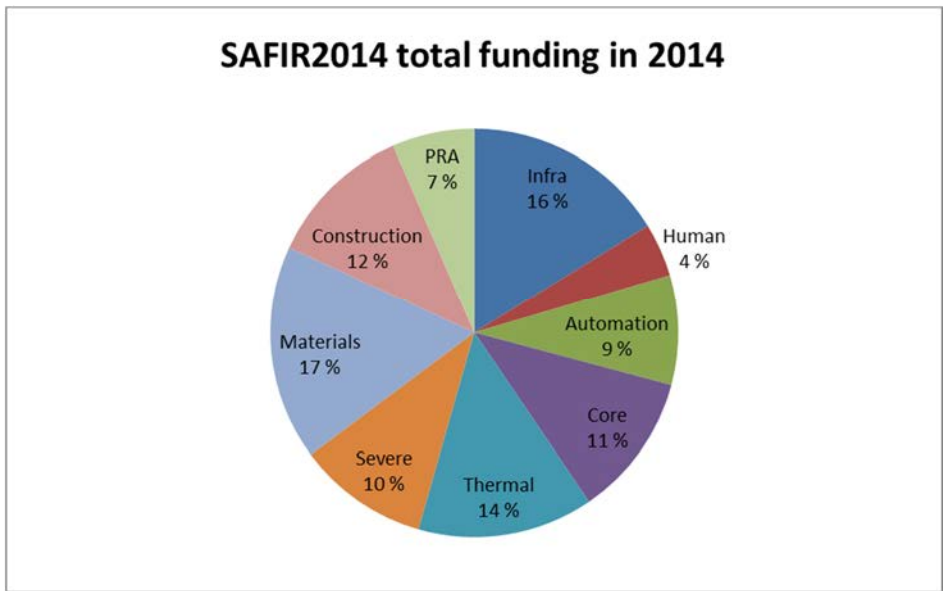


Figure 5. Distribution of total funding in the SAFIR2014 research areas in 2014.

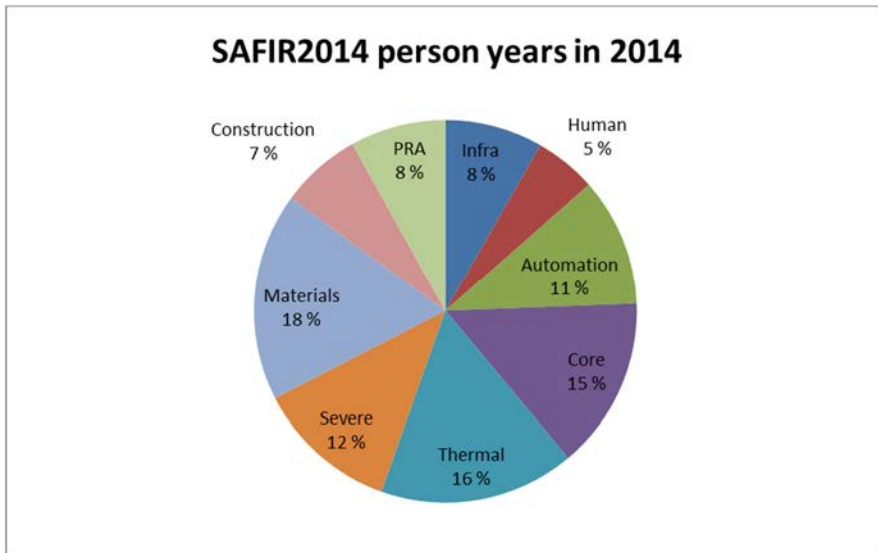


Figure 6. Distribution of person years in the SAFIR2014 research areas in 2014.

Figures 7 and 8 illustrate the funding sources and cost structure of SAFIR2014 in the year 2014.

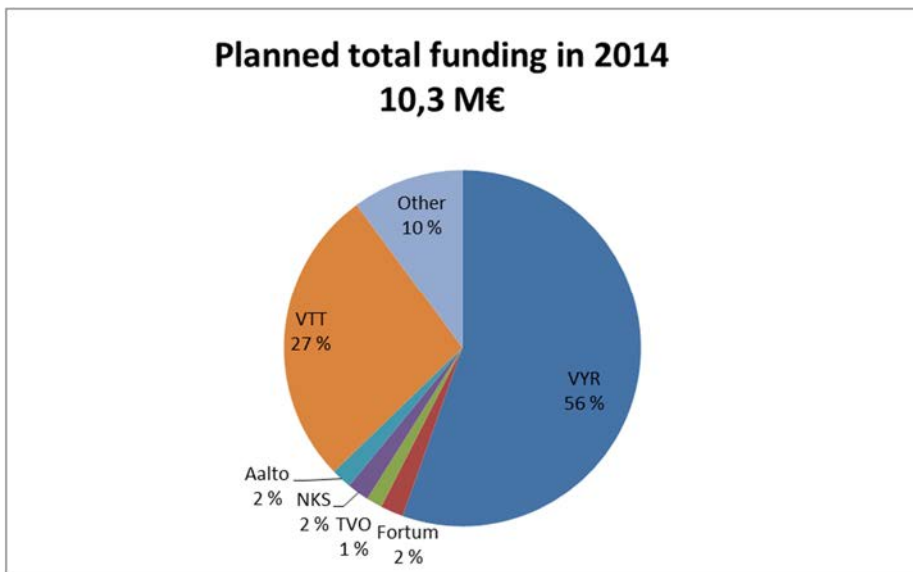


Figure 7. SAFIR2014 funding sources in 2014.

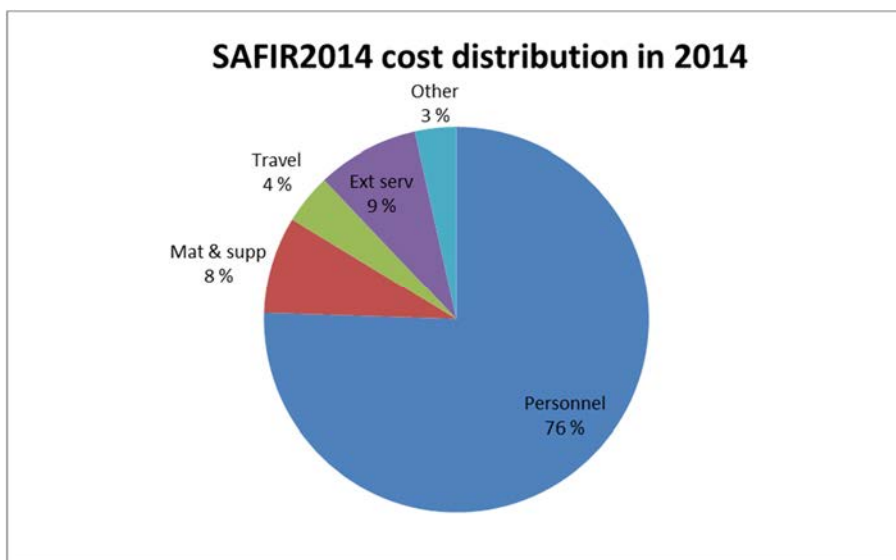


Figure 8. SAFIR2014 cost structure in 2014.

The programme has produced 1244 publications in 2011-2014 (Table 3). Major part of the publications consisted of conference papers and extensive research institute reports. The number of publications varied greatly between the projects. The average number of publications is 4,4 per person year, and the average number of scientific publications is 0,6 per person year which is greater than in the SAFIR2010 programme (0,5 per p.y.). Many projects have deliberately aimed at publication of the results as extensive research institute reports that are found to be more useful to the end-users than scientific publications, which has to be taken into account when judging the numbers of publications in different categories.

Table 3. Publications in the SAFIR2014 projects in 2011-2014.

Project	Scientific	Conference papers	Res. Inst. reports	Others	Total	Volume pers. year
MANSCU	15	9	8	4	36	8,74
SAFEX2014	2	6	1	12	21	3,74
SISIANS	7	2	2	1	12	1,6
CORSICA	0	9	17	7	33	5,03
HACAS	9	23	16	7	55	5,33
SARANA	10	21	14	18	63	11,59
SAREMAN	0	6	6	20	32	5,93
IFAPROBE	1	4	1	0	6	1,69
CRISTAL	7	6	17	4	34	7,56
KOURA	0	7	24	14	45	8,35

KÄÄRME	25	26	6	2	59	6,58
NEPAL	11	2	2	8	23	6,85
PALAMA	6	15	35	8	64	11,6
RASTA	0	0	1	1	2	0,55
BEPUE	0	0	1	0	1	0,8
ESA	4	4	22	4	34	13,27
EXCOP	7	2	14	6	29	8,06
NUFOAM	1	5	24	1	31	6,55
NUMPOOL	0	0	4	1	5	3,27
PACSIM	0	1	3	1	5	0,76
PAX	2	2	12	4	20	10,59
SGEN	0	1	9	1	11	2,75
UBEA	0	0	5	1	6	2,87
SPEFU	0	0	4	0	4	1,29
COOLOCE	1	1	4	0	6	1,22
COOLOCE-E	3	3	10	1	17	4,04
FISKE	0	0	7	1	8	2,6
FISKES	0	0	8	1	9	1,91
TERMOSAN	4	4	14	4	26	4,66
TRAFI	2	20	11	3	36	9,47
VESPA	0	2	12	2	16	3,74
PCCS	0	0	4	0	4	2,37
ENVIS	3	13	29	7	52	19,43
FAR	8	4	18	2	32	5,81
MAKOMON	1	9	19	3	32	4,76
RAIPSYS	5	3	13	2	23	3,91
SURVIVE	9	4	14	2	29	3,64
WAPA	3	3	15	4	25	4,83
FRESH	1	2	14	1	18	3,13
RICO	0	1	3	0	4	1,58
IMPACT2014	3	6	6	1	16	9,05
MANAGE	0	17	10	8	35	4,12
SMASH	5	5	14	2	26	5,57
SESA	0	2	12	6	20	3,43
EXWE	14	9	11	9	43	6,7
LARGO	5	14	16	4	39	4,88
PRADA	1	10	17	8	36	7,16
FINPSA-TRANSFER	0	4	21	1	26	4,45
ELAINE	0	0	4	6	10	7,11
REHOT	0	0	13	4	17	10,48
ADMIRE	0	1	7	0	8	3,94
TOTAL	175	288	574	207	1244	279,34

Education of new experts has been an important task in SAFIR2014. The academic degrees obtained in the projects is given in Table 4. There were altogether 12 Doctoral, 2 Licentiate and 27 Master level degrees.

Table 4. Academic degrees obtained in the projects in 2011-2014.

Project	Doctor	Licentiate	Master
CORSICA			1
HACAS			1
SARANA	2		1
SAREMAN			1
CRISTAL	1*		
KÄÄRME	1*		
NEPAL	1		1
PALAMA		1	2
ESA			1
EXCOP	1		2**
PAX	1		1
UBEA			2
TERMOSAN			1
TRAFI	1		
ENVIS			3
FAR			1
RAIPSYS		1	
WAPA			3
IMPACT2014			1
MANAGE	1		
EXWE	2		2
LARGO	1		
PRADA			1
ELAINE			2**
TOTAL	12	2	27

*) one Doctoral thesis jointly in CRISTAL and KÄÄRME

***) one Master's thesis jointly in EXCOP and ELAINE

1.4 Administration, seminars and international evaluation

The programme management bodies, the Steering Group and the nine Reference Groups, met on regular basis 4-5 times annually. The ad hoc groups met upon the needs of the specific projects and had a vital role for several projects. The programme was managed by the coordination unit VTT, the programme director, the project co-ordinator and the project managers of the individual research projects.

The information on the research performed in SAFIR2014 was communicated formally quarterly via the progress reports of the projects, the annual plans and reports of the programme and the SAFIR2014 website. Additional information was given in seminars organised by several research projects. The detailed scientific results were published as articles in scientific journals, conference papers, and separate reports.

A combined brochure of the SAFIR2010 & SAFIR2014 programmes was produced by the programme management. General presentations on the structure and goals of the SAFIR2014 programme were given abroad by the programme director.

Major events during the SAFIR2014 have been the Interim Seminar in March 2013 [12] with some 200 participants, approximately 10% from abroad, the international evaluation of the programme in March 2014 with project presentations, interviews of the steering and reference group members, exit meeting and final evaluation report [13]. The evaluation also gave recommendations for the planning seminar of SAFIR2018 held in April 2014. SAFIR2018 has a new structure and it is described in detail in the SAFIR2018 Framework Plan [14].

In addition to conducting the actual research according to the yearly plans, SAFIR2014 has been an efficient forum for information exchange with all organisations operating in the nuclear energy sector in Finland: It has also been an open discussion forum for participation in international projects and planning of new projects.

1.5 Structure of the report

The report contains presentation of the main scientific achievements of the projects in Chapters 2-45. Both project overviews and special technical articles are included. For the statistical information on publications, academic degrees and project personnel as well as list of the Steering Group, Reference Group and Ad Hoc Group members, reference is made to the Annual Plans and Annual Reports that can be found on SAFIR2014 website.

1.6 Acknowledgements

The results of the SAFIR2014 programme have been produced by all who have been involved in the research projects. Their work is highly esteemed.

The contributions of project managers and researchers that form the essential contents of this report are acknowledged with gratitude.

The work of the persons in the Steering Group, Reference Groups and Ad Hoc Groups that has been carried out with the expense of their own organisations is highly appreciated.

Jari Hämäläinen and Vesa Suolanen

References

1. National Nuclear Power Plant Safety Research 2011-2014. SAFIR2014 Framework Plan. Publications of the Ministry of Employment and the Economy, Energy and the climate 50/2010 (also available on <http://safir2014.vtt.fi/>).
2. Simola, K. & Suolanen, V. SAFIR2014 Annual Plan 2011. VTT Research Report VTT-R-03783-11. 34 p. + app. 227 p.
3. Simola, K. & Suolanen, V. SAFIR2014 Annual Plan 2012. VTT Research Report VTT-R-03343-12. 36 p. + app. 262 p.
4. Simola, K. & Suolanen, V. SAFIR2014 Annual Plan 2013. VTT Research Report VTT-R-02683-13. 38 p. + app. 273 p.
5. Hämäläinen, J. & Suolanen, V. SAFIR2014 Annual Plan 2014. VTT Research Report VTT-R-03911-14. 38 p. + app. 295 p.
6. SAFIR2014 toimintakäsikirja (SAFIR2014 Operations manual, living document at the programme www-pages. In Finnish.)
7. Puska, E.K. & Suolanen, V. (eds.) SAFIR2010, The Finnish Research Programme on Nuclear Power Plant Safety 2007-2010. Final Report. VTT Research Notes 2571. Espoo 2011. 578 p. ISBN 978-951-38-7689-0; 978-951-38-7690-6.
8. Simola, K. (ed.) SAFIR2014 Annual Report 2011. VTT Research Report VTT-03188-12. Espoo 2012. 120 p. + app. 60 p.
9. Simola, K. (ed.) SAFIR2014 Annual Report 2012. VTT Research Report VTT-R-02682-13. Espoo 2013. 130 p. + app. 77 p.
10. Simola, K. & Suolanen, V. (eds) SAFIR2014 Annual Report 2013. VTT Research Report VTT-R-02526-14. 144 p. + app. 89 p.
11. Hämäläinen, J. & Suolanen, V. (eds.) SAFIR2014 Annual Report 2014. VTT Research Report. (To be published in April 2014.)
12. Simola, K. (ed.) SAFIR2014. The Finnish Research Programme on Nuclear Power Plant Safety 2011-2014. Interim Report. VTT, Espoo, 2013. VTT Technology 80. 447 p. ISBN 978-951-38-7918-1; 978-951-38-7919-8.
13. Evaluation of the Finnish Nuclear Safety Research Programme SAFIR2014. Publication of the Ministry of Employment and the Economy, June 2014.
14. National Nuclear Power Plant Safety Research 2015-2018. SAFIR2018 Framework Plan. Publications of the Ministry of Employment and the Economy, Energy and the climate 34/2014 (also available on <http://safir2018.vtt.fi/>).

2. Managing safety culture throughout the lifecycle of nuclear plants (MANSCU)

2.1 MANSCU summary report

Pia Oedewald¹, Nadezhda Gotcheva², Kaupo Viitanen¹, Mikael Wahlström¹

¹VTT Technical Research Centre of Finland Ltd
P.O. Box 1000, FI-02044 Espoo

²VTT Technical Research Centre of Finland Ltd
P.O. Box 1300, FI-33101 Tampere

Abstract

Nuclear industry organisations should employ safety management practices that allow them to develop a good safety culture. Recent safety science theories emphasise that safety management should not focus solely on avoidance of incidents and increasing controls but rather it should focus more on building organisational capabilities that allow them to succeed in varying conditions. This may require some modifications on the typical safety culture thinking that evolved in the nuclear industry in the 80's and 90's which has a fairly mechanistic view on organisational development and management. A second need for continuing research on safety culture and safety management stems from the current challenges in developing a sound safety culture in design and construction phases of the new build projects and major modernisations which are carried out by network of subcontractors instead of a single licensee organisation. In MANSCU project a set of case studies was carried out to study the practical challenges that the safety management practices should be able to handle and to test some of the safety management concepts proposed by scientists and practitioners.

Introduction

Organisations involved in nuclear power production in its various lifecycle stages are expected to have a good safety culture (see e.g. The Finnish Government Degree 2013). Previous research has put significant effort in defining what is safety culture as a phenomenon, what is *good* safety culture, and how to evaluate if the organisations' culture fulfils the criteria of a good safety culture. VTT has developed a methodology DISC (Design for integrated safety culture) (Reiman and Oedewald 2009, Oedewald et al. 2011a) which has been used in safety culture assessments and event investigations. During the last years safety culture assessments have become a common practice in the Nordic nuclear industry. The next challenge has been to understand how to develop safety culture in organisations i.e. what kind of management philosophies and organisational development practices should be applied in order to foster nuclear safety, and organisational culture which supports it. There are two major questions that scientists and practitioners face; firstly, what is safety i.e. what is the desired state of the organisation they want to achieve, and secondly, how to achieve transitions in organisational culture towards the desired direction. In MANSCU project we took the standpoint that safety is more than absence of accidents and incidents (cf. Woods & Hollnagel 2006). Safety can be viewed as organisational ability to succeed in varying conditions (Hollnagel 2009). Therefore development of safety culture should be about building positive capabilities in the organisation rather than focusing solely on building barriers to prevent failures.

Safety culture is embedded in all activities in the organisations, and thus, any development of organisational practices and structures may change its culture. However, in many safety critical domains safety culture development has become a goal oriented activity which uses various methods developed by practitioners and scientists (Table 1).

Table 1. Typical methods used in safety culture development activities in the nuclear industry (adopted from Viitanen, forthcoming).

Safety culture development methods	Function/scope	Target group
Safety culture trainings, seminars	Create awareness of importance of safety culture and a forum for reflecting own culture	Entire organisation
Safety culture assessment and related development targets	Address weaknesses identified in e.g. a safety culture survey	Entire organisation, typically local actions
Behavioural-based safety programs	Behaviour modification	Shop-floor workers
Human performance programs	Reduce human errors and manage controls	Usually shop-floor workers, potentially also management
Operating experience processes	Learn the contributing factors of actualised safety problems and determine corrective actions	Technology and work processes and working practices
Human resource management	Select suitable and competent workers, recompensing, ensure continuity of culture	Entire organisation
Safety leadership development	Develop safety leadership skills and implement tools	Management

In the nuclear industry risk and quality management are very well established. Researchers have argued that sometimes this has led to a tendency to overemphasise plans, rules and procedures in guaranteeing safety of the nuclear plants (Vicente 1999, Perin 2004). Nuclear industry culture has been described as “culture of control” (Perin 2004) where organisations do not always appreciate the inherent uncertainties. This has also been recognised by some of the Fukushima accident investigations (Epstein 2012; Diet 2012). In reality many activities in the nuclear industry, for example maintenance, design work, construction of new plants and emergency management involve dealing with unforeseen situations and performing underspecified work tasks. In order to smoothly cope with these the culture of the organisation need to support flexibility and adaptability to some degree. It is everyday reality for example in the maintenance work that rules and instructions do not cover all circumstances thus the actions or decisions are based on worker or management expertise. We state that safety management practices should not assume that all activities are – or could be – prescribed in a nuclear power plant. Instead, *safety management practices should support organisational mindfulness: vigilance and attentiveness to unexpected situations and means for coping with them in a flexible manner* (Weick & Sutcliffe 2007).

In order for the actions and decision to be safe they need to be *based on sound understanding of the possible risks and safety impacts of the decisions and actions.*

Achieving and maintaining that understanding across the organisation is not self-evident, however. Partly this relates to very nature of nuclear hazards: the nuclear safety related risks are intangible and they realize infrequently thus not all workers really employ realistic understanding of them. The hazards may also be considered distant due to multiple technical barriers and strict distribution of responsibilities among different actors. Therefore we claim that safety culture models and safety management practices which aim at developing safety culture should not focus solely on attitudinal aspects (employees' and management attitudes towards safety) but include the knowledge component as well (see also Kirwan 2008). This is a topical question since the new power plant projects and modernisations of the operating units require such an amount of employees and services that it's necessary to utilise subcontractor companies and new workers with little or no previous experience in nuclear industry.

All in all, the question of *how to create safety culture in a supply chain or a network of organisations* is one of the practical challenges the power companies and regulators face at the moment. In modernisation or new build projects the work is typically carried out by a virtual organisation which consist of workers from multiple organisations. It is a temporary group with little shared history and thus little shared cultural norms and assumptions. Often these project organisations are multicultural (IAEA 2012). Safety management practices and safety culture models have their roots in single company context and thus it may be challenging to understand how to manage safety and what kind of cultural features to facilitate in a supply chain may be challenging.

Goals and tasks of MANSCU project

The generic objective of the MANSCU project (2011-2014) was to create knowledge that can be used in developing safety management approaches in such a way that they would better take into account the recent developments in safety science. Manscu project focuses on three topics which are relevant practitioners in the Nordic nuclear industry. Safety management approaches should:

1) support the development of sufficient *understanding and knowledge of nuclear safety* and risks as well as nuclear industry specific working practice demands.

2) take into account the needs of *other contexts than the operating units*. Especially we focus on creating knowledge on how safety culture should be understood in a) design activities and b) complex networks of subcontractors. The networks and supply chains may be multicultural and interdisciplinary.

3) support *organisational alertness (mindfulness)* to new risks or other unexpected conditions which are based on either technical or social phenomena. It also means avoidance of complacency and constant effort of continual improvement.

MANSCU project carried out both theoretical work and case studies in Finland and Sweden. The case studies were designed based on interests of the power companies and regulators and thus, they were not directly structured according to the MANSCU project generic goals. During 2011 and 2014 the case studies focused in:

- Understanding *design* activities from safety culture point of view (subtask SADE/DESIGN).
- Understanding how unexpected daily situations are handled and could be supported in maintenance activities (subtask MoReMo). Various concepts stemming from *resilience engineering* paradigm (cf. Hollnagel 2006) were applied, and their applicability in nuclear domain were illustrated.
- Understanding the expected and experienced benefits of *Human Performance Programmes*, which become a popular safety management approach also in the Nordic countries during the last decade (subtask HUMAX).

In addition to the case studies MANSCU project studied how the concept of safety culture could be utilised in networked activities, which are typical in the pre-operational and post-operational stages of a nuclear power plant lifecycle (Gotcheva et al. 2011, Oedewald et al. 2011b, Oedewald 2012, Oedewald & Gotcheva, forthcoming). In this chapter we will focus on reporting the main results of the three sub-tasks; DESIGN, MoReMo and HUMAX.

Subtask DESIGN: Safety culture in the design activities

Design issues have often been found as contributing to accidents across different industrial domains. In the nuclear industry, between 1985 and 1997, more than 3100 licensee event reports in the United States have identified and reported design-based issues (Lloyd et al., 2000). Also the major nuclear accidents have revealed shortcomings related to the design process. For example the Three Mile Island accident revealed a design flaw for pressurizer relief valve as well as design problems in the control room. Various design issues (e.g. the location of the emergency diesel generators) emerged in the analysis of the Fukushima nuclear disaster in 2011 as well (The National Diet of Japan, 2012). As design flaws can contribute to serious nuclear power accidents, it is important to also consider how safety culture affects the design activity and how the design work can be supported from this perspective. The DESIGN subtask was an opening to this complex and understudied research area. It aimed at providing general understanding on design activities from safety culture perspective and mapping current cultural challenges and opportunities.

Literature review on theoretical concepts and methods available to prevent design errors, and review of international standards on human factors engineering (HFE) were performed. Interview studies with regulators, licensees and designers were carried out. Altogether 35 semi-structured in-depth individual interviews, as well as some workshop interviews were conducted.

The results highlight that design is a conceptual, creative, analytical and uncertain process. In the beginning of the process there are various possible paths to be followed to come up with a specific practical solution. This kind of conceptual and creative activity is difficult to standardize or support with detailed instructions. The study showed that the organisational challenges, for which the nuclear industry should pay attention to when developing safety culture in design activities, can be grouped into three main categories:

Firstly, design activities require effective *collaboration* between multiple parties, which also means a risk of blurred responsibilities and various communication challenges concerning safety requirements and priorities. The customer (e.g. the licensee), design organisation and the regulatory body are the core actors of the design activity. In major modernization projects and new build the design activities are carried out by large network of design organisations which sets even more demands on collaboration activities. Secondly, design activities call for effective *requirements management*. Identifying, finding, understanding and balancing the various requirements was described as one of the core activities by the designers interviewed in the study. In the operating units understanding the design basis of some existing systems may be challenging since there may be discontinuity of the documentation. In the new build project e.g. the different national regulatory requirements should be thoroughly understood by foreign designers. Thirdly, the designers' sense of *responsibility* of safety and functioning of the end-product may be challenged due to multiple reasons which are related to the designers' geographical, contractual or psychological distance from the end-users. This may lead to solutions which are suboptimal, although the designers formally fulfil the demands of their assignment. When design activities are dispersed to multiple companies - often from different countries - special attention is needed both to encourage that the designers study the local contexts of the end-product. A culture where any safety or quality concerns would be openly reported can be facilitated by enhancing the designers knowledge on the broader context and use of the systems.

Subtask MoReMo: Can resilience engineering approach help in managing safety in maintenance activities?

The MoReMo subtask described maintenance organisations' practices in coping with underspecified, unanticipated multi-actor work tasks (Oedewald et al. 2012, Macchi et al. 2013). These situations are prone to so called human errors but in most cases the organisations cope well with them. The purpose was to find means to support adaptive work processes at the nuclear plants without sacrificing the safety of the decisions or the culture of complying with procedures.

MoReMo carried out field observations, interviews and document reviews concerning working practices during outages in three Nordic plants. In addition to that observations and interviews covered the field operator's work in one plant. The main goal was to identify what kinds of ad hoc adjustments are done, are there goal conflicts, are the adjustments good from the safety point of view or are some of them risky.

The observations and interviews confirmed the expectations that maintenance is an activity where tasks are underspecified and unexpected situations are part of everyday work. The unexpected situations we observed included following (Macchi et al. 2013):

- the equipment the working group was using did not work and the working group had to find new equipment which postponed the task until the next day

- a major overhaul and modification was scheduled to be carried out in a short timeframe during the outage which required new working arrangements: extra workers were borrowed from other unit and two shift system was implemented
- field operators struggled in finding the valves they were supposed to close in order to ensure isolation and maintenance working group fell behind the schedule
- a component was installed upside down during the overhaul which resulted in delays of start up after the outage
- recent modifications in the building have not been taken into account in the work planning and that caused challenges for the maintenance crew when they were lifting a big component
- when a system was opened the piping did not match with the drawings.

Supporting the handling of these kinds of typical unexpected situations was found to be challenged by the fact that the interviewed maintenance supervisors and workers seldom noticed that they were facing a situation which required a local adaptation. These situations were experienced so mundane that the observed workers seldom explicitly considered the different options they had in the situations. For most of the occurrences there was no specific instruction on how to proceed; what is a good practice or risky behaviour in that kind of a situation. If these situations would have ended up in an unavailability of the technical system they would have been – most likely - labelled as human errors. If they do not result in any technical problems the actions taken are considered as normal organisational practice. From safety management perspective this kind of a hindsight approach is not fruitful. There should be means to identify adjustments points as they are happening and tools to evaluate the safety effects of the possible actions.

Thus we came up with an evaluation framework (see Macchi et al. 2013, appendix A2) which on one hand evaluates *whether the practice or ad hoc decision is done according to the core task demands and on the other hand whether the way it is carried out complies/violates the safety culture criteria* (based on the DISC model, see Oedewald et al. 2011). Based on the evaluation framework we developed a first version of a checklist tool which might be useful for the power plant organisations. The checklist could be used for, first of all, helping the maintenance organisation to pay attention to the fact that they do frequently carry out work process adjustments. Secondly, when a situation which needs adjustment is recognised the checklist could help in evaluating whether the decision would be problematic in a long turn. Thus the checklist could serve as one practical safety management tool for supporting resilience in maintenance and outages.

During the MoReMo study it seemed evident that the nuclear industry organisations still seem to find human error reduction as a more natural safety management approach than resilience engineering type of approach which emphasis the need for human performance variability. Therefore, in order to study this issue more deeply we carried out the subtask HUMAX, which is described next.

Subtask HUMAX: Expected and experienced effects of human performance programmes

In recent years most Nordic nuclear power plants have implemented so called human performance programmes. According to Department of Energy (DOE 2009a, 2009b) the goal of human performance programmes is to *reduce error and manage controls*. Error reduction focuses on work execution and includes such means as preparation of work task, improving performance during task execution, and reporting feedback after task completion. Management of controls on the other hand focuses on making sure that there are sufficient safeguards and that hazard or opportunities for error are eliminated. There are various approaches on how to develop, implement and conduct human performance programmes (e.g. IAEA 2001, 2005; Pershing 2006), but typically human performance programmes consist of choosing and implementing a particular set of human performance tools (HU tools). HU tools are simple aids or working practices to be used on all levels of the line organisation, although shop-floor maintenance and control room workers are most often in focus. The HU tools include, for example, peer checking, three-way-communication, pre-job-briefing and post-job review. The different nature of the various HU tools is illustrated in Figure 1 where the typical HU tools are grouped in accordance to the purpose of the tools.

- **Promoting adherence to procedures/instructions**
 - Procedure Use and Adherence
- **Catching errors**
 - Clear Communication
 - Peer-Checking
 - Independent Verification
- **Sharing insights and experiences to promote performance**
 - Pre-job Briefings
 - Post-Job Debriefings
 - Task Observation
 - Operational Experiences
- **Sensitizing to unexpected states/events**
 - Self-Checking - STAR
 - Questioning Attitude



Figure 1. Most commonly used HU tools grouped according to their purpose. The tools in the up control or prescribe the human actions to large degree. The tools in the bottom provide more freedom for the actors to decide on how to proceed and they rather aim at sensitising to possible errors (Oedewald et al. 2014).

Despite the prominence of human performance programmes there is little scientific literature on the premises behind the HU programmes. Also, the concrete beneficial effects from using HU tools in nuclear power plants remain elusive. HUMAX subtask aimed at providing knowledge of the impacts of the HU programmes and to support implementation of effective HU tools. The focus was especially on maintenance activities. In 2013 and 2014 HUMAX project carried out three case studies in Nordic nuclear power plant maintenance. Furthermore HUMAX disseminated an international survey to human performance experts around the world to gain insights into the motives underlying the human performance programmes and the benefits received.

The results show that HU tools are introduced as error prevention techniques and it is believed that reducing the number of human errors improves nuclear safety. However, the study suggests that it may be difficult to prove measurable improvements in nuclear safety indicators. The benefits of HU tools included other than directly nuclear safety related benefits such as decreased number of occupational safety incidents and less rework. There was a general fairly positive attitude towards the use of HU tools amongst the maintenance personnel when the tools were seen as supporting the quality of work rather than as controlling methods. If not carefully planned, HU tools may complicate and slow down work processes and cause frustration among workers. A risk that task execution becomes mechanistic and HU tools dampen workers' self-initiative was reported. In this regard the results of the HUMAX subtask partially resonate with the scientist concerns with error or individual worker focused safety management approaches.

In order to facilitate mindful use of the tools it is crucial that the implementation process starts by thorough discussion on why, how and when each of the tools should be used in the unique cultural context. The national context and organisational culture may affect the implementation process markedly. The study also pointed out the need to emphasise that HU tools should not be used for compensating system problems, such as poor working conditions or leadership issues. The results of the study were summarised in a set of recommendations to support the HU programme implementation process (Oedewald et al. 2015).

References

- Diet, 2012. The National Diet of Japan The official report of the Fukushima Nuclear Accident Independent Investigation Commission
- DOE 2009a. "Human performance improvement handbook. Volume 1: concepts and principles". DOE Standards. Washington, D.C.: U.S. Department of energy.
- DOE 2009b. Human performance improvement handbook, DOE-HDBK-1028-2009. (Vol. 2: Human performance tools for individuals, work teams, and management). Department of Energy Washington, DC.
- Epstein, S. 2011. A Probabilistic Risk Assessment Practitioner looks at the Great East Japan Earthquake and Tsunami. A Ninokata Laboratory White Paper. Tokyo Institute of Technology.
- Hollnagel, E. 2006. Resilience – the challenge of the unstable. In: E. Hollnagel, D.D. Woods, and N. Leveson, eds. Resilience Engineering. Concepts and Precepts. Aldershot: Ashgate, 55–65.
- Hollnagel, E. 2009. The ETTO Principle: Efficiency-Thoroughness Trade-Off. Burlington, VT: Ashgate.
- IAEA 2012. Safety Culture in Pre-operational Phases of Nuclear Power Plant Projects. Safety report series 74.
- IAEA 2001. A systematic approach to human performance improvement in nuclear power plants: Training solutions. IAEA-TECDOC-1204. Vienna : International Atomic Energy Agency.
- IAEA 2005. Human performance improvement in organizations: Potential application for the nuclear industry. IAEA-TECDOC-1479. Vienna : International Atomic Energy Agency.
- Kirwan, B. 2008. From Safety Culture to Safety Intelligence. In proceedings of Euro-control international conference, Bretigny 2008.
- Lloyd R., Boardman, J. and Pullani S. 2000. Causes and Significance of Design-Basis Issues at U.S. Nuclear Power Plants. NUREG-1275. U.S. Nuclear Regulatory Commission, Washington, D.C.
- Gotcheva, N., Oedewald, P., Reiman, T. & Pietikäinen, E. (2012). Enhancing network safety through network governance, shared understanding and inter-firm heedfulness. In Proceedings of the 11th International Probabilistic Safety Assessment and Management Conference and The Annual European Safety and Reliability Conference, Helsinki, Finland 25–29 June.

Government Decree on the Safety of Nuclear Power Plants, 717/2013, 28 §.

Macchi, L., Gotcheva, N., Alm, H., Osvalder, A-L., Pietikäinen, E., Oedewald, P., Wahlström, M., Liinasuo, M., Savioja, P. 2014. Improving design processes in the nuclear domain. Insights on organisational challenges from safety culture and resilience engineering perspectives. NKS report 301, Roskilde, Denmark.

Macchi, L., Eitrheim, M., Gotcheva, N., Axelsson, C. Oedewald, P. & Pietikäinen, E. 2013. Modelling resilience for maintenance and outage. Final report of Moremo project. NKS report 279, Roskilde, Denmark.

Mark, G., Lyytinen, K., & Bergman, M. 2007. Boundary objects in design: An ecological view of design artifacts. *Journal of the Association for Information System*, 8, 34.

Oedewald, P. & Gotcheva, N. (forthcoming). Safety culture and subcontractor network governance in a complex safety critical project.

Oedewald, P., Skjerve, AB., Axelsson, C., Viitanen, K. & Bisio, R. 2015. Human performance tools in nuclear power plant maintenance activities - Final report of HUMAX project. NKS report 328. Roskilde, Denmark.

Oedewald, P. 2012. Network safety culture. Presented in IAEA Technical meeting on Safety culture in pre-operational phases. 26-30 November 2012, Cape Town.

Oedewald, P., Macchi, L., Axelsson, C. & Eitrheim, M. H. R. 2012. Intermediate report of MoReMO Modelling Resilience for Maintenance and Outage, NKS Nordic Nuclear Safety Research, NKS-262.

Oedewald, P., Pietikäinen, E. & Reiman, T. 2011a. A guidebook for evaluating organisations in the nuclear industry - an example of safety culture evaluation. SSM.

Oedewald, P., Gotcheva, N., Reiman, T., Pietikäinen, E. and Macchi, L. 2011b. Managing safety in subcontractor networks: The case of Olkiluoto3 nuclear power plant construction project. 4th Resilience Engineering International Symposium, Sophia-Antipolis, France, 8-10 June.

Perin, C. 2004. *Shouldering Risks: The Culture of Control in the Nuclear Power Industry*. University Press. Princeton, NJ.

Pershing, J.A. (eds.) 2006. *Handbook of human performance technology. Principals, practices and potential*. 3rd edition. San Francisco: Pfeiffer.

- Reason, J. 1998. Achieving a safe culture: theory and practice *Work and Stress*, 12, 293 – 306.
- Reiman, T. 2011. Understanding maintenance work in safety-critical organizations – managing the performance variability. *Theoretical Issues in Ergonomics Science*.
- Reiman, T. and Oedewald, P. 2009. Evaluating safety-critical organizations – emphasis on the nuclear industry. SSM: Swedish Radiation Safety Authority, Research Report 2009:12.
- Vicente, K. 1999. *Cognitive work analysis: Toward safe, productive, and healthy computer-based work*. Erlbaum, Mahwah, NJ.
- Viitanen, K. (forthcoming). Developing safety culture in nuclear power plants. In Oedewald et al. (forthcoming). *Facilitating safety culture in nuclear industry – challenges and practical approaches*. VTT publication.
- Weick, K. E. and Sutcliffe, K. M. 2007. *Managing the unexpected – Resilient performance in an Age of Uncertainty*, second edition. John Wiley & Sons. Inc.
- Woods, D.D., Hollnagel, E., 2006. Prologue: resilience engineering concepts. In: Hollnagel, E., Woods, D.D., Leveson, N. (Eds.), *Resilience Engineering. Concepts and Precepts*. Ashgate, Aldershot.

2.2 Supporting safe design in the nuclear industry by understanding cultural features of design organizations

Nadezhda Gotcheva¹ and Pia Oedewald²

¹ VTT Technical Research Centre of Finland Ltd
P.O. Box 1300, FI-33101 Tampere

² VTT Technical Research Centre of Finland Ltd
P.O. Box 1000, FI-02044 Espoo

Abstract

Safe and functional nuclear power design is a topic of growing interest due to new builds and modernizations projects in the operating plants. This report highlights and extends some of the main points identified in the SADE DESIGN/MANSCU project by addressing the cultural features that influence the design organizations' activities in the nuclear industry: co-design of end-products by interacting with multiple stakeholders, management of stringent safety requirements, and systemic understanding of design and its effects on safety. It is suggested that these main cultural characteristics should be better understood and taken into account by practitioners and scientists alike to support design organizations for delivering safe and functional end-products in the context of large nuclear projects.

Introduction

Design is a goal-oriented iterative process composed of multiple steps, which aims at developing an artefact to solve a practical problem and achieve a desired performance (Gero, 1990, 1996; Mark et al., 2007; Veland, 2010). The engineering design process of developing new functionalities involves creative and analytical skills for inventing and implementing technical artefacts, while balancing between many constraints. Veland (2010) argues that design in the nuclear industry requires "design thinking", which is a solution-focused approach for exploring the parameters of the problem and possible practical solutions at the same time. Design thinking is also seen as a balance between the right- and left-brain thinking (Martin, 2009). Design involves dealing with uncertainty and navigating in an open problem space, where different solutions might be possible in the beginning, yet then it is difficult to know how the chosen solution will turn out from safety perspective. IAEA (2007) defined design as "the process and the result of developing a concept, detailed plans, supporting calculations and specifications for a facility and its parts".

It has long been acknowledged that safety culture should be taken into account and continuously developed in operational nuclear power plants. Before becoming operational, plants have been planned, designed, constructed and commissioned by involving multiple organizations. The existing safety management approaches have

not been specifically focused on the needs and purposes of design organisations, although design flaws have been identified as important contributors to serious nuclear accidents (Kinnersley & Roelen, 2007). Design work is inherently complex and uncertain; thus evaluating relevant safety-related solutions and tracing safety flaws is challenging. Design error is defined as a design feature, which makes it “unable to perform according to its specification” (Taylor, 2007: 62). For example, the analysis of the Three Mile Island reactor accident in 1979 revealed design flaws in the pressurizer relief valve, as well as in the control room (Lloyd et al., 2000). The Fukushima nuclear accident analysis highlighted the height of the tsunami protection wall and location of the emergency diesel generators (The National Diet of Japan, 2012). The Fukushima disaster also brought increased regulatory scrutiny on the robustness of the designs of proposed new nuclear plants around the world. In some cases this resulted in designers needed to re-engineer additional safety features to withstand unwanted events. Still, in the nuclear industry it is not an easy task to perform design enhancements, e.g. digital versus analog controls, since fundamentally design is largely based on familiar and proven technologies.

However, Kinnersley & Roelen (2007) indicated that risks might be hidden beyond the proved technology since misconceptions between designers and operators have contributed to incidents in safety-critical domains as well. The fact that the designers are influenced by cultural issues as much as the other actors involved in a nuclear power project have not been extensively discussed in the nuclear industry research. From the nuclear power lifecycle perspective, management decisions taken during the conceptual design phase could have a substantial impact and consequences, for example, on maintenance, waste handling and even final decommissioning costs (IAEA, 2002). In that sense design phase offers valuable opportunities to identify and correct possible problems, which could later be actualized in the operating phase and thereby jeopardize safety. Design is a critical phase in the lifecycle because it sets requirements for the whole nuclear plant lifecycle, ranging from manufacturing and construction to maintenance and decommissioning. However, the relevance of the safety culture concept in design of new builds is challenged by the fact that the nuclear fuel and the associated hazards are not yet present at the site.

In modernization projects in the operating plants the challenges are rather related to the need to test newly designed features or align new features in the context of interconnected systems within an operational plant, which has its unique history of various modifications, aging phenomena and organisational practices of the operating staff. If safety culture principles and practices are not adequately understood and applied from the very beginning of the design project, there is a risk of latent and actualized safety deficiencies, which might actualize unexpectedly during the subsequent operation of the plant (IAEA, 2012). Therefore, understanding safety culture in design creates technical and organizational preconditions for a good safety culture in operational and even decommissioning phases. In order to support design organizations in delivering safe artefacts it is important to understand how their organizational and cultural features influence their activities.

Objectives and scope of the report

The report focuses on highlighting *the core cultural features that influence the design organizations' activities in the nuclear industry*, e.g. shared conceptions, assumptions, norms, practices, etc. The aim is to assist the licensees when, for example they need to audit design organizations during the contractual process: what they should take into account when contracting companies for delivering various aspects of design in a future plant? It is expected that this report will be beneficial for licensees to be better able to support design organizations for delivering safe artefacts.

The SADE DESIGN sub-project (January 2011-December 2013) under the MANSCU project (see Macchi et al., 2012, 2013, 2014) was organized in three phases and focused on the following set of activities: a) identifying the organizational challenges in the design and implementation activities, and understanding how they affect the safety of the operating power plant; b) safety culture characteristics required during the design of new technological and organizational solutions to contribute to resilient nuclear power plants; and c) the role of resilience engineering and safety culture theory for improving design practices. Extensive literature review on theoretical concepts and methods available to prevent design errors and to assess risks, and review of international standards on human factors engineering (HFE) were performed under these sub-projects. A number of case studies, consisted of altogether 35 semi-structured in-depth individual interviews, as well as some workshop interviews were carried out with the regulators, licensees and various experts involved in design and implementation activities in the Nordic nuclear domain. The interview themes were related to respondent's work and tasks, definition of nuclear safety, evaluation of nuclear safety, contribution of design to nuclear safety, understanding of design principles, human factors engineering, and safety culture in design organizations. In the current report, some main points related to this study are summarized and highlighted.

Cultural features of design in the nuclear industry

Culture develops gradually in the organization as it learns ways to deal with pressures, concerning external adaptation and internal integration (Schein, 1990). Accordingly, the culture of an organization frames all activities in the organization and has widespread impacts on the performance. Practitioners and scientists have defined the concept of *safety culture* in different ways. In this report safety culture is understood as those aspects of an organization's culture that define how safety is viewed and handled on a daily basis. Reiman & Oedewald (2009) stated that safety culture can be seen as *organization's potential for safe activities*. Furthermore, Reiman et al. (2012) have defined safety culture as an organization's ability and willingness to understand the nature of safety and hazards inherent in their activities, and the ability and willingness to act in a manner that the hazards are taken care of and safety is created. In that sense, certain cultural features prevail in the nature of design activities in the nuclear industry as well.

Co-designing artefacts through interaction of multiple stakeholders

Design in the nuclear industry is developed both by in-house personnel of the power company and outsourced design companies. Such engineering design companies may serve multiple customers in various industrial domains and they might not necessarily be familiar with the nuclear industry context and its specific requirements. Many of the design companies may not be familiar with the term 'safety culture' and related behavioural and management expectations concerning e.g. open reporting, quality assurance and personnel training. One of the most complex issues facing design in safety-critical domains is the involvement of multiple stakeholders with various tasks and responsibilities, who interact to ensure development of the final artefact (Menon & Kelly, 2010). This interaction can be particularly challenging in the beginning of the design phase, since there might be misunderstandings due to ill-established or no pre-existing relationships. Different countries may use different design terminology, which may challenge the smoothness of collaboration. Furthermore, international subcontractors or suppliers may not have a sound understanding of national or local nuclear requirements and context.

The interview results showed that the process of co-designing was sometimes experienced as challenged because *organizations involved do not always share safety philosophies and understand safety requirements in the same way* (Macchi et al., 2014). For example, if designers do not understand the principle of continuous improvement of nuclear safety, they may not be aware of the need to design enough buffers for upgrade of the components. This need stems from the fact that throughout the long lifecycle of a nuclear power plant, from its design to decommissioning and dismantling, major changes usually happen in the engineering and scientific knowledge that underpin the design, construction, operation and maintenance of the plant (OECD, 2011).

Furthermore, in this context *distributing roles and responsibilities between different stakeholders in design was sometimes experienced as challenging* (Macchi et al., 2014). When the design activities are purchased from several different subcontractors, responsibilities might get blurred, especially regarding the management of technical and organizational interfaces. Overcoming one's own immediate responsibility area, and for example raising a concern of an interface issue, necessitates that the persons involved have a high sense of responsibility over the functioning of the entire system. The interview results suggested that subcontracting and the fact that nuclear safety may be an intangible concept for some design partners could hinder development of such overall responsibility. Also the roles and responsibilities between buyers and vendors and the involvement and oversight strategy of the regulator were perceived sometimes unclear. Very prescriptive regulatory strategy and heavy involvement in reviewing the design from the early stages, may be perceived by the licensee as the regulator would be available for consulting and coordinating the design process and solutions.

However, the involvement of multiple actors with various competences and perspective affects also positively the safety of design. Different actors provide unique mix of technical competencies, and involvement of multiple actors provide requisite

variability of viewpoints and iterative checks which may reduce the likelihood of design error. Because the design activities involve interaction of multiple stakeholders, measures should be taken to define carefully and clearly the scope of responsibilities, consider the management and leadership style of the design project, create and elaborate means for collaboration with different stakeholders and perform training on differences between national regulatory requirements. In addition, various means to support openness and willingness to admit own problems are needed, taking into account the characteristics of the design project network, which consists of possibly competing partners and commercial contracts which may have been tight to schedules.

Management of stringent safety requirements

Design in the nuclear power industry is highly regulated and the role of the regulator is more emphasised than in conventional industries. The need to balance between economy and safety is well-known in the nuclear industry, and the requirements are developed to ensure that systems take all safety considerations into account. However, the design process requires also that attention is paid to feasibility, or the economic aspects of the chosen solution. In the interviews the designers described this balancing between various needs and constraints as one of the core issues in their work. Some of the requirements are issued by the regulator, others stem from design basis of the plant, some from international standards and codes and also from the end users. In practice major effort in design activities is related to collecting, reading, analysing and interpreting requirements, and respectively producing extensive written documentation. Interpretations of the requirements among design companies and individual designers might differ (Menon & Kelly, 2010). The designers communicate their work through documents where they should be able to illustrate that all the requirements have been taken into account. The interview study pinpointed the inherent tension in the design activity between the innovative concept building stage and the rigorous documentation and regulatory approval stage. Communication process between designers and the regulator involves tedious paper work and formal interaction. This process is sometimes experienced as bureaucratic, and the interview results suggested that sometimes it might remove the collective focus from the overall solution to the details of argumentation of the fulfilment of the requirements.

To summarize, as the design activity involves understanding and management of wide range of safety requirements, measures should be taken through adequate communication to ensure that the focus on the requirements does not jeopardize the ability to see the big picture in the design project. The uncertainties in the design process should be appreciated and therefore, preparedness for possible changes and iteration in schedules, for instance, should be kept up to date.

Systemic understanding of design and its effects on safety

In general, a systemic view on safety involves an awareness on the dynamic nature of safety, the interrelation of human, organizational and societal factors, and the non-linear nature of their interactions. A holistic understanding of safety in design is needed as it is not sufficient for designers to understand the specific requirements of certain component or system. They need to understand not only the requirements per se but also the underlying assumptions of the requirements.

Many of the safety challenges related to design are result of a suboptimal understanding of the context and possible usability conditions of the systems, rather than e.g. calculation errors. If a designer has never been or worked at an operating power plant, it may be difficult to consider some relevant issues and understand the operational context. It is thus important to support designers in understanding the specifics of the end-product context and the operators' needs and constraints. One aspect which challenges the systemic view on safety is the duration of the design process: for example, in new builds or in major modernisations the design phase usually takes many years, during which staff turnover is likely and knowledge transfer and sense of continuity may become an issue. In turn, these may hinder the ability of designers to understand the role of that particular component or system for the functioning of the end product and the overall safe operation of the plant. Hence, in long-term nuclear power projects the organisational learning mechanisms, such as mentoring of newcomers and documentation management within design organisations, as well as between the design and operating organisations, need to be well developed.

Summary and conclusions

This report provides suggestions for practitioners and researchers on how to support safe design in the nuclear industry by understanding cultural features of design organizations. Following the work of Reiman & Oedewald (2009) and Oedewald et al. (2011), safety culture is seen as formed by a safety conscious mindset, organizational systems and structures, which create preconditions for good quality work, and understanding of the hazards and safety consequences of the work. This perspective tries to provide insights into elements that are required from the organization to be able to prioritize safety in a sensible manner. In practice, when the licensees need to audit a set of design organizations during the contractual process, they need to ensure their ability and willingness to deliver safe and functional end-products for the nuclear industry. What safety culture features they should pay attention to when approaching and contracting design companies for delivering various aspects of design in a future nuclear power plant, or a modernization project in existing plants? The cultural features that influence the design organizations' activities in the nuclear industry are integrated here into three main "pillars": 1) co-design of end-products through interaction of multiple stakeholders; 2) management of safety requirements; and 3) systemic understanding of design and its effects on safety.

Regarding the fact that major design activities are about *interacting with multiple stakeholders in a project setting* the collaboration between different design organizations and the operating organization should be supported by various means. Attention should be paid, on one hand, to designers' shared feelings of responsibility for safety and on the other hand on clear roles between partners. Responsibility can manifest for example in efforts put in studying the end user's needs and the operational context, and identifying differences between national regulatory requirements. Interacting with multiple actors in a competitive and dynamic project environment under a tight time schedule requires developing good leadership skills from different parties to support openness and willingness to report any safety and quality concerns.

The *amount of requirements* associated with nuclear industry design brings along not only the need for a rigorous requirements management approach but also the need to acknowledge uncertainties and the iterative nature of design work. This necessitates organisational preparedness for changes and adjustments e.g. in schedules and in documentation. In addition, measures should be taken so that the required focus on dealing with a broad range of requirements does not threaten the ability of designers to see the big picture in the design project.

Concerning the challenge of a *systemic understanding of design and its effects on safety*, means should be in place for developing designers' sense of engagement and awareness of the need to continuously gain the necessary knowledge for designing safe and functional future end-product, even when faced with slight uncertainties. The long timeframe of the nuclear power projects requires special attention to be devoted to enhancing the organisational learning mechanisms both within design organisations and between different actors in the project network to ensure that despite personnel changes, there is continuity of knowledge and understanding of "how it all fits together".

References

- Gero, J.S. 1990. Design prototypes: A knowledge representation schema for design. *AI Magazine*, 11(4): 26-36.
- Gero, J.S. 1996. Creativity emergence and evolution in design. *Knowledge-Based Systems*, 9: 435-448.
- IAEA, 2002. Safe and effective nuclear power plant life cycle management towards decom-missioning, IAEA, Vienna, IAEA-TECDOC-1305.
- IAEA, 2007. IAEA safety glossary. Terminology used in nuclear safety and radiation protection. Vienna: International Atomic Energy Agency.
- Kinnersley, S. & Roelen, A., 2007. The contribution of design to accidents, *Safety Science*, 45, 31-60.
- Lloyd R., Boardman, J. & Pullani S., 2000. Causes and Significance of Design-Basis Issues at U.S. Nuclear Power Plants. NUREG-1275. U.S. Nuclear Regulatory Commission, Washington, D.C.
- Macchi, L., Gotcheva, N., Alm, H., Osvalder, A-M., Pietikäinen, E., Oedewald, E., Wahlström, M., Liinasuo, M. & Savioja, M. 2014. Improving design processes in the nuclear domain. Insights on organisational challenges from safety culture and resilience engineering perspectives, NKS Nordic Nuclear Safety Research, NKS-301.
- Macchi, L., Pietikäinen, E., Liinasuo, M., Savioja, P., Reiman, T., Wahlström, M., Kahlbom, U. & Rollenhagen, C. 2013. Safety Culture in Design, NKS Nordic Nuclear Safety Research, NKS-278.
- Macchi, L., Reiman, T., Savioja, P., Kahlbom, U. & Rollenhagen, C. 2012. Organizational factors in design and implementation of technological and organizational solutions in the nuclear industry, NKS Nordic Nuclear Safety Research, NKS-263.
- Mark, G., Lyytinen, K. & Bergman, M. 2007. Boundary objects in design: an ecological view of design artifacts, *Journal of the Association for Information Systems*: Vol. 8(11), 34.
- Martin, R. L. 2009. *The Design of Business: Why Design Thinking is the Next Competitive Advantage*. Harvard Business Press.
- Menon, C. & Kelly, T. 2010. Managing safety requirements across supply chains, 5th IET International Conference on System Safety, October, Manchester, UK.

- OECD, 2011. Improving Nuclear Regulation. NEA Regulatory Guidance Booklets, Vol. 1-14, Improving Versus Maintaining Nuclear Safety. Organisation for Economic Co-Operation and Development.
- Reiman, T. & Oedewald, P., 2009. Evaluating safety-critical organizations – emphasis on the nuclear industry. SSM: Swedish Radiation Safety Authority, Research Report 2009:12.
- Reiman, T., Pietikäinen, E., Oedewald, P. & Gotcheva, N., 2012. System modelling with the DISC framework: Evidence from safety-critical domains, Work. IOS Press. 41, 3018-3025.
- Schein, E. H., 1990. Organizational culture. *American Psychologist*, 43(2), 109-119.
- Taylor, J. R. 2007. Statistics of design error in the process industries. *Safety Science*, 45(1), 61-73.
- The National Diet of Japan, 2012. The official report of the Fukushima nuclear accident independent investigation Commission. The National Diet of Japan, Tokyo, Japan.
- Veland, O. 2010. Design patterns in the nuclear domain: theoretical background and further research opportunities. OECD Halden reactor project. HWR-932.

3. Sustainable and future oriented expertise (SAFEX2014)

3.1 SAFEX2014 summary report

Eerikki Mäki¹, Krista Pahkin²; Anna-Leena Kurki², Sara Lindström²

¹Department of Industrial Engineering and Management, Aalto University
P.O.Box 15500, FI-00076 Aalto – Finland

²Centre of Expertise for the Development of Work and Organizations
Finnish Institute of Occupational Health
Topeliuksenkatu 41 a A, FI-00250 Helsinki – Finland

Abstract

SAFEX2014 aimed at producing information and knowledge that can be applied for improving organizational performance in the areas of expertise development, knowledge and competence management and human resource management (HRM). Large-scale surveys, and targeted interviews and workshops were used for collecting data. SAFEX2014 has produced longitudinal data that help nuclear industry organization to evaluate and develop their managerial and organizational practices. The project has also produced an assessment tool that can be used for assessing and developing organizational HRM practices.

Introduction

SAFEX2014 research project aimed to analyze and understand how organizations in the nuclear energy industry maintain and develop expertise that is needed for guaranteeing safe operations. The focus was both on current and future organizational practices and human resource management methods that will help organizations in this challenging task. The importance of human resource management and management of knowledge and expertise has been recognized in many IAEA reports (IAEA 2004, 2006, 2008). The aims of knowledge management are several including

e.g. identifying valuable knowledge both inside and outside of the organization, providing access to knowledge, developing new knowledge and enhancing usage of existing knowledge, maintaining and updating knowledge resources and expertise (e.g. McAdam & McCreedy 1999, Bhatt 2001, DeTienne et al. 2004, Huysman & de Wit 2004).

Every organization manages its human resources somehow. Human resource management (HRM) includes several areas including e.g. human resource planning, personnel recruitment and selection, personnel appraising, and training and development (Schuler & MacMillan 1984). Even though organizations typically have separate HR-unit, more and more often HRM practices are implemented in the front line by unit and group supervisors (Purcell & Hutchinson 2007).

Nevertheless, front line managers and supervisors may lack skills and methods to manage and lead their employees (Larsen & Brewster 2003). To be successful they need feedback on their own human resource management performance so that they know what works and what needs to be improved. Employees and the work performance are the good indicators of that, but then front line managers and supervisors must have a feedback channel to gather that information. A rough illustration of the project context can be illustrated as in Figure 1.

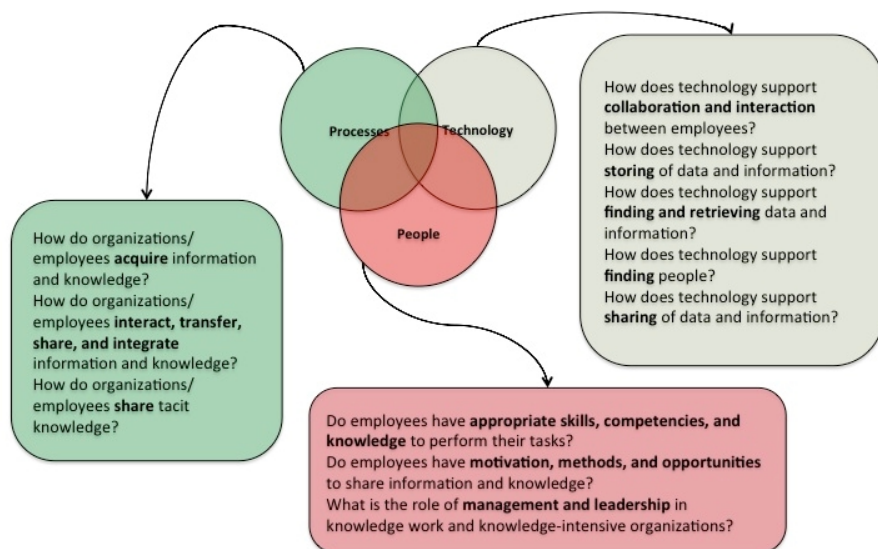


Figure 1. Safex2014 aimed to understand the different elements that enable organizations to utilize and develop their employees' expertise.

So, organizations (and people responsible for management and leadership) must be capable to understand how their processes, technology and people help at achieving the objectives of the organization.

Safex2014 research project was mostly focusing on people and their interaction on work. Safex2014 research project aimed to generate results that are easily applicable in the Finnish nuclear energy organizations, and which may improve the development and utilization of organizational expertise.

Two practical publications (Pahkin et al. 2014a, Pahkin et al. 2014b,) (in Finnish) are publicly available through the websites of Finnish Institute of Occupational Health. Both publications will advise HR-personnel and managers / supervisors on how to take care of the employees: giving them opportunities to develop in their areas of expertise and how to develop well-being of employees.

Main objectives

As already stated in the research proposal, the purpose of SAFEX2014 was to generate new knowledge on

- evaluation methods of HR practices,
- knowledge and competence management in nuclear power industry and
- good practices in the area of human resource management, leadership and collaboration between organizations.

In addition, the SAFEX2014 aims at creating practices for

- the development of leadership and management of human resources
- guaranteeing expertise and
- promoting collaboration of experts across organizational boundaries.

Human resource management in this project includes both HR-department /specialists and team/group leaders or supervisors. SAFEX2014 aimed at delivering and disseminating information and results in many forms. *Research reports* summarized subproject's results and conclusions. Research reports were either public or available only for the participant organizations. *Workshops* and interactive discussion and development forums were targeted for the members of the participating organizations and researchers. Short articles in *practically oriented journals* (e.g. ATS Ydintekniikka) (i.e. Mäki et al. 2013, Linström et al. 2015) disseminate the findings for the broader public interested in research topics. National and international *science forums* (scientific conferences and scientific journals) are used to disseminate and discuss the results. And finally, SAFEX2014 aimed to produce results that can be *implemented into daily work practices* by active participation of the participating organizations.

Assessment and follow-up of well-being and expertise development and collaboration capabilities of the nuclear power expert network

In the funding period 2011-2014 Safex2014 research project conducted two surveys in the Finnish nuclear power organizations. Six organizations participated the survey

2012 and four 2014. The number of respondents was 770 and 639, respectively. The survey results have produced valuable information to the participating organizations on many aspects on their HRM practices and expertise development opportunities. The survey study has been conducted every second year since 2008 and some of the Finnish nuclear industry organizations have participated to the survey every time. Therefore the survey results have provided helpful information on the development and progress of the studied themes on the participating organizations. For example, Figure 2 depicts the experienced stress of employees in two case organizations in years 2008, 2012, and 2014.

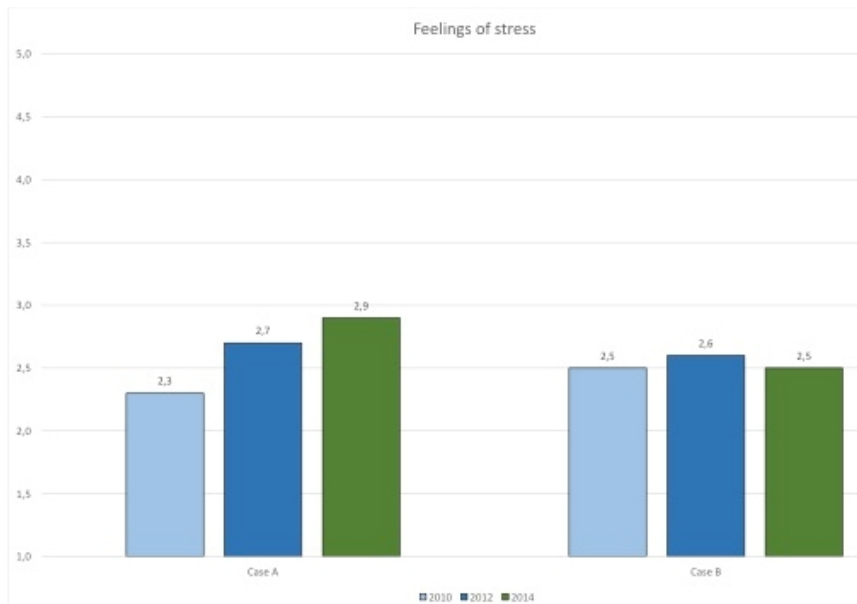


Figure 2. Experience of work related stress in two case organizations.

Moreover, as an example Figure 3 explains how work engagement is associated with several work related features (based on survey 2012) This kind of information is a powerful tool for human resource specialist and managers, because it enables to target actions that need to be taken to take care of the employees and improve performance of the organization.

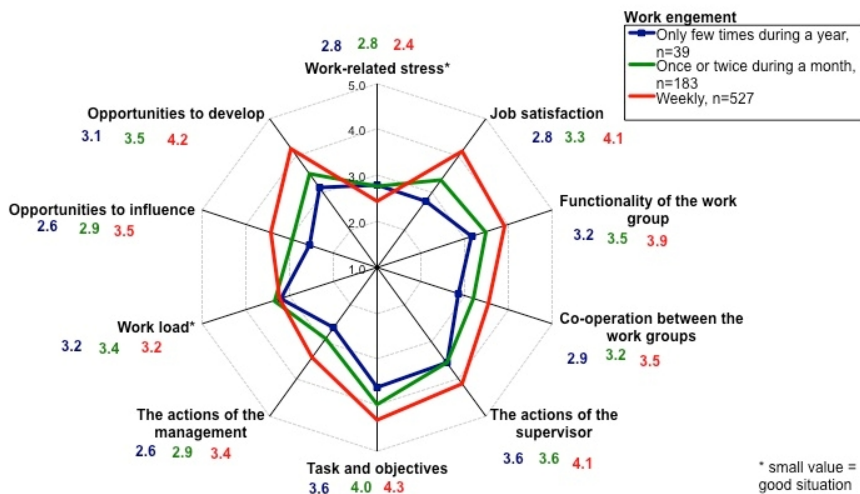


Figure 3. Experience of work engagement and its relation with some job related factors.

Assessment method for evaluating HRM practices

The second major contribution of Safex2014 project was a self-assessment method that organizations can use for analyzing their HRM practices and targeting the efforts of development. The assessment method is easy to use and apply in different small groups. It is a structured and interactive method for collecting views and opinions on how different HRM practices are applied in organization. Different HRM practices are to be evaluated in scale 1-3 (1=practice needs to be improved, 2=practice works well, 3=practice works excellently). The assessment method consists of four different HRM related theme areas:

- Management of career development (covered with 9 different aspects/statements) e.g.: "Consequences of employee exit on unit's competence base are evaluated"
- Management of competence development and knowledge sharing (covered with 9 different aspects/statements) e.g.: "Enough time and other resources are reserved for developing expertise"

- Management of performance (covered with 10 different aspects/statements) e.g.: “Duties and responsibilities are clearly defined, and updated when needed”
- Management of organizational and safety culture (covered with 9 different aspects/statements) e.g. “We celebrate/show happiness when having good insights/results”

The assessment method and the information it produces have several benefits. First, it gives employees an easy way to give feedback to supervisors. Second, use of the assessment method offers new perspectives for the supervisors and HR-personnel and facilitates learning. Third, it generates valuable discussion and learning opportunities (sharing of best practices), which maybe does not occur otherwise. Fourth, it gives direction to the development actions.

The use of the assessment method does not require a lot of time or other resources and it is easily implemented according the following steps:

- Deciding the participants
- Participants’ individual assessment of HRM practices
- Organizing 2-3 hour workshop for the participants in order to make the results of the evaluation visible and deciding the actions that need to be taken

Figure 4 depicts the visual outcome of the combined assessment results. The picture is taken from one actual pilot study that was organized in one nuclear energy organization in 2013.

Tavoitteiden asettaminen	◆ käytännössä kehitettävää	◆◆ hyvä käytäntö	◆◆◆ edistysellinen käytäntö
Tehtävänkuvat (roolit, tehtävät ja vastuut) on määritelty.	✂ ✂ ✂ ✂	✂ ✂ ✂ ✂	✂
Yksilön/työryhmän/projektin suoritumisodotukset on määritelty.	✂ ✂	✂ ✂ ✂ ✂	
Työntekijöillä on mahdollisuus viestiä johdolle, mikäli työssä ilmenee jotain sellaista, joka vaikuttaa yksilön/ ryhmän/ projektin suoritumisodotusten määrittelyyn.	✂ ✂	✂ ✂ ✂ ✂	✂
Suoritumisodotuksiin kuuluu hyvän turvallisuuskulttuurin...		✂ ✂ ✂ ✂	

Figure 4. Workshop participants’ evaluations on different HRM practices (in the figure employees, managers, and HR-personnel have used different colors in their answers).

Practical implications

SAFEX2014 research project has produced nuclear industry organization specific information and tools that can be applied to improve performance of the organizations. To be able to benefit from the results, nuclear industry organizations need to be able to allocate time and effort to utilize the findings of the SAFEX2014 project. Usually the most demanding part of organizational development is to implement the development efforts and embed new practices into organizational routines.

References

- Bhatt, G. 2001. Knowledge Management in Organizations: Examining the Interaction Between Technologies, Techniques, and People. *Journal of Knowledge Management*, vol. 5 (1), 68-75.
- DeTienne, K., Dyer, G., Hoopes, C. & Harris, S. 2004. Toward a Model of Effective Knowledge Management and Directions for Future Research: Culture, Leadership, and CKOs. *Journal of Leadership & Organizational Studies*, vol. 10 (4), 26-43.
- Huysman, M. & de Wit, D. 2004. Practices of Managing Knowledge Sharing: Towards a Second Wave of Knowledge Management. *Knowledge and process management*, vol. 11 (2), 81-92.
- IAEA 2004. The nuclear power industry's ageing workforce: Transfer of knowledge to the next generation, IAEA-TECDOC-1399
- IAEA 2006. Knowledge Management for Nuclear Industry Operating Organizations. IAEA-TECDOC-1510
- IAEA 2008. Planning and Execution of Knowledge Management Assist Missions For Nuclear Organizations, IAEA-TECDOC-1586
- Larsen, H. H., Brewster, C., 2003. Line management responsibility for HRM: what is happening in Europe. *Employee Relations*, 25 (3), pp. 228-244.
- Lindström S., Kurki A-L., Mäki E. & Pahkin K. 2015. Urapolut ydinvoima-alalla ATS Ydintekniikka
- McAdam, R. & McCreedy, S. 1999. The Process of Knowledge Management within Organizations: A Critical Assessment of both Theory and Practice. *Knowledge and Process Management*, vol. 6 (2), 101-113.
- Mäki, E., Pahkin, K., Kurki, A-L., & Lindström, S. 2013. Arviointimalli henkilöstövoimavarojen johtamisen tueksi. *ATS-lehti* 4/2013.

- Pahkin, K., Mäki, E., Kurki, A-L. & Lindström, S. 2014a. Kestävää ja kehittyvää tulevaisuuden osaamista ydinvoima-alalla. Työterveyslaitos ja Aalto-yliopisto, 2014. ISBN: 978-952-261-517-6 (PDF). 31 pages.
- Pahkin, K., Mäki, E., Kurki, A-L. & Lindström, S. 2014b. Kohti yhtenäisiä henkilöstövoimavarojen johtamiskäytäntöjä. Opas johtamiskäytäntöjen arvioimiseksi ja kehittämiseksi turvallisuuskriittisessä organisaatiossa. Työterveyslaitos ja Aalto-yliopisto, 2014. ISBN 978-952-261-381-3 (pdf). 27 pages.
- Purcell, J., Hutchinson, S., 2007. Front-line managers as agents in the HRM-performance causal chain: theory, analysis and evidence. *Human Resource Management Journal*, Vol. 17 (1), pp. 3-20.
- Schuler, R. S., MacMillan I. C., 1984. Gaining competitive advantage through human resource management practices. *Human Resource Management*, Vol. 23 (3), pp. 241–255.

4. Signalled and silenced aspects of nuclear safety (SISIANS)

4.1 SISIANS summary report

Marja Ylönen

University of Jyväskylä
P.O. Box 35, FI-40014 Jyväskylä

Abstract

This summary synthesizes the results of two year research project on Signaled and Silenced Aspects of Nuclear Safety (SISIANS). Signaled refers to well-articulated and silenced means underdeveloped or downplayed sides of safety. The study shows that nuclear safety that is approached predominantly from a technical perspective is also affected by societal and cultural factors. Culture is understood here as consisting of institutional dimensions, i.e. how organisations, such as the regulatory body, act with regard to safety. Culture includes normative (how safety should be dealt with), cognitive (what is relevant for safety), social (how the relationships among the inspectors and between inspectors and industry have been arranged) dimensions. The main conclusion is that even though international nuclear safety regime affects national safety regime, the cultural characteristics give eventual form of safety regulation. Within Finnish safety regulation there are many features which contribute to nuclear safety. At the same there is a need to balance between relatively detailed regulation and to ensure that it gives space for the operators' own safety developments. Obviously grass-root level interaction between inspectors and operators provides a fruitful space for both control and motivation tasks.

Introduction

Nuclear safety is societal, cultural, organizational and technical phenomenon by nature. Recently there has been a growing international interest in the impact of national culture on safety attitudes and safety performance within the nuclear sector. The more new challenges nuclear safety and the regulatory field encounter in the form of accidents, new nuclear power countries, several subcontractors and workers, the more important an understanding of cultural aspects becomes. In addition, the ongoing harmonization efforts in the field of nuclear safety (e.g. by the WENRA) requires understanding of national cultures. Moreover, in the Finnish context, nuclear sector is expanding and new construction projects with various actors coming from different cultures make understanding of national culture relevant, and particularly, culture of nuclear safety regulation. Understanding of features of Finnish nuclear safety regulation may contribute to safety, and decrease misunderstandings between various actors.

This two year project's objectives of the year 2013 were to 1) identify the international and national nuclear safety regimes after the Fukushima accident 2) identification of national cultural features that could affect safety 3) analysis of the concept of safety based on the IAEA Safety Standards. The results of the year 2013 can be found in the report (Ylönen 2015a).

In 2014 research task was to analyse further the Finnish nuclear safety regulation and identify cultural characteristics and their implications on safety. The research was based on 18 interviews with personnel of the Radiation and Nuclear Safety Authority (STUK). The background of interviewees varied from those who had an experience in working in other organisations to those who had worked only in the STUK. There were 7 interviewees who had worked in the STUK at least 10 years or more and 11 interviewees had worked in the STUK nine years or less.

Interview themes included background information, education of the inspectors, their expertise, independence of the STUK, role of trust in regulation, attitudes as regards mobility from a regulator to regulatee and vice versa, characteristics of Finnish safety regulation, experiences as regards different generations, knowledge gaps, and targets of development.

Each interview took about 1 hour and 30 minutes. Interviews were recorded and transcribed. All together there were about 270 pages texts. Through interviews I traced inspectors' understandings of how safety regulation is dealt with and how it should be developed and what aspects could be strengthened or avoided. I looked at contents, their consistencies or inconsistencies, whether there were aspects, which complemented each other or which were in contradiction with each other. Naturally, chosen themes affect what is discussed, but also new topics emerged during the interviews. The interview talk is not equated with action, but it gives hint of inspectors' thinking and practices.

Findings of 2014 research

Trust norm

General features related to Finnish culture, such as trust in other people and institutions (science, technology and education), obedience to the law, appreciation of honesty, promptness and diligence, recur and get amplified in Finnish nuclear safety inspectors' interviews.

Interviews with the inspectors show that trust is a corner stone of Finnish nuclear safety regulation. It is a precondition for the functioning of the safety regulatory system. It is a norm that provides a framework for an interaction between the inspectors and operators. According to the interviews, trust requires reciprocity and if trust turns to distrust, it will take a long time to gain trust again. In Finnish cultural context trust is not blind, but functional one. Hence, a combination through which trust and distrust function within the STUK is through functional trust i.e. based on verification that operators act as they have said, and functional distrust that refers to justified cautions in some regulatory situations. An indication of functional trust is when inspectors think that operators are honest but still it is good to verify that operators have dealt with things in a pertinent way. These can be seen beneficial to the safety regulation. Instead, dysfunctional trust and dysfunctional distrust were seen avoidable by inspectors.

Furthermore, the inspectors described also situations where trust norm is questioned, and when trust may turn to distrust. Situation of distrust may be due to newcomers both within industry and authority. Newcomers have not yet internalized functional trust norm, and they are prone to enter into relationships that may be more adversarial. In addition, situations of distrust may have related to delays in timetables or divergent interpretations of the requirements, such as the safety technical terms and conditions (TTKE, Turvallisuustekniset käyttöehdot). Instructions have been open to interpretations and the licensees have interpreted them in a different way than the inspectors.

Even though this combination of functional trust and distrust is desirable, it may be that some specific features in Finnish safety regulation may cause embarrassment among actors coming from different cultures. It may be that outsiders feel that Finnish inspectors are too strict and carriers of dysfunctional distrust rather than functional trust. This may be due to the YVL-guides, which include relatively detailed requirements, which force inspectors to adopt strict, detailed control. The Figure 1 illustrates different forms of trust and distrust and the risk that functional trust is understood as dysfunctional distrust by outsiders. That could undermine outsiders' trust in Finnish inspectors.

FINNISH NUCLEAR SAFETY REGULATION BASED ON FUNCTIONAL TRUST

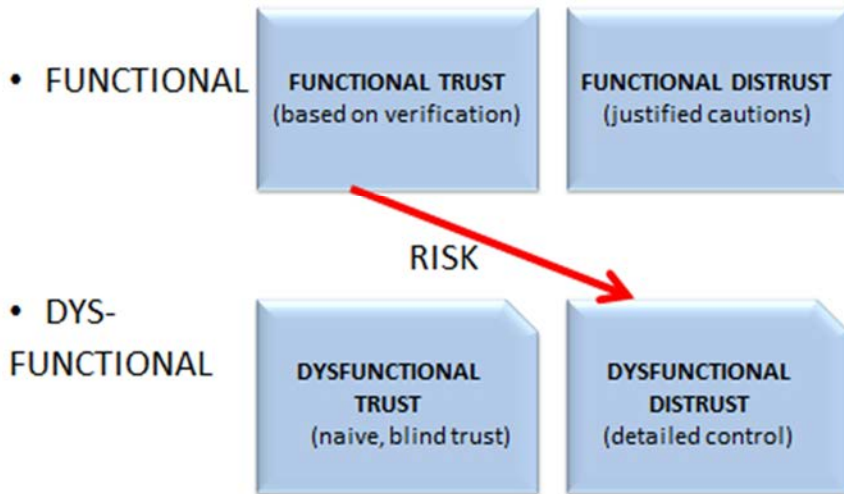


Figure1. Risk that the inspectors' functional trust can be mixed up with dysfunctional distrust.

Independence of the regulatory body

After the Fukushima accident the IAEA emphasised the need of independence of the regulatory authority from the outside pressures. The STUK inspectors were asked to reflect how independence comes true in Finland. The interviews showed that Finnish nuclear safety inspectors feel they are independent from outside pressures and are able to act independently despite the fact that within the nuclear sector in a small country there are relatively few actors and that the inspectors and the operators may know each other. The inspectors based their independence arguments on three types of justifications: Institutional arrangements, which separate regulatory body from the body that allows licenses; Inspectors' practices and decisions, which do not follow the expectations of licensees; Inspectors' high professionalism and focus on pertinent things, facts, which guarantee the independence.

In addition, the report on Characteristics of an Effective Regulator (OECD NEA 2014) distinguishes between different dimensions of independence, one being economy. In the face of current cut of the work force within the research department of the Radiation and the Nuclear Safety Authority, there is a need to consider the independence of the regulatory body in terms of economy. This question becomes

urgent in the current situation in which Finnish nuclear sector is changing fast because of furthering new nuclear power capacity and there would be a need of more personnel within the regulatory body.

Two types of inspectors and relationships between the operators and the inspectors

Related closely to the independence item, but still forming an own separate field of discussion is the relationship between the operators and the inspectors. From the point of view of safety regulation, too close as well as too distant relationships between the inspectors and the operators would be avoidable. If relationships are too close then there is a risk of "regulatory capture" i.e. inspectors would start to promote interests of the industry. Whereas, in the case of too distant relationships, inspectors would not be aware about what is happening in the facilities and that would not contribute to safety either (Baldwin et al. 2012). The question is how to balance between adequate proximity and distance in relationships.

Two types of inspectors were identified on the basis of inspectors' opinions on belonging to Finnish Nuclear Society (ATS) and whether the closeness between the inspector and the operator would be desirable or avoidable (see Figure 2). There are inspectors who are members of the ATS, and found it useful as regards their engineering skills. In addition, there were also inspectors who have recently joined in or are considering of joining in the ATS. Some non-members have recently left the membership due to their position that requires neutrality and some non-members have never considered a membership because of their willingness to maintain their neutrality. The two types of inspectors are the public servant type of inspectors who are collectively oriented and to whom the neutrality is the main principle and they want to keep good relationships but adequate distance to operators. Instead the informal and open type of inspectors is more individually and technical fact-oriented and focused on inspector-operator relationship and is less concerned about the public. They believe they are able to be more efficient in regulation by being more open and informal in their relations with the industry. It is their technical expertise that guarantees their neutrality. Often these inspectors seem to be more open also to other job opportunities or they have a background in working in industry.

These two types of inspectors could be contradictory in some circumstances and they may have different responsiveness to safety matters. Hence, there arises a need to reflect upon the balance between two opposite types of inspectors so that adequate uniformity is found and that there would be adequately close and adequately distant relationships between the inspectors and operators.

TWO TYPES OF INSPECTORS



Figure 2. Two types of inspectors based on their opinions on the belonging to the Finnish Nuclear Society (ATS).

Different roles of inspectors

Studies on safety regulation have emphasized that over the last thirty years there has occurred a shift from a command and control type of regulation towards a de-centered regulation, where safety is an outcome of actions of different actors and networks (Baram and Lindoe et al. 2014). In decentered regulation knowledge is fragmented, which means that no actor has all the relevant knowledge required to deal with complex and multifaceted safety problems or no actor has overview about safety regulation and ability to employ all means necessary to effective regulation (Baldwin et al. 2012). The decentered understanding of regulation also stresses interactions and interdependencies between actors, and a challenge to coordinate actions of different, autonomous actors who are involved in, for instance nuclear activities. In a situation of decentered regulation, where the outcome of the safety regulation is a consequence of actions of several actors and networks, the role of a motivator is emphasised. How did the different roles of inspectors come out in the Finnish context? What kinds of meanings did inspectors attach to roles?

The role of inspector came out in different contexts in the interviews. It was associated mostly with neutrality and independence. In addition, four additional roles related to inspector were mentioned. Two of them were desirable roles related to

controller and motivator, and two others were avoidable roles related to advisor and quality controller (see Figure 3). The inspectors identified themselves most frequently with the role of a controller that means ensuring that the industry complies with the requirements.

Instead the role of a motivator did not come out of interviews, at least not directly. One can ponder why the motivator role seemed to be weaker, or not as strong as the role of a controller. Is it because YVL-guides strengthen the role of a controller and there is therefore not so much space left to the role of a motivator? Or is it just that the role of a motivator did not come out verbally even though it would have been adopted in regulatory practices?

The following features in Finnish safety regulation could suggest that motivator role is also present. Finnish inspectors work close to operators in the facilities. There is a site inspector, who works continuously in a facility. This kind of solution differs from many other nuclear power countries. In addition, Finnish inspectors follow closely also the modernization works in facilities. Grass-root level interaction may open up several opportunities to motivate the operators. In addition, inspectors' willingness to follow the process because they are interested to see and learn how things are done, tells about inspectors' strong motivation. And that practice may also motivate operators to find better solutions.

When the inspector follows so closely the process, the benefit is that they acquire deep understanding about what is happening in the installations and that is an advantage as regards controlling overall safety. However, there might lurk also a risk in that the inspectors are too closely involved in development processes that belong to power companies, and inspectors may easily take a role of an advisor that does not belong to their mandate. As well the role of quality controller is a risk if authorities visit producers to ensure that the structures of devices and components are according to the requirements (see Figure 3).

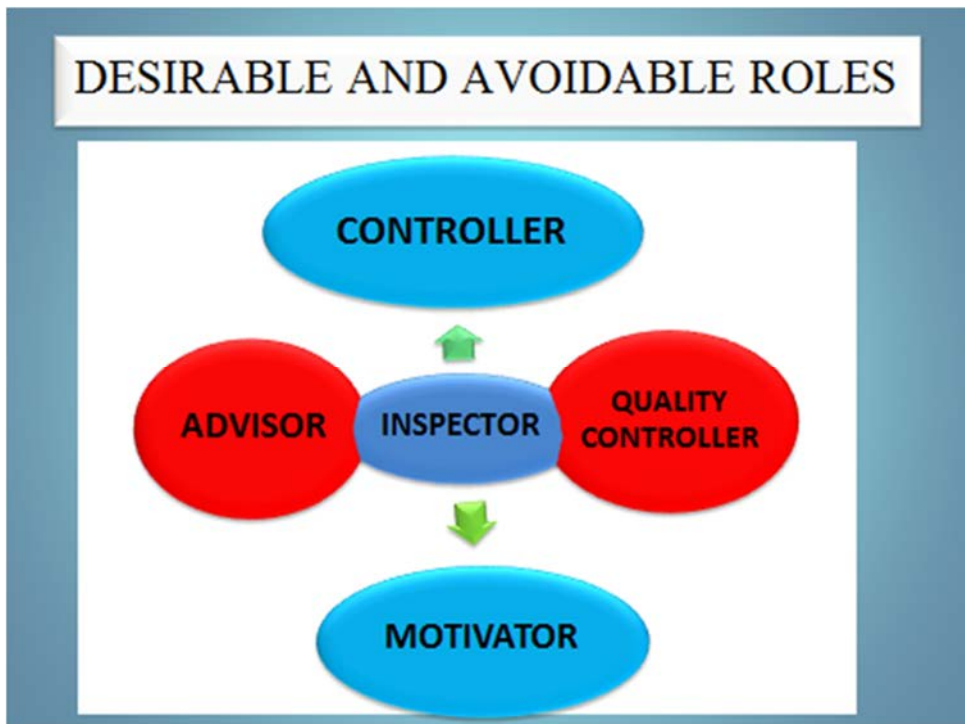


Figure 3. Two desirable roles (controller and motivator) and two avoidable roles of inspector.

Mechanisms that maintain similar understanding of safety stem from the YVL-guides and expert structure of the regulatory body. Majority of the inspectors have a technical education, which contribute to homogeneous understanding of safety. At the same, however, there are various areas of technical expertise and different offices within the regulator body that have promoted somewhat different practices. In addition, there are differences in safety practices between the newcomers and more experienced inspectors. For this reason, efforts have been made to streamline the safety regulation and to make it more focused on safety-significant matters.

Interviews indicate that safety regulation is under pressure to become more uniform, coordinated, and focused on upper level safety issues i.e. plant and system level safety. These efforts are in accordance with the OECD NEA's Characteristics of the Effective Regulator (2014), with uniformity and predictability in their action. The relevant question is how to support individual thinking and at the same promote more uniform, coordinated regulation.

Characteristics of Finnish safety regulation

Even though the international nuclear safety regime with technical, co-regulative and safety-intensifying features affect Finnish regime, this happens at a general level. The national cultural features give the eventual form to safety regulation. Cultural characteristics of Finnish nuclear safety regulation as well as nuclear safety regime entail trust and control-based, risk-informed, ambitious, technical and professional, relatively detailed, proceduralised, grass-root level regulation that is both rigid and flexible.

In the safety regulation continuum Finnish safety regulation could be set on the command and control end of the continuum instead of the self-regulation end. Even though Finnish regulation has been described to be rigid, it entails also flexibility. There is always space for negotiations about the procedures. This kind of duality might not be visible to outsiders.

However, all the regulatory systems are combination of command and control type and self-regulation type of instruments, there does not exist pure self-regulatory or pure command and control type of regulation. Possibly within a high risk industrial sector in the small country, there is a need to apply relatively stable and rigid, command and control type of regulation, that is however combined with some features of flexibility and relatively close grass-root-level regulation. Finnish regulatory style is a unique combination of principles and practices that have developed over the decades. The regulatory style is in a continuous process. The question arises how to maintain adequate command and control type of regulation and at the same ensure that it gives space for the operators' own developments? Or are the inspectors at grass-root-level so closely following what is happening in the facilities that it may be difficult to distinguish between command and control and motivation or command and control and self-regulation?

The national cultural characteristics are important to detect and understand if the safety will be improved at national and international level. This study cannot be regarded as exhaustive. Further inquiry is therefore needed into different stakeholders' understanding of Finnish inspectors' safety regulation. In addition, international comparisons between nuclear safety inspectors' practices in other countries would be useful for getting better understanding of cultural features, both similarities and differences, consistencies and inconsistencies between them. Moreover, further research would be needed in order to understand the conditions under which both the inspectors and operators operate daily when dealing with safety.

Nuclear safety is a complex phenomenon, cultural and socio-technical by nature. Therefore there would be an urgent need for a multidisciplinary research, a true co-operation between the engineering sciences and social sciences in a concrete research. Through that it would be possible to gain a better understanding how cultural, social and technical are participating in the end result of nuclear safety.

Acknowledgement

The support of SAFIR2014 Research Programme and all members of the RG1 is gratefully acknowledged. Special thanks to Ann-Mari Sunabacka-Starck and Kirsi Levä who have made valuable comments on this study. In addition, without the support of the STUK and expert interviewees this paper would never have been written. I take responsibility for the content of the reports and summary.

References

- Baldwin, R., Cave, M. and Lodge, M. (2012) *Understanding Regulation*. Second Edition. Oxford University Press, New York.
- Baram, M. and Lindoe P.H. (2014) Modes of risk regulation for prevention of major industrial accidents. In Lindoe, P.H., Baram, M. and Renn, O. (eds.) *Risk Governance of Offshore Oil and Gas Operations*. Cambridge University Press, New York.
- Ylönen, M. 2015a) Signalled and Silenced Aspects of Nuclear Safety. International nuclear safety regime and the national cultural features. Project report. (Forthcoming, to be published in JYKS).
- Ylönen, M. 2015b) Signalled and Silenced Aspects of Nuclear Safety. Characteristics of Finnish Nuclear Safety Regulation. SAFIR2104 Final report. (Forthcoming, to be published in JYKS).

5. Coverage and rationality of the software I&C safety assurance (CORSICA)

5.1 CORSICA summary report

Jussi Lahtinen¹, Risto Nevalainen², Janne Valkonen¹, Timo Varkoi²

¹VTT Technical Research Centre of Finland Ltd
P.O. Box 1000, FI-02044 Espoo

²Finnish Software Measurement Association FiSMA ry
Tekniikantie 14, 02150 Espoo

Abstract

The aim of the CORSICA research project is to improve the safety evaluation of I&C software in nuclear industry by improving consciousness of process assessment and rationality of integrated evaluation methods. Main issues that were addressed are: support of process assessments in supplier evaluation and pre-qualification; consciousness of coverage and rationality of V&V-methods in software evaluation; and novel technologies that require new qualification approaches. The research produced methods that will benefit the industry by providing concrete solutions to the identified issues. The research was organised in tasks with specific topics. In addition to the methods, the tasks produced scientific and technical reports. Dissemination of the results took place in meetings addressed to the SAFIR2014 community and in international conferences.

Introduction

There is a general need to perform qualification of I&C safety systems as effectively as possible, keeping still the necessary formalism and accuracy of the qualification. Early notification of potential problems is the most effective and proactive way to perform qualification. Good knowledge of nuclear standards, professional application

of sophisticated methods and good ability to adopt novel technologies is essential for qualification.

In previous SAFIR2010 program we developed approaches to qualify and certify software intensive I&C systems for nuclear power plants. This work was continued in SAFIR2014 program, extending previous results for general evaluation for example in following topics:

- adequacy and relevance of process capability assessment in technical product evaluation,
- coverage and rationality of required development and assurance methods,
- certification and evaluation issues in using new technologies, for example FPGA,
- use of new standards in technical safety evaluation of nuclear I&C systems

The topics have been addressed by corresponding tasks within the CORSICA project. To meet process assessment needs in the nuclear domain, the Nuclear SPICE assessment method was developed. The method supports assessment of safety critical I&C systems and software development processes. The need for assurance methods led to analysis of review techniques and development of test set generation for function block based systems. Increasing complexity and demands for safety were covered by studying certification and evaluation issues in using new technologies, like FPGA. The tasks were dynamically planned to adapt to the changing needs of the research domain. The evolution of tasks is depicted in Figure 1.

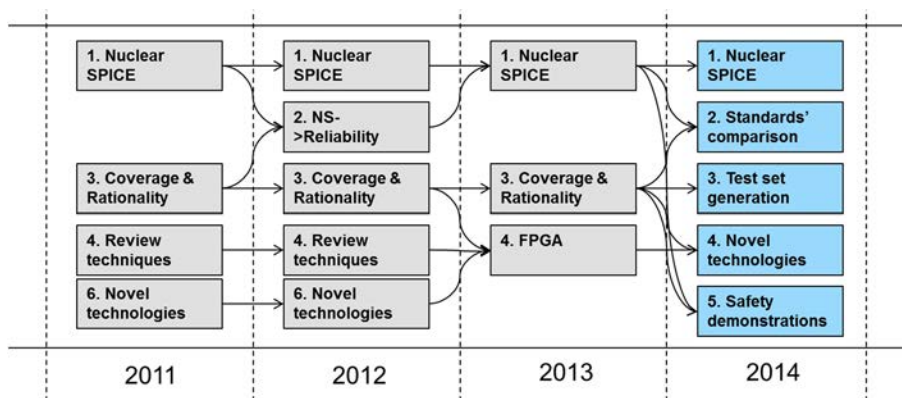


Figure 1. Tasks in CORSICA 2011 – 2014.

The CORSICA project is a partnership between VTT and FiSMA. FiSMA is responsible for process related topics, mainly the development of new process assessment model called Nuclear SPICE. Also integration of Nuclear SPICE with reliability and software quality concepts belongs to FiSMA. VTT is responsible for selected V&V methods in qualification, for example new kinds of review techniques. VTT has also worked with novel technologies, like FPGA and multicore platforms in nuclear power plants.

Use of evaluation concepts, methods and tools from other domains is also important in CORSICA, because nuclear power standards are not adequate alone for all qualification and certification needs. Experiments in pilot projects are also used to validate our results of CORSICA tasks.

Assessment of system and software development process with Nuclear SPICE

The main standard in functional safety is IEC 61508:2010 (3rd edition). It has seven parts. Software requirements are mainly in Part 3 [IEC 61508]. The safety concept in IEC 61508 is called “safety related”. In nuclear domain it would mean safety system in lower level safety classes 2 and 3. Our concept “safety critical” in CORSICA means more or less the same.

Software standards in nuclear domain are IEC 60880 [IEC 60880] for safety-critical software (Category A) and IEC 62138 [IEC 62138] for safety-related software (Category B and C). They can be classified as “second level” standards, referring directly to IEC 61513 [IEC 61513] but only indirectly to IEC 61508.

The generic solution in process assessment is the standard called “SPICE”. It is currently in transition period from previous ISO/IEC 15504 (10 parts) into ISO/IEC 330xx series [ISO/IEC 330xx].

One major task in CORSICA was to create an integrated family of methods to assess the degree of compliance with system and software standards. SPICE provides a generic framework and by adding content and criteria from generic safety standards and from nuclear standards we created Nuclear SPICE, a holistic method to assess process capability and compliance. This idea is presented in Figure 2.

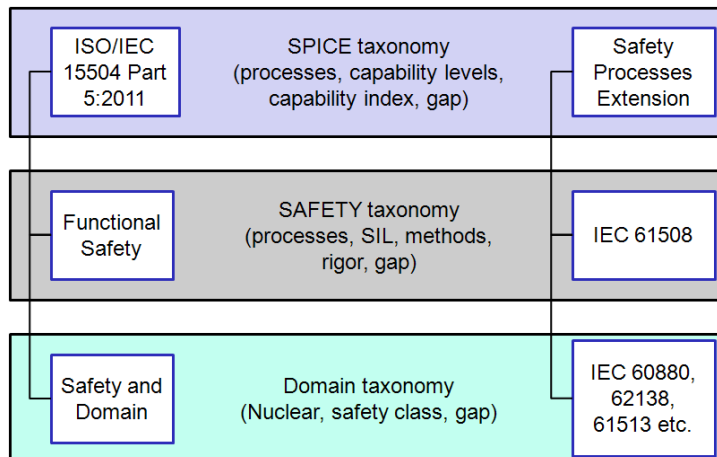


Figure 2. The integration layers of standards and criteria in Nuclear SPICE.

The main challenge is integration between the layers. SPICE, IEC 61508 and IEC 60880 can be kept separate and leave space for ad hoc integration in each assessment and qualification case. Also deeper integration is made in small steps, for example by combining methods from IEC 61508 with software engineering processes.

The continuous development of the Nuclear SPICE framework produced a novel solution to a specific business need i.e. the need to assess processes that are used to develop software with utmost safety requirements. Altogether, FiSMA has published nine technical reports about the Nuclear SPICE in the years 2012-2014:

- FiSMA 2011-1: S4N Method Description - Nuclear SPICE PRM and PAM (2012)
- FiSMA 2011-2: S4N Assessment Process - Requirements for Nuclear SPICE assessment (2012)
- FiSMA 2012-1: Nuclear SPICE PAM for pre-qualification process assessment (2013)
- FiSMA 2012-2: Nuclear SPICE assessment process (2013)
- FiSMA 2012-3: Framework to evaluate software reliability based on Nuclear SPICE (2013)
- FiSMA 2013-1: Nuclear SPICE PAM for pre-qualification, annex (2014)
- FiSMA 2013-2: Nuclear SPICE assessment process, update of FiSMA 2012-2 (2014)
- FiSMA 2014-1: Integrated Nuclear SPICE Process Assessment Model (2014)
- FiSMA 2014-2: Advanced Nuclear SPICE assessment process (2014)

FiSMA reports 2011-1 and 2012-1 are mainly process reference models (PRM) and process assessment models (PAM). The full Nuclear SPICE PRM and PAM are included in 2011-1 report. The second Nuclear SPICE model report 2012-1 is more detailed and is limited to pre-qualification in software intensive I&C systems mainly in Category A. It means more detailed mapping of Nuclear SPICE with IEC 61513 and IEC 60880. FiSMA report 2013-1 presents the relationship of the updated national regulatory requirements [STUK 2013] as well as the Common Position 2013 [Common Position 2013] requirements to the assessment model. FiSMA report 2014-1 integrates the previous assessment models and presents the final result.

Four other FiSMA reports are about the assessment process. Report 2011-2 is the set of requirements for assessment process to be compliant with previous and current requirements of SPICE standards (mainly ISO/IEC 15504-5:2012 and DIS version ISO/IEC 33002). Report 2012-2 describes in detail an assessment process to meet the requirements specified in report 2011-1. The assessment process is intended for performing systems and software process assessment in highly safety-critical environments in the nuclear industry domain. Report 2012-3 presents selected articles and assumptions related to software reliability, and defines a framework to support evaluation of risks for software reliability using process assessment. FiSMA report 2014-2 supplements the assessment process with practical guidance to support selection of appropriate assessment scope and rigour. Additionally, a number of conference and journal articles and tutorials were prepared of the Nuclear SPICE topic, e.g. [Varkoi et al. 2013].

FiSMA report 2012-3 studies the applicability of process assessment in evaluating software reliability. It specifies tentative sets of process quality attributes for process assessment in safety domain. The basic set includes attributes that meet the elementary requirements for trustworthy software development.

The Nuclear SPICE method has been validated with pilot assessments. Currently, the method defines a process assessment based approach to ensure quality in systems and software development for nuclear domain. It can be used to identify potential safety risks that are related to the development processes. The main strengths of the method are: it relies on international process assessment standards; assessments are flexible in scope and rigour; and it delivers pre-qualification results fast, typically in 1 month.

Structure-based test generation

Functional testing plays a major role in the V&V of safety critical software of instrumentation and control (I&C) in nuclear power plants (NPPs). Functional testing aims to check whether there are any program errors in meeting particular aspects of the given specification and whether all specified requirements have been met.

However, functional testing has some challenges. Firstly, as a test is derived from the specification, it can only detect non-conformance to that specification, and cannot be used to prove software correctness. The second challenge is that full test coverage with respect to completeness and correctness is practically impossible.

In CORSICA we have looked into structure-based testing as a complementary testing method. Unlike specification-based testing, structure-based tests are derived directly from the structure of the system. We have examined function block diagrams as the design formalism since many nuclear safety automation systems are designed using function block based descriptions.

In our work, we used previously developed structure based test criteria [Jee et al. 2010] as a basis, and developed an automatic technique for generating structure-based test suites for function block diagrams. See also [Lahtinen 2014] and [Lahtinen et al. 2014] for details. The generic technique is illustrated in Figure 3.

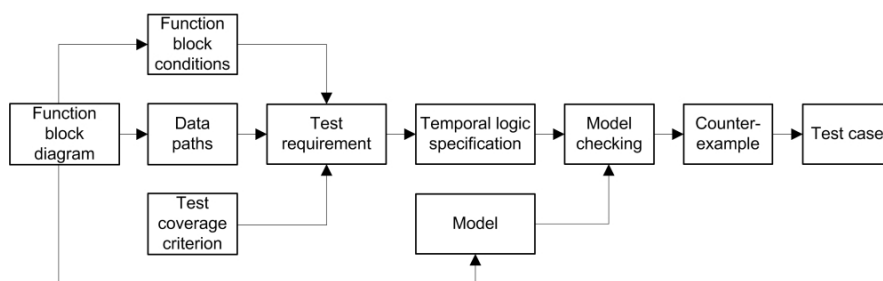


Figure 3. The technique used for generating structure-based test cases using model checking.

We also developed a simple greedy algorithm for generating a set of test cases that has high structure-based coverage. The resulting test set is efficient in the sense that the number of test cases is small and the tests are concise, i.e. a single test case can fulfil multiple test requirements. We implemented the algorithm using the Python programming language and have experimented with test generation on a small group of function block diagrams.

The developed test set generation technique is valuable, since manual structure-based test design can become infeasible on more complex system designs that contain memories, timers and feedback loops. Furthermore, in larger systems the number of test requirements can be rather high.

The main application of our technique are safety-critical function block based systems, but the technique can be used for other relatively simple function block based systems consisting of Boolean logic, timers and memories. Based on our experience the technique should scale to typical nuclear domain safety systems, as long as only the behaviour of the single system is included in the analysis.

Standards and regulatory requirements

Standards are important and widely accepted references in assessing safety of software intensive I&C systems. Practically all countries have also additional and complementary regulatory requirements. The consistency and timely relevance of standards and regulatory requirements has not been always in balance, because they are also changing according to their own timetables.

CORSICA project has been active in nuclear standardisation by participating in CENELEC working group SC45A. The goal has been to exchange information and experiences in Europe in using IEC nuclear safety standards. Some work has been done in comparing European and Finnish recommendations and policies with U.S. Nuclear Regulatory Commission NRC policies and guidance. NRC refers mainly to IEEE standards and has prepared several guidelines to interpreting these standards. STUK mainly refers to IEC 60880, and has added requirements to YVL guides about software development. However, both approaches do not deny using other standards than IEC and IEEE.

A detailed analysis of IEC 62138 next generation draft has been made [Teikari and Nevalainen 2014], to improve its overall quality and consistency with relevant YVL new guides (mainly B.1 and E.7) and Common Position 2013 document.

Use of novel technologies and methods in nuclear power plants

In CORSICA, we have continuously strived for finding and evaluating potential new technologies and methods to be used in the Finnish nuclear I&C domain. Over the four year period we have looked into e.g. field-programmable gate arrays (FPGAs), multi-core processors, reading techniques, fault injection techniques, novel hazard analysis techniques, and new practices for safety demonstration.

Reading techniques

In software development it is very useful to locate defects in the early phases of the development life-cycle. The cost of an error found in requirements specification is much less than an error that is found in the testing phase.

Reviews and inspections are typically used to locate software defects in the early life-cycle phases. The most effective strategies have been advanced reading techniques that consist of a written guidance or a procedure that the inspector should follow.

Many perspective-based reading techniques exist. One variant is Perspective-Based Reading (PBR). The idea in perspective-based reading is to examine a software artefact description from the perspectives of the artefact's stakeholders in order to identify defects. The second key characteristic of the PBR method is the active role of reviewers in the inspection. The idea is that each reviewer creates some high-level version of a work product that the user would normally create from their perspective. The intention is that, by producing work products themselves, the reviewers obtain a more profound understanding of the system, and thus are able to detect more defects that are difficult to find and not just superficial errors.

In CORSICA, we have applied the generic PBR ideas to the review of nuclear domain conceptual design plans, see [Lahtinen, 2012]. Separate review instructions (i.e. a scenario) were written for five perspectives: an automation designer scenario, a control room designer scenario, an electrical designer scenario, a safety designer scenario, and a regulator scenario. The developed method was considered to be effective as the technique was used to review a real conceptual design document by an automation designer.

Field-Programmable Gate Arrays

Interest in the use of field programmable gate array (FPGA) technology in nuclear power plant (NPP) automation has increased in recent years. FPGA technology is considered less complex since it does not involve a microprocessor, or an operating system. Instead the FPGA circuit consists of a large array of logic gates and memories, and can be configured by the user to perform custom operations.

CORSICA has followed FPGA developments throughout the entire project. First, a literature survey on FPGA technology was conducted [Ranta, 2011]. The report covers technological aspects, application design, reliability considerations, and the situation of currently existing FPGA based safety related systems.

Further on, a case study was developed to take a closer look at application design, implementation and verification. A logic circuit called the Stepwise Shutdown System (SWS) was implemented on actual FPGA hardware. The case study is initially documented as a research report, see [Lötjönen, 2012]. The SWS case study was later expanded to a larger case study involving two separate FPGA circuits. Multiple V&V methods were successfully used on the system. The work in general is described in [Lötjönen, 2013] and [Lötjönen et al. 2013]. The use of model checking to verify various design stages of the FPGA system was also examined. The work is described in [Lahtinen et al. 2014]. One important result of this work was the notion that implementing second-scale timers using the typical nanosecond-scale clock

frequencies of the FPGA chip may be problematic in the verification of these systems.

Novel hazard analysis techniques

Traditional hazard analysis techniques such as FTA, FMEA, and HAZOP focus on various components and their failures. The System-Theoretic Process Analysis (STPA) method on the other hand offers a rather different approach on hazards analysis. The method is based on control theory, and it was designed to also take into account communication faults between system components and the societal structure surrounding the system. It widens the scope of traditional methods and should theoretically enable the identification of new kinds of flaws. Real-world experiences in the use of the method have been very positive so far. STPA also shows potential regarding its use for licensing purposes in the nuclear domain. But despite the positive experiences, STPA is still a fairly young method with a limited use base. Also, quite a significant amount of knowledge about the method is required for one to be able to apply it to real-world cases. The method has, however, created major interest in many fields and its use can be expected to increase in the future. [Teikari 2014]

Safety demonstrations

Licensees are required to demonstrate in a clear and unarguable way that nuclear power plants and the related systems are safe. In the current practice, a Safety Analysis Report (SAR) provides an overall view of the safety of the plant or system. However, SARs are not formally structured and their focus is on the solutions with less emphasis on requirements and safety arguments. Thus, the information needed to demonstrate safety may be scattered.

The objective of the very small task was to introduce and demonstrate the idea of formal, structured safety demonstration templates (patterns) that could be used to argue that a system (or part of it) has certain properties and features. In addition to reporting on the safety demonstration templates, also general terminology and aspects on justifying safety were summarized in the task.

Conclusions

CORSICA project improved the safety evaluation of I&C software in nuclear industry by developing a method for process assessment and applicability of integrated evaluation methods. The Nuclear SPICE method supports assessment of safety critical I&C systems and software development processes. The need for assurance methods led to analysis of review techniques and development of test set generation for function block based systems. Increasing complexity and demands for safety were covered by studying certification and evaluation issues in using new technologies. The research produced methods that will benefit the industry by providing concrete solutions to the identified issues.

References

- Common Position 2013. European Commission's Advisory Experts Group, Nuclear Regulators Working Group, Licensing of safety critical software for nuclear reactors - Common Position of seven European nuclear regulators and authorized technical support organizations, Revision 2013 (2013).
- IEC 60880:2006 Nuclear power plants – Instrumentation and control systems important to safety – Software aspects for computer-based systems performing category A functions. IEC 2006.
- IEC 61508-3:2010 Functional safety of electrical / electronic / programmable electronic safety-related systems Part 3: Software requirements, IEC 2010.
- IEC 61513 (FDIS 2011) Nuclear power plants - Instrumentation and control for systems important to safety - General requirements for system. IEC 2011.
- IEC 62138:2004 Nuclear Power Plants – I&C Systems Important to Safety – Software Aspects for Computer Based Systems Performing Category B and C Functions, 2004.
- ISO/IEC 330xx Information technology – Process assessment. Family of new standards for Process Assessment. ISO 2013.
- Jee, E., Kim, S., Cha, S., and Lee, I. 2010. Automated test coverage measurement for reactor protection system software implemented in function block diagram. In Proceedings of the 29th International Conference on Computer Safety, Reliability, and Security, ser. SAFECOMP'10. Berlin, Heidelberg: Springer- Verlag, pp. 223–236.
- Lahtinen, J. 2012. Development of a review technique for conceptual design plans, VTT. 29 p. Research Report; VTT-R-08337-12. Available online: <http://www.vtt.fi/inf/julkaisut/muut/2012/VTT-R-08337-12.pdf>.
- Lahtinen, J. 2014. Automatic test set generation for function block based systems using model checking. In: 9th International Conference on the Quality of Information and Communications Technology (QUATIC 2014), 23 – 26 September, Guimarães, Portugal.
- Lahtinen, J., Ranta, J., and Lötjönen L. 2014. CORSICA 2013 work report: Test set generation, FPGA model checking, and fault injection, VTT Technical Research Centre of Finland, Espoo, Finland, Research report VTT-R-00212-14.

- Lötjönen, L. 2012. FPGA Implementation of the Stepwise Shutdown System. VTT Research report. VTT-R-06053-12. Espoo, Finland.
- Lötjönen, L. 2013. Field-Programmable Gate Arrays in Nuclear Power Plant Safety Automation. Master's Thesis. Aalto University, 2013. Available online: <https://aaltodoc.aalto.fi/handle/123456789/10921>
- Lötjönen, L., Ranta, J., Lahtinen, J., Valkonen, J., Holmberg, J.-E. 2013. Use of Field-Programmable Gate Arrays in Nuclear I&C Safety Systems – Case Stepwise Shutdown System. Automaatio XX seminar, Helsinki.
- Ranta, J. 2011. Current state of FPGA technology in a nuclear domain, VTT Technology 10. Espoo, Finland.
- STUK 2013. Radiation and Nuclear Safety Authority, Regulatory Guides on nuclear safety (YVL), 2013. (<http://plus.edilex.fi/stuklex/en/>)
- Teikari, O. 2014. CORSICA Task 4.1 Hazard analysis methods of digital I&C systems. VTT Research Report, VTT-R-03821-14, 2014.
- Teikari, O., Nevalainen, R. 2014. Comparison of software safety standards IEC 61508-3 and IEC 62138. VTT Research Report, VTT-R-03820-14, 2014.
- Varkoi, T., Nevalainen, R. and Mäkinen, T. 2013. Toward Nuclear SPICE – integrating IEC 61508, IEC 60880 and SPICE. Journal of Software: Evolution And Process (2013).

6. Human-automation collaboration in incident and accident situations (HACAS)

6.1 HACAS summary report

Jari Laarni, Paula Savioja, Iina Aaltonen, Maiju Aikala, Hannu Karvonen, Hanna Koskinen, Timo Kuula, Jari Lappalainen, Paula Laitio, Marja Liinasuo, Leena Norros, Markus Porthin, Teemu Tommila and Mikael Wahlström

VTT Technical Research Centre of Finland Ltd
P.O. Box 1000, FI-02044 Espoo

Abstract

The HACAS project studied operator work, human-technology interaction and control room (CR) design from different perspectives. More specifically, the project focused on studying how digital automation (I&C) and CR upgrades affect resilient performance of CR personnel, how Human Factors Engineering (HFE) activities should be organized in order to support plant safety and productivity, and how humans and automation systems collaborate to accomplish safety and production goals of nuclear power plants (NPPs). As a result, tools and guidelines have been developed for resilient-based analysis of work practices, for an integrated approach to HFE, for a multi-stage approach to verification & validation (V&V) and for the measurement of automation awareness. Empirical simulator tests have been conducted in which novel interactive wall-mounted displays and automation awareness and competence were studied.

Introduction

Effective and efficient performance of the operating personnel plays a key role in the safe production of nuclear power. Currently, the general view is that the main objective in safety management is to ensure the resilient functioning of the whole socio-technical system, especially during events which have some characteristics difficult to anticipate.

Resilience at the operational level is mainly based on continuous and active monitoring of the power process, supported by regular training of personnel.

Main objectives

In 2011-14, the main objectives of the HACAS project have been to study:

- 1) Operating procedures in incident and accident management;
- 2) Development of an integrated approach to HFE and CR V&V;
- 3) Automation awareness and its development.

Regarding the first main task, the specific aim has been to study the effect of routines of procedure usage on the management of severe accidents, the parallel use of EOPs and safety HSIs in accident management, and the procedure design process from the HF perspective. Regarding the second main task, the aim has been to investigate the effect of digital I&C systems on operator practices in accident situations, review approaches for more integrated and unified HFE processes, identify challenges in the design of interactive wall-mounted displays for the simulator environment, and develop an integrated validation concept for multi-stage modernization projects. Regarding the third main task, we have studied operators' automation awareness and the effect of automation complexity on automation awareness and skills, designed an AproS-based simulation demonstrator for testing automation awareness in experimental settings, outlined a method for measuring automation awareness and competence, and studied automation competence among automation maintenance personnel.

Main results

Proceduralized activity in the new accident management

Emergency operating procedures (EOPs) help CR operators to perform their tasks safely and efficiently even in high workload situations; on the other hand, strict adherence to EOPs may even hamper operators' situation monitoring and process control in accident situations.

We have studied the usage of EOPs in digital CRs, and the requirements for procedure-based activities in the implementation of safety management Concept of Operations (ConOps). In an interview study, operators' conceptions on procedures, structured under three themes relevant to the role of the operator's autonomy in relation to the official guidance. The interviews were analysed by classifying each interview answer into one of three predefined categories: reactive, confirmative or interpretative orientation (Norros, Liinasuo & Savioja, 2014). The results show striking similarities in the orientations of the operators of two different NPPs (Norros et al., 2011). Interestingly, the orientation of turbine operators seems to differentiate from the ones of the other operators (i.e., shift supervisor and reactor operator)

We have studied the effect of EOPs on the operators' situation awareness in different phases of the accident management process and the effect of routines of procedure usage on the management of severe accidents by analysing the usage of EOPs in a simulated accident scenario in a detailed fashion (Norros, Savioja, et al., 2014; Savioja et al., 2014). The variance between the operator crews concerns the functions of information usage, interpretation of the situation, dealing with automation, decision making, communication, and leadership. The different habits of action for each function were described, and the habits were graded according to their capability of producing system level resilience in the operating activity. According to the results, procedure usage should be actively trained and in the training attention should be paid, not only to following the procedure but also to the way of utilising the procedure in a manner which does not detach proceduralized tasks from the environment.

We have also developed new practices for procedure design based on interview results. As a result of the interview study, procedure design was found to be mainly technically oriented, not usage centric, although operator feedback is also considered in developing procedures (Wahlström et al., 2014). Themes that were raised in interviews include the following: the importance of (1) utilising usage-centric approach in procedure design, (2) defining the basics of procedure design, (3) developing a shared understanding of the relationship between operator's professional competence and the usage of procedures and (4) training in the usage of procedures in unexpected situations.

Development of an integrated approach to HFE

In order to support system resilience, there is a need for more integrated systemic approaches to HFE that are tightly integrated into the engineering design process from the beginning. The main goals for a unified comprehensive HFE process are to define appropriate roles and responsibilities for personnel, to support the design and development of usable and functional HSIs and to ensure the safety and reliability of human performance.

We have studied operator practices in accident management in wholly or in partly digitalized control rooms. Based on the literature review, it was found that differences in operator performance are quite small between traditional analogue and digital control rooms in design-based accident situations (Laarni & Liinasuo, 2011). Even though computer-based human-system interfaces and new techniques in process control open new possibilities for process control, a general finding is that in traditional analogue CRs situation awareness at the team level is higher and communication more fluent than in digital CRs.

Two reviews of the HFE implications of the level of the HSI modernization and of the migration strategy have been prepared. According to the results, a fully modernized digital CR provides a plenty of benefits over the old analogue one, but the risks involved in the modernization project itself are high to such a degree that it has to be carefully think about whether they are worth the benefits (Laarni & Savioja, 2012). In addition, there are several challenges for successful implementation of HFE work,

such as the proper timing of implementation of HFE activities, the use of screening and graded approach to HFE evaluation, the importance of skills of participating stakeholders, early integration of operators into development, and appropriate sharing of knowledge among designers, HFE experts, and management (Laarni & Savioja, 2013). Guidelines and recommendations are offered in order to open up a route for a more systematic application of HFE practices in the nuclear domain in the future.

Together with Fortum we have outlined a HFE process that is more tightly integrated into the systems engineering process from the beginning (Salo et al., in press). In the described case there was a need to develop an HFE process that would guide HFE management and ergonomics design in different types of projects from upgrades to new builds. In addition, we propose ConOps as a useful collaboration tool in the design and licensing of automation systems and control rooms (Laarni & Tommila, in preparation). Since safety is a key issue in the nuclear domain, ConOps should be adapted to its safety practices. In particular, ConOps should be combined with the concept of Defence-in-Depth (DiD) in order to provide a practical boundary object to represent and discuss the high-level safety architecture.

Testing the Virtual Panel system

Touch-sensitive wall-mounted displays provide new opportunities for process monitoring and control. The Fortum virtual panel concept was realized as a part of the training simulator's human system interface by introducing a set of touch sensitive wall mounted displays for the CR of the training simulator. Based on an interview with the designers and an interface walkthrough, it was addressed what kind of challenges and compromises the designers needed to account for in the transition from the analogue to the digital interface medium, and how they envision the interactive surface technologies could be used in the future CR environments (Koskinen et al., 2012). A descriptive model of the innovative features of the Virtual panel concept within the System Usability framework was developed.

In order to assess the usability and functionality of the virtual panel system a simulator test on the interactive large-screen usage was conducted (see Fig. 1). Based on the results of the tests, some guidelines have been prepared for testing of the fidelity of interactive LSDs for the CR environment. The functionality and usability of the virtual panel system was founded to be quite high, and the participating operators could well identify the HSI components of the turbine side, even though the total HSI system of the turbine side was slightly changed (Koskinen et al., in press).

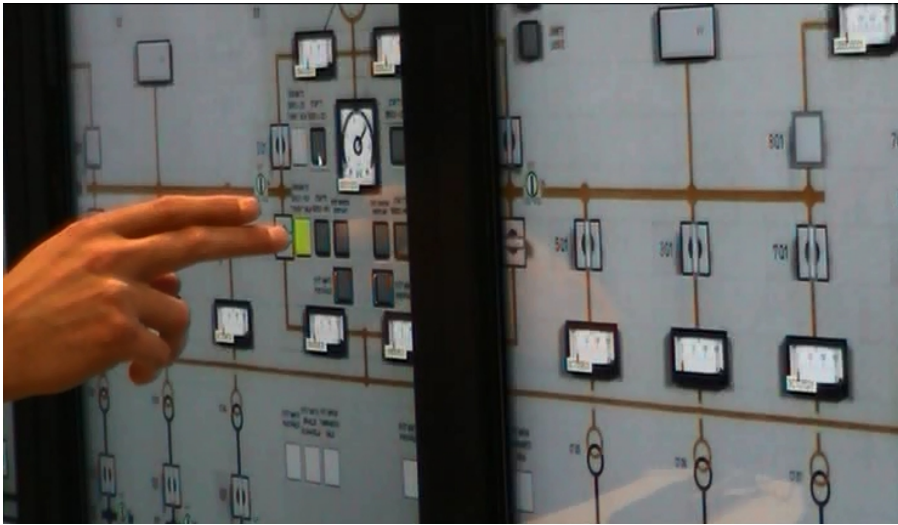


Figure 1. Testing the virtual panel system in the Fortum Loviisa training simulator.

The designed virtual panel system will have an impact on simulator fidelity. A methodology has been outlined for the evaluation of the simulator fidelity of NPP training simulators for operator training and validation purposes (Laarni & Koskinen, 2014). We propose that the assessment of simulator fidelity is conducted in an iterative fashion, and it should consist of three subsequent stages: The first round of the evaluation is conducted after the completion of the sub-system level validation tests/simulator performance validation testing and before the execution of Integrated System Validation (ISV) and operator training activities. The latter two evaluation rounds should not be conducted until the completion of operator training/ISV and until commissioning and until the new MCR has been under operation for some period of time.

Development of a contextual multi-stage approach to V&V

In several projects VTT has developed its own methodology for the system validation of CR systems. This work has been continued in HACAS, in which a resilience engineering –based approach for the analysis of work practices has been outlined (Norros, 2012, 2014; Savioja, 2014; Savioja & Norros, 2013; Savioja et al., 2012). There are five main steps in the resilience-based analysis approach: analysis of the work system, modeling the domain and control demands, modeling situational task demands, analysis of actual behaviour, and identification of generic tool functions. The systems usability analysis tools have been applied for empirical evaluations of NPP CRs. In these studies it has been found that performance-based criteria deliver important information of the tool's instrumental capabilities, and the practice-based

and user experience-based measures are particularly valuable in informing of the tool capabilities with regard to the psychological and communicative functions.

In addition, the methodological basis of the sub-system validation (SSV) activity has been developed, and the application of the SSV approach to the evaluation of the safety HSIs has been presented (Laarni et al., 2014). We have advocating a continuous and phased/multi-staged V&V of NPP CR systems. We propose that phased V&V is conducted in several stages in sequence so that cumulative evidence of the validity of the new CR systems is achieved. The approach provides continuous support for ongoing iterative design of CR systems by producing regular feedback to design. In addition, by accumulating validation evidence over test activities more thorough evaluation of the CR systems is possible. The phased approach to V&V is well suited to continuous iterative systems engineering process, in which human-system characteristics are incrementally discovered during the design process; there is a cyclic ongoing specification of system requirements and design solutions; and system requirements and design solutions are concurrently developed.

Because a lot of data is collected during the V&V process, systematic methods are needed for the accumulation and systematization of validation evidence and drawing conclusions from the evidence. During the development of the multistage HF validation approach, it was reasoned that a case-based approach is particularly suitable approach when the system to be evaluated is unique and comparison to other systems is difficult. It also supports formative evaluation, in which the interest is to steer the development of the system by successive evaluations, and nevertheless remain independent of the design process itself. In case-based reasoning, a Systems Usability Case is created. For managing the case an appropriate software tool is used (i.e., Adelard ASCE).

We have also assessed the applicability of HRA in CR system validation by examining how HRA should be considered in the design and implementation of CR system validation activities, and how HRA results should be considered in the evaluation process, e.g., in the evaluation of possible system deficiencies and in the prioritisation of required changes (Liinasuo & Porthin, 2014). The results of validation results have been rechecked in order to find out whether they could be utilised for updating HRA. As a result, it was firstly found that validation data is relevant for HRA but it should be re-categorised in order to be usable for updating HRA. We performed the re-categorisation based on the effect of the identified weakness in design on operator performance, and named the categories according to the imperfection in the technical solution. The new categorisation comprises of display related, performance demands related and concept related issues. By using this type of categorisation, validation data can be used for naming performance shaping factors in HRA.

Automation awareness and automation competence development

New safety automation based on digital technology is more complex on its architecture and functionality which may have an impact on automation awareness and automation skills. Apparently, the introduction of digital automation and HSIs has safety

implications, and therefore new tools and practices are needed to help to manage possible problems caused by digital I&C systems. There is, however, little knowledge and research on safety risks associated with accident management based on digital automation; nor is there much knowledge about training challenges caused by the new I&C and HSIs.

Parallel to the concept of situation awareness, automation awareness can be defined as the operator's conception of the utilized automation system's state in such a manner that it enables the operator to observe, control, and anticipate the process events initiated by the automation. The development of automation awareness is considered to be a continuous process that consists of perceiving the current status of the automation, comprehending the status and its meaning to the system behaviour and estimating its future status and its meaning. The question of what is sufficient automation awareness and how to examine automation awareness is addressed and a preliminary model on automation awareness has been developed. According to our findings, the complexity of the automation system has a great impact on the development and maintaining of automation awareness (Laitio, 2013; Laitio et al., 2013). Other factors that have to be taken into account are the usability and functionality of human-system interfaces, personnel's trust in automation and various situation-specific factors.

We have developed an Apros-based simulator environment which was used in the experimental testing of automation awareness. The test results indicate that especially the digital presentation of the measurement values, graphical format of the values' status and their automation-related limits, and illustrative trend displays were seen to improve automation awareness (Karvonen et al., 2014). Furthermore, the results suggest that in addition to factors, such as the operators' automation-specific education, experience and provided training, the quality of the automation system's user interface is a significant contributor to the development of automation awareness. We also created a preliminary version of a versatile tool to study automation awareness.

Automation maintenance personnel at the two Finnish NPPs were interviewed about their work tasks and tools, as well as training practices at the plants, on-the-job-learning and the challenges of modernization. The training needs described by the interviewees are categorized in six themes: 1) language skills, 2) analog vs. digital systems, 3) use of computers and new technology, 4) retirement of personnel, 5) emerging collaboration and 6) multi-skilled workers (Aaltonen et al., in press). Interestingly, knowledge on analog automation may pose a greater challenge than of digital, because analog automation is no longer taught at schools, and the automation modernization does not necessarily mean full digitalization of I&C systems.

International collaboration

The project has collaborated with OECD/Halden Reactor Project (HRP) and Institute for Energy Technology (IFE), EdF (*Electricité de France*), the Human Factors research team at IRSN (L'Institut de Radioprotection et de Sûreté Nucléaire) and with the stakeholders of the NUGENIA (Nuclear Generation II & III Association). In addition, it has collaborated with several foreign universities, and research institutes, such as Chalmers University, Danmarks Tekniske Universitet, Kyoto University and Université Lumière Lyon 2. The project work has contributed to OECD/NEA Working Group of Human and Organisational Factors (WGHOFF) and its task group work (Human Intervention and Performance under Extreme Conditions and Integrated System Validation).

Applications and implications

Research conducted in the HACAS project has been continued in confidential contract projects in which more innovative practical methods for operating personnel training, HFE plan development and CR system validation have been developed. Especially, the developed method for a multi-stage contextual assessment of systems usability has been used in several commission projects during 2011-2014. We have participated in the verification of design documents and in the pre-validation of CR systems and HSIs.

Ad hoc seminars and workshops on the themes of the project (autonomy vs. guidance in NPP operations, human factors in safety automation design, operator practices from the resilience-engineering perspective, cross-sectoral safety design and management) have been arranged. The discussions with the stakeholders of Finnish nuclear power companies and the Finnish regulator have been useful in providing feedback and suggestions for future studies.

Conclusions

The project's main results can be summarized as follows:

- Development of modelling and analysis tools for the ecological investigation of activity;
- Profound understanding of the usage of emergency operating procedures and EOP design;
- Development of guidelines for a more integrated approach to HFE;
- Development of a multi-stage approach to V&V of control-room systems;
- Profound understanding of the usability and functionality of the virtual panel system;
- Thorough understanding of automation awareness and its measurement;
- Better understanding of automation competence among automation maintenance personnel.

In the future projects the aim is to further develop operational capabilities for resilience and specify in a more detailed fashion 1) what the characteristics of resilient activity are; 2) how the indicators of resilience can be identified; 3) what characteristics and features promote resilience, and 4) what the potential consequences, prospects, and weaknesses of resilience are from the perspective of safety.

References

- Aaltonen, I., Kuula, T., Wahlström, M. & Aikala, M. in press. Training needs of NPP maintenance personnel. Paper to be presented in ANS NPIC&HMIT 2015.
- Karvonen, H., Lappalainen, J. & Liinasuo, M. 2014. Automation awareness user interface study – preliminary results. Proceedings of Enlarged Halden Programme Group Meeting, Roros, Norway, September 7-12, 2014.
- Koskinen, H., Laarni, J., Markkanen, P., Näveri, J., Paananen, A. & Torkkeli, K. 2012. From analogue to digital in training simulator: The design and implementation of a new interactive panel system. Proceedings of ANS NPIC&HMIT 2012, San Diego, USA, July 22-26, 2012.
- Koskinen, H., Laarni, J., Torkkeli, K. & Vesaoja, E. in press. Pre-validation of a new interactive operating panel system for a nuclear power plant training simulator. Paper to be presented in ANS NPIC&HMIT 2015.
- Laarni, J. & Koskinen, H. 2014. Method for fidelity evaluation of nuclear power plant simulators from the Human factors point of view. Proceedings of the 5th International Conference on Applied Human Factors and Ergonomics AHFE 2014, Kraków, Poland 19-23 July 2014
- Laarni, J. & Liinasuo, M. 2012. Operointikäytännöt onnettomuustilanteissa. [In English: Operator practices in accident situations]. VTT-R-00768-12.
- Laarni, J., & Savioja, P. 2013. Developing an integrated Human Factors Engineering process for the nuclear domain. VTT-R-00536-14.
- Laarni, J., Savioja, P., Norros, L., Liinasuo, M., Karvonen, H., Wahlström, M. & Salo, L. 2014. Conducting stepwise HFE validations to support control room modernization. Proceedings of ISOFIG/ISSNP 2014, Jeju, Korea, August 24-28, 2014.
- Laarni, J. & Tommila, T. in preparation. Concept-of-Operations as a boundary object in knowledge sharing across stakeholders in nuclear industry. Paper to be submitted to the Applied Human Factors and Ergonomics Conference (AHFE) 2015.

- Laitio, P. 2013. User interface solutions for supporting operators' automation awareness in nuclear power plant control rooms. Master's thesis. Espoo: Aalto University.
- Laitio, P., Savioja, P. & Lappalainen, J. 2013. Exploring the concept of automation awareness in nuclear power plant control rooms. In Proceedings of the Enlarged Halden Programme Group Meeting, Storefjell, Norway, March 11-15, 2013.
- Liinasuo, M. & Porthin, M. 2014. Updating Human Reliability Analysis – insights from Human Factors oriented control room validation. VTT-R-05278-14.
- Norros, L. 2012. Analysis of work practices from the resilience engineering perspective. *Nuclear Safety and Simulation* 3(4). [Online]
- Norros, L. 2014. Developing human factors/ergonomics as a design discipline. *Applied Ergonomics* 45, 61-71.
- Norros, L., Liinasuo, M. & Savioja, P. 2011. Operators' conceptions of procedure guidance in NPP process control. Proceedings of the Enlarged Halden Project Group Meeting, Sandefjord, October 2-7, 2011. Vol 1, p. C1.7.
- Norros, L., Liinasuo, M. & Savioja, P. 2014. Operators' orientations to procedure guidance in NPP process control. *Cognition, Technology & Work* 16, 487-499.
- Norros, L., Savioja, P., Liinasuo, M. & Wahlström, M. 2014. Can proceduralization support coping with the unexpected? *Nuclear Safety and Simulation* 5(3). [Online]
- Salo, L., Savioja, P. & Laarni, J. in press. Developing a Human Factors Engineering process for control room upgrades. Paper to presented in ANS NPIC&HMIT 2015.
- Savioja, P. 2014. Evaluating Systems Usability in Complex Work. Development of a Systematic Usability Concept to Benefit Control Room Design. Espoo: VTT. VTT Science 57. 168 p. + app. 116 p.
- Savioja, P. & Norros, L. 2013. Systems usability framework for evaluating tools in safety-critical work. *Cognition, Technology & Work* 15, 255-275.
- Savioja, P., Norros, L. & Salo, L. 2012. Functional situation models in analyses of operating practices in complex work. Proceedings of ECCE 2012: European Conference on Cognitive Ergonomics, Edinburgh, UK, August 29-31, 2012.

Savioja, P., Norros, L., Salo, L. & Aaltonen, I. 2014. Identifying resilience in proceduralised accident management activity. *Safety Science* 68, 258-274.

Wahlström, M., Liinasuo, M., Norros, L. & Savioja, P. 2014. Symbiosis of rule-following and flexible acting? Procedure designers' views on NPP operating work. Proceedings of Enlarged Halden Programme Group Meeting, Roros, Norway, September 7-12, 2014.

6.2 Studying automation awareness in nuclear power plants

Hannu Karvonen, Iina Aaltonen, Jari Lappalainen, Marja Liinasuo, Timo Kuula, Mikael Wahlström, Maiju Aikala, Paula Laitio, Paula Savioja, Jari Laarni

VTT Technical Research Centre of Finland Ltd
P.O. Box 1000, FI-02044 Espoo

Abstract

This paper summarizes the automation awareness user studies conducted in the HACAS project. Automation awareness can be defined as a user's conception of the utilized automation system's state in such a manner that it enables the user to appropriately observe, control, and anticipate the process events mediated by the automation. We conducted two separate, but interrelated studies where automation awareness was investigated. First, we interviewed automation mechanics on the challenges and training needs in nuclear power plant automation maintenance. Second, we conducted a simulator study with field operators and automation mechanics. The results suggest that in addition to factors such as the users' automation-specific education, work experience, and the provided training, the quality of the automation system's user interface is a significant contributor to the development of automation awareness. As a conclusion, automation awareness should be taken into account especially in the design of user interfaces, personnel training, and operating procedures in nuclear power plant modernization and new building projects.

Introduction

The role of automation systems is continuously increasing in nuclear power plants (NPPs). Therefore, in addition to understanding the basic process phenomena, there is a growing need for different workers to understand also the underlying functioning principles of the automation, which is to monitor, control, and protect the process. This understanding is applied in operating situations when interpreting the current (and possibly also foreseeing the future) state of the automation. We see that this kind of activity requires what we call 'automation awareness' (AA). The intention of

the AA concept is to emphasize that in the world of digital automation, the users' situation awareness is growingly related to the state of the automation instead of only process parameters (see our previous publications about AA: Aaltonen et al., 2012; Laitio, 2013; Laitio et al., 2013; Karvonen, Lappalainen & Liinasuo, 2014; and Karvonen, Liinasuo & Lappalainen, 2014).

As a concept, automation awareness is close to the concept of situation awareness. In line with the definition of the situation awareness (SA) stages by Endsley (1995), we see the development and maintenance of automation awareness in an NPP control room (CR) to be a continuous process that comprises of perceiving the current status of the automation, comprehending this status and its meaning to the system behaviour, as well as projecting its future status and meaning (Laitio et al., 2013). In other words, AA is the user's conception of the utilized automation system's state in such a manner that it enables the user to observe, control, and anticipate the process events mediated by the automation. If this conception is on a correct level (i.e., matches with reality accurately enough), the user understands sufficiently the automation's role in the on-going process control events. This enables the user to use the automation system in an appropriate way, taking into account the demands of the situation at hand. Therefore, good AA presumes the user to have the ability to pay attention to the cues indicating the automation's state, interpret these cues correctly, make correct conclusions based on them, and act accordingly.

In addition to the provided user interface and user training, we see that there are also other factors contributing to the development of the user's AA in an NPP control room. Many of them are rather properties of the automation itself than characteristics of the presentation of automation in a user interface and should be taken into account already when designing the automation. Laitio's (2013) master's thesis lists, for example, the following factors: level of automation, automation complexity, modes of automation, functions of automation, processes of automation, flexibility of automation, reliability of automation, other automation properties (e.g., inbuilt correction and compensation functions and failure masking), feedback about the state of automation, and user workload. For the purposes of this paper, we do not go into details of these factors here. More detailed design guidelines for supporting good automation awareness can be found also in Karvonen, Liinasuo & Lappalainen (2014).

Next, we present two studies we have conducted in order to study AA. The first one is about the challenges and training needs in NPP automation maintenance, and the second one about an AA simulator user interface study.

Challenges and training needs in NPP automation maintenance

Interview study of automation maintenance personnel

Automation maintenance personnel at two Finnish NPP sites were interviewed about their school education, work tasks and tools, as well as training practices at the sites, on-the-job-learning and the challenges of automation modernization. Altogether

er nine interviews were conducted in person using a semi-structured interview method. The aim was to acquire knowledge of how the personnel sees its training needs and what its' future work expectations are (see Aaltonen et al., 2015).

The interviewees described their maintenance work on a practical level. In addition to doing preventive maintenance, repairing failures, performing periodic tests, and implementing new systems, the interviewees mentioned that their work also includes supporting the control room operators in solving reasons for abnormal system behaviour and in providing the operators results of measurements that they can rely on while operating the process.

In the interviewees' opinion, the control room operators have varying levels of understanding of automation. There were also varying opinions on who possesses the best knowledge of the state of the automation in case of a failure; some suggested the control room staff, others the automation mechanics or their supervisors, or automation engineers, or a combination of them. Regarding their own work, the mechanics emphasized the importance of understanding the role of automation in the energy production process, although they felt they could benefit from knowing more about the process.

The interviewees thought that revision and equipment installation are the most effective opportunities for learning. Some mechanics had experience on simulation-based training, but there were mixed opinions about the benefits of it, depending on how profoundly the learner was actually able to test and examine the equipment. Some thought the training was very beneficial, and is actually the best way of learning, while others evaluated the training to be almost useless.

The training needs described by the interviewees were categorized into four themes: 1) language skills, 2) analog vs. digital systems, 3) use of computers and new technology, 4) retirement of personnel, 5) emerging collaboration, and 6) multi-skilled workers. Themes 2), 3), 5) and 6) are considered further below from the viewpoint of AA.

The automation mechanics familiar with the digital automation preferred the digital system to the analog system on several accounts. The digital system (especially the function block diagram) was, for example, estimated to be more informative to both the mechanics and the control room operators. On the other hand, failures in the digital system were found to be more difficult to identify. Interestingly, in the long run, knowledge on analog automation may pose a greater challenge than of digital, because analog automation is no longer taught at schools, and the automation modernization does not necessarily lead to a complete digitalization of I&C systems.

The use of computers and other new technology has increased in NPPs. An example of this new technology is the multi-calibrator, which is a smart measurement and signal generation device that does a lot of the reasoning and manual work that was previously required by the mechanics. This may introduce a new challenge for maintaining AA, especially for the less experienced mechanics.

The emerging collaboration with other groups and teams at the NPPs (automation engineers, the process-IT department and other information technology specialists) can be seen as a learning and training need as well. The interviewees noted that the process-IT department could benefit from increased automation understanding.

Along the same line, some mechanics suggested they should know more about the nuclear energy production process.

And finally, the requirement to master and perform multiple work tasks instead of profoundly specializing in one area of work, has been recognized as a learning challenge at both sites. Traditionally, the maintenance personnel have had their own, strictly focused areas of responsibility, but are currently required to master multiple work tasks, which may also have an effect on maintaining a good level of AA.

Automation awareness simulator study

Development of the automation awareness simulator

In order to investigate AA, we have developed an automation awareness simulator, which simulates the emergency diesel generator (EDG) system and its control user interface (UI) (see Figure 1) for Loviisa NPP with periodic testing functionality. EDGs automatically ensure the power supply to the NPP's safety-critical systems in case of a failure in the normal power supply. The Loviisa NPP units have four EDGs, which means two EDGs per redundancy. To each of the EDGs a periodic test is conducted once every four weeks. The first EDG in the first redundancy (a system called EY01) was chosen as the target of the AA simulator system. The simulator featured a new, digital design for the operator user interface, in contrast to the analogue system used currently at the Loviisa plant.

Technically, the simulator environment consisted of the Apros (www.apros.fi) simulator and ProcSee (www.ife.no/procsee) user interface software, which communicate between each other via OPC. The simulator uses the Apros model of Fortum's Loviisa Engineering and Development Simulator, but was restricted to include only the emergency diesel generator system.

The design of the simulator UI was based on three guidelines derived from the literature: good observability of automation, minimized workload, and transparent failure management (Laitio et al., 2013). For a detailed description of the simulator (and how the principles are taken into account in the design), please see Laitio et al. (2013) and Laitio (2013).

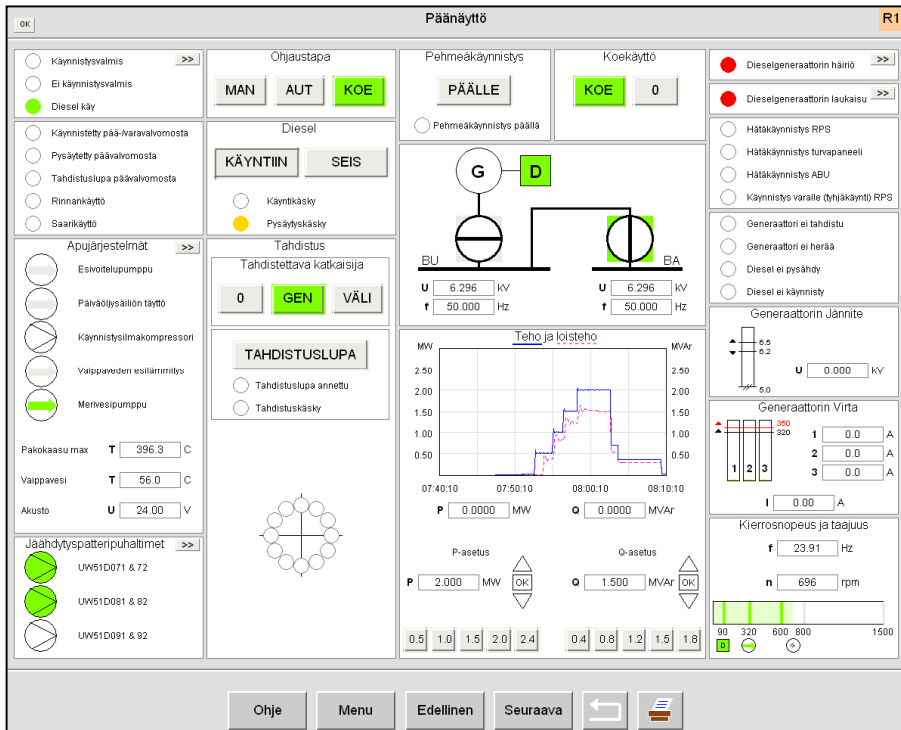


Figure 1. AA simulator main display (in Finnish). A diesel trip has occurred in the system.

Research questions

The research aims of our user study were two-fold: 1) to study automation awareness with the simulator and 2) to identify usability issues related to the UI. In order to support these aims, we had the following research questions in the studies:

- How automation awareness can be studied with the simulator?
- Do the developed simulator solutions support the user in achieving good automation awareness, and if so, how?
- What kind of usability issues are related to the developed simulator?

Method

In the studies, we had six test sessions with two participants in each session. Therefore, we had 12 participants in total, of which five were turbine field operators, one was a main control room turbine operator, and six were automation mechanics from the turbine side. In the studies, we utilized a pair testing approach (see, e.g., Kallio & Kekäläinen, 2004).

The participants' work experience in the Loviisa NPP varied between two and 37 years. Some of the participants had previous work experience, for example, from the paper industry. All the operators had conducted a periodic testing of an EDG within the last month, so they remembered the actual testing procedure quite well.

The user study test sessions took place during three consecutive days in May 2014 in the meeting rooms of the gate building of the Loviisa NPP. The researchers, who conducted the tests, sat next to a meeting room table (see Figure 2) with a laptop, which was running the EDG system's Apros model and ProcSee software to provide the UI. One of the researchers (see the left side of Figure 2) managed a command interface, from which he could do required field actions in the simulator and introduce fault situations in appropriate points during the test.

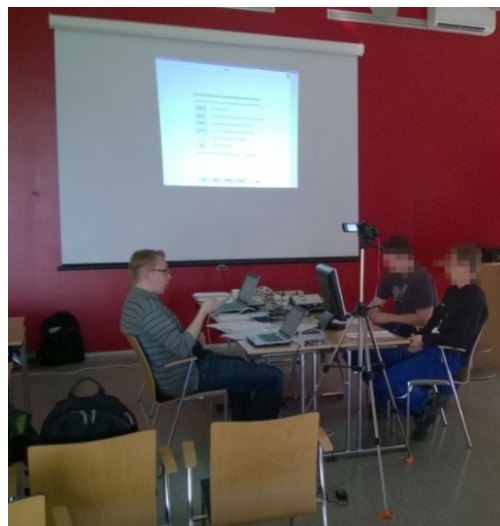


Figure 2. The facilities and the technical setup of the user studies.

The participants (see the right side of Figure 2) sat on the other side of the meeting room table in front of a 24 inch LCD, which showed the UI of the simulator. The test setup included also a duplicated version (see the video projector image on top of Figure 2) of the participants' UI view in order for the researchers to observe better what the participants were doing with the UI, and to video record discussions and everything what is happening in the UI with a video camera (see the middle part of Figure 2). The participants were operating the UI with a regular PC mouse.

Our research approach in the study was exploratory (Stebbins, 2001). In the spirit of exploratory research, we utilized mostly qualitative methods in the user studies. First, before starting the actual test tasks, a pre-test interview was conducted. In this interview, the participants were asked, for example, about their backgrounds and EDG and automation-related experience. Second, the test instructor did a short walkthrough of the UI for the participants by showing and explaining each display.

Third, the participants could briefly practice navigating in the UI by themselves. The walkthrough and navigation without any specific task were performed for familiarizing the participants with the new system so that there would not be difficult problems in using the system as such.

After these phases, the actual test tasks with the simulator were started. The participants were first instructed to do a normal periodic testing with the system according to the printed periodic testing procedures, the same they normally use in the testing. The participants were also instructed to think aloud (Bainbridge & Sanderson, 1995) while using the system, so that the researchers could hear how the participants understood the UI and how their mental model about its behaviour developed. After the first fault-free periodic testing, a second round with different (fault) scenarios was performed. These scenarios ranged from minor departures from standard practice to distinct faults in the system.

After each task step or scenario, the test instructor asked questions to find out more about, for example, what the participants were thinking while using the UI. After all the test tasks, a semi-structured post-test interview was conducted, which included questions about the UI and the participants' automation awareness during the test. Finally, an automation awareness questionnaire, which we had developed, was filled in by the participants.

Results and discussion

The simulator UI and the data it provided were considered to be realistic by the participants. Most of the participants managed to conduct the given test tasks successfully and the designed UI displays were generally well accepted, although the displays also received many suggestions for improvements from the participants. If the participant had experience of other NPP systems or systems in other industries (e.g., paper machines), it seemed to affect positively their visions about how the UI could improve the user's AA.

The automation awareness questionnaire results indicate that the participants had a fairly good level of automation awareness with the simulator. When asked how well (1–10 scale, 1 being not at all and 10 being entirely) the participants understood the state and functioning of the automation in different situations during the tests, the average score was 7.4. In addition, when asked about the extent of the UI in helping to understand the state of the automation (1–10 scale, 1 being not at all and 10 being extensively), the average score was 7.7. The participants also felt that the simulator UI presented the automation's state and functioning in simple rather than in complex way.

When interviewed about EDG's automation, most of the participants answered that automation is primarily utilized in the synchronization phase of the diesel to the BU and BA buses. This is to say that the user does not have to do the synchronization manually, but only wait until the synchronization is done automatically by the system. One of the participants also mentioned that during the start-up of the EDG,

a lot of automated sequences take place. Furthermore, the protection signals that caused the diesel system to trip were seen to involve automation.

The educational background of the participants seemed to have an effect on how automation was understood in the context of nuclear process control. For example, participants with background in electrical engineering seemed to understand automation in the EDG system to be very low level technical operations, such as the functioning of the relays. If the understanding was on a high level, the participants understood automation to be a whole consisting of automatic information processing, logic, and control features of the system.

In summary, to support AA better the participants emphasized especially the importance of 1) the presentation of digital and exact measurement values, 2) graphical presentation styles of the values' status and their minimum and maximum limits, 3) illustrative trend displays in understanding the state of the automation, and 4) presenting clear alarm indications. It can be inferred from the results that particularly the trend displays work as a powerful tool in interpreting the previous, current, and future state of the automation (besides the state of the process).

The studies showed that UI is the main contributor to the development of AA. Therefore, we see that different UI means to support the users in understanding the automation more deeply need to be investigated and utilised in design. However, the current technological limitations of the available automation platforms often constrain the possible UI solutions in the field of nuclear power.

In addition to UI features and solutions, AA and understanding in the test sessions was affected considerably by the amount of work experience and received training. For example, if the participant had only a few years of experience with EDG systems, it seemed (according to the thinking aloud comments) that he was not able to keep track with our new UI of what automation was doing in different phases of the scenarios. Furthermore, if the participant had previous experience of logic displays, or bar and trend graphs, from other systems, he could also easily understand their meaning in our simulator, which resulted in a good level of AA while using the system.

Some of the automation mechanics with good AA in the studies emphasized the connection between solving automation-related faults and understanding the actual process (i.e., EDG's functioning). Understanding of the process is very important in the troubleshooting of automation-related issues too. That is why in practice, the automation mechanic and the field operator are, and also should be, working together in case of a fault in the system. Therefore, it can be concluded that good AA requires also a deep understanding of the actual process itself.

Summary and conclusions

We see that a user's understanding about automation is an essential part of situation awareness in any modern industrial environment. We call this understanding as conception automation awareness and state that it creates the prerequisites for appropriate user activity in monitoring and controlling a highly automated process. It

is no longer enough for the user to understand only the process and its states, but he/she also needs to understand and follow the progress of the automated functions in order to operate the plant properly. Without sufficient automation awareness, the user has no ability to observe the functioning of the system as a whole. This leads to a situation where the user is 'out-of-the-loop' and therefore loses the hands-on touch both to the automation and to the process control. Consequently, the user's ability to act in demanding exceptional situations is also diminished.

Automation awareness is a phenomenon, which is developed especially in the interaction between the user and automation. The quality of this interaction is dependent from the system's part most importantly on the ability of the automation system's user interface to provide the user the needed information about the functioning of the automation, factors affecting its current state, the system's general structure (i.e., architecture), and the system's functioning principles. This also affects, e.g., the development of user trust in the automated system, which we see to be an important determinant of, for example, misuse of automation or whether the user uses it at all (if optional). In addition, automation awareness is built upon the basic knowledge regarding the automation, which is learned during training and with experience gained by operating the system in hands-on work.

In the work presented in this paper, we have studied automation awareness by analysing the way operators and mechanics talked about automation and how they actually conducted tasks in simulator user study sessions. Therefore, for example the terms participants used and their conceptions about the state of the automation and how they actually operated the system were regarded as indicators of the participants' current AA. Another way of studying AA could have been, for instance, to stop the test (and freeze the simulation) at certain points in time, and ask the participants about the state of the automation, as is done in the traditional studies of situation awareness (see, e.g., Stanton et al., 2013). However, we see that our approach is a more subtle way of studying the SA or AA (as it does not intervene with the participants' tasks) and also takes more deeply into account the interpretation of actual activity of the participants. Guidelines for AA method development can be found in detail in Karvonen, Liinasuo & Lappalainen (2014).

We conclude that it is not reasonable to try to develop a fully generalizable method for the measurement of automation awareness. The measurement of AA needs always to be customized for taking into account the system that the users are using and also the specific situation where the method is utilized. Therefore, neither the HACAS project nor this paper does end up with a finalized fit-all method for the measurement of AA. Instead, we presented ways to approach how we perceive automation awareness could be studied and measured.

Finally, it can be said that both the short- and long-term implications of digitalization and increasing level of NPP automation need to be carefully considered. According to our experience, potential problems can be largely avoided by increasing the workers' understanding of automation, skills to interact with it and willingness to cooperate with it. This can be done, for example, by involving the users early-on to the design and implementation of the user interfaces, level of automation, and the automation itself.

References

- Aaltonen, I., Karvonen, H., Laarni, J., Lappalainen, J., & Savioja, P. 2011. Kirjallisuuskatsaus: Automaattitietoisuus prosessinhallinnassa (in Finnish). VTT Research Report VTT-R-00675-12, 59 p.
- Aaltonen, I., Kuula, T., Wahlström, M., Aikala, M., & Laarni, J. 2015. Challenges and training needs in NPP automation maintenance. To be presented at the ANS NPIC & HMIT Conference in Charlotte, North Carolina, US, Feb 2015.
- Bainbridge, L., & Sanderson, P. 1995. Verbal Protocol Analysis. In: J. Wilson and E.N. Corlett (Eds.), *Evaluation of human work: A practical ergonomics methodology*, pp. 159-184. Taylor & Francis.
- Endsley, M. R. 1995. Toward a theory of situation awareness in dynamic systems. *Human Factors: The Journal of the Human Factors and Ergonomics Society*, Vol. 37, No. 1, pp. 32-64.
- Kallio, T., & Kekäläinen, A. 2004. Improving the effectiveness of mobile application design: User-pairs testing by non-professionals. In: *Mobile Human-Computer Interaction – MobileHCI*, pp. 315-319, Springer Berlin Heidelberg.
- Karvonen, H., Liinasuo, M., & Lappalainen J. 2014. Assessment of situation and automation awareness. VTT Research Report VTT-R-05997-14, 38 p.
- Karvonen, H., Lappalainen, J., & Liinasuo, M. 2014. Automation Awareness User Interface Study – Preliminary Results. In: *Proceedings of the Man-Technology-Organisation Sessions at the 2014 Enlarged Halden Programme Group Meeting, C2.4, OECD Halden Reactor Project*.
- Laitio, P., Savioja, P., & Lappalainen, J. 2013. Exploring Automation Awareness in Nuclear Power Plant Control Rooms. In: *Proceedings of the Man-Technology-Organisation Sessions at the 2013 Enlarged Halden Programme Group Meeting, C5.8, OECD Halden Reactor Project*.
- Laitio, P. 2013. User interface solutions for supporting operators' automation awareness in nuclear power plant control rooms. Master's thesis. Aalto University, School of Electrical Engineering.
- Stanton, N. A., Salmon, P. M., Rafferty, L. A., Walker, G. H., Baber C., & Jenkins, D. P. 2013. *Human Factors Methods. A Practical Guide for Engineering and Design*. Surrey: Ashgate Publishing Limited.

Stebbins, R. A. 2001. *Exploratory Research in the Social Sciences*. Sage Publications.

7. Safety evaluation and reliability analysis of nuclear automation (SARANA)

7.1 SARANA summary report

Björkman Kim¹, Heljanko Keijo², Kähkönen Kari², Lahtinen Jussi¹, Pakonen, Antti¹, Porthin Markus¹, Tyrväinen Tero¹, Valkonen Janne¹

¹VTT Technical Research Centre of Finland Ltd
P.O. Box 1000, FI-02044, VTT, Finland

²Helsinki Institute for Information Technology and Department of Computer Science,
Aalto University
P.O. Box 15400, FI-00076 Aalto, Finland

Abstract

The objective of the SARANA project was to develop methods and tools for safety and reliability analysis of digital systems and utilize them in practical case studies. The project provided guidelines to analyse and model digital systems in PRA context, brought together deterministic and probabilistic analyses for safety assessment of plant designs, developed the reliability analysis tool YADRAT, investigated the applicability of probabilistic model checkers, used model checking for analysing high-level design architecture, developed an iterative and automatic algorithm for modular model checking of large systems, developed methods for systematic model checking of complex asynchronous systems, and investigated how different modelling approaches and tools can be used and suited for the safety analysis of I&C in different phases of the plant lifecycle. The project followed and participated in the work of several international working groups and conferences in its application areas.

Introduction

The overall objective of the SARANA project was to develop methods and tools for safety and reliability analysis of digital systems and to utilize them in practical case studies. The project covered various topics and built bridges between risk analysis and automation experts. SARANA provided guidelines to analyse and model digital systems in Probabilistic Risk Assessment (PRA) context, brought together deterministic and probabilistic analyses for safety assessment of plant designs, developed the reliability analysis tool YADRAT, developed an iterative and automatic algorithm for modular model checking of large systems, and developed more efficient methods for systematic model checking of asynchronous systems. Strong emphasis was put on finding links between the different approaches, developing modelling and algorithmic links, developing common concepts and improvement of communication between different disciplines. This summary report introduces the main results of the project.

Reliability analysis of digital systems in PRA context

The objective of this task was to develop guidelines to analyse and model digital systems in PRA context for nuclear power plants. The project consisted of three interrelated activities. A taxonomy for failure modes of digital I&C systems was developed by a task group of OECD/NEA Working Group RISK (WGRISK) (WGRISK 2014). In the parallel Nordic activity, a fictive digital I&C PSA model was developed for the demonstration and testing of modelling approaches (NKS-230, NKS-261, NKS-277, NKS-302). An example of a four-redundant digital I&C protection system architecture is presented in Figure 1. The third activity was to develop a method for the quantification of software reliability in the context of PRA (NKS-304).

The scope of the failure mode taxonomy included both protection and control systems of a nuclear power plant focusing on protection systems. The taxonomy was divided into hardware and software related failure modes. The needs from PRA guided the work, i.e. that I&C system and its failures are studied from their functional significance point of view. The developed example model included basic events for both detected and undetected failures of hardware and software components. Different fail safe principles and intelligent voting logics were incorporated in the model. Common cause failures between I&C components were also included. In most cases, common cause failures of I&C components were dominant over single failures. Hence, the estimation of CCF parameters for I&C components has to be studied carefully. The proposed software evaluation and quantification method will use operational history to estimate the fatal failure probability within system software (operating system, runtime), and use another method for estimation of failure probability within application software. The quantification for application software is based on

two main measures, complexity and the degree of verification and validation of the software.

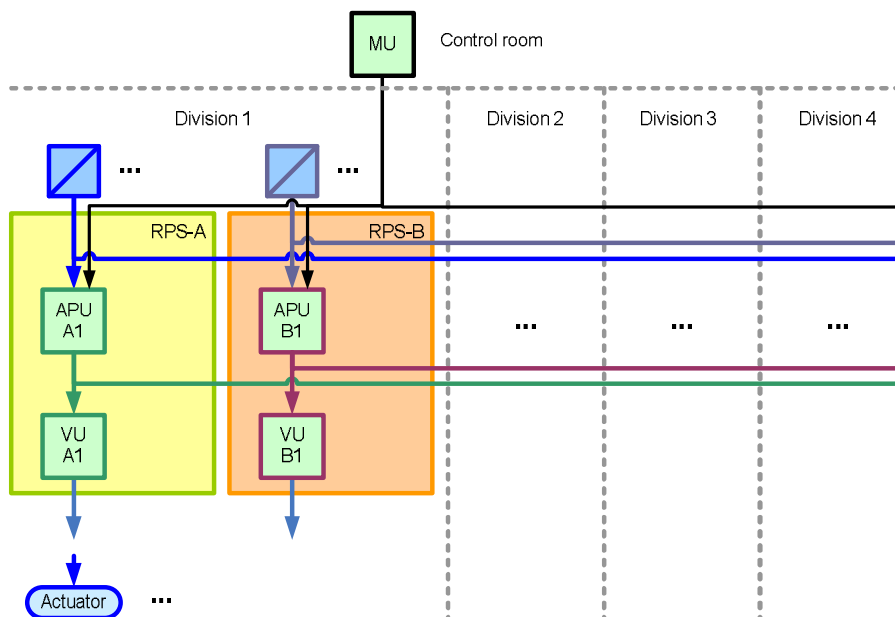


Figure 1. Example of a four-redundant digital I&C protection system architecture (NKS-302).

YADRAT development

The dynamic flowgraph methodology (DFM) is an approach for reliability analysis of dynamic systems such as digital I&C systems. The Yadrat tool (Björkman 2013) developed at VTT is an implementation of the DFM methodology. An example Yadrat model is shown in Figure 2. Yadrat is based on interpreting the DFM model as a binary decision diagram. YADRAT has been implemented so that the DFM model can be translated into SMV (symbolic model verifier) code that can further be examined with the formal model checking tool NuSMV. The applicability of the tool was analysed and a comparison between FinPSA (a unique software tool developed at STUK for PRA) and YADRAT was performed (Björkman & Tyrväinen 2014). The benefits and limitations of both tools in modelling digital I&C systems were analysed. Finally, different ways to utilise dynamic flowgraph methodology and particularly Yadrat tool as part of PRA were studied (Björkman & Tyrväinen 2015). The study focused on FinPSA and Yadrat, but the conclusions should be applicable also for alternative DFM and PRA software. The results indicate that DFM could in principle be used in PRA as such but for practical use it should at least be possible to auto-

mate the integration of DFM results into the PRA tool. Possibilities for developing a simple interface between YADRAT and FinPSA to exchange information between the tools were investigated.

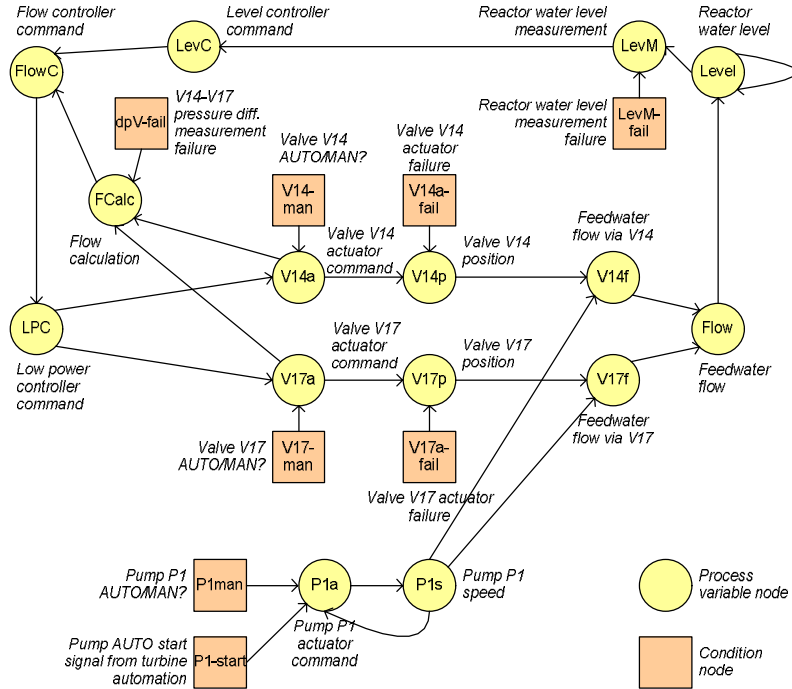


Figure 2. An example Yadrat model of a feedwater control system.

Formal analysis of large systems

Model checking (Clarke et al. 2001) has been successfully used to analyse individual functions of safety-critical I&C systems, see e.g., (Lahtinen et al. 2012a). In the nuclear domain, it is common to cope with hardware failures by implementing several subsystems that execute the same physical function using design diversity in software and/or hardware. It may be necessary to examine these diverse subsystems simultaneously, e.g., because the specifications may in fact cover their combined behaviour, and to also additionally check that the diverse subsystems have no unintended interactions. Currently available classical model checking methods do not always scale to analysing these large and complex combined systems.

An iterative technique for model checking large modular systems was developed in the project. The technique uses abstraction based over-approximations of the model behaviour, combined with iterative refinement.

In the technique, we require that the system is structured into modules. Abstractions of the model are created by replacing a subset of the modules with stubs that can at each time point non-deterministically give any value from any of their outputs.

We employ an abstraction refinement technique based on the modular structure of the model, the dependency graph of the model, and a refinement sampling heuristic. In iterative abstraction refinement, an initial abstraction is first generated and model checked. If the examined property produces a counter-example, the model is refined and the resulting new model is verified again. The process is continued until the property is proved or no further model refinement is possible. The iterative refinement loop used in our technique is illustrated in Figure 3.

In the model checking step of our abstraction refinement technique, three model checking algorithms (BDD-based, k-induction, PDR) are run in parallel in a portfolio-based manner. The abstractions in our technique are refined using a two-phase procedure. First, in the preliminary refinement phase, we obtain a computationally manageable subset of the modules that is sufficient for proving the given state invariant. This part of the refinement procedure is based on traversing the dependency graph of the modules. After the preliminary refinement phase we attempt to minimise the size of the needed model refinement using an iterative sampling procedure based on a technique called delta debugging (Zeller & Hildebrandt 2002).

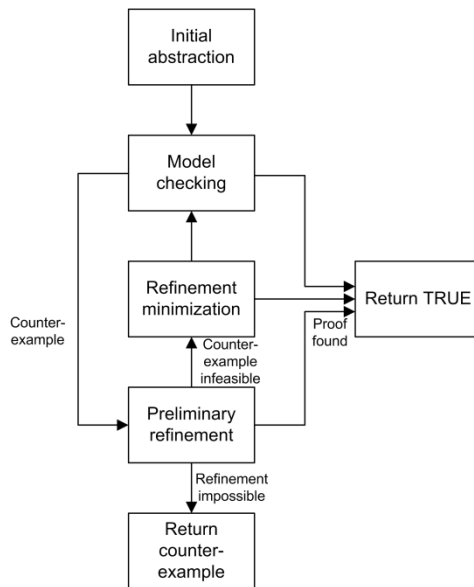


Figure 3. The iterative refinement loop used in our technique.

Our technique will: (i) significantly reduce the amount of manual work needed to create abstractions, (ii) prove the system correctness based on verification runs automatically performed on these abstractions, and (iii) reduce the overall computational effort required for model checking, enabling the model checking of larger sys-

tem models. Our approach is designed to be efficient at finding proofs for properties, as we expect most of the designs at this stage of inspection to actually be correct.

We have tested our technique by verifying two different systems with it. The first system is a fictional case study that consists of two diverse safety systems. The second system is an actual industrial emergency diesel generator control system that is used for evaluating the performance of our technique on a real life system. In both case studies we have compared our technique against three other model checking approaches: classical BDD-based model checking, SAT-based k-induction, and PDR-based model checking. The results show that for most of the properties our technique is able to find a proof of correctness of the system more efficiently than the other three approaches. For more details on this work see e.g. (Lahtinen et al. 2012b, Lahtinen et al. 2012c, Lahtinen et al. 2010).

System level interfaces and timing issues

In the earlier development of model checking methodology for nuclear I&C verification, the usual assumption has been that the analysed system is one fully synchronous entity through which all signals are able to traverse within a single system clock cycle. However, this assumption does not hold especially for distributed systems, where the subsystems employ different clocks, and the signals do not always carry over from one part of the distributed system to another during a single clock cycle. Assuming synchronous behaviour can leave some errors undetected when verifying the model.

In SARANA, we have modelled a case study system consisting of an asynchronous control circuit with both analogue and digital signals (Lahtinen et al. 2012b). The system was modelled using both the UPPAAL model checker and the NuSMV model checker, using both the traditional timing assumptions and the more accurate asynchronous timing. We were able to analyse the model in greater detail using the accurate timing model, while still keeping the model size small enough to fit into memory.

One of the challenges in model checking I&C systems is that they combine timers with large input non-determinism due to the large number of sensors that typical system designs contain. We have evaluated the use of a model checker called ATMOC (Aalto Timed Model Checker) (Kindermann et al. 2012) that allows timers to be used in modelling systems in an extended version of the NuSMV language. We have also developed a modelling approach to convert I&C designs efficiently into ATMOC-specific model checking models, and the initial experimental results are very promising.

Plant-level models and failure modelling

Our previous research has shown that model checking is a viable technique for verifying individual I&C systems. There is, however, also need to examine the overall system safety and fault-tolerance on the plant-level. The Finnish regulatory

guides on nuclear safety (YVL guides) require that all individual safety systems are single-failure tolerant. For some systems it should also be possible to perform the safety function even if any single component fails and any other component is simultaneously out of operation due to repair or maintenance.

The traditional plant-level architecture analysis methods such as fault tree analysis (FTA), failure mode and effects analysis (FMEA) and probabilistic risk assessment (PRA) are not intended for exhaustively examining the complex functionality of the digital automation systems. Model checking, on the other hand, can be used to verify the logical designs exhaustively. Thus, it is tempting to try to expand the scope of model checking to the plant-level so that the overall system behaviour could be analysed in more detail. This approach could be beneficial in finding potential errors in system design that arise from a combination of a hardware failure and a software design error.

In order to enable the analysis of fault-tolerance requirements, we have developed in the SARANA project a methodology for modelling hardware failures. The intention is to model failures in e.g. telecommunication links, microprocessors, measurement devices, pumps and valves. The operation of the actuators and the effects of failures to how signals are interpreted in the I&C systems are modelled. The developed methodology serves as a framework for verification of high-level system properties and fault-tolerance, which has previously been quite difficult.

First we experimented with a simple case study model (see Lahtinen et al. 2012b). Later on we used the fictitious PRA model also used in the DIGREL project (see Authén et al. 2013) and created a corresponding model that can be used for model checking. The PRA model depicts a boiling water reactor (BWR) type nuclear power plant, which has four-redundant safety systems.

We successfully verified system level safety properties on the plant model, and analysed the level of fault-tolerance the plant model had with regard to these properties. We also used simple abstractions, and simplifications to make the verification more feasible. The biggest simplification when compared to a real system was that no time delays were implemented in the safety system logics. We also assumed that all hardware failures were permanent. The methodology is quite compatible with PRA, and it serves as a basis for further integration between the two approaches. More details on our work can be found in (Lahtinen 2014a) and in (Lahtinen 2014b).

The main challenge in verifying large plant-level models is that the resulting model can become very large. The biggest current limitation of using our methodology in practice is that adding timing behaviour to the logic modules significantly increases the complexity of the model checking problem. Using the IC3 algorithm (Bradley 2011) for verification is a potential approach, as well as the portfolio based approach (Sterin et al. 2011). For liveness properties, a liveness to safety reduction, as described in (Kuismin & Heljanko 2013), could be used.

Model checking tool portfolio

If the model checker reports no errors found, one may doubt the correctness of the result. If two model checkers containing no shared code give the same result, confidence is naturally higher. Another way to get increased confidence is to provide an independently checkable proof from the model checker. A prototype tool chain to model check SMV models without using any code from NuSMV model checker was developed. This was done by first converting the model from SMV to AIGER, which is the input format used in the Hardware Model Checking Competition. After this conversion, a number of tools can be used for the actual model checking. Additional benefit is the possibility to use multiple different model checking algorithms in parallel and using the result of the one that finishes first. In this case, some confidence is traded for speed. Also initial proof checking support was integrated to the work flow.

Formal analysis of source code

The digital nuclear I&C systems contain a fair amount of source code (e.g., C code) in platform software, application software and in smart instruments. Many approaches exist for analysing source code. Static code analysis methods analyse code without executing the program. Typically static analysis tools produce false warnings that need to be ruled out manually, making them laborious to use. Dynamic symbolic execution (DSE) is a hybrid method that combines benefits from static analysis and automated testing. A brief state-of-the-art report on source code analysis was prepared and the applicability of the different methods was analysed through an academic case study.

Acknowledgements

The project group acknowledges the representatives of the Finnish power companies and STUK who have contributed to the successful accomplishment of SARANA project by providing case studies, giving comments and reviewing reports.

References

- Authén, S., Björkman, K., Holmberg, J.-E., Larsson, J., 2010, Guidelines for reliability analysis of digital systems in PSA context — Phase 1 Status Report, NKS-230 Nordic nuclear safety research (NKS), Roskilde, 2010.
- Authén, S., Gustafsson, J., Holmberg, J.-E., 2012, Guidelines for reliability analysis of digital systems in PSA context — Phase 2 Status Report, NKS-261 Nordic nuclear safety research (NKS), Roskilde, 2012.

- Authén, S., Gustafsson, J., Holmberg, J.E., 2013, Guidelines for reliability analysis of digital systems in PSA context - Phase 3 status report. NKS Report NKS-277, Nordic Nuclear Safety Research (NKS)
- Authén S., Holmberg J-E., Lanner L., Tyrväinen T., 2014, Guidelines for reliability analysis of digital systems in PSA context - Phase 4 Status Report. NKS-302. Nordic nuclear safety research (NKS), Roskilde, 2014.
- Björkman, K., 2013, Solving dynamic flowgraph methodology models using binary decision diagrams. *Reliability Engineering and System Safety*. 2013; 111:206-16.
- Björkman K, Tyrväinen T., 2014, Modelling a digital I&C system with Yadrat and FinPSA. VTT Research Report, VTT-R-08750-13. Espoo, 2014.
- Björkman K, Tyrväinen T., 2014, Dynamic flowgraph methodology as a part of PRA. VTT Research Report, VTT-R-04222-14. Espoo, 2015.
- Bradley, A.R., 2011, SAT-based model checking without unrolling. In Jhala, R., Schmidt, D.A., eds.: *VMCAI*. Volume 6538 of *Lecture Notes in Computer Science*., Springer 70 – 87.
- Bäckström O., Holmberg J.-E., Jockenhövel-Barttfeld, M., Porthin, M., Taurines, A., 2014, Software Reliability Analysis for PSA, NKS-304, Nordic nuclear safety research (NKS), Roskilde (2014)
- Clarke E. M., Grumberg O., Peled D., 2001, Model checking. MIT Press; ISBN 978-0-262-03270-4.
- Kindermann, R., Junttila, T. J., Niemelä, I., 2012, SMT-based induction methods for timed systems. In Jurdzinski, M., Nickovic, D, editors, *FORMATS 2012*. *Lecture Notes in Computer Science* 7595, Springer, p. 171-187.
- Kuismin, T. & Heljanko, K., 2013, Increasing confidence in liveness model checking results with proofs. In Bertacco, V., Legay, A., eds.: *Haifa Verification Conference*. Volume 8244 of *Lecture Notes in Computer Science*., Springer 32 – 43.
- Lahtinen et al. 2010, Lahtinen J., Björkman K., Valkonen J., Frits J., Niemelä I., 2010, Analysis of an emergency diesel generator control system by compositional model checking. VTT Working Papers 156; VTT Technical Research Centre of Finland.
- Lahtinen et al. 2012a, Lahtinen J, Valkonen J, Björkman K, Frits J, Niemelä I, Heljanko K., 2012, Model checking of safety-critical software in the nuclear

engineering domain. *Reliability Engineering & System Safety*;105:104 – 113.

Lahtinen et al. 2012b, Lahtinen J., Launiainen T., Heljanko K., 2012, Model checking methodology for large systems, faults and asynchronous behaviour. *VTT Technology* 12; VTT Technical Research Centre of Finland.

Lahtinen et al. 2012c, Lahtinen J., Björkman K., Valkonen J., Niemelä I., 2012, Emergency diesel generator control system verification by model checking and compositional minimization. In: Kucera A, Henzinger TA, Nesetrl J, Vojnar T, Antos D, editors. *MEMICS 2012*. ISBN 978-80-87342-15-2; 2012, p. 49 – 60.

Lahtinen, J., 2014a, Verification of Fault-Tolerant System Architectures Using Model Checking. In: *DEVVARTS - 1st International Workshop on DEvelopment, Verification and VALidation of cRiTical Systems*. 195 – 206.

Lahtinen, J., 2014b, Hardware failure modelling methodology for model checking. Research report: VTT-R-00213-14, VTT Technical Research Centre of Finland Available online: <http://www.vtt.fi/inf/julkaisut/muut/2014/VTT-R-00213-14.pdf>

Sterin, B., Een, N., Mishchenko, A., Brayton, R., 2011, The benefit of concurrency in model checking. In: *In Proceedings of the International Workshop on Logic Synthesis, IWLS'11*. 176 – 182.

WGRISK 2014, Failure modes taxonomy for reliability assessment of digital I&C systems for PRA, report prepared by a task group of OECD/NEA Working Group RISK, OECD/NEA/CSNI, Paris. October, 2014.

Zeller A., Hildebrandt R., 2002, Simplifying and isolating failure-inducing input. *IEEE Trans Software Eng*;28x(2):183 – 200.

7.2 Formal verification of nuclear power plant I&C

Jussi Lahtinen¹, Keijo Heljanko²

¹VTT Technical Research Centre of Finland Ltd
P.O. Box 1000, FI-02044 Espoo

²Helsinki Institute for Information Technology and Department of Computer Science,
Aalto University
P.O. Box 15400, FI-00076 Aalto, Finland

Abstract

Model checking is a formal method that has proven useful for verifying e.g., logic designs of safety systems used in nuclear plants. However, redundant subsystems are implemented in nuclear plants in order to achieve a certain level of fault-tolerance. A formal system-level analysis that takes into account both the detailed logic design of the systems and the potential failures of the hardware equipment is a difficult challenge. In the SARANA project we have created new methodology for modelling hardware failures, and used it to enable the verification of the fault-tolerance of the plant using model checking. We have used an example probabilistic risk assessment (PRA) model of a fictional nuclear power plant as reference and created a corresponding model checking model that covers several safety systems of the plant. Using the plant-level model we have successfully verified several safety properties of the nuclear plant. We have also analysed the fault-tolerance of the plant with regard to these properties. Our work is a step towards being able to exhaustively verify properties on a single model that covers the entire plant. The developed methodology follows closely the notations of PRA analysis, and serves as a basis for further integration between the two approaches.

Introduction

The verification of digital instrumentation and control (I&C) systems is challenging because of complicated control functions, and because the state spaces of the designs easily become too large for comprehensive manual inspection. Formal methods can provide more confidence on the correctness of I&C systems.

Model checking (Clarke et al. 2001) is a computer-aided formal verification method that uses models quite similar to those used in simulation. However, unlike simulation, model checkers examine the behaviour of the system design exhaustively and compare it with the system specification. The specification is expressed in a suitable language, such as temporal logics, describing the permitted behaviours of a system. Given a model and a specification as inputs, a model checking algorithm determines whether the system has violated its specification. If a violating behaviour is found the model checker will give a counter-example execution of the system

demonstrating how the specification has been violated. In this work, we have used the model checking tool NuSMV (FBK-IRST et al. 2012), and formalised the requirements as state invariants.

We have previously applied model checking to the verification of logic designs of individual safety systems, see e.g., Lahtinen et al. 2012a. There is, however, also a need to examine the overall system safety and fault-tolerance on the plant-level. The Finnish regulatory guides on nuclear safety (YVL guides) require that all individual safety systems are single-failure tolerant. For some systems it should also be possible to perform the safety function even if any single component fails and any other component is simultaneously out of operation due to repair or maintenance.

The traditional plant-level architecture analysis methods such as fault tree analysis (FTA), failure mode and effects analysis (FMEA) and probabilistic risk assessment (PRA) are not intended for exhaustively examining the complex functionality of the digital automation systems. Model checking, on the other hand, can be used to verify the automation logic designs exhaustively. Thus, it is tempting to try to expand the scope of model checking to the plant-level so that the overall system behaviour could be analysed in detail. This approach could be beneficial in finding potential errors in system design that arise from a combination of a hardware failure and a software design error.

In our earlier work (Lahtinen et al. 2012b) we have developed preliminary methodology for hardware fault models using a small fictitious model. Here we have improved on this methodology. The intent is to model failures in e.g., telecommunication links, microprocessors, measurement devices, pumps and valves. The operation of the actuators and the effects of failures to how signals are interpreted in the I&C systems are modelled. The developed methodology serves as a framework for verification of high-level system properties and fault-tolerance, which has previously been quite difficult.

We have used a fictitious PRA model and created a corresponding model that can be used for model checking. The PRA model depicts a boiling water reactor (BWR) type nuclear power plant, which has four-redundant safety systems.

We have successfully verified system level safety properties on the plant model, and have analysed the level of fault-tolerance the plant model had with regard to these properties. We have also used simple abstractions, and simplifications to make the verification more feasible. The biggest simplification when compared to a real system is that no time delays have been implemented in the safety system logics. We have also assumed that all hardware failures are permanent. The methodology is quite compatible with PRA, and it serves as a basis for further integration between the two approaches. More details on our work can be found in a workshop paper (Lahtinen 2014a) and in a research report (Lahtinen 2014b).

Related work

Model checking has been previously used to analyse system faults and fault-tolerance. FSAP/NuSMV-SA (Bozzano & Villafiorita 2007) is a safety assessment

platform that can be used for injecting faults into a system model and verifying the system fault-tolerance using model checking. A similar fault injection approach is described in (Joshi & Heimdahl 2005), where a wheel brake system is verified using SCADE.

The Altarica language (Arnold et al. 1999) was designed for formally specifying the behaviour of failing systems. Altarica is used in e.g., (Bieber et al. 2002) in combination with model checking to assess safety requirements of the AIRBUS A320 hydraulic system. Other work combining model checking and analysis of fault-tolerance is covered in e.g., (Schneider et al. 1998), (Bernadeschi et al. 2002), and Bruns & Sutherland, 1997).

Our work, in contrast to the ones above, is about modelling larger systems in which many types of hardware faults are possible. The modelling methodology is built on top of the NuSMV modelling language. Our work also has a connection to PRA analysis.

Description of the example system

The case study model used in this work is based on a PRA model of a nuclear power plant. The model depicts a fictive and simplified boiling water reactor (BWR) type nuclear power plant (NPP). Detailed information on the PRA model can be found from (Authén et al. 2013).

The plant model includes eight different safety systems that are mostly four-redundant. The safety systems are divided into two separate subsystems: Reactor Protection System (RPS) and Diverse Protection System (DPS), which are implemented on different automation hardware.

The RPS safety systems are: automatic depressurisation system (ADS), component cooling water system (CCW), emergency core cooling system (ECC), service water system (SWS) and residual heat removal system (RHR). The DPS safety systems are: emergency feed water system (EFW), and main feed water system (MFW). In addition, the AC power system belongs to both RPS and DPS.

The model describes the operation logic of the safety systems, the hardware equipment used to implement each system, and the associated failure modes for each piece of equipment.

The safety systems read measurements, and actuate their dedicated pumps and valves when necessary to prevent damage in the reactor core. The actuation logic of the safety systems is implemented in four separate acquisition and processing unit (APU) computers. Measurements, which are also four-redundant, are separately brought to each APU. The control signals calculated by the redundant APUs are collected in several voting units (VU) that decide on sending the actuation commands to the pumps and valves.

The safety systems are designed so that the plant can survive a set of potentially hazardous events called initiating events. Five initiating events are defined: loss of coolant accident (LOCA), loss of feed water due to e.g. main feed water pump failures (LOFW), loss of online power (LOOP), disturbances in normal plant operation

without the loss of primary coolant (Transient), and the loss of DC power. Depending on the initiating event there are different success criteria for the safety systems. The success criteria can be derived from event trees that exist for each initiating event.

Modelling

We used the PRA model as reference and created a corresponding model using the NuSMV modelling language that can be used for model checking. We modelled seven out of the eight safety systems that are part of the PRA model. Only the AC power system was not included in the model due to excessive modelling effort required. For more details on modelling, see (Lahtinen 2014a).

We modelled the plant as a discrete time model in which signal propagation is instantaneous, i.e. inputs from measurements reach the outputs of a safety system on the same clock cycle if delays are not implemented in the safety system logic. The modelling methodology was kept as modular as possible.

The modular composition of the model is illustrated in Figure 1. The main components of the model are the logic modules (APU and VU), the various link modules, process module, and a failure module. The connections in Figure 1 are either one-to-one or one-to-many, and should be read as ‘creates an instance of’. For example, the main module creates a single instance of the failure module. Figure 1 also shows some of the variables calculated and output by the modules. For example, the main module calculates the success criteria for individual safety systems and scenarios. Successful operation means for e.g. ECC that in one of the four redundancies, the pump is running and the corresponding valve is open. A large LOCA scenario is survived when both ECC and RHR systems operate successfully.

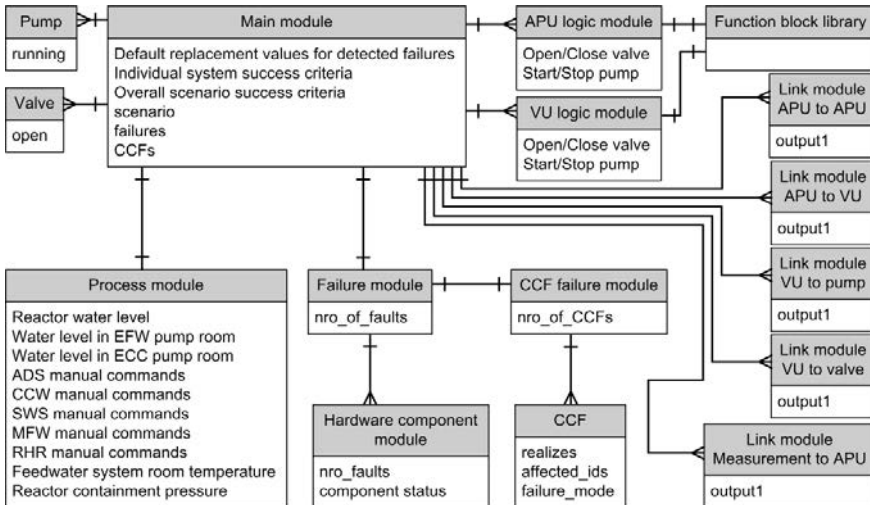


Figure 1. Modular composition of the case study model.

When compared to our previous modelling techniques three new components can be found from the model in Figure 1: the process module, the failure module (and the modules it refers to), and the various link modules.

Link modules are used whenever some piece of information is transferred from one place to another in the plant automation. The link module executes this transfer of information but simultaneously the effects of possible faults affecting the information are taken into account. Since there are only a small number of different type of links (e.g., APU-to-APU, measurement to APU, etc.) link type modules were created that can be parameterised with equipment related to the particular link.

The process module plays the role of an environment model, and decides on the values of the physical parameters of the plant. These values are the actual physical values independent from the measured values which are suspect to faults.

The failure module manages common cause failures, and determines which of the hardware components experience failures. This failure information is passed on the link modules.

Simplifications

In order to simplify the model we did some over-approximating abstractions on the model. We also concentrated on verifying simple state invariant properties only that can be proved efficiently in NuSMV.

The PRA model did not include any descriptions of time delays used in the I&C systems, and thus no timers were added to the logic modules. However, in real I&C systems timers are regularly used. Adding timers into the function block diagrams is straightforward but doing so may lead to a model that is computationally more challenging.

In our methodology we assumed that all failures were permanent. This assumption simplifies modelling and verification times significantly. Also, in our model the environment model is quite free. For example, the operational states of pumps and valves do not affect the physical parameters, so there are no feedbacks implemented in the model environment.

Results

We verified several safety requirements on the case study model, formalised the requirements as state invariants, and analysed the fault tolerance of the plant with respect to these specifications. The checked requirements are listed in Table 1. The first four requirements are plant-level requirements that require several safety systems to be examined in parallel in order to be verified.

Four different failure assumptions were used: 1) no single failures assumed, 2) one single failure assumed, 3) two single failures allowed, and 4) three single failures assumed.

Table 1. Requirements checked on the plant model.

Number	Requirement
1	In case of a LOCA initiating event, the plant safety systems shall fulfil the related success criteria.
2	In case of a LOFW initiating event, the plant safety systems shall fulfil the related success criteria.
3	In case of a LOOP initiating event, the plant safety systems shall fulfil the related success criteria.
4	In case of a TRANSIENT initiating event, the plant safety systems shall fulfil the related success criteria.
5	In case of a LOFW/LOOP/TRANSIENT initiating event, the EFW safety system shall start a pump and open a valve in at least one of the four redundant subsystems.
6	In case of a LOCA/LOFW/LOOP/TRANSIENT initiating event, the ECC safety system shall start a pump and open a valve in at least one of the four redundant subsystems.
7	In case of a LOOP/TRANSIENT initiating event, at least two out of the three MFW pumps shall be started.
8	In case of a LOFW/LOOP/TRANSIENT initiating event, at least four out of the eight ADS release valves shall be opened.
9	In case of a LOCA/LOFW/LOOP/TRANSIENT initiating event, at least one out of the four RHR pumps shall be started.

All requirements in Table 1 except requirement 7 are true even if two simultaneous failures are assumed. Requirement 7 becomes false in the case of two single failures. This is because unlike the other safety systems, the MFW system is only three-redundant. If the voting modules on redundancies 1 and 2 fail because of a single failure, only a single pump on the third redundancy is started. For more detailed results, see (Lahtinen 2014a).

Improving reliability of model checking results

One of the challenges in using model checking to verify the correctness of safety critical systems is the reliance on the correctness of the model checking tools themselves. In the case the model checking tool is able to find a violation to one of the requirements of the system, it is usually fairly straightforward to verify that the counterexample execution provided by the model checker is indeed an incorrect behaviour of the system by simulating the counterexample in a simulation environment. However, in the case the model checking tool claims that all the requirements of the system are fulfilled, the situation is more complex, as the model checking tools could contain bugs themselves that hide some incorrect behaviours of the system. One

approach to combat this is to use several independent model checking tool chains with disjoint code bases and algorithms to verify the same model, which gives us better confidence in the model checking results. We can, however, do even better as we have shown in the paper (Kuismin & Heljanko 2013), which shows how one can generate proofs from model checking results that can be verified by external tools, and which prove that the model checking process itself contains no errors.

Summary and conclusions

We have briefly presented new methodology for modelling failures. The methodology serves as a framework for the verification of the fault-tolerance of the plant by taking into account the hardware configuration of the system and the various failure modes of the hardware components. We used a PRA model of a nuclear power plant as reference and created a corresponding model that can be used for model checking. We then verified the fault-tolerance of the model with respect to several properties.

The main challenge in verifying large plant-level models is that the resulting model can become very large. The biggest current limitation of using our methodology in practice is that adding timing behaviour to the logic modules significantly increases the complexity of the model checking problem. Using the IC3 algorithm (Bradley 2011) for verification is a potential approach, as well as the portfolio based approach (Sterin et al. 2011). For liveness properties, a liveness to safety reduction, as described in (Kuismin & Heljanko 2013), could be used.

Our work intends to bridge the gap between model checking and PRA methods. The model is entirely based on PRA reference material. This suggests that a single well-defined system-level model of the plant could be used for both PRA and model checking. We are also planning to find more synergy between the methods. For example, it may be possible to generate parts of the model checking models based on PRA analysis data sheets. We also want to find out whether the two methods can provide inputs for one another.

References

- Arnold, A., Point, G., Griffault, A., Rauzy, A. 1999. The AltaRica formalism for describing concurrent systems. *Fundam. Inf.* 40(2,3) 109 – 124
- Authén, S., Gustafsson, J., Holmberg, J.E. 2013. Guidelines for reliability analysis of digital systems in PSA context - Phase 3 status report. NKS Report NKS-277, Nordic Nuclear Safety Research (NKS)
- Bernardeschi, C., Fantechi, A., Gnesi, S. 2002. Model checking fault tolerant systems. *Softw. Test., Verif. Reliab.* 12(4) 251 – 275
- Bieber, P., Castel, C., Seguin, C. 2002. Combination of fault tree analysis and model checking for safety assessment of complex system. In: *In Proc. 4th Euro-*

pean Dependable Computing Conference, volume 2485 of LNCS, Springer-Verlag

- Bozzano, M., Villaflorita, A. 2007. The FSAP/NuSMV-SA safety analysis platform. *International Journal on Software Tools for Technology Transfer* 9(1) 5 – 24
- Bradley, A.R. 2011. SAT-based model checking without unrolling. In Jhala, R., Schmidt, D.A., eds.: *VMCAI*. Volume 6538 of *Lecture Notes in Computer Science*., Springer 70 – 87.
- Bruns, G., Sutherland, I. 1997. Model checking and fault tolerance. In Johnson, M., ed.: *Algebraic Methodology and Software Technology*. Volume 1349 of *Lecture Notes in Computer Science*. Springer Berlin Heidelberg 45 – 59
- Clarke, E.M., Grumberg, O. & Peled, D. 2001. *Model checking*. MIT Press.
- FBK-IRST, Carnegie Mellon University, University of Genova and University of Trento. 2012. NuSMV model checker v.2.5.4
- Joshi, A., Heimdahl, M.P.E. 2005. Model-based safety analysis of Simulink models using SCADE design verifier. In: *Proceedings of the 24th International Conference on Computer Safety, Reliability, and Security. SAFECOMP'05*, Berlin, Heidelberg, Springer-Verlag. 122 – 135
- Kuismin, T. & Heljanko, K. 2013. Increasing confidence in liveness model checking results with proofs. In Bertacco, V., Legay, A., eds.: *Haifa Verification Conference*. Volume 8244 of *Lecture Notes in Computer Science*., Springer 32 – 43.
- Lahtinen et al. 2012a, Lahtinen, J., Valkonen, J., Björkman, K., Frits, J., Niemeä, I., Heljanko, K. 2012. Model checking of safety-critical software in the nuclear engineering domain. *Reliability Engineering & System Safety* 105(0) 104 – 113.
- Lahtinen et al. 2012b, Lahtinen, J., Launiainen, T., Heljanko, K. 2012. Model checking methodology for large systems, faults and asynchronic behaviour - SARANA 2011 work report. VTT Technology 12, VTT Technical Research Centre of Finland Available online: <http://www.vtt.fi/inf/pdf/technology/2012/T12.pdf>.
- Lahtinen, J. 2014a, Verification of Fault-Tolerant System Architectures Using Model Checking. In: *DEVVARTS - 1st International Workshop on DEvelopment, Verification and VALidation of cRiTical Systems*. 195 – 206.

- Lahtinen, J. 2014b, Hardware failure modelling methodology for model checking. Research report: VTT-R-00213-14, VTT Technical Research Centre of Finland Available online: <http://www.vtt.fi/inf/julkaisut/muut/2014/VTT-R-00213-14.pdf>.
- Pakonen, A., Mätäsniemi, T., Lahtinen, J., Karhela, T. 2013. A toolset for model checking of PLC software. In: IEEE 18th Conference on Emerging Technologies & Factory Automation (ETFA). 1 – 6.
- Schneider, F., Easterbrook, S.M., Callahan, J.R., Holzmann, G.J. 1998. Validating requirements for fault tolerant systems using model checking. In: ICRE, IEEE Computer Society 4 – 13
- Sterin, B., Een, N., Mishchenko, A., Brayton, R. 2011. The benefit of concurrency in model checking. In: In Proceedings of the International Workshop on Logic Synthesis, IWLS'11. 176 – 182.

8. Safety requirements specification and management in nuclear power plants (SAREMAN)

8.1 SAREMAN summary report

Teemu Tommila¹, Eero Uusitalo², Antti Pakonen¹, Jarmo Alanen¹, Janne Valkonen¹

¹VTT Technical Research Centre of Finland Ltd
P.O. Box 1000, FI-02044 Espoo

²Aalto University, Department of Computer Science and Engineering
P.O. Box 15400, 00076 Aalto

Abstract

The aim of the SAREMAN project was to develop practices for requirements definition and management. We describe here first the fundamental modelling concepts for requirements and nuclear power plant systems. To present the more practical contents of the project, we then give examples of some requirements engineering approaches applicable to the design and licensing of nuclear automation systems.

Introduction

Requirements are a prerequisite not only for successful implementation but also for demonstrating the safety of nuclear power plant systems. However, requirements engineering is an abstract and multi-disciplinary area and still widely considered as a challenge. Therefore, the SAREMAN project developed practices for requirements definition and management. Our approach was founded on well-defined models of both systems and engineering processes. From a consistent terminology we proceeded to modelling and documentation methods, working practices and finally towards information technology tools. Our focus was on the safety of instrumentation and control (I&C) systems and the early stages of design. This emphasises the

multi-disciplinary nature of requirements engineering involving, for example, safety analysis, process engineering and human factors. The challenges in nuclear energy domain are similar to many other areas of industry. So, their standards and guidelines can be applied.

Requirements in systems modelling and design

The main job of engineers is to provide descriptions according to which a system can be purchased, built, installed, operated and maintained. Traditionally, design data is represented in drawings and written documents. Today, information should preferably be in a well-structured, electronic form that allows it to be stored, processed and transferred with computers. Even if documents continue to be necessary, design is more and more driven by structured, or even formal *models*. In the future, we expect to see integrated data repositories of all engineering artefacts, including documents and models (**Figure 1**).

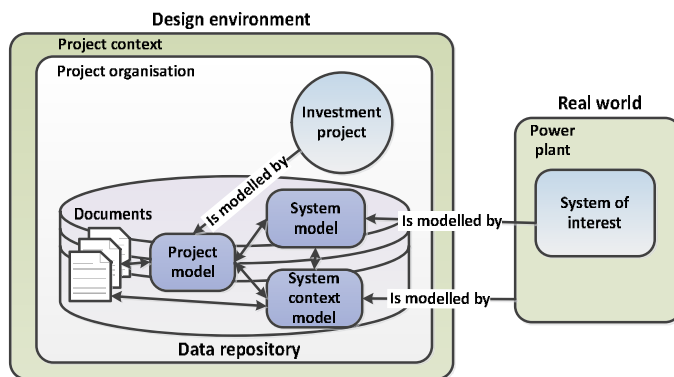


Figure 1. A real-world system is engineered by a project organisation creating various engineering artefacts stored in a project data repository.

Requirements are *statements* about entities in the system of interest and its environment. To be able to express requirements in an unambiguous way, it is necessary to have a sound model of the system. In addition to the system, requirements often concern the processes of its development, operation and maintenance. Therefore, several models is needed, e.g. *system* and *context models* and an associated *project model* (Tommila & Alanen 2015).

We see *systems* as man-made, real-world entities consisting of, e.g., sub-systems, devices, structures, pieces of software and humans (ISO/IEC 15288 2008). As we see it, the practices of system operation and maintenance are part of the solution developed by designers. For example, operators are elements of the power plant system. Therefore, operation and maintenance are included in the system model.

Systems participate in various *activities*, such as producing energy or controlling process parameters. To do this, a system must be designed to have suitable capabilities, in particular *system functions*. Their availability and service level depends on the current *operational state* and *operating mode* of the system. Activities can be performed by combining the capabilities of one or more redundant systems. In the early stages of design, only high-level concepts of these entities are outlined. However, they make it possible to express clearly the requirements for their properties, relationships and behaviour, for example, in the form of textual statements, tables or scenarios.

Investment projects implement life-cycle processes that are discussed in many standards (e.g. ISO/IEC 15288 2008, ISO/IEC 29148 2011). It seems, however, difficult to find one widely accepted and conceptually sound life-cycle model. In its widest sense, our *project model* describes

- technical and management activities to be carried out
- design artefacts and information flows between activities
- scheduling, phases and milestones
- participating organisations and their responsibilities
- practices, methods and tools to be applied

Developing a system involves many activities carried out by various organisations. The consecutive *life-cycle phases* separated by decision gates, *milestones*. Parts of the project organisation are responsible for certain areas of the system model. So, system and project models are linked to each other. In a way, the project organisation is a “system” to which requirements can be attached. Different from *product requirements* concerning the system being developed, *process requirements* specify properties of the project organisation and its working practices.

Requirements and requirements engineering

We see *requirement* as a capability or property that a system must have to satisfy a contract, standard or specification (Tommila & Alanen 2015). A requirement expresses a mandatory feature without unnecessarily constraining the possible solutions. Requirements are found on all levels of detail and throughout the life-cycle. A specification on one level typically sets requirements for the next one.

Like all design information, requirements are concerned with communication between stakeholders. So, we understand a requirement as a *statement* of a stakeholder, e.g., a regulator or user, concerning a product or its development process. Statements are communicated in spoken form or coded as documents and delivered by a tool, such as e-mail or a design database. For successful communication, the interpretation should be easy and unambiguous. Design is iterative, and requirements are mixed with other types of statements, e.g. facts and design solutions. Consequently, documents containing only requirements don't exist. To serve their purpose of communicating relevant information to the selected audience, documents must also describe the system environment and design solutions made so far.

In addition to requirements, engineers must express, e.g., facts, intentions and design solutions. So, a statement should indicate clearly, whether it is a soft goal, requirement, design constraint, an assumption or something else. Consistent use of words like “shall” and “should” are recommended for textual specifications. This is, however, not practical when specifications are in graphical or tabular form. Therefore, we model the *communicative intent* of a statement as a separate attribute. In this way any description, such as a logic diagram, can be labelled with the intent “requirement” to represent a requirement instead of a design solution.

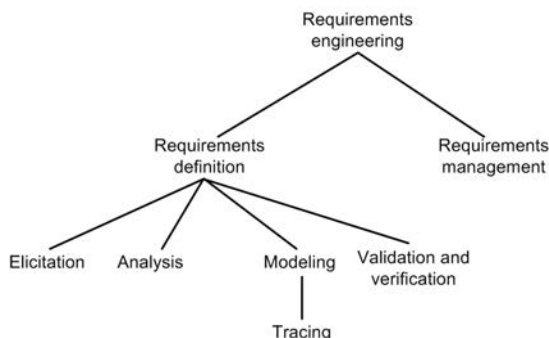


Figure 2. Main activities of requirements engineering.

The purpose of *Requirements Engineering* (RE) is to produce a consistent set of requirements to be used in many other activities such as detailed design and test planning (Figure 2). RE contains two main activities, requirements definition and requirements management. *Requirements definition* includes discovering, analysing, documenting and validating and verifying the requirements. Analysis includes negotiation and prioritization processes that lead to a set of agreed requirements. Requirements definition also includes maintaining the traceability of requirements. *Requirements management*, in turn, can be seen as part of *configuration management*, e.g. identification and change control applied to requirements.

As shown in Figure 2, *tracing* is part of system modelling. We interpret *traceability* as a characteristic of design data that makes it possible to find out how and why requirements and solutions have been derived from various sources (Tommila & Alanen 2015). Traceability should cover both derivation paths and the progress of artefact versions in time (Figure 3). Traceable design data can give answers to questions like: What information is the artefact based on?; How will it be verified?; How has it seen modified?; and What are the impacts of a change? The design data itself, combined with intelligent queries, can give answers to some of these questions. However, additional information must be added that records the history and the reasoning of the designers. A *traceability information model* defines the contents and well-formedness criteria for the traceability links.

Even if the idea is old, no single definition or a way to implement traceability can be found (Tommila 2013). Advanced traceability is rarely applied in the industry due

to its complexity and costs. Commercial software tools for requirements management and engineering provide some but fairly limited support for traceability.

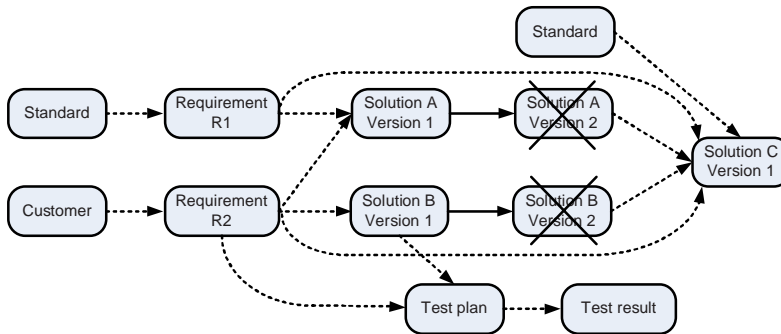


Figure 3. Examples of traceability links between engineering artefacts.

The discussion above implies that requirements can't be considered in isolation. Instead, they should be attached to an integrated system model continuously evolving during the design process. Therefore, we tried to clarify the concepts needed for describing a system and expressing its requirements. We also looked for practical solutions based on modelling principles and domain-specific terminology. The main findings were summarised in a short guide (Tommila 2015). The sections below highlight some of the work.

Concept of Operations as a basis of requirements

Requirements definition is a multi-disciplinary activity. Therefore, we studied the idea of *Concept of Operations* (ConOps) in conceptual design and requirements definition (Tommila, Laarni & Savioja 2013). It was introduced in late 1980's and then refined in many guidelines and standards. ConOps describes on a high level how the elements of the system and entities in its environment collaborate to achieve their goals. It communicates the overall system functions and properties among the user, regulator, developer and other stakeholders. ConOps contains the following information:

- overall goals and constraints of the (socio-technical) system
- business or production processes to be carried out
- interfaces to external entities (e.g. company headquarters)
- system elements (technical systems, structures, human organisation)
- main functions the system and its elements
- operational states and operating modes, including abnormal situations
- allocation of responsibilities and tasks to the system elements
- operating scenarios (e.g. plant start-up)
- high-level user requirements (if not covered by the scenarios)

ConOps provides a basis for defining the more technical *system requirements* of I&C systems (Figure 4). The user requirements and the allocation of responsibilities, i.e. the degree of automation, determine the functional requirements of the I&C system, control room and human operators. With this allocation, also the performance requirements flow down to individual system elements.

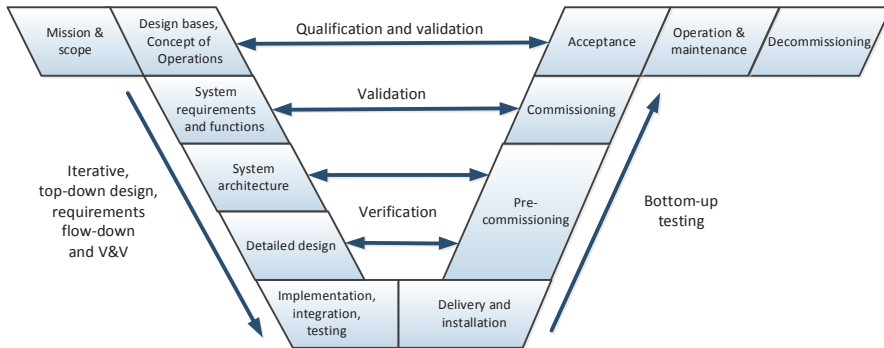


Figure 4. Position of ConOps in the V-model of system life-cycle.

The origin of ConOps is in complex, information-intensive systems. It has not been explicitly applied to nuclear power plants. However, corresponding elements can be identified in most Human Factors Engineering (HFE) guidelines and standards. To be a practical design artefact, ConOps should be adapted to the engineering and licensing processes applied in the nuclear domain. When safety is concerned, this boils down to the idea of *Defence in Depth* (DiD). There is a need for structured ways to describe the DiD architecture and methods to analyse its safety performance. ConOps could be a practical boundary object to work with in a multi-disciplinary way in defining the overall safety architecture.

Writing well-formed requirements

A good requirement is unambiguous, complete, verifiable and easy to understand. In the one end, there are formal methods that try to make requirements unambiguous or even computer understandable. More practical approaches give guidance for well-structured natural language requirements. For example, Boilerplates (Hull, Jackson & Dick 2002) is a collection of templates for expressing requirements in natural language. Despite the existing guidance, industry experts are not necessarily well prepared for writing good requirements.

As a practical approach, we studied the Easy Approach to Requirements Syntax (EARS) described in (Mavin et al. 2010). EARS has been successfully applied to a variety of complex, safety-critical systems, including regulatory safety requirements, at Rolls-Royce Control Systems. The method was developed primarily for stakeholder requirements, as opposed to technical system requirements. The hypothesis

of EARS is that a small set of simple requirement structures is an efficient and practical way to enhance the writing of high-level stakeholder requirements. In EARS, the requirements are based on five sentence templates (Figure 5). Basic templates can be combined to create compound statements. One strength of the approach is that requirements remain in a form that is readable by anyone. Special training is not required, as opposed to formal methods. The results reported by Mavin et al. suggest that EARS can alleviate many common problems in requirements, such as wordiness, complexity, untestability and ambiguity.

Ubiquitous	<ul style="list-style-type: none"> •The <system name> shall <system response> •<i>The kitchen system shall have an input hatch.</i>
Event-driven	<ul style="list-style-type: none"> •When <optional preconditions> <trigger>, the <system> shall <system response> •<i>When the chef inserts a potato to the input hatch, the kitchen system shall peel the potato.</i>
State-driven	<ul style="list-style-type: none"> •While <in a state>, the <system> shall <system response> •<i>While the kitchen system is in maintenance mode, the kitchen system shall reject all input.</i>
Unwanted behavior	<ul style="list-style-type: none"> •If <optional preconditions> <trigger>, then the <system> shall <system response> •<i>If a spoon is inserted to the input hatch, then the kitchen system shall eject the spoon.</i>
Optional	<ul style="list-style-type: none"> •Where <feature>, the <system> shall <system response> •<i>Where the kitchen system has a food freshness sensor, the kitchen system shall detect rotten foodstuffs.</i>

Figure 5. Templates of the Easy Approach to Requirements Syntax (EARS).

We experimented with EARS several times. First, a selection of YVL regulatory guides and white papers was targeted and feasibility of EARS ascertained (Uusitalo et al. 2011). Later, we found that teaching EARS as a requirements documentation “crash course” in a single brief one-to-one session was possible, and we also experimented with groups of nuclear domain experts (Uusitalo & Raatikainen 2014).

We also applied EARS templates to the 485 requirements in YVL B.1 draft 2 (Uusitalo et al. 2014a). This work resulted in 900 EARS requirements. We found that EARS can be applied to regulatory requirements in the nuclear domain with reasonable effort. Additionally, applying the EARS templates worked as a requirements analysis tool: Many deficiencies were found in the requirements and the resulting requirements were of higher quality than the originals.

As was seen above, guidelines and templates are the fastest way to improve designers’ skills in requirements writing. However, also computer tools are needed. They, in turn, require formalisation, e.g. use of a Controlled Natural Language (CNL) with a restricted vocabulary and grammar. Our literature review on the topic and a tool concept for model checking I&C functions can be found in (Tommila & Pakonen 2014). We also used an experimental tool that guides the user with a vocabulary, elements of the particular application and a collection of templates (Figure 6). For

example, the requirement “Condition (FLUSH) is false before condition (LEVEL_T10 > 85).” matches to the template “Absence before” and is automatically transformed into the temporal logic formula “LTLSPEC F(LEVEL_T10 > 85) -> (!(FLUSH) U (LEVEL_T10 > 85))”. This formula can then be used in a model checker tool to see whether the requirement holds in the model of the I&C functions.

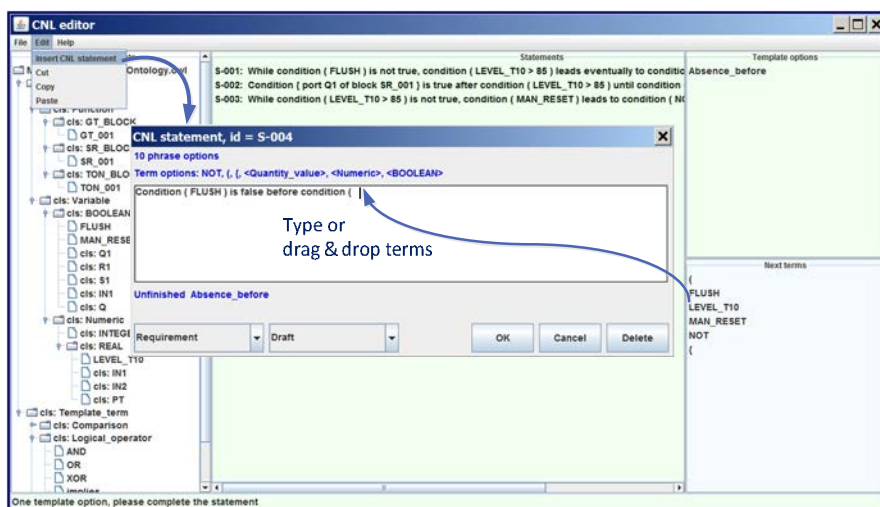


Figure 6. In our syntax controlled editor statements can be assembled by dragging and dropping allowed next terms to the text area (Tommila & Pakonen 2014).

The VAHA-A initiative for annotating regulatory requirements

As a follow-up to the renewal of YVL guides, a joint effort called VAHA-A was started by the nuclear safety authority STUK, nuclear license holders and license applicants. This initiative aims to annotate the entire body of Finnish nuclear regulation (approximately 9000 requirements and other items) with metadata that enables efficient requirements management. The metadata includes attributes for requirements identification (i.e. number, version, unique ID) and for contextual data such as the safety classes effected by the requirement, and the life-cycle phases the requirement pertains to. At the time of writing, the effort is still ongoing as the work is 75% complete.

As regulations are an essential source of safety requirements, SAREMAN collaborated with the VAHA-A initiative. Aalto University designed, implemented and maintained a web-based tool called KLAD with over 200 users to facilitate setting the metadata for all requirements. In addition, VTT organized a collaboration repository for the documents. More detailed results and experiences of the effort are described in (Uusitalo et al. 2014b) and (Uusitalo et al. 2014c).

Regulatory requirements and licensing

Requirements are an essential element in the overall life-cycle processes of nuclear facilities (Figure 7). There is an increasing demand for the utilities to demonstrate the safety of their plants by showing that all hazards have been adequately managed. *Safety demonstration* is understood as a set of arguments and evidence which support claims on the safety of a system. Structured approaches and tools exist to organise this information. On a generic level, *assurance case* is a reasoned, auditable artefact created to support (or challenge) its top-level claims (ISO/IEC 15026-2 2011). Arguing through multiple levels of sub-claims, this argumentation connects the top-level claims to the evidence and assumptions. When the top-level claim is about safety, security, dependability, assurance cases are called *safety cases*, *security cases*, *dependability cases*, respectively.

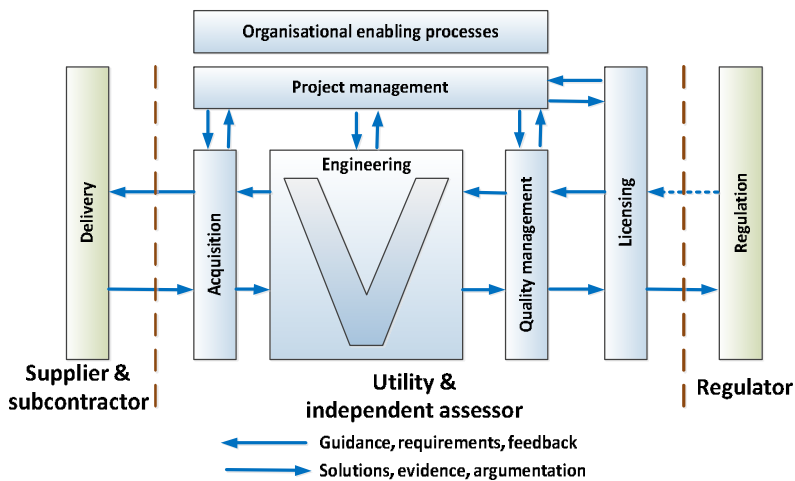


Figure 7. V-model embedded in the major life-cycle processes.

In SAREMAN, we reviewed the literature on licensing practices and safety demonstrations (Tommila, Savioja & Valkonen 2014). On the basis of the review and discussions with domain experts, it seems that the current practices are not fully satisfactory. For example, requirement specifications, traceability and safety argumentation are not always clearly explicated. Therefore, we plan to continue work on terminology, safety architectures and systems engineering practices and tools needed in the design and licensing of instrumentation and control systems.

References

Hull, E., Jackson, K. & Dick, J. 2002. Requirements Engineering. Springer-Verlag, 2002.

- ISO/IEC 15026-2 2011. Systems and software engineering -- Systems and software assurance -- Part 2: Assurance case. International Organization for Standardization (ISO), 2011.
- ISO/IEC 15288 2008. Systems and software engineering - System life cycle processes. International Organization for Standardization (ISO), 2nd edition.
- ISO/IEC 29148 2011. Systems and software engineering - Life cycle processes – Requirements engineering. International Organization for Standardization (ISO).
- Mavin, A. & Wilkinson, P. 2010. Big ears (the return of easy approach to requirements engineering). In: Proceedings of the 18th IEEE International Requirements Engineering Conference (RE'10), pp. 277-282, 2010.
- Tommila, T. 2013. On modelling traceability in requirements engineering. Working report of the SAREMAN project, 25 p.
- Tommila, T., Laarni, J. & Savioja, P. 2013. Concept of operations (ConOps) in the design of nuclear power plant instrumentation & control systems. Working report of the SAREMAN project, 68 p.
- Tommila, T. & Pakonen, A. 2014. Controlled natural language requirements in the design and analysis of safety critical I&C systems. Research report VTT-R-01067-14, 66 p.
- Tommila, T., Savioja, P. & Valkonen, J. 2014. Role of requirements in safety demonstrations. Working report of the SAREMAN project, 49 p.
- Tommila, T. & Alanen, J. 2015. Conceptual model for safety requirements specification and management in nuclear power plants. VTT Technology no. xx, to be published, ~140 p.
- Uusitalo, E., Raatikainen, M., Tommila, T. & Männistö, T. 2011. Structured natural language requirements in nuclear energy domain: Towards improving regulatory guidelines. In: Fourth International Workshop on Requirements Engineering and Law (RELAW), . IEEE, 2011. p. 67-73.
- Uusitalo, E. & Raatikainen, M. 2014. Applying structured natural language to regulatory requirements in nuclear domain. SAREMAN working report, 8 p.
- Uusitalo, E., Raatikainen, M. & Männistö, T. 2014a. Piloting Lightweight Requirements Engineering Training. SAREMAN working report, 6 p.
- Uusitalo, E., Raatikainen, M., Ylikangas, M. & Männistö, T. 2014b. Experiences from an industry-wide initiative for setting metadata for regulatory requirements in the nuclear domain. In: 7th International Workshop on Requirements Engineering and Law (RELAW), IEEE, 2014. p. 2-9.
- Uusitalo, E., Ylikangas, M., Raatikainen, M. 2014c. Annotating regulatory requirements – a summary report of VAHA-A. SAREMAN working report, 9 p.

9. Identification of fault situations propagating between different systems and disciplines (IFAPROBE)

9.1 IFAPROBE summary report

Nikolaos Papakonstantinou

VTT Technical Research Centre of Finland Ltd
P.O. Box 1000, FI-02044 Espoo (On behalf of Aalto University)

Abstract

The aim of the project is to develop methodology for identifying fault propagation between automation systems, the process and the physical layout. For early phase designs, it is important to be able to identify interactions between systems that were not expected and can lead to unsafe situations. Additionally, generic methods and tools were developed in the domain of safety of complex systems. These methodologies describe the automated generation of event trees, the discovery of critical event scenarios using genetic algorithm and human computation, and the generation of data sets for fault detection and identification systems.

Introduction

Some examples of interactions between different aspects of a system which can cause unforeseen failure propagation are shown in Figure 1. During 2013 the interactions between process, automation and environment were studied (Sierla, O'Halloran et al. 2013). The modelling aspects and the application of the method proposed in IFAPROBE was demonstrated using the spent fuel pool cooling system of nuclear power plant as a case study.

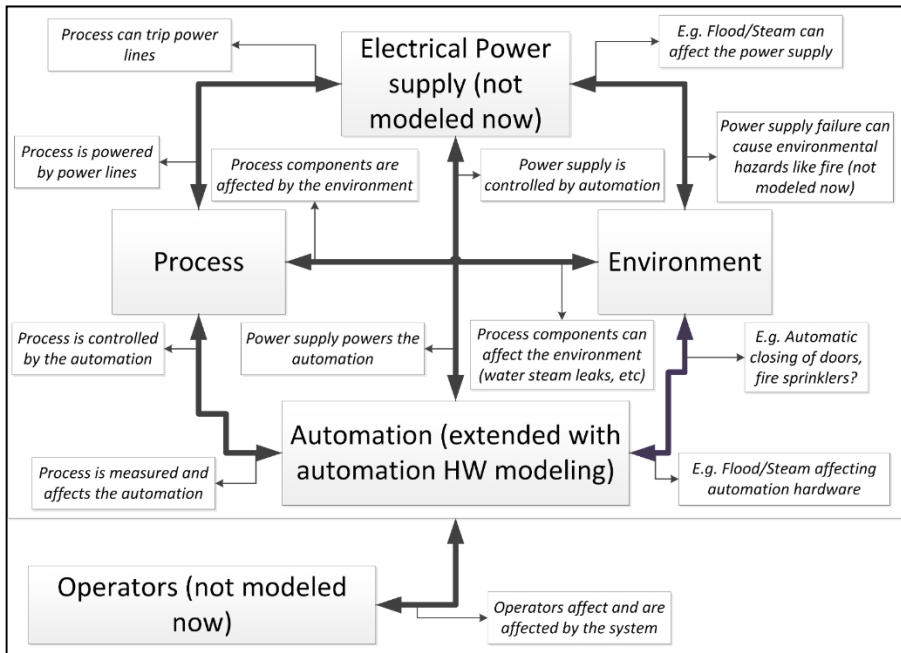


Figure 1. Examples of interactions between different aspects of a complex system which can cause unforeseen failure propagation.

A framework was developed to support this research goal which was able to:

- transition components to failure modes when exposed to environmental hazards
- recognize component failures modes such as “leaking” as sources of environmental hazards
- capture propagation of failure between environment, automation and the physical process

An early version of this framework, which is based on the Apros 6 simulation platform, was first applied on a small example case and then it was applied to the spent fuel pool cooling system case study. The case study is presented in this project summary.

Failure propagation through the environment (Case study, spent fuel pool cooling system)

The case study of the project is the spent fuel pool cooling system of nuclear power plant. The information for this case was provided by Fortum Power and Heat. An overview of the process is shown in Figure 2. The spent fuel pool (Pool A1-3) is

connected during the last phase of a long outage with the reactor pool (Pool D) and Pool B1-2 for the process or refuelling.

The system uses two main redundant cooling systems (MCS A and B) and one emergency cooling system (ECS) to control the spent fuel pool temperature. These systems are connected to the Pools A and B. To keep the spent fuel pool temperature at safe levels only one main cooling system is enough.

After a long outage the spent fuel is more active and then both main cooling systems are used in order to further lower the operating temperature of the spent fuel pool. The initiating event for the critical event scenario of this case is a major water leak in the main cooling system A.

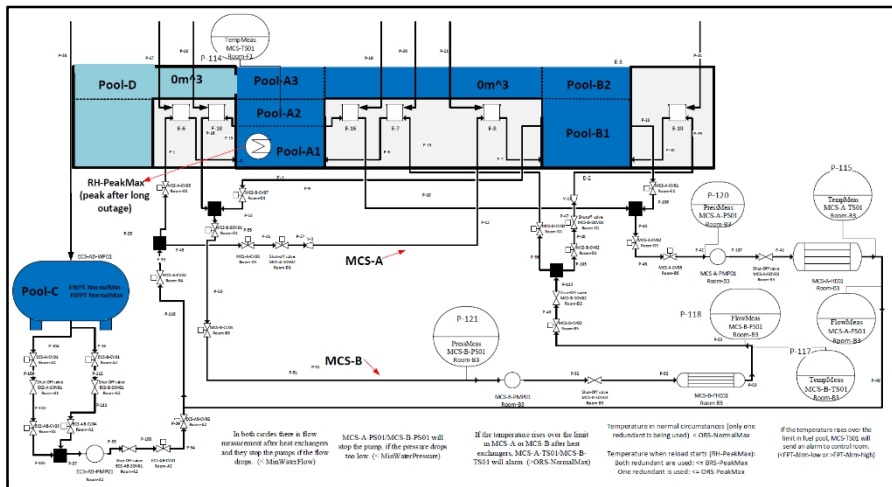


Figure 2. Spent fuel pool case study basic P&I diagram. Two main redundant systems and one emergency system are used to control the spent fuel pool temperature.

The layout of the plant, with only the rooms relevant to this case study, is shown in Figure 3. The main process components of the three cooling systems are located in room on two plant levels, level A and level B (below the spent fuel pool). Under level A there is level A- (basement) and between level A and level B are two more levels (A+ and A++).

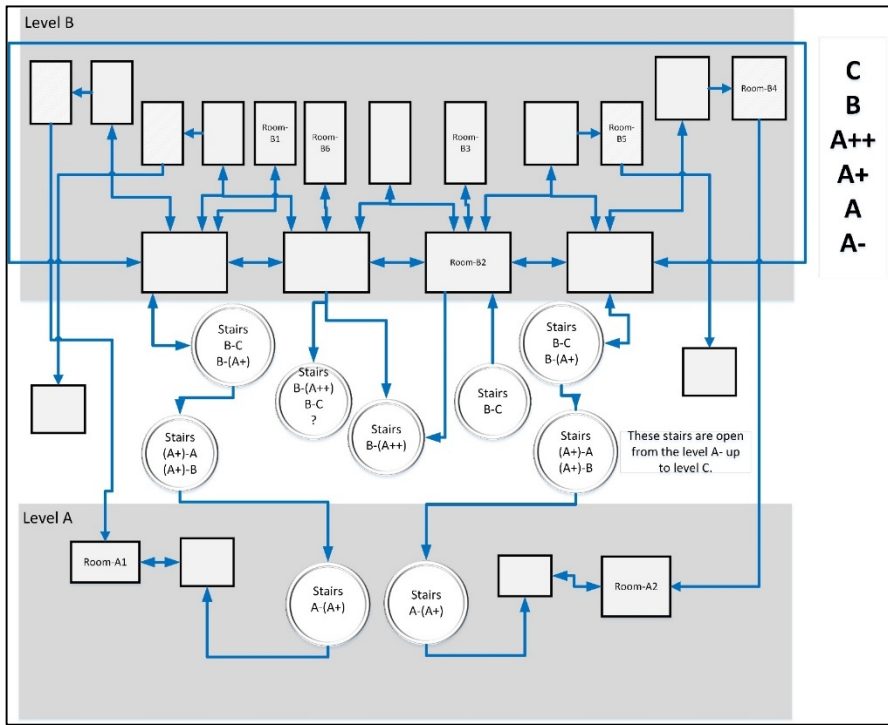


Figure 3. Plant layout relevant to the spent fuel pool cooling systems of the case study. The most basic automation actuator components of the main cooling systems are located at level B and the emergency cooling system automation actuator components are located at level A.

The spent fuel pool process model in Apris 6 for the case study is shown in Figure 4. Severe leaks are modeled in addition to the basic process for the two main cooling systems. These severe leaks, if triggered, will enable the flow of water from the spent fuel pool to the room B3 where many automation and process components of the main cooling systems are located.

The simple automation controlling this process is shown in Figure 5. On the left in the automation logic and on the right are the automation actuator control components. These components are encapsulated in custom components which add the capability of triggering a failure mode ("Failed?" input). The signals between the logic (left) and the automation (right) are routed through cables modeled in the automation hardware to environment mapping diagram shown later on in Figure 6. This simple automation controls only some key process components of the three cooling systems. It keeps active both main cooling systems and contains a simple on-off control for the emergency cooling system.

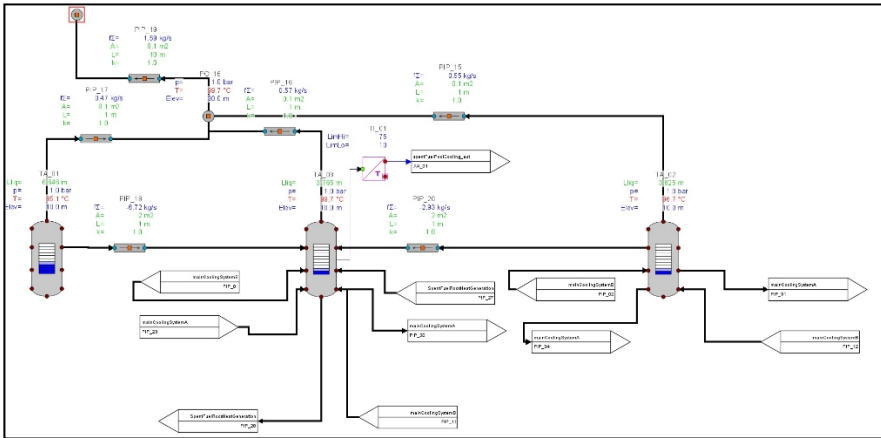


Figure 4. Process diagram of the spent fuel pool (Pool A, center), reactor pool (Pool D, left) and Pool B (right) in Apris 6.

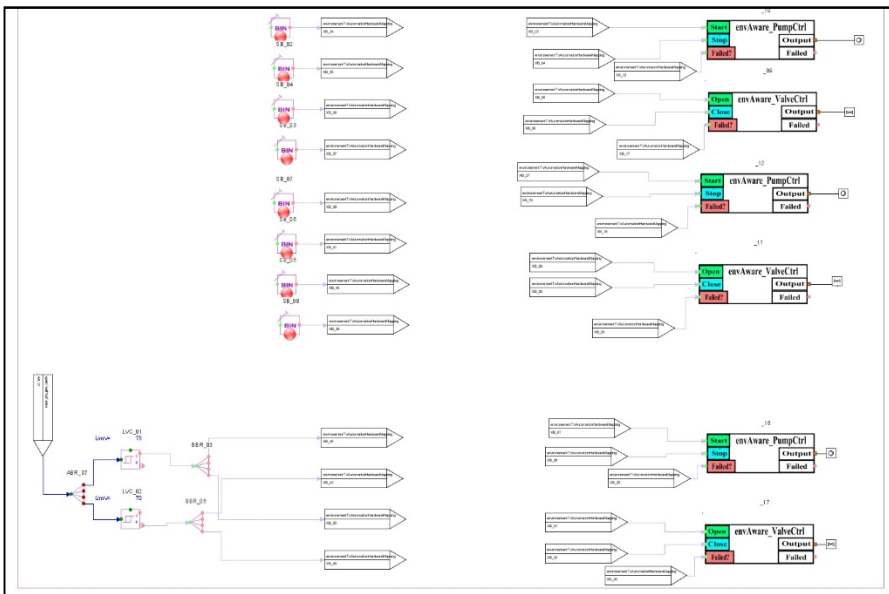


Figure 5. Automation diagram for the case study, custom components are used to encapsulate the valve end pump actuator control components.

The mappings between the automation, automation hardware and the environment are presented in Figure 6. Custom components are used to model the cable shelves, cables and the actuator automation hardware. The signals from the environment (left side, in this case the room water levels) are connected to the cable

shelves and actuator hardware components. If the environmental conditions can cause failures to the automation hardware, then the “Failed” outputs are activated.

In this version of the automation hardware model the cables fail if the cable shelves are under water or are under extreme temperature. If a cable fails, then the automation signals it carries are no longer transmitted. The actuator automation control hardware will fail if it is under water, under extreme temperature or under extreme humidity. For the case study the temperature, humidity and water level of the rooms B3 and A2 are monitored. The signals from the room B3 are connected to the automation hardware components of the main cooling systems A and B while the signals from the room A2 are connected to the automation components of the emergency cooling system. If the automation hardware component fails, the “Failed?” output, driven to the “Failed?” input of the custom component shown in Figure 5, will force the component into a failure mode.

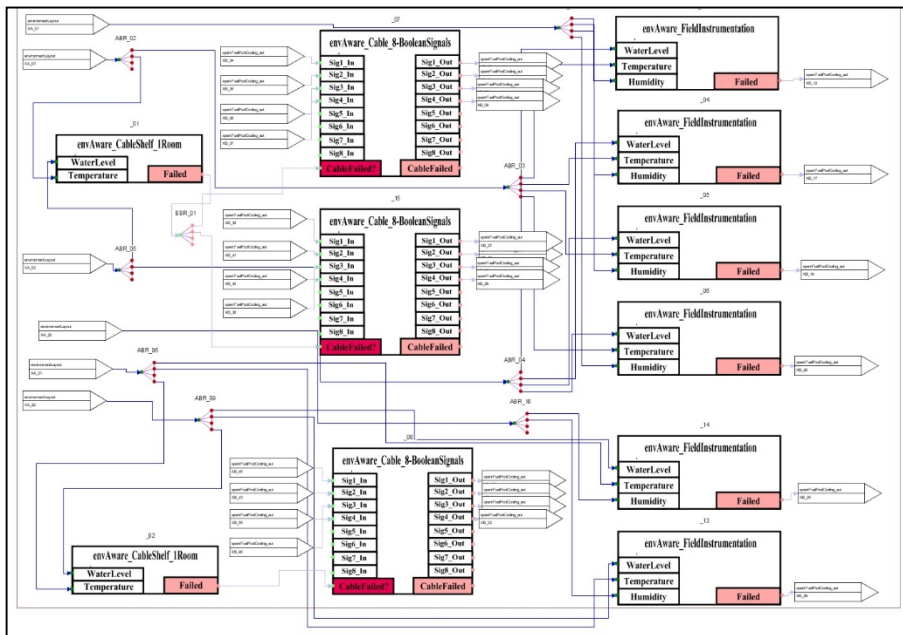


Figure 6. Mappings between environment, automation hardware and automation.

The last diagram for the case study is the environment model, a partial view is presented in Figure 7. The complete diagram uses 16 containment nodes to model the 16 rooms relevant to the case study. Water branches are used to model the flood propagation paths between the rooms and between levels A and B (through staircases).

Water flow from the major leak process components is added to the rooms using thermo-hydraulic components. The water level, temperature and humidity measurements from the rooms A2 and B3 are driven to the environment, automation hard-

ware and automation mappings diagram and are used to trigger failure modes of the automation hardware components.

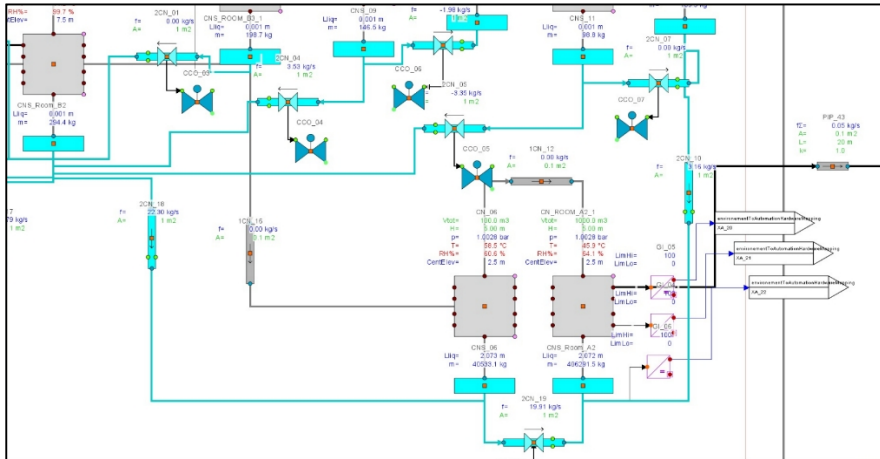


Figure 7. Model of the environment, using containment nodes, detail of room A2.

The charts with the results of the simulation of a severe water leak in main cooling system A are shown in Figures 8 (Pools A, B and D water levels) and 9 (Pool A and B temperature). The water level in the Pools A, B and D start dropping when water starts leaking from the main cooling system A. The water from that leak causes flood in room B3 which disables both main cooling systems. Flood propagating from the room B3 to the room A2, through the staircases, disables the pump and valve actuator control automation hardware of the emergency cooling system too. The Pool A and Pool B water level drops to the level of the connection to the main cooling system piping and water from no cooling system can be transferred because the main and emergency systems are in rooms which are flooded. The result is that the water in the spent fuel pool (Pool A) reaches the boiling point in about 40 minutes after the initiating event.

This case study was used to further test the failure propagation modeling capabilities of the simulation environment. These models are not accurate and the results should only be used to evaluate the potential of modeling additional system aspects (in this case the environment) in order to capture cross-discipline failure propagation mechanisms. The result of the case study is that adding a model of the environment and of the automation hardware to the process and automation models already traditionally developed, can lead to the identification of additional failure propagation paths.

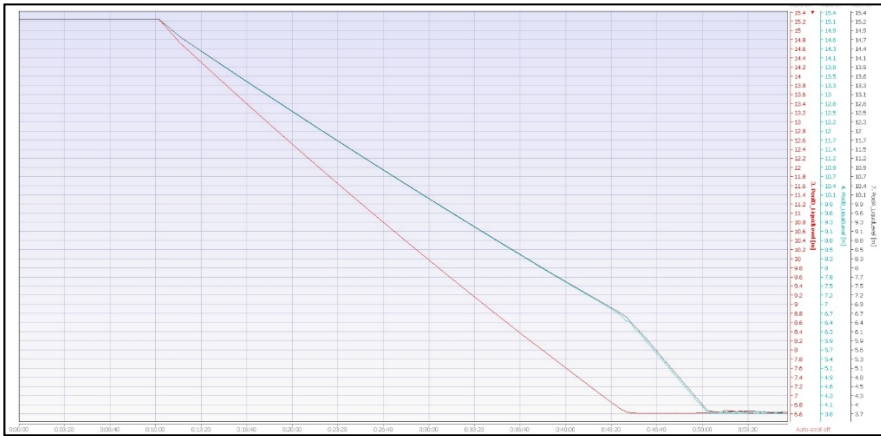


Figure 8. The Pool A and B water levels (light blue and black lines) drop to the level of the cooling system piping. The water level in Pool D (red line) falls to the level it is connected to Pool A. The scale of the signals is not the same.



Figure 9. The Pool A and B temperature levels (red and yellow lines) rise to the boiling point 40 minutes after the initiating event. The scale of the signals is not the same.

Generic simulation based methods and tools related to nuclear safety

Simulation Based automatic event tree generation

A functional model based methodology was developed for the generation of event trees with the addition of functional failure simulation results and simulation results

for critical process parameters (Papakonstantinou, Sierla et al. 2013). The case study was the early simulation model of a generic boiling water reactor.

Security assessment using genetic algorithm

A methodology was developed for the selection of multiple fault critical event scenarios with significant impact to the operation of the plant (Papakonstantinou, Sierla et al. 2014). The faults of the critical event scenarios are used as “genes” and the scenarios as “chromosomes” for the genetic algorithm. A “fitness function” outputs a fitness score for every scenario using simulation results as inputs. The case study was a generic model of a nuclear power plant.

Using non-expert humans for the identification of critical event scenarios for complex systems

An experiment was setup in which engineering students from the Oregon State University (Corvallis, OR, USA) were able to perform remote simulations and try the effects of different multiple fault scenarios. Their performance was compared to a random scenario generator. An overview of the experiment setup is shown in Figure 10. The case study was a generic model of a nuclear power plant.

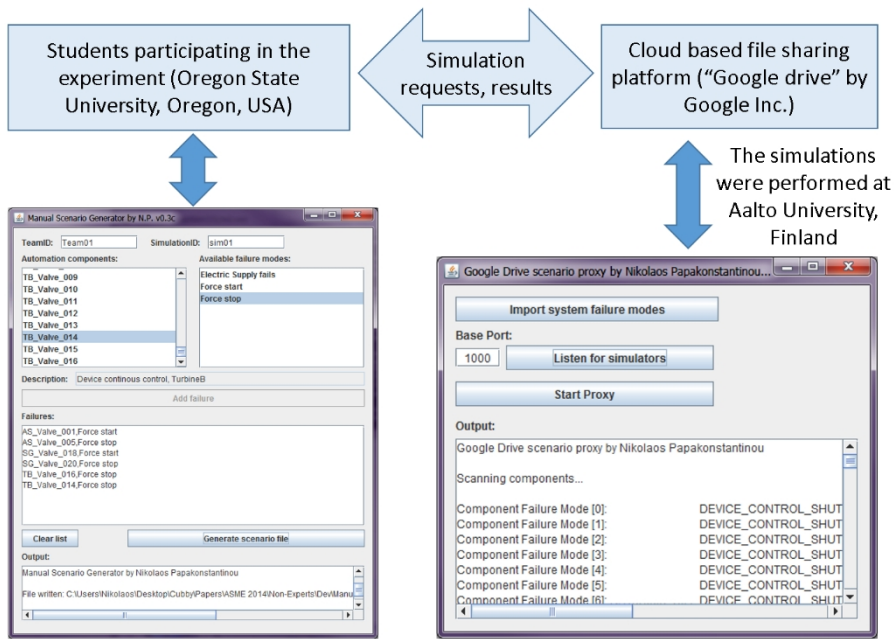


Figure 10. An intercontinental experiment to test the ability of non-expert humans for identification of critical event scenarios.

Data set generation for the development of machine learning based fault detection and identification systems

Fault Detection and Identification (FDI) for complex systems is a challenging task. Machine learning techniques can support the development of FDI systems. A methodology was proposed to generate the necessary training and testing data sets for the development of data-driven FDI systems (Papakonstantinou, Proper et al. 2014). Figure 11 presents a generated data set in the Weka tool. The case study was a generic model of a nuclear power plant.

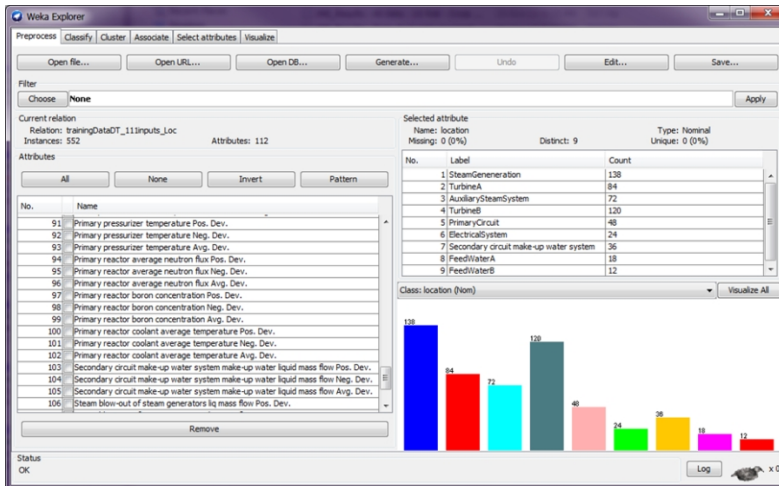


Figure 11. Training data set when imported in the Weka tool.

References

- Papakonstantinou, N., S. Proper, B. O'Halloran and I. Y. Tumer (2014). Simulation Based Machine Learning For Fault Detection In Complex Systems Using The Functional Failure Identification And Propagation Framework. ASME CIE. Buffalo NY, USA.
- Papakonstantinou, N., S. Sierla, K. Charitoudi, B. O'Halloran, T. Karhela, V. Vyatkin and I. Turner (2014). Security impact assessment of industrial automation systems using genetic algorithm and simulation. Emerging Technology and Factory Automation (ETFA), 2014 IEEE.
- Papakonstantinou, N., S. Sierla, B. O'Halloran and I. Y. Tumer (2013). A Simulation Based Approach to Automate Event Tree Generation for Early Complex System Designs. ASME IDETC/CIE 2013. Portland, Oregon, USA.
- Sierla, S., B. O'Halloran, T. Karhela, N. Papakonstantinou and I. Tumer (2013). "Common cause failure analysis of cyber-physical systems situated in constructed environments." Research in Engineering Design 24(4): 375-394.

10. Criticality safety and transport methods in reactor analysis (CRISTAL)

10.1 CRISTAL summary report

Karin Rantamäki, Petri Kotiluoto, Maria Pusa, Tuomas Viitanen

VTT Technical Research Centre of Finland Ltd
P.O. Box 1000, FI-02044 Espoo

Abstract

During the last 6 years the reactor physics group at VTT has gone through a change in generation as researchers have left and new, young persons have joined the group. Consequently, the main aim of the project has been to educate and train new researchers in the field. The project has covered inventory and activation calculations as well as research on sensitivity and uncertainties. A small but significant task has been education of a new person into reactor dosimetry. Alongside with the education, the improvement and updating of the calculation tools had a strong emphasis. On this side, most of the work was done in neutron dosimetry and criticality safety. Setting up a package for criticality safety validation is a tedious and long-lasting task and was the main aim in this field.

Introduction

Reactor physics is a base element in nuclear power safety. Many safety analyses need input from reactor physics codes. The dynamics codes rely on input from stationary codes, and together they have to cover a wide range of applications dealing with both normal operation and transient conditions. In order to maintain a high level of competence in reactor safety analysis, it is important to keep up to date both the code system and the know-how about the codes.

The expertise in the field is an important issue in order to ensure appropriate and adequate safety analyses. A lot of expertise at VTT has been lost during the last ten

years. New researchers have joined the group but much effort and time is needed to train them into qualified reactor physicists.

The project has two major tasks and two smaller ones. The larger ones in which most of the work is done, are calculation methods and criticality safety. The smaller ones are reactor dosimetry, and international co-operation including participation in training courses.

The calculation methods task is divided into two parts: transport methods, and sensitivity and uncertainty analysis. The former covers a variety of tasks related to both the reactor itself and components outside the reactor with duties ranging from cross-section calculation for fuel assemblies to activation analysis of the pressure vessel. Determination of the uncertainty of various parameters and their importance to the final results is necessary in order to understand the accuracy of computer codes. Tools for this purpose are created in the latter part. Criticality safety has become more and more important especially as the enrichment of the fuel increases. In addition to the knowledge, special attention needs to be paid to the calculation system that needs to be brought to an appropriate level. As a small task, reactor dosimetry has focused on updating the data and procedures.

International co-operation involves work within AER and the OECD/NEA. The participation in the Nuclear Science Committee as well as the Working Party on Nuclear Criticality Safety and its expert groups is covered. The contribution has been especially strong in the Uncertainty Analysis in Modelling (UAM) group.

Main Objectives

The main objective of this project is to improve the knowledge in various fields of reactor physics and areas close to it. The knowledge on various calculation methods must be maintained and improved as new researchers have joined the reactor physics team, and it takes time to train the newcomers to qualified staff. The main aim in the calculation methods task is to educate new experts into the field of inventory calculation and activation analysis. Criticality safety is an increasingly important subject where more experts are needed. In addition to expertise, the code system needs to be improved. An important subtask is the criticality validation which needs to be brought to an appropriate level. In reactor dosimetry the main goal was in updating the calculation system and educating a new expert after the retirement of the former one.

Applications of Deterministic Transport Codes

In order to increase the knowledge on basic reactor physics codes and macroscopic cross sections, a study on the dependence of the cross sections on various reactor parameters was performed [1]. The basic reactor parameters, the fuel temperature, the moderator temperature and density, and the boron concentration were varied. Their effect on various two-group macroscopic cross sections was studied. The results obtained from the calculations were compared to the polynomial fits used in

the dynamics codes made at VTT. Within the parameter range the results behave roughly linearly so it was concluded that the fits describe the system well enough.

The cross sections are used in the dynamics codes or system codes as source data. Two-group cross sections have been produced for this purpose using CASMO-4/4E. A script using in-house utility codes was written to take care of the calculation chain in the case of BWRs including their specific features [2]. The script uses given CASMO-inputs as a source and produces the material constants in the HEXBU-format. As a first application of this package, a cross-section set was prepared for the BWR stability benchmark studied in KOURA. A similar package was written for EPR cross sections [3] which were later used in contract work.

Knowledge of inventory calculations was enhanced by calculating an EPR assembly [4] and two benchmarks: the EPRI benchmark [5] and the CB6 benchmark [6]. In all three cases a 17×17 assembly was considered with various burnups and decay times, e.g. in the CB6 up to 1 000 000 years. Thus, inventory data was calculated for both reactor accident analysis and long term safety analysis of final disposal.

The calculations were mostly made with NEWT, TRITON and ORIGEN-S codes from the SCALE-6.1 package. In the CB6 benchmark the multiplication eigenvalue was calculated using TORT. In this case, the major issue was that due to serious internal convergence problems of the available TORT code version, criticality eigenvalue results from several time points did not converge [7]. Despite the difficulties, new experience on decay and 3D discrete ordinates radiation transport calculations was gained, which was the main aim of this study. In the EPRI benchmark, 11 cases were considered varying enrichment, concentration of burnable absorbers, boron content, and fuel and coolant temperatures. The calculations agreed well with the benchmark results [8].

Deterministic radiation transport methods are often needed for out-of-core fluence calculations and deep penetration problems. The TORT 3D discrete ordinates code has been the main deterministic computational tool for such purpose. A large 3D geometry model for TORT of one quarter of the Olkiluoto BWR reactor with reflective boundaries was generated with BOT3P [9]. Axially the model includes part of the steam separators, and extends radially to the outer surface of the concrete biological shield.

The knowledge of deterministic codes was further increased by calculating the C5G7 benchmark using the TORT code [10]. The geometry shown in Figure 1 was generated with BOT3P and the 7-group cross sections needed for TORT were processed by the GIP code. The calculated criticality eigenvalue agreed well within 80 pcm compared to eigenvalue given in the benchmark specifications [11]. However, the rod-wise fission powers had large variation compared to the values given in the specifications, even though the average relative error was below 6.5% for all fuel assemblies. The main reason for large rod-wise variation was that due to memory allocation problems, the TORT mesh could not be made fine enough for moderator areas between the fuel rods.

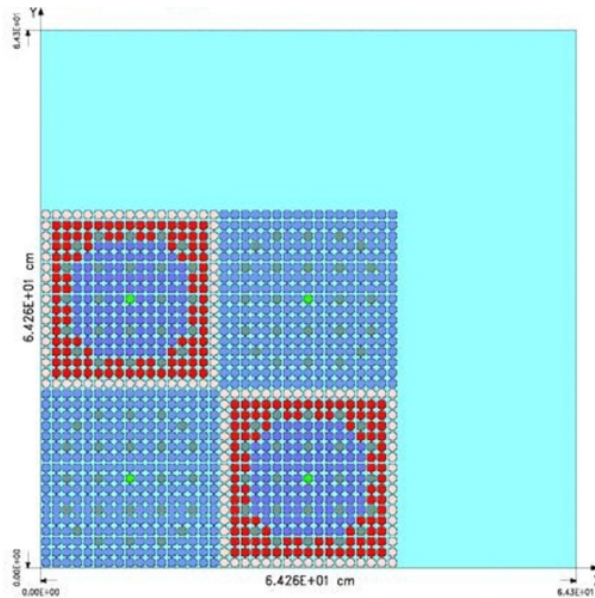


Figure 1. Cross section of the TORT geometry of the C5G7 benchmark of UO₂ and MOX fuel elements without spatial homogenisation.

Sensitivity and Uncertainty Analysis

When uncertain parameters are used in computation, also the calculation results contain uncertainty. In order to estimate the reliability of these calculations, it is necessary to develop uncertainty analysis methods enabling the propagation of the uncertainty through the calculations. In reactor physics, the imprecision of neutron interaction data is believed to be one of the most significant sources of uncertainty and there has been an increasing interest to be able to propagate this uncertainty through all stages of coupled neutronics/thermal-hydraulics computations. As a first step this requires developing uncertainty analysis methods to reactor physics codes that are used to produce homogenized data for the following full-core computations.

To advance this goal, an uncertainty analysis capability based on classical perturbation theory was previously [12] implemented in CASMO-4. This implementation enables the sensitivity and uncertainty analysis of the multiplication factor in lattice physics calculations. In this project, the work continued by adding generalized perturbation theory (GPT) as a new feature [13] to CASMO-4. GPT enables the uncertainty analysis of responses that can be presented as reaction rate ratios. In GPT, the responses of interest are first linearized with respect to the uncertain parameters. The uncertainty analysis can then be carried out deterministically in an efficient manner.

The calculation system developed in the project allows the uncertainty analysis of all relevant assembly data that is passed on to the following full-core calculations with the considered responses including two-group homogenized cross-sections, diffusion coefficients and assembly discontinuity factors. In addition, an automated calculation system enabling the propagation of nuclear data uncertainty through the CASMO-4 – SIMULATE-3 calculation sequence was developed. The project has participated actively in the UAM benchmark [14] with new results presented at the annual work shop every year. The work done in this context is described in more detail in Section 10.2.

Criticality Safety

Criticality safety was the other large task in this project. The aim was to broaden the knowledge base in the field. An even more important goal is to bring the calculation system to a stage where it meets the international standards and guides. This is a tedious and long-lasting work that will need to be continued after this programme.

General Understanding of Reactivity and Burnup Credit

In order to increase the general knowledge and understanding in criticality, a study on the dependences of reactivity on various VVER-440 assembly parameters was carried out in the early phase of the project [15]. Although many results were obvious, the study gave more confidence in how the various parameters affect reactivity. In addition to qualitative behaviour, the study also gave quantitative results. As this study was done with both Serpent and MCNP it also gave data for code comparison.

Work on burnup credit was started with participating in the OECD/NEA Burnup Credit benchmark Phase IIIC for a BWR fuel assembly [16]. It offered a good opportunity to further train experts in the field of criticality calculations, and to validate the in-house expertise and calculation methods against an international reference case. The benchmark case consisted of a square shaped 9x9 BWR assembly with a water channel in the centre, irradiated up to 50 MWd/kgU and cooled for 15 years.

At VTT, the benchmark was calculated with both CASMO-4E and Serpent. In general, good agreement between the codes was found when the same cross-section library was used. However, differences were observed. In k_{eff} the differences were larger between libraries than between codes while in rod-wise exposure it was the opposite. The nuclide compositions agreed very well except for Gd and Eu isotopes, which is attributed to different Gd treatment in the two codes.

Criticality Safety Validation

Criticality safety validation of the calculation system, i.e. the code, the cross-section library, and the platform, is essential for criticality safety analyses. The objective is to find the bias of the calculation system which is extremely important as it determines the extra safety margin needed due to the uncertainty of the calculation system.

Consequently, the main task in criticality safety has been to bring the criticality safety validation to an appropriate level by setting up a criticality safety validation

package. Such a package consists of a set of critical experiments to be modelled by the code used for the safety analyses, and a script to take care of running the calculations and performing the statistical analysis used to obtain the bias. The number of critical benchmarks should be large enough to fulfil the requirements of the statistical analyses used to treat the results. The goal is to have 100 to 200 such cases adequately covering the target to be analysed. The evaluated benchmarks are picked from the International Handbook of Evaluated Criticality Safety Benchmark Experiments [17].

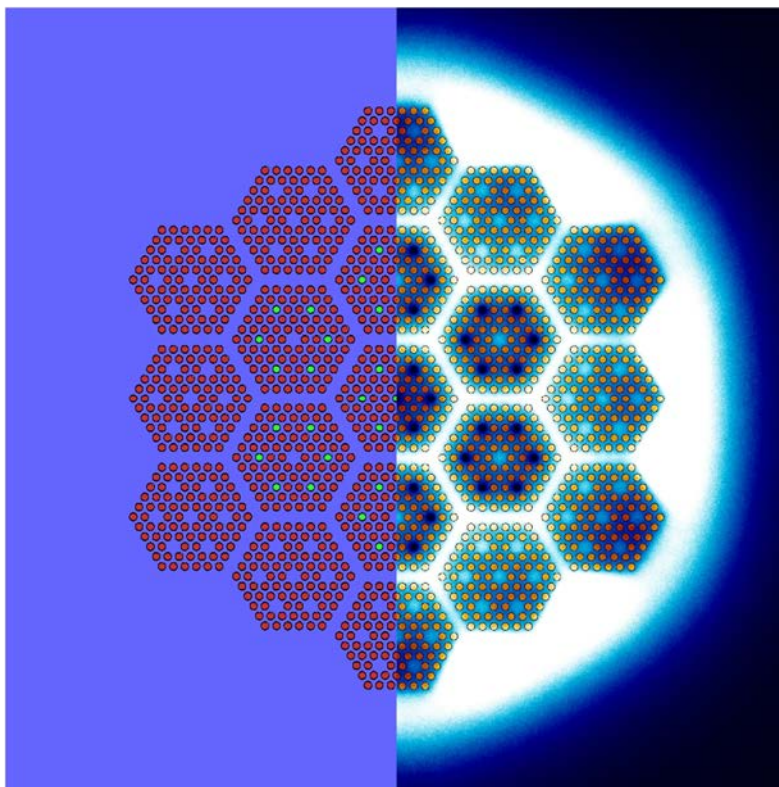


Figure 2. The Serpent geometry (left) and thermal flux/fission rate (right) for a ZR6M case in the validation package. This case consists of assembly imitators, with empty positions and B4C absorber rods (green).

The assembling of such a package [18] for the VVER-440 reactors was interrupted for over a decade but has been resumed during this project. The work was started by revising the initial set of 23 inputs for critical experiments from the ZR-6 reactor modelled with the MCNP-code. The set of modelled benchmarks was then increased by 25 new cases from the LR-0 reactor. In 2013, the set of cases in the package for MCNP was further increased by 14 new cases from the SF-9 reactor. The package was also extended to Serpent. As the work on the Serpent inputs has

started later, it follows the steps of the package for MCNP. The first inputs to be written were those of the ZR-6 reactor followed by the ones for the LR-0 reactor.

The number of cases has grown large enough for the statistical analysis to become possible. Therefore, also a script has been written. This script finalises the inputs for the cases, runs the calculations and collects the resulting k_{eff} -values. It also plots the data to enable trend analyses for various parameters. Eventually, this script should make the whole validation analysis and write a validation report automatically. The package should then be run for the specific code, library and platform combination used for the criticality safety analyses.

A small but significant task was to update the upper safety limit obtained for criticality safety calculations at VTT over ten years ago. This update [19] repeated the old calculation method for the same cases recalculated with the new code and library versions. It was important to update the value as both code versions and cross-section libraries have changed since the value was last calculated.

Reactor Dosimetry

Reactor dosimetry studies the neutron exposure of critical reactor components, such as the pressure vessel. The estimates for the exposure are usually determined semi-empirically, meaning that the computational results are adjusted according to measurement data from neutron dosimeters. Consequently, reactor dosimetry requires mastering of, for example, gamma spectrometry and spectrum adjustment techniques, on top of methods typically used in reactor physical analyses.

The competence of VTT in neutron dosimetry related activities has been maintained and developed in the CRISTAL project. In 2011 the main emphasis was on activities related to the 14th International Symposium on Reactor Dosimetry (ISRD). T. Serén took part in the organization of the symposium and was the second author of an article on the neutron dosimetry in a UK PWR reactor [20].

In 2012 VTT participated in a Round Robin exercise in which the calibration of gamma spectrometers was compared between various European institutions. Specific activities of Ag, Co, Fe, Ti and Nb samples were determined at each institution and the results were collected by an independent partner. The results were published anonymously at the 15th ISRD conference in 2014 [21]. The results agreed within the uncertainty margins reported by the institutions.

During 2012 and 2013 a lot of effort was put in the updating of cross section libraries based on a new release of the International Reactor Dosimetry and Fusion File (IRDFF). A "master" cross section library in 640-group SAND-II format was first prepared [22] from the IRDFF data, with a few additions from ENDF/B-VII nuclear data files. The library includes also uncertainty information in the form of relative uncertainties and correlation matrices. The cross section libraries of PREVIEW and LSL-M2 codes were updated by condensing the 640-group cross sections in the master library to BUGLE-80 format, which has 47 neutron groups.

Because of the retirement of T. Serén in 2013, VTT needed a new responsible for the neutron dosimetry related activities. To familiarize the new responsible in the field, a simple hands-on neutron dosimetry study was performed in 2014 in collaboration with the KÄÄRME project. In this study, the spatial distribution of the neutron flux in the FIR 1 research reactor was measured using Mn and Ni dosimeters and the measurements were compared to a Serpent model of the reactor [23].

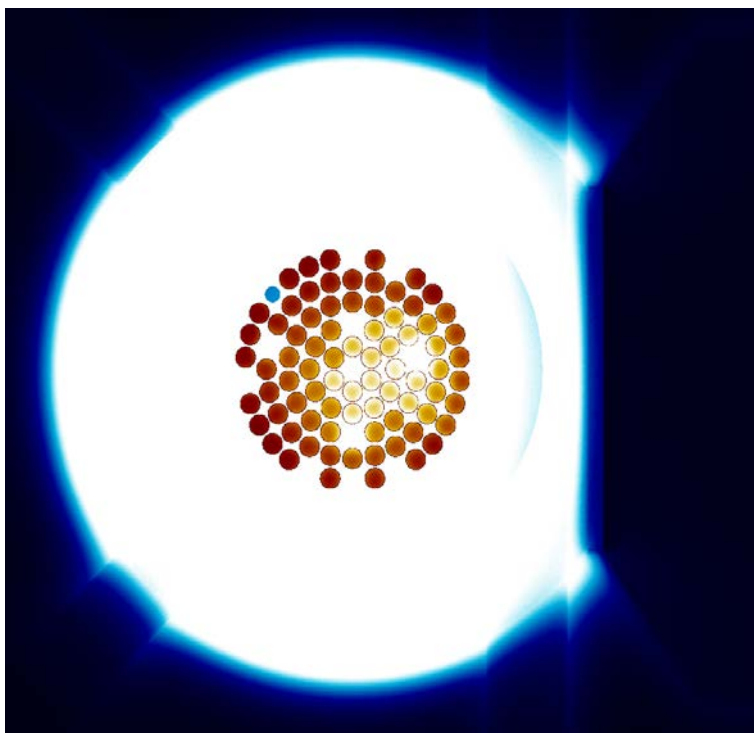


Figure 3. The neutron flux distribution within the FIR 1 reactor was calculated using Serpent 2 Monte Carlo neutron transport code.

Conclusions

The main aim of the project was to educate new researchers in various fields of reactor physics and areas close to it. Another objective was to improve and update the calculations systems. In criticality safety the main aim was to bring the calculations system to a stage where it meets the international standards and guidelines.

Most of the education was covered by calculating benchmarks, which are a very good source for this purpose as they make it possible to compare the obtained results. The project has been active also in international co-operation mainly through

OECD/NEA. Especially the participation in the UAM benchmark has been very active.

Calculation systems have been updated and improved. The work in neutron dosimetry has served also in educating a new expert into the field. The work on the validation package needs still a lot of work but it is well on its way in order to meet the international standards.

References

1. Rätty, A. & Rantamäki, K. 2012. VTT Research Report VTT-R-00457-12.
2. Rantamäki, K. & Rätty, A. 2013. VTT Research Report VTT-R-00778-13.
3. Häkkinen, S. & Rantamäki, K. 2013. VTT Research Report VTT-R 08039-13.
4. Rätty, A. 2014. VTT Research Report VTT-R-00057-14.
5. Machiels, A. 2011. Benchmark for Quantifying Fuel Reactivity Depletion Uncertainty. EPRI Technical Report 1022909.
6. Markova, L. April 2010. Specification for CB 6 Benchmark on VVER-440 Final Disposal. NRI.
7. Rätty, A. & Kotiluoto, P. 2013. VTT Research Report VTT-R-08653-12.
8. Rätty, A. 2014. VTT Tutkimusraportti VTT-R-04186-14.
9. Rätty, A. "Three-Dimensional Discrete Ordinates Calculations with TORT", in the XV Meeting on Re-actor Physics Calculations in the Nordic Countries, Helsinki, Finland, April 12-13, 2011.
10. Lewis, E.E. et al. 2003. Benchmark Specification for Deterministic 2-D/3-D MOX Fuel Assembly Transport Calculations without Spatial Homogenisation, C5G7 MOX Benchmark. OECD/NEA, NEA/NSC/DOC(2003)16.
11. Rätty, A. 2015. C5G7 benchmark BOT3P- ja TORT-koodeilla. VTT Tutkimusraportti VTT-R-05771-14.
12. Pusa, M. 2012. Incorporating sensitivity and uncertainty analysis to a lattice physics code with application to CASMO-4. *Ann. Nucl. Energy*, 40(1), 153—162.
13. Pusa, M. 2012. Perturbation-theory-based sensitivity and uncertainty analysis with CASMO-4. *Sci. Technol. Nucl. Install.* 2012. and Pusa, M. 2014. Adjoint-Based Sensitivity and Uncertainty Analysis of Lattice Physics Calculations with CASMO-4. In *Proc. PHYSOR 2014*, Kyoto, Japan.

14. Ivanov, K. et al. 2013. Benchmark for Uncertainty Analysis in Modeling (UAM) for Design, Operation, and Safety Analysis of LWRs. NEA/NSC/DOC(2013)7
15. Viitanen, T., Rantamäki, K. & Häkkinen S. 2012. VTT Research Report VTT-R-00786-12.
16. Valtavirta V. & Rätty A. 2014. VTT Research Report VTT-R-09014-13.
17. International Handbook of Evaluated Criticality Safety Benchmark Experiments, NEA/NSC/DOC/(95)03/IV, Volume IV, OECD/NEA, 2010.
18. Valtavirta V. & Juutilainen P. 2015. VTT Research Report VTT-R-00405-15.
19. Rantamäki, K., Juutilainen, P. & Valtavirta, V. 2014. VTT memorandum VTT-M-03118-14.
20. Thornton, D.A., et al. 2011. "Dosimetry Assessment for the RPV and Core Barrel in UK PWR Plant", Proceeding of the 14th International Symposium on Reactor Dosimetry, Bretton Woods, New Hampshire, USA, May 22-27.
21. Thornton, D.A. et al. 2014. "The EWGRD Round Robin Measurement Exercise", In Proc. 15th ISR, Aix-en-Provence, France, May 18-23.
22. Serén, T. 2013. "A dosimetry cross section library mainly based on IRDFF", VTT Research Report VTT-R-00948-13.
23. Viitanen, T. & Leppänen, J. 2014. "Validating the Serpent Model of FiR 1 Triga Mk-II Reactor by Means of Reactor Dosimetry." In proc. 15th ISR, Aix-en-Provence, France, May 18-23.

10.2 Adjoint-based uncertainty analysis of lattice-physics calculations with CASMO-4

Maria Pusa

VTT Technical Research Centre of Finland Ltd
P.O. Box 1000, FI-02044 Espoo

Abstract

This article describes the development of sensitivity and uncertainty analysis capabilities in the lattice physics code CASMO-4 in the context of the UAM benchmark. The developed calculation system enables the uncertainty analysis of homogenized assembly constants passed on to nodal codes simulating a full reactor core. The uncertainty analysis methodology is deterministic, meaning that the sensitivity profiles of the responses are computed first after which uncertainty is propagated by combining them with the covariance matrices of the uncertain nuclear data. The developed calculation system has been applied to the CASMO-4 -- SIMULATE-3 code sequence.

Introduction

This article considers the development of a sensitivity and uncertainty (S&U) analysis calculation system for lattice physics calculations in the context of the UAM (Uncertainty Analysis in Best-Estimate Modelling for Design, Operation and Safety Analysis of LWRs) benchmark (Ivanov et al., 2013). The UAM benchmark was initiated in 2006 with the goal of being able to propagate uncertainty through all stages of coupled neutronics/thermal-hydraulics calculations. The imprecision of nuclear data is considered to be one of the most significant sources of uncertainty in reactor physics calculations and therefore there is a special emphasis on this uncertainty. The first phase of the benchmark concentrates on lattice physics calculations used to produce data for the following full-core computations. At VTT, CASMO-4 (Rhodes and Edenius, 2001) is one of the standard tools for assembly level calculations and therefore it was decided to begin developing uncertainty analysis capability to it. The long-term goal of this work is to be able to routinely propagate nuclear data uncertainty through full-core calculation sequences.

Uncertainty analysis methods can be divided into statistical and deterministic methods. In statistical methods, the values of the uncertain parameters are sampled according to their uncertainty distributions, and, for each sample of parameters, the calculation is repeated to provide an uncertainty distribution for the responses under consideration. In deterministic methods, on the other hand, the sensitivity profiles of the responses with respect to uncertain parameters are computed first, after which the parameter uncertainty is propagated deterministically by combining the sensitivity profiles with the covariance matrices of the parameters. These sensitivity

profiles can be computed efficiently by utilizing the adjoint system of the forward system. This approach is generally well-suited when the number of responses is small compared to the number of uncertain parameters. It is also beneficial that this type of uncertainty analysis yields detailed information on the sources of uncertainty in the computation.

In lattice physics calculations the number of uncertain parameter is of the order of 10 000 whereas the number of responses is typically of the order of 10. For this reason, it was decided to start developing an adjoint-based uncertainty analysis capability to CASMO-4. During the TOPAS project of the SAFIR2010 programme, classical perturbation theory was implemented to CASMO-4 to enable the uncertainty analysis of the critical eigenvalue (Pusa, 2012a). In this context, a methodology was devised for processing the covariance matrices from SCALE-6 to become compatible with the cross-section libraries of CASMO-4 (Pusa, 2012a). This work continued in the CRISTAL project by adding generalized perturbation theory (GPT) as a new feature to the code (Pusa, 2012b). GPT allows the uncertainty analysis of responses that can be presented as reaction rate ratios thus enabling the uncertainty analysis of most of the homogenized few-group constants generated with CASMO-4. Ideally, the outcome of the uncertainty analysis should be a global covariance matrix corresponding to the entire cross-section library generated with a lattice physics code. This covariance matrix can then be used to define input uncertainties for the following nodal calculations.

This paper is organized as follows. First the theoretical background of the adjoint-based uncertainty analysis is reviewed. Then the developed methodology and implementation are considered in more detail with some example results illustrating the capabilities of the modified CASMO-4 code.

Theory

In lattice physics calculations, the neutron transport eigenvalue problem is solved on assembly-level and the solution is used to homogenize and collapse data for the following nodal calculations. The responses of the uncertainty analysis comprise of homogenized few-group cross-sections, diffusion coefficients and assembly discontinuity factors (ADFs). In adjoint-based uncertainty analysis, the adjoint-system of the forward problem is utilized in linearizing the responses with respect to uncertain nuclear data.

The neutron transport eigenvalue problem can be written in operator form as

$$\mathbf{A}\Phi = \frac{1}{k}\mathbf{B}\Phi, \quad (1)$$

where $\Phi \in H_\Phi$ is the neutron flux, H_Φ is a Hilbert space and k is the critical eigenvalue. The uncertain parameters consist of nuclear data, and they are denoted by the vector $\sigma \in E_\sigma$. Since nuclear data, such as neutron cross-sections, are functions of energy and location, it is necessary to use a functional derivative to define the response sensitivities. The sensitivity of the response R to the

perturbation $\mathbf{h} = [\delta\Phi, \delta\sigma] \in D = H_\Phi \times E_\sigma$ at the point $\hat{\mathbf{e}} = [\hat{\Phi}, \hat{\sigma}] \in D$ can be defined as the Gâteaux variation:

$$\delta R(\hat{\mathbf{e}}; \mathbf{h}) = \lim_{t \rightarrow 0} \frac{R(\hat{\mathbf{e}} + t\mathbf{h}) - R(\hat{\mathbf{e}})}{t}. \quad (2)$$

In practice, however, Eq. (1) and the system responses are discretized meaning that the sensitivity profiles to nuclear data are reduced to vectors containing conventional partial derivatives.

In perturbation theory, the sensitivities of system responses with respect to all uncertain parameters are computed based on solving one additional adjoint system for each response. The adjoint of Eq. (1) is defined as the system satisfying the following relation:¹

$$\left\langle \mathbf{A}\Phi - \frac{1}{k}\mathbf{B}\Phi, \Psi \right\rangle = \left\langle \Phi, \mathbf{A}^*\Psi - \frac{1}{k}\mathbf{B}^*\Psi \right\rangle, \quad (3)$$

where the brackets $\langle \cdot, \cdot \rangle$ denote an inner product, i.e. integrals over energy, space and direction. The solution of the adjoint problem

$$\left(\mathbf{A}^* - \frac{1}{k}\mathbf{B}^* \right) \Psi = 0 \quad (4)$$

is called the *fundamental adjoint*. In classical perturbation theory, the response under consideration is the critical eigenvalue k . By utilizing the fundamental adjoint the following expression can be derived for the relative sensitivity of k with respect to a perturbation $\delta\sigma$ (For derivation, see e.g. Williams, 1986 or Pusa, 2012a):

$$\frac{\delta k(\hat{\mathbf{e}}; \mathbf{h})}{k} = - \frac{\left\langle (\mathbf{A}'_\sigma(\hat{\mathbf{e}}) - \frac{1}{k}\mathbf{B}'_\sigma(\hat{\mathbf{e}})) \delta\sigma, \Psi \right\rangle}{\left\langle \frac{1}{k}\mathbf{B}\Phi, \Psi \right\rangle}. \quad (5)$$

For functional responses that are Fréchet-differentiable with the gradient orthogonal to the forward flux, the *generalized adjoint* can be defined as the solution to the following inhomogeneous system

$$\left(\mathbf{A}^* - \frac{1}{k}\mathbf{B}^* \right) \Gamma = \frac{\nabla_\Phi R}{R}. \quad (6)$$

If the generalized adjoint problem has a solution, it follows that an infinite number of solutions exist. Out of these solutions, it is possible to choose the one orthogonal to the forward fission source. (For further details, see e.g. Pusa, 2012b) This particular solution is denoted by Γ_p in this paper.

Generalized perturbation theory considers responses of the form

$$R(\mathbf{e}) = \frac{\langle \Phi, \Sigma_1 \rangle}{\langle \Phi, \Sigma_2 \rangle}, \quad (7)$$

where $\Sigma_1, \Sigma_2 \in H_\Phi$. In Eq. (7) it is assumed that Σ_1 and Σ_2 do not depend on Φ . It is straight-forward to show that in this case the relative gradient of the response can be written

$$\frac{\nabla_\Phi R}{R} = \frac{\Sigma_1}{\langle \Phi, \Sigma_1 \rangle} - \frac{\Sigma_2}{\langle \Phi, \Sigma_2 \rangle} \quad (8)$$

¹In some cases the adjoint relation needs to be written in the form $\langle \mathbf{A}\Phi - \frac{1}{k}\mathbf{B}\Phi, \Psi \rangle = \langle \Phi, \mathbf{A}^*\Psi - \frac{1}{k}\mathbf{B}^*\Psi \rangle + [\mathbf{P}(\Psi, \Phi)]_{x \in \partial\Omega}$, where $[\mathbf{P}(\Psi, \Phi)]_{x \in \partial\Omega}$ is a bilinear form associated with the system. We will only consider cases where it is straightforward to force this term to vanish.

and that this gradient is orthogonal to the forward flux Φ . The following expression can now be derived for the sensitivity of a GPT response (For derivation, see e.g. Williams, 1986 or Pusa, 2012b):

$$\frac{\delta R(\hat{\mathbf{e}}, \mathbf{h})}{R} = \frac{R_{\sigma'}(\hat{\mathbf{e}}) \delta \sigma}{R} - \left\langle \Gamma, \left(\mathbf{A}'_{\sigma}(\hat{\mathbf{e}}) - \frac{1}{k} \mathbf{B}'_{\sigma}(\hat{\mathbf{e}}) \right) \delta \sigma \right\rangle_{\Phi}, \quad (9)$$

where the direct sensitivity term can further be written

$$\frac{R_{\sigma'}(\hat{\mathbf{e}}) \delta \sigma}{R} = \frac{\sigma \Sigma_1(\hat{\sigma}) \delta \sigma \Phi}{\Sigma_1 \Phi} - \frac{\sigma \Sigma_2(\hat{\sigma}) \delta \sigma \Phi}{\Sigma_2 \Phi}. \quad (10)$$

Homogenized two-group cross-sections and pin powers can be written in the form of Eq. (7) and therefore Eqs. (8), (9) and (10) can directly be applied to their sensitivity analysis. When diffusion coefficients are considered as responses, Eq. (8) needs to be modified to take into account that the homogenized diffusion coefficient to be collapsed depends on the forward flux (Pusa, 2014). Also, in the sensitivity analysis of ADFs, the assembly surface flux is approximated by the volume-averaged flux near the boundary.

The uncertainty related to nuclear data is typically reported as covariance matrices. These covariance matrices should be understood in terms of Bayesian probability interpretation. In this framework, all knowledge about uncertain parameters is assumed to be incorporated into probability distributions defined so that the integral $\int_a^b p(\sigma_j) d\sigma_j$ corresponds to the probability of the value of σ_j belonging to the interval $[a, b]$. When no other information is available, it is assumed that nuclear data parameters follow Gaussian distributions whose second moments are equal to reported covariance matrices.

In deterministic uncertainty analysis, the objective is to estimate the covariance matrix of the system responses \mathbf{R} by linearizing the response vector $\mathbf{R} \approx \mathbf{R}(\hat{\mathbf{e}}) + \mathbf{S}\sigma$. Here $\mathbf{S} \in J \times K$ is the response vector sensitivity matrix, J is the number of responses and K is the number of uncertain parameters. After linearizing the response, the covariance matrix can be computed simply using the identity

$$[\mathbf{R}] \approx [\mathbf{R}(\hat{\mathbf{e}}) + \mathbf{S}\sigma] = \mathbf{S}[\sigma]\mathbf{S}^T \quad (11)$$

known as the first-order uncertainty propagation formula or the *Sandwich rule*.

Implementation and applications

Before the start of the CRISTAL project, classical perturbation theory had been implemented to CASMO-4. This implementation enabled the sensitivity analysis of the multiplication factor with respect to multi-group nuclear data. In addition, the covariance matrices from SCALE 6 had been processed to become compatible with the cross-section library (Rhodes and Edenius, 2005) of the code. In this project, this work continued by adding GPT to CASMO-4 to allow responses that can presented as reaction rate ratios (Pusa, 2012b and 2014).

As a first step, a generalized adjoint solver applicable to Eq. (6) was implemented to the code. Luckily, the method of characteristics used in CASMO-4 is applicable to the solution of adjoint problems so only moderate changes were needed to implement this capability. The guidelines of the implementation are described in (Pusa, 2014). The main difficulty with generalized adjoint problems is to find the

solution that is orthogonal to the fission source. In this work this was accomplished by forcing the orthogonality with each outer iteration. After obtaining the generalized adjoint solutions, the sensitivities of the responses can be computed in an efficient manner based on Eq. (9).

The sensitivity and uncertainty analysis methodology has been implemented for the following responses: two-group homogenized cross-sections, pin powers, diffusion coefficients and assembly discontinuity factors. Figure 1 shows the pin-power values and uncertainties of a BWR assembly as an example of uncertainty analysis results. In addition to the individual uncertainties, the GPT methodology yields the correlations between all the output responses. The correlation matrix for the pin-powers shown in Figure 1 is shown in Figure 2.

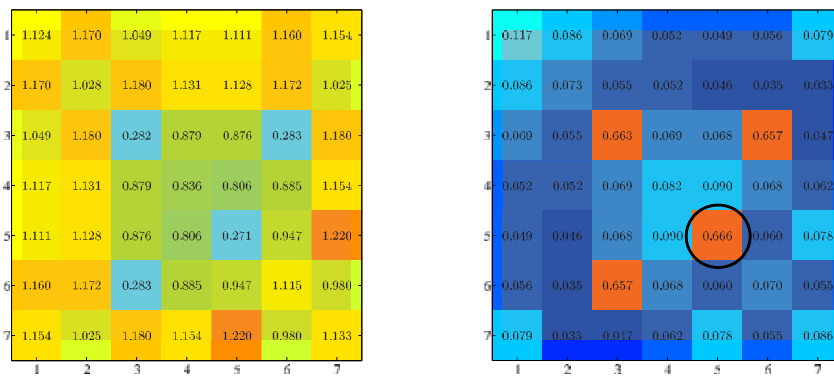


Figure 1. Relative pin-powers and their uncertainties (%) for a BWR fuel assembly with 4 Gd pins.

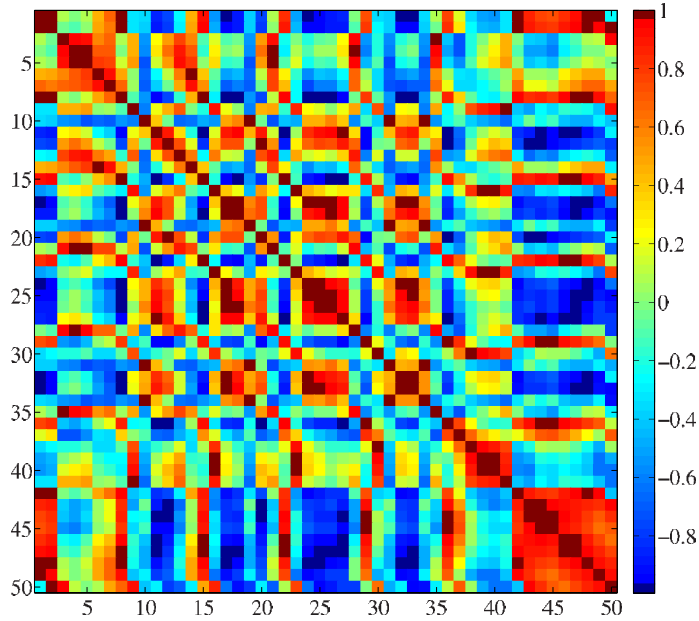


Figure 2. Correlation matrix of the pin-power uncertainties shown in Fig.1.

In addition to computational efficiency, a definite advantage of the adjoint-based approach is that it yields very detailed information on the responses and their uncertainties. For example, it is easy to see which nuclear data parameters contribute most to the uncertainty of a particular response and this study can also be carried out energy-group-wise. To illustrate this, Table 1 shows the uncertainty break-down for the fast ADF of a PWR fuel assembly. The sensitivity profiles describing the first-order dependence of the responses with respect to nuclear data also bring valuable insight into the application. Figure 3 shows the sensitivities of the same ADF with respect to the top three contributors to its uncertainty.

Table 1. Top five contributors to the uncertainty of the fast ADF for a PWR fuel assembly. For this application, the value of the response is $f_1 = 0.980$ with a relative uncertainty of $\Delta f_1 = 2.96 \times 10^{-2} \%$.

Nuclide	Param. pair	Contr. to $\Delta R/R$
^{235}U	χ, χ	1.955×10^{-2}
^{238}U	$\sigma_{s'}, \sigma_s$	1.525×10^{-2}
^1H	$\sigma_{s'}, \sigma_s$	1.359×10^{-2}
O	$\sigma_{s'}, \sigma_s$	7.542×10^{-3}
^{157}Gd	$\sigma_{c'}, \sigma_c$	2.110×10^{-3}

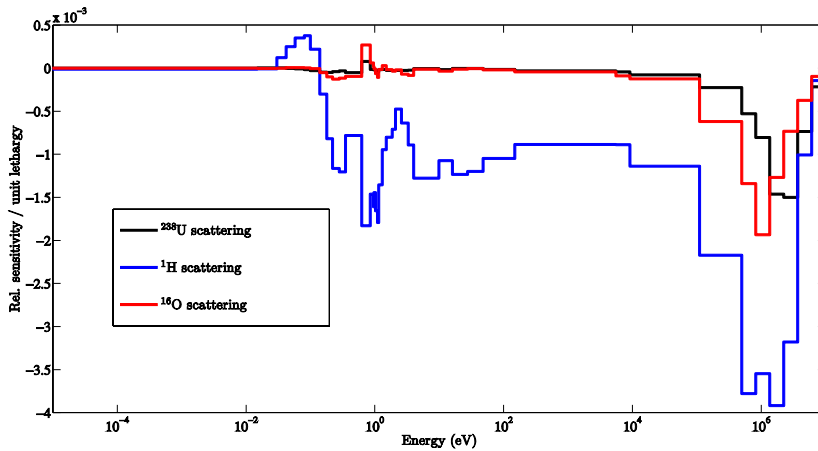


Figure 3. Sensitivity profiles of the fast ADF for a PWR fuel assembly.

The usefulness of uncertainty analysis depends greatly on the completeness of the uncertainty quantification for the employed nuclear data. To establish the current state of covariance libraries, the project has collaborated with Aalto University where a significant research effort has been put into covariance studies (Vanhanen 2015a, 2015b). During this collaboration, multi-group covariance libraries based on ENDF/B-VII.1, JEFF 3.2 and JENDL 4.0u have been connected with the modified CASMO-4 and the prediction capabilities of them have been compared in the context of the UAM benchmark (Vanhanen and Pusa, 2015). During the course of the study, it was for example found that the uncertainty estimates can differ by an order of magnitude for several important pieces of nuclear data.

The ultimate goal of the described work is to be able to produce a complete set of uncertainty data for SIMULATE-3 and nodal transient codes. In order to achieve this objective, depletion needs to be included in the uncertainty analysis methodology. However, only fresh fuel applications have been considered in this project. As mentioned previously, the purpose of lattice physics calculations is to produce assembly-specific group constants for the following nodal calculations by modeling the fuel assemblies of a reactor separately in different operating conditions. When propagating the nuclear data uncertainty through these calculations, it needs to be taken into account that all the responses become correlated due to depending on the same uncertain data. Therefore, in addition to the individual uncertainties related to the responses, the global covariance matrix corresponding to the entire cross-section library needs to be computed. This requires that the sensitivity profiles of the selected responses are computed and stored for each lattice calculation after which the covariance matrix can be built element-wise based on the Sandwich rule. Even without depletion, the number of responses in the global covariance matrix becomes of the order of ten thousand, making the calculations computationally intensive.

The propagation of nuclear data uncertainty through the CASMO-4 -- SIMULATE-3 sequence has been studied in this project. Because of the computational challenges related to the global covariance matrix, the problem was approached by developing a calculation system where each assembly type is considered separately, i.e. the correlations between different assembly types are ignored. After this approximation, the size of each covariance matrix becomes of the order of 900×900 . The uncertainty can then be propagated through SIMULATE-3 by drawing random samples for each assembly separately. The calculation system has been applied to one of the PWR core-exercises of the UAM benchmark.

Summary, conclusions and future work

When uncertain parameters are used in computation, also the calculation results contain uncertainty. In nuclear safety calculations, the imprecision of nuclear data is believed to be one of the most significant sources of uncertainty. In order to propagate this uncertainty through calculation sequences simulating a full reactor core, uncertainty analysis methods need to be developed for lattice physics calculations that are used to produce homogenized assembly data. In this project, an adjoint-based uncertainty analysis methodology has been developed in the lattice physics code CASMO-4 that is one of the standard tools for group constant preparation at VTT. The work has been carried out in the context of the UAM benchmark.

Before the start of the project, classical perturbation theory had been implemented to CASMO-4 to enable the uncertainty analysis of the critical eigenvalue. This work was continued by adding generalized perturbation theory as a new feature to the code. In this framework, the responses of interest are linearized with respect to the uncertain parameters in an efficient manner by utilizing the adjoint system of the original forward problem. The uncertainty analysis can then be carried out by combining the covariance matrices of the uncertain nuclear data with these sensitivity profiles. The calculation system developed in the project allows the uncertainty analysis of all relevant assembly data that is passed on to the following full-core calculations with the considered responses including two-group homogenized cross-sections, diffusion coefficients and assembly discontinuity factors. In addition, an automated calculation system enabling the propagation of nuclear data uncertainty through the CASMO-4 - SIMULATE-3 calculation sequence has been developed.

The ultimate goal of the described work is to be able to produce a complete set of uncertainty data for SIMULATE-3 and nodal transient codes which eventually requires extending the adjoint-based methodology to burnup calculations. This goal is fairly ambitious as depletion can not be included to the GPT formalism in a straight-forward manner without the computation time becoming prohibitive and therefore the number of adjoint solutions computed during a burnup step needs to be somehow restricted. Once accomplished, the calculation system will make it possible to routinely produce the global covariance matrix corresponding to a cross-section library for the uncertainty analysis of the following full-core calculations.

References

- Ivanov, K. et al. 2013. Benchmarks for uncertainty analysis in modelling (UAM) for the design, operation and safety analysis of LWRs. OECD Nuclear Energy Agency.
- NEA Data Bank, 2011. ZZ-SCALE6.0/COVA-44G, a 44-group cross section covariance matrix library retrieved from the SCALE-6.0 package, NEA Data Bank code package USCD1236/03.
- Pusa, M. 2012a. Incorporating sensitivity and uncertainty analysis to a lattice physics code with application to CASMO-4. *Ann. Nucl. Energy* 40(1), 153-162.
- Pusa, M. 2012b. Perturbation Theory Based Sensitivity and Uncertainty Analysis with CASMO-4. *Sci. Technol. Nucl. Install.* 2012.
- Pusa, M. 2014. Adjoint-based Uncertainty Analysis of Lattice Physics Calculation. In *Proc. of: PHYSOR 2014 - The Role of Reactor Physics toward a Sustainable Future*, Kyoto, Japan.
- Rhodes, J. and Edenius, M. 2001. CASMO-4, A Fuel Assembly Burnup Program, User's Manual. Studsvik Scandpower.
- Rhodes, J. and Edenius, M. 2005. JEF 2.2 and ENDF/B-IV 70 group neutron data libraries. Studsvik Scandpower.
- Vanhanen R. 2015a. Computing more consistent multigroup nuclear data covariances. *Nucl. Sci. Eng.* (in press)
- Vanhanen R. 2015b. Computing positive semidefinite multigroup nuclear data covariances," *Nucl. Sci. Eng.* (in press)
- Vanhanen R and Pusa, M. 2015. Survey of Prediction Capabilities of Three Nuclear Data Libraries for a PWR Application. submitted to *Ann. Nucl. Energy*.
- Williams, M. 1986. Perturbation Theory for Nuclear Reactor Analysis. In Ronen, Y. Ed., *CRC Handbook of Nuclear Reactors Calculations Vol 3*. SRC Press.

11. Three-dimensional reactor analyses (KOURA)

11.1 KOURA summary report

Ville Hovi, Anitta Hämäläinen, Mikko Ilvonen, Hanna Rätty, Ville Sahlberg,
Veikko Taivassalo, Elina Syrjälähti

VTT Technical Research Centre of Finland Ltd
P.O. Box 1000, FI-02044 Espoo

Abstract

KOURA was a four-year project focused on reactor dynamics and thermal hydraulics. Focus of the project has been on modelling of the boiling water reactors and coupling of 3D thermal hydraulics with reactor dynamic codes.

Introduction

The fundamental objective of KOURA project is to have a truly independent transient calculation system, which can be utilized by the safety authority and other end-users for safety analyses that are independent from those of power plant designers and fuel vendors.

Main codes for transient analysis at VTT are HEXTRAN (Kyrki-Rajamäki, 1995) for VVER reactors and TRAB3D (Kaloinen, 1997) for PWR and BWR reactors. Both codes include a three-dimensional nodal model for the core, coupled to parallel one-dimensional hydraulics channels and radial heat transfer in the fuel and cladding. TRAB3D includes also models for the rest of the BWR pressure vessel thermal hydraulics using one-dimensional channels, as well as models for steam lines, pumps and control systems. The core models of TRAB3D and HEXTRAN can be coupled to the system code SMABRE (Miettinen, 2000) for analyses of VVER, PWR and HPLWR reactors.

One of the main objectives of the KOURA project has been supplementing the code system with three-dimensional thermal hydraulics modelling. For that purpose CFD-style 3D thermal hydraulics solver PORFLO (Hovi et al., 2012) has been developed. Other main objective has been the enhancement of VTT's boiling water

reactor modelling capabilities. In addition, neutronics and fuel rod modelling of the reactor dynamics codes have been improved.

3D Thermal hydraulics

3D two-phase CFD code PORFLO

The PORFLO code is a two-phase 3D flow simulation tool. It is mainly targeted at coupled reactor dynamics applications but also serve as a stand-alone CFD code. Its main applications are such that 3D phenomena may be significant but geometrical complexity does not allow for a CFD-style structure fitted grid all around the computational domain, e.g. fuel bundles, internal structures of reactor pressure vessels, steam generators and heat exchangers. PORFLO utilizes the concept of porous medium to model structural features not represented explicitly in a computational mesh. In the porous medium approach, the fluid fraction of the total cell volume is defined as the porosity and the effects of the porous medium are modelled explicitly as source terms in the scalar transport equations that govern the fluid flow. A complete rewrite of the PORFLO code was done during 2011, in which two major improvements were introduced: the ability to handle unstructured meshes and parallelization. In addition to that, during the KOURA project iterative solution using the phase-couple SIMPLE algorithm and $k-\epsilon$ turbulence modelling has been further developed (Hovi et al., 2014). Main stand-alone applications have been EPR fuel assembly and EPR pressure vessel (Takasuo et al., 2012).

The AER-7 benchmark

The capability of PORFLO to function as the 3D thermal-hydraulic part of a reactor dynamic transient calculation system is tested by simulations of the AER 7. benchmark with the coupled code system PORFLO-HEXTRAN/SMABRE. The benchmark considers start-up of a cold loop of a VVER-440. The objective is to predict core power when it receives coolant that was first mixed in the downcomer and then in the lower plenum.

Used CFD mesh is based on a mesh provided by Fortum. Geometrically defined subblocks of the Fortum mesh were used to define boundaries for new meshing of the internal volumes between the boundaries. The meshes contain a small portion of the 6 cold leg inlets, the downcomer and lower plenum, up to the inlet level of the core. Three different-sized meshes were generated: coarse (N1, 14012 cells), medium (N2, 108752) and fine (N3, 363276). They have 2, 4 and 6 cells across the downcomer width, respectively. N2 is shown in Figure 1.

HEXTRAN and SMABRE models are based on that used in the earlier AER benchmark. The primary loop includes six separate loops. The pressure vessel is divided into six parallel channels except the upper head. The total number of nodes and junctions is 516 and 663, respectively. By the nodalization and the turbulent mixing model, 30 % mixing is provided in the pressure vessel before the core and 10 % after the core.

The PORFLO 3D domain is connected with SMABRE plant model at the 6 cold leg inlets, and will be with HEXTRAN core TH & neutronics at core lower end. So far

only one-way coupling from SMABRE to PORFLO is used. The mass flow rates and temperatures of the cold leg inlets of the 6 loops are calculated by HEXTRAN-SMABRE and they are used as time-dependent boundary conditions in the PORFLO simulation. The inlet boundary of the PORFLO simulation is located in the cold legs of the 6 loops, relatively near the downcomer. It is expected in near future to have a coupling, where the mixed temperature field from PORFLO is transferred to HEXTRAN at each time step. In addition to the PORFLO-HEXTRAN/SMABRE simulation, the benchmark has been calculated with HEXTRAN/SMABRE to get comparison data for PORFLO simulation.

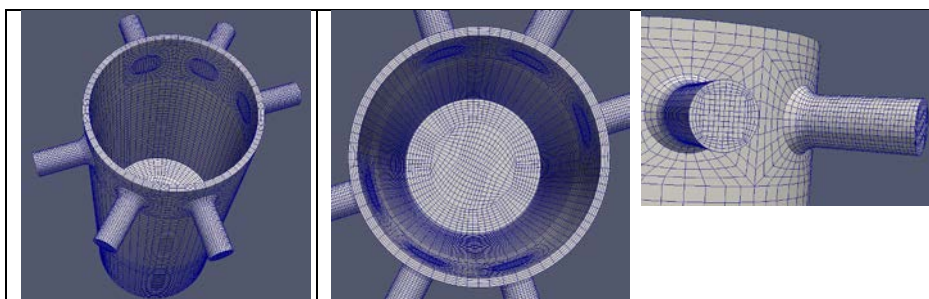


Figure 1. Medium-grained 3D CFD mesh (N2) used in the PORFLO simulations.

At the initial state reactor power is 87% of nominal. Loop 1 has been isolated and its temperature is 100 °C. According to the definition of the benchmark (Kotsarev et al., 2010) the initial main events of AER-7 are:

1. A main isolation valve (MIV) in hot leg 1 opens.
2. The main circulation pump (MCP) of loop 1 starts operation.
3. After the MCP has reached full flow, the MIV in the cold leg starts to open.
4. Reactor power increases when the slug of cooler liquid enters the core.
Fission is stopped by SCRAM at 110 % of nominal power (1375 MWt).

At appr. 30 s, the mass flow rate of loop 1 increases from zero to the level of the others. Due to assumptions on the secondary circuit, the temperature of loop 1 remains at a low level. Transient was simulated up to more than 200 s of physical time. Temperature fields at core inlet at three time points are shown in Figure 2. It can be seen that in general the locations and levels of the cold plume coincide quite well, but the mixing by SMABRE is very coarse-grained due to using only 6 sectors. In addition, Figure 2 contains the PORFLO-predicted downcomer temperature fields for the same time points.

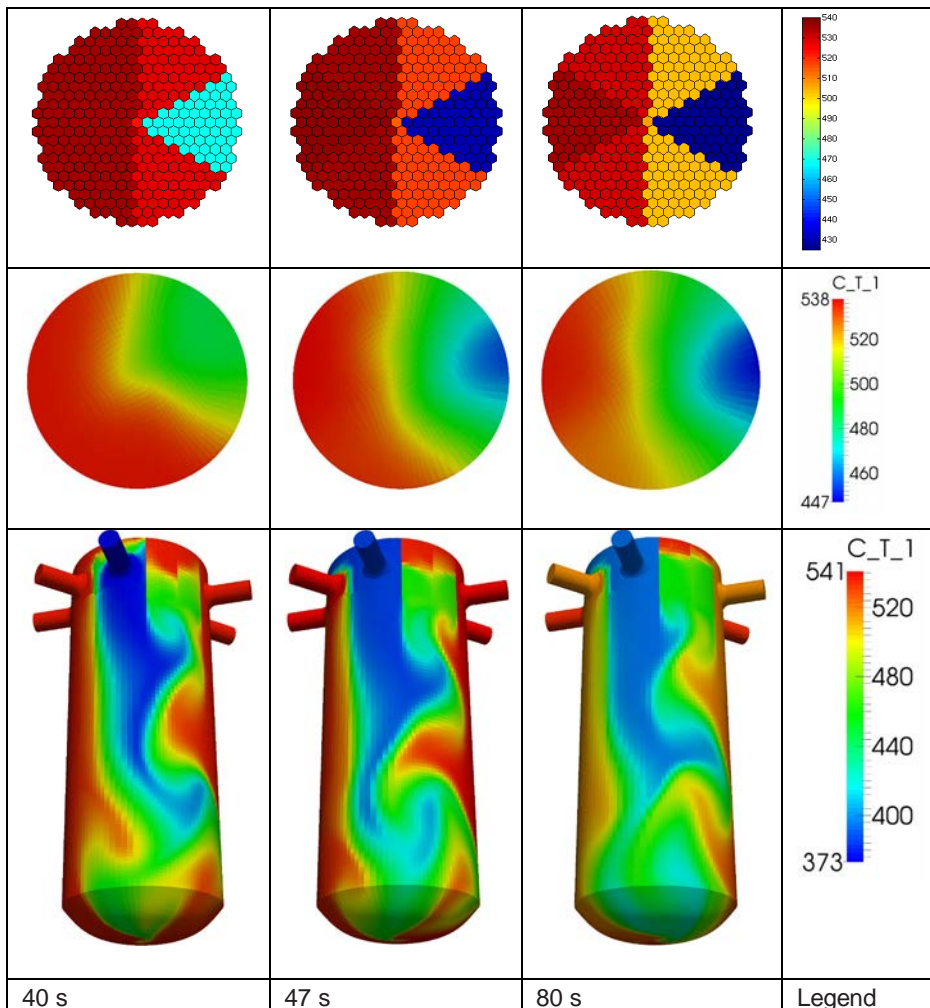


Figure 2. Results of temperature mixing in AER-7 benchmark by SMABRE (top row) and PORFLO (two lower rows). Comparison of SMABRE and PORFLO results can be made between the first two rows, which show the temperature field at core inlet level. Additionally, the bottom row shows the downcomer temperature field by PORFLO. Three time points are shown: 40 s, 47 s and 80 s. The PORFLO results shown were calculated with the finest (N3) mesh.

BWR modelling

Enhancement of boiling water reactor modelling capabilities has been one focus area in the KOURA project. OECD/NEA launched new boiling water reactor benchmark in 2011. The benchmark is based on the stability event at the Oskarshamn-2 nuclear power plant in February 1999. VTT decided to participate in the benchmark

with the aim of challenging and enhancing its BWR modelling capabilities, with special emphasis on deepening the expertise on BWR phenomena and further training of reactor dynamics specialists on using TRAB3D for BWR analyses.

In 2012 the TRAB3D model for Oskarshamn-2 power plant was created from scratch that was a very useful lesson in the modelling of BWRs. Main difference to the TRAB3D's usual BWR application, Olkiluoto power plant, is that the recirculation pumps are located in

external recirculation lines. The cross section data was modified in co-operation with the CRISTAL project to the format that can be used in TRAB3D. Transient modelling was started in 2013, but it revealed still many deficiencies in the specifications. In 2014 updated specifications were delivered to participants and with that data it has been possible to continue calculation to the unstable period (Syrjälähti, 2015).

The stability event was initiated by loss of feedwater pre-heaters and a control system logic failure that resulted in a condition with high feedwater flow and low feedwater temperature without reactor scram. In addition to the initiating event, an interaction of the automatic power and flow control system caused the plant to move into the low flow - high power regime. A combination of the above events led to diverging power oscillations which triggered an automatic scram at high power. The reactor was initially at full power. Behaviour of the fission power is shown in Figure 3. TRAB3D calculation is terminated due to a channel dryout.

TRAB3D and SMABRE have earlier been connected with parallel coupling (Daavittila et al, 2003) and recently with internal coupling (Syrjälähti et al, 2011). With parallel coupling the core thermal hydraulics is calculated by both codes in parallel. In internal coupling TRAB3D performs the neutronics calculation, the heat transfer calculation is carried out either by SMABRE or TRAB3D, and SMABRE takes care of the hydraulics calculation of the whole cooling circuit including the reactor core, and the automation and control logic.

The internal coupling of TRAB3D and SMABRE has in the KOURA project been validated against measurements at the Olkiluoto (OL) NPP: OL1 overpressurization transient of 1985 (Räty et al., 2013) and OL1 load rejection test of 1998 (Hämäläinen & Räty, 2014).

Results of the internally coupled TRAB3D-SMABRE for the overpressurization transient were in good agreement with the TRAB3D standalone calculation and measurements, Figure 4.

The load rejection transient starts with a closure of the turbine valve, opening of the turbine dump valves and startup of partial scram. The partial scram involves insertion of two control rod groups, one with a fast hydraulic insertion, the other with

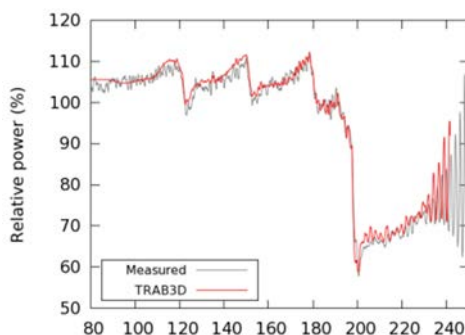


Figure 3. Local power measurement APRM during O2 transient.

a slow electrically driven insertion. Local power measurements from the core are available.

Small differences in the positions of the steam line valves can be seen in the early stage of the transient, Figure 5, as SMABRE is not inside of the iteration process of TRAB3D. For the rest of the transient the calculated dump valve position is well simulated. The 3-D power behaviour is well predicted with the internally coupled TRAB3D-SMABRE code. The LPRM results indicate relatively good results with the internal-coupling, Figure 5 even though general slowness in changes is seen.

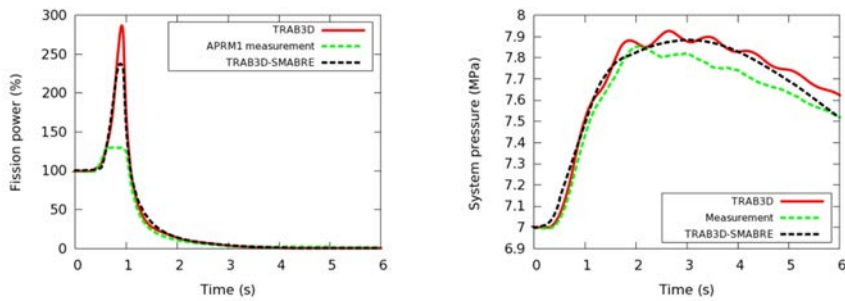


Figure 4. Measured and calculated reactor power and system pressure with TRAB3D and TRAB3D-SMABRE in Olkiluoto 1 overpressurization transient 1985.

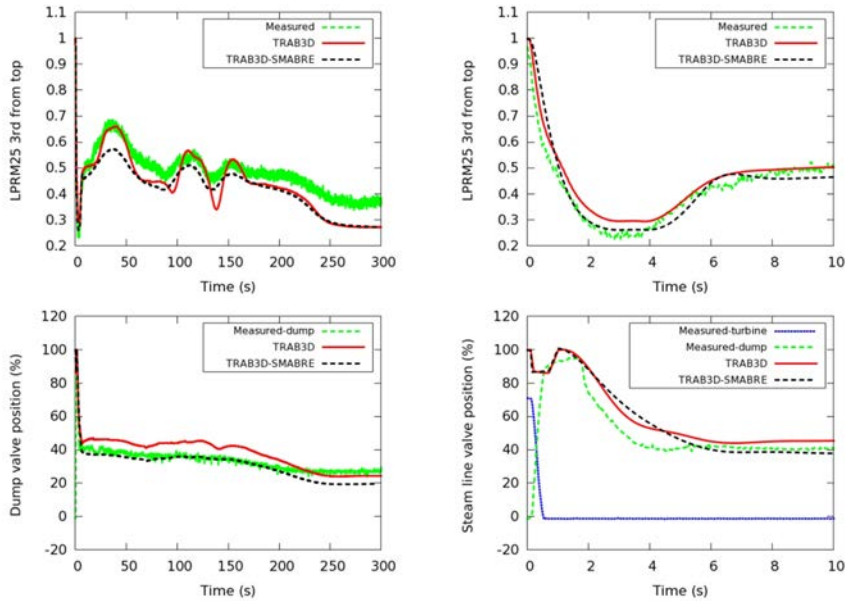


Figure 5: Measured and calculated local power (top) and steam line valve positions (bottom) in OL load rejection test with TRAB3D and TRAB3D-SMABRE.

Development of improved submodels

Neutronics

Previously HEXTRAN and TRAB3D have calculated only the nodewise power distribution. However, more accurate safety analyses and modern thermal hydraulic solvers, such as PORFLO, require a pinwise power distribution. In the KOURA project TRAB3D code has been supplemented with a pin power reconstruction model. Model is based on the previous work, in which external code is used for the simulation of the simple test cases. (Mattila, 1999) The method is based on combining the homogeneous power distribution by a nodal code and a heterogeneous power distribution, which is achieved by using precalculated intranodal power distributions. This is an effective and relatively accurate method, which is commonly used in different nodal codes around the world.

To validate a pin power reconstruction model added to TRAB3D, Serpent 2 was chosen as a reference source. A TRAB3D –Serpent 2 code sequence was developed in cooperation with KÄÄRME project, allowing the use of group constants generated by Serpent 2 for TRAB3D calculations, (Sahlberg, 2014).

During the process it was noted that the difference between the radial power distributions of TRAB3D and Serpent 2 full core results could hamper the validation of the pin power reconstruction model and work began to improve the results of the TRAB3D – Serpent 2 code sequence. By solving albedos for the system with Serpent 2 with fewer assumptions about the surrounding geometry, an average reduc-

tion of one third of the differences between TRAB3D and Serpent 2 results was achieved with the difference vanishing at certain parts of the core.

The improvements to results near core boundaries enable continuation of the pin power validation and work is underway to implement TRAB3D pin power reconstruction using results from Serpent 2 as a base.

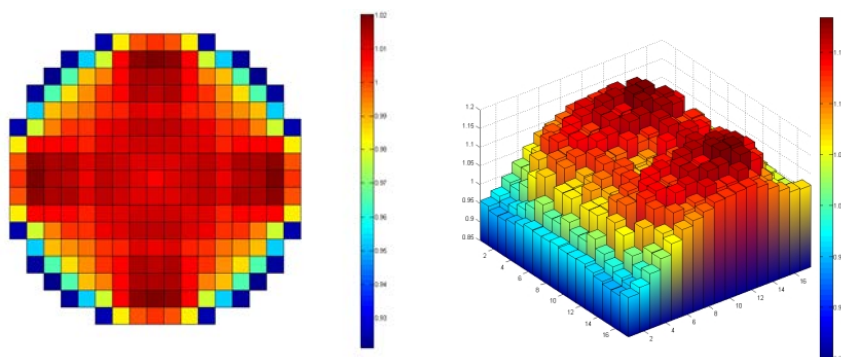


Figure 6. Relative difference between radial power distributions of Serpent 2 and TRAB3D results at the axial peak power layer of an EPR core (left) and relative power distribution of a top of a fuel assembly at the second outermost radial layer of an EPR core (right), reconstructed by TRAB3D using CASMO results as a base.

Fuel rod modelling

FINIX is a new light-weight fuel behavior code that has been developed in PALAMA project during SAFIR2014 (Ikonen et al., 2013). FINIX solves the time-dependent temperature distribution in the rod and the heat flux from the cladding to the coolant. Elastic and thermal mechanical deformations of the cladding can also be solved with FINIX. In the KOURA project the FINIX fuel module has been coupled to the reactor dynamics codes TRAB-1D, TRAB3D, and HEXTRAN. FINIX has been used in the simulation of fast power transients and a PWR main steam line break in different types of reactors (Ikonen et al., 2014).

With the HEXTRAN-FINIX coupling for example 3rd dynamical AER benchmark, control rod ejection transient in standard VVER-440 power plant was simulated. Figure 7 shows the gas gap conductance and fuel temperature during the transient using FINIX module and original simple correlations used in the benchmark. Due to the lower conductance fuel temperatures calculated by FINIX are higher than those calculated with old correlations.

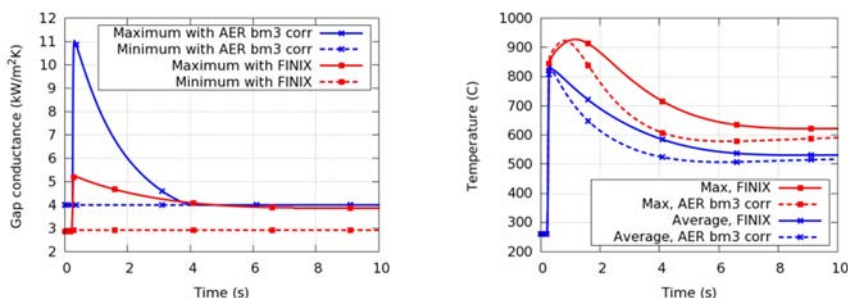


Figure 7. Minimum and maximum conductance of the gas gap (left) and maximum fuel temperature and maximum of fuel pellet radial average temperature (right) during the control rod ejection in the 3rd AER benchmark with the FINIX module and with original correlation used in the 3rd AER benchmark.

Quality assurance and documentation

One aim of the project is to maintain and improve usability of the code system. During the KOURA project reactor dynamic codes TRAB3D, HEXTRAN and SMABRE have been transferred to Linux environment, and in that connection several deficient and non-standard features of the source code have been replaced. Branched versions of reactor dynamics codes, especially TRAB3D versions used in internal and parallel couplings with SMABRE as well as benchmark specific versions of the HEXTRAN and TRAB3D have been merged to product versions. Several types of transients in different power plants have been recalculated with up-to-date code versions.

Usability of the code system has been improved also by updating and documenting the reactor dynamics codes, analysis methods and auxiliary codes developed in the KOURA project and its predecessors.

International co-operation

Participation in the OECD Nuclear Energy Agency (NEA) working groups and benchmarks is one of the most important ways of validating the methods and codes used in reactor analysis. This project includes the participation in the meetings of the NEA Working Party on the Scientific Issues of Reactor Systems (WPRS), which is responsible for the organization of the reactor dynamics benchmarks among other activities and included participation to the work of Nuclear Science Committee (NSC) in 2011. In the frame of the KOURA project VTT has participated in the OECD/NEA BWR stability benchmark (O2) and Uncertainty analysis benchmark series (UAM).

The cooperation and information exchange on VVER safety within the AER framework together with other countries that use VVER reactors has been continued. Conference papers have been presented in AER symposium (Rintala, 2011;

Syrjälähti, 2012). Project has also included participation to FJOH summer school and to the international scientific workshop on reactor dynamics and safety.

References

- Daavittila, A., Hämäläinen, A. & Kyrki-Rajamäki, R. Effects of secondary circuit modeling on results of PWR MSLB benchmark calculations with new coupled code TRAB-3D/SMABRE. Nuclear Technology, Vol. 142, No. 2, pp. 116-123, May 2003.
- Hovi, V., Taivassalo, V., Ilvonen, M., Manninen, M., Takasuo, E. EPR-related applications of the PORFLO code on rectilinear and unstructured meshes. VTT Research report, VTT-R-01142-12, 2012.
- Hovi, V., Ilvonen M. and Taivassalo V. 3D Core Thermal Hydraulics With the PORFLO Code - Turbulence Modeling and Porous Medium With Porosity Steps. In: Proceedings of ICONE-22, Paper ICONE22-30731., Prague, Czech Republic, July 7 – 11, 2014
- Hämäläinen, A. and Rätty, H.. BWR load rejection transient with internally coupled TRAB3D-SMABRE. Research report VTT-R-00925-14, 2014
- Ikonen, T., Tulkki, V., Syrjälähti, E., Valtavirta, V., Leppänen, J. FINIX – fuel behavior model and interface for multiphysics applications. In: 2013 Fuel Performance Meeting / TopFuel, Charlotte, USA. 2013.
- Ikonen T., Loukusa H., Syrjälähti E., Valtavirta V. , Leppänen J., Tulkki V. Module for thermomechanical modeling of LWR fuel in multiphysics simulations. Annals of Nuclear Energy, in press, 2014
- Kaloinen, E. and Kyrki-Rajamäki, R., 1997. TRAB3D, a new code for three-dimensional reactor dynamics. In Proceedings of ICONE-5, Nice, France, May 26-30, 1997.
- Kotsarev, A., Lizorkin, M. and Petrin, R. Definition of the 7th Dynamic AER Benchmark – VVER-440 Pressure Vessel Coolant Mixing by Re-connection of an Isolated Loop, Proceedings of the 20th Symposium of AER on VVER Reactor Physics and Reactor Safety, Espoo, Finland, September 2010.
- Kyrki-Rajamäki, R. . Three-dimensional reactor dynamics code for VVER type nuclear reactors. VTT Tech. Rep. 246, 1995.
- Mattila, R. Pin power reconstruction module for TRAB-3D nodal code, VTT/Helsinki University of Technology, Master's thesis, 1999.

- Miettinen, J. Thermohydraulic model SMABRE for light water reactor simulations, Licentiate's thesis, Helsinki University of Technology, 2000.
- Rintala, J. Overview of the validation of the new 3-D neutronics model in Apros. In: Proceedings of the twenty-first Symposium of AER, Dresden, Germany, September 19-23, 2011
- Räty, H., Hämäläinen, A., Syrjälähti, E. TRAB3D and TRAB3D-SMABRE code updates and validation status. Research report VTT-R-00788-13, 2013
- Sahlberg V. Development of Serpent 2 - TRAB3D code sequence. Research report VTT-R-04538-14, 2014.
- Syrjälähti, E., Hämäläinen, A., Räty, H. Tridimensional Core Transient Analysis Methods (TRICOT). TRICOT summary report. SAFIR2010 Final Report. VTT Research Notes 2571. pp. 145-159, 2011.
- Syrjälähti, E. Characterization of a representative VVER-440 fuel rod with the statistical ENIGMA. In: Proceedings of the twenty-second Symposium of AER, Pruhonice, Czech Republic, October 1-5, 2012. pp 721-734., 2012.
- Syrjälähti, E. TRAB3D calculation of the O2 BWR stability benchmark. Research Report VTT-R-00227-15., 2015.
- Takasuo, E., Hovi, V., Ilvonen, M. Applications and Development of the PORFLO 3D Code in Nuclear Power Plant Thermal Hydraulics. In: Proceedings of ICONE-20. Paper ICONE20-5416. Anaheim, California, USA, 2012.

12. Development of Finnish Monte Carlo reactor physics code (KÄÄRME)

12.1 KÄÄRME summary report

Jaakko Leppänen, Maria Pusa, Tuomas Viitanen, Ville Valtavirta,
Toni Kaltiaisenaho

VTT Technical Research Centre of Finland Ltd
P.O. Box 1000, FI-02044 Espoo

Abstract

The development of the Serpent Monte Carlo reactor physics code was started at VTT in 2004, and has continued with the support of the Finnish national SAFIR research programmes. In SAFIR 2014 the work was gathered under its own project, during which the code established a large international user basis and the range of applications expanded beyond the project boundaries. The work carried out within the KÄÄRME project converged into a few specific topics, introduced in the following, together with a special article covering the use of Serpent for spatial homogenization.

Introduction

The KÄÄRME project in SAFIR 2014 was established to continue the development of the Serpent Monte Carlo reactor physics burnup calculation code, started at VTT in 2004. When the project was initiated in 2011, the code had been in public distribution for two years, and had a small but active user basis of about 60 users in 40 universities and research organizations around the world. The source code was managed by two developers at VTT, with additional contribution from M.Sc. students at Aalto University.

During the past four years the user basis has increased to almost 400, and the development is currently carried out by a five-member team. The initial work carried out in SAFIR 2014 and the previous SAFIR programmes has expanded to entirely

new fields, which connect to various research projects in Finland and abroad. The KÄÄRME project, started with the re-writing of the Serpent source code, consequently converged towards a few specific research topics. The primary goal of the project was to complete the methodology for spatial homogenization, and demonstrate that the continuous-energy Monte Carlo method is a feasible option for producing input data for deterministic nodal diffusion codes. This topic is covered separately in a special article in this report, and the remaining tasks are described in the following.

Background

Work on the Serpent code started at VTT in 2004, with the purpose of developing a new Monte Carlo code for spatial homogenization, i.e. the production of input parameters for deterministic reactor core simulator calculations. The idea of using the Monte Carlo method for this task was not new, but Serpent is one of the first codes specifically developed for the purpose. The advantages of the method in spatial homogenization include the capability to model complicated three-dimensional geometries and to use continuous-energy cross sections in the transport simulation, without any application-specific limitations. These advantages can be considered particularly valuable for the development of advanced fuel types and reactor technologies, some of which lie completely beyond the capabilities of conventional deterministic lattice transport codes.

Developing a Monte Carlo based calculation code dedicated to spatial homogenization required a certain level of specialization, including the capability to perform fuel depletion and the calculation of few-group constants in an automated manner. The early work is described in a doctoral thesis completed in 2007 (Leppänen, 2007) and a novel method developed for the solution of Bateman depletion equations in another thesis, completed in 2013 (Pusa, 2013b).

Serpent was released into public distribution for non-commercial research and educational use via the OECD/NEA Data Bank in 2009 and RSICC in the US one year later. As soon as the user basis began to grow, so did the applications, and the code was found to be a useful calculation tool for a variety of reactor physics applications, including depletion studies, research reactor modelling and the validation of deterministic transport codes. Spatial homogenization still remains as one of the main research topics, but considerable efforts are devoted to coupled multi-physics simulations and extending the scope of applications into new fields beyond reactor analysis, including radiation shielding and fusion neutronics.

The early work was mainly funded from the EMERALD and TOPAS reactor physics projects in the SAFIR and SAFIR 2010 research programmes. In SAFIR 2014, the development of Serpent was gathered under the KÄÄRME project. Serpent is currently developed by a five-member team, with significant contributions from active users around the world. Development of Serpent continues in SAFIR 2018 under the MONSOON and KATVE projects. A comprehensive and up-to-date description of

the code is found at Serpent website (<http://montecarlo.vtt.fi>) or a summary review to be published in *Annals of Nuclear Energy* (Leppänen, 2015a).

Goals and accomplishments of the KÄÄRME project

The main goal of the KÄÄRME project was to complete the methodology for spatial homogenization, and to demonstrate the feasibility of the continuous-energy Monte Carlo method in the production of input data for deterministic reactor simulator calculations. This topic is covered in a special article in this report, and the following subsections focus on other major tasks.

Development of Serpent 2

When the KÄÄRME project was launched in 2011, it had become apparent that certain features developed in Serpent originally for the purpose of optimizing the calculation routines for 2D assembly-level calculations resulted in serious limitations when the code was used for large-scale problems. The main issue was the excessive memory demand in burnup calculations, which became a limiting factor when the applications moved from 2D to 3D geometries. Similar limitations resulted from the methodology used for parallel calculation. Parallelization was based on the Message-Passing Interface (MPI), a distributed-memory technique, which meant that the memory demand was multiplied by the number of parallel tasks. These limitations made it practically impossible to run burnup calculations for research reactors or 3D fuel assembly geometries. Even more importantly, the parallelization scheme based on MPI meant that Serpent was unable to fully utilize the computing power of multi-core workstations and computer clusters.

In order to fix the problems with excessive memory usage, the source code was completely re-written, starting from October 2010. The capability to run large burnup calculation problems was accomplished by introducing different optimization modes for assembly- and core-level calculations (Leppänen, 2012), and parallelization based on shared-memory OpenMP allowed the calculations to be distributed over multiple CPU cores without increasing the memory footprint. Serpent is currently capable of handling tens or even hundreds of thousands of depletion zones in burnup calculation, without limitations in parallelization.

The new version became to be known as Serpent 2, and it was made available by request to registered users of Serpent 1 for beta-testing purposes in early 2012. Development of new features and capabilities was completely shifted to Serpent 2 by the end of the KÄÄRME project, and public release is scheduled for late 2015. Further work on Serpent 1 is not completely frozen, but there has been no new updates since April 2013.

Supporting work for coupled multi-physics simulations

Work on multi-physics simulations started within the KÄÄRME project, but was later moved into its own project outside SAFIR 2014, when funding specifically devoted to the development of coupled neutronics / thermal hydraulics calculations was granted by the Academy of Finland in 2012 (Leppänen, 2015b). Most of the early work was focused on a new temperature treatment routine, capable of performing temperature corrections (Doppler-broadening) on microscopic cross sections on-the-fly (Viitanen, 2012a, 2012b). This routine currently forms the basis of the multi-physics coupling scheme developed for Serpent 2. The work also became the topic of a doctoral thesis, recently submitted for pre-examination (Viitanen, 2015).

In addition to thermal hydraulics coupling, Serpent has been successfully coupled to fuel performance codes. Much of this work has been carried in KÄÄRME, in collaboration with the PALAMA project of SAFIR 2014 (Viitanen, 2011; Valtavirta, 2012a, 2012b, 2013). The work continues within the MONSOON project of SAFIR 2018, with studies on the effects of realistic fuel temperature distributions on group constant generation.

Photon transport simulation mode

The transport routine in Serpent has shown good performance in neutron transport simulations involving reactors and other complex geometries, and the same routines are applicable to other particle types as well. Extending the transport capabilities from neutrons to photons was started in the KÄÄRME project already in 2011, but the development was put on hold for more than two years because of more urgent priorities. The work was finally continued in 2014, with the implementation of new photon interaction physics routines as part of an M.Sc. thesis project. The development was completed by the end of 2014 (Kaltiaisenaho, 2015).

The original motivation for developing photon transport capability is the simulation of gamma heating for coupled multi-physics applications. The methodology also makes it possible to run radiation shielding calculations, which became one of the topics of the KATVE project in SAFIR 2018.

Development of other features and capabilities

When the SAFIR 2014 programme was started in 2011, it was the only source of funding for Serpent development. Even though the topics later converged to spatial homogenization and photon transport, there are other significant features and capabilities developed in the Serpent code within the scope of the KÄÄRME project. This includes in particular the Chebyshev Rational Approximation Method (CRAM), used for solving the Bateman depletion equations in burnup calculation problems (Pusa, 2011, 2012, 2013a, 2013b, 2013c, 2013d, 2014).

Other major features include the calculation of adjoint-weighted delayed neutron fractions and point-kinetics parameters (Leppänen, 2014a) and statistical tests for the validity of Monte Carlo error estimates (Kaltiaisenaho, 2014a, 2014b). The idea

of extending the applications of Serpent from reactor physics to new fields, such as radiation shielding, has brought new challenges for geometry modelling as well. Work began in 2013 on the development of new unstructured mesh- and surface-based geometry routines, capable of reading the output from CAD and other engineering tools without conversion to standard CSG-based Monte Carlo geometry (Leppänen, 2014b, 2014c, 2015d). Part of this work has been carried out within scope of the KÄÄRME project.

International collaboration

Since the public release of Serpent 1 in May 2009, the user community has grown to almost 400 users in 125 universities and research organizations in 33 countries around the world. The applications of Serpent range from spatial homogenization and assembly-level burnup calculations to research reactor modelling and coupled multi-physics simulations.

Daily communication between the developer team and serpent users is handled via e-mail and a public discussion forum (<http://ttuki.vtt.fi/serpent/>). International user group meetings have been organized in different locations since 2011:

- 2011 – 1st International UGM in Dresden, Germany, Sept. 15-16, 2011
- 2012 – 2nd International UGM in Madrid, Spain, Sept. 19-21, 2012
- 2013 – 3rd International UGM in Berkeley, California, USA, Nov. 6-8, 2013
- 2014 – 4th International UGM in Cambridge, UK, Sept. 17-19, 2014

The last two meetings in Berkeley and Cambridge were three-day events, gathering some 35 active Serpent user from 20 different organizations around to world.

The Serpent team has actively participated in international conferences, such as M&C, PHYSOR, SNA and TopFuel, and a half-day Serpent workshop was organized in the latest PHYSOR 2014 reactor physics conference in Kyoto, Japan, in September 2014. Smaller invited lectures and workshops have been organized at three locations in Korea (2011), Ben-Gurion University of the Negev in Israel (2012), Culham Centre for Fusion Energy in the UK (2012), University of California, Berkeley (2012) and Texas A&M University (2014). The project manager takes part in the scientific activities of the American Nuclear Society (ANS), as an Executive Committee member of the Reactor Physics Division (RPD).

Education of new experts

The five-member project staff includes three young persons / graduate students and one member graduated with a doctoral degree in 2013. The typical Serpent user is an M.Sc. or Ph.D. student, using the code for academic research and thesis work. A total of 50 Doctoral, Master's and Bachelor-level theses have been written on Serpent-related topics worldwide since 2007, more than 20 of which in Finnish universi-

ties. The total number of peer-reviewed journal and conference publications is around 200.

Summary and future work

The development of the Serpent Monte Carlo reactor physics burnup calculation code was continued in the KÄÄRME project of SAFIR 2014. During the duration of the project the uses basis was increased from 60 to almost 400, and the range of applications was consequently considerably diversified. The KÄÄRME project, which started out as a general development project for the Serpent code eventually converged into a few specific research topics, including spatial homogenization and photon interaction physics.

These two topics also form a significant part of two research projects in SAFIR 2018: the MONSOON project, in which the Serpent code is developed into a practical tool for group constant generation and independent safety analyses of Finnish power reactors, and the KATVE project, in which the photon transport capabilities in Serpent are developed to cope with the needs and challenges of radiation shielding applications.

The work also continues outside the SAFIR 2018 research programme, under topics related to coupled multi-physics simulations and fusion neutronics. This work supports the common goals of developing advanced calculation methods for nuclear and radiation transport applications, enabling more rigorous safety analyses and education of a new generation of experts.

References

- Kaltiaisenaho, T. 2014a. Statistical tests and the underestimation of variance in Serpent 2. VTT-R-00371-14, VTT Technical Research Centre of Finland, 2014.
- Kaltiaisenaho, T. and Leppänen, J. 2014b. Analysing the Statistics of Group Constants Generated by Serpent 2 Monte Carlo Code. In proc. PHYSOR 2014, Kyoto, Japan, Sep. 28 - Oct. 3, 2014.
- Kaltiaisenaho, T. 2015. Implementing a photon physics model in Serpent 2. M.Sc. Thesis, Aalto University, 2015. (on-going).
- Leppänen, J. 2007. Development of a new Monte Carlo reactor physics code. D.Sc. Thesis, Helsinki University of Technology, 2007. (VTT Publications 640).
- Leppänen, J. and Isotalo, A. 2012. Burnup calculation methodology in the Serpent 2 Monte Carlo code. In proc. PHYSOR 2012, Knoxville, TN, Apr. 15-20, 2012.

- Leppänen, J., Aufiero, M., Fridman, E., Rachamin, R., and van der Marck, S. 2014a. Calculation of effective point kinetics parameters in the Serpent 2 Monte Carlo code. *Ann. Nucl. Energy*, 65 (2014) 272-279.
- Leppänen, J. and Aufiero, M. 2014b. Development of an Unstructured Mesh Based Geometry Model in the Serpent 2 Monte Carlo Code. In *proc. PHYSOR 2014, Kyoto, Japan, Sep. 28 - Oct. 3, 2014*.
- Leppänen, J. 2014c. Development of a CAD Based Geometry Model in Serpent 2 Monte Carlo Code. *Trans. Am. Nucl. Soc.*, 111 (2014) 663-667.
- Leppänen, J., Pusa, M., Viitanen, T., Valtavirta, V. and Kaltiaisenaho, T. 2015a. The Serpent Monte Carlo code: Status, development and applications in 2013. *Ann. Nucl. Energy*. (in press).
- Leppänen, J., Hovi, V., Ikonen, T., Kurki, J., Pusa, M., Valtavirta, V. and Viitanen, T. 2015b. The Numerical Multi-Physics project (NUMPS) at VTT Technical Research Centre of Finland. *Ann. Nucl. Energy*. (in press).
- J. Leppänen. 2015c. CAD-based geometry type in Serpent 2 – Application in fusion neutronics. In *proc. M&C 2015, Nashville, TN, April 19-23, 2015*. (submitted).
- Pusa, M. 2011. Rational approximations to the matrix exponential in burnup calculations. *Nucl. Sci. Eng.*, 169 (2011) 155-167.
- Pusa, M. and Leppänen, J. 2012. An efficient implementation of the Chebyshev rational approximation method (CRAM) for solving the burnup equations. In *proc. PHYSOR 2012, Knoxville, TN, Apr. 15-20, 2012*.
- Pusa, M. 2013a. Accuracy considerations for Chebyshev rational approximation method (CRAM) in burnup calculations. In *proc. M&C 2013, Sun Valley, ID, May 5-9, 2013*.
- Pusa, M. 2013b. Numerical methods for nuclear fuel burnup calculations. D.Sc. Thesis, Aalto University, 2013. (VTT Science 32)
- Pusa, M. and Leppänen, J. 2013c. Solving linear systems with sparse Gaussian elimination in the Chebyshev rational approximation method (CRAM). *Nucl. Sci. Eng.*, 175 (2013) 250-258.
- Pusa, M. 2013d. Correction to partial fraction decomposition coefficients for Chebyshev rational approximation on the negative real axis. [arXiv:1206.2880v1](https://arxiv.org/abs/1206.2880v1) [math.NA].
- Pusa, M. 2014. Higher-Order Chebyshev Rational Approximation Method (CRAM). In *proc. PHYSOR 2014, Kyoto, Japan, Sep. 28 - Oct. 3, 2014*.

- Valtavirta, V. 2013a. Internal Neutronics-temperature coupling in Serpent 2 -- Reactivity differences resulting from choice of material property correlations. In proc. M&C 2013, Sun Valley, ID, May 5-9, 2013.
- Valtavirta, V., Tulkki, V., Leppänen, J., and Viitanen, T. 2013b. The universal fuel performance code interface in Serpent 2. In proc. TopFuel 2013, Charlotte, NC, Sept. 15-19, 2013.
- Valtavirta, V., Viitanen, T., and Leppänen, J. 2014. Internal neutronics-temperature coupling in Serpent 2. Nucl. Sci. Eng., 177 (2014) 193-202.
- Viitanen, T. 2011. Serpent-ENIGMA - Combining Monte Carlo reactor physics with fuel performance. VTT-R-06265-11, VTT Technical Research Centre of Finland, 2011.
- Viitanen, T. and Leppänen, J. 2012a. Explicit treatment of thermal motion in continuous-energy Monte Carlo tracking routines. Nucl. Sci. Eng., 171 (2012) 165-173.
- Viitanen, T. and Leppänen, J. 2012b. Explicit temperature treatment in Monte Carlo neutron tracking routines – First results. In proc. PHYSOR 2012, Knoxville, TN, Apr. 15-20, 2012.
- Viitanen, T. 2015. Development of a stochastic temperature treatment technique for Monte Carlo neutron tracking. D.Sc. Thesis, Aalto University, 2015. (in pre-examination).

12.2 Group constant preparation with Serpent

Jaakko Leppänen, Maria Pusa

VTT Technical Research Centre of Finland Ltd
P.O. Box 1000, FI-02044 Espoo

Abstract

The Serpent Monte Carlo reactor physics code has been developed at VTT since 2004, and the code is currently distributed to 125 universities and research organizations in 33 countries around the world. One of the main user applications is the production of input parameters for deterministic fuel cycle and transient simulator codes, used for the design and safety analyses of nuclear reactors. This procedure is known as spatial homogenization, and Serpent is one of the first Monte Carlo codes specifically developed for this task. Development of calculation methods and techniques for Monte Carlo based homogenization also forms the main content of the KÄÄRME project in SAFIR2014, and the work continues in the new SAFIR2018 programme as well.

Introduction

The work on a Monte Carlo reactor physics code currently known as Serpent was started at VTT in 2004, with the idea of developing a simplified Monte Carlo based lattice physics code for spatial homogenization, i.e. the production of input parameters for full-scale fuel cycle and transient simulator calculations. The main reason for starting the work from scratch was the fact that general-purpose Monte Carlo codes available at the time were not particularly well suited for this task, which requires a certain level of specialization and the capability to simulate changes in fuel composition over the reactor operating cycle. The applications of Serpent have considerably diversified over the years along with the growing user community, but spatial homogenization still remains as one of the two major topics in code development. The early work was largely funded from the EMERALD and TOPAS reactor physics projects within the SAFIR and SAFIR2010 research programmes, and in SAFIR2014 Serpent development was carried out within its own project, with a special emphasis in spatial homogenization.

Serpent was released to public distribution for non-commercial research and educational use in 2009, and during the past six years the code has gathered an active user community of almost 400 users in 125 universities and research organizations in 33 countries around the world. The typical Serpent user is an M.Sc. or Ph.D. student, using the code for academic research, and a total of 50 doctoral, master's and bachelor-level theses have been written on Serpent-related topics since 2007. The total number of peer-reviewed journal and conference publications is around 200.

The code is currently developed by a five-member team at VTT, supported by feedback and contributions from active users around the world.

Spatial homogenization

The modelling of an operating nuclear reactor deals with a complicated problem, involving tight coupling between core neutronics, heat transfer and coolant flow. Fuel depletion and physical feedbacks between fission power and material temperatures and densities turn an already difficult-to-solve linear neutron transport problem into a non-linear problem, which in practice requires iterative solution. Obtaining a full-scale solution for a single operating state using heterogeneous high-fidelity transport methods is barely within the capabilities of modern super-computers, but since reactor design and safety analyses often necessitate repeating the calculations for a number of different operating conditions, this type of direct approach is not expected to become feasible in practice within the foreseeable future.

Instead, the traditional calculation chain applied in reactor analysis proceeds in stages, in which the physics of the problem is gradually simplified, while simultaneously moving towards larger spatial scale. This multi-stage calculation scheme can be roughly divided in three steps:

- 1) Production of nuclide-wise microscopic interaction data for neutron transport codes from evaluated nuclear data
- 2) Solution of the heterogeneous transport problem at fuel assembly level, and production of assembly-specific group constants
- 3) Solution of the homogeneous full-scale transport problem, coupled to heat transfer and coolant flow

The output from each step serves as the input for the next step in the chain. Evaluated nuclear data, which represents the best available knowledge on neutron interactions with matter, is first processed into reaction cross sections, which together with a detailed geometry description are used to obtain a heterogeneous solution to the transport problem at fuel assembly level. This solution is then used to condense the physics into a handful of parameters called homogenized group constants, which are used for obtaining the full-scale solution in final stage of the calculation chain. When the procedure is performed by preserving the local reaction rate balance at each stage, the solution to the coupled problem can be obtained at an acceptable computational cost without compromising the accuracy.

In LWR analyses the core-level calculations are typically performed using deterministic fuel cycle and transient simulator codes, based on two-group nodal diffusion methods. The input data consists of spatially homogenized group constants, including:

- 1) Reaction cross sections, representing the rates of absorption, fission, fission neutron and energy production, etc.

- 2) Scattering removal cross sections, determining the transfer of neutrons from fast to thermal energy group
- 3) Diffusion coefficients, characterizing the migration distance of neutrons in the homogenized medium
- 4) Assembly discontinuity factors, used for coupling the intra-nodal flux solutions together into a global full-core solution

The cost of reducing the complexity of transport physics by homogenizing the geometry at assembly level is that the dependence of the solution on local operating conditions is lost. This information is needed for modelling fuel depletion and reactivity feedbacks, and in order to recover the necessary dependencies the data is provided separately for different fuel burnups and state points. In practice this implies repeating the homogenization calculations for different assembly types, accounting for the changes in fuel composition with increasing burnup, and performing a number of branch calculations by varying fuel temperature, moderator density, boron concentration, insertion of control rods and other parameters reflecting the dependence of neutronics on local operating conditions.

Spatial homogenization is traditionally performed using 2D deterministic lattice transport codes. The idea of replacing these codes with continuous-energy Monte Carlo simulation is not new, but Serpent is one of the first codes specifically developed for this task. Monte Carlo codes are inherently three-dimensional, and capable of handling complex geometries without approximations. Neutron interaction data used in the transport simulation can be obtained from the evaluated nuclear data files without converting cross sections into application-specific multi-group form, which means that the same calculation code can be used for producing group constants for any fuel or reactor type.

The Monte Carlo method also has its drawbacks. The transport simulation is computationally expensive to run, and covering all assembly types, burnups and reactor operating conditions takes considerable time. Since the method has not been used for spatial homogenization in a routinely manner, accomplishing this task has required developing new calculation techniques, often by method of trial and error.

Methodology developed in Serpent

When the KÄÄRME project was launched in 2011, Serpent had the capability to perform transport simulations and produce some of the group constants required for nodal diffusion calculations (Leppänen, 2007). The code also had a built-in fuel depletion module, based on the Chebyshev Rational Approximation method (CRAM), which was the topic of a doctoral thesis completed during the project (Pusa, 2013). The code also had some serious problems with excessive appetite for computer memory, and the parallel calculation scheme was not well adapted to computer clusters with a large number of CPU cores. In order to correct these flaws,

the source code was completely re-written. The development of a new code version, Serpent 2, became the first major topic of the KÄÄRME project.

The most difficult group constant to produce using the Monte Carlo method is the diffusion coefficient, which essentially requires combining rigorous transport simulation with a crude deterministic approximation. There are several techniques derived for calculating this coefficient, implemented in Serpent and other Monte Carlo codes, which, however, produced less than satisfactory results. The problem was eventually solved by revising the entire methodology used for group constant generation and switching to a semi-deterministic approach used successfully in deterministic lattice transport codes (Fridman, 2013a).

Other standard methodologies adopted from deterministic codes include the calculation of leakage-corrected cross sections by solution of the B_1 equations (Fridman, 2011, 2012) and implementation of a homogeneous diffusion flux solver for producing assembly discontinuity factors and form factors for pin-power reconstruction in geometries homogenized by accounting for their immediate surroundings. Serpent users, in particular at the Helmholtz-Zentrum Dresden-Rossendorf (HZDR) provided invaluable contribution and feedback in the development of these methodologies.

Taking the semi-deterministic approach ensured compatibility with state-of-the-art core simulator codes, while still maintaining the advantages of the Monte Carlo method, and the option to develop the methodology of spatial homogenization beyond its current capabilities. By the end of 2014, Serpent was capable of producing all input parameters needed for full-core nodal diffusion calculations. The last year of the project was largely devoted to code validation and development of an automated calculation sequence capable of performing branch calculations necessary for covering all reactor operating conditions with minimal user effort.

Applications

The main motivation for using the continuous-energy Monte Carlo method for reactor analysis is its inherent capability to handle geometry and interaction physics without major approximations. When used for spatial homogenization, Monte Carlo codes also have the advantage of being able to model the full-scale heterogeneous problem, which represents the best available reference solution for the calculation scheme. Serpent-generated group constants have been validated in particular for the Serpent-DYN3D code sequence at HZDR. Test calculations involving various PWR (Fridman, 2011, 2012, 2013a, 2013b; Duerigen 2012), SFR (Fridman 2013c, 2013d; Rachamin 2013; Nikitin, 2015) and HTGR (Baier, 2014) cores have shown good agreement in both full-scale comparisons to three-dimensional Serpent calculations and assembly-level comparisons to deterministic lattice transport codes HELIOS 1.9 and ECCO/ERANOS 2.1.

Other similar comparisons include full-scale calculations with Serpent-PARCS at the Paul Scherrer Institute (PSI) (Hursin, 2013) in Switzerland, the Royal Institute of Technology (KTH) (Ghasabyan, 2013) in Sweden, and University of Michigan (Hall,

2013, 2014) and Brookhaven National Laboratory (BNL) (Brown, 2013b, 2014) in the U.S. Assembly-level comparisons to CASMO-5 lattice code have been performed at PSI (Hursin, 2013; Canepa, 2013), comparisons to WIMSD at Institut Josef Stefan (IJS) (Ćalić, 2012) in Slovenia, comparisons to DRAGON at the École Polytechnique de Montréal, (Harrisson, 2012) and comparisons to TRITON-NEWT and BOXER at BNL (Brown et al., 2013a).

The advantages of continuous-energy Monte Carlo calculation also become apparent when used to support the development of new methods for core analysis (Duerigen, 2013; Baier, 2014; Daeubler, 2014; Hou, 2015, Jareteg, 2014, Bilodid 2014). Moving from two- to three-dimensional methods in homogenization becomes important in the modelling of complicated systems, and practically a necessity when generating group constants for next-generation fuel and reactor types with strong axial heterogeneities (Herman, 2011). A good example of extending the conventional methods of homogenization to three dimensions is the introduction of axial discontinuity factors in nodal diffusion calculations performed for Resource-Renewable BWR (RBWR) cores, with alternating seed and blanket layers inside the fuel assemblies (Hall, 2013; Fridman, 2013b; Ward, 2014).

One of the long-term goals for Serpent development is to use the code as the primary tool for producing group constants for fuel cycle and transient simulator codes used for reactor safety analyses at VTT. The work started in the KÄÄRME project in 2013, with the validation of the Serpent-ARES calculation sequence using the MIT BEAVRS benchmark (Horelik, 2013) as the test case. In the first phase of the study, the ARES core simulator was used to model the hot zero-power initial core of a 1000 MW Westinghouse PWR using Serpent-generated group constants (Leppänen, 2014). The calculations were compared to a Serpent 3D reference solution. The results turned out to be in good agreement at both assembly and pin-level. Differences in radial assembly-wise power distributions ranged from -1.6 to 0.6% at core mid-plane, and the reconstructed pin-powers were off by less than 1% in 82% of all fuel pins. Axial power distributions were also in good agreement, and the dominating error source was the local depression in thermal flux caused by grid spacers, which in the ARES model were homogenized in the group constants.

The study has been continued to hot full-power calculations with thermal hydraulic feedback, and work is currently under way for simulating the first operating cycle of the BEAVRS core. The overall computational cost of using Monte Carlo for producing the full set of group constants was assessed in separate study (Leppänen, 2014), in which it was concluded that although computationally expensive, accomplishing this task is within the capabilities of modern computer clusters. Serpent has also been used for producing group constants for the initial core of the EPR reactor, modelled using the TRAB3D transient simulator code (Sahlberg, 2014).

Summary, conclusions and future work

The Serpent Monte Carlo reactor physics code has been developed at VTT since 2004, and the code is currently used in 125 universities and research organizations

in 33 countries around the world. One of the main applications is spatial homogenization, i.e. the production of input parameters for deterministic fuel cycle and transient simulator codes. Serpent is one of the first Monte Carlo codes specifically developed for this task, which also forms the main content of the KÄÄRME project in SAFIR2014.

Serpent has been used for generating group constants for various core simulators, such as DYN3D and PARCS, mainly for the purpose of developing new transport methodologies and validating the calculation sequence for various applications involving contemporary and advanced LWR and Gen-IV reactor technology. At VTT, work is currently under way for the validation of the Serpent-ARES code sequence for LWR fuel cycle simulations.

The work on Monte Carlo based group constant generation continues in the MONSOON project of the SAFIR2018 research programme. One of the major goals is to develop Serpent into a routine calculation tool capable of producing input data for all deterministic core simulators used at VTT, including ARES, TRAB3D, HEXTRAN and HEXBU. These codes provide the means to perform independent safety analyses for Finnish power reactors using state-of-the-art calculation methods, supported by comprehensive understanding of the underlying physics.

Whereas the KÄÄRME project focused on group constant generation for conventional nodal diffusion calculations, the MONSOON project proceeds to new methodologies, taking advantage of the specific features of Serpent and continuous-energy Monte Carlo simulation. This includes moving from 2D to 3D geometries in spatial homogenization, for the purpose of better accounting for strong axial heterogeneities in core-level calculations, and new options for state-point parametrization, taking advantage of the multi-physics capabilities in the Serpent code.

References

- Baier, S., Fridman, E., Kliem, S. and Rohde, U. 2014. Extension and application of the reactor dynamics code DYN3D for Block-type High Temperature Reactors. *Nucl. Eng. Design*, 271 (2014) 431-436.
- Bilodid, Y., Fridman, E., Margulis, M., Kotlyar, D. and Shwageraus, E. 2014. Verification of the Spectral History Correction Method with Fully Coupled Monte Carlo Code BGCore. In *proc. PHYSOR 2014, Kyoto, Japan, Sep. 28 - Oct. 3, 2014*.
- Brown, N., Ludewig, H., Aronson, A., Raitses, G., and Todosow, M. 2013a. Neutronic evaluation of a PWR with fully ceramic microencapsulated fuel. Part I: Lattice benchmarking, cycle length, and reactivity coefficients. *Ann. Nucl. Energy*, 62 (2013) 538-547.
- Brown, N., Ludewig, H., Aronson, A., Raitses, G., and Todosow, M. 2013b. Neutronic evaluation of a PWR with fully ceramic microencapsulated fuel.

Part II: Nodal core calculations and preliminary study of thermal hydraulic feedback. *Ann. Nucl. Energy*, 62 (2013) 548-557.

- Brown, N., Aronson, A., Todosow, M., Brito, R. and McClellan, K. 2014. Neutronic performance of uranium nitride composite fuels in a PWR. *Nucl. Eng. Design*, 275 (2014) 393–407.
- Čalić, D., Trkov, A., and Kromar, M. 2012. Neutron multigroup homogenized cross section determination with the Monte Carlo method. In *proc. 21st International Conference Nuclear Energy for New Europe 2012*, Ljubljana, Slovenia, Sept. 5-7, 2012.
- Canepa, S., Hursin, M., Ferroukhi, H., and Pautz, A. 2013. Preparation of nuclear libraries with deterministic and stochastic methods for for LWR reflectors. In *proc. M&C 2013*, Sun Valley, ID, May 5-9, 2013.
- Daeubler, M., Jimenez, J. and Sanchez, V. 2014. Generation and Application of Interface Discontinuity Factors in the Reactor Simulator DYN3D. In *proc. ICAPP 2014*, Charlotte, NC, Apr. 6-9, 2014.
- Duerigen, S. and Fridman, E. 2012. The simplified P3 approach on a trigonal geometry of the nodal reactor code DYN3D. *Kerntechnik*, 77 (2012) 226-229.
- Duerigen, S. 2013. Neutron Transport in Hexagonal Reactor Cores Modeled by Trigonal-Geometry Diffusion and Simplified P3 Nodal Methods. Ph.D. Thesis, Karlsruhe Institute of Technology, 2013.
- Fridman, E. and Leppänen, J. 2011. On the use of the Serpent Monte Carlo code for few-group cross section generation. *Ann. Nucl. Energy*, 38 (2011) 1399-1405.
- Fridman, E. and Leppänen, J. 2012. Revised methods for few-group cross section generation in the Serpent Monte Carlo code. In *proc. PHYSOR 2012*, Knoxville, TN, Apr. 15-20, 2012.
- Fridman, E., Leppänen, J., and Wemple, C. 2013a. Comparison of Serpent and HELIOS-2 as applied for the PWR few-group cross section generation. In *proc. M&C 2013*, Sun Valley, ID, May 5-9, 2013.
- Fridman, E., Duerigen, S., Bilodid, Y., Kotlyar, D., and Shwageraus, E. 2013b. Axial discontinuity factors for the nodal diffusion analysis of high conversion BWR cores. *Ann. Nucl. Energy*, 62 (2013) 129-136.
- Fridman, E. and Shwageraus, E. 2013c. Modeling of SFR cores with Serpent-DYN3D codes sequence. *Ann. Nucl. Energy*, 53 (2013) 354-363.

- Fridman, E., Rachamin, R., and Shwageraus, E. 2013d. Generation of SFR few-group constants using the Monte Carlo code Serpent. In proc. M&C 2013, Sun Valley, ID, May 5-9, 2013.
- Ghasabyan, L. 2013. Use of Serpent Monte Carlo code for development of 3D full-core models of Gen-IV fast-spectrum reactors and preparation of group constants for transient analyses with PARCS/TRACE coupled system. M.Sc. Thesis, Royal Institute of Technology, 2013.
- Hall, A., Xu, Y., Ward, A., Downar, T., Shirvan, K. and Kazimi, M. 2013. Advanced neutronics methods for analysis of the RBWR-AC. *Trans. Am. Nucl. Soc.*, 108 (2013) 771-774.
- Hall, A., Downar T., Ward A., Jarret M., Wysocki A., Xu Y. and Shirvan K. 2014. Advanced Methods Development for Equilibrium Cycle Calculations of the RBWR. In proc. ICAPP 2014, Charlotte, NC, Apr. 6-9, 2014.
- Harrison, G. and Marleau, G. 2012. Computation of a Canadian SCWR unit cell with deterministic and Monte Carlo codes. In proc. PHYSOR 2012, Knoxville, TN, Apr. 15-20, 2012.
- Herman, B., Shwageraus, E., Leppänen, J. and Forget, B. 2011. Cross section generation strategy for advanced LWRs. In proc. ICAPP 2011, Nice, France, May 2-5, 2011.
- Horelik, N., Herman, B., Forget, B. and Smith, K. 2013. Benchmark for Evaluation and Validation of Reactor Simulations (BEAVRS), v1.0.1. In proc. M&C 2013, Sun Valley, ID, May 5-9, 2013.
- Hou, J., Choi, H. and Ivanov, K. 2015. Development of an iterative diffusion-transport method based on MICROX-2 cross section libraries. *Ann. Nucl. Energy*, 77 (2015) 335-342.
- Hursin, M., Vasiliev, A., Ferroukhi, H. and Pautz, A. 2013. Comparison of Serpent and CASMO-5M for pressurized water reactors models. In proc. M&C 2013, Sun Valley, ID, May 5-9, 2013.
- Jareteg, K., Vinai, P. and Demazière, C. 2014. Fine-mesh deterministic modeling of PWR fuel assemblies: Proof-of-principle of coupled neutronic/thermal-hydraulic calculations. *Ann. Nucl. Energy*, 68 (2014) 247–256.
- Leppänen, J. 2007. Development of a new Monte Carlo reactor physics code. D.Sc. Thesis, Helsinki University of Technology, 2007. (VTT Publications 640).

- Leppänen, J., Mattila, R., and Pusa, M. 2014. Validation of the Serpent-ARES code sequence using the MIT BEAVRS benchmark - Initial core at HZP conditions. *Ann. Nucl. Energy*, 69 (2014) 212-225.
- Leppänen, J. and Mattila, R. 2014. On the Practical Feasibility of Continuous-Energy Monte Carlo in Spatial Homogenization. In *proc. PHYSOR 2014*, Kyoto, Japan, Sep. 28 - Oct. 3, 2014.
- Nikitin, E., Fridman, E. and Mikityuk, K. 2015. Solution of the OECD/NEA neutronic SFR benchmark with Serpent-DYN3D and Serpent-PARCS code systems. *Ann. Nucl. Energy*, 74 (2015) 492-497.
- Pusa, M. 2013. Numerical methods for nuclear fuel burnup calculations. D.Sc. Thesis, Aalto University, 2013. (VTT Science 32).
- Rachamin, R., Wemple, C., and Fridman, E. 2013. Neutronic analysis of SFR core with HELIOS-2, Serpent, and DYN3D codes. *Ann. Nucl. Energy*, 55 (2013) 194-204.
- Sahlberg, V. 2014. Development of Serpent 2 - TRAB3D code sequence. Special assignment, Aalto University, 2014. (VTT-R-04538-14).
- Ward, A., Hall, A. and Downar, T. 2014. A Preliminary analysis of the accuracy of homogenized 2D cross sections in 3D nodal calculation of BWRs. In *proc. PHYSOR 2014*, Kyoto, Japan, Sep. 28 – Oct. 3., 2014.

13. Neutronics, nuclear fuel and burnup (NEPAL)

13.1 NEPAL summary report

Pertti Aarnio¹, Jarmo Ala-Heikkilä¹, Aarno Isotalo¹, Markus Ovaska¹, Antti Rintala^{1,2},
Ville Valtavirta^{1,2} & Risto Vanhanen¹

¹Aalto University School of Science
P.O. Box 11000, FI-00076 AALTO

²Current affiliation: VTT Technical Research Centre of Finland Ltd
P.O. Box 1000, FI-02044 Espoo

Abstract

Our first focus area in the NEPAL project has been accurate burnup calculations that aim at finding rare but potentially problematic nuclides like strong absorbers or other reactor-physically important nuclides. Additionally, it is important to know accurate concentrations of nuclides that are important for spent fuel disposal or nuclear safeguards. Using the most accurate methods, one can naturally opt for the old accuracy that can be reached with a reduced computational time.

Our second focus area has been the behaviour of nuclear fuel in a quasi-stationary situation. Traditionally the characteristics of fuel pellets are described on the basis of empirical data. Reliable modeling outside of the normal operating parameter range necessitates thorough understanding of the phenomena and their modelling in a mesoscopic scale. Still, behaviour of a porous, chemically complex medium in a radiation field is a challenge to model. We have developed a novel mesoscopic model of the thermal creep failure of fuel pellets. The model includes damage accumulation from radiation-induced fission gas buildup and the behaviour of the gases themselves.

Introduction

The Fission and Radiation Physics Group at Aalto University School of Science concentrates on developing calculation methods for reactor physics, modeling basic physical and chemical phenomena in nuclear fuel, and researching new fuel cycles and next generation nuclear reactors. The activities seamlessly combine education and research of nuclear engineering. The essential field of know-how of the group covers physics-based analyses and numerical computation.

In the SAFIR2014 research programme, we had a 4-year project named NEPAL (Neutronics, nuclear fuel and burnup). The volume was 1.5-2 person-years per calendar year. We had three main themes: accurate methods for burnup calculations, coupling of the temperature distribution in a fuel pellet to neutronics, and joint modeling of thermal creep and fission gas diffusion in nuclear fuel. In this summary, we concentrate on the first and third theme, since the second theme was continued at VTT from 2012 onwards. The NEPAL share of this research has been documented in the SAFIR2014 mid-term proceedings and its references.

Accurate methods for burnup calculations

Most burnup calculations, and in particular all Monte Carlo burnup calculations, combine sequential steady state neutronics and depletion calculations with a coupling scheme. On each step, the scheme uses one or more neutronics solutions and possible preliminary depletion calculations to predict representative step average values for the one-group cross sections and flux for use in the depletion calculations. Traditionally coupling schemes have used only zeroth or first order predictions.

We have developed new higher order neutronics-depletion coupling schemes (Isotalo & Aarnio 2011a). These methods are based on using data from the previous step to form higher order predictions about the future development of the cross sections and flux. This allows linear extrapolation to replace the old constant one on the predictor and quadratic interpolation to replace linear one on the corrector.

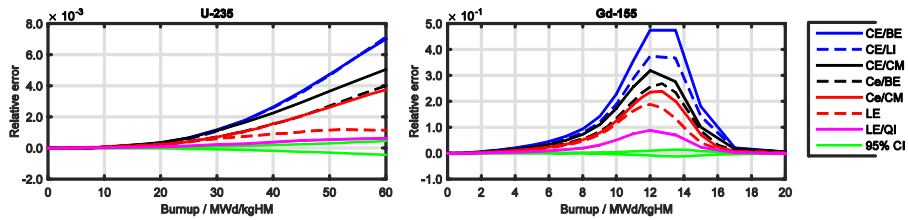


Figure 1. Relative errors for U-235 and Gd-155 in a PWR assembly test case with various methods using nearly equal amounts of CPU time. LE and LE/QI are some of our new methods.

The coupling is further improved by dividing the steps to substeps which are solved sequentially (Isotalo & Aarnio 2011b). This allows piecewise constant, rather than constant, approximation of the predicted behavior to be used in the actual depletion calculations. Higher order predictions and substeps complement each other, and together greatly improve the performance of burnup calculations. The higher order coupling schemes and substeps were implemented to the release branch of Serpent Monte Carlo code (Leppänen 2013) starting from version 2.0. The results are, however, not Serpent-specific and can be applied to other codes using similar methods.

Existing Monte Carlo burnup codes suffer from xenon driven spatial oscillations in large geometries (Isotalo et al. 2013). This instability was shown to be, at least in some cases, inherent to the simulation models typically used, and hence cannot be removed simply by reducing step lengths. Forcing xenon and flux to a mutual equilibrium offers a simple solution to these oscillations. Since the equilibrium calculation can be integrated to normal Monte Carlo neutronics, it has only a minor effect on running times and can be used with any burnup calculation algorithm. Furthermore, at least the equilibrium iteration algorithm of Serpent can significantly improve flux convergence in large geometries with a high dominance ratio.

Oscillations driven by fuel burnup still arise if too long steps are used, but unlike xenon oscillations, these only occur with long steps, allowing calculations to be performed with reasonable step lengths. This is a major improvement, especially in cases where stable solutions simply could not be obtained without the equilibrium method.

The work on advanced coupling schemes and equilibrium xenon was summed up in the doctoral dissertation of Aarno Isotalo (Isotalo 2013). After the completion of the thesis, work has continued on a more comprehensive comparison of different coupling schemes. There was a severe lack of comparisons between even the oldest methods. Moreover, we found out that there are significantly more methods in use than could be inferred from the literature, since authors have failed to make a distinction between several different schemes.

A two part study (Isotalo & Sahlberg 2014, Isotalo 2014) has largely amended the shortcomings of prior research and shows our new methods to be superior to all the

tested old methods. The results also allow the old methods to be ranked by accuracy, which is valuable for the wide range of users still relying on these methods. However, one more old method as well as other new methods still remain unaccounted for, and will hopefully be remedied in future studies.

After some delays, a post-doc (Aarno Isotalo) was sent to the Oak Ridge National Laboratory in the USA. He started there in June 2014. The research at ORNL has thus far focused on the CRAM depletion solver developed at VTT. CRAM is an extremely promising method for depletion calculations, i.e., solving the Bateman equations with constant coefficients. However, the original method does have two limitations. First, it cannot be used for problems with external feed. Second, while CRAM is generally very accurate in terms of absolute errors, it may produce essentially unbounded relative errors in pure decay problems, which limits the generality and reliability of the method. Similar behavior is also possible with non-zero flux if the initial composition contains short-lived nuclides that are far from their secular equilibrium levels. Solutions were developed for both of these limitations.

External feed can be modeled by representing the source term as the decay of imaginary nuclides with no removal (Isotalo & Wieselquist 2015a). By chaining such nuclides, even polynomially time dependent feed rates can be modeled. When this is done correctly, the new system can be solved with CRAM as accurately as problems without external feed. It was also discovered that while the accuracy of CRAM is unaffected by step lengths, it improves rapidly and reliably over subsequent steps with identical lengths and reaction rates (Isotalo & Wieselquist 2015b). This can be exploited by dividing steps to equidistant substeps (not to be confused with the substeps in the coupling schemes). This allows even decay problems, where CRAM has previously been less accurate and reliable, to be solved with ten correct digits for all nuclides with atomic fraction above an arbitrary threshold. Furthermore, such substeps can be solved much faster than an equal number of regular steps by recycling the LU-decompositions required in CRAM (Isotalo & Wieselquist 2015b).

Combined, the new capabilities mean that CRAM can now be used for any and all depletion calculations with extremely high accuracy and reliability. CRAM depletion solver with the above-mentioned source term and substepping capabilities was implemented to the widely used ORIGEN code developed at ORNL.

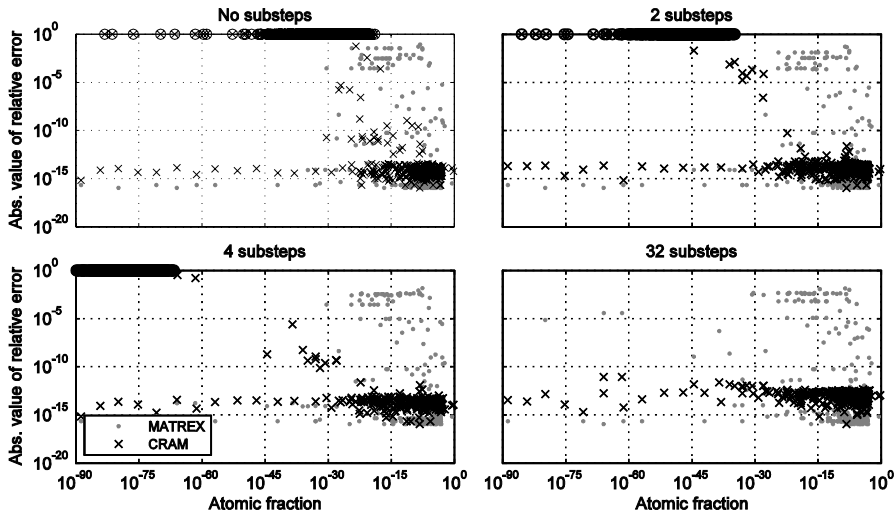


Figure 2. Relative errors for individual nuclides after decaying used fuel over a single 365-day step with different numbers of substeps with CRAM and MATREX (the original solver of ORIGEN). Circles mark errors that have been reduced to 1 for plotting.

Joint modelling of thermal creep and fission gas diffusion in nuclear fuel

The microstructure of nuclear fuel changes significantly during reactor operation. As fuel undergoes fission, heat and fission products are released. Since oxide fuels have low heat conductivity, the center of a fuel pellet becomes hotter than the outer region. An uneven temperature distribution causes radial fragmentation during early stages of a fuel pellet's lifetime. Thermal creep due to thermal stress leads to further microcracking over time.

In addition to thermomechanical effects, fission products play an important role in the microstructural evolution of fuel. Stable gases, such as several isotopes of xenon and krypton, make up a significant portion of all fission products. Gas atoms diffuse inside the pellet, and eventually form bubbles both within grains (intragranular) and grain faces (intergranular). The formation of bubbles increases the porosity of fuel, causing swelling and lowering the thermal conductivity. Gas released from the fuel mixes with the fill-gas (pressurized helium) in the pellet-cladding gap, decreasing thermal conductivity between the pellet surface and cladding. The behavior of fission gases is an important safety issue, since they can potentially cause the fuel assembly to overheat, or lead to pellet-cladding interactions due to swelling. Economically it makes sense to use fuel up to higher burnups, but the amount of gaseous fission products increases with burnup as well.

Gas diffusion and thermal creep are coupled together. Both gas bubbles and microcracks make the fuel more porous over time. This can affect the rate of gas release due to gas diffusion occurring through pore networks in addition to atomistic diffusion. There is evidence of fission gas release via coalescing gas bubbles along the grain boundaries. The goal of this subproject is to combine porosity formation from thermal creep fracture and gas accumulation to the diffusion of generated gas within a fuel pellet.

We are developing a computational model for simulating the microstructural evolution of nuclear fuel (Ovaska 2013). The model includes damage accumulation from thermal creep deformation and from fission gas buildup within the pellet. Damage accumulation is linked with increasing porosity of the fuel, as microcracks and gas bubbles are formed. Diffusion of fission gases is simulated from the viewpoint of percolation theory: gas flows through interlinked pores, and can only reach the surface of the pellet through continuous pore pathways.

The basic components of the model were implemented into a computer code and tested in 2012, after which the model has been gradually improved in order to make it more realistic. Simultaneous evolution of porosity and gas concentration has been added to the model, as well as a mechanism for damage repair through pore closure. A main feature of simulation results is a rapid transition from low to high fission gas release, as the porosity of the pellet reaches the percolation threshold. The role of different damage accumulation mechanisms was studied in detail. It was found that the more homogeneously spread damage from gas bubble generation leads to significantly faster gas release than the randomly distributed creep damage due to microcracks (Ovaska & Alava 2014a).

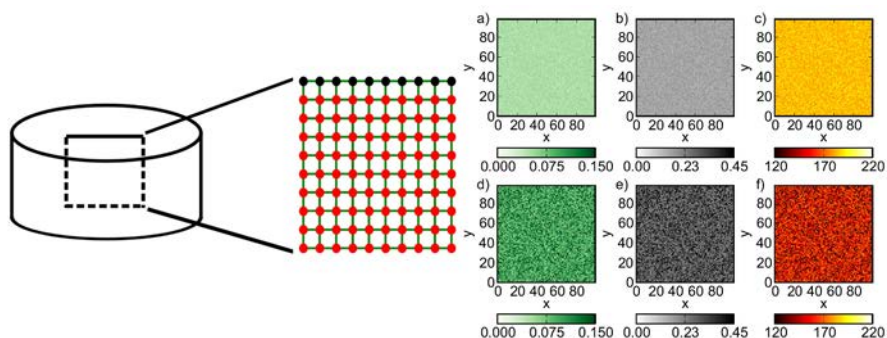


Figure 3. On the left: Schematic of the simulation system: A rectangular cross-section from a pellet. Gas nodes (red) are interconnected through bonds (green). Fission gas is released through the top boundary (black nodes). On the right: Example snapshots of porosity (a & d), damage (b & e) and Young's modulus in GPa (c & f). The top row (a-c) corresponds to the initial state, and the bottom row (d-f) shows a later stage when creep and radiation damage have weakened the pellet. (Ovaska & Alava 2014a)

The model was further refined in 2014. Damage accumulation from microcracks and fission gas bubbles are now treated as separate variables, and thus the pore geometry can be taken into account. Instead of a global percolation threshold, local percolation thresholds are calculated for each bond in the system according to the ratio of creep and gas damage it has sustained. An increase in relative microcrack density wrt. gas bubble density expedites gas release, as this effectively lowers the local percolation thresholds.

Another interesting result was obtained in simulations with creep damage accumulation coupled to damage repair. Varying the repair rate separated the release dynamics into two phases. With a slow repair rate, all gas is eventually released from the system, but a sufficiently high repair rate limits the gas release to the region close to the top boundary.

Instead of explicitly solving the diffusion equations, gas diffusion is now approximated by periodically searching for all boundary-connected bond clusters, and emptying all gas nodes linked to these clusters. The speed-up gained through this approximation allows us to use much larger system sizes without significantly affecting the accuracy of simulation results. The latest results were presented at the Nuclear Materials 2014 conference (Ovaska & Alava 2014b).

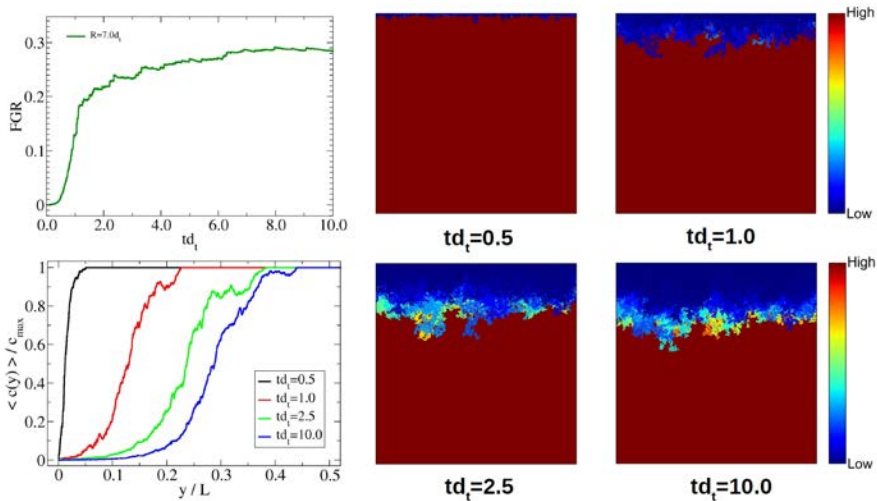


Figure 4. Example of a simulation run with creep damage and repair. Fractional gas release as a function of scaled time is shown in the top left panel. Snapshots of gas concentration at four different times reveal how gas gets released through the top boundary. The y-directional concentration profiles corresponding to these snapshots are also plotted in the bottom left panel. Here the damage repair rate is sufficiently high to limit gas release to the top part of the system. (Ovaska & Alava 2014b)

Conclusions

The objectives of the NEPAL project can be defined primarily as new calculation methods and scientific publications documenting them. Moreover, the new expertise in the field and the new experts themselves are important deliverables of the project. One DSc thesis, one MSc thesis and one BSc thesis were produced in the project, and all by different authors, so the project has reached its main objective.

Acknowledgement

The fruitful collaboration with the KÄÄRME and PALAMA projects of VTT in the SAFIR2014 programme, as well as with Oak Ridge National Laboratory is acknowledged.

References

- Isotalo, A.E., Aarnio, P.A., 2011a. Higher order methods for burnup calculations with Bateman solutions. *Annals of Nuclear Energy* 38, 1987--1995.
- Isotalo, A.E., Aarnio, P.A., 2011b. Substep methods for burnup calculations with Bateman solutions. *Annals of Nuclear Energy* 38, 2509--2514.
- Leppänen, J., 2013. Serpent – a Continuous-energy Monte Carlo Reactor Physics Burnup Calculation Code, VTT Technical Research Centre of Finland. (March 6, 2013). Serpent web site: <http://montecarlo.vtt.fi>.
- Isotalo, A.E., Leppänen, J., Dufek, J., 2013. Preventing xenon oscillations in Monte Carlo burnup calculations by enforcing equilibrium xenon distribution. *Annals of Nuclear Energy* 60, 78--85.
- Isotalo, A.E., 2013. Computational Methods for Burnup Calculations with Monte Carlo Neutronics. Doctoral dissertation, Aalto University (2013).
- Isotalo, A.E., Sahlberg, V., 2014. Comparison of Neutronics-Depletion Coupling Schemes for Burnup Calculations. Accepted for publication in *Nuclear Science and Engineering*.
- Isotalo, A.E., 2014. Comparison of Neutronics-Depletion Coupling Schemes for Burnup Calculations 2. Accepted for publication in *Nuclear Science and Engineering*.
- Isotalo, A.E., Wieselquist, W.A., 2015a. Method for Including External Feed in Depletion Calculations with CRAM and Implementation to ORIGEN. Submitted to *Annals of Nuclear Energy* (2015).
- Isotalo, A.E., Wieselquist, W.A., 2015b. Implementation of CRAM Depletion Solver with External Feed and Improved Accuracy into ORIGEN, Submitted to the M&C2015 conference to be held in Nashville, TN, April 19-23, 2015.
- Ovaska, M., 2013. Joint modelling of thermal creep and fission gas diffusion in nuclear fuel, Aalto University Technical Report FF-2013-01, 2013.
- Ovaska, M., Alava, M.J., 2014a. Joint modeling of thermal creep and radiation damage interaction with gas permeability and release dynamics: the role of percolation. Submitted to *Physica A* (2014).
- Ovaska, M., Alava, M.J., 2014b. Joint modelling of fission gas transport and creep fracture in nuclear fuels. The Nuclear Materials Conference NuMat2014, Clearwater Beach, Florida, 27-30 October, 2014.

14. Extensive fuel modelling (PALAMA)

14.1 PALAMA summary report

Asko Arkoma, Silja Häkkinen, Anitta Hämäläinen, Timo Ikonen, Seppo Kelppe,
Joonas Kättö, Henri Loukusa, Anna Nieminen, Jan-Olof Stengård,
Elina Syrjälahti, Ville Tulkki, Ville Valtavirta,
Tuomas Viitanen

VTT Technical Research Centre of Finland Ltd
P.O. Box 1000, FI-02044 Espoo

Abstract

PALAMA was a four-year project focused on fuel behaviour analysis. The scope contained traditional analysis and model development for fuel behaviour during normal operations and accidents, the fuel description in multiphysics analysis, sensitivity and uncertainty analysis, and own code development. The Halden Reactor Project, the French IRSN organization and the OECD/NEA WGFS working group are among the international research partners.

Introduction

Reactor fuel, as regards both its construction and materials, is a product under continuous development. The progress largely stems from measures for improved efficiency, particularly through striving for higher fuel discharge burnups. Revisions of the regulatory guides will set new limits for acceptable ranges of fuel use, and improved models and codes are required for assessments.

Investigation into the effects of increasing burnup has been ongoing for years with strong ties to experimental work performed at the OECD Halden Reactor Project. Methods for statistical approach at steady state conditions have been created but need to be implemented to the latest code versions. A statistical tool for transient analysis was created during SAFIR2010, and a verification of its capabilities was

performed in PALAMA. In-house development of the FINIX fuel behaviour module for multiphysics applications has been initiated as a part of the project. Active collaboration tasks with the US Pacific Northwest National Laboratory (PNNL) regarding the FRAPCON/FRAPTRAN code line, as well as with the IRSN and the SCANAIR RIA code are ongoing. These tools need to be developed and validated further, while their areas of application are concurrently widened.

The general goal of PALAMA project has been to develop and maintain competence and tools required for independent nuclear fuel behaviour assessment in both normal operation and accident conditions. The update to the regulatory guides created a need to better understand, describe and model phenomena related to increasing burnup and the statistical nature of the fuel rod behaviour. Investigation into so-called design extension conditions requires fuel behaviour studies broadened to include thermal hydraulics, reactor dynamics and severe accident phenomena. The increasing volume of the Finnish nuclear power production is posing new challenges as the load following operation may be required and its effects to the fuel performance must be understood. The fuel performance codes need to be systematically validated, and the creation of a framework for that purpose is one of the goals of the project.

The scope of PALAMA as presented in this report is divided between the basic fuel behaviour addressing issues of improved fuel performance modelling, statistical analysis relating to development and use of various statistical tools and methods, multiphysics work, and work done on validation and international benchmarking.

Fuel Behaviour

SCANAIR development

The SCANAIR code, developed by the Institut de Radioprotection et de Sûreté Nucléaire (IRSN), is designed for modelling the behaviour of a single fuel rod in the fast transient conditions during a reactivity initiated accident (RIA) in a PWR. In SCANAIR, the available fuel material properties and the thermal-hydraulics model are for PWR fuel and coolant conditions, respectively, but there are no similar models for BWR to be applied in a BWR RIA, the rod drop accident (RDA). Specifically, the code has lacked properties of Zircaloy 2 (Zry-2), the predominant BWR cladding material, and thermal hydraulic models for two-phase flow – the basic condition of the coolant in BWRs.

In a collaborative effort, new yield strength (YS) and ultimate tensile strength (UTS) laws based on the PROMETRA tests (a French cladding mechanical properties test programme) were fitted and implemented into SCANAIR. The new and old laws were compared by simulating the LS-1 and FK-1 tests performed in the NSRR facility in Japan (Arffman 2012).

The Zry-2 PCMI failure criterion was also addressed: a criterion based on Critical Strain Energy Density (developed by EPRI) was applied. Rods of the FK test series (11 tests on BWR fuel performed in NSRR) were simulated with SCANAIR using the

new UTS correlation. The results were found to be in alignment with those gained by EPRI using the FALCON code. The thermal hydraulic model of SCANAIR for the conditions in the NSRR tests (room temperature, atmospheric pressure, zero flow) was deduced to be adequate to describe the worst initial condition for an RDA, cold zero power (CZP).

The prospects of coupling a dedicated thermal hydraulic code to SCANAIR were investigated, and as a proof-of-concept case, GENFLO was coupled to SCANAIR. This allows for the simulation of two-phase (boiling) coolant.

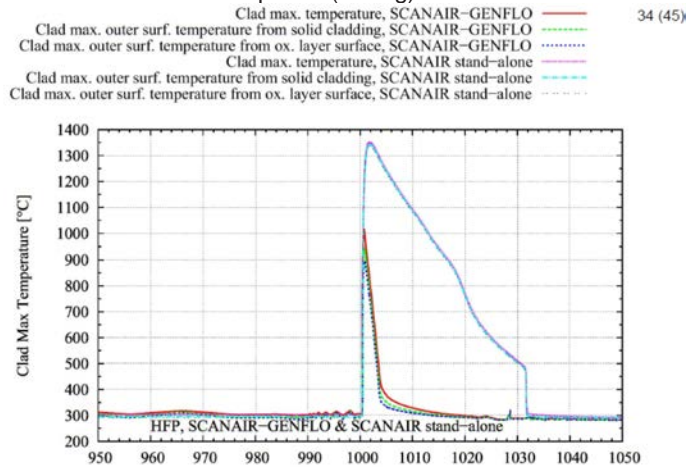


Figure 1. Comparison between the cladding maximum temperatures during RIA as given by standalone SCANAIR and SCANAIR-GENFLO.

Cladding creep

High temperatures and stress differential across the cladding wall causes the cladding tubes to plastically deform during its reactor life. This slow plastic deformation is called creep, and it is often separated into primary and secondary creep. Primary creep acts right after the stress change, and the secondary creep is the steady phase after the primary creep has actualized. Creep caused by static stress is relatively straightforward, but transient stress brings additional complications. Conventionally the stress changes are modelled assuming the strain hardening rule. However, the observations on the primary creep behaviour made in Halden experiments with on-line measurements do not support such assumption. A model based on the viscoelastic behaviour of materials has been developed in PALAMA (Tulkki 2011, Tulkki & Ikonen 2013, 2014a, 2014b, 2015). This model can reproduce the experimentally observed behaviour in a self-consistent way. Usually viscoelastic deformation in metals is thought to be small and fade under plastic primary creep. The operating environment, however, appears to enhance the viscoelastic behaviour in nuclear fuel cladding.

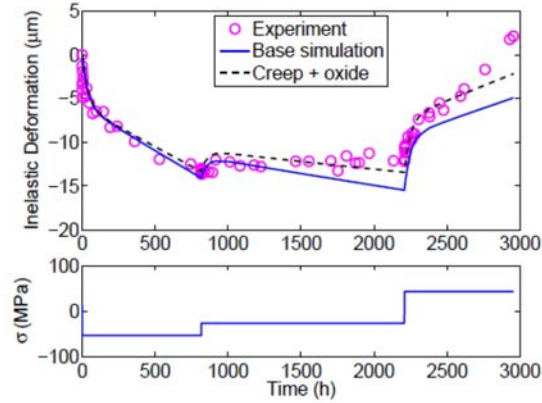


Figure 2. Performance of the new creep model in simulating Halden IFA-699 Zirc-4 creep experiment.

Cladding oxidation

A new model describing Zircaloy-4 cladding corrosion in steady-state reactor environment was created (Kättö 2013). In this model the cladding waterside surface oxide layer thickness is a function of oxide-metal interface temperature and exposure time. This model was programmed as a part of the ENIGMA fuel performance code, and simulation runs with the updated ENIGMA code were performed. The results were compared with measurement data and predictions provided by other corrosion models and show a distinct improvement on the old ENIGMA models.

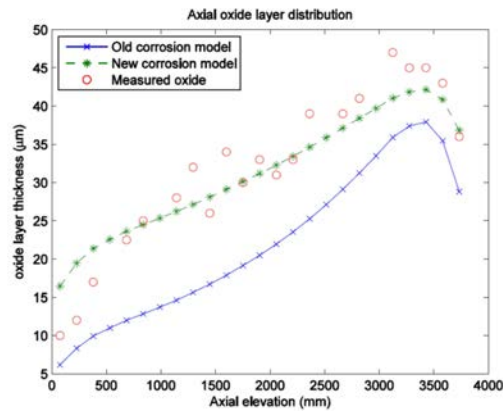


Figure 3. Comparison between the old and new corrosion model.

Chemistry of a fuel pellet

A computational module was developed in PALAMA for the calculation of thermo-chemical equilibria bearing in mind the application of the module to chemical phenomena in nuclear fuel (Loukusa 2014). Gibbs energy minimization principles set forth by Gunnar Eriksson in the SOLGASMIX program were applied for the calcula-

tion of thermochemical equilibria along with some improvements published in the literature. The program developed was tested and in many cases was found to calculate results comparable to other, established programs. Even difficult cases possible in the application of irradiated nuclear fuel were evaluated with the new program. Also, a simulation of oxygen potential in a nuclear fuel rod under irradiation was performed.

Other phenomena of interest

Introducing Finnish future reactors and recent amendments to the regulatory guides may require that advanced modes of operation and wider ranges of conditions be considered. New nuclear capacity combined with the planned wind power production would make a load following operation of NPPs a possibility. New regulatory guides allow fuel rod internal overpressure, as long as re-opening of the pellet-to-clad gap or “lift-off” is avoided. This brings additional requirements to the analysis codes, as the rod behaviour must be understood better than before in such an off-normal situation. Also, as severe accidents are a separate field of study, there exists a gap between the disciplines that should be bridged. All these subjects have been studied under PALAMA to gain better understanding of the phenomena involved (Kelppe et al. 2011, Tulkki et al. 2013, Arkoma & Tulkki 2013).

After Fukushima Daiichi accident there has been an increased interest in the development of Accident Tolerant Fuels. These fuel designs aim to improve fuel performance during accidents, and take after the development of both GenIV and actinide management designs. To keep abreast of these developments, the actinide fuels have been reviewed.

Statistical analysis

Numerical analysis

As a part of PALAMA, a statistical script for numerical analysis for the two steady state codes, ENIGMA and FRAPCON, has been created. A novel statistical method, the so-called Sobol' variance decomposition, was employed in the uncertainty and sensitivity analysis of the FRAPCON-3.4 code. A benchmark steady-state case was studied with both conventional correlation methods and with the variance decomposition technique (Ikonen & Tulkki 2014). It was shown that the variance decomposition method performs better in the case where the model has strong interactions between the uncertain input variables. For example, in the case of the gap width and gap conductance, these non-additive interactions can account for a significant amount of the output uncertainty. This result highlights the importance of considering case-appropriate uncertainty and sensitivity measures in the analysis of fuel performance codes. The script has been extended also to the transient code FRAPTRAN.

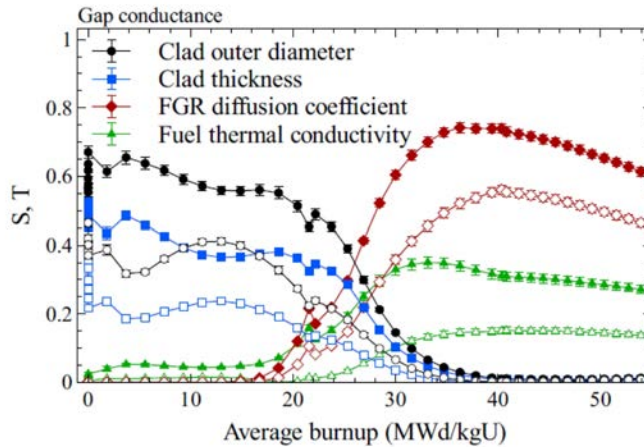


Figure 4. Contributors to the uncertainty in gap conductance. The open symbols refer to results given by traditional first-order methods, the filled symbols to the results from the variance decomposition technique.

Multiphysics

FINIX

In PALAMA, a new light-weight fuel behaviour code FINIX has been developed (Ikonen et al. 2013, 2014). FINIX is specifically designed for modeling of LWR fuel rods in multiphysics simulations and has been coupled with VTT's Monte Carlo reactor physics code Serpent 2, and reactor dynamics codes TRAB-1D, TRAB3D, and HEXTRAN. FINIX solves the time-dependent temperature distribution in the rod and the heat flux from the cladding to the coolant, allowing two-way coupling of the fuel behaviour simulation with both neutronics and thermal hydraulics simulations. Elastic and thermal mechanical deformations of the cladding can also be solved with FINIX. The stand-alone FINIX has been compared with FRAPTRAN-1.4 simulations and data from Halden experiments. The comparison reveals a good agreement in both cases. Coupled with Serpent, we have simulated both steady-state cases and a fast reactivity transient with the fuel temperature and fission power solved self-consistently. With VTT's reactor dynamics codes, FINIX has been used in the simulation of fast power transients and a PWR main steam line break. The latter serves as an example of coupled fuel behaviour, neutronics and system-level thermal hydraulics simulation.

Fuel codes for Serpent

FINIX has been integrated to the Serpent Monte Carlo neutronics code (Ikonen et al. 2014, Valtavirta et al. 2014, Leppänen et al. 2014). Concurrently, an interface for externally coupled fuel performance code has been developed (Valtavirta et al. 2013). Several studies on the coupling between the Serpent reactor physics code and the ENIGMA steady-state fuel performance code have been performed (Vi-

tanen & Tulkki 2012). In both the internal and the external coupling, the fuel models are used to model the dynamical behaviour of the fuel, i.e. changes in the fuel dimensions and temperature distribution. This information is forwarded to Serpent, which is responsible of the burnup and power distribution calculations. The radial power distribution data is returned to the fuel code to be utilized by its power depression routines. The coupling provides for detailed temperature and geometry modelling in a burnup calculation. Hence, it can be utilized to examine the errors originating from the usual approximation of stationary thermo-mechanical properties of the fuel. The new code can also be used in the verification of models and input parameters of a fuel behaviour code.

FRAPTRAN-GENFLO

FRAPTRAN is a fuel code continually developed by PNNL for accident analysis. It has been combined with VTT's GENFLO thermal hydraulics code to better simulate the dynamical effects during loss of coolant accidents. The combination has lately been used in analysis of Halden LOCA experiments (Manngård 2013).

In the Safir2010/POKEVA and Safir2014/PALAMA projects, VTT has developed a new method for statistical analysis of fuel failures in accident conditions (Arffman et al. 2011). The VTT approach applies neural networks and methods developed for uncertainty and sensitivity analyses.

According to the VTT method, evaluating fuel failures starts with 59 system code simulations of the accident with varying global parameters in the input deck. The results are applied as boundary conditions for a FRAPTRAN-GENFLO analysis where the number of failed fuel rods is calculated. The FRAPCON code calculates the burnup dependent and fuel manufactory parameter dependent data into a restart file used in FRAPTRAN. The rest of the local parameters are varied in the FRAPTRAN-GENFLO analysis. Instead of calculating all the rods, a neural networks method has been used, where only a fraction of the rods are analysed. This work has culminated in applying it to an EPR large break LOCA analysis (Arkoma et al. 2015).

Most recently, the FRAPTRAN-GENFLO coupling was updated to simulate several fuel rods simultaneously. This has its application in simulating e.g. a case of a fuel bundle with a flow blockage.

Validation and Benchmarks

Validation tools development

Validation is an essential yet tedious part of any model development. To ease the task, a new validation system for models in the ENIGMA fuel performance code was developed that can make major parts of the procedure run automatically. The validation system consists of three parts. The first part is the validation code called Simulation Performance Analysis Code for ENIGMA (SPACE). The second part is a database that contains all the measurement and input data that are available. The third

part of the system is comprised of different MATLAB routines that are used to graphically illustrate the SPACE output. The development of the validation system started in 2011 and continues in the future with the extension of the tool for other fuel performance codes.

Benchmarks

During PALAMA, VTT has participated in two reactivity initiated accident (RIA) focused benchmarks, OECD/NEA RIA benchmark Phase I (2011–2013) and Phase II (2014–2015). VTT participates to the benchmark with the IRSN-developed SCANAIR code.

In the first benchmark, four distinct RIA tests were simulated. As findings of the benchmark simulations, a few deficiencies in the results of the base irradiation initialization made with the ENIGMA code were pointed out: some FGR data produced by the VTT-developed ENIGMA-SCANAIR interface module was found non-realistic, and the oxide layer thicknesses calculated by ENIGMA (with the default parameters) were consistently underestimated. This was later addressed by recoding the ENIGMA oxide layer model. The user effect was also one of the subjects to be quantified in the benchmark; it was discovered that the SCANAIR results delivered by IRSN, VTT, SSM and CIEMAT were quite close to each other.

The second benchmark focuses on the open issues from the first one. Especially the sensitivity and uncertainty of the codes will be analysed, as well as the more simple cases in order to better ascertain the effect of the individual models.

VTT participated in the IAEA Coordinated Research Programme FUMEX-III that took place in 2008–2011, first part of the SAFIR2010 project POKEVA and then with PALAMA. FUMEX-III had over 30 participants using various fuel behaviour codes, and the exercise ranged over a wide variety of cases and topics of interest. A state-of-the-art review of VTT's fuel performance code ENIGMA and a Licentiate of Technology thesis were prepared as a part of VTT's benchmark work. In 2014, the spiritual successor of the IAEA FUMEX line, Coordinated Research Programme FUMAC (Fuel Modelling in Accident Conditions) was initiated with VTT participation.

OECD Benchmark for Uncertainty Analysis in Best-Estimate Modelling (UAM) benchmark consists of three phases, out of which the first, neutronics calculations, has nearly finished by 2013. The second phase, announced in the UAM-5 workshop in 2011, is to include an exercise focusing on fuel behaviour modelling. Thus far these benchmarks have been participated in and VTT has contributed to the definition of the fuel exercise. The work done on uncertainty and sensitivity analysis in PALAMA is the basis of VTT participation. The workshop is also an appropriate venue for presenting and getting feedback on cross-disciplinary studies such as the FINIX development and multiphysics coupling.

References

- Arffman, A. and Rintala, J. Statistical Analysis of Fuel Failures in Accident Conditions, 2011 Water Reactor Fuel Performance Meeting, Chengdu, China, Sept. 11-14, 2011.
- Arffman, A. Recent RIA and LOCA Analyses Performed at VTT Using Fuel Performance Codes SCANAIR and FRAPTRAN-GENFLO, IAEA Technical Meeting on Fuel Behaviour and Modelling Under Severe Transient and LOCA Conditions, Mito, Ibaraki-ken, Japan, Oct. 18-20, 2011.
- Arffman, A., MOAL A., GEORGENTHUM V.. EVALUATION AND ADAPTATION OF THE RIA CODE SCANAIR FOR MODELLING BWR FUEL AND CONDITIONS. TopFuel2012, Manchester, United Kingdoms, Sept. 3-6 2012.
- Arkoma, A., Tulkki V., "Release of radioactive nuclides from spent WWER fuel", 10th International Conference on WWER Fuel Performance, Modelling and Experimental Support, 7.-14.9.2013, Bulgaria.
- Arkoma, A., Hänninen M., Rantamäki K., Kurki J., Hämäläinen A., Statistical analysis of fuel failures in large break loss-of-coolant accident (LB-LOCA) in EPR type nuclear power plant. Nuclear Engineering and Design, accepted manuscript (2015).
- Ikonen T., Tulkki V., Syrjälähti E., Valtavirta V., Leppänen J., "FINIX – fuel behaviour model and interface for multiphysics applications", LWR Fuel Performance Meeting TopFuel 2013, 16.-18.9.2013, Charlotte NC, USA.
- Ikonen T., Loukusa H., Syrjälähti E., Valtavirta V., Leppänen J., Tulkki V. 2014. Module for thermomechanical modeling of LWR fuel in multiphysics simulations. Annals of Nuclear Energy, in press (2014).
- Ikonen T., Tulkki V. 2014. The importance of input interactions in the uncertainty and sensitivity analysis of nuclear fuel behaviour. Nuclear Engineering and Design Vol. 275 (2014) No: August, 229 – 241.
- Kelpe, S., Klecka, L., Tulkki, V. ENIGMA modeling of IFA-610 overpressure series, Enlarged Halden Programme Group Meeting 2011, Sandefjord, Norway, Oct. 3-6, 2011.
- Kättö, J. Corrosion and its Modeling in Nuclear Reactor Fuel Cladding, Master's Thesis. Aalto University School of Engineering, 7 July 2013, 80 p.
- Leppänen J., Hovi V., Ikonen T., Kurki J., Pusa M., Valtavirta V., Viitanen, T. "The Numerical Multi-Physics Project (NUMPS) at VTT Technical Research Centre of Finland", Annals of Nuclear Energy, accepted (2014).

- Loukusa H. Computational module for the calculation of thermochemical equilibria in nuclear fuel, Master's Thesis, Aalto University School of Chemistry, 2014, 134 p.
- Manngård, T., Stengård, J.-O., Jernkvist, L. Evaluation of Halden IFA-650 loss-of-coolant accident experiments 2, 3, 4, 5, 6 and 7. Enlarged Halden Programme Group Meeting 2013, Gol, Norway, March 10-15, 2013.
- Tulkki, V. Development of VTT ENIGMA creep models, Enlarged Halden Programme Group Meeting 2011, Sandefjord, Norway, Oct. 3-6, 2011.
- Tulkki, V., Ikonen T., "Implementation of model for primary creep derived from Halden experimental results", Enlarged Halden Programme Meeting 2013, 11.-15.3.2013, Storefjell, Norway.
- Tulkki V., Nieminen A., Rätty A., "Radionuclide Release from High Burnup Fuel", IAEA Technical Meeting on modelling of water-cooled fuel including design basis and severe accidents, 28.10.-1.11.2013, Chengdu, China.
- Tulkki V., Ikonen T. 2014a. Modeling of Zircaloy cladding primary creep during load drop and reversal. *Journal of Nuclear Materials*, Volume 445, Issues 1–3, February 2014, Pages 98–103.
- Tulkki V., Ikonen T. 2014b. Effect of underlying assumptions to the publication and display of creep data, F4.7, EHPG 2014, 7.-12.2014 Norway.
- Tulkki, V., Ikonen, T. 2015. Viscoelastic modeling of Zircaloy cladding in-pile transient creep. *Journal of Nuclear Materials*, Volume 457, February 2015, Pages 324-329.
- Valtavirta V., Tulkki V., Leppänen J., Viitanen T., "The Universal Fuel Performance Code Interface in Serpent 2" LWR Fuel Performance Meeting TopFuel 2013, 16.-18.9.2013, Charlotte NC, USA.
- Valtavirta V., Ikonen T., Viitanen T., Leppänen J., "Simulating fast transients with fuel behavior feedback using the Serpent 2 Monte Carlo code", in *Proceedings PHYSOR 2014*, September 28 - October 3 2014, Kyoto, Japan.
- Viitanen, T. and Tulkki, V. COMBINING REACTOR PHYSICS AND FUEL PERFORMANCE CALCULATIONS, TopFuel2012, Manchester, United Kingdoms, Sept. 3-6 2012.

14.2 FINIX fuel behaviour module: development and applications

Timo Ikonen, Henri Loukusa, Elina Syrjälähti, Ville Valtavirta, Jaakko Leppänen,
Ville Tulkki

VTT Technical Research Centre of Finland Ltd
P.O. Box 1000, FI-02044 Espoo

Abstract

In PALAMA, a new light-weight fuel behavior code FINIX has been developed. FINIX is specifically designed for modeling of LWR fuel rods in multiphysics simulations and has been coupled with VTT's Monte Carlo reactor physics code Serpent 2, and reactor dynamics codes TRAB-1D, TRAB3D, and HEXTRAN. The coupling work has been partially done within the KOURA and KÄÄRME projects in SAFIR2014. FINIX is used to solve the time-dependent temperature distribution in the rod and the heat flux from the cladding to the coolant, allowing two-way coupling of the fuel behavior simulation with both neutronics and thermal hydraulics simulations. Elastic and thermal mechanical deformations of the cladding can also be solved with FINIX. The stand-alone FINIX has been compared with FRAPTRAN-1.4 simulations and data from Halden experiments. The comparison reveals good agreement in both cases. Coupled with Serpent, we have simulated both steady-state cases and a fast reactivity transient with the fuel temperature and fission power solved self-consistently. With VTT's reactor dynamics codes, FINIX has been used in the simulation of fast power transients and a PWR main steam line break. The latter serves as an example of coupled fuel behavior, neutronics and system-level thermal hydraulics simulation.

Introduction

In light water reactors, the thermal and mechanical behaviour of the fuel rods strongly influences the behaviour of the reactor in both steady state and transient conditions. For example, the power of the reactor is sharply affected by the fuel temperature due to the absorption of neutrons by Doppler-broadened cross sections. This coupling is important both in the steady state and, even more so, in transients. Similarly, transient heat transfer to the coolant and avoiding departure from nucleate boiling is dependent on the heat conductance of the pellet-cladding gap. The gap conductance is a notoriously complicated function of both thermal and mechanical properties of the fuel rod. Therefore dedicated fuel behaviour codes are often used

in multiphysics simulations to solve the heat transfer in the rod self-consistently with, for example, the reactor power calculated by a neutronics code.

However, the fuel performance code or the expertise for its use is not always available for the multiphysics modeller. Therefore a somewhat simpler approach has been studied at VTT, where the fuel behaviour module FINIX has been recently developed (Ikonen, 2013; Ikonen et al., 2013; Ikonen et al., 2014). The FINIX module adopts a middle-ground between elaborate fuel performance codes and thermal elements in order to give a “simple but sufficient” description of the fuel rod’s thermal and mechanical behaviour. The aim is to make fuel behaviour modelling more easily approachable to multiphysics modellers without imposing on them the complete fuel behaviour phenomenology, but still provide significant improvements to stand-alone simulation methods.

The current modeling capabilities of FINIX are aimed towards calculating the fuel rod’s thermal behavior in fast transient simulations, although more limited capabilities to model also steady state behavior exist. At present, FINIX solves the time-dependent heat transfer across the pellet, gas gap and the cladding, taking into account elastic and thermal deformations and their coupling to the gap conductance. Material correlations are taken from public literature. Initialization for accumulated burnup can be done using a FRAPCON simulation for the steady state irradiation. For a more easy-to-use initialization, a parameterization method for burnup-dependent quantities is also under development.

FINIX is designed to be integrated as a subprogram into a larger simulation code, such as Serpent or TRAB3D, where FINIX replaces the existing fuel model. While multiphysics capabilities can also be achieved with direct code-to-code coupling, such approach is often laborious when highly specialized software is involved. Thus, in the design of the FINIX code, flexibility of the interface between FINIX and the main simulation code has been prioritized. This facilitates integration into a wide range of different simulation codes.

The main models and the interface to the main simulation (host) code is illustrated in Figure 1. For a description of the FINIX models and their capabilities, the interested reader is referred to the descriptions given in Ikonen, 2013 and Ikonen et al., 2014.

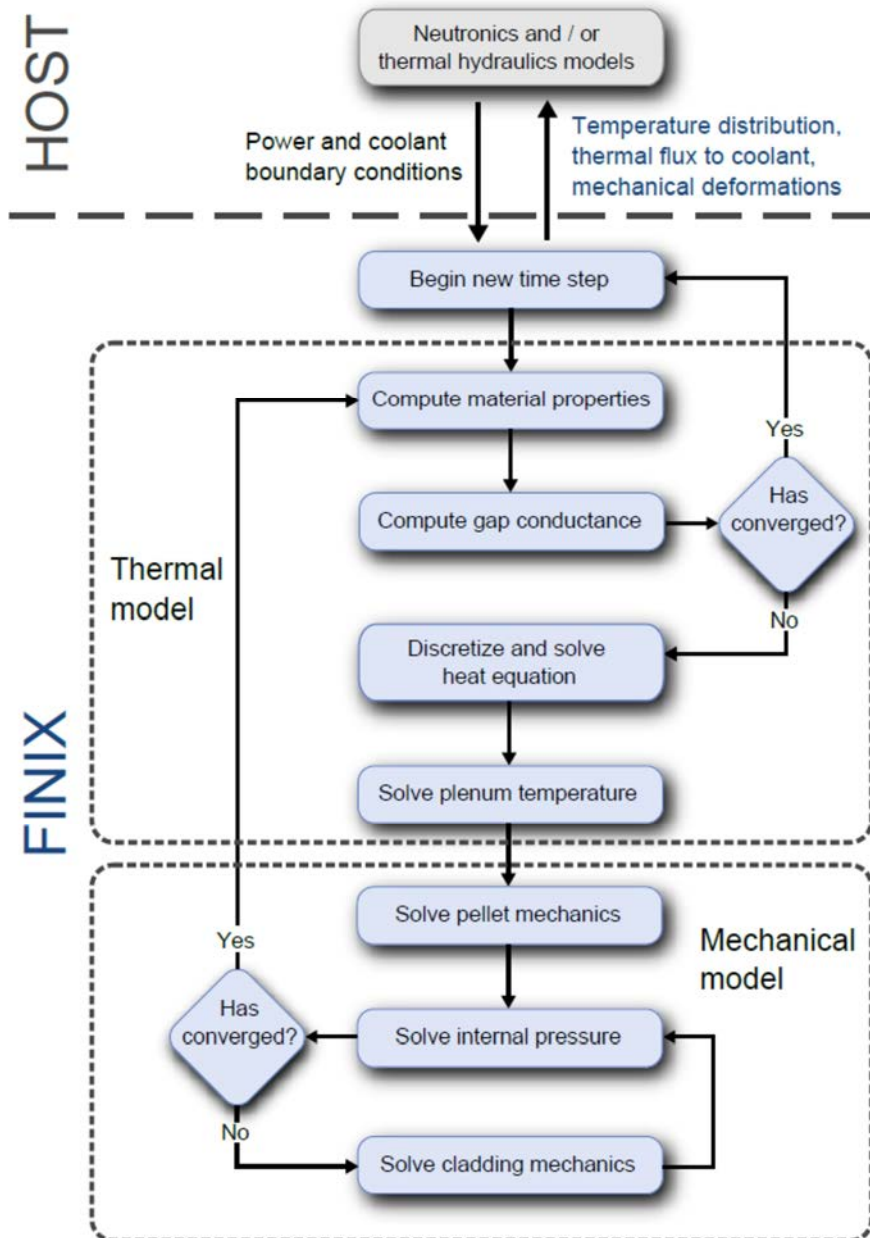


Figure 1. Schematic illustration of the FINIX module and its role in a multiphysics simulation. The iteration of the thermal and mechanical solutions is indicated by the flowchart. The convergence checks are assumed to automatically fail on the first iteration.

Verification and validation of stand-alone FINIX

Arguably the most important quantity that a fuel performance module calculates in a coupled multiphysics simulation is the time-dependent temperature distribution in the pellet and in the cladding. This is especially true in coupled neutronics simulations, where the fuel temperature determines the reactivity change due to Doppler broadening. Also in thermal hydraulics simulations, the temperature distribution directly affects the heat flux from the cladding to the coolant.

The temperature calculation of FINIX has been compared against both the FRAPTRAN-1.4 fuel performance code and experimental data from Halden IFA-429 and IFA-432 test series. The former involves code-to-code comparisons with similar inputs, and is useful in verifying FINIX's overall behavior in the tested scenarios. In these comparisons, one can look at any calculated quantities, including gap conductance, pressure, mechanical deformations, and so on. The comparison with experimental data, on the other hand, is limited to quantities that have been measured in the experiment. However, the comparison is truly quantitative and reveals the model's accuracy with respect to real-world data.

The results of the comparisons have been reported in full by Loukusa, 2013. The comparison with the experimental steady-state centreline temperature data finds good match between FINIX and the measurements, as shown in Figures 2 and 3. The deviation of the simulated results from the experimental ones at moderate to high burnup are due to steady-state phenomena such as cladding creep, pellet swelling, etc., which are not currently modelled in FINIX.

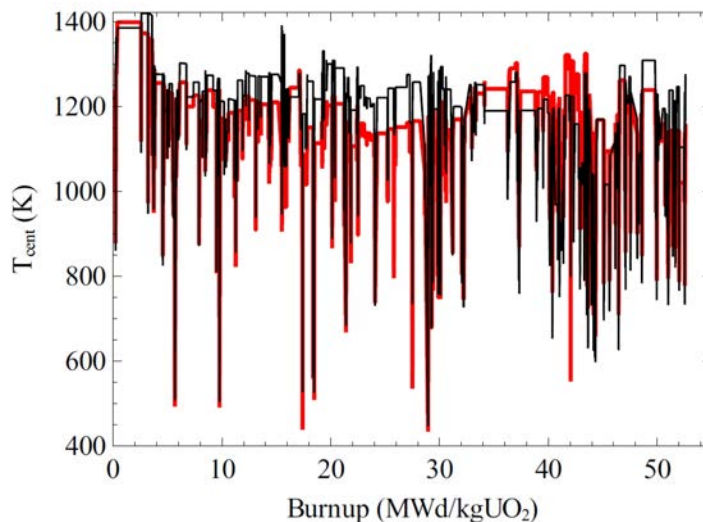


Figure 2. Fuel centerline temperatures as a function of burnup for the IFA-429 experiment rod BC as calculated by FINIX (black line) and as measured in the experiment (thick red line).

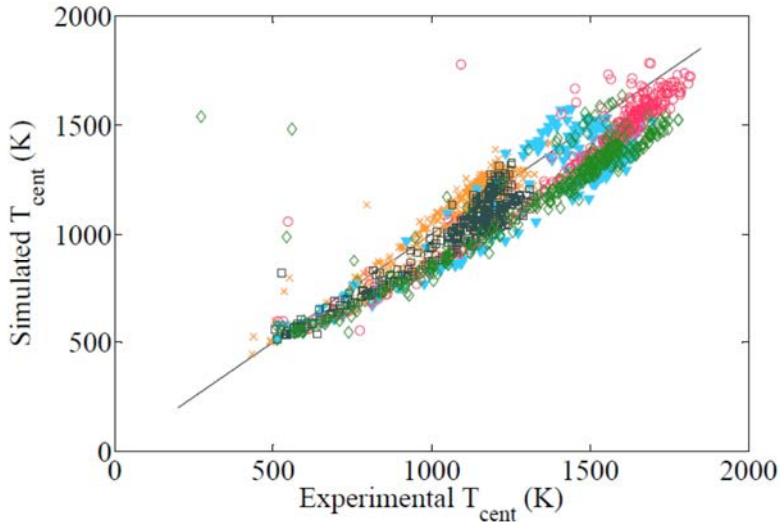


Figure 3. Measured vs. calculated fuel centerline temperatures from the IFA-429 and IFA-432 test series. Different symbols correspond to different rods.

The comparison between FRAPTRAN-1.4 and FINIX shows very close match for all the cases with small cladding plastic deformations. An example of such a case is presented in Figure 4. Plastic deformations of the cladding are not modelled in FINIX, but even in scenarios where FRAPTRAN predicts significant plastic cladding deformation, the temperature distributions are reproduced by FINIX quite well (Loukusa, 2013; Ikonen et al. 2014).

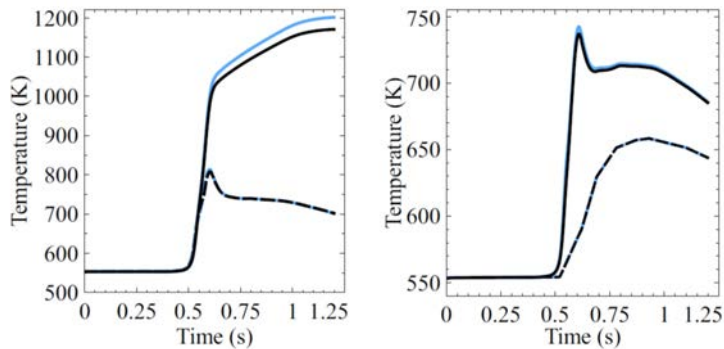


Figure 4. Temperatures in the fuel and cladding for the CABRI REP-Na4 scenario as a function of time calculated by FINIX (black lines) and FRAPTRAN (blue curves). Left panel: Fuel centerline temperatures (solid lines) and outer surface temperatures (dashed line). Right panel: Clad inner surface temperatures (solid lines) and outer surface temperatures (dashed lines).

Integration with Serpent

FINIX has been integrated into Serpent 2, where it complements Serpents' multiphysics coupling capabilities as an interval fuel temperature solver (Leppänen et al, 2014). The integration is described in detail by Valtavirta, 2014. Serpent-FINIX models have been constructed for the Three Mile Island Unit 1 (TMI-1) assembly, which was simulated in the steady state mode in Ikonen et al., 2013. Here the temperatures and powers were solved self-consistently, with FINIX receiving the power distribution as an input from Serpent, and the temperature distribution solved by FINIX is passed to Serpent. The system is iterated until a solution is found. For the TMI-1 assembly, the average temperatures of the rods solved in this way are shown in Figure 5.

976	960	978	995	1006	1013	1011	1010
960	733	966	996	1013	1029	1015	1007
978	966	994	1027	1041		1032	1012
995	996	1027		1049	1044	1022	1012
1006	1013	1041	1049	1040	1044	1024	1015
1013	1029		1044	1044		1041	1024
1011	1015	1032	1022	1024	1041	1035	1043
1010	1007	1012	1012	1015	1024	1043	

Figure 5. The volume averaged temperatures of the fuel rods in the top left quarter of the TMI-1 assembly calculated by Serpent 2 and FINIX (black squares correspond to the guide tubes and the instrumentation tube).

A new feature in Serpent 2 that can also utilize FINIX's time-dependent solution capabilities is the new dynamical simulation mode. With FINIX, this mode was used to demonstrate a Monte Carlo neutronics simulation of a fast transient in a 2D TMI-1 pin-cell. The system is initially set up as supercritical, but the exponential increase in power is shut down by the negative reactivity from the increased fuel temperature. (see Figure 6 and Ikonen et al., 2014).

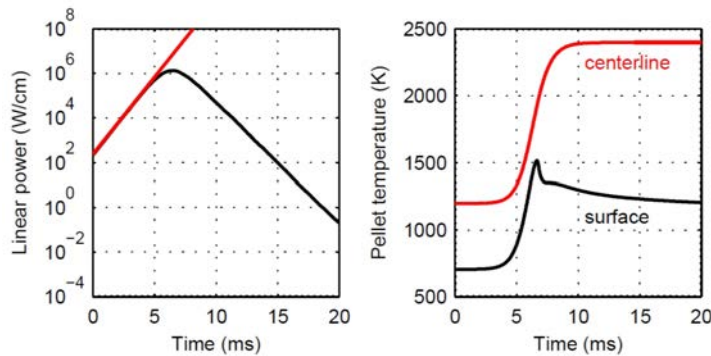


Figure 6. System linear power (left panel) with no-feedback prediction (red line) and pellet surface temperature (right panel) as a function of time for the coupled transient calculated by Serpent 2 and FINIX.

Integration with reactor dynamics codes

Several types of transients and plants have been simulated with FINIX and VTT's reactor dynamics codes TRAB-1D (see, for example, Ikonen et al. 2014), TRAB3D (Syrjälähti, 2013), and HEXTRAN (Syrjälähti 2015). For example, a fast power peak in a PWR fuel rod has been simulated with FINIX-TRAB-1D. Here the results with stand-alone TRAB-1D were contrasted with the simulation of the coupled codes. FINIX predicts slightly lower peak temperatures and slower decay of the over time than TRAB-1D (see Figure 7). Further comparison of the models of FINIX and TRAB3D in an EPR control rod ejection accident reveals that FINIX improves the existing models and gives results that are closer to fuel-specific correlations (Syrjälähti, 2013).

With HEXTRAN-FINIX, scenarios in the AER 3rd benchmark concerning a control rod ejection accident in a VVER-440 reactor have been simulated. A representative fuel rod from each of the 349 fuel assemblies was modelled with FINIX. Figure 8 shows the FINIX-calculated gap widths during a control rod ejection accident. The distribution of the minimum gap width is shown 0.3 seconds after the control rod ejection. The simulation is done with fresh fuel and zero initial power.

In addition to the fast transients, FINIX integrated into TRAB3D/SMABRE has been used to simulate a main steam line break accident in TMI-1 (Syrjälähti, 2013; Ikonen et al., 2014). In that case TRAB3D/SMABRE was used to run 177 instances of FINIX, each representing the rods in one assembly.

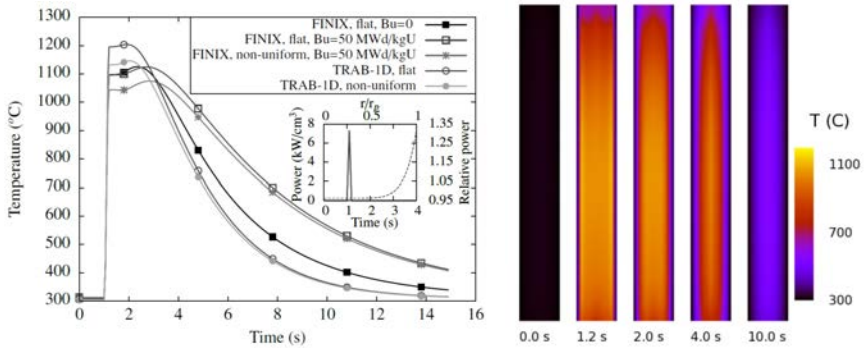


Figure 7. Left: Maximum fuel centerline temperature during power peak transient with TRAB-1D. Inset: the average power density during the transient (solid) and radial heat generation in the fuel pellet as a function of radius (dashed), r =radius, r_p =pellet outer radius. Right: Temperature distribution in the fuel rod during the power peak transient using FINIX with TRAB-1D. Non-uniform radial heat generation, burnup 50 MWd/kgU.

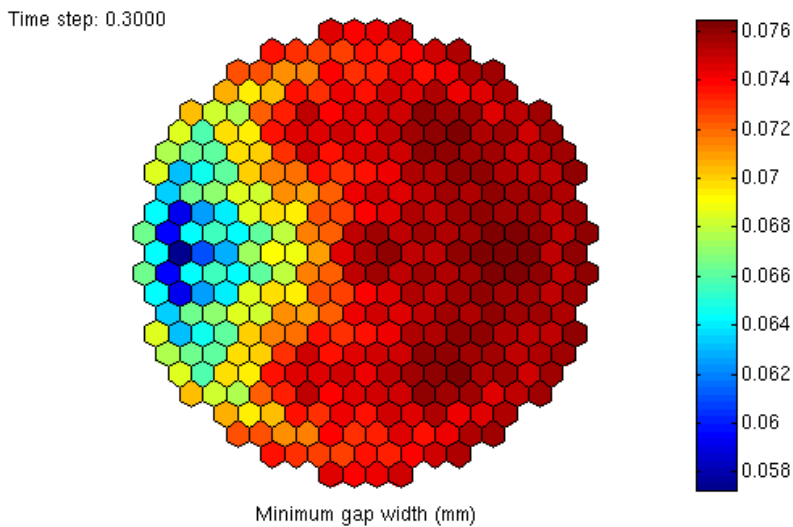


Figure 8. Minimum gap width 0.3 seconds after control rod ejection in a VVER-440 reactor according to HEXTRAN-FINIX simulation. The location of the ejected rod in the figure is near the left edge.

Summary and outlook

A light-weight fuel behavior module FINIX has been developed. FINIX is aimed especially for multiphysics simulations, where it takes the role of the simulation's fuel behavior model. FINIX has been designed to be integrated into a wide array of simulation codes, and to provide an identical description of the fuel thermal behavior across different disciplines such as reactor physics and thermal hydraulics. In cases where the role of fuel performance simulations has been taken by simple correlations and thermal elements, calculation of the thermal response can be significantly improved by including mechanical feedback and power history dependence. Towards such a goal, we use FINIX to simulate the transient thermal and mechanical behavior of the rod, and show that FINIX can be used to provide improved estimates for the rod's thermal behavior in multiphysics simulations.

FINIX models have been validated against experimental centerline temperature data and verified against FRAPTRAN-1.4 simulations of several RIA experiments. The comparison shows good performance, especially for the calculation of the temperature distribution. For the temperatures, the agreement with FRAPTRAN remain good even when significant plastic deformations are predicted by FRAPTRAN, despite FINIX's lack of nonelastic models for the cladding. However, to extend FINIX's validity to simulation of steady state irradiation or loss of coolant accidents (LOCA), improvements such as fission gas modeling, cladding creep, and plastic deformations are required.

To demonstrate the applicability of FINIX to multiphysics simulations, we have integrated FINIX to Serpent 2, a Monte Carlo reactor physics code, and to TRAB3D, TRAB-1D and HEXTRAN, VTT's in-house reactor dynamics codes. With Serpent, we have done a steady-state simulation of a TMI-1 assembly, and a test case of an initially supercritical PWR pin-cell, where the exponential increase of power is terminated by the negative reactivity feedback from the increasing fuel temperature. With TRAB-1D, an artificial power peak without neutronics feedback has been modeled, revealing the difference between the temperatures calculated by FINIX and simple benchmark correlations. With TRAB3D, a main steam line break of the TMI-1 has been simulated, and with HEXTRAN, a control rod ejection accident in a VVER-440 reactor. The cases involve running multiple (several hundred) instances of FINIX in one simulation, and show how FINIX can be used to model the fuel thermal behavior of a whole reactor.

Development of the FINIX module is an on-going work. Future work follows two parallel paths, with the first focusing on improving the fuel performance capabilities in LOCAs and in steady state, and the second concentrating on developing methods for uncertainty propagation and system initialization with incomplete information. The aim of both is in keeping with FINIX's general goal to enhance the accessibility and reliability of fuel performance modeling in multiphysics simulations.

References

- Ikonen, T. 2013. FINIX Fuel behavior model and interface for multiphysics applications. Code documentation for version 0.13.9. Technical Report VTT-R-06563-13; VTT Technical Research Centre of Finland; 2013.
- Ikonen, T., Tulkki, V., Syrjälähti, E., Valtavirta, V., Leppänen, J. 2013. FINIX – fuel behavior model and interface for multiphysics applications. In: 2013 Fuel Performance Meeting / TopFuel, Charlotte, USA. 2013.
- Ikonen, T., Loukusa, H., Syrjälähti, E., Valtavirta, V., Leppänen, J., Tulkki, V. 2014. Module for thermomechanical modeling of LWR fuel in multiphysics simulations. *Annals of Nuclear Energy*, in press.
- Leppänen, J., Hovi, V., Ikonen, T., Kurki, J., Pusa, M., Valtavirta, V., Viitanen, T., 2014. The numerical multi-physics project (NUMPS) at VTT Technical Research Centre of Finland. *Annals of Nuclear Energy*, in press.
- Loukusa, H. 2013. Validation of the FINIX fuel behavior code version 0.13.9. Technical Report VTT-R-06565-13; VTT Technical Research Centre of Finland; 2013.
- Syrjälähti, E., 2013. Coupling of the FINIX fuel module to the reactor dynamics codes TRAB3D and TRAB-CORE. Technical Report VTT-R-08967-13 ; VTT Technical Research Centre of Finland; 2013.
- Syrjälähti, E., 2015. Updates in the reactor dynamics code system and validation matrix in 2014. Technical Report VTT-R-00223-15 ; VTT Technical Research Centre of Finland; 2015.
- Valtavirta, V., 2014. Coupling Serpent and FINIX for neutronics – fuel behavior multiphysics calculations. Technical Report VTT-R-05942-14 ; VTT Technical Research Centre of Finland; 2014

15. Enhancement of safety evaluation tools (ESA)

15.1 ESA summary report

Ismo Karppinen, Seppo Hillberg, Risto Huhtanen, Jarno Kolehmainen, Joonas Kurki, Sampsala Lauerma, Ari Silde, Pekka Urhonen

VTT Technical Research Centre of Finland Ltd
P.O. Box 1000, FI-02044 Espoo

Abstract

System analysis codes (Apros and TRACE) and containment analysis methods (Apros containment and Fluent CFD) were validated in large range of experiments ranging from separate effect tests to fullscale power plant models. The multi-node LP nodalization of Apros containment was used successfully to simulate gas stratification.

Introduction

New nuclear power plant concepts have new passive and active emergency heat exchangers. Especially in the passive systems the driving forces are small and therefore evaluation of their performance with computational methods requires models that are validated for these conditions. Boiling water reactor concepts ABWR and ESBWR have isolation condensers (IC) to control reactor circuit pressure and passive containment condensers (PCCS) to cool containment atmosphere. The APWR PWR concept has also containment coolers. Modelling of condensers was studied in the ALWR research program some 10 years ago, but the models and codes have been further developed and new validation is needed.

Finland participates in the OECD/NEA research programs and in the EU SARNET research activities. The experimental results and information received through these research programs can best be utilized by modelling and simulating the experiments. Northnet co-operation with Swedish organizations facilitates code development and validation based on PPOOLEX experiments in Lappeenranta University.

International co-operation is also necessary for training young experts and for maintaining the know-how.

Main objectives

The objective of the project was to develop and validate calculation methods for safety evaluation of nuclear power plants. Both thermal hydraulic system analysis codes, containment lumped parameter (LP) codes and CFD calculation methods were used. Apros and TRACE codes were validated with both separate effect and integral tests concentrating on the phenomena important for the new plant concepts offered for the OL4 and the Fennovoima plants. CFD methods for analysing containment behaviour were enhanced. Condensation models and modelling of containment condensers were validated. An important objective was to train new thermal hydraulic code users and educate young experts. Participation in large international OECD/NEA and USNRC thermal hydraulic projects and Nordic co-operation were essential parts of the project.

Validation of system analysis codes

A systematic and thorough validation of codes is a prerequisite for their use in safety analysis. Calculation of the validation cases and analysis of the results is also an effective means to educate young experts. The thermal hydraulic system analysis codes Apros and TRACE have been validated with experimental data from Lappeenranta University, EU and OECD research programs (Table 1).

Table 1. System code validation with LUT, EU and OECD experiments.

Experiment or case	Phenomena or scenario	Code
NOKO EU series	passive horizontal condenser	Apros
PANDA PCC	passive vertical condenser	Apros
PACTEL NCg experiments	Horizontal SG with non-condensable gas	Apros
ROCOM tests 2.1, 2.2	Fluid mixing in reactor vessel down-comer	TRACE
ROSA-2 test 3	Hot leg SBLOCA (1.5%)	Apros, TRACE
ROSA-2 test 2 and 7	Cold leg intermediate size LOCA	Apros, TRACE
PWR PACTEL benchmark	Blind SBLOCA	Apros
AER DYN-006 benchmark	Steam line break	TRACE/PARCS
LUT PCC	Condensation efficiency of passive containment condenser system	Apros
FLECHT-SEASET	Reflooding	Apros, TRACE

PWR PACTEL CNC-01, CNC-02	Cool down with natural circulation with isolated steam generator	Apros
PKL3 test G7.1	Hot leg SBLOCA	Apros
PKL3 test H2.1	Station black out	Apros
PWR PACTEL SBO-02	Station black out, supplement to PKL3 H2.1	Apros
FONESYS benchmark 1	Boiling in a channel	Apros
FONESYS benchmark 2	Critical flow	Apros
ABWR plant model	Integrated plant model with isolation condenser and passive containment cooler.	Apros

Validation of Apros with condenser experiments

Most of the new power plant concepts offered to TVO and Fennovoima have passive condenser systems, operation of which is based on natural circulation. The ability of Apros code to simulate behaviour of those condensers was tested by calculating NOKO [Hillberg 2011] and PANDA PCC experiments [Hillberg 2012]. The German NOKO experiment facility is a model of the passive emergency condenser of the Kerena plant concept (Figure 1), but quite similar condensers with horizontal heat exchangers are used also in other power plant designs.

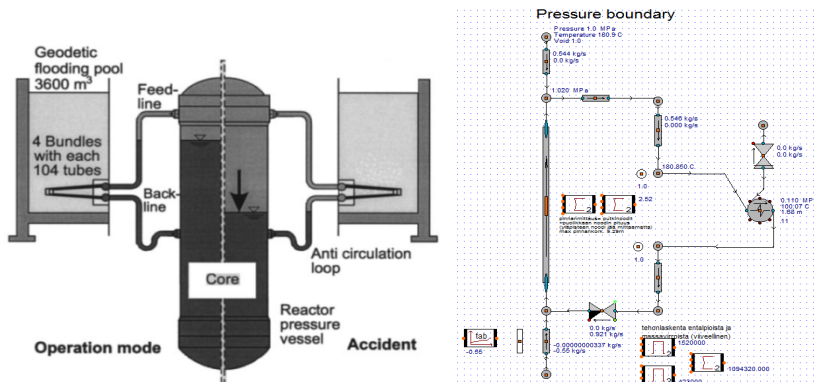


Figure 1. Principal diagram of Emergency Condenser and Apros model of NOKO experiment.

Measured and calculated condenser performance was compared in 10 different operation conditions using 3 alternate condensation correlations available in Apros code. The results show reasonable agreement with the experiments although the comparison to the data suggests that there may be some over prediction of heat transfer in some of the simulated cases with the default correlation (Shah). On the

basis of Apros calculations Nusselt model for condensation is recommended for this kind of condensers.

PANDA facility is a large scale containment test facility located at Paul Scherrer institute in Switzerland. A set of isolation condenser (IC) tests were simulated with Apros using both a detailed model of the IC heat exchanger (Figure 2) and a heat exchanger process component available in Apros. Both modelling approaches gave the same results. The tests and simulations were run at 3, 6 and 9 bar pressure ranges so that each range had a pure steam test along with three tests with different amounts of non-condensable gas mixed in the steam flow. Suitability of three different interfacial heat transfer correlations was evaluated. Chen and Nusselt correlations produced results that are very close to each other but also in a reasonably good agreement with the test results.

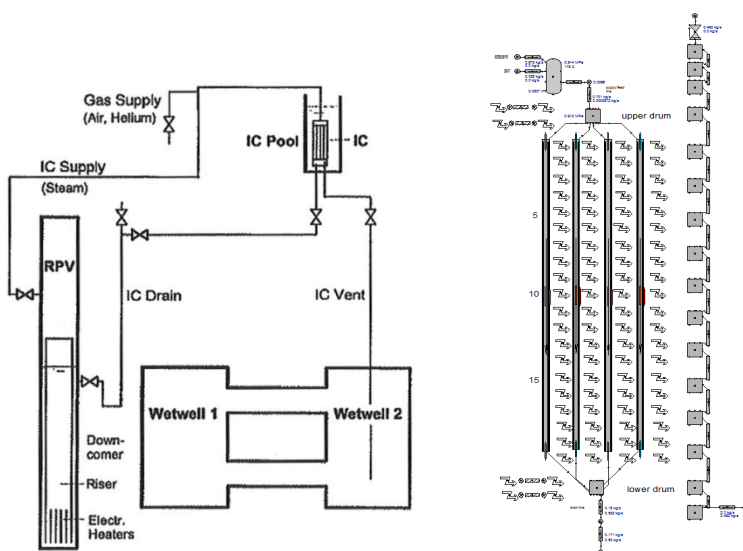


Figure 2. The PANDA facility in the test configuration and the detailed Apros model of the condenser.

Validation of Apros with PACTEL test

Both configurations VVER PACTEL and PWR PACTEL have been used in Apros validation. Effects of non-condensable gas on heat transfer in horizontal steam generator (Figure 3) were studied in PACTEL experiments NCg-1, NCg-3, NCg2-04 and NCg2-05 [Kolehmainen 2012]. Heat transfer degradation by stepwise injections of non-condensable gas was well reproduced by Apros simulation. PWR PACTEL experiments CNC-01, CNC-02, SBO-2 and PWR PACTEL Benchmark [Kouhia] were modelled with Apros to validate code modelling capabilities of the system with vertical steam generator (Figure 4).

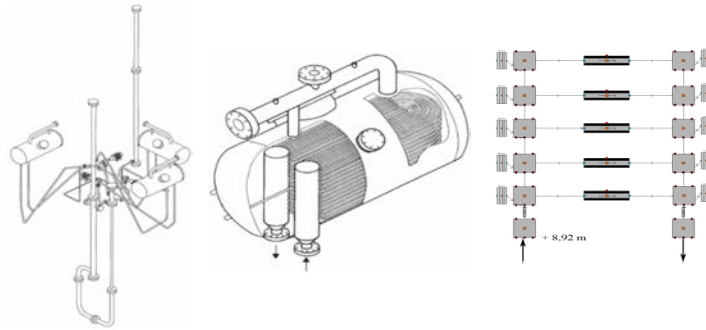


Figure 3. PACTEL facility, horizontal steam generator and Apros model of the steam generator tubes.

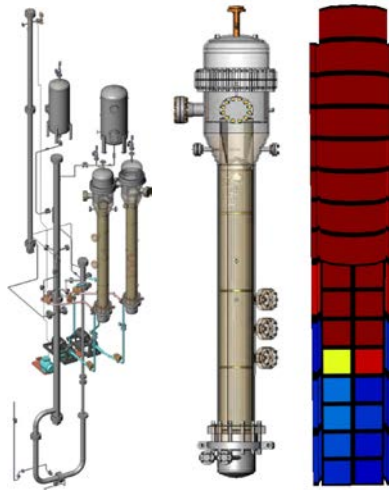


Figure 4. PWR PACTEL facility, vertical steam generator and visualization of calculated void fraction in the steam generator secondary side model.

Validation of Apros and TRACE with OECD research data

Experimental data received through OECD/NEA research programs ROSA-2, PKL-2 and PKL-3 was used in validation of Apros and TRACE codes. The experiments conducted in large scale integral test facilities studied plant transients and accident scenarios found important for accident management and code validation. The OECD/ROSA-2 Test 3 and the counterpart test PKL-2 G7.1 described a hot leg small break loss-of-coolant accident. Simulation of the ROSA test with both Apros and TRACE [Inkinen 2012] enabled in addition to code to code comparison also comparison to simulation and findings of the the counterpart test. Both Apros and TRACE models (Figure 5) predicted reasonably well the major events of the experiment.

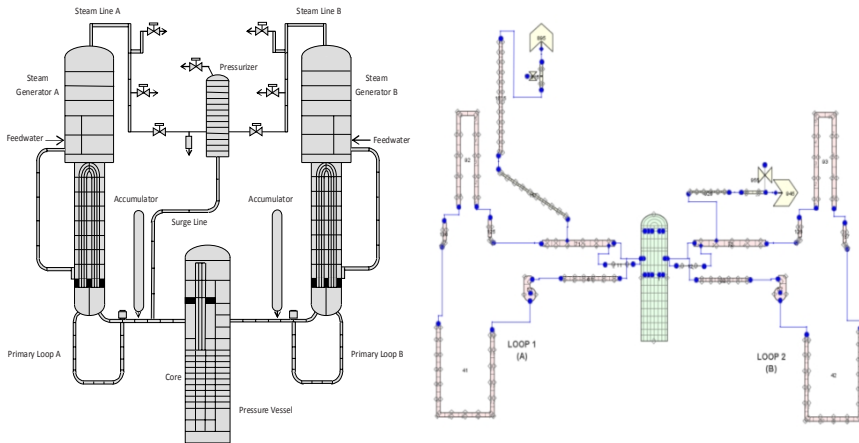


Figure 5. ROSA/LSTF model nodalizations in Apros (left) and TRACE (right).

Validation of containment analysis methods

Apros lumped parameter (LP) containment code was validated both with separate effect and integral tests. Models utilized in CFD analysis were tested with well defined separate effect tests like SARNET spray benchmark and finally simulation capabilities were benchmarked in the OECD CFD exercise (Table 2).

Table 2. Containment code verification and validation cases.

Experiment or source	Phenomena or Scenario	Code
GEKO	Building condenser efficiency	Apros containment
CONAN	Wall condensation under forced convection conditions	Apros containment
Areva RECO data	Efficiency of passive auto-catalytic recombiner (PAR)	Apros containment
SARNET generic containment benchmark	Pressurization, H ₂ concentration and operation of PAR system in a large dry containment	Apros containment
SARNET elementary spray benchmark	Heat and mass transfer of single droplet	Apros containment, Fluent
PANDA ST4.1	Containment cooler experiment	Fluent
THAI test TH24	Break up of stratified steam/air layer	Apros containment, Fluent
THAI test HM-2	Stratification of hydrogen	Apros containment, Apros 6eq
OECD CFD benchmark	Gas stratification in PANDA test	Fluent

	facility	
MISTRA HM2-1	Gas mixture stratification and mixing with a PAR system	Apros containment

SARNET Generic Containment Benchmark

A Generic Containment Benchmark exercise was organised in the frame of the European Network of Excellence SARNET2 (Severe Accident Research Network) [Kelm 2013a, 2013b]. In total, 14 European organisations applying 10 different, the most common LP codes, were contributing to this activity. The benchmark basic nodalization was developed for a German pressurized water reactor (PWR) with 1300 MW_{el} and provided by GRS (Figure 6). All participants tried to build an identical nodalization concept/simulation model.

The benchmark consisted of three phases with increasing complexity from SBLOCA (run-0) to severe accident conditions with release of hydrogen, carbon monoxide and carbon dioxide (run-1) and activation of passive auto-catalytic recombiners (PAR) (run-2) [Kelm 2014]. The nodalization was similar in all phases of the benchmark exercise.

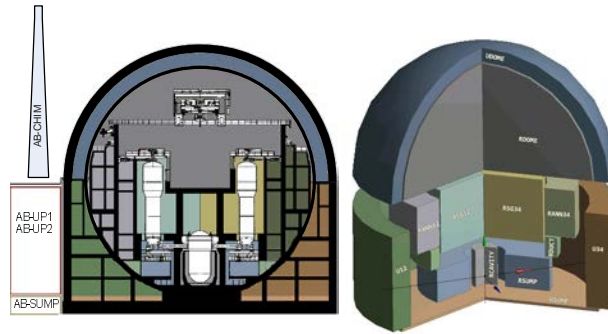


Figure 6. Nodalization for the German pressurized water reactor containment.

The Apros simulation results of dome pressure and gas temperature are compared with the mean values and standard deviation band of the other calculations in Figure 7. The Apros results were well within the deviation band. Similar trend was observed in other important compared target variables. One observation of the benchmark was that there were differences between some calculation results, even if the same computer code with similar nodalization were used.

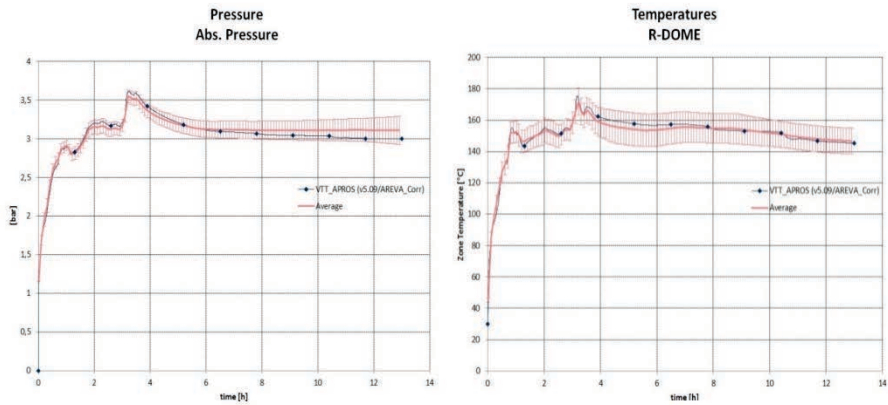


Figure 7. Calculated dome pressure and gas temperature of Apros compared to the mean values and standard deviation band of the other calculations in the SARNET Generic Containment benchmark.

SARNET elementary spray benchmark

A single droplet heat and mass transfer tests conducted at IRSN CARAIDAS facility (SARNET spray benchmark) was calculated using the Apros containment code and Fluent CFD code [Malet 2013]. Both evaporation and condensation cases were studied in condition, where monosized spray drops were generated in the top of the facility. The main goal of the work was to validate the containment spray heat and mass transfer models of Apros and to verify that the droplet models in Fluent are suitable for modelling containment spray [Malet 2015].

Calculated and experimental droplet size is presented as a function of distance from the spray nozzle (Figure 8). Generally speaking, the drop size predicted by APROS at two different levels during the drop fall agreed well with the measurements, but the evaporation rate in the weak evaporation cases was slightly under predicted [Silde 2012].

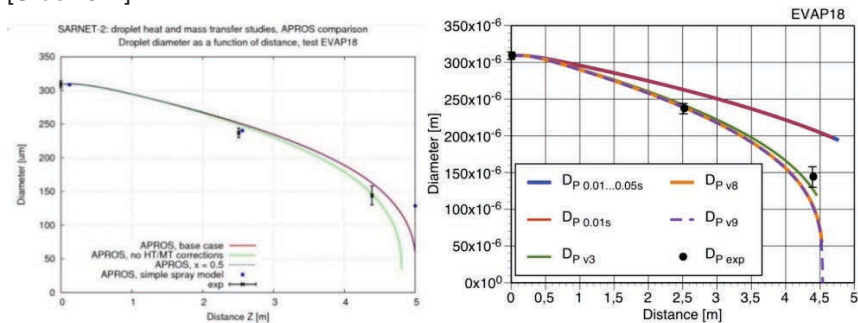


Figure 8. Calculated droplet size evolutions with Apros (left) and Fluent (right) using different modelling options, and the measurement data in test EVAP18.

THAI test TH24

VTT participated in blind and open calculations of German THAI experiment TH24 with the Fluent CFD code and the lumped parameter containment code Apros containment. Experiment TH24 was intended to investigate the dissolution of a steam layer subject to natural convection in the atmosphere of the THAI test vessel [Freitag 2012]. Conventionally, CFD simulation tools are used to solve complicated natural circulation and gas stratification phenomena. However, during the last years also LP containment models have been used more and more in modeling the gas stratification phenomena. The blind calculation of TH24 gave a great opportunity to test the nodalization concept without knowing the experimental results beforehand.

The main component of the THAI facility is a cylindrical steel vessel of 9.2 m height and 3.2 m diameter, with a total volume of 60 m³ (Figure 9).

In the Apros model (totally 140 nodes); the vessel was divided into 28 vertical node levels (Figure 9). Each node level was further divided horizontally into 5 nodes forming so called “pseudo 3-D” nodalization. The steam injection zone had an own 8-node nodalization.

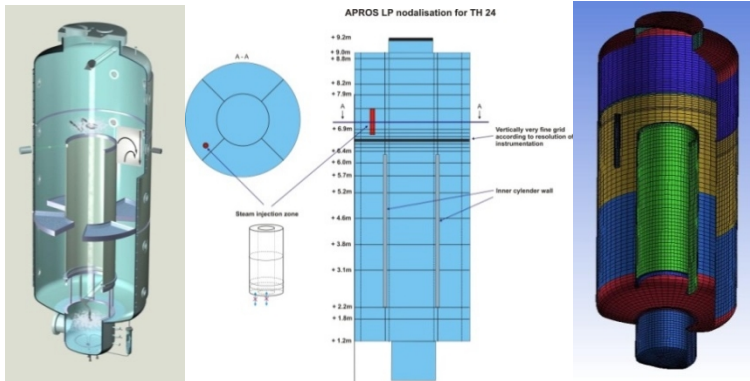


Figure 9. THAI test facility (left) [17]. APROS (middle) and Fluent (right) nodalizations for TH24.

The results of the benchmark show that the main features of the simulated field distributions are qualitatively comparable to the measured data. This is shown in both the CFD and LP simulation (Figure 10). A general conclusion of the exercise was that the pressure increase is qualitatively well simulated by most LP and CFD models, but quantitative comparison indicates that there is still a need for further model improvements. It was found that Apros LP code could simulate the steam stratification with a very good quality as well as the mixing of the steam until $t = 700$ s. The fact that the later mixing occurs quicker than in the experiment, is most likely due to an over-prediction of the convective flows. The multi-node LP modelling approach was further tested in modelling the THAI HM-2 experiment with Apros containment [Kolehmainen 2014]. Similar nodalization was used as in the THAI TH-24

experiment. The results showed that the code was able to model hydrogen stratification, if the vertical nodalization was dense enough.

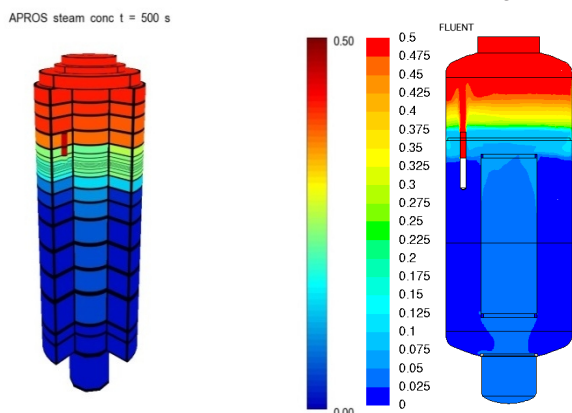


Figure 10. Steam molar fraction at $t = 500$ s calculated by the Apros (left) and Fluent (right) codes.

Conclusions

Both system analysis codes (Apros and TRACE) and containment analysis methods (Apros LP and Fluent CFD) were validated in large range of experiments ranging from separate effect tests to full-scale power plant models. The multi-node LP nodalization of Apros containment was used successfully to simulate the gas stratification phenomena reasonably in the MISTRA and THAI containment test facilities. The validation and benchmark cases were selected keeping in mind the new power plant concepts offered to TVO OL4 and Fennovoima projects.

References

- Freitag, M. Comparison Report for Blind Simulations of THAI Test TH24 (CV5) "Dis-solution of Steam Stratification by Natural Convection". Report no. 150 1361 – TH24 – VB. Becker Tech-nologies GmbH, Eschborn, 2012.
- Hillberg S., Simulation of NOKO emergency condenser EU experiments with APROS, VTT-R-06319-11, Technical Research Centre of Finland, 2011.
- Hillberg S., PANDA steady state isolation condenser experiments with APROS, VTT-R-01259-12, Technical Research Center of Finland, 2012
- Inkinen P., Lauerma S., ROSA-2 Test 3 Simulation with TRACE and Apros, VTT-R-01120-12, Technical Research Centre of Finland 2012.

- Kelm St. (editor), Broxtermann Ph., Krajewski S., Allelein H.-J., Preusser G., Sangiorgi M., Klein-Hessling W., Bakalov I., Bleyer A., Bentaib A., Kljenak I., Stempniewicz M., Jonnet J.R., Kostka P., Morandi S., Burkhardt J., Denk L., Parduba Z., Paci S., Manfredini A., Silde A., Jancovic J., Juris P., 2013a, Generic Containment, a Detailed Comparison of Containment Simulations Performed on Plant Scale, NURETH-15, May 12-17, Pisa, Italy, 2013
- Kelm St., Klauck M., Krajewski S., Allelein H.-J., Preusser G., Sangiorgi M., Klein-Hessling W., Bakalov I., Bleyer A., Bentaib A., Kljenak I., Stempniewicz M., Kostka P., Morandi S., Ada del Corno B., Bratfisch C., Risken T., Denk L., Parduba Z., Paci S., Manfredini A., Silde A., Jancovic J., Juris P., Lele H.G., Ganju S., 2013b, Generic Containment: Detailed Comparison of Containment Simulations Performed on Plant Scale, ERMSAR-2013, October 2-4, Avignon, France, 2013
- Kelm, St., Silde A. et al. Generic Containment: Detailed Comparison of Containment Simulations Performed on Plant Scale. *Annals of Nuclear Energy* 74 (2014)
- Kolehmainen J., Simulation of the PACTEL non-condensable gas experiments NCG-1, NCG-3, NCG2-04 and NCG2-05 with APROS 5.11.02, VTT-R-07223-12, Technical Research Center of Finland, 2012
- Kolehmainen, J. Modelling of hydrogen stratification and gas mixing in containment using the APROS code. Master's thesis. Lappeenranta University of Technology. March 2014.
- Kouhia, V.; Riikonen, V.; Kauppinen, O.-P.; Purhonen, H.; Austregesilo, H.; Bánáti, J.; Cherubini, M.; D'Auria, F.; Inkinen, Pasi; Karppinen, Ismo; Kral, P.; Pelto Korpi, L.; Peltonen, J.; Weber, S; Benchmark exercise on SBLOCA experiment of PWR PACTEL facility, *Annals of Nuclear Energy*. Elsevier. Vol. 59 (2013), 149 - 156
- Malet J., Mimouni S., Manzini G., Xiao J., Vyskocil L., Siccama N.B., Huhtanen R., Gas entrainment by one single French PWR spray, SARNET-2 spray benchmark, NURETH-15, May 12-17, Pisa, Italy, 2013
- Malet J., Huhtanen R. et. all, Gas entrainment by one single French PWR spray, SARNET-2 spray benchmark, *Nuclear Engineering and Design* 282 (2015)
- Silde, A. Validation of containment spray modelling of APROS on single droplet heat and mass transfer tests. VTT Research Report VTT-R-08953-11, 31.1.2012.

16. Experimental studies on containment phenomena (EXCOP)

16.1 EXCOP summary report

Markku Puustinen, Jani Laine, Antti Räsänen, Vesa Tanskanen, Lauri Pyy,
Elina Hujala, Joonas Telkkä

Lappeenranta University of Technology
School of Energy Systems
Nuclear Engineering
P.O. Box 20, FI-53851 Lappeenranta

Abstract

The EXCOP project has focused on experimentally studying at well controlled conditions different phenomena occurring in a scaled down BWR containment during steam/gas discharge into sub-cooled water and modelling these phenomena with CFD codes. Direct contact condensation as well as thermal stratification and mixing have been investigated both with straight vent pipes and with a SRV sparger. Sophisticated measuring solutions i.e. a Particle Image Velocimetry (PIV) system and high speed cameras have been used. Condensation models used in NEPTUNE_CFD and Fluent codes have been tested at Lappeenranta University of Technology (LUT) and VTT by comparing the simulation results with the measured data obtained in the PPOOLEX experiments. Furthermore, the experiment data has formed the basis for the development and improvement of the Effective Momentum Source (EMS) and Effective Heat Source (EHS) models to be implemented in GOTHIC code by Kungliga Tekniska Högskolan (KTH). Validation of certain system code models has also benefited from the experiment campaign of the EXCOP project.

Introduction

The PPOOLEX test facility at LUT, including models of a Boiling Water Reactor (BWR) drywell and wetwell compartments and withstanding proto-typical system pressure, has been extensively used in thermal hydraulic experiments dealing with different aspects of the suppression pool operation. Direct-contact condensation (DCC) at the vicinity of the blowdown pipe outlet, stratification/mixing during a long-lasting steam discharge condition and the behaviour of a safety relief valve (SRV) sparger under different flow modes among other topics have been studied in PPOOLEX. Numerical simulations with NEPTUNE_CFD, OpenFOAM, ANSYS Fluent and TransAT codes of several POOLEX and PPOOLEX tests have been performed.

Networking among international research organizations has been enhanced via participation in the NORTHNET framework and the NKS/ENPOOL project. Analytical and numerical work at KTH has been combined to the EXCOP, ELAINE, NUMPOOL and ESA projects of SAFIR2014. The EXCOP project has also a connection to the nuFoam project of SAFIR2014, where PPOOLEX data on DCC has been used in the validation of an OpenFOAM-solver.

Main objectives

The main objective of the EXCOP project has been to improve understanding and increase fidelity in quantification of different phenomena inside the drywell and wetwell compartments of BWR containment during steam discharge. The behaviour at the blowdown pipe outlet during air/steam discharge still needs to be investigated experimentally in more detail in order to improve simulation models. To achieve the project objectives, a combined experimental/analytical/computational study programme has been carried out. The experimental part at LUT has been responsible for the development of a database on condensation pool dynamics and heat transfer at well controlled conditions in the PPOOLEX test facility. Sophisticated measuring solutions i.e. a PIV system and modern high speed cameras have been used. The analytical/computational part at VTT, KTH and LUT has used the developed experiment database for the improvement and validation of models and numerical methods including CFD and system codes such as Fluent, NEPTUNE_CFD, TransAT, OpenFOAM, GOTHIC, APROS and TRACE. Also analytical support has been provided for the experimental part by pre- and post-calculations of the experiments.

PPOOLEX test facility

The PPOOLEX facility consists of a wetwell compartment (condensation pool), drywell compartment, inlet plenum and steam line piping. An intermediate floor separates the compartments from each other but a route for gas/steam flow from the drywell to the wetwell is created by a vertical blowdown pipe attached underneath the floor.

The main component of the facility is the ~31 m³ cylindrical test vessel, 7.45 m in height and 2.4 m in diameter. The test facility is able to withstand considerable structural loads caused by rapid condensation of steam. The removable vessel head and a man hole in the wetwell compartment wall provide access to the interior of the vessel for maintenance and modifications of internals and instrumentation. The drywell is thermally insulated. A sketch of the test vessel is shown in Figure 1. Steam needed in the experiments is produced with the nearby PACTEL test facility, which has a core section with 1 MW heating power and three horizontal steam generators [Tuunanen et al.]. Steam is led through a thermally insulated steam line from the PACTEL steam generators to the test vessel.

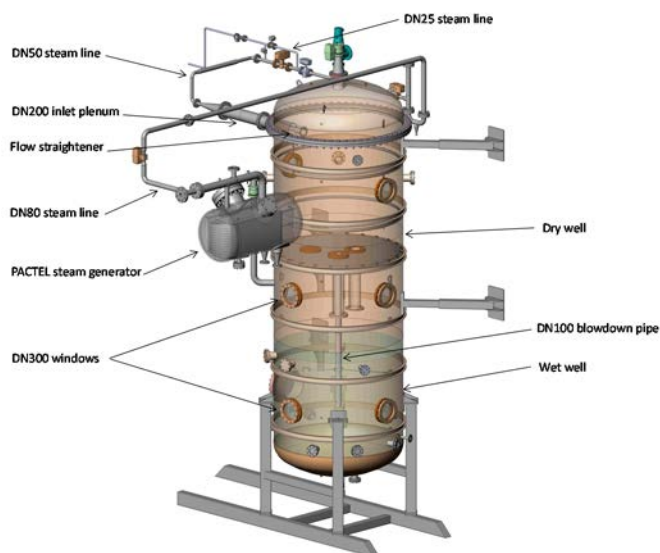


Figure 1. PPOOLEX test facility.

The applied instrumentation depends on the experiments in question. Normally, the test facility is equipped with several thermocouples for measuring steam, pool water and structural temperatures and with pressure transducers for observing pressures in the drywell, inside the blowdown pipes, at the condensation pool bottom and in the gas phase of the wetwell. Steam flow rate is measured with a vortex flow meter in the steam line. Additional instrumentation includes, for example, strain gauges on the pool outer wall and valve position sensors. A Particle Image Velocimetry system and up-to-date high speed cameras were added to PPOOLEX in 2011-2012. National Instruments PXIe PC-driven measurement system is used for data acquisition. The system enables high-speed multi-channel measurements.

Stratification and mixing experiments

In case of small steam flow rates, thermal stratification could develop above the blowdown pipe exit and significantly impede the pressure suppression capacity of the condensation pool. Pressure of the containment, determined by the temperature of free surface of water pool in the wetwell, will increase with development of thermal stratification and cause safety concerns in the containment.

Experimental studies have shown that once steam flow rate increases significantly, momentum introduced by the steam injection can destroy stratified layers and lead to mixing of the pool water. However, accurate and computationally efficient prediction of the pool thermal-hydraulics with thermal stratification, mixing, and transition between them, presents a computational challenge.

KTH is developing and implementing the EMS and EHS models in GOTHIC code [Li et al.]. The models have been proposed to simulate thermal stratification and mixing during a steam injection into a large pool of water. To provide necessary data for the development of the models, several experiments (MIX series) in the PPOOLEX facility were carried out in the framework of the SAFIR2014 and NORTHNET RM3 programs [Laine et al. 2013 & Laine et al. 2014]. A detailed test matrix, put together on the basis of pre-test calculations, was provided by KTH [Vil-lanueva et al. & Li et al.]. All experiments had clearing, stabilization, stratification and mixing periods.

In the MIX-01...06 experiments a DN200 blowdown pipe was used whilst in the MIX-07...12 experiments a DN100 pipe was used. Furthermore, the outlet of the DN100 pipe was about 300 mm higher than the outlet of the DN200 pipe. The submergence depth of the pipes was the same. An extensive net of temperature measurements was installed inside the blowdown pipe to accurately record the frequency and amplitude of steam/water-interface oscillations during the chugging condensation mode [Lahey & Moody]. This data is needed for the assessment of the EMS term.

The development of temperature stratification was very similar in both experiment series but differences were observed during the mixing period. With the DN200 blowdown pipe complete mixing was achieved in every experiment. However, the water pool began to stratify again despite of the high steam mass flux if the water bulk temperature was let to reach ~ 50 °C. In the DN100 case, the temperature difference between the pool bottom and surface decreased at first by 2–3 °C but then began to increase again. Complete mixing was thus not achieved. The main reason for this was the longer distance between the pool bottom and the outlet of the blowdown pipe which prevented internal circulation created by the steam jet from reaching the pool bottom to enhance mixing. Figures 2 and 3 present the vertical temperature profile of the pool during the stratification and mixing period in the MIX-11 experiment.

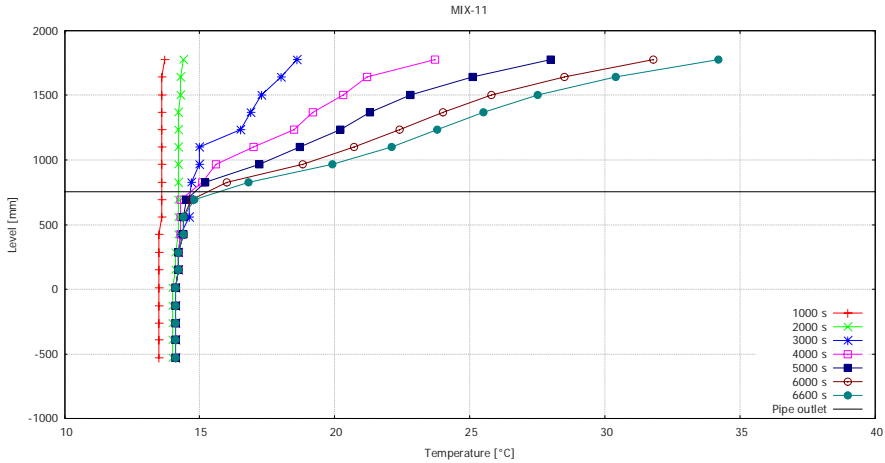


Figure 2. Vertical temperature profile of pool during the stratification period.

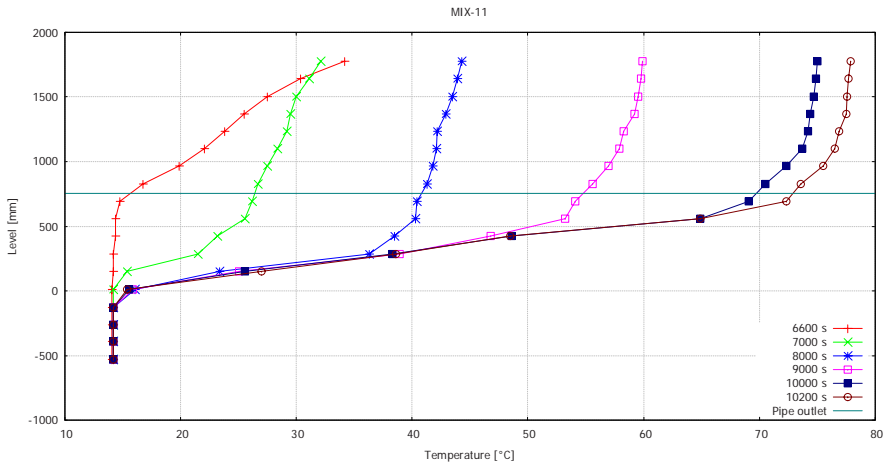


Figure 3. Vertical temperature profile of pool during the mixing period.

Sparger experiments

To obtain additional data for the development of the EMS and EHS models an experiment series with a safety relief valve (SRV) sparger was performed in the PPOOLEX facility [Laine et al. 2015]. The design and scaling of the model of the sparger was done by KTH [Gallego-Marcos et al.]. A detailed test matrix and procedure put together on the basis of the pre-test calculations was also provided by KTH [Villanueva et al. 2014].

The sparger model has 32 Ø8 mm holes drilled radially in the sparger head of the DN65 (Ø76.1x4.0) sparger pipe. The load reduction ring (LRR) is 700 mm above the pipe outlet and it has 8 axially drilled Ø8 mm holes. However, during the actual sparger experiments all the LRR holes were plugged. For detecting vertical tempera-

ture distribution in the pool and inside the sparger pipe several thermocouples were added to the existing instrumentation.

The sparger experiments consisted of two small steam flow rate stratification periods and of two higher (or lower) flow rate mixing periods. During the stratification phase steam flowed through the injection holes of the sparger head as small jets and condensed mainly outside the sparger pipe. Complete mixing of the pool succeeded either with a quite small steam flow rate when enough turbulence was created by external chugging or with a high flow rate when the momentum created by the horizontal steam jets was so strong that the resulting internal circulation hit the pool wall and partly turned downwards thus mixing also the elevations far below the sparger head, Figure 4. In the intermediate flow rate cases the created momentum was sufficient to cause mixing only along a small distance below the sparger head outlet elevation. In all cases the elevations above the sparger head outlet were, however, well mixed.

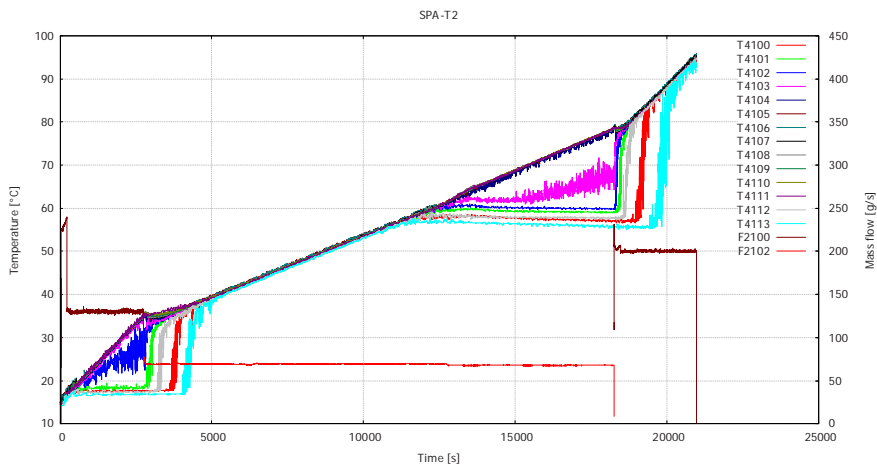


Figure 4. Complete mixing of the suppression pool with external chugging mode (at 5000 s) and with ellipsoidal jet mode (at 20000 s) in a sparger experiment.

PIV tests

A Particle Image Velocimetry measurement system was installed to the PPOOLEX facility at the end of 2011 for capturing the details of DCC related phenomena. The idea was to get CFD grade measurement data for validation of numerical models.

For the PIV measurement system to work correctly, clear raw particle images need to be recorded. For time-averaging purposes close to a constant velocity field should exist. Otherwise the fluctuations will diminish average velocity field close to zero.

It was soon found out that even with the use of fluorescent tracer particles and short pass filters the reflections from steam bubbles created huge problems in the field-of-view, FOV. With a big steam release to the FOV the reflections oversaturat-

ed the particle image so much that it was unusable. The long pass filters were replaced with common red band pass filters which let through only 0.4 % of 532 nm wavelength compared to the old long pass filters. However, steam created major optical problems that couldn't be conquered even with the new red band pass filters. The only way to present any PIV results from the DCC experiments is with individual vector images when there are optically intact raw images available, Figure 5.

The main finding from the DCC experiments was that PIV cannot be applied successfully for velocity measurements near the blowdown pipe outlet with the current PPOOLEX measuring set-up [Pyy & Telkkä]. The character of the flow in most steam discharge experiments is fluctuating and chaotic. These fluctuations make the time-averaging of PIV images impossible because there is no constant flow direction to be found. In addition, when there are optical distortions present, the PIV vector result is corrupted. At the moment there is not a way to get around these optical distortions even though the new filters succeeded well by cutting the reflections from the actual steam bubbles.

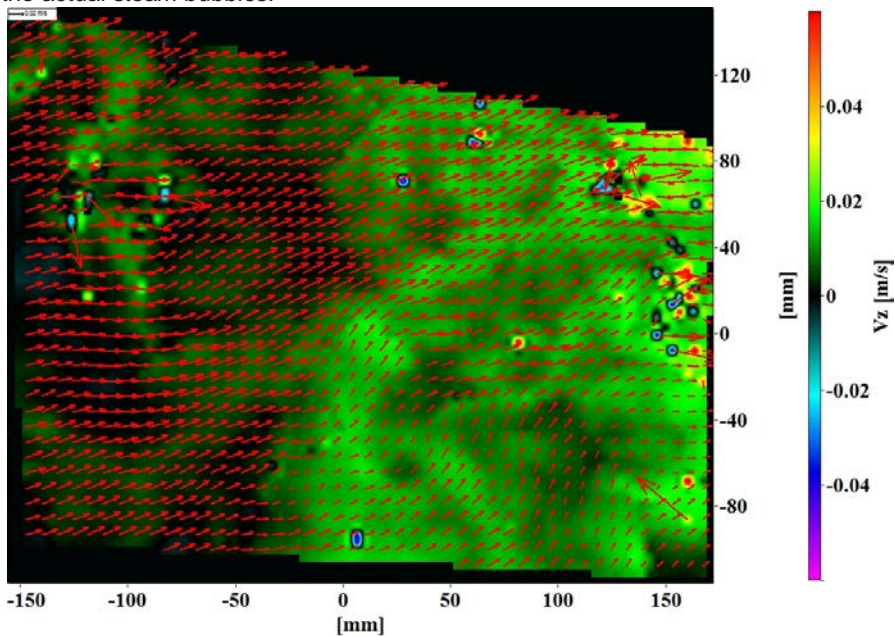


Figure 5. A vector image from a PIV measurement from the DCC-07 experiment.

Pattern recognition and CFD simulations

Macroscopic information of vapour-liquid interface and its changes obtained with a high-speed camera system does not directly apply to the CFD models but data of bubble size, surface deformation rate and frequency of bubble formation can be indirectly compared to field data of CFD simulations with the help of a pattern recognition algorithm. Experiment data on the DCC phenomenon obtained with the

POOLEX and PPOOLEX facilities has been utilized in the development work of such an algorithm.

The pattern recognition algorithm originally developed for a one camera system has been updated to be able to handle data from three high speed cameras [Hujala]. The idea of the algorithm is to subtract the background image from the image of interest and only the steam bubbles should remain. The algorithm consists of two parts: the first part is for the pattern recognition of bubbles and the second part is for the analysis of the recognized bubble images.

Chugging frequencies calculated with the help of the algorithm are realistic and of the same size as the average frequency calculated from the experimental data. However, some approximations are still needed due to nonhomogeneous lighting and disruptive visible objects of instrumentation. The method to be used in the evaluation of volume and surface area of steam bubbles has been chosen and the size distribution estimation with Sauter mean diameter should be ready in the near future. An example result of traced bubble boundaries is shown in Figure 6.

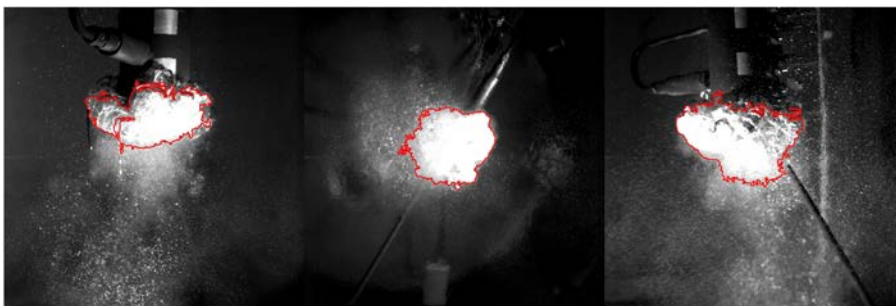


Figure 6. Recognized bubble patterns from three different camera angles in a PPOOLEX test.

Several NEPTUNE_CFD simulations of POOLEX and PPOOLEX direct contact condensation experiments have been done in the framework of the EXCOP and EU/NURESAFE projects. The aim has been to improve condensation models using the current separated flow condensation models as a starting point.

The value of indirectly obtainable quantities, such as those with the use of pattern recognition algorithms, is emphasized, because the condensation rates cannot be directly measured on highly oscillating interfaces even with modern instrumentation. In case of turbulent chugging mode condensation, it is necessary to simulate relatively long periods of time to obtain enough statistical data of chugging for reliable comparison with the pattern recognition data gathered from the experiments.

The Reynolds Averaged Navier-Stokes (RANS) simulations by using the Eulerian-Eulerian NEPTUNE_CFD code with steam tables have been promising. However, the 3D NEPTUNE_CFD v.2.0.1 simulation model of PPOOLEX did not lead to such strong chugging conditions as observed in the reference test. This outcome was general for all the condensation models tested. The result differs negatively from the

earlier NEPTUNE_CFD v.1.0.8 POOLEX chugging simulations. Despite of missing chugging, the condensation rates of all the models were high enough to condensate the detaching steam bubbles in the vicinity of the blowdown pipe outlet. Weak chugging or weak condensation rate in the PPOOLEX simulations is not a new challenge. Similar problems were encountered in previous studies by Pättikangas and his colleagues [Pättikangas et al.]. Turbulence kinetic energy (TKE) levels and turbulence production by chugging, initial state in the blowdown pipe, computational grid resolution, and the accuracy of calculated interfacial area will be plausible issues when addressing next the problem of too weak chugging. An example of the calculation of TKE in a DCC case is shown in Figure 7.

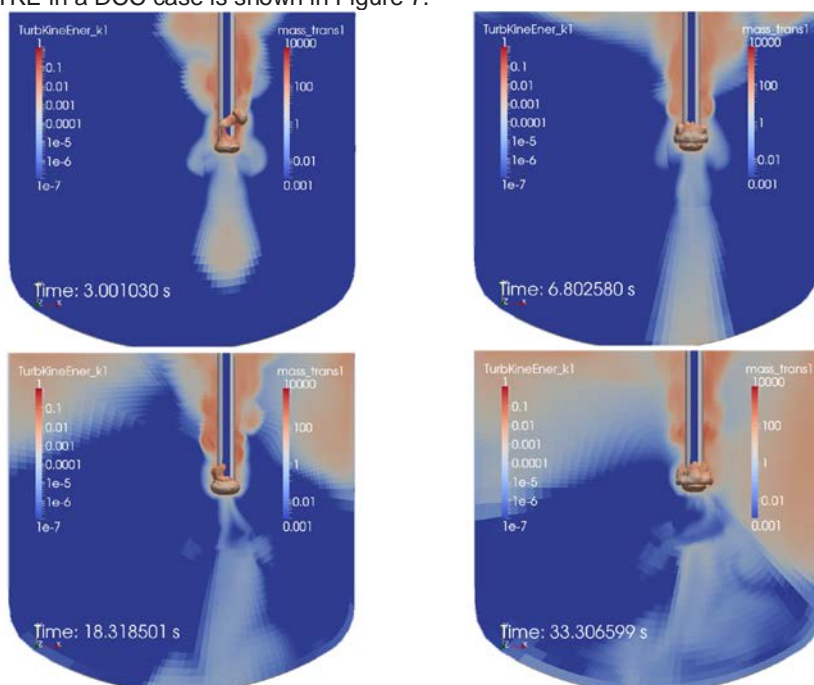


Figure 7. Development of turbulence kinetic energy field of liquid in the wetwell of PPOOLEX in a DCC simulation case.

References

- Tuunanen, J., Kouhia, J., Purhonen, H., Riikonen, V., Puustinen, M., Semken, R. S., Partanen, H., Saure, I. & Pylkkö, H. 1998. General Description of the PACTEL Test Facility. Espoo: VTT. VTT Research Notes 1929. ISBN 951-38-5338-1.

- Li, H., Villanueva, W. & Kudinov, P. 2014. Effective Models for Simulation of Thermal Stratification and Mixing Induced by Steam Injection into a Large Pool of Water. Division of Nuclear Power Safety, KTH.
- Laine, J., Puustinen, M. & Räsänen, A. 2013. PPOOLEX Experiments on the Dynamics of Free Water Surface in the Blowdown Pipe. Lappeenranta: Lappeenranta University of Technology. Nuclear Safety Research Unit. Research Report EXCOP 2/2012.
- Laine, J., Puustinen, M. & Räsänen, A. 2014. PPOOLEX Mixing Experiments. Lappeenranta: Lappeenranta University of Technology. Nuclear Safety Research Unit. Research Report EXCOP 1/2013.
- Villanueva, W., Li, H. & Kudinov, P. 2012. Proposed tests in PPOOLEX facility for the development of EMS model. Division of Nuclear Power Safety, KTH.
- Li, H., Villanueva, W. & Kudinov, P. 2013. Proposed Conditions for PPOOLEX Test in 2013. Division of Nuclear Power Safety, KTH.
- Lahey, R. T. & Moody, F., J. 1993. The Thermal-Hydraulics of a Boiling Water Reactor. American Nuclear Society, Illinois. 2nd edition.
- Laine, J., Puustinen, M. & Räsänen, A. 2015. PPOOLEX Experiments with a Sparger. Lappeenranta: Lappeenranta University of Technology. Nuclear Safety Research Unit. Research Report EXCOP 1/2014.
- Gallego-Marcos, I., Filich, L., Villanueva, W. & Kudinov, P. 2014. Scaling Analysis for Design of a Sparger in PPOOLEX Facility Tests. Division of Nuclear Power Safety. KTH.
- Villanueva, W., Gallego-Marcos, I. & Kudinov, P. 2014. Preliminary Test Matrix. Division of Nuclear Power Safety. KTH.
- Pyy, L. & Telkkä, J. 2015. PIV Measurements of DCC-06 and DCC-07 PPOOLEX Experiments. Lappeenranta: Lappeenranta University of Technology. Nuclear Safety Research Unit. Research Report EXCOP 2/2014.
- Hujala, E. 2013. Evaluation of Bubble Formation and Break Up in Suppression Pools by Using Pattern Recognition Methods. Lappeenranta: Lappeenranta University of Technology. Master's Thesis.
- Tanskanen, V. 2012. CFD modelling of direct contact condensation in suppression pools by applying condensation models of separated flow, Acta Universitatis Lappeenrantaensis 472., Lappeenranta University of Technology, ISBN: 978-952-265-221-8, ISBN: 978-952-265-222-5 (PDF), ISSN: 1456-4491.

Tanskanen V., Jordan A., Puustinen M. & Kyrki-Rajamäki R. 2014. CFD simulation and pattern recognition analysis of the chugging condensation regime, *Annals of Nuclear Energy* 66 (2014) pp. 133–143.

Pättikangas T., Niemi J., Laine J., Puustinen M. & Purhonen H. 2010. CFD modeling of condensation of vapour in the pressurized PPOOLEX facility. *CFD for Nuclear Reactor Safety Applications (CFD4NRS-3) Workshop*, Bethesda, MD, USA, 14-16 September 2010.

16.2 PPOOLEX Experiments with a Sparger

Jani Laine, Markku Puustinen, Antti Räsänen

Lappeenranta University of Technology
School of Energy Systems
Nuclear Engineering
P.O. Box 20, FI-53851 Lappeenranta

Abstract

The sparger experiments were carried out in 2014 with the scaled down PPOOLEX test facility designed and constructed at Lappeenranta University of Technology (LUT). Steam was blown through the vertical DN65 sparger type blowdown pipe to the condensation pool filled with sub-cooled water.

The main objective of the experiments was to obtain validation data for the development of the Effective Momentum Source (EMS) and Effective Heat Source (EHS) models to be implemented in GOTHIC code by Kungliga Tekniska Högskolan (KTH) [Li et al.]. The EHS and EMS models have been proposed to simulate thermal stratification and mixing during a steam injection into a large pool of water. A detailed test matrix and procedure put together on the basis of the pre-test calculations was provided by KTH.

Altogether five experiments, consisting of two stratification periods and two mixing periods, were carried out. The initial water bulk temperature in the condensation pool was 14–19 °C. During the stratification periods a mass flux of about 60–80 kg/m²s was used. With these flows steam condensed mainly outside the sparger pipe and no chugging kind of phenomenon existed. However, steam jets outside the sparger injection holes were too weak to create turbulence in the pool. As a result temperatures remained constant below the blowdown pipe outlet but increased towards the pool surface layers indicating strong thermal stratification of the wetwell pool water.

During the mixing periods the steam mass flux was increased rapidly to 80–165 kg/m²s or decreased to 25–43 kg/m²s to mix the pool water inventory. Total mixing of the pool was not obtained in every experiment. Mixing efficiency depended on the

flow mode in question i.e. on the used steam mass flow rate and on the pool bulk temperature. If not enough turbulence was created in the pool, the water volume below the sparger pipe outlet remained unmixed. In all cases the elevations above the sparger head outlet were, however, well mixed.

Introduction

The main objective of the EXCOP project was to improve understanding and increase fidelity in quantification of different phenomena inside the drywell and wetwell compartments of BWR containment during steam discharge. These phenomena could be connected, for example, to bubble dynamics issues, thermal stratification and mixing, wall condensation, direct contact condensation (DCC) and interaction of parallel blowdown pipes. Steam bubbles interact with pool water by heat transfer, condensation and momentum exchange via buoyancy and drag forces. Pressure oscillations due to rapid condensation can occur frequently.

To achieve the objectives, a combined experimental/analytical/computational research programme was carried out in the SAFIR2014, NORTHNET RM3 and NKS ENPOOL framework. The experimental part at LUT was responsible for the development of a database on condensation pool dynamics and heat transfer at well controlled conditions. The analytical/computational part at VTT, KTH and LUT used the developed experiment database for the improvement and validation of models and numerical methods including CFD and system codes. Also analytical support was provided for the experimental part by pre- and post-calculations of the experiments.

During a postulated accident or transient situation in a typical BWR plant the automatic depressurization system (ADS) could be activated and a large amount of steam would be blown from the reactor pressure vessel (RPV) to the condensation pool through the safety relief valve (SRV) sparger pipes. The wetwell pool serves as the major heat sink for condensation of steam. In November–December 2014 a series of experiments (labelled as SPA-T2...T6) focusing on the behaviour of a SRV sparger was carried out with the PPOOLEX test facility at LUT.

Test facility

The PPOOLEX test facility was taken into use at LUT in the end of 2006. PPOOLEX models the containment of a BWR plant. During the years the facility has gone through several modifications and enhancements as well as improvements of instrumentation. For the sparger experiments described here the facility was equipped with a model of a safety relief valve sparger pipe.

The PPOOLEX facility consists of a wetwell compartment (condensation pool), drywell compartment, inlet plenum and air/steam-line piping, Figure 1. An intermediate floor separates the compartments from each other. Usually a route for gas/steam flow from the drywell to the wetwell is created by a vertical blowdown pipe attached underneath the floor. In the sparger experiments the drywell was, however, by-

passed and steam was blown directly into the wetwell via the sparger pipe. Steam needed in the experiments is generated with the nearby PACTEL test facility, which has a core section with 1 MW heating power and three horizontal steam generators.

The main component of the facility is the $\sim 31 \text{ m}^3$ cylindrical test vessel, 7.45 m in height and 2.4 m in diameter. The test facility is able to withstand considerable structural loads caused by rapid condensation of steam. The dry and wetwell sections are volumetrically scaled according to the compartment volumes of the Olkiluoto 1 and 2 containment (ratio approximately 1:320).

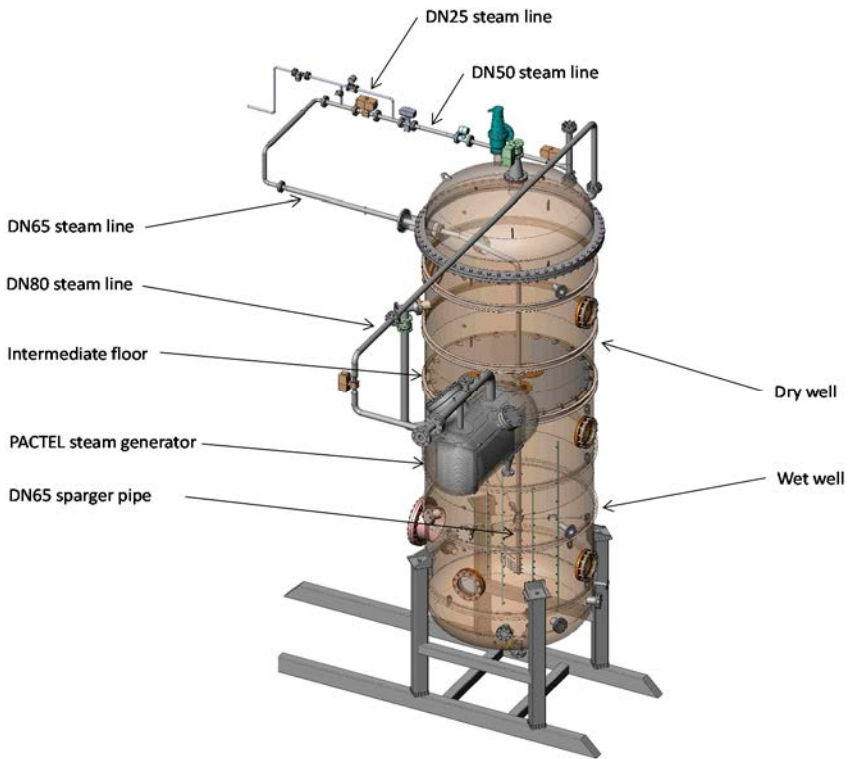


Figure 1. PPOOLEX test vessel.

The model of the sparger used in the experiments was designed and scaled by KTH. The goal of the scaling was to develop an approach for defining the scale and conditions of the PPOOLEX experiments with a sparger in order to cover the ranges of thermal hydraulic phenomena and regimes relevant to a steam discharge into a water pool in prototypical conditions of a BWR pressure suppression pool operation. The experiments should provide data for the validation of simulation models. However, the scaling does not aim to model experimentally the temperature profiles that could occur in a steam discharge in a BWR [Gallego-Marcos et al.].

The scaling approach has three levels: macro scale, meso scale and micro scale. In macro scale the goal was to determine pool water level, sparger submergence depth, steam flow rate, injection conditions and total exit hole area. Furthermore, the aim was to preserve characteristic ratios of mechanical and thermal energies to respective momentum and heat sources injected into the pool. In meso scale the goal was to determine the diameter of the sparger pipe and the location and dimensions of the load reduction ring (LRR) in order to control condensation regime in the steam line and distribution of heat and moment sources in the pool. In micro scale the goal was to determine the total exit hole area and the diameters of the LRR and sparger holes to cover the ranges of micro scale phenomena so that mass fluxes and ratios of buoyant, inertial and viscous forces are similar as in a typical BWR sparger. The PPOOLEX sparger experiments were designed to cover the maximum possible range of steam mass fluxes and injection conditions which can be scaled with the given limitations of the PPOOLEX facility. GOTHIC code was used to estimate the steam mass flow rate and injection conditions [Gallego-Marcos et al.].

As a result of the selected scaling approach the sparger model used in the PPOOLEX experiments has 32 $\varnothing 8$ mm holes drilled radially in the lower part (sparger head) of the DN65 ($\varnothing 76.1 \times 4.0$) sparger pipe, Figure 2. The load reduction ring is 700 mm above the pipe outlet and it has 8 axially drilled $\varnothing 8$ mm holes. However, during the actual sparger experiments all the LRR holes were plugged.

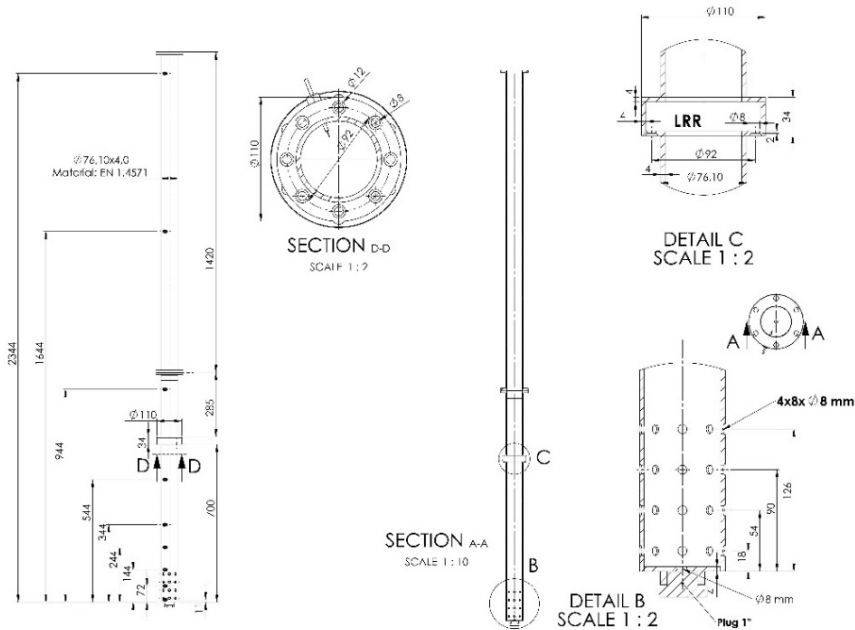


Figure 2. Scaled sparger model used in the PPOOLEX experiments.

The applied instrumentation depends on the experiments in question. Normally, the test facility is equipped with several thermocouples (T) for measuring steam, pool water and structure temperatures and with pressure transducers (P) for observing pressures in the drywell, inside the blowdown pipes, at the condensation pool bottom and in the gas space of the wetwell. Steam flow rate is measured with a vortex flow meter (F) in the steam line. Additional instrumentation includes, for example, strain gauges (S) on the pool outer wall and steam line valve position sensors.

For the sparger experiments a 6x7 grid of temperature measurements was installed in the pool in front of the injection holes of the sparger head. For measuring vertical temperature distribution inside the sparger pipe temperature measurements were installed with a varying interval. Four trains of temperature measurements (thermocouples T4100...T4113, T4200...T4219, T4300...T4319 and T4400...T4413) were installed in the pool below the water level for detecting vertical temperature distribution, Figure 3

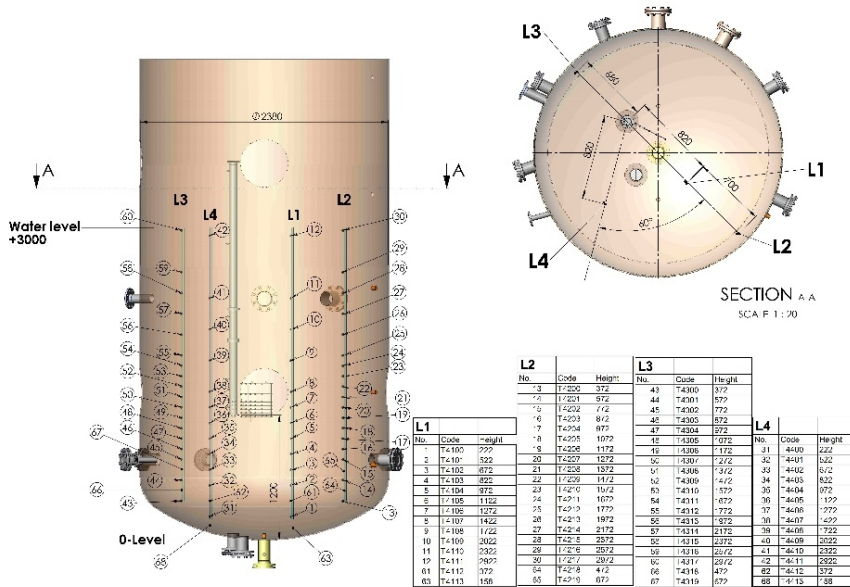


Figure 3. Four trains of temperature measurements in the wetwell.

Test program

The sparger test program in 2014 consisted of five experiments (labeled from SPA-T2 to SPA-T6). Before the actual experiments a characterization test (SPA-T0) was carried out. The main purpose of the SPA experiment series was to obtain additional data for the development of the EMS and EHS models to be implemented in GOTH-IC code by KTH. A detailed test matrix and procedure put together on the basis of

the pre-test calculations was provided by KTH before the experiments [Villanueva et al.]. During the experiment campaign the test parameters for the next test were updated on the basis of an initial analysis of the results of the previous tests. All the experiments had two stratification periods and two mixing periods.

The path of each experiment defined by steam mass flux and pool bulk temperature is marked on the condensation mode map for a sparger of Chan and Lee [Chan and Lee] in Figure 4. In the map the steam mass flux is determined as the mass flow rate through the injection holes of the sparger head divided by the cross-sectional area of the holes.

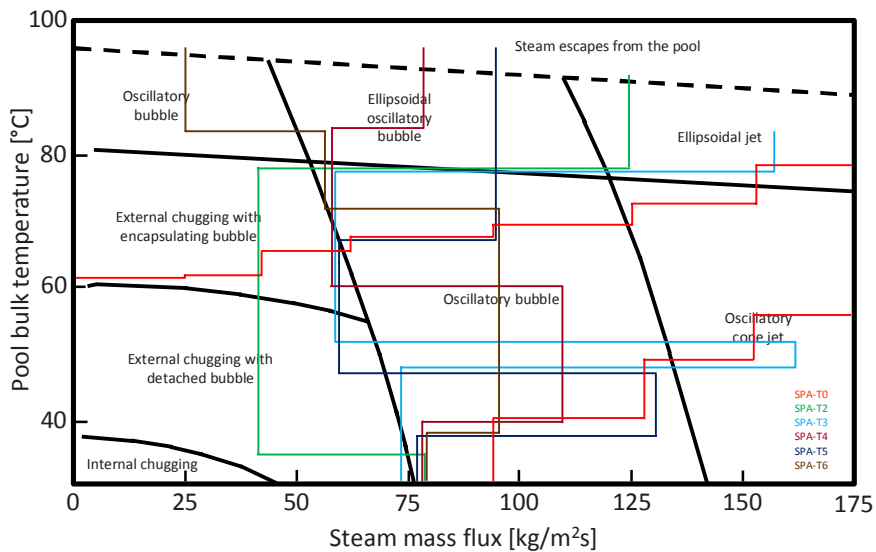


Figure 4. Paths of the SPA experiments marked on the direct condensation mode map for pure steam discharge of Chan and Lee.

Experiment results

The SPA experiments consisted of two small steam flow rate stratification periods and of two higher (or lower) flow rate mixing periods. In the beginning of the experiments air was removed from the steam line and the piping structures were heated up for 200 seconds with a steam mass flow rate of 220–240 g/s. Before the experiments, the wetwell pool was filled with isothermal water (14–19 °C) to the level of 3.0 m i.e. the sparger pipe outlet was submerged by 1.8 m.

After the steam line had been heated up the steam flow rate was rapidly decreased to the level of 120–130 g/s (corresponding to the mass flux of about 80 kg/m²s) in order to start the first stratification period. With this kind of mass fluxes steam flowed through the injection holes of the sparger head as small jets and condensed mainly outside the sparger pipe. Because no chugging kind of phenomenon

existed and the steam jets were too weak to create much turbulence in the pool suitable conditions for thermal stratification to occur prevailed. As a result temperatures below the sparger pipe outlet remained constant while they rose towards the pool surface layers indicating strong thermal stratification of the wetwell pool water, Figure 5 and Figure 6. The heat-up process was driven by the flow of warm condensed water upwards from the sparger outlet as well as by conduction through the pipe wall. The stratification period was continued as long as the temperature difference between the pool bottom and surface had reached the target value given by KTH i.e. 15–30 °C depending on the test.

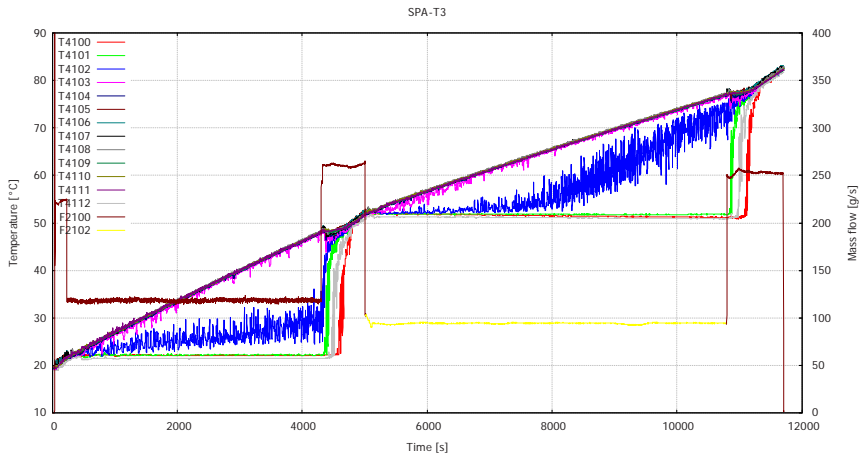


Figure 5. Vertical temperature distribution in wetwell water (T4100–T4112) and steam flow rate (F2100 and F2102) in SPA-T3.

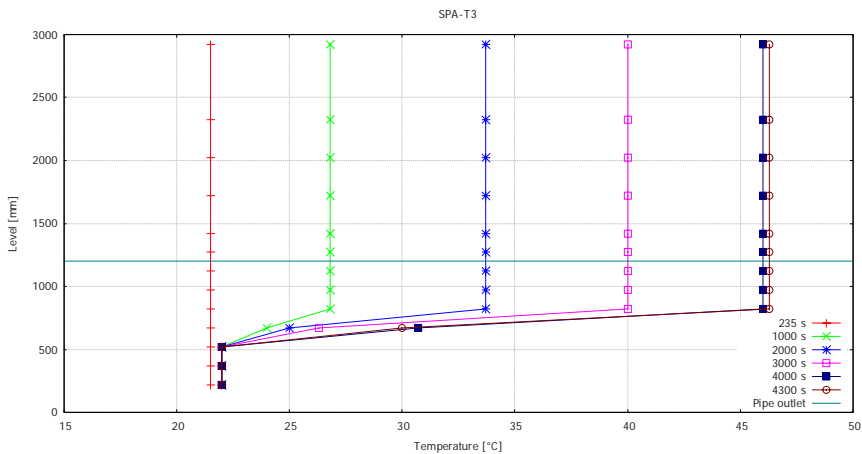


Figure 6. Development of vertical temperature profile of pool water in SPA-T3 during the first stratification period.

After the desired temperature difference between the pool bottom and surface was attained the steam mass flow rate was rapidly increased up to 150–260 g/s (about 95–165 kg/m²s) to create turbulence in the pool with the help of the steam jets and thus to mix the condensation pool water inventory totally. In SPA-T2 the steam flow rate for the first mixing period was decreased to 70 g/s (about 43 kg/m²s) to find out if the pool water inventory can be mixed with external chugging condensation mode, Figure 4 and Figure 7. With the highest used flow rates as well as with the 70 g/s flow rate enough turbulence was created to mix the pool water volume completely. Depending of the used steam flow rate and initial pool water temperature it took 500–2950 s to achieve total mixing of the pool. With the intermediate flow rate (150 g/s) mixing was observed only along a small distance below the sparger head outlet elevation. The elevations above the sparger head outlet were, however, well mixed.

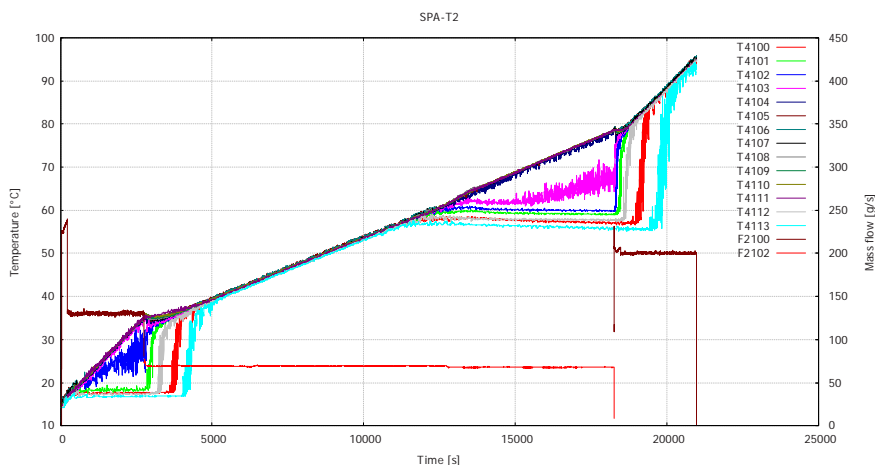


Figure 7. Vertical temperature distribution in wetwell water (T4100–T4112) and steam flow rate (F2100 and F2102) in SPA-T2.

After the pool water inventory had mixed totally the second stratification period was initiated by decreasing the steam flow rate to the level of 90–97 g/s (round 60 kg/m²s). With this flow rate steam condensed again mainly outside the sparger pipe thus creating suitable conditions for thermal stratification to occur. Because the pool water bulk temperature was 20–40 °C higher than in the beginning of the first stratification period lower steam flow rate could be used without the risk of ending up in the chugging region of the condensation mode map, see Figure 4. The second stratification period was continued as long as the temperature difference between the pool bottom and surface had reached the target value of 20–30 °C depending on the test.

After the desired temperature difference between the pool bottom and surface was attained the second mixing period was initiated by increasing the steam flow

rate rapidly to the level of 130–250 g/s (about 80–160 kg/m²s). Total mixing of the pool water inventory was achieved only in SPA-T2 and SPA-T3 with 200 and 250 g/s steam flow rate, correspondingly. In SPA-T2 it took 2250 s and in SPA-T3 530 s before the pool water had mixed totally. In SPA-T6, the steam flow rate was decreased to 40 g/s (round 25 kg/m²s) for the second mixing period in order to find out if the pool water inventory could be mixed with oscillatory bubble condensation mode. However, with this flow rate the temperature difference between the pool bottom and surface increased from 65 °C to 72 °C since condensation took place inside the sparger pipe and there was no mixing effect at all.

Summary and conclusions

The sparger experiments were carried out in 2014 with the scaled down PPOOLEX test facility designed and constructed at Lappeenranta University of Technology. The main objective of the experiments was to obtain validation data for the development of the Effective Momentum Source and Effective Heat Source models to be implemented in GOTHIC code by KTH.

Altogether five experiments were carried out according to a test plan written by KTH. The experiments consisted of two small steam flow rate stratification periods and of two higher (or lower) flow rate mixing periods.

During the first stratification period a 120–130 g/s steam flow rate was used. With this flow rate steam flowed through the injection holes of the sparger head as small jets and condensed mainly outside the sparger pipe. No chugging kind of phenomenon existed and the steam jets were too weak to create turbulence in the pool. As a result temperatures remained constant below the sparger pipe outlet but increased towards the pool surface layers indicating strong thermal stratification of the wetwell pool water. In the end of the first stratification period the temperature difference between the pool bottom and surface was 18–26 °C depending on the test in question. In the second stratification period a 70–97 g/s steam flow rate was used. In the end of this period the temperature difference between the pool bottom and surface was 20–31 °C.

During the mixing periods the steam flow rate was increased rapidly to 130–260 g/s or decreased to 40–70 g/s to mix the pool water inventory. Total mixing of the pool was not obtained in every experiment. Mixing efficiency depended on the flow mode in question i.e. on the used steam mass flow rate and on the pool bulk temperature. With the highest used flow rates (from 175 to 260 g/s) complete mixing was achieved. Complete mixing was also achieved with the 70 g/s flow rate. With the used intermediate flow rates (130 and 150 g/s) and with the lowest used flow rate (40 g/s) mixing was incomplete. One reason for this kind of behavior is the horizontal direction of the injection holes in the sparger head. When the flow rate is very low (in the range of 40 g/s) condensation takes place inside the sparger pipe and there is no mixing effect at all. When the flow rate is in the region of 70 g/s the flow mode is external chugging, where steam jets out and water suction into the sparger head through the injection holes alternate. This creates enough turbulence in the

pool so that also the water volume below the sparger pipe outlet is finally mixed. With the intermediate and high flow rates steam jets through the injection holes prevail and there is no water ingress back into the sparger head. In the high flow rate cases the momentum created by the horizontal steam jets is so strong that the resulting internal circulation hits the pool wall and partly turns downwards thus mixing also the elevations far below the sparger head. In the intermediate flow rate cases the created momentum is sufficient to cause mixing only along a small distance below the sparger head outlet elevation. In both cases the elevations above the sparger head outlet were, however, well mixed.

References

- Li, H., Villanueva, W. & Kudinov, P. 2014. Effective Models for Simulation of Thermal Stratification and Mixing Induced by Steam Injection into a Large Pool of Water. Division of Nuclear Power Safety. KTH.
- Gallego-Marcos, I., Filich, L., Villanueva, W. & Kudinov, P. 2014. Scaling Analysis for Design of a Sparger in PPOOLEX Facility Tests. Division of Nuclear Power Safety. KTH.
- Villanueva, W., Gallego-Marcos, I. & Kudinov, P. 2014. Preliminary Test Matrix. Division of Nuclear Power Safety. KTH.
- Chan, C. K. & Lee, C. K. B. 1982. A Regime Map for Direct Contact Condensation. *Int. J. Multiphase Flow*.

17. OpenFOAM CFD-solver for nuclear safety related flow simulations (NUFOAM)

17.1 NUFOAM summary report

Juho Peltola¹, Juhaveikko Ala-Juusela², Tomas Brockmann², Karoliina Ekström⁴, Giteshkumar Patel³, Timo Pättikangas¹, Timo Siikonen², Vesa Tanskanen³, Timo Toppila⁴

¹VTT Technical Research Centre of Finland Ltd
P.O. Box 1000, FI-02044 Espoo

²Aalto University
P.O. Box 11000, FI-00076 AALTO, Finland

³Lappeenranta University of Technology
P.O. Box 20, FI-53851 Lappeenranta, Finland

⁴Fortum Power and Heat Oy
P.O. Box 100, FI-00048 FORTUM

Abstract

OpenFOAM is the most popular open source computational fluid dynamics code. It is not a monolithic program like most commercial CFD solvers, but more of a library of C++ modules that can be used to create specialized solvers for different applications. However, it does come with a large number of pre-built solvers that can be used as-is in many applications. In this project, solvers based on the library have been used to simulate single phase flow in fuel rod bundles and in a T-junction. Simulation results were submitted to the blind OECD/NEA MATIS-H fuel rod bundle benchmark. Existing OpenFOAM multiphase solvers have been adapted and extended for simulation of subcooled nucleate boiling. These solvers have been tested against experimental data and results of alternative CFD codes. The same solvers have also been modified and tested for simulation of direct-contact condensation.

Introduction

In the field of nuclear reactor safety analysis, Computational Fluid Dynamics (CFD) has become an increasingly popular tool for thermal hydraulic investigations. There are several suitable, commercial and open-source, CFD-codes available, but in recent years the open-source CFD-library called OpenFOAM has been gaining popularity worldwide. These days, it is clearly the most widely used open source CFD code. The code originated in Imperial College London in late 1980's and was published as open-source in 2004. It is distributed by the OpenFOAM Foundation.

Compared to commercial solvers, the benefits of an open source CFD code are transparency, infinite customizability and lack of licensing fees, which brings the cost of massively parallel computation down to a feasible level. Compared to other open source CFD codes, the benefits of OpenFOAM® are a large, active and growing user base, modern approach to mesh handling with unstructured and polyhedral meshes, parallelization and an object oriented code structure that makes it fast and easy to implement new models and solvers in the top level code.

Distinct drawbacks of OpenFOAM are the lack of public, formal documentation and – partially because of the previous point – a very steep learning curve. Generally it can also be said that many of the features of OpenFOAM represent the state-of-the-art, but often lack the polish to directly apply them to practical engineering problems. In this project we try to alleviate these drawbacks from the perspective of nuclear reactor safety analysis to make OpenFOAM a practical tool for these applications. Initial work was carried out in 2010 by validating turbulent near-wall treatments in pipe flows, developing a version of two-phase solver that is suitable for dispersed bubbly flows and by participating in the OECD/NEA T-junction benchmark.

Main objectives

The main aim of the project has been to validate components of OpenFOAM® as tools for nuclear reactor safety related simulations. An application oriented approach for validation has been used. The first goal has been to be able to simulate transient single-phase flows and heat transfer in a complex geometry, especially in the fuel assembly and its head parts, more accurately using efficient parallel computing. As a result, a more detailed understanding of the coolant mixing is expected and the results can be used, e.g., in verifying safety issues when increasing the burn up of the fuel.

Another branch of the project has been to adapt and extend OpenFOAM® two-phase flow capabilities for nuclear safety analysis applications, specifically to two-fluid turbulent gas-fluid flow simulations with heat transfer, boiling and condensation. In this project, the goal has been to successfully simulate subcooled nucleate boiling in a PWR fuel rod bundle and direct contact condensation (DCC) in a suitable test case.

An important goal of the project has also been to strengthen the Finnish CFD community in the field of nuclear safety and to participate in Northnet and other international cooperation.

Simulation of single phase flows

The work on single phase simulations has been carried out at Aalto University and Fortum. Fortum took part in the MATIS-H benchmark, simulating a horizontal fuel rod bundle with a spacer grid utilizing RANS turbulence modelling. Aalto University has mainly concentrated on studies of the VVER-440 fuel rod bundle. It has been simulated with different turbulence modelling approaches, including more advanced approaches like Large-Eddy Simulation (LES) and Detached-Eddy Simulation (DES). A new inflow boundary condition was implemented that is able to generate the transient turbulent inflow that is required in LES and DES simulations, without need for inlet recirculation or long inflow sections.

OECD/NEA MATIS-H Benchmark

OECD/NEA MATIS-H benchmark (Measurement and Analysis of Turbulent Mixing in Subchannels - Horizontal) was a blind CFD benchmark exercise, where the flow in a cold 5x5 fuel rod bundle with a spacer grid was solved. The test facility, MATIS-H, is located at the Korea Atomic Energy Research Institute (KAERI) in Daejeon, South Korea. The test participants were given details of the test geometry and operating conditions. The velocity components, turbulent intensity and vorticity information inside the fuel rod bundle and in the vicinity of the spacer grid were calculated. Fortum contributed to the benchmark by calculating the test case with OpenFOAM 2.1.0.

The mesh of CFD model was created using ANSYS Gambit 2.4.6. The mesh contained 14 million cells of which 87 % were hexahedral and 13 % tetrahedral. The case was calculated using different solvers and turbulence models and for comparison, the case was also calculated using the commercial CFD code ANSYS Fluent 13.0. The computation mesh is presented in Figure 1.

The results of the different simulations were compared against the experimental data from a test without a spacer grid that was available for the participants. The κ - ϵ turbulence models in Fluent and OpenFOAM seemed to give quite coherent results, whereas the Reynolds stress model in Fluent differed to some extent. The κ - ϵ model results gave good agreement with the experiment. The Fluent steady state and time dependent results were identical. In OpenFOAM, the SimpleFoam (steady state) and PimpleFoam (time dependent) results were very similar as well. After comparisons of the different cases, the OpenFOAM - SimpleFoam - κ - ϵ results were chosen as those to be submitted to the benchmark organisers. A report on the benchmark participation including a summary of results was written (Ekström, 2014).

Summary of the results of all participants was presented in OECD/NEA & IAEA workshop CFD4NRS-4 in September 2012 (Smith et al., 2013). The total of 25 par-

Participants had submitted simulation results. Commercial codes CFX, STAR-CCM+ and Fluent were used by most participants, only one had used OpenFOAM code. Different approaches were used for the turbulence modelling; LES, hybrid approaches, RSM and RANS with SST $k-\omega$ or $k-\epsilon$. Our results were selected as the "best estimations case of $k-\epsilon$ turbulence model", and most of the main flow features were presented satisfactory by our simulation, as demonstrated by the well captured mean flow profiles shown in Figure 2. As a feedback for the NuFoam project, it was clear that OpenFOAM is as good as any CFD code for this kind of CFD simulations.

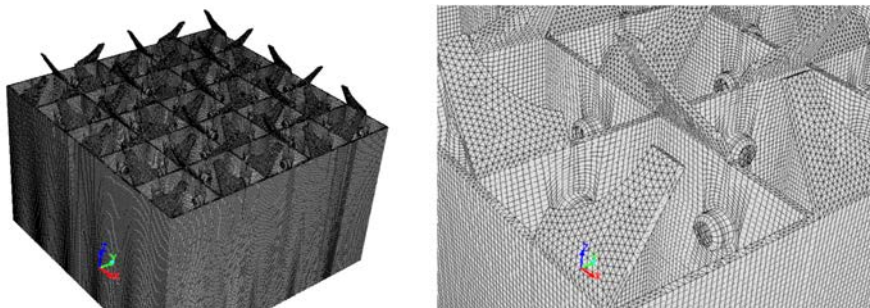


Figure 1. Computational mesh at the surface of spacer grid in the MATIS-H simulations. Whole spacer grid (left) and one mixing vane (right).

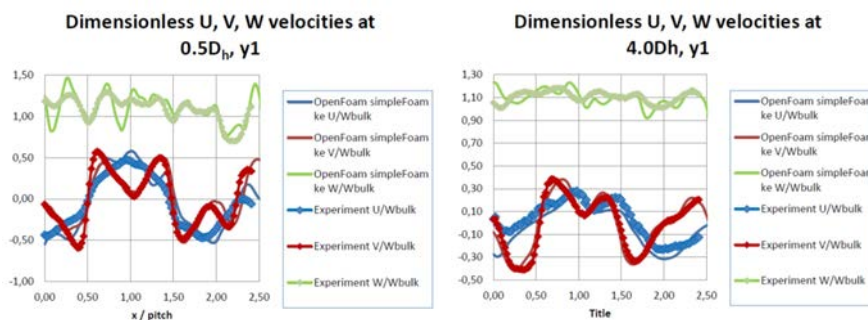


Figure 2. Flow inside the MATIS-H fuel rod bundle without a spacer grid. Comparison of measured and calculated mean velocity components.

VVER-440 fuel rod bundle

Simulations of VVER-440 fuel rod bundle were started by applying OpenFOAM and FINFLO CFD-codes to isothermal one spacer grid interval models. OpenFOAM RANS simulations were carried out with traditional 30 degree sectional models as well as with a single sub-channel model.

In these simulations, the standard $k-\epsilon$, SST $k-\omega$ and Launder-Gibson Reynolds stress models were applied to include the turbulent effects. The Reynolds stress

turbulence model predicted stronger vorticity structures in the sub-channels than the two-equation models. Furthermore, a single spacer interval DES simulation was done with FINFLO-code by applying the SST $k-\omega$ turbulence model. The simulation gives some time varying flow patterns, but otherwise the results were close to the RANS results which were used as an initial guess. Large-scale turbulent fluctuations did not appear with the applied mesh resolution. Initial full rod length RANS simulations were also performed with FINFLO-code.

Simulations of VVER-440 fuel rod bundle were continued by finally applying OpenFOAM also to the full-length bundle, both in isothermal and heat transfer cases. At first, the same computational grid as with FINFLO-code was utilized, but it was found to cause severe instability in heat transfer simulation. Nominally sufficient aspect ratios in certain cells were too large with the added complexity in the solution due to the solution of the energy equation. A new denser grid was created that consists of 56.6 million cells. The largest aspect ratios were cut to one half compared to the original grid. It was also found out that velocity distributions predicted by simpleFoam-solver, used in the isothermal case and the velocity distributions of heat transfer capable buoyantSimpleFoam-solver, were different, even when the latter was used in an isothermal case. This study was carried out with OpenFOAM release 2.3.0. While simpleFoam distributions are slightly closer to measurements, buoyantSimpleFoam results are almost identical to the earlier FINFLO-code results. All RANS simulations, except the simpleFoam ones, share similarities with earlier simulations, showing sharp peaks in velocity distributions above the spacers which hold the fuel rods. A large velocity peak also tends to appear above the 'O'-shape sub-channel, which is not there in the measured flow distributions. However, it should also be noted that the velocity distributions in this case are extremely sensitive to location. Moving the sampling line by just 0.1 mm across the stream direction causes large changes in the velocity distributions.

Heat transfer simulations were carried out by utilizing constant heat flux from the rods. In real applications the heat fluxes are rod and location dependent but these features were left for future investigations. Fairly good heat balance was achieved and the influence of turbulent mixing in temperature distribution could be observed. Heating up of the coolant as it flows through the rod bundle can be seen in Fig 3.

Revised single sub-channel simulations were carried out by applying the RANS, LES and DES turbulence modelling approaches with OpenFOAM (Figure 4). The model was reduced to a minimal size in order to save computational time while studying the turbulent behaviour. It was also important to avoid excessive computational difficulties related to the complexity and the size of the computational grid. The simulations were carried out with a coarse near-wall mesh resolution ($y^+=2\dots22$). The LES/DES grid had to be fine enough to capture the large-scale turbulent behaviour, which requires significantly more cells than the RANS simulations. The RANS simulations using a grid with 0.39 million cells took 15 hours of a wall-clock time and the LES and DES simulations with 2.9 million cells took 14 days. The mean flow passes the model 7 times during the simulated time period. In the DES and LES simulations, SST-SAS and self-implemented version of the dynamic Smagorinsky turbulence models were applied, respectively (Menter & Egorov, 2009; Piomelli & Liu, 1995).

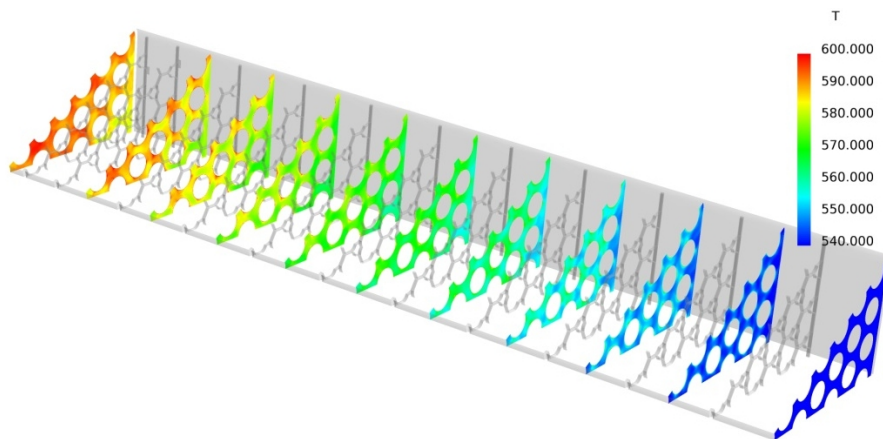


Figure 3. Temperature distributions on planes normal to flow direction in the denser full-rod-length RANS simulation. Rod spacers are shown in grey. OpenFOAM-code with SST k- ω turbulence model. Geometry is scaled for visualization purposes.

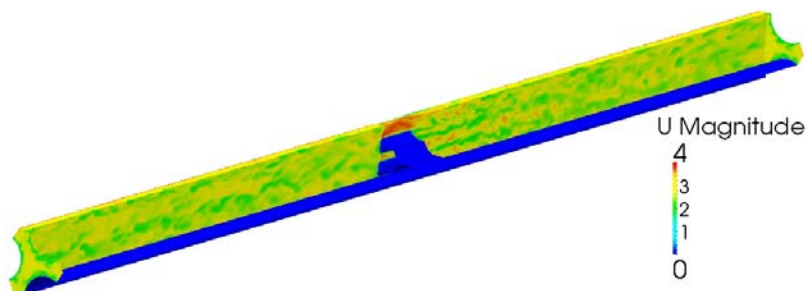


Figure 4. Velocity distributions in the single sub-channel DES simulation. SST-SAS turbulence model. Periodic boundary conditions.

Static inflow conditions are often inadequate in time dependent LES and DES simulations. In order to make realistic LES and DES simulations of turbulent flows, it is necessary to describe properly the incoming turbulent flow. In this work a pre-processing utility was developed to create synthetic flow fluctuations on boundary surfaces of OpenFOAM simulations. This approach eliminates the need for recirculations of the inflow or a long inflow section. The fluctuating velocity components are based on sums of Fourier series to include the energy spectrum between the smallest and largest resolvable scales. In present work, the fluctuations are isotropic which is seldom an accurate representation of actual flow conditions. Regardless, the method was demonstrated in a channel flow case shown in Figure 5 as a useful way of initialising turbulent flows (Davidson, 2007).

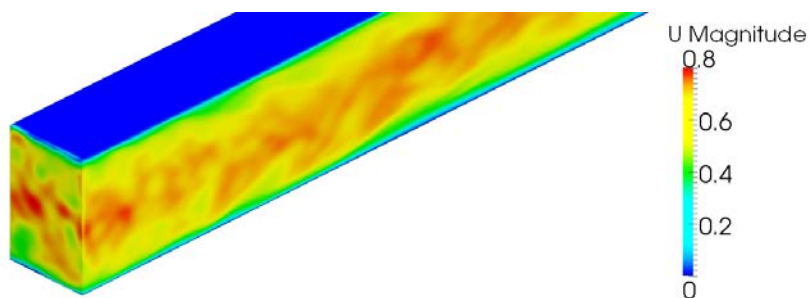


Figure 5. Velocity distributions in a channel flow LES simulation with isotropic synthetic turbulent inflow. Dynamic Smagorinsky turbulence model. $Re_b=2800$.

Modelling of two-phase flows

In two phase flows, the work in the project has been more oriented towards code development simply because the publicly available OpenFOAM solvers were not capable of simulating two-phase flows with boiling and condensation. The development effort of the main solver and simulations of dispersed bubbly flows and sub-cooled nucleate boiling has been carried out at VTT. This work is presented in more detail in an accompanying special report. LUT has concentrated on adapting the two-phase solver for simulations of direct-contact condensation (DCC) and relevant test simulations, implementing Hughes and Duffey (1991) surface renewal model and Lakehal et al. (2008) surface divergence DCC model into the two-phase solver.

Direct-contact condensation

The initial validation of implemented DCC models was performed in CFD simulations of the STB-31 experiments of steam discharge into sub-cooled water. These experiments were carried out with the scaled-down condensation pool test facility (POOLEX) at LUT. This stable steam-water interface at blowdown pipe mouth experiment was successfully simulated with an OpenFOAM 1.7 based, incompressible two-phase solver developed in this project.

The next step was simulations of a more challenging STB-28 experiment. The POOLEX STB-28 experiment consisted of one long-running steam blowdown. The purpose of this test was to analyze the formation and condensation of steam bubbles at the blowdown pipe outlet as a function of pool water temperature. The experiments were recorded with high-speed and standard video cameras. Promising results have previously been obtained with the NEPTUNE CFD code utilizing the Hughes-Duffey heat transfer model for direct-contact condensation.

There were seven intervals of about 12 - 30 s recorded during the blowdown with a higher sampling rate. These were labelled from STB-28-1 to STB-28-7. During the test, the temperature of pool water rose from 47 C° to 77 C°. The steam mass flow rate was kept at $0.3 \text{ kg}\cdot\text{s}^{-1}$ during the whole blowdown.

The STB-28-4 test of the POOLEX facility of LUT was simulated. In order to solve the case as 2D-axisymmetric one with a 3D solver, a 2° sector of the POOLEX pool was modelled. A grid of hexahedral cells was generated by rotating a quadrilateral grid with respect to z-axis to contain a single cell thickness. In the present simulations, the interfacial heat transfer between steam and water was modeled by using the surface renewal theory based condensation model of Hughes and Duffey (HD). Flow turbulence was solved by employing the standard k- ϵ turbulence model. The available standard OpenFOAM thermodynamic libraries were not well-suited to the simulation of thermal phase change. However, this limitations can be avoided by disabling the steam phase enthalpy transport solution and by setting suitable saturation state enthalpies and temperatures while matching the steam phase thermal capacitance to the saturated state.

Only the initial 30 s period of STB-28-4 test was simulated. The volume fraction fields of Figure 6 show the first bubble of the OpenFOAM simulation. The early phase of the simulation seems promising, as the initial hyperboloid jet condenses quite rapidly. A toroidal bubble is formed after that as was expected. However, it can be seen that the size of the bubble is relatively large. As simulation is continued, it can be seen that the bubble still oscillates at the blowdown pipe outlet, never collapsing totally. This indicates that the predicted condensation rate is high enough to condense the steam before any bubbles detach from the steam outlet, but at the same time too low to initiate proper chugging.

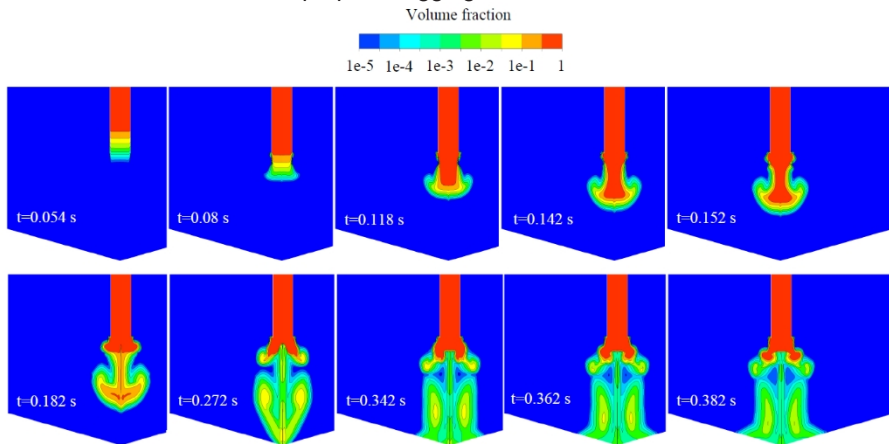


Figure 6. Volume fraction field in the 2D-axisymmetric OpenFOAM CFD simulation of the STB-28-4 experiment by using the HD condensation model.

Figure 7 displays the predicted condensation mass flow rate in the STB-28-4 experiment with the HD condensation model. The condensation rate oscillates quite symmetrically around the inlet steam mass flow rate value, whereas the mean DCC rate is lower than the circa 0.3 kg s^{-1} obtained in the NEPTUNE CFD simulation (Tanskanen et al. 2014). Due to this, the condensation model implemented in OpenFOAM resembles more the “condensation oscillations” or the “quasi-steady conden-

sation” modes than the “chugging” mode. Despite this result, a promising outcome is that the DCC rate is high enough to condensate the steam in the vicinity of the blow-down pipe outlet. Promisingly, the stability of the solver was also good during the simulation. Concerning the future work, the following matters should be considered:

- Comparison of the near-interface turbulence kinetic energies between the NEPTUNE_CFD and OpenFOAM results.
- Use of a compressible flow solver
- Modelling of interfacial area

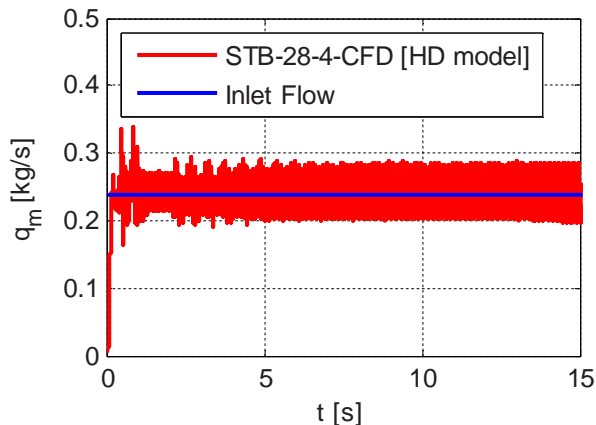


Figure 7. Condensation mass flow rate and inlet vapour mass flow rate in the 2D-axisymmetric OpenFOAM CFD simulation of the STB-28-4 experiment by using the HD condensation model. The amount of wall condensate is deducted from the inlet steam mass flow rate.

Conclusions

OpenFOAM has been shown to be a potential CFD code for the simulation of the investigated applications, but some more work is still needed.

In single phase flows, the most important development needs are establishment of best practices in single phase flows, optimizations of meshing workflow and determination of the critical mesh quality criteria in different applications.

In two phase flows, while the official OpenFOAM release now offers competitive capability for simulation of isothermal multiphase flows, many features needed for meaningful simulation of multiphase heat transfer are still missing. The two-phase solver developed in this project offers a baseline implementation of the missing features, but a lot more work is still needed to refine the models, to improve solver efficiency and to make the solver more robust in challenging simulations. To realize these goals, efficient international co-operation – enabled by the open-source nature of the platform – is essential.

References

- Davidson, L. 2007. Using Isotropic Synthetic Fluctuations as Inlet Boundary Conditions for Unsteady Simulations. *Advances and Applications in Fluid Mechanics* Volume 1, Issue 1, pp. 1-35.
- Ekström, K. 2014. Simulation of MATIS-H Benchmark Using OpenFOAM and Fluent. Fortum Power and Heat Oy. Report FPWR-TERMO-402784.
- Hughes, E.D., Duffey, R.B., 1991. Direct contact condensation and momentum transfer in turbulent separated flows. *Int. J. Multiphase Flow* 17, 599-619.
- Laine, J., Puustinen, M. 2006. Condensation Pool Experiments with Steam using Insulated DN200 Blowdown Pipe. Research Report POOLEX 3/2005, Lappeenranta University of Technology.
- Lakehal, D., M, Fulgosi, and G, Yadigaroglu. 2008. DNS of Condensing Stratified Steam Water Flow. *ASME J. Heat Transfer*, 130, pp. 021501-10.(2008b).
- Menter, F. R., Egorov, Y 2009. DESider: Notes on Numerical Fluid Mechanics and Multidisciplinary Design).
- Piomelli, U., Liu, J. 1995. Large-eddy Simulation of Rotating Channel Flows Using a Localized Dynamic Model" *Phys. Fluids* 7 (4), April.
- Smith, B. L & Song, C.-H. & Chang, S.-K. & Lee, J. R. & Kim, J. W. 2013. Report of the OECD/NEA-KAERI rod bundle CFD benchmark exercise. OECD, Nuclear energy agency report NEA/CSNI/R(2013)5.
- Tanskanen, V., Jordan, A., Puustinen, M., Kyrki-Rajamäki, R., 2014. CFD simulation and pattern recognition analysis of the chugging condensation regime. *Annals of Nuclear Energy* 66, 133-143.

17.2 OpenFOAM and subcooled nucleate boiling in fuel rod bundles

Juho Peltola¹, Timo Pättikangas¹

¹VTT Technical Research Centre of Finland Ltd
P.O. Box 1000, FI-02044 Espoo

Abstract

The capability of OpenFOAM multiphase solvers has been extended to simulation of subcooled nucleate boiling. New features such as non-drag interfacial forces, inter-phase mass transfer, compressibility, alternative turbulence models and interfacial models suited for the application have been implemented in the solvers. These features have been tested against experiments and the results have been documented. During the project, the multiphase solvers of the official OpenFOAM release have evolved significantly. The decision was made to maintain compatibility with the official release and an effort has been made to migrate the features implemented in this project into the newest available platforms. As the capability of the official release has evolved, some of the features implemented in this project have become obsolete, but the public OpenFOAM release still lacks support for the simulation of boiling and condensation. This paper presents the latest modified solver which incorporates the experiences gained from the previous solver to the latest OpenFOAM release. Results from different test simulation are used to illustrate modelling choices that have to be made in simulations of boiling in fuel rod bundles. The capabilities and the limitations of the present solver are discussed.

Introduction

In the present project, an effort has been made to adapt OpenFOAM multiphase solvers for the simulation of subcooled nucleate boiling in PWR fuel rod bundles. The goal has been a competitive solver that could be used in real applications, while providing a basis for a general purpose, open source multi-phase solver for nuclear reactor safety related thermal hydraulic investigations.

The boiling flow in a fuel rod bundle presents several challenges for CFD modelling. The CFD simulations provide additional value over 1D simulations, if the results additional information on the lateral distribution of flow properties and transport between the sub-channels. To achieve this, the simulation has to be able to capture the complex physical phenomena of multiphase flow adequately. Another requirement is that in practical applications the computational effort has to be feasible. This is a very strict limitation considering the scale and the operational parameter of the applications. The fundamental principles of the multiphase flow are well known and – in theory – it would be possible to simulate the phenomena very accurately by applying

these principles. In practice however, such direct simulation approach is limited to the scale of a few nucleating vapour bubbles.

A commonly used modelling approach for practical simulation of multiphase applications is the dispersed Eulerian approach, also known as the two-fluid model. In this approach, both continuous and dispersed phase are modelled as interpenetrating continua in terms of mean velocities and volume fractions of phases. The interaction between the phases is modelled with statistical models that describe things like drag force and heat transfer between the phases.

The NUFOAM project

In the beginning of the project in 2011, the public OpenFOAM released offered a two-phase Eulerian solver called `twoPhaseEulerFoam`. The solver provided basic capability for the simulation of turbulent two-phase flows with a selection drag models. However, the solver only supported constant material properties, constant dispersed phase diameter and it did not include any kind of heat transfer capability. It also lacked bubble specific drag models, supported only constant lift and virtual mass coefficients and did not include any models for turbulent dispersion or wall lubrication force. The $k-\epsilon$ turbulence model was hard coded into the solver and could only be turned on or off.

During 2011 and 2012, an extended version of the solver called `twoPhaseNuFoam v0.4` was developed independently in this project, which addressed most of the above limitations. It includes user selectable framework for all the interfacial models with a large selection of closure models widely used in bubbly flows. It includes enthalpy based heat transfer solution with two-resistance interfacial heat transfer model and support for thermal phase change, non-uniform material properties and compressibility. It also includes alternative turbulence models and an implementation of the RPI wall boiling model (Kurul & Podowski, 1991) and it can be used for the simulation of subcooled nucleate boiling, as was demonstrated by Pelton & Pättikangas (2012).

At the same time, active development of the official OpenFOAM release multiphase solvers had begun after a few dormant years. OpenFOAM 2.1.0 was released in December 2011. It included a multiphase solver that included temperature based heat transfer solution, supported compressibility and a non-uniform dispersed phase diameter. In May 2012, OpenFOAM 2.1.1 improved boundedness of the volume fraction solution by incorporating MULES solution algorithm for it. In March 2013, 2.2.0 release extended thermophysical libraries to multiphase solvers, allowing non-uniform material properties and enthalpy based heat transfer solution. In February 2014, the 2.3.0 release consolidated dispersed two-phase solvers into a single, general solver with runtime selectable interfacial and turbulence model libraries and an extensive selection of closure models. In December 2014, 2.3.1 release included a new version of the general two-phase solver that is fully conservative for mass, momentum and energy.

It was decided that the multiphase solvers developed in the NUFOAM project should remain compatible with the official OpenFOAM release. Considering the limited resources of the present project, maintainability and desire to benefit from the improvements in new OpenFOAM releases, it did not make sense in longer term to maintain and develop a separate fork of the code. Not to mention, that a code that significantly differs from the public release in structure and functionality makes it more difficult to co-operate with the OpenFOAM developers and hinders efficient co-operation with third-parties. Another important aspect is that a large user base is important for credible validation of the solvers.

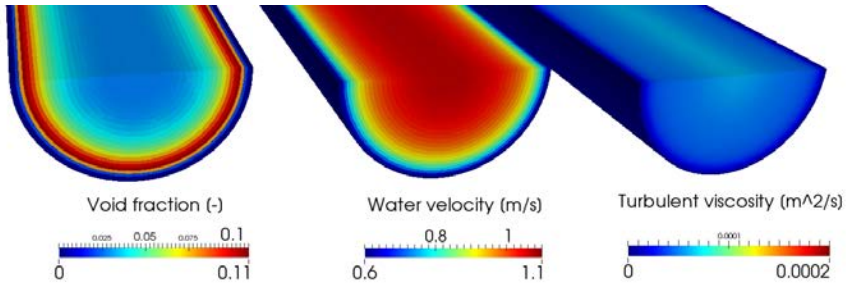
By the release of OpenFOAM 2.3.0, the interfacial, turbulence and thermodynamic framework implemented in twoPhaseNuFoam v0.4 and v0.5 (2013) had become obsolete. However, the public OpenFOAM 2.3.1 release still has limited heat transfer models, lacks support for the simulation of boiling and condensation and the hydrodynamic models have not been tested in applications similar to the fuel rod bundles.

The results shown in this paper have been calculated with a newly developed twoPhaseNuFoam v0.6 solver that is based on the fully-conservative OpenFOAM 2.3.1 twoPhaseEulerFoam solver. The modified solver applies the experiences gained with previous twoPhaseNuFoam solvers to address some identified weaknesses in the 2.3.1 twoPhaseEulerFoam. It extends the closure model selection and includes enhanced heat transfer modelling. It also incorporates support for wall boiling as well as interfacial boiling and condensation. In future, the goal is to increase co-operation with the OpenFOAM developers and the role of the present solver is to serve as a test bed to establish key development areas that are most important for nuclear reactor safety assessment.

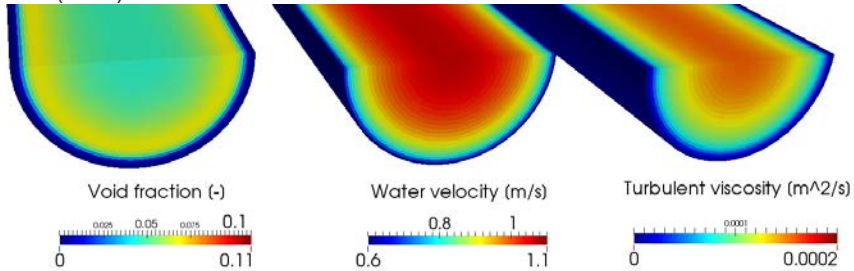
Modelling of interfacial forces

In bubbly flows, there are several important interaction mechanisms between the phases that determine the void and velocity distributions: buoyancy, drag, virtual mass, velocity gradient induced lift force, turbulent dispersion and wall lubrication force. The buoyant force is straight-forward to calculate, but all the other mechanisms require modelling. In simulations of vertical channel flows, the lateral void distribution is mainly a result of the balance between the selected lift, wall lubrication and turbulent dispersion models. The drag force is dominantly aligned with the buoyant force and has limited direct influence on the lateral distribution, but a large influence on the gas hold-up. All the non-drag closure models also depend on the slip velocity between the phases, creating a strong indirect link between drag and the lateral void distribution. All-in-all, the interaction between the different mechanisms is complex and changing any one of them affects all the others.

1. Std. $k-\epsilon$ turbulence, Burns et al (2004) dispersion, Frank (2005) wall lubrication force:



2. $k-\omega$ SST + Sato (1981) turbulence, Burns et al (2004) dispersion, Frank (2005) wall lubrication force:



3. $k-\omega$ SST + Sato (1981) turbulence, Lopez de Bertodano (1992) dispersion, Antal (1991) wall lubrication force:

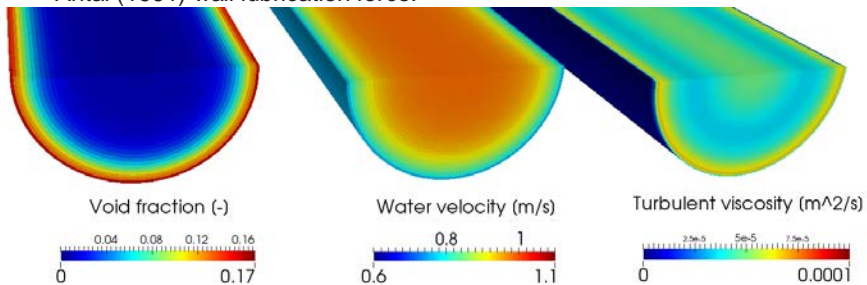


Figure 1. Contours of void fraction, water velocity and turbulent viscosity from twoPhaseNuFoam v0.6 simulations of DEDALE 11-01 experiment with different interfacial closure models.

In the twoPhaseNuFoam v0.6, a cell face based numerical treatment is used to avoid numerical oscillations when the interfacial forces are large and the lift force is damped in near-wall cells to avoid excessive lift forces when bubbles are large compared to the mesh resolution. Some of the interfacial models have been modified to better match the original papers and the selection of models has been extended.

Figure 1 shows the results from simulations of the DEDALE 11-01 experiment (Grossete, 1995) that illustrates the influence of different sub-model variations on the results.

In Figure 2 these results are compared to experimental results. In this case, the standard $k-\epsilon$ turbulence model provided the best results with the Burns et al. (2004) dispersion and Frank (2005) wall lubrication force models. However, the standard $k-\epsilon$ model has proven sensitive to near-wall void fraction, which can make the results unpredictable in some applications.

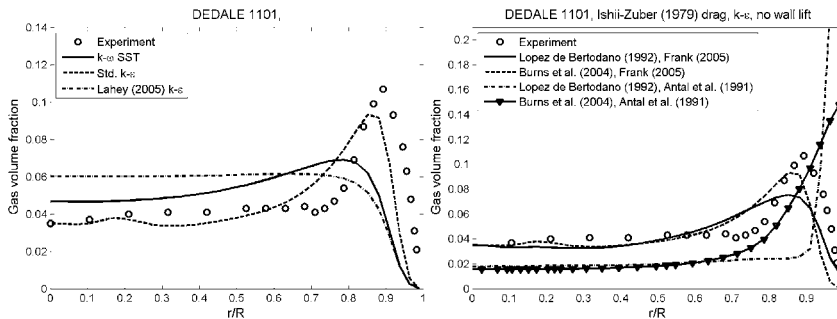


Figure 2. Radial void fraction and liquid velocity distributions from a twoPhaseNuFoam v0.6 simulation of DEDALE 11-01 experiment with different turbulence models (left) and combinations of wall lubrication force and turbulent dispersion models (right).

Multiphase heat transfer and boiling

The modified solver includes several enhancements in heat transfer modelling. It applies thermal wall functions to wall heat transfer and the turbulent Prandtl number is accounted for in the effective thermal diffusion coefficient. The interfacial heat transfer is now modelled with a two-resistance model, where the interfacial heat flux is calculated between the bulk of each phase and the interface between the phases.

When thermal phase change model is active, the interfacial temperature is set to saturation temperature. The interfacial boiling or condensation mass flux can then be calculated from the heat balance across the interface. The solver also includes an implementation of the RPI wall boiling model (Kurul & Podowski, 1991) with alternative sub-models for nucleation site density, bubble departure diameter and frequency. The inclusion of the thermal phase change mass flux requires additional terms in the momentum, enthalpy and pressure equations to account for the mass energy and momentum carried over by the transferred mass. The inclusion of these source terms can affect the convergence of the solver and it has been noted that the convergence of the pressure equation becomes challenging if the source terms are large. How large they are, depends on the wall heat flux, the latent heat and resolution of the computational mesh.

Figure 3 shows results from a simulation of DEBORA5 subcooled nucleate boiling experiment (Manon, 2000). The simulated geometry is a 5 m long vertical pipe with a diameter of 19.2 mm. The heated section is 3.5 m tall and flowing liquid is R-12 at 26 bar pressure. The contours in Figure 3 illustrate the generation of vapour on the heated wall and how the vapour is transported away from the wall and condensed. The condensing vapour heats up the liquid phase and an increasing vapour build-up is seen near the end on the heated section.

The DEBORA5 simulation results are compared to the experiment in Figure 4, which also shows the evolution of simulation results during this project. The results obtained with twoPhaseNuFoam v0.6 and $k-\omega$ SST turbulence model match quite well with the experimental values. In the isothermal DEDALE simulations the standard $k-\epsilon$ turbulence model produced the best results, but in this case its sensitivity to near-wall void fraction leads to severe under prediction of dispersion and excessively high near-wall vapour concentration.

Challenges of the dispersed Eulerian approach in complex geometries

Simulations of pipe flows seen in the previous examples are highly useful in testing and validation of all the closure models, but the complex geometries seen in real applications create additional challenges for the modelling.

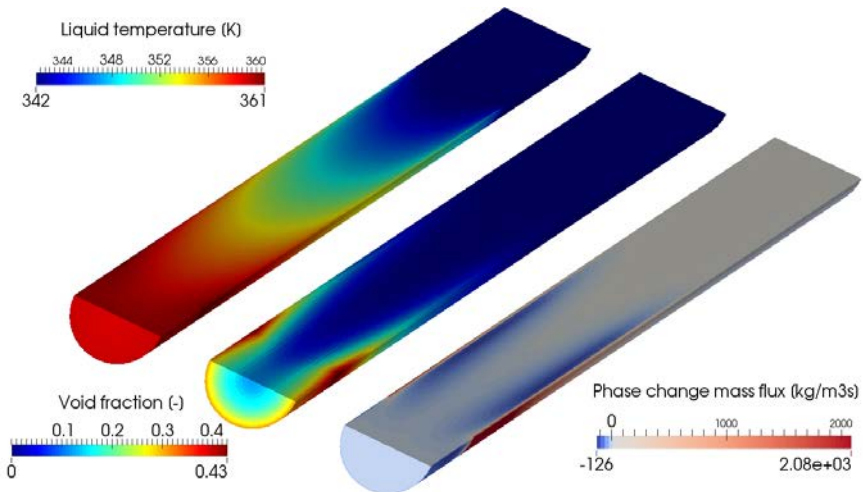


Figure 3. Contours from a simulation of the DEBORA5 subcooled nucleate boiling experiment with twoPhaseNuFoam v0.6 with the $k-\omega$ SST turbulence model.

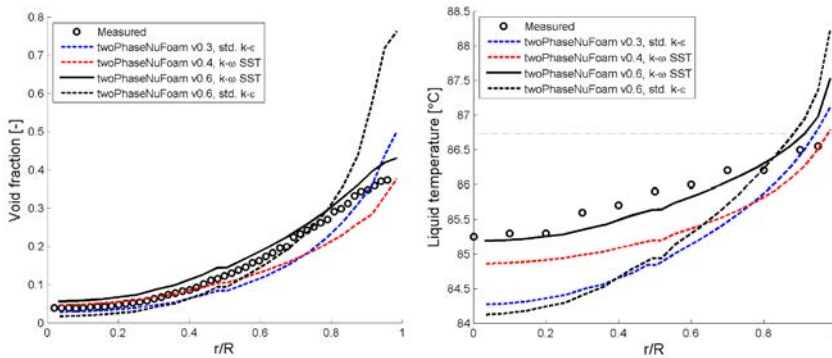


Figure 4. Comparison of calculated radial void fraction and liquid temperature obtained with different versions of the solver to experimental results. Simulation results are shown for twoPhaseNuFoam v0.3, v0.4 and v0.6 with $k-\omega$ SST and standard $k-\epsilon$ turbulence models.

In the dispersed Eulerian approach, the void fraction indicates probability of finding gas phase at specific location in time and space. Positions of individual bubbles are not known and the bubbles are typically characterized by their assumed or predicted diameter and aspect ratio. These principles are relatively straightforward as long as the resolution of the simulation is large compared to the diameter of the bubbles, i.e., it can be assumed that the local flow properties describe the environment experienced by the bubble. If the bubbles are large compared to the resolution of the simulation, it is no longer possible to correctly determine, for instance, a velocity gradient experienced by the bubble based on the local velocity field. The sampling should occur on the scale larger than the dispersed phase diameter. Implementation of such an algorithm in the dispersed Eulerian framework with low computational cost is not easy and generally the local properties are used to update the interfacial models. In such cases, care should be taken to choose closure models that do not produce unphysically small flow structures.

Further complications arise when spacer grids of fuel rod bundles are considered. The smallest gaps between the spacer and fuel rods can be smaller than the bubbles that collide with the spacer. These bubbles are either split into smaller bubbles or deformed so that they can squeeze through the gaps.

Figure 5 illustrates the issue by showing examples of dispersed and interface tracking simulations of bubbly flow through a spacer grid. In the interface tracking simulation, individual bubbles are simulated and their deformation break-up and coalescence are simulated based on the balance between bubble surface tension and forces exerted on the bubble by the surrounding flow. The image in Figure 5 shows how the bubbles are first split by the spacer and heavily deformed by the mixing vanes. It is difficult to imagine generally applicable closure models for the dispersed Eulerian approach that could correctly describe the interfacial forces acting on those large, heavily deformed, strand or plane like bubbles near the mixing vanes.

Figure 6 compares a dispersed Eulerian simulation of a bubbly flow through a spacer grid to experiments carried out by Hyvärinen (2014). In this case, the mean bubble size before the spacer is 3.8 mm and the rod pitch is 34 mm. In the simulation, the bubble diameter is kept constant and the mesh resolution is approximately 0.7 mm. Despite the limited ability of the closure models to describe the interaction between the phases, the simulated void fraction distribution after the spacer matches very well with the experiment. Perhaps the good result is an indication that the mechanistic approach of CFD simulation can work surprisingly well, despite the approximations inherent in the closure models. However, the results might not be as good if the bubble size were increased further.

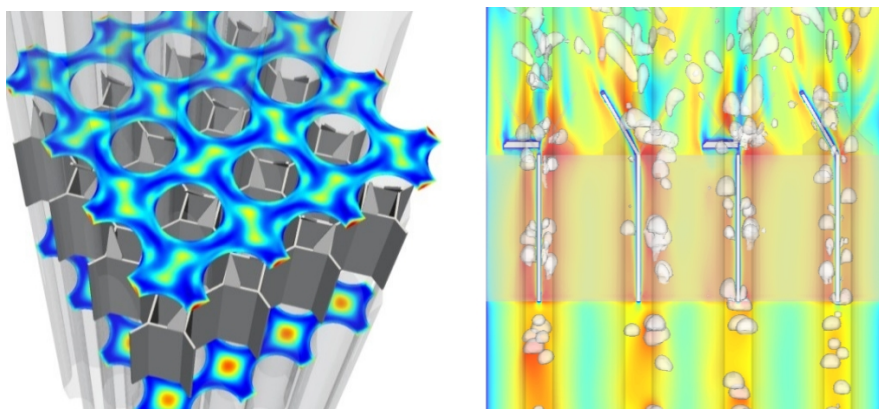


Figure 5. Illustration of two different simulation approaches for multiphase flow through the spacer grids of fuel rod bundles: Void fraction of a dispersed Eulerian model (left, twoPhaseNuFoam) and an interface tracking VOF-simulation (right, interFoam).

A hybrid CFD solver could be a viable route to improve modelling capability in the cases, where at least some of the flow structures are large compared to the geometry. In such a solver, the structures too small to be resolved are represented with the dispersed closure models and the larger structures are resolved with an interface tracking approach. The challenge here is to determine, when to switch between the modelling approaches.

Conclusions and outlook

During the project a few versions of modified dispersed Eulerian two-phase solvers were developed based on different generations of OpenFOAM two-phase solvers. The latest one of them is based on OpenFOAM 2.3.1 twoPhaseEulerFoam and is called twoPhaseNuFoam v0.6. It has been modified in terms of interfacial force treatment, extended closure model selection and improved modelling of heat trans-

fer. It also includes the capability to simulate wall boiling and interfacial boiling and condensation.

The solver has been tested in different isothermal and boiling simulation and comparatively good results have been obtained. Compared to the previous solver versions developed in this project, the present version provides a much more flexible and general platform for further development. It appears, however, that the new solver is a bit less robust than the previous versions. Some more development is needed to improve the ease of use and robustness, without sacrificing the general purpose capability of the solver.

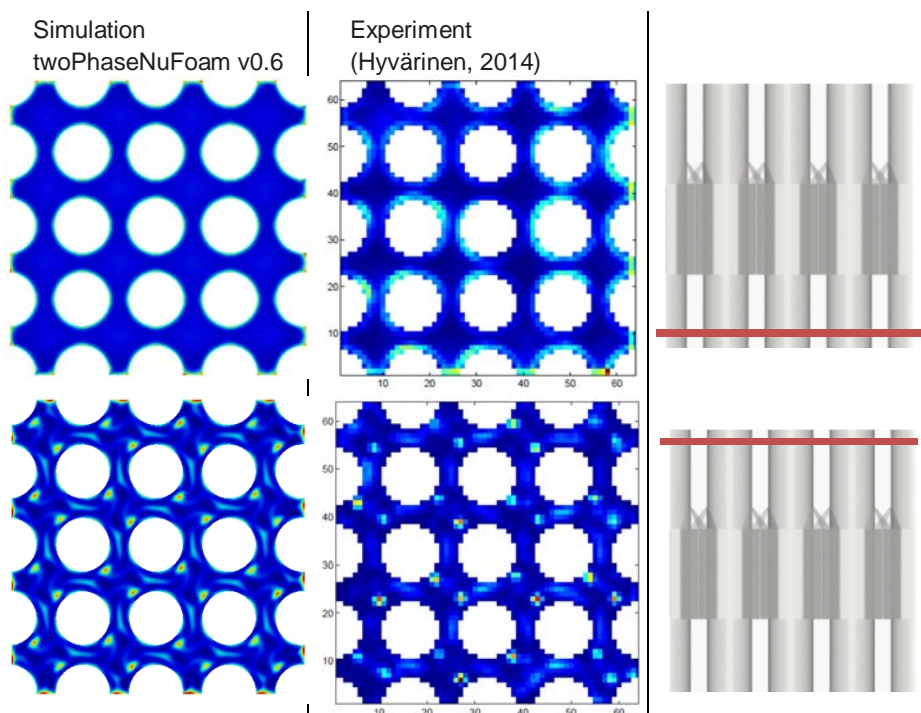


Figure 6. Comparison void fraction distribution obtained with twoPhaseNuFoam v0.6 to the experiment carried out by Hyvärinen (2014).

In near future, we plan to increase the co-operation with the OpenFOAM Foundation to integrate the boiling and condensation capability into the official OpenFOAM release. This would then serve as a transparent and commonly available computational platform for the nuclear reactor safety applications.

In this project, we have collaborated with the KTH Royal Institute of Technology and Helmholtz-Zentrum Dresden-Rossendorf (HZDR). We hope that the inclusion of the multiphase boiling and condensation capability to the public OpenFOAM release will motivate more organizations to contribute to further development and validation of the platform.

References

- Antal, S.P., Lahey, R.T., Flaherty, J.E., Analysis of phase distribution in fully developed laminar bubbly two-phase flow. *International Journal of Multiphase Flow* 17, No. 5, pp. 635-652, 1991.
- Burns, A.D., Frank, T., Hamill, I., Shi, J.-M., The Favre averaged drag model for turbulent dispersion in Eulerian multi-phase flow. 5th International Conference on Multiphase Flow ICMF 2004, 17 p. Yokohama, Japan, May 30-June 4, 2004.
- Frank, T. Advances in computational fluid dynamics (CFD) of 3-dimensional gas-liquid multiphase flows. NAFEMS Seminar "Simulation of Complex Flows (CFD)", Wiesbaden, Germany, April 25-26, 2005.
- Grossete, C., Experimental investigation and numerical simulations of void profile development in a vertical cylindrical pipe, 96NB00120, EdF, ISSN 1161-0611, 289 p., 1996.
- Hyvärinen, J.-P., Two-phase flow measurements with spacer grid in a rod bundle geometry. M.Sc. Thesis, Lappeenranta University of Technology, 107 p., 2014.
- Kurul, N., Podowski, M. Z., On the modeling of multidimensional effects in boiling channels. *ANS Proceedings, National Heat Transfer Conference*, Minneapolis, Minnesota, USA, July 28-July 31, 1991, ISBN: 0-89448-162-2, pp. 30-40, 1991.
- Lopez de Bertodano, M., Turbulent bubbly two-phase flow in a triangular duct, Ph.D. Thesis, Rensselaer Polytechnic Institute, New York, USA, 1991. Cited in Burns (2004).
- Manon, E., Contribution à l'analyse et à la modélisation locale des écoulements bouillants sous-saturés dans les conditions des réacteurs à eau sous pression. Ph.D. Thesis, Ecole Centrale Paris, 2000.
- Peltola, J., Pättikangas, T., Development and validation of a boiling model for OpenFOAM multiphase solver.CFD4NRS-4 conference, Daejeon, South Korea, September 10-12, 2012.
- Sato, Y., Sadatomi, M.; Momentum and heat transfer in two-phase bubble flow – I, Theory. *International Journal of Multiphase Flow* 7, pp. 167-177. 1981.

18. Numerical modelling of condensation pool (NUMPOOL)

18.1 NUMPOOL summary report

Timo Pättikangas, Antti Timperi & Qais Saifi

VTT Technical Research Centre of Finland Ltd
P.O. Box 1000, FI-02044 Espoo

Abstract

In the NUMPOOL project, two-phase computational fluid dynamics (CFD) and Fluid-Structure Interaction (FSI) calculation methods have been developed that can be used for modeling of a pressure suppression pool of a BWR. In particular, the direct-contact condensation occurring in the pool during a postulated large-break loss-of-coolant accident has been modeled. The loads on the wall structures have been calculated with CFD codes and the structural behavior has been calculated with Finite Element Method (FEM). Coupled CFD-FEM calculations have been performed to analyze the effect of the loads on wall structures. The numerical calculations have been validated by comparing the results to the experiments performed with the PPOOLEX facility in the EXCOP project.

Introduction

In boiling water reactors (BWR), the major function of the containment is to protect the environment if a loss-of-coolant accident (LOCA) should occur. The containment is designed to accommodate the loads generated in hypothetical accidents, such as sudden rupture of a main steam line. In such an accident, a large amount of steam is suddenly released in the containment. An essential part of the pressure suppression containment is a water pool, where condensation of released steam occurs.

In a BWR, the pressure suppression containment typically consists of a drywell and a wetwell with a water pool. In a hypothetical LOCA, steam and air flow from the drywell through vent pipes to the wetwell, where the outlets of the vent pipes are

submerged in the water pool. When steam flows into the water pool, so-called chugging effect may occur, which means periodic formation and rapid condensation of large vapor bubbles at the vent outlets. The rapid condensation of the vapor bubbles may induce significant pressure loads on the structures in the pressure suppression pool and on the containment.

In the NUMPOOL project, computational fluid dynamics (CFD) simulations of chugging have been performed by using the Euler-Euler two-phase model of the commercial ANSYS Fluent code. Experiments performed with the PPOOLEX facility (Puustinen et al., 2011) at the Lappeenranta University of Technology have been modelled. The direct-contact condensation in the water pool has been modelled with user-defined functions implemented in the ANSYS Fluent code.

During the discharge of steam into the condensation pool, the rapid condensation of large vapor bubbles may induce significant pressure loads on the pool structures. The collapse of a vapor bubble and the loads have been modelled with the Abaqus Finite Element Method (FEM) code. Fluid-Structure Interaction (FSI) calculations of the PPOOLEX facility have been performed by coupling Abaqus with the Star-CD CFD code. In the early phases of the NUMPOOL project, the coupling was performed by using the MpCCI middleware developed at the Fraunhofer Institute (MpCCI, 2015). MpCCI makes possible using so-called explicit coupling of FEM and CFD codes.

In the explicit coupling, the loads and displacements between the FEM and CFD codes are exchanged only once per time step, i.e., without iteration of the coupled solution within the time step. In several situations, the explicit coupling is numerically unstable, which hampers, for instance, the FSI calculations of PPOOLEX experiments. The numerical instability can usually be prevented with implicit coupling, where iteration within time step is performed by exchanging the boundary data several times during time step. The Star-CCM+ CFD and the Abaqus FEM codes can be coupled without middleware, and the implicit method is also available. Therefore, these codes were studied to achieve numerically stable, fully coupled FSI simulations of condensation pools.

The performance of Star-CCM+ for modelling a propagating pressure wave in water was first studied. The explicit and implicit coupling methods were then tested with a simplified FSI problem and the results were compared with an acoustic-structural Abaqus FSI simulation. Finally, implicit FSI simulations of the PPOOLEX facility and a realistic BWR containment pool were performed.

The pressure suppression pools of boiling water reactors (BWRs) typically have a large number of vent pipes. Experiments have shown that the pressure loads originating from different vent pipes are slightly desynchronized (Kukita & Namatame, 1985; Puustinen et al., 2011). The desynchronization reduces the overall pressure load compared to the case in which the chugging occurs simultaneously in all vent pipes. The experimental results for desynchronization were studied by using the acoustic FSI model of the Abaqus code and the results were applied to a model of a BWR containment.

Fluid–Structure Interaction modelling of PPOOLEX experiments

The PPOOLEX experiment SLR-05-02 was considered, where air was injected into the condensation pool through the drywell (Laine & Puustinen, 2008). The Volume Of Fluid (VOF) model was used for tracking the water surface and the standard k - ϵ model and wall functions were used for the modelling of turbulence. Air was treated as compressible ideal gas while water was assumed either incompressible or compressible. A linear structural model consisting of shell and beam elements including damping was used.

Time step in the simulations was 0.2 ms. The number of inner iterations in the CFD model and of implicit FSI iterations within time step was 20, i.e., one FSI iteration per one inner iteration of the CFD model was performed. The motion of the internal CFD mesh due to the structural displacements was handled by the mesh morpher of Star-CCM+.

With incompressible water, the solution diverged in spite of the implicit FSI algorithm. The stability of the FSI solution has been found to decrease with decreasing fluid compressibility or with decreasing ratio of structure density to fluid density. Stable calculations might be obtained by decreasing the time step further and/or by adjusting Under-Relaxation Factor (URF) of the FSI solution and performing more iterations within time step.

With compressible water, the FSI solution remained stable with the default settings of the URF of the FSI solution. However, pressure at the pool bottom wall showed considerable high-frequency oscillations, where the period corresponded to the time step size. The effect of the URF, number of iterations and whether Star-CCM+ or Abaqus leads the simulation on the oscillations was studied. The number of iterations was varied by changing the number of inner iterations in the CFD model while keeping one FSI iteration per one inner CFD iteration. Increasing the number of iterations and decreasing the URF reduced the oscillations slightly. However, the best results in this case were obtained by increasing the URF. A non-oscillatory solution was obtained with a constant URF of 0.7.

Formation of the first bubble in the pool after the vent pipe clearance is shown in Figure 1 for the experiment and for simulations with Star-CD and Star-CCM+. Charging of the drywell with air was found to be too slow in the calculations, viz., the first bubble appeared at the pipe outlet later in the calculations than in the experiment. Therefore, in the figures times between the calculations and experiment have been synchronized to the moment when the first bubble appears. The delays are about 0.39 s and 0.32 s in the simulation with Star-CD and Star-CCM+, respectively.

The bubble shape and rise velocity are slightly better in the simulation with Star-CCM+ than with Star-CD, although the same mesh has been used. The Star-CCM+ simulation has a shorter time step and higher-order time discretization. In addition to the better time-accuracy, the results may also be affected by better spatial discretization and improved VOF model. The VOF method of Star-CCM+ was, however, found to be less stable than that of Star-CD which was used earlier.

Wall pressures and displacements are compared in Figure 2. The Star-CCM+-Abaqus simulation shows qualitatively correct behavior but predicts too large dis-

placements in the late phase. This may be caused by a resonance situation, since the simulation with rigid walls shows pressure oscillations with a frequency similar to the natural frequency of the pool wall vertical motion. The earlier Star-CD calculations show lower pressure oscillations due to lower accuracy.

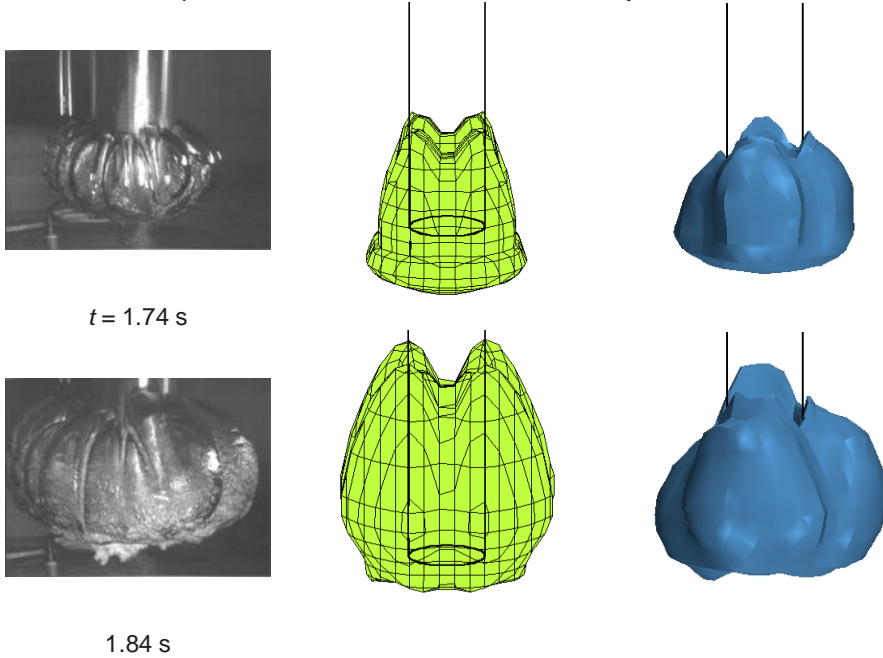


Figure 1. Air bubble at vent outlet in the PPOOLEX experiment (left) and in the calculations with Star-CD (middle) and Star-CCM+ (right).

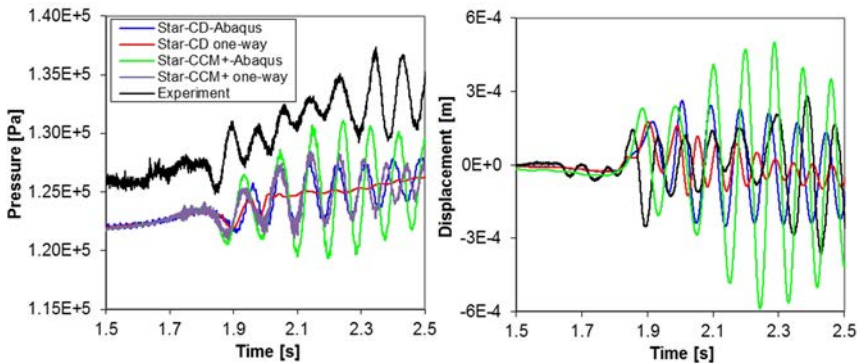


Figure 2. Wall pressure below pipe and wall displacement in the PPOOLEX experiment and in the calculations.

FEM analysis of a BWR containment

The behavior of a pressure suppression containment of a BWR has been studied under application of stochastic loading caused by blowdown of steam into the pressure suppression pool. The stochasticity is caused by desynchronization of the vent pipes, i.e., differing times of formation of bubbles and different size and condensation rate of the bubbles in different vent pipes.

The study has been carried out in several phases, where the data have been provided by experiments performed with PPOOLEX and JAERI facilities. FSI calculations with the acoustic FSI model of Abaqus have been performed by using explicit, implicit and model dynamic analyses.

The FEM model of the BWR containment has 16 vent pipes. The standard deviation of the desynchronization time between different chugging events has been determined to be 42 ms in the JAERI experiments (Kukita & Namatame, 1985). The average time between chugging events was set to 2 s. In earlier studies, the effect of statistically desynchronized chugging between vent pipes on the overall pressure load has been investigated. The behavior of the BWR containment was calculated for different load shapes and water sonic velocities in the pressure suppression pool.

In the last phase of the study, the statistical investigations were expanded further by randomization of load period lengths and amplitudes. The FEM simulations in this phase of the study were divided into three cases of statistical loadings that are discussed in the following.

Case 1 has amplitude variation derived from Kukita and Namatame (1985), who considered large chugs with load amplitudes greater than 10 kPa. Normalized mean load amplitude value of 1 unit was assumed with standard deviation of 0.233 units. The BWR simulations were carried out with single load shape and two sonic velocities (450 and 1412 m/s). The desynchronization between chugging and load amplitudes was randomized with the mean values and standard deviations determined from experiments.

In Case 2, a mean load period of 142 ms and standard deviation of 14 ms were used that were calculated from the JAERI experiments presented by Kukita and Namatame (1985). The same load shape and sonic velocities in water were assumed as in Case 1. Simulations of BWR containment were performed with randomized chugging desynchronization and load periods. It should be noted that in Case 1 the load period was kept constant and in Case 2 the load amplitude.

Finally in Case 3 all three randomizations (desynchronization, load amplitude and load period) were combined with the stated mean and standard deviation values. The FEM simulations were performed for the given load shape and two sonic velocities as in previous cases.

The results from all three cases and previous study phase were compared. Average of root mean squared (RMS) and maximum horizontal displacement results were calculated for a given time history on the inner surface of the BWR containment. The FEM model and the monitored nodes are illustrated in Figure 3.

In all the simulations, multiple chugging events were considered to get realistic normal distribution curves for each stochastically varying parameter. Thus, for a

single pipe 100 chugging events were considered, which means that the total number of chugging events for 16 pipes rises to 1600 events.

Typical load shape at the vent pipes and the resulting Von Mises stress and deformation are illustrated in Figure 4.

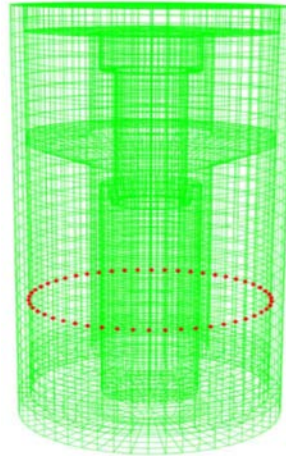


Figure 3. FEM model and node set for gathering displacement statistics on the inner surface of BWR containment.

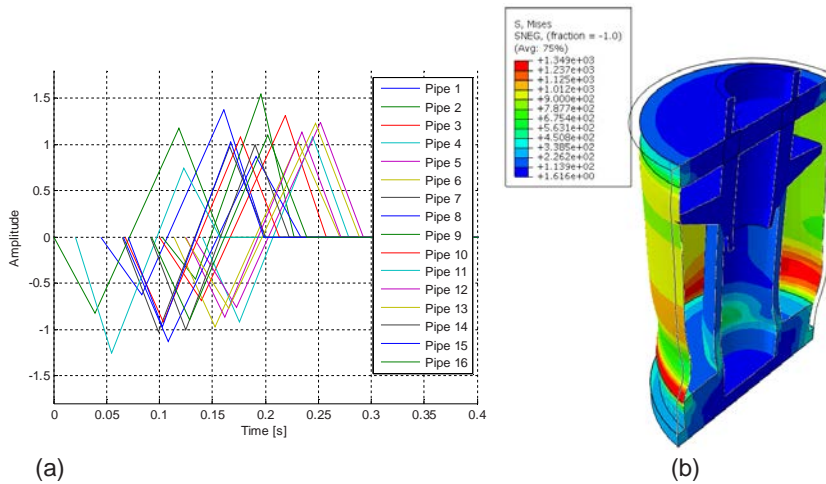


Figure 4. (a) Load shape of 16 vent pipes for the first chugging events with randomized desynchronization time, amplitude and period. (b) Von Mises stress distribution and deformation in the BWR containment model.

CFD modelling of blowdown of air and steam into pressure suppression pool

Two different approaches exist for solving two-phase flow of gas and liquid. In the Volume Of Fluid (VOF) model, the interface between the immiscible liquid and gas is tracked during the simulation. The interface is kept sharp with a numerical algorithm in order to reduce the effect of diffusion and to avoid mixing of the phases. In the Euler-Euler method, mixture of small gas bubbles and continuous liquid phase is considered, but the interface of the bubbles and the liquid is not solved in detail. Instead, the volume fraction of the bubbles in each grid cell is solved from so-called two-fluid equations, where continuum approximation is used for the flow of small bubbles.

In modelling of the behavior of large steam bubbles during blowdown of vapor into water pool, both tracking the surface of large bubbles and the volume fraction of small bubbles would be beneficial. Therefore, a hybrid method of VOF and Euler-Euler method would be useful, where the interfaces of large bubbles are tracked but only volume fraction of small bubbles is solved.

Laviéville (2008) and Coste (2013) have introduced the Large Interface Model, where “large interfaces” between the phases are resolved. In the present project, some of the features of the Large Interface Model have been combined with the Euler-Euler model of ANSYS Fluent by using the user-defined functions of Fluent. The implemented model has been used in modelling the condensation of vapor bubbles in PPOOLEX experiments.

The formation and condensation of one bubble is shown in Figure 5, where the volume fraction of vapor is shown at different instants of time. At time $t = 6.225$ s, a large vapor bubble has formed at the outlet of the vent pipe. The bubble is only partly condensed at the outlet of the vent pipe; a fraction of the vapor rises upwards and is condensed before it reaches water surface. Later, the interface between vapor and liquid water moves somewhat inside the vent pipe. Then, formation of a new bubble starts.

In the bottom part of Figure 5, the results from locating the large scale interface between the phases is shown. Three-cell stencil at the interface between gas and liquid water is determined. The grid cell at the interface (yellow), the grid cell on the liquid side (red) and the grid cell on the gas side (cyan) are shown. The interface tracking algorithm is able to locate the bubble and the water level of the pool at almost every location, where large surface exists. At a few locations, however, gaps can be seen in the tracking results, which do not exist in the simulation result shown in the top part of Figure 5.

The implemented large scale interface model contains the basic functionality for the tracking of the large scale interfaces between gas and liquid. Improvements are, however, still needed in the modelling in order to achieve quantitatively satisfactory results. In particular, a better model for the surface area between the phases should be implemented. The stability of the algorithm also needs some improvements.

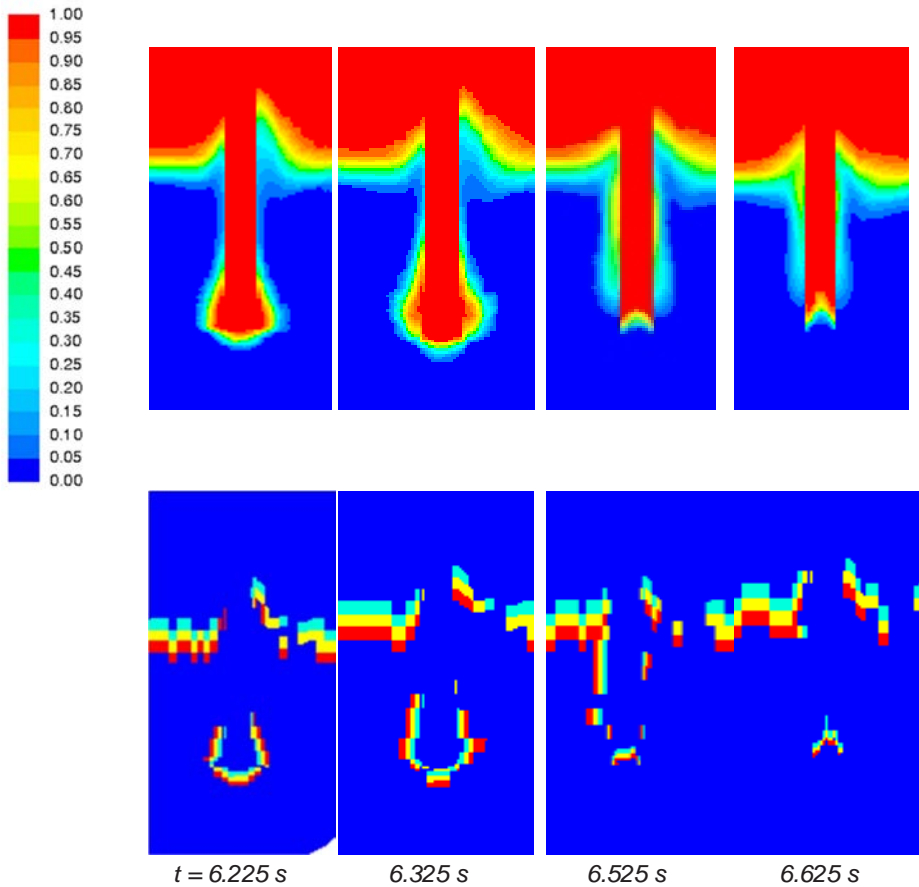


Figure 5. Volume fraction of gas (top) and the calculated “large interface” between the gas and liquid phase (bottom) at different instants of time.

Summary and discussion

FSI calculations using explicit and implicit two-way coupling of Star-CCM+ and Abaqus have been performed. In CFD modelling of a pressure wave in water, numerical damping was considerable with first-order time discretization unless a very short time step was used. Second-order time discretization preserved the pulse amplitude well, but resulted in oscillatory solution. Both the explicit and implicit FSI simulations agreed well with acoustic-structural FEM solutions in a simplified test case. The implicit simulations enabled the use of fairly large time steps for cases where the explicit solution became unstable. In FSI simulations of the PPOOLEX facility, test calculations with incompressible water were unstable also with implicit

coupling while finding a proper under-relaxation factor was required with compressible water. Time and spatial accuracy of the CFD model was found important in modelling the pool loading during the air discharge. Simulations of the early non-condensable phase for a realistic BWR containment showed stable calculations also with explicit coupling when compressible water was assumed. The effect of FSI was small in the BWR containment for the early phase probably due to small displacements and relatively low load frequency.

FEM calculations by using acoustic model of Abaqus were performed for BWR containment with different load shapes, water sonic velocities and stochastic loadings. Loadings of BWR model through 16 vent pipes was randomized in different ways with estimated mean values and standard deviation values from experiments performed at JAERI (Kukita & Namatame, 1985). Stochastic randomizations of load amplitude, load period length and desynchronization between chug events was performed and simulations for the different stochastic combinations were done. The effect of load shapes on the structural response of the containment was found to be small compared to the effect of sonic velocity. For higher sonic velocities lower structural displacement response and von Mises stresses were obtained. Maximum von Mises stress response was considerably higher for the case where chugging occurred simultaneously with constant amplitude and period compared to the statistical cases. Between different statistical simulations relatively highest maximum von Mises stress was detected in the case, where chugging desynchronization, load period and load amplitude were randomized. However, if the random amplitude case was compared to a case with constant amplitude set according to the maximum experimental value, then the more realistic case with amplitude variation resulted in lower stresses.

In modelling of the direct-contact condensation of large vapor bubbles, the basic features of the large scale interface model was implemented in ANSYS Fluent by using User-Defined Functions. In the large scale interface mode, the surfaces of vapor bubbles larger than the grid size are tracked and resolved. The bubbles that are smaller than the grid size are modelled by using continuum approximation of the Euler-Euler two-phase model. In this sense, the model is a mixture of Volume Of Fluid and Euler-Euler model.

Acknowledgement

The authors thank Mr. Markku Puustinen and the EXCOP project for co-operation and for providing experimental data on the PPOOLEX experiments.

References

- Abaqus, 2010. Analysis User's Manual, Dassault Systèmes, Providence, RI, Version 6.10-2.
- Kukita, Y. & Namatame, K. 1985. The vent-to-vent desynchronization effects on LOCA steam condensation loads in BWR pressure suppression pool. Nuclear Engineering and Design, **85**, 141–150.
- Laine, J. and Puustinen, M. 2008. Steam line rupture experiments with the PPOOLEX test facility. Research report CONDEX 2/2007, Nuclear Safety Research Unit, Lappeenranta University of Technology.
- Coste, P., 2013. A Large interface model for two-phase CFD, Nuclear Engineering and Design, **255**, 38–50.
- Laviéville, J. & Coste, P., 2008. Numerical modelling of liquid-gas stratified flows using two-phase Eulerian approach, Proc. 5th Symposium on Finite Volumes for Complex Applications, Aussois, France, June 8-13.
- MpCCI, 2015. MpCCI Home Page, Fraunhofer SCAI.
<http://www.mpcci.de/mpcci-software.html>
- Namatame, K. et al., 1980. Full-Scale Mark II CRT Program: facility description. Japan Atomic Energy Research Institute, JAERI-M 8780, 1980.
- Puustinen, M., Laine, J. & Räsänen, A. 2011. Multiple blowdown pipe experiments with the PPOOLEX facility. Lappeenranta University of Technology, Nuclear Safety Research Report CONDEX 2/2010, 28 p. + app. 8 p.

19. PWR PACTEL experiments (PAX)

19.1 PAX summary report

Vesa Riikonen, Virpi Kouhia, Otso-Pekka Kauppinen,
Joonas Telkkä, Heikki Purhonen

Lappeenranta University of Technology
P.O. Box 20, FI-53851 Lappeenranta, Finland

Abstract

Traditionally the experimental work in Finland has focused on the horizontal steam generators. The new EPR type nuclear power plant under construction in Olkiluoto, Finland, contains vertical steam generators. Hence, the PWR PACTEL facility with vertical steam generators was constructed and taken into operation in the PAOLA project in 2009 to fulfil the new research needs.

The objective of the SAFIR2014 PAX project was to utilize the PWR PACTEL test facility in an effective way in nuclear safety research in Finland and internationally. One of the main goals of the PAX project was also to provide valuable data for code validation. Analyses with thermal hydraulic computer codes were also an essential part of the experiment preparation.

Introduction

The new EPR type nuclear power plant in Olkiluoto will contain vertical steam generators. The experimental work in Finland has focused on the horizontal steam generators. The PWR PACTEL facility [1] with vertical steam generators was constructed and taken into operation to fulfill the new needs. The PWR PACTEL test facility is designed and constructed to be utilized in the safety studies, especially related to the thermal-hydraulics of PWRs with EPR type vertical steam generators.

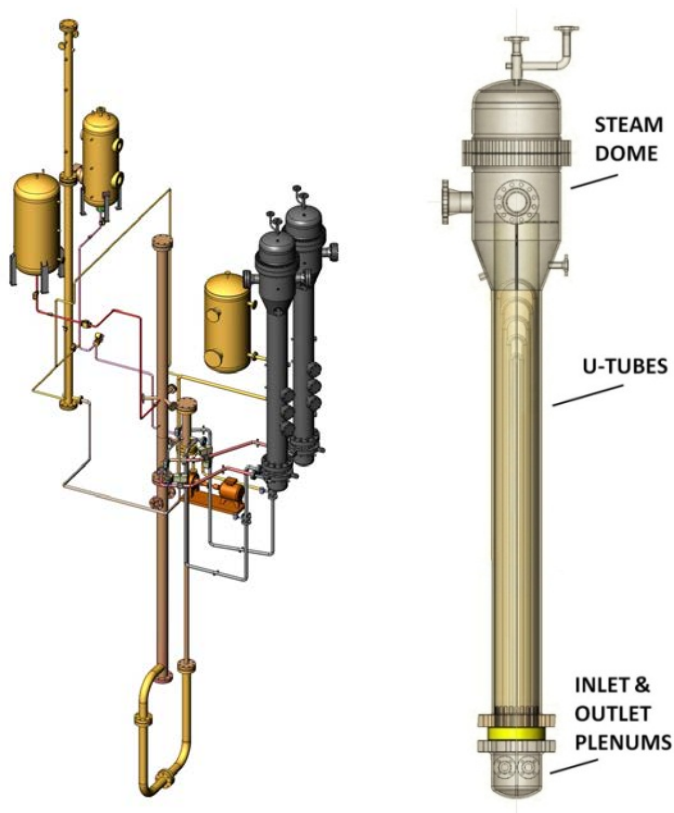


Figure 1. PWR PACTEL facility and general view of the steam generators.

The first experiments with PWR PACTEL were carried out in 2010 after the facility characteristics (pressure losses, heat losses etc.) had been defined. One of these first experiments was chosen as a test transient for an international benchmark calculation exercise coordinated through the SAFIR2014 PAX project. The exercise offered a possibility to check the skills of the analysts in organizations performing thermal hydraulic safety analyses of nuclear power plants.

The PWR PACTEL test program continued in the PAX project with two other test series in 2011. These tests focused on supporting the earlier characterizing experiments in higher pressure and on experimentally verifying the flow reversal in the steam generator tubes. The PAX project continued with one U-leg draining test series and participating in the OECD/NEA PKL Phase 3 project [2] in 2012 - 2014 with two PWR PACTEL experiment series. The OECD/NEA PKL Phase 3 project will continue to end of April 2016. Code simulations were used in the pre-test and post-test analyses of the experiments.

In 2013 the main circulation pumps for the PWR PACTEL facility were installed in the ELAINE project. The pressure and heat losses of the modified parts were defined and the facility description was updated in the PAX project.

The knowledge on two-phase flow behavior would increase if measured data of the void fraction in the secondary side of steam generators was available. This kind of data would be useful in the computer code validation and analysis. Anyhow, such experimental data is not currently available. Furthermore, especially in vertical steam generators the measuring of the void fraction is extremely challenging e.g. due to the triangle array of the tubes. Possibilities of measuring the void fraction in the secondary side of vertical steam generators were studied in the PAX project also. Possibilities of using different measuring and instrumentation systems as well as using separate effects test facilities was studied to find a solution for this problem [3].

Benchmark

The PWR PACTEL benchmark exercise [4] was organized in Lappeenranta by Lappeenranta University of Technology. The benchmark consisted of a blind and an open calculation phase. Seven organizations from the Czech Republic, Germany, Italy, Sweden and Finland participated in the benchmark exercise, and four system codes were utilized in the benchmark simulation tasks. Two workshops were organized for launching and concluding the benchmark, the latter of which involved presentations of the calculation results as well as discussions on the related modeling issues.

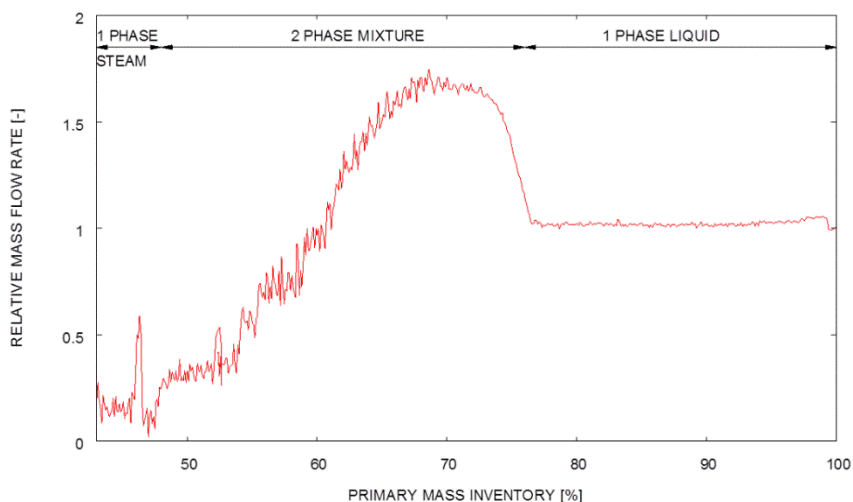


Figure 2. Measured loop flow rate as a function of the primary mass inventory in the PWR PACTEL benchmark experiment.

The chosen experiment for the benchmark was a small break loss of coolant accident experiment which was performed to study the natural circulation behavior over a continuous range of primary side coolant inventories. For the blind calculation task, the detailed facility descriptions, the measured pressure and heat losses as well as the results of a short characterizing transient were provided. For the open calculation task part, the experiment results were released.

As a main conclusion of the benchmark we can say that there is a need for user guidelines or for a collection of best practices in modelling for system codes that could be utilized when different types of transients and situations are to be analyzed.

Experiments at low pressures

Various SBLOCA experiments have revealed a strong dependence of natural circulation behavior on the primary coolant inventory. Natural circulation in test facilities is characterized by three distinct modes: single phase flow for a near maximum primary inventory, two phase circulation for intermediate inventories, and reflux condensation or a boiler condenser mode for low inventories. Transitions between these flow types are usually relatively smooth. Very low mass flow rates are observed for the reflux condensation and boiler condenser modes, but the energy transport is still sufficient to provide core cooling. To observe the natural circulation flow behavior under quasi steady state conditions over a range of primary side inventory levels at a low pressure two stepwise inventory reduction experiments (SIR-32 and SIR-33) [5] were performed with the PWR PACTEL facility.

The ROSA/LSTF experiments have revealed the system wide oscillation with the mass inventories between 40 % and 50 %, a characteristic C-shape vertical temperature distribution in the steam generator secondary side, and a “stagnant two-phase stratification” at low pressures [6]. These phenomena were not observed in the PWR PACTEL SIR experiments. In the PWR PACTEL SIR experiments only one steam generator was used. That might have had an effect on the system behavior. The power level in the SIR experiments was lower than in the ROSA/LSTF experiments and the internal circulation in the steam generator secondary side was therefore also smaller. The EPR features and others differences in the construction of the PWR PACTEL compared to the ROSA/LSTF facility might also have had effect on the results.

Flow reversing in vertical heat exchange tubes

Four steady state experiments (RF-01, RF-02, RF-03, and RF-04) [7] were carried out to experimentally verify the flow reversal in the steam generator tubes for single phase liquid flow. In the first experiment air was discovered in the heat exchange tubes of one steam generator. It showed that it is impossible to distinguish the flow stagnation caused by air in the tube from the possible reversed flow from a uniform temperature distribution. With the new differential pressure measurements between the inlet and outlet plenum and with the new temperature measurements in the

steam generator plenums the non-uniform flow characterized by the coexistence of the normal and reversed flow was observed directly in the experiments for single phase liquid flow (Figure 3).

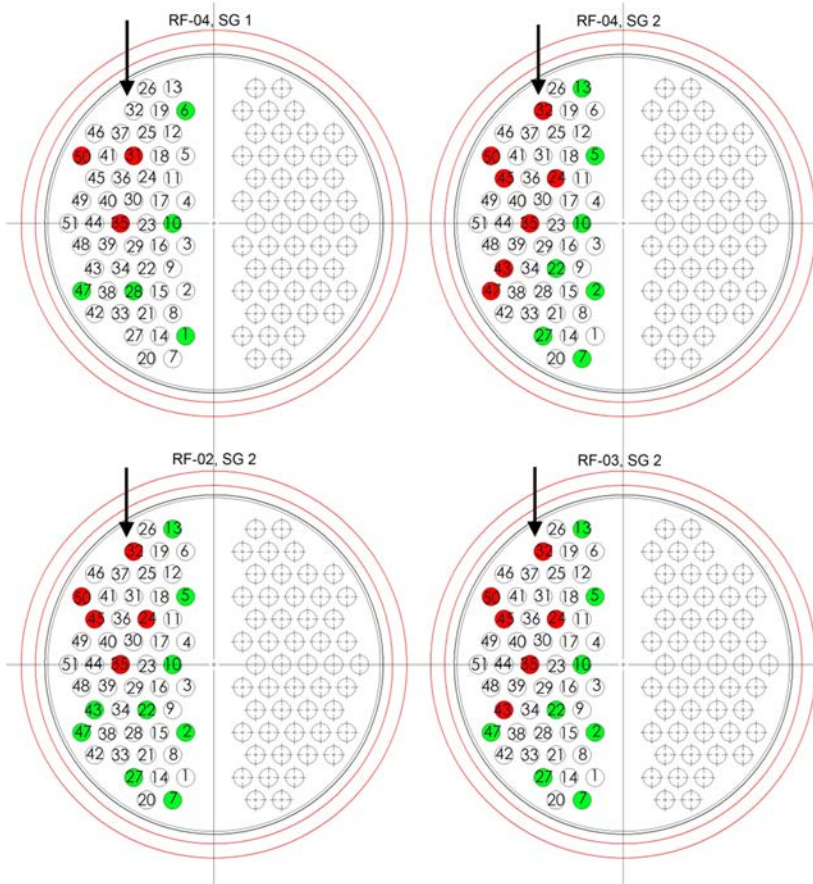


Figure 3. Flow direction in the instrumented heat exchange tubes of the steam generators in the RF-02, RF-03, and RF-04 experiments. Tubes having normal flow (from hot plenum to cold plenum) are marked with green color and tubes where the reversed flow is possible according to the measurements with red color. The flow direction from the hot leg is indicated with an arrow.

From the measured data was estimated that the flow reversed in about 30 % of the heat exchange tubes. According to these experiments the amount of tubes where flow was reversed is independent of the secondary side conditions. The location of the hot leg connection has an effect on the flow reversing in the heat exchange tubes.

According to a theory the flow direction changes in the longest U-tubes with small mass flow rates. To investigate how the flow velocity gradient affects the flow reversing the RF-10 experiment [8] was carried out. Before the main circulation pumps were installed to the PWR PACTEL test facility, it was not possible to investigate a situation where the flow is unquestionably to the forward direction inside the steam generator tubes.

Two problems were observed regarding the reliability of the experiment. The cooling of the main circulation pump influenced on the temperatures in the primary loop, causing the fluctuation of the steam generator inlet temperature. Moreover, during the experiment there was an unknown amount of air inside some of the steam generator tubes, which prevented the flow. For these reasons the results of the experiment are not reliable in order to make valid conclusions about the flow reversing inside the U-tubes. Hence, the investigated dependence of the flow reversing on the flow velocity gradient was not fully observed in this experiment.

Loop seal experiments

The U-leg draining phenomenon is well known and it has been observed on different test facilities. EPR type nuclear power plant analyses have shown that the peak cladding temperature depends not only on the core uncover depth and duration but also on the number of U-legs drained. The U-leg draining phenomenon is mainly driven by the size and location of the break.

A series of experiments (LSC-01, LSC-02, and LSC-03) [9] were proposed by TVO to validate the EPR FSAR analyses, to determine the effect of break size on U-leg draining during intermediate break loss-of-coolant accident conditions and to test the suitability of the PWR PACTEL facility for the U-leg draining studies. Parameter values, boundary conditions as well as initial break sizes for the experiments were chosen based on the results of the pre-test calculations with TRACE.

In the experiments both U-legs opened but as soon as one U-leg was opened, the pressure difference across the U-leg that was the main driving force leading to clearing was strongly reduced, and the second U-leg did not remain open. The U-leg that remained open was not always the same in the experiments. In these experiments the effect of break size on U-leg draining could not be verified as the safety limit for heater rod temperature was exceeded in one experiment and it had to be terminated too early. Despite of this these experiments showed that the PWR PACTEL facility is suitable for U-leg draining studies with some limitations characteristic to the facility. The experiments also showed that small breaks can be more serious for the core than bigger ones and confirmed the results of EPR analyses.

The simulations of the LSC-03 experiment were performed with the APROS and TRACE codes. The U-leg draining was visible in both simulations.

Defining pressure and heat losses

In 2013 the main circulation pumps for the PWR PACTEL facility were installed in the ELAINE project. Experiments PL-20, PL-21, PL-22, PL-23 and PL-24 [10] were performed to define the pressure losses over the main circulation pumps in the cold legs of the PWR PACTEL test facility. The pressure losses were determined by means of circulating cold water in the test facility in both flow directions. An external pump was used to circulate the water.

Experiment HL-40 [10] was performed to define the heat losses of the main circulation pumps. During the experiment the test facility was heated up from the environment temperature to 250 °C. Also cold and hot steady state conditions were measured. Heat losses were determined with the help of the pump energy equilibrium.

Experiments in OECD/NEA PKL Phase 3 project

The PWR PACTEL CNC experiments in the OECD/NEA PKL Phase 3 Project [2] were performed in December 2012 and January 2013 as a supplement to the H4.1 experiment in the PKL facility. The objective of the experiments was to investigate cool down under natural circulation conditions in presence of secondary side isolated steam generators (Figure 4). Especially, the aim was to find the maximum continuous cool down rate while maintaining the natural circulation in the loops with isolated steam generators and water-filled on the secondary side.

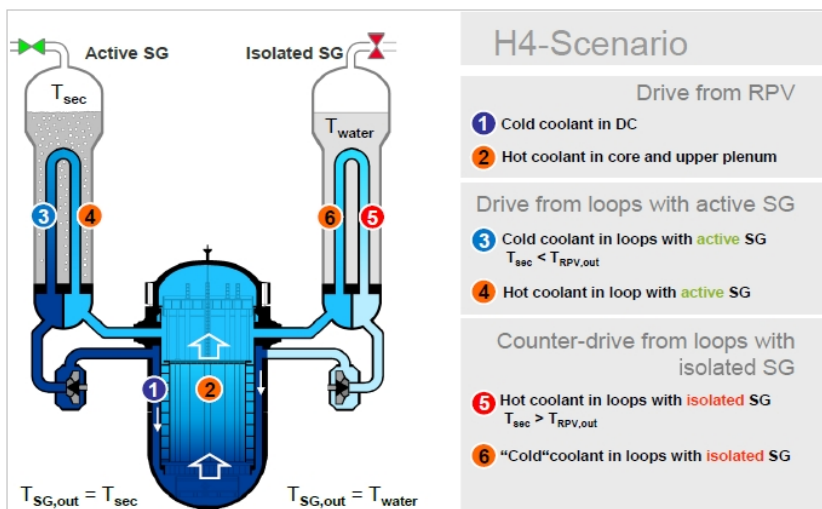


Figure 4. Cool down under natural circulation condition [11].

In December 2012 a preliminary experiment with the cool down rate of 25 K/h was carried out to test the systems and experiment procedure and to get more infor-

mation for planning the final experiment in January 2013. Several pre-test analyses with the APROS and TRACE codes were done using different pressure, core power, and cool down rate values to find suitable experiment parameters. None of the pre-test analyses gave results where the natural circulation in the isolated loop would reverse or stagnate. After discussions with Areva the cool down rate of 50 K/h was decided to be used in the final experiment. Then the results can be compared with the results of the PKL H4.1 experiment.

In the experiment with the cool down rate of 25 K/h, the temperature difference between the inlet and outlet of the isolated steam generator was positive during the whole experiment and the loop flow reversing in the loop was not possible. In the experiment with the 50 K/h cool down rate the driving force for the reverse direction was not enough to stop the natural circulation. The maximum continuous cool down rate while maintaining natural circulation in the loop with isolated steam generator and water-filled on the secondary side cannot be found with PWR PACTEL. The flow cannot reverse in the isolated loop of PWR PACTEL with any available experiment conditions and procedures. The most important reason seems to be the small height of the steam generators in the PWR PACTEL facility. However, the experiments provide valuable data for code validation.

The PWR PACTEL station blackout experiments (SBO) [12] in the OECD/NEA PKL Phase 3 Project were performed in the beginning of 2014 as a supplement to the H2.1 experiment with the PKL facility. In the experiments very lately initiated measures to prevent a core melt down scenario were studied. Without any operator actions a total loss of the secondary side heat sink leads to a core uncover and a core damage. The objectives of the experiments were to evaluate the effectiveness of accident management measures and to test the performance of the core exit temperature measurement for the detection of core heat up.

The secondary side depressurization of one steam generator did not have any significant effect on the primary side behavior. It serves as a preliminary measure for the later actions in the power plant. The capacity of the pressurizer relief valve was enough to keep the primary side pressure below the allowed maximum pressure of the facility. The core exit temperatures began to rise later than the core cladding temperatures. The core cladding temperatures were then higher than the core exit temperatures. There is no shield tube in the PWR PACTEL facility as in the PKL facility and the core exit temperatures are measured from the free flow.

The primary side depressurization proved to be an efficient accident management measure but timing is crucial. The peak cladding temperature during the core heat up depends on the core uncover depth and duration. The later the primary side depressurization was executed the higher the peak cladding temperature was during the core heat up. The initial accumulator pressure has also a significant effect. In the experiments much lower initial primary and secondary side pressures were used than in the real power plants. With the full power plant pressures it takes longer for the primary side pressure to reach the accumulator pressure. Then the core temperatures could rise high before the accumulator injection begins.



Figure 5. Condensation pipes used in the SBO experiments.

Acknowledgement

The project was performed with the financial support of the Finnish Research Programme on Nuclear Power Plant Safety 2011–2014 (SAFIR2014), the Finnish power company Teollisuuden Voima Oy (TVO), and the partners participating in the OECD/NEA PKL Phase 3 project. The authors are grateful for their support to OECD Nuclear Energy Agency (NEA), the members of the SAFIR2014 Reference Group 4 and the members of the Program Review Group and the Management Board of the OECD/NEA PKL Phase 3 project. The data from the experiments in the OECD/NEA PKL Phase 3 project will be available to the NEA member countries via their CSNI representative organisations three years after the end of the PKL3 project.

References

1. Virpi Kouhia, Vesa Riikonen, Harri Partanen, Antti Räsänen, Otso-Pekka Kauppinen, Joonas Telkkä, Lauri Pyy, General Description of the PWR PACTEL test facility - third edition, Technical report, PAX 2/2014, Lappeenranta University of Technology / Nuclear Safety Research Unit, Lappeenranta, 2014, 28 p. + app. 118 p.
2. OECD/NEA PKL-Phase 3 Project. <<http://www.oecd-nea.org/jointproj/pkl-3.html>>

3. Joonas Telkkä, Aukko-osuuden mittausmenetelmien kartoitus PWR PACTEL -koelaitteiston pysty-höyrystimen sekundääripuolella, Diplomityö, Lappeenranta teknillinen yliopisto, LUT Energia, Lappeenranta, 2012.
4. Virpi Kouhia, Vesa Riikonen, Otso-Pekka Kauppinen, Heikki Purhonen, Henrique Austregesilo, József Bánáti, Marco Cherubini, Francesco D'Auria, Pasi Inkinen, Ismo Karppinen, Pavel Kral, Lauri Peltokorpi, Joanna Peltonen, Sebastian Weber, Benchmark exercise on SBLOCA experiment of PWR PACTEL facility, Annals of Nuclear Energy, Volume 59, September 2013, Elsevier, 2013, p. 149-156.
5. Vesa Riikonen, Virpi Kouhia, PWR PACTEL experiments at low pressures. Research Report, Lappeenranta University of Technology, LUT Energy, Nuclear Safety Research Unit, PAX 3/2011. Lappeenranta, 2011.
6. Taisuke Yonomoto, ROSA/LSTF Experiments on PWR Natural Circulation and Validation of RELAP5/MOD3.3, Japan Atomic Energy Research Institute, IAEA's Second Research Coordination Meeting on the CRP on Natural Circulation Phenomena, Modelling, and Reliability of Passive Safety Systems that Utilize Natural Circulation, Oregon State University, Corvallis, Oregon, USA, 2005.
7. Vesa Riikonen, Virpi Kouhia, Juhani Vihavainen Study of flow reversing in vertical heat exchange tubes. Research Report, Lappeenranta University of Technology, LUT Energy, Nuclear Safety Research Unit, PAX 4/2011. Lappeenranta, 2011.
8. Joonas Telkkä, Vesa Riikonen, Quick look report of the PWR PACTEL RF-10 experiment, Technical report, PAX 4/2014, Lappeenranta University of Technology / Nuclear Safety Research Unit, Lappeenranta, 2014, 7 p.
9. Vesa Riikonen, Virpi Kouhia, Otso-Pekka Kauppinen, Loop seal experiments with PWR PACTEL, Research Report, PAX 1/2012, Lappeenranta University of Technology / Nuclear Safety Research Unit, Lappeenranta, 2012.
10. Lauri Pyy, Joonas Telkkä, Vesa Riikonen, Pressure and heat loss experiments of the PWR PACTEL main circulation pumps, Technical report, PAX 3/2013, Lappeenranta University of Technology / Nuclear Safety Research Unit, Lappeenranta, 2013, 24 p.
11. Agreement on the OECD/NEA PKL Phase 3 Project.
12. Vesa Riikonen, Virpi Kouhia, Otso-Pekka Kauppinen, Station blackout experiments, Research Report, PAX 1/2014, Lappeenranta University of Technology / Nuclear Safety Research Unit, Lappeenranta, 2014, 20 p. + app. 18 p.

19.2 Loop seal experiments and calculations

Otso-Pekka Kauppinen, Virpi Kouhia, Vesa Riikonen

Lappeenranta University of Technology
P.O. Box 20, FI-53851 Lappeenranta

Abstract

The loop seal clearing (LSC) can occur in the U-leg part of the cold leg during a loss-of-coolant accident. A series of PWR PACTEL experiments and related computer analyses with the APROS and TRACE codes have been performed to study the LSC phenomenon. The objective of this research was to determine the effect of break size on LSC, to test the suitability of the PWR PACTEL facility for the LSC studies, and to validate PWR PACTEL system code models. The results of the experiments showed that the PWR PACTEL facility is suitable for the LSC studies and that the small breaks can be more serious for the core than bigger ones. The effect of break size on LSC could not be verified because the safety limit for heater rod temperature was exceeded in one experiment and it had to be terminated too early. Regarding overall behavior of the code calculations, both system codes gave reasonable results. Yet, the analysis of the calculation results revealed some possible needs for model improvement.

Introduction

The loop seal clearing (LSC) (or U-leg draining) is the well-known phenomenon in pressurized water reactors during a loss-of-coolant accident (LOCA) and it has been observed with several test facilities during the LOCA experiments [Aksan, 2008]. EPR type nuclear power plant analyses have shown that the peak cladding temperature depends not only on the core uncover depth and duration but also on the number of loop seals drained. The LSC phenomenon is mainly driven by the size and location of the break. The more detailed presentation of the development of the small or intermediate break LOCA can be found in reference [Pochard and Lewis, 1989].

Three PWR PACTEL experiments (LSC-01, LSC-02, and LSC-03) with different break sizes were performed to test the suitability of the PWR PACTEL facility for the LSC studies and to determine the effect of break size on LSC [Riikonen et al., 2012].

The PWR PACTEL test facility [Kouhia, V. et al., 2014] has been designed and constructed in 2009 to be used in the safety studies related to the thermal hydraulics of the pressurized water reactors with EPR type vertical steam generators. PWR PACTEL is a two-loop facility with the loops representing hot legs, steam generators, loop seals, primary coolant pumps (the primary coolant pumps were not yet installed

to the facility during these loop seal experiments), cold legs, and emergency core cooling systems (ECCSs).

The thermal hydraulic system code calculations with the APROS and TRACE codes were performed simulating the LSC-03 experiment. The aim was to assess the general accuracy of code model predictions against the experiment results.

In this report the results of the PWR PACTEL experiments and code calculations are briefly presented.

Experiment procedure and main results

The parameter values, the boundary conditions as well as the initial break sizes for the experiments were chosen based on the results of the pre-test calculations with the TRACE code. The initial conditions of the LSC-01, LSC-02, and LSC-03 experiments are presented in Table 1.

Orifice plates with the diameters of 5 mm (LSC-01 experiment), 5.5 mm (LSC-02), and 6 mm (LSC-03) are used to simulate the break size and control the loss rate. The break sizes are about 0.9 %, 1.1 %, and 1.3 % of the PWR PACTEL cold leg cross sectional area and correspond the break sizes of 80 cm², 100 cm², and 115 cm² in the EPR scale, respectively. The break is located in the cold leg 2 between the loop seal and the downcomer on the top side of the pipe.

In the experiments two emergency core cooling systems, i.e. a safety injection system with a pump and a separate accumulator with piping is used. Both of these ECCSs inject water to the top part of the downcomer. The pressurizer is connected to the hot leg 2. In the PWR PACTEL facility there is no by-pass between the upper plenum and the downcomer. Hence, the pressure difference between the downcomer and the upper plenum can stabilize only through the loop seals.

Table 1. Initial conditions in the loop seal experiments of the PWR PACTEL facility.

Parameter	LSC-01	LSC-02	LSC-03
Primary side pressure	75 ± 1 bar	75 ± 1 bar	75 ± 1 bar
Secondary side pressure	40.0 ± 0.6 bar	40.0 ± 0.6 bar	40.0 ± 0.6 bar
Core power	180 ± 6 kW	180 ± 6 kW	180 ± 6 kW
Total mass flow rate	1.1 ± 0.3 kg/s	1.3 ± 0.3 kg/s	1.3 ± 0.3 kg/s
Pressurizer level	5.4 ± 0.2 m	5.6 ± 0.2 m	5.7 ± 0.2 m
SG collapsed level	3.90 ± 0.12 m	3.94 ± 0.12 m	3.90 ± 0.12 m
Feed water temperature	23 ± 1 °C	20 ± 1 °C	22 ± 1 °C
Feed water mass flow rate	1.8 ± 0.4 l/min 1.4 ± 0.4 l/min	1.8 ± 0.4 l/min 1.5 ± 0.4 l/min	1.8 ± 0.4 l/min 1.6 ± 0.4 l/min
Break size	Ø5 mm	Ø5.5 mm	Ø6 mm
Accumulator pressure	30 ± 1 bar	30 ± 1 bar	30 ± 1 bar
Accumulator temperature	54 ± 4 °C	60 ± 4 °C	54 ± 4 °C
Accumulator level	1.33 ± 0.05 m	1.34 ± 0.05 m	1.32 ± 0.05 m
Safety injection flow rate	5.9 ± 0.3 l/min	6.0 ± 0.3 l/min	6.0 ± 0.3 l/min
Safety injection temperature	21 ± 2 °C	17 ± 2 °C	19 ± 2 °C

The experiments were started by first establishing a steady state operation mode at a full inventory for 1000 seconds. The following transient mode started with opening the break in the cold leg 2. The pressurizer heaters were switched off when the water level in the pressurizer reached the top of the pressurizer heaters (at the elevation of 2.3 m). The safety injection system pump was started manually when the primary pressure fell to 40 bar. In the LSC-03 experiment the starting of the SIS pump was slightly delayed. The accumulator injection started when the primary pressure fell to 30 bar. The secondary side water levels were maintained in the 3.9 m by feed water injection systems. The two-phase mixture leaked from the primary system was condensed and collected in a tank with a capacity of about 700 l, setting a limit to the duration of the experiments.

The progression of the transient was almost similar in each experiment. In the beginning of the transient the primary pressure dropped sharply (Figure 1) until the saturation temperature reached the core outlet temperature. This drop in the primary side pressure caused water in the core region to boil and water in the upper plenum to flash to steam. The steam created in the core slowed down the primary side pressure drop rate until the water level in the upper plenum fell below the hot leg elevation and steam began to flow through the hot legs into the steam generators. After that the primary side pressure dropped nearly to the level of the secondary side pressure.

At this point the water level in the core was determined by manometric effect (Figure 2). Steam produced in the core could not escape from the primary side through the break since the primary side water was stratified in the loop seals. Water in the core and downcomer was in hydrostatics equilibrium.

Increased steam generation kept the primary side pressure near the secondary side pressure in spite of the break flow from the primary side. Due to boiling in the primary side and the mass inventory reduction through the break, the core water level decreased steadily and led finally to the core heat up (Figure 3). The second core heat up peak visible in Figure 3 is the result of the delayed starting of the SIS pump in the LSC-03 experiment. When the SIS pump was injecting the flow rate was sufficient to compensate the break flow and the water level of the core was restored.

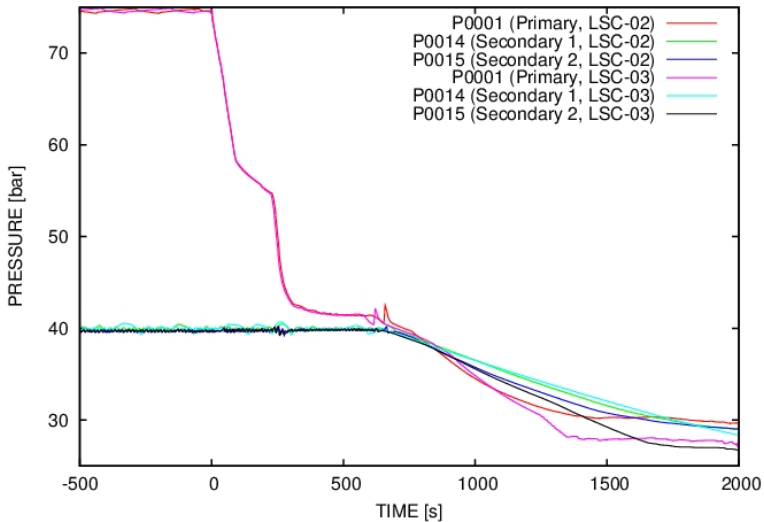


Figure 1. Primary and secondary side pressures in the LSC-02 and LSC-03 experiments.

The peak cladding temperature depends on the core uncover depth and duration. In the LSC-01 experiment where the break size was smallest the maximum core temperature exceeded facility safety limit of 400 °C and the experiment was terminated at that time. In the LSC-02 and LSC-03 experiments the core dry out was halted by the LSC before the maximum core temperature reached the facility safety limit. Once the LSC occurred, steam could flow through the loop seals and the break restoring a normal water distribution in the primary side (Figure 2). After the LSC, the primary side pressure began to decrease again.

In the LSC-02 and LSC-03 experiments both loop seals opened (Figures 4 and 5). As soon as one loop seal opened, the pressure difference across the loop seal that was the main driving force leading to the clearing was strongly reduced, and the second loop seal did not remain open. The loop seal of the cold leg 1 remained open in the LSC-02 experiment whereas in the LSC-03 experiment it was the loop seal of the cold leg 2. Due to the low core power the steam generation rate was relatively low. The small steam flow could not totally clear the loop seals. The up flow sides of the loop seals were at least partly filled with water.

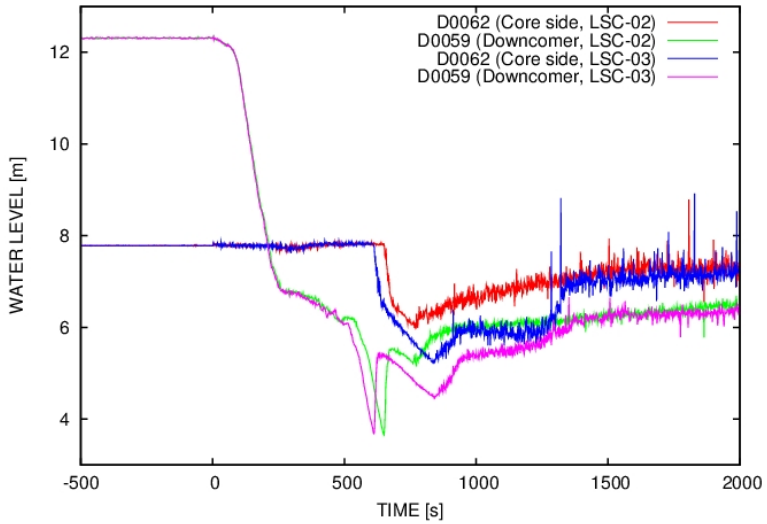


Figure 2. Collapsed water levels on the primary side in the LSC-02 and LSC-03 experiments.

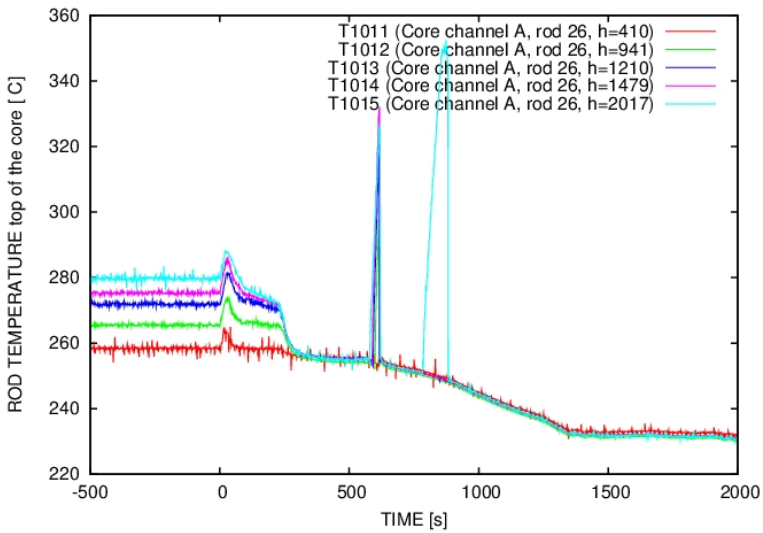


Figure 3. Core temperatures in the LSC-03 experiment.

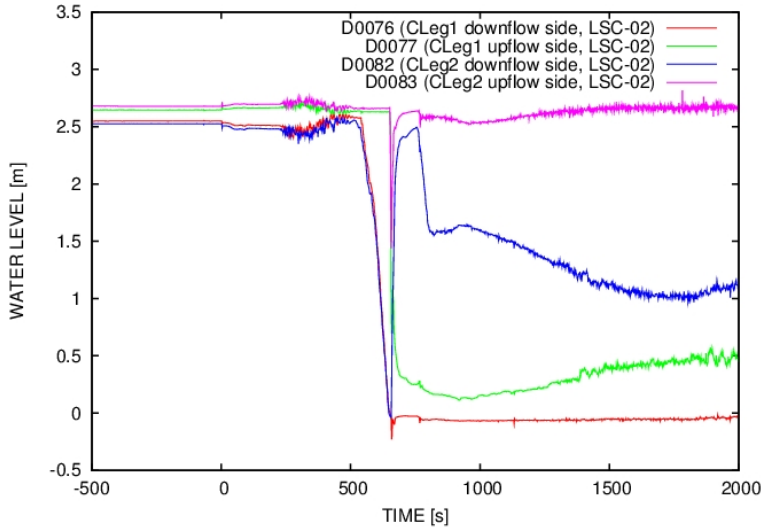


Figure 4. Collapsed water levels in the loop seals in LSC-02 experiment.

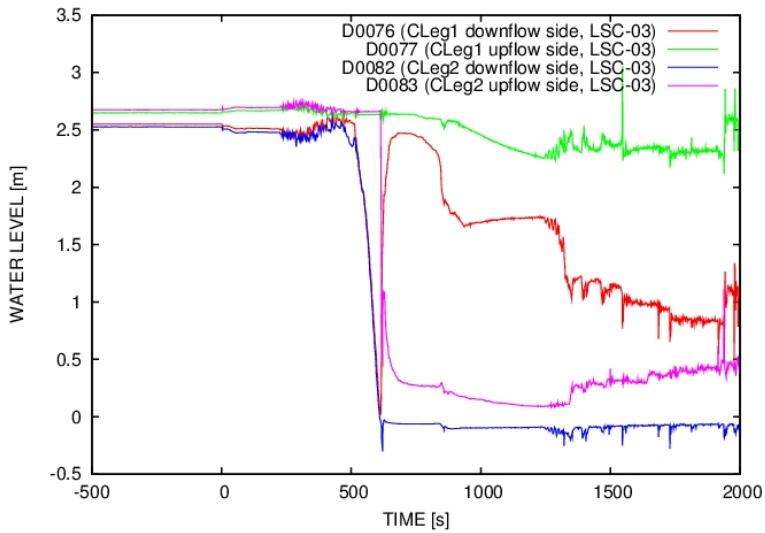


Figure 5. Collapsed water levels in loop seals in the LSC-03 experiment.

System code calculations

The system code calculations were carried out to simulate the LSC-03 experiment as it was considered an interesting and challenging modelling task with the two core dry outs and the two temperature excursions. The calculations were performed with the TRACE (code version 5.0 patch 3) and APROS (version 5.11.08) system codes.

The principles of the TRACE and APROS nodalizations are almost similar. Both nodalizations are 1D models including all the main components of the PWR PACT-EL facility. The heat exchange tubes of the steam generators are partly lumped together, i.e. modeled with five parallel U-tube groups based on their lengths.

The Break line with the orifice plate was modelled in detail in both nodalizations until the orifice plate. In the TRACE nodalization the form loss was determined only for the orifice plate, not separately for the valves or the bend of the break line. The form loss coefficient of the orifice plate was adjusted so that the break flow rate and the total break water inventory of the simulation matched the experiment as well as possible. In the APROS nodalization, the geometry of the break line with the orifice plate was modeled in detail with approximated form losses included taken into account also the critical flow modelling with discharge coefficient at the break part. With both codes the total amount of leaked water from the primary side was well predicted.

The overall behavior of both calculations match relatively well with the experiment results. The primary side depressurization (Figure 6) and water level decrease (Figure 7) are in a relatively good agreement with experiment results. The LSC was also visible and well predicted with both codes. One loop seal was drained while other one did not remain open. In the APROS and TRACE calculations the drained loop seal was same as in the LSC-03 experiment, however, it was noticed that the draining order was very sensitive to the initial conditions and nodalization changes.

Compared to the experiment results some differences were noticed in the peak cladding temperatures (Figure 8) and the behavior of the secondary side pressure (Figure 6). In both calculations the peak cladding temperatures were underestimated and, in the TRACE calculation, the second temperature peak did not exist. The possible reason for this was too early SIS pump injection which flooded the core too early. In the APROS calculation both peaks can be seen in the results, even though the peak temperatures are underestimated.

The secondary side pressures in both steam generators were overestimated in both codes after the primary side pressure dropped beneath the secondary side pressure. Possible reason for this overestimation could be in the inaccurate modeling of the heat transfer between the primary and secondary side, secondary side nodalization, or the heat losses of the secondary sides.

More detailed description of the calculation results is intended to publish in a nuclear engineering related journal during 2015.

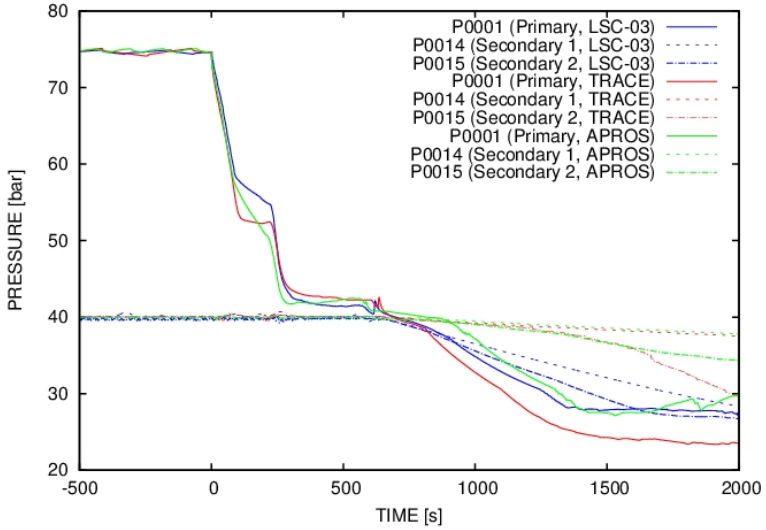


Figure 6. Primary and secondary side pressures of LSC-03 experiment and code calculations.

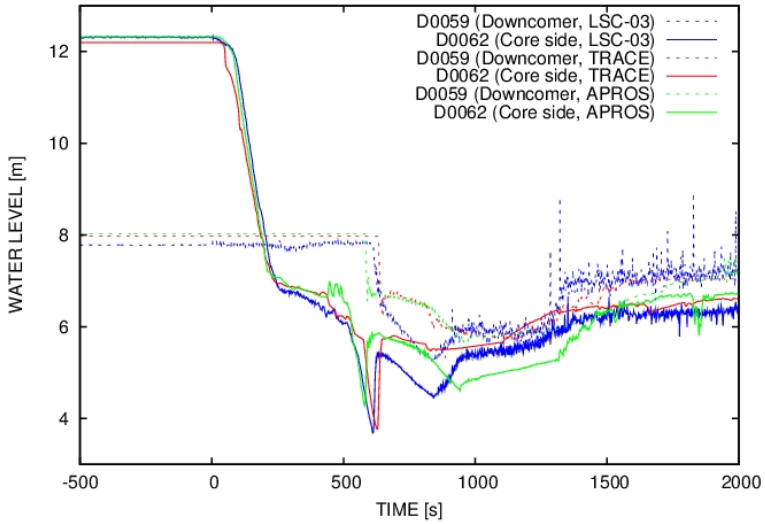


Figure 7. Pressure vessel and downcomer water levels of LSC-03 experiment and code calculations.

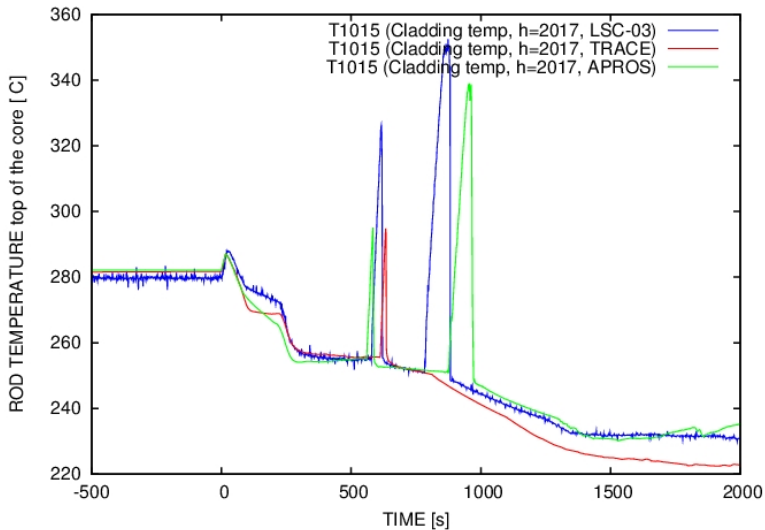


Figure 8. Cladding temperatures of LSC-03 experiment and code calculations.

Summary and conclusions

Three loop seal experiments with the PWR PACTEL test facility and thermal hydraulic system code calculations with the APROS and TRACE codes were performed to study the LSC phenomenon. The objective of the experiment series with PWR PACTEL was to test the suitability of the PWR PACTEL facility for the LSC studies and determine the effect of break size on the LSC. The objective of the code calculations was to validate the PWR PACTEL simulation models created with the system codes.

In the loop seal experiments the effect of break size on LSC could not be verified as the safety limit for heater rod temperature was exceeded in one experiment and it had to be terminated too early. However, these experiments showed that the PWR PACTEL facility is suitable for the LSC studies. These experiments also showed that small breaks can be more serious for the core than bigger ones. The threshold break size was found to be between $\text{Ø}5.0$ mm and $\text{Ø}5.5$ mm (80 cm^2 and 100 cm^2 in the EPR scale).

The system code calculation results with both codes matched relatively well with the results of the LSC-03 experiment. The LSC was well predicted by both codes. Some discrepancies were founded in the cladding temperatures and the secondary side behavior. The analysis of the calculation results revealed some possible needs for model improvement, such as modeling of the break line, heat losses, and the secondary side.

References

- Aksan, N. 2008. International Standard Problems and Small Break Loss-of-coolant Accident (SBLOCA). *Science and Technology of Nuclear Installations*, Vol. 2008, Article ID 814572.
- Kouhia, V., Riikonen, V., Partanen, H., Räsänen, A., Kauppinen, O-P., Telkkä, J., Pyy, L. 2014. General description of the PWR PACTEL facility – third edition. Technical report, Lappeenranta University of Technology, Nuclear safety unit, PAX 2/2014, Lappeenranta, 2014.
- Pochard, R., Lewis, M.J. 1989. LOCA Scenarios and ECC Phenomenology, in: Lewis, M.J. (Eds.), *Thermohydraulics of emergency core cooling in light water reactors—a state of the art report*. Tech. Rep. 161, OECD/NEA, Paris, France, October 1989.
- Riikonen, V., Kouhia, V., Kauppinen, O-P. 2012. Loop seal experiments with PWR PACTEL, Research Report, PAX 1/2012, Lappeenranta University of Technology / Nuclear Safety Research Unit, Lappeenranta, 2012.

20. Modeling of steam generators of nuclear power plants (SGEN)

20.1 SGEN summary report

Timo Pättikangas¹, Ville Hovi¹, Sampsa Lauerma¹, Ismo Karppinen¹,
Tommi Rämä² & Timo Toppila²

¹VTT Technical Research Centre of Finland Ltd
P.O. Box 1000, FI-02044 Espoo

²Fortum Power and Heat Oy
P.O. Box 100, FI-00048 FORTUM

Abstract

A three-dimensional CFD simulation tool has been developed for modeling pressure transients and heat loads on the secondary sides of steam generators of nuclear power plants. The model has been validated against experiments performed with the PWR PACTEL test facility at Lappeenranta University of Technology.

The goal has been to develop models that can be used for the calculation of pressure and heat loads and transport of impurities in steam generators. The models can be used in the analysis of postulated accidents and in the life time management of steam generators.

The developed models have been applied to steam generators of VVER-440 and EPR power plants. The models have been tested by calculating full power stationary states of the VVER-440 and EPR steam generators. In addition, transient behavior of the steam generators in hypothetical accident scenarios have been simulated.

Introduction

Steam generators are used in pressurized water reactors to convert water of the secondary circuit into steam. Most western reactors employ vertical steam generators, where the heat transfer tubes are arranged vertically, parallel to the flow of the

mixture of water and steam rising between the tubes on the secondary side. Examples of such an arrangement are the steam generators of the European Pressurized Reactor (EPR) and the steam generators of the PWR PACTEL experimental facility (Kouhia et al., 2012). In the eastern VVER-440 reactor, the heat transfer tubes are arranged horizontally. Therefore, the rising steam flows perpendicular to the primary tubes.

In the SGEN project, three-dimensional computational fluid dynamics (CFD) models have been developed for the simulations of steam generator secondary sides. The models have been applied to both experimental devices and steam generators of nuclear power plants (NPPs), which contain thousands of primary tubes. Therefore, it is not possible to model them in detail in three-dimensional calculations, but some approximative approach has to be used. The porous medium approximation has been applied to the region containing the heat transfer tubes, i.e. the flow resistance caused by the primary tubes on the secondary side flow has been described with experimental correlations. The heat transfer from the primary tubes has been modelled with source terms of enthalpy. Similar approach has previously been applied to VVER-1000 steam generators by Stosic and Stevanovic (2002).

The flow in the primary circuit has been solved with the Apros system code (Apros, 2015) and the outer wall temperatures of the primary tubes have been interpolated into the CFD mesh. The heat transfer from the primary to the secondary side has been included in the boiling model implemented in the ANSYS Fluent CFD code (ANSYS, 2013). In addition, the drag forces and the heat and mass transfer between vapor and liquid-water have been implemented in Fluent as User Defined Functions (UDFs). In order to model transient situations, a wall condensation model and proper steam tables were also implemented in Fluent as UDFs.

In the following, the porous media model is briefly described. Then, simulations performed for the steam generator of the VVER-440 nuclear power plant are presented. The behavior of the EPR steam generator is studied during the transient caused by the loss of offsite power. Finally, the results are briefly discussed.

Steam generator model

The CFD model is based on the basic conservation laws of mass, momentum and energy for the vapor and the liquid-water phases. The model equations are written in the form used in the Euler-Euler two-phase model of the commercial CFD code ANSYS Fluent version 14.5. Earlier versions of the model have been presented by Pättikangas et al. (2010a; 2013).

Conservation of mass of phase q can be written as

$$\frac{\partial}{\partial t}(\gamma\alpha_q\rho_q) + \nabla \cdot (\gamma\alpha_q\rho_q\mathbf{v}_q) = S_{\text{mass},q} \quad (1)$$

where γ is porosity, α_q is the volume fraction, ρ_q is the density and \mathbf{v}_q is the velocity of phase q . Porosity, γ , is defined as the fluid fraction of total volume, i.e., the fraction available for liquid flow on the secondary side. Therefore, $1 - \gamma$ is the volume fraction of the primary tubes. Indices $q = 1$ and $q = 2$ stand for the liquid and vapor

phases, respectively. The sum of volume fractions is $\alpha_1 + \alpha_2 = 1$. Evaporation and condensation are described with the source term $S_{\text{mass},q}$.

Conservation of momentum of phase q is

$$\frac{\partial}{\partial t}(\gamma\alpha_q\rho_q\mathbf{v}_q) + \nabla \cdot (\gamma\alpha_q\rho_q\mathbf{v}_q\mathbf{v}_q) = \mathbf{S}_{M,q} \quad (2)$$

The source term $\mathbf{S}_{M,q}$ on the right-hand side contains interphase momentum transfer, lift force and virtual mass force. In addition, it includes the gravitation and the flow friction caused by the primary tubes, which is modelled using the experimental correlations of Simovic et al. (2007).

Conservation of energy is

$$\frac{\partial}{\partial t}(\gamma\alpha_q\rho_q h_q) + \nabla \cdot (\gamma\alpha_q\rho_q\mathbf{v}_q h_q) = S_{E,q} \quad (3)$$

where h_q is the specific enthalpy of phase q . The source term $S_{E,q}$ on the right-hand side includes the interphasial heat exchange and the heat source from the primary tubes. The surface heat transfer is modelled with the Thom pool boiling correlation. The mass transfer between the phases is included in equation (1) as source and sink terms. The drag and the heat and mass transfer terms have been implemented as UDFs in the Fluent code.

ANSYS Fluent version 14.5 does not have proper steam tables which are essential when pressure transients in steam generators are modelled. Therefore, steam tables of the Apros code were implemented with the user-defined real gas model of Fluent. In pressure transients, the heat capacity of the solid structures is important. Therefore, a wall condensation model developed earlier for containment analysis (Pättikangas et al., 2010b) has been adopted in the steam generator model.

Modelling of a VVER-440 steam generator

The horizontal steam generator consists of hot and cold collectors, tube bundles supported by thin support plates and a steam dryer above the bundles. The primary circuit consists of more than 5 000 tubes that are connected to the hot and cold collectors. The computational mesh for the Loviisa VVER-440 steam generator is presented in Figure 1(a). The mesh consists of 220 000, mostly hexahedral, cells.

The feed water injection manifold is the flow inlet boundary of the model and it is located above the tube bundles. The flow outlet boundary, located at the top of the computational domain, is defined as a pressure outlet.

The transient caused by the major steam line break (MSLB) was first modelled with the Apros system code (Apros, 2015) model of the Loviisa nuclear power plant in order to get the boundary conditions for the more detailed Apros model of the steam generator. The time-dependent inflow and outflow boundary conditions for the Fluent model were taken from the Apros plant model. The time-dependent temperature boundary conditions for the tube bundles were obtained from the detailed Apros steam generator model and then interpolated to the Fluent mesh, Figure 1(b).

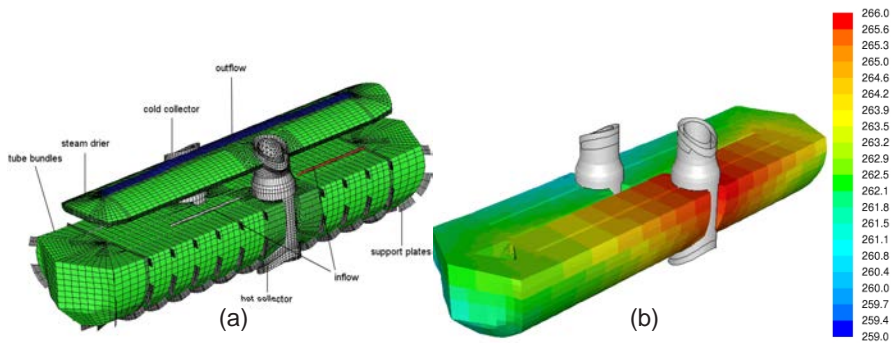


Figure 1. (a) Computational mesh and the inside parts of the VVER-440 steam generator. (b) Temperatures [°C] on the outer walls of the primary tubes interpolated to the Fluent mesh.

In the operational state, the primary side water is at the pressure of 124 bars. Approximately 1400 kg/s of water enters the primary tubes of the steam generator at the temperature of 300 °C and leaves at the temperature of 266 °C. Secondary side of the steam generator is at the pressure of 45.3 bars. Feed water injection is approximately 140 kg/s at the temperature of 257 °C. Thermal power produced is approximately 250 MW. The void fraction distributions at the operational state and after 50 seconds of the MSLB transient are presented in Figure 2.

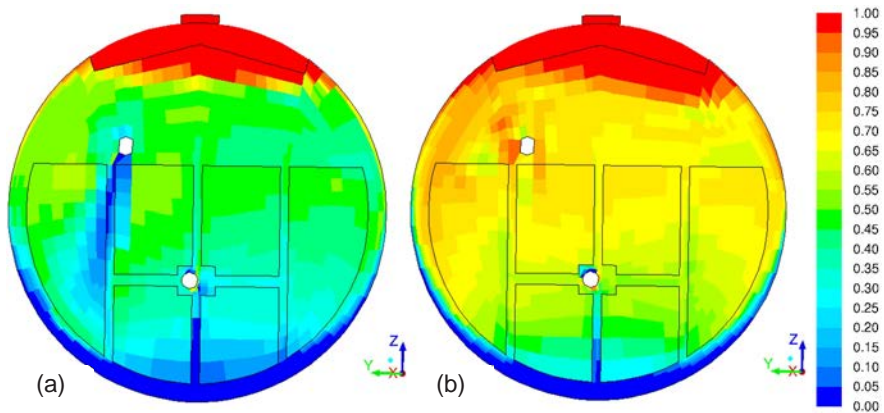


Figure 2. (a) Void fraction at the operational state and (b) 50 seconds after the MSLB of the SG.

According to the void fraction distribution in Figure 2, water rises almost to the outflow level at the hot collector side of the steam generator. The rapid pressure drop during the transient contributes to the steam generation increasing the void fraction in the steam generator, as seen in Figure 2(b).

Modelling of an EPR steam generator

The outer shell and some of the internal parts of an EPR steam generator are shown on the left side of Figure 3 (Areva, 2008). The corresponding parts of the CFD model are illustrated on the right side of Figure 3: wall structures are shown in grey tones and the porous tube regions in green. The plate between the hot and cold sides of the riser tube and the tube support plates are shown in the middle of Figure 3. The CFD mesh consists of approximately 295 000 grid cells; almost all cells are hexahedral but polyhedral and tetrahedral cells are used in the vicinity of the dryer unit.

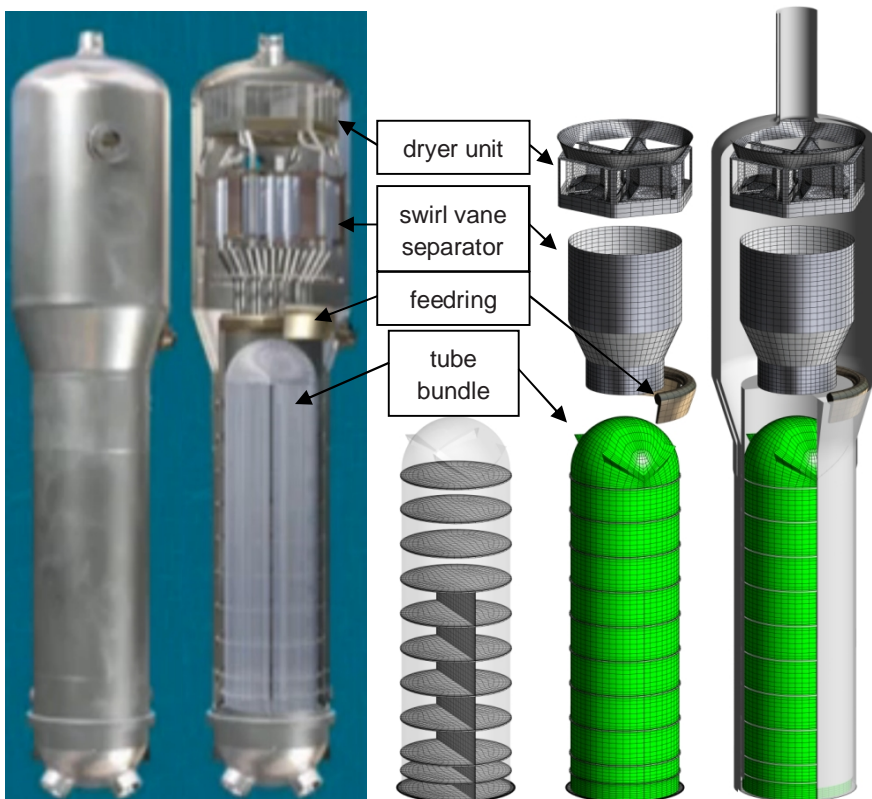


Figure 3. Outer shell and internal parts of an EPR steam generator (on the left) and the corresponding parts of the CFD model (on the right).

The behavior of the steam generator during the early phase of the transient caused by the loss of offsite power (LOOP) was analyzed with the steam generator model. The behavior of the nuclear power plant was first calculated with an Apros model for the power plant. Then, the behavior of the steam generator primary tubes was calculated with the Apros steam generator model using the results of the plant model as boundary conditions. Finally, a CFD simulation of the secondary side of

the steam generator was performed by using the temperatures of the primary tubes as the boundary condition for the simulation.

When the offsite power is lost, the feed water pumps of the steam generator stop. Then, coastdown of the reactor coolant pumps (RCPs) occurs followed by a reactor trip triggered by low RCP speed. After these events, isolation of the steam lines occurs, which causes the pressure on the secondary side of the steam generator to rise rapidly. Eventually, the steam relief valves open due to high steam generator pressure, which leads to a decrease in secondary pressure until the relief valves close.

A full power steady state condition was calculated before initiating the LOOP. After the isolation valves are closed at 5 s, the secondary pressure starts to rise rapidly. It reaches its maximum at 14 s just before the steam relief valves are opened. Then the pressure starts to decrease until it reaches its minimum at 47 s, when the steam relief valves are closed. Finally, the pressure starts gradually rising again.

Contours of vapor fraction [-] on the vertical plane on the centerline of the steam generator are shown in Figure 4. The hot side is on the left and the cold side is on the right. During the initial steady state (5.0 s), a significant difference in the vapor content between the hot and cold sides of the bundle wrapper is visible: high vapor fractions on the hot side and low vapor fractions on the cold side. The rapid increase in secondary pressure, due to the isolation of the steam lines, causes the voids to collapse (maximum pressure at 14 s). The subsequent decrease in the secondary pressure (up to 47 s) occurs due to the opening of the steam relief valves, and causes significant vapor generation all over the steam generator secondary side.

Evaporation rate on the vertical plane on the centerline of the steam generator is shown in Figure 5. During the initial steady state, the highest evaporation rates are found in the lower part of the hot side of the bundle wrapper, where the primary coolant first enters the heat transfer tubes (not clearly visible due to the clipping). Significant evaporation is seen all around the secondary side during the pressure drop (time frames 17.5 to 40 s).

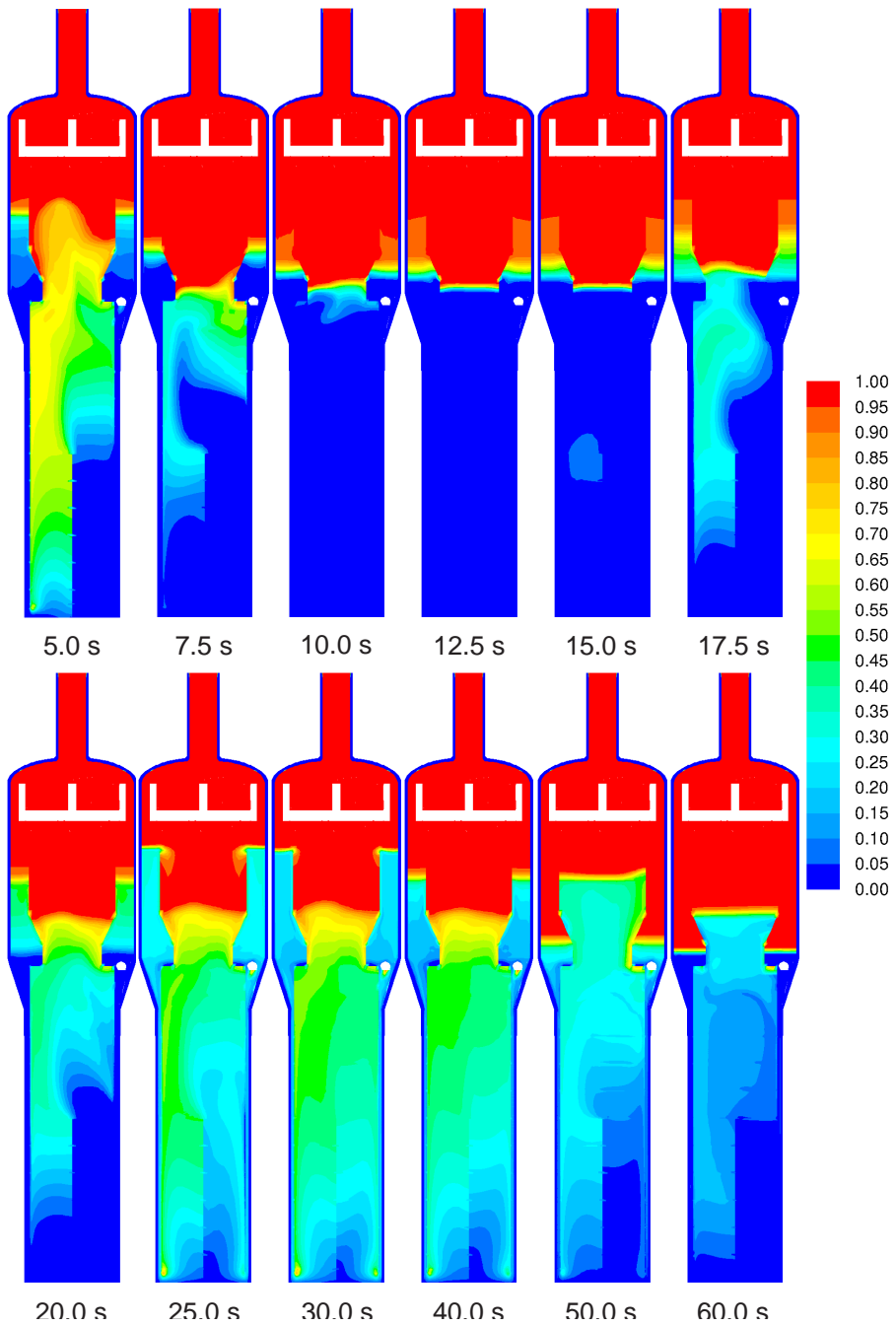


Figure 4. Vapor fraction [-] on the vertical plane on the centerline of the steam generator.

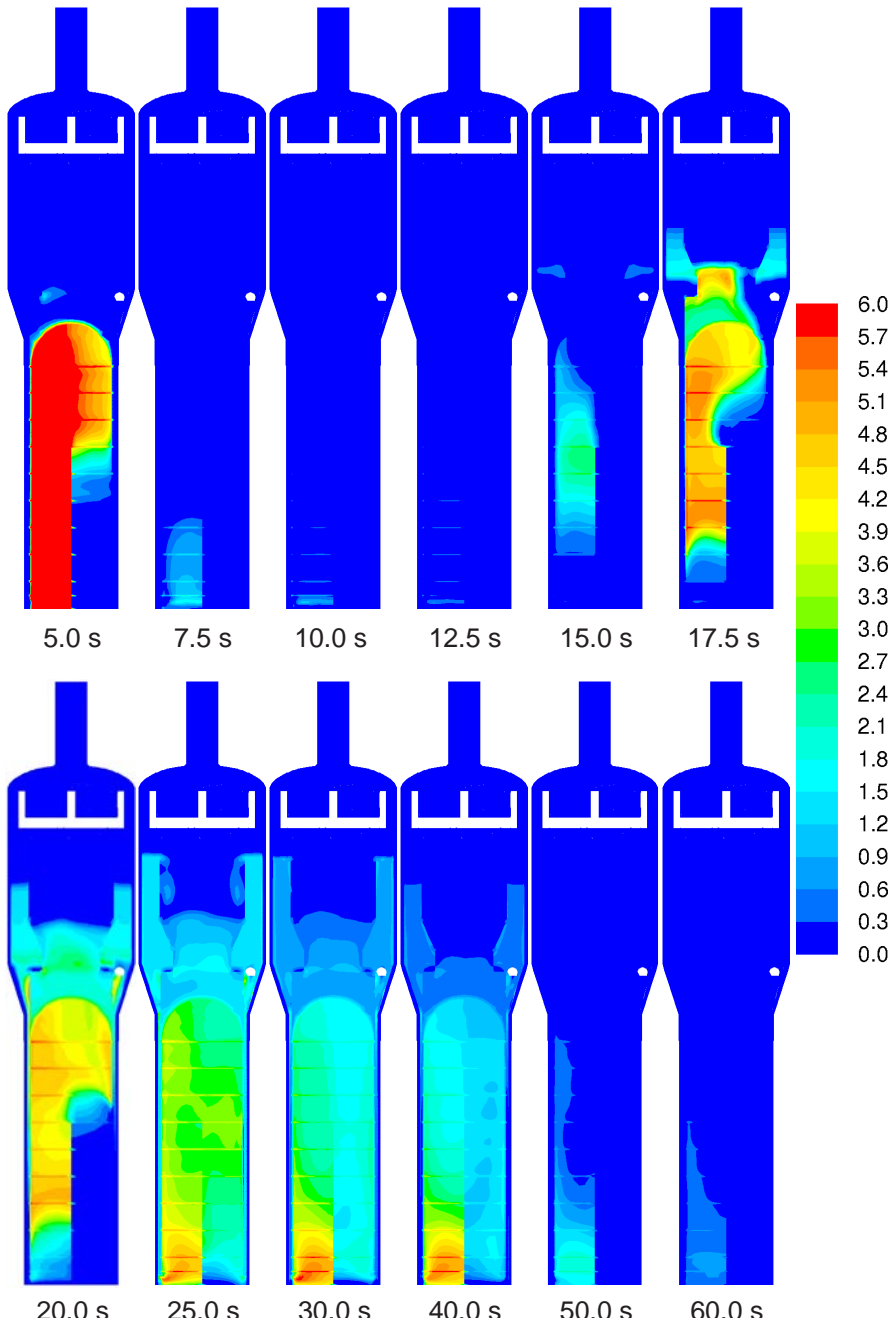


Figure 5. Evaporation rate [$\text{kg/m}^3\text{s}$] on a vertical plane on the centerline of the steam generator, clipped to the limits of the colorbar [0, 6].

Summary and discussion

Numerical methods have been developed for modelling transients in steam generators. The primary side of the steam generator is calculated with a one-dimensional Apros model. Three-dimensional modelling of the secondary side has been performed with the commercial ANSYS Fluent CFD code. The geometry of the secondary side has not been described in detail, but the tubes of the primary circuit have been modelled as a porous media, for which the pressure losses, mass exchange rates and enthalpy sources have been defined explicitly. One-way coupling has been used between the two code counterparts.

The models have been used for simulating VVER-440 and EPR steam generators. Stationary states of the steam generators have been resolved and the results have been compared to available experimental data. In addition, transient situations have been calculated. Loss of feed water and main steam line break transients have been calculated for a VVER-440 steam generator. The behavior of the EPR steam generator in the early part of the loss of offsite power transient was calculated. It was demonstrated that the present simulation model is capable of producing spatially and temporally resolved data on the heat and pressure loads on the secondary sides of steam generators.

Acknowledgement

The authors thank Mr. Vesa Riikonen and the PAX project for co-operation and for providing experimental data on the PWR PACTEL steam generators.

References

- ANSYS, 2013. ANSYS Fluent 15.0 User's Guide, Ansys Inc., USA.
- Apros, 2015. Homepage of the Apros Process Simulation Software, 28.1.2015, www.apros.fi.
- Areva, 2008. Areva 3D animation "In the heart of an EPR steam generator", http://cdn.streamlike.com/hosting/areva/index.php?med_id=f93d57d607cd59c8&subtitlePath=http://de.areva.com/mediatheque/liblocal/docs/sous-titres/11758_EN.xml&skincolor=CC0033 (accessed 25.2.2014).
- Kouhia, V., Purhonen, H., Riikonen, V., Puustinen, M., Kyrki-Rajamäki, R. & Viha-vainen, J. 2012. PACTEL and PWR PACTEL Test Facilities for Versatile LWR Applications, Science and Technology of Nuclear Installations, Volume 2012, Article ID 548513.
- Pättikangas, T.J.H., Niemi, J., Hovi, V., Toppila, T. & Rämä, T. 2010a. Three-Dimensional Porous Media Model of a Horizontal Steam Generator, CFD for Nuclear Reactor Safety Applications (CFD4NRS-3) Workshop, Bethesda, MD, USA, 14–16 September 2010, 12 p.
- Pättikangas, T.J.H., Niemi, J., Laine, J., Puustinen, M. & Purhonen, H. 2010b. CFD modelling of condensation of vapour in the pressurized PPOOLEX facility. CFD for Nuclear Reactor Safety Applications (CFD4NRS-3) Workshop, Bethesda, MD, USA, 14–16 September 2010, 12 p.
- Pättikangas, T.J.H., Hovi, V., Niemi, J., Toppila, T. & Rämä, T. 2013. CFD modelling of horizontal and vertical steam generators (SGEN). SAFIR2014, The Finnish Research Programme on Nuclear Power Plant Safety 2011–2014, Interim Report, Ed. Kaisa Simola, VTT Technology 80, Espoo, Finland, p. 204–211.
- Simovic, Z.R., Ocokoljic, S., & Stevanovic, V.D. 2007. Interfacial Friction Correlations for the Two-Phase Flow across Tube Bundle, International Journal of Multiphase Flow, 33, 217–226.
- Stosic, Z.V. & Stevanovic, V.D. 2002. Advanced Three-Dimensional Two-Fluid Porous Media Method for Transient Two-Phase Flow Thermal-Hydraulics in Complex Geometries, Numerical Heat Transfer, B 41, 263–289.

21. Uncertainty evaluation for best estimate analyses (UBEA)

21.1 UBEA summary report

Torsti Alku, Joonas Kurki

VTT Technical Research Centre of Finland Ltd
P.O. Box 1000, FI-02044 Espoo

Abstract

Propagation of input uncertainty through code runs and statistical analysis of the results has proven to be the method of choice for VTT when performing Best-Estimate Plus Uncertainty (BEPU) analysis of nuclear installations with APROS. To use the method the uncertainties of the inputs need to be defined. A difficult task in this respect is the uncertainty of the constitutive equations of a code and for this reason VTT took part in the PREMIUM benchmark with APROS to research the uncertainties of reflooding related correlations.

The work has been performed under the Uncertainty evaluation for Best Estimate Analyses (UBEA) SAFIR 2014 project. First some analyses were performed with the statistical BEPU method to familiarize with its use with APROS. Some topics of development were identified and addressed to perform the analyses, after which the focus of the project turned to the quantification of the uncertainties of APROS and the possible methodologies for this purpose.

The methodologies proposed in the PREMIUM benchmark were evaluated, tried and found wanting in some respects. Still, important headway was made into the quantification of APROS' uncertainties and the focus of future work required was cleared.

Introduction

Best Estimate Plus Uncertainty approach to deterministic safety analyses is maturing to be a viable option for the licensing needs of nuclear power installations. Unlike

in the conventional, so-called conservative approach, effort is put into modelling all physical phenomena and initial and boundary conditions of the simulations as realistically as possible, avoiding conservative assumptions to the largest possible extent. Fulfilment of the required safety margins are demonstrated by calculating bounding uncertainty curves for the output parameters of interest through statistical techniques.

A Best Estimate Plus Uncertainty analysis requires first of all a best estimate code, and secondly quantification of the uncertainties of all the parameters influential to the simulation. These influential parameters include coefficients in the physical phenomena models within the best estimate code, initial state variables within the simulation model representing the nuclear installation, and other parameters used as boundary and initial conditions within the model. While the quantification of the uncertainties related to the boundary and initial conditions should be relatively easily available from plant data, the uncertainties related to the physical modelling within the simulation code are often more difficult to quantify: some of the physical models are based on simple separate effect tests (SETs) in which case the quantification of the model uncertainty should in most cases be quite straight forward.

On the other hand, some phenomena cannot be measured directly from separate effect tests, such as is the case for most of the physical models dealing with interfacial phenomena, and the physical models describing these phenomena within the simulation codes are typically based on measurement of the secondary effects. In these cases, the quantification of the associated uncertainties has to be deduced from comparisons between simulation results and experimental data of integral tests. Methods aiming at accomplishing this task have been studied in the OECD/NEA PREMIUM benchmark exercise.

The name of the SAFIR2014 subproject dealing with Best Estimate Plus Uncertainty approach was originally BEPUE (application of Best Estimate Plus Uncertainty Evaluation method) but was changed to UBEA (Uncertainty evaluation for Best Estimate Analyses) in the beginning of year 2012 to better reflect the focus of the project: research related to the quantification of the uncertainties needed in a BEPU analysis, instead of mere application of the BEPU approach.

The Best-Estimate Plus Uncertainty approach to safety analyses

There are several ways to practically implement the Best Estimate Plus Uncertainty approach, including CSAU (Code Scaling, Applicability and Uncertainty) developed by the U.S Nuclear Regulatory Commission [IAEA, 2008], CIAU (Code with the capability of Internal Assessment of Uncertainty) proposed by the University of Pisa [Petruzzi, D'Auria, 2008], and the "GRS method" developed at the Gesellschaft für Anlagen- und Reactorsicherheit [Glaeser, 2008]. Due to its simplicity, and the fact that the computational complexity is independent of the number of uncertain parameters, the "GRS method" is probably the most widely used of the available methods.

In the "GRS method" all uncertain parameters are associated with a predefined probability density function (PDF). The analysed scenario is then simulated multiple

times, with randomly sampling the values of all the uncertain parameters from their specific PDF's at the beginning of each simulation. The number of required simulations depends only on the desired confidence level, and can be deduced using the well-known Wilks' formula:

$$1 - na^{n-1} - (1 - n)a^n \geq b,$$

where n is the number of required simulation runs and a is the probability that all the results will be enveloped with the confidence level b . With the defacto standard 95 %/95 % probability and confidence level, the required number of simulation runs becomes 93, which may take a considerable amount of time depending on the analysed scenario, and the computer system used to run the simulations. As a result of the simulation a family of curves is obtained for all output parameters, from which the bounding curves can be extracted.

Applications of the BEPU approach

While best estimate thermal-hydraulic system codes have been applied to safety analyses at the VTT Technical Research Centre of Finland for decades, the simulations have still been of the conservative type due to the use of conservative values for initial and boundary conditions. The study of the application of the BEPU approach has been properly started only within the BEPUE/UBEA project. To gain insight on the method, and to develop the required tools and knowledge, a few best estimate plus uncertainty analyses were first carried out within the project.

Simulation of loss-of-coolant accident at a APR1400 power plant

The first analysed scenario was a large-break loss-of-coolant accident in one of the cold legs of a generic reactor model similar to the Korean APR1400 power reactor. [Luukka, 2012] The list of varied parameters was created based on findings of the international BEMUSE programme, and included parameters such as the coefficient of critical flow limitation, initial pressures and temperatures in various parts of the reactor coolant system, maximum power of the hottest fuel assembly, and the coefficient of critical heat flux. All of the parameters suggested in the BEMUSE reports could not be varied because there was no variables for them in APROS.

An uncertainty analysis tool [Peltokorpi, 2009] developed earlier at Fortum as a module of the Testing Station software, was utilized to carry out the best estimate plus uncertainty analyses, and to calculate the bounding curves and sensitivity measures. Some results of the analysis are presented in Figure 1.

As a result of the study some development needs were identified; namely the importance of parallelization, ability to manipulate data, and the accessibility to some physical model coefficients within the code.

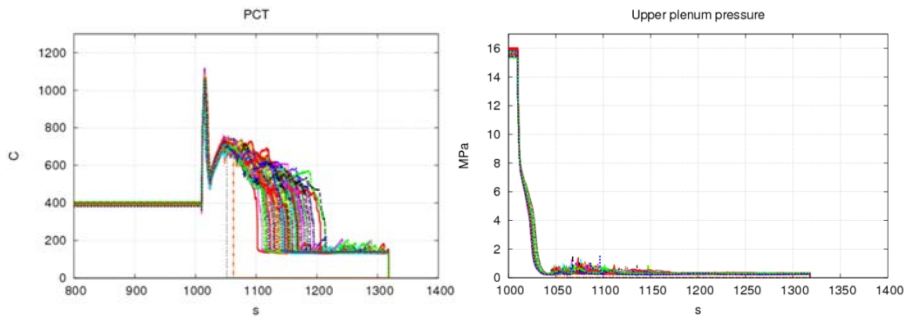


Figure 1. Some results from the BEPU analysis of the LOCA at a APR1400 power reactor: the peak clad-ding temperature (left) and the pressure in the upper plenum (right). Portrayed are all the 93 output curves, while the bounding curves are extracted as the lowest and highest values at each time point.

Simulation of the International Standard Problem number 50

The next analysed case was the International Standard Problem number 50 (ISP-50), which had previously been calculated with APROS at the VTT Technical Research Centre of Finland. [Inkinen, 2011, Alku 2012/1]

Because the Testing Station software was under development at the time and thus the uncertainty analysis tool, which was a part of it, was unable to parallelize the simulation runs, simple Python scripts were written specifically for the purpose of arranging the best estimate plus uncertainty analyses with APROS, using all the available computer cores on a single desktop computer. This enabled local parallelization to the four computer cores available on a typical desktop PC, which was deemed adequate for the present needs. Also at the same time, effort was put into adding the possibility to vary the most important physical model parameters within APROS, which were not available for the APR1400 simulations.

The list of varied parameters was again created based on the recommendation of the BEMUSE project, but this time a longer list of varied parameters could be considered thanks to the code improvements. The BEPU analysis of 93 runs was applied three times to the transient scenario to provide for internal comparison of the method and the achieved results. The output parameter variations in the BEPU analyses were all in accordance with one another and no dramatic differences were found in this respect.

The ISP-50 analysis provided a basis for future research into best-estimate methods using APROS and laid out the general workflow for a BEPU analysis. What was found out was that to achieve reliable results with the BEPU method it is extremely important to use a model that is able to reproduce the real situation very precisely. A recommendation was made of applying the BEPU method to APROS validation cases to provide more information on the usage of the method with APROS.

Participation in the PREMIUM benchmark

The PREMIUM (Post BEMUSE Reflood Models Input Uncertainty Methods) benchmark exercise has been organized by OECD/NEA/WGAMA beginning in 2012. By the end of 2014 all actual work by benchmark participants has been performed with the remaining work being to draft the synthesis report of the project completed by the benchmark organizers.

The focus of PREMIUM is the quantification of the uncertainties of the physical models in system thermal hydraulic codes related to modelling of the reactor reflooding scenario. Different methods for quantification of the uncertainties of the physical model parameters have been introduced, and within the PREMIUM benchmark these methods have been put into use with reflooding test data from two separate test facilities: FEBA and PERICLES-2D. VTT Technical Research Centre of Finland has participated in the PREMIUM benchmark using the APROS code within the UBEA project.

During the year 2012, the focus in the PREMIUM was to identify all the influential parameters that affect the outcome of a reflooding simulation of the FEBA facility [Alku, 2012/2] followed in 2013 by the largest and most demanding phase of the benchmark: the evaluation of the methods for the quantification of the uncertainties and finally the actual quantification with the data from the same facility [Alku, 2013]. After the quantification, in the end of 2013 onto 2014, the next phase of the benchmark, a blind verification of the defined uncertainties with the PERICLES-2D tests, was performed. In 2014 the results were gathered and reported to the benchmark organizers, who released the PERICLES-2D experimental data allowing participants to compare their results to the data.

Identification of the influential parameters

An initial list of all parameters that could be influential to the main responses of interest such as cladding temperatures, rewetting time instant, quench front elevation and pressure distribution within the channel was first drafted. The initial list included practically all physical parameters of the experiment that have been modelled in the APROS code. Next, the overall influence of all parameters was evaluated by simulating the reflooding experiment numerous times, varying a single uncertain parameter at a time, at the limits of its predetermined PDF. To determine which of the parameters on the initial list were influential, a set of criteria related to the maximum cladding temperature and the rewet time variation, proposed in the benchmark specification, was applied. In the end 30 out of the 40 parameters on the initial list were pruned out.

With the initial quantification of the influential input parameters, the experimental results were not enveloped by the bounding curves obtained as a results of the BEPU simulation, and it seems that APROS underestimates the rise of the cladding temperatures, and the quench times. Examination on the probable cause for the observed behaviour suggested that the interfacial heat transfer and friction models

used above the quench front are in their current form inadequate to properly describe the reflooding phenomena at least in the case of the FEBA experiment.

During the preparatory work for the quantification of the uncertainties the list of parameters chosen for quantification was modified from the one reported before. Two parameters were dropped due to a bug that was found in the calculation of entrainment, which caused some physical models to be calculated wrong in reflooding conditions; after new sensitivity runs were performed and with the same criteria for parameter influence as were used before two parameters were deemed to not be influential. Also because there were dependencies between some parameters two more parameters were dropped from the list leaving six influential parameters.

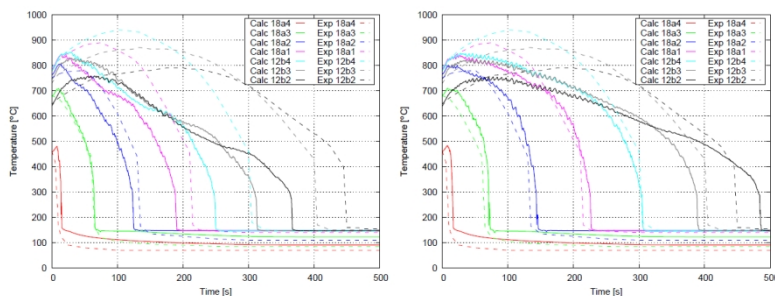


Figure 1. FEBA experiment number 216 cladding temperatures before (left) and after (right) correcting the bug in the calculation of entrainment in the APROS code.

Evaluation of quantification methods

Although not directly a part of the benchmark an evaluation of three of the methods proposed was conducted and two of them were used with data from the FRIGG-loop experiments for a paradigm application. The two methodologies, CIRCE and FFTBM, used in the paradigm application were described in detail and the steps to conduct an analysis with them were outlined. The third one, a method developed at the Karlsruhe Institute of Technology (KIT), was only briefly introduced because it resembles CIRCE, but is more complex. No ready software to use the method exists either, unlike in the case of CIRCE. [Alku, 2013]

Some issues arose in the application of the methodologies, partly due to the nature of the data, but also due to shortcomings of the methods themselves. As it stands, though, both the FFTBM and CIRCE methods were found to be applicable to researching the uncertainties of the physical models of APROS. Although issues were identified, no impediments to using the methods in the PREMIUM benchmark and in further studies were found.

Quantification of parameters' uncertainty with FEBA data

For the quantification of the uncertainty of the parameters both CIRCE and FFTBM were utilized. Additionally several thousands of simulations were run while randomly

varying all parameters with the idea of finding out which possible combinations of the varied parameters could produce results that were consistent with experimental values.

None of the methods provided reasonable results on their own; all had their deficiencies. FFTBM was not able to capture some biases that were known to exist in the code, CIRCE failed in providing meaningful standard deviations and the random simulations were found to be excessively costly considering computer time to see through and showed signs of not converging. Thus, an effort was made to produce a quantification of the parameter uncertainties with the help of all available and achievable information in a cost effective way.

The logic of the final quantification was roughly the following. CIRCE was used to find the biases (or mean values) of the parameters. With the help of the knowledge gained from the random simulations, biases that were known to exist in the code and running some checkup runs, a best-estimate of the parameter biases was tuned. Then, the FFTBM method was employed, taking into account the biases, and this way ranges for the PDFs were found.

An immediate observation of the uncertainty ranges identified for the parameters was that they were very wide. Further work into finding the optimal mean values for the parameters could have had an impact on the broadness of the definitions, but the possible improvements were not seen to be worthwhile taking into account the resources required and the time frame of the PREMIUM benchmark. Moreover, this suggested that the biases troubling APROS were not simply a matter of magnitude.

Another approach into improving the precision of the uncertainties associated to the parameters would be to fully repeat the analysis starting with the simulation model of the FEBA facility built with APROS. Yet, even then, the issues with the correlations of APROS relating to reflooding would exist and would burden the results. Also, the CIRCE and FFTBM methods would still be limited in their usefulness.

Verification of the PDFs with PERICLES-2D experiments

The fourth phase of the PREMIUM benchmark consisted of building a simulation model of the PERICLES-2D facility and running BEPU analyses of several reflooding experiments performed at the facility. The PERICLES-2D facility was built with the purpose of investigating thermal hydraulic phenomena in a reflooding situation in radial direction. Most experiments before PERICLES-2D had used tubes or single bundles, which mainly exhibit axial phenomena. This was also true for the FEBA experiments.

While according to the BEPU methodology 93 runs are to be run for 95 %/95 % bounding limits the benchmark organizers asked for 200 simulation runs to be performed and the 5th and 195th value to be extracted as the bounding limits. Additionally during the process of defining the uncertainties for the parameters the PDFs were cut at certain distances from the mean value, but when calculating the results for the benchmark it was imposed that no truncation be used. This most likely had only minor effect on the bounds, though.

The limits for the cladding temperatures reported to the benchmark organizers were very wide. Full quench does not even occur in most cases during calculated time frame, though maximum cladding temperatures are contained. In some cases the lower limits of quenching are also almost immediate after the start of transient.

The reason for the wide cladding temperature limits are the wide uncertainty distributions for the input parameters defined previously. It can be said that the PERICLES-2D results confirm that the uncertainty distributions do not have to be wider, at least when extrapolating the uncertainties defined with the FEBA experiments to PERICLES-2D experiments. The idea of the quantification of the uncertainties is in essence that they can be applied to any case and all real values would be covered by the resulting limits and in the extent of the PREMIUM benchmark this goal was fulfilled by VTT.

VEERA uncertainty study

In the VEERA uncertainty study the same methodologies that were utilized in PREMIUM for quantification of the uncertainties were used with data from Lappeenranta VEERA reflooding experiments [Alku, 2014]. Several issues arose during the building and validation of the APROS model of the VEERA facility, which caused difficulties during the application of the methodologies and doubts about the ability to produce results.

The largest problem, presumably caused mostly by thermocouple attachment to the heater rods, was that quenching occurred much earlier in the experimental data than in the simulations. Because of this, experimental data only until the moments before rewetting could be taken into account in the analyses, which in turn caused the uncertainties of parameters with the largest influence in the rewetting times to be difficult to define. Another issue was with the experimental procedure, because the experiments were so fast that the full spectrum of phenomena evident in reflooding could not properly be demonstrated. Notwithstanding the issues with the data, all the same six parameters were found influential in the VEERA experiments as during PREMIUM.

The FFTBM method was not able to produce meaningful uncertainty distributions for the input parameters. Application of the CIRCE method, on the other hand, was successful after some modifications to its previous use, the results are shown in Figure 3. Uncertainties of four out of the six parameters were quantified with calibrated best-estimate values close to the ones deduced in PREMIUM, while the other two were more influential in rewetting and thus the same could not be expected of them.

Comparisons with PREMIUM probability distribution functions and BEPU analyses performed with them revealed that even with the issues with the data interesting results could be reached. The quantification part of the study is presented in more depth in the UBEA project special article.

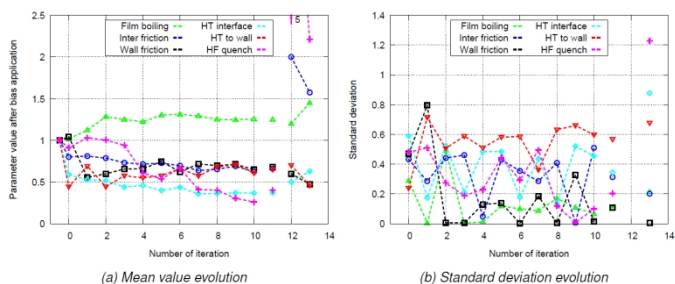


Figure 2. Results of the CIRCE iterations in the VEERA uncertainty study, where at point -0.5 on the x-axis are the nominal values and at 0 the original CIRCE application results. At point 10 are the results of the last CIRCE application and at 11 the final chosen calibrated mean/best-estimate and standard deviation values for the parameters. Points 12 to 13 present a trial with the PREMIUM results.

Conclusions

During the first part of the SAFIR 2014 UBEA project the workflow of a BEPU analysis with APROS was outlined and experience on using the statistical method was gained. It also became apparent that further development of the Testing Station software was required for parallelization and data output in order to perform BEPU analyses with it. Uncertainty coefficients of the correlations were also added to APROS for BEPU analyses.

After this the focus of the project turned to the quantification of the uncertainties required for the BEPU analyses. VTT took part in the PREMIUM benchmark to study the different methods for the quantification, while also performing a paradigm application of the methods to familiarize with the methods before the more complex application within the benchmark. After the benchmark another study into the quantification of the uncertainties of APROS was performed with data from the VEERA experiments and the results were compared to the PREMIUM results.

Future work is required to be able to use BEPU methodologies with APROS in safety analyses. More experiments must be used to evaluate the uncertainties existing in APROS. The optimal scenario would be to use all the experiments that are a part of APROS validation and verification to define and validate the uncertainties. This is especially important for reflooding experiments, because of the complex nature of the phenomena taking place in them.

The methods used for the quantification of the uncertainties in APROS should also be studied further and refined to reduce the amount of expert judgment required. Additionally it would be useful to be able to take already known uncertainties into account when defining the uncertainties for other parameters.

The findings of the UBEA project are of great value and work as a basis for both code improvement as well as further studies into refining the use of BEPU methods with APROS. In fact a proposition has already been presented within the SAFIR2018 USVA project plan to develop a new methodology for the quantification of the uncertainties.

References

- IAEA, 2008. Best estimate safety analysis for nuclear power plants: uncertainty evaluation. Safety reports series 52. STI/PUB/1306. Vienna: International Atomic Energy Agency. ISBN: 978-92-0-108907-6.
- Petruzzi, A., & D'Auria, F., 2008. Approaches, Relevant Topics, and Internal Method for Uncertainty Evaluation in Predictions of Thermal-Hydraulic System Codes (Oct. 2007). Science and Technology of Nuclear Installations. Article ID 325071.
- Glaeser, H., 2008. GRS Method for Uncertainty and Sensitivity Evaluation of Code Results and Applications. Science and Technology of Nuclear Installations (Feb. 2008). Article ID 798901.
- Luukka, J., 2012. LOCA epävarmuusanalyysi APROS Testing Station -ohjelmistolla, Tutkimusraportti VTT-R-00782-12, Teknologian tutkimuskeskus VTT. (In Finnish)
- Peltokorpi, L., 2009. Developing of Uncertainty Analysis System for APROS Safety Simulation Environment. Master's Thesis, Helsinki University of Technology, Faculty of Information and Natural Sciences.
- Inkinen, P., 2011. Simulation of ISP-50 with APROS. Research Report VTT-R-00749-11, VTT Technical Research Centre of Finland.
- Alku, T., 2012/1. Best-Estimate Plus Uncertainty Analysis of the ISP-50 Problem, Research Report VTT-R-08027-12, VTT Technical Research Centre of Finland.
- Alku, T., 2012/2. Identification of Influential Uncertain Parameters of PREMIUM Benchmark. VTT-R-08026-12. VTT.
- Alku, T., 2013. Quantification of APROS' physical model uncertainties in the context of the PREMIUM benchmark. MSc. thesis. Aalto University.
- Alku, T., 2014. Quantification of uncertainties related to APROS modeling of reflooding using VEERA experiments. VTT-R-05342-14. VTT.

21.2 The use of VEERA test results in uncertainty quantification

Torsti Alku

VTT Technical Research Centre of Finland Ltd
P.O. Box 1000, FI-02044 Espoo

Abstract

Propagation of input uncertainty through code runs and statistical analysis of the results has proven to be the method of choice for VTT when performing best-estimate plus uncertainty analysis of nuclear installations with APROS. To use the method the uncertainties of the inputs need to be defined. A difficult task in this respect is the uncertainty of the constitutive equations of a code and for this reason VTT took part in the PREMIUM benchmark with APROS to research the uncertainties of reflooding related correlations.

In the work presented in this report, the same methodologies that were utilized in PREMIUM for quantification of the uncertainties, have been used with data from VEERA reflooding experiments. Several issues arose during the building and validation of the APROS model of the VEERA facility, which caused difficulties during the application of the methodologies and doubts about the ability to produce results.

The FFTBM method was not able to produce meaningful uncertainty distributions for the input parameters. Application of the CIRCE method, on the other hand, was successful with some modifications to its previous use and finally uncertainties of four out of six parameters were quantified with calibrated best-estimate values close to the ones deduced in PREMIUM.

Introduction

The research of using Best-Estimate Plus Uncertainty (BEPU) methodologies in conjunction with APROS thermal hydraulic system code has been an area of interest at VTT for some years now. It has risen from the global tendency towards taking uncertainties into account to provide more comprehensive safety analyses of nuclear installations [IAEA, 2008, Prošek & Mavko, 2003, Bucalossi & al., 2010].

At VTT the research has focused on a statistical method to evaluate the uncertainties related to simulation results by propagation of input uncertainty through the code runs. This method is sometimes also referred to as the GRS method after the German research organization Gesellschaft für Anlagen- und Reaktorsicherheit [Glaeser, 2008].

To provide reliable results the statistical method requires the uncertainties of the inputs to be well defined. In the case of physical parameters, such as inlet water velocity or pipe diameters, the uncertainty can be related directly to their measurement or manufacturing error. With parameters relating to the correlations, which a

thermal hydraulic system code is built upon, the definition of uncertainties is not as straightforward.

The quantification of thermal hydraulic system codes' uncertainties has been the goal of the Post BEMUSE REflood Models - Input Uncertainty Methods (PREMIUM) benchmark organized by OECD/NEA in which VTT has been taking part using APROS within the SAFIR2014 UBEA project. The specific focus of the PREMIUM benchmark is with closure equations relating to reflooding since most of the phenomena these correlations describe can not be separated in experimental setups from other phenomena. [de Crécy & Skorek, 2011]

In the PREMIUM benchmark the quantification of the uncertainties was performed with the help of experimental data from the German FEBA tests performed in the 1980's [Skorek, 2012] and verified with the French PERICLES 2D tests also performed in the 1980's [Deruaz, Clement & Veteau, 1985]. Within the UBEA project a similar quantification of the uncertainties of APROS was performed with data from the Finnish VEERA reflooding experiments performed in the 1990's as a joint task between Lappeenranta University of Technology and VTT.

The methods used for the quantification were the same as in the PREMIUM benchmark, FFTBM (Methodology for characterizing the range of input uncertainty parameters by the use of the FFTBM) and CIRCE (Calcul des Incertitudes Relatives aux Corrélations Élémentaires, English: Calculation of the Uncertainties Related to the Elementary Correlations) [Alku, 2013], to provide results that can be compared to assess the functionality and reliability of the methods.

In this special report the quantification of the uncertainties of the parameters is presented. It was started by determining, which parameters were influential in the simulations of the reflooding experiments after which an analysis was performed with the two different methods to quantify the uncertainties based on the VEERA reflooding experiments.

Identification of influential parameters

The identification of the influential parameters that would be quantified was performed similarly as in the PREMIUM benchmark [Alku, 2012]. In PREMIUM each parameter was varied according to a predefined variation range and the results were compared to each other and to the best-estimate run with nominal, or best-estimate (BE), parameter values. The output parameter that was used was cladding temperature at the hottest measured point in one experiment including quenching time extracted from the temperature curve.

The criteria used in the PREMIUM benchmark with the FEBA experiments to determine whether a parameter was influential needed to be adjusted according to the differences of the VEERA experiments. Most importantly quenching times could not be taken into account due to large differences between experimental and calculated values, which were in turn most likely caused by an inappropriate way of attaching the thermocouples to the heater rods leading to thermocouples quenching before the cladding.

Because the VEERA experiments are much faster than the FEBA experiments the criteria used to determine influence, a minimum difference of 50 °C of the variation runs to the best-estimate run in PREMIUM, was changed to 25 °C. Additionally to rule out spurious effects, where both negative and positive change in the input parameter would cause change in the same direction, the maximum difference between the negative and positive increment runs was required to be at least 50 °C.

Two experiments were used in the identification of the influential parameters of the VEERA calculations. The output parameter that was considered was at approximately middle elevation of the bundle, which was the hottest measurement point out of the five points used in the analyses and at the same time the one that took most time to quench. Similarly as in the FEBA analysis, in the case of the VEERA experiments the temperature curves were cut right before the quenching occurred in the experimental results.

The final list of the parameters identified as influential was *minimum film boiling temperature, interfacial friction droplet, wall friction coefficient / liquid, heat transfer between gas and interface, heat transfer to dry wall / forced convection to gas and additional heat flux near quench front*. These are all the same parameters that ultimately were identified as influential and the uncertainty of which was quantified in the PREMIUM benchmark analyses [Alku, 2013].

FFTBM analysis

The application of the FFTBM methodology was conducted similarly as for the FEBA experiments in the PREMIUM benchmark [Alku, 2013]. Namely the error function that was used was the shortest distance of each experimental point from the calculated points, taking into account both magnitude and time variation, and all of the 15 experiments used in the analyses were used at the same time to define the global average amplitude value for each variation of the input parameters. The workflow for the application of the FFTBM methodology as described in [Alku, 2013] is as follows:

1. Run reference case
2. Select output parameters
3. Derive all the $AA_{R_i}^{REF}$
4. Select uncertain input parameter
5. Run sensitivity cases for the input parameter
6. Derive all the $AA_{R_i}^{*,IP}$ (one per output parameter) and the $AA_G^{*,IP}$ (one per sensitivity calculation)
7. Define threshold value and identify the variation range
8. Discard input parameter, if it is not relevant

The sensitivity runs were also performed in the same fashion as before by running seven simulations with each input parameter from the lower limit of the range to the higher limit at evenly spaced intervals. The sensitivity runs were performed for all experiments for all parameters after which the results were aggregated to produce the global average amplitudes for each variation. All five cladding temperature curves as defined in the identification phase were used in the aggregation.

Figure 1 presents the FFTBM analysis results with the nominal value for each parameter set at 1. According to the figures the nominal value is not the best value for any of the parameters. This in turn would require a new iteration of the analysis to be performed with new nominal values. It was already discovered with the FEBA experiments that iterating the FFTBM method was not a viable way of reaching a convergence of the results and that a better form to find the optimal nominal values would be with trial-and-error, CIRCE or expert judgment.

In fact after the CIRCE application, the results of which are presented in the next chapter, was completed, a FFTBM analysis was performed with the new nominal values for the parameters. The results of the analysis are portrayed in Figure 2.

It is evident from comparing Figure 1 and Figure 2 that even after defining new nominal values, which are supposed to produce a better best-estimate run, the FFTBM method does not produce usable results in the case of the VEERA experiments. The forms of the global average amplitude curves are very similar to the original FFTBM analysis and the optimal values of the parameters specified with the new analysis do not coincide with the values defined in the CIRCE analysis.

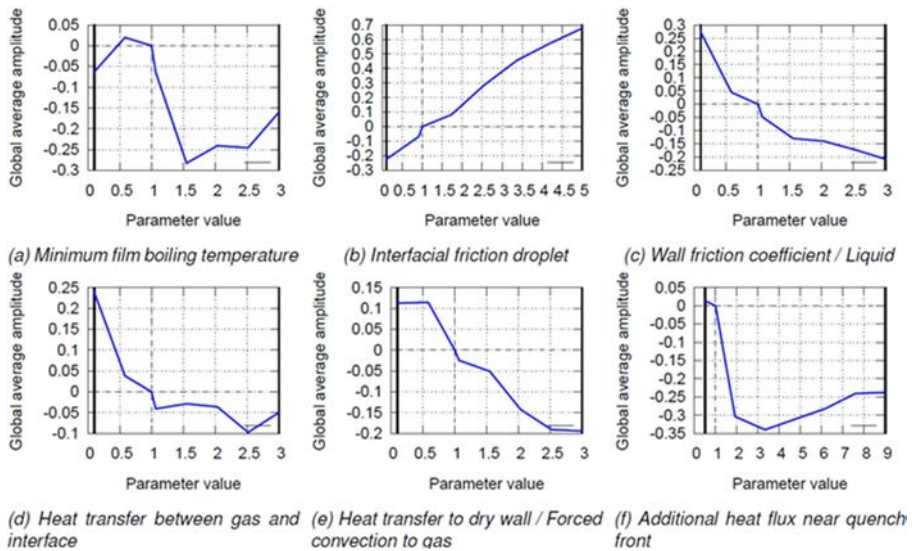


Figure 1. FFTBM analysis results for the different input parameters. The black vertical lines define the ranges of the variation.

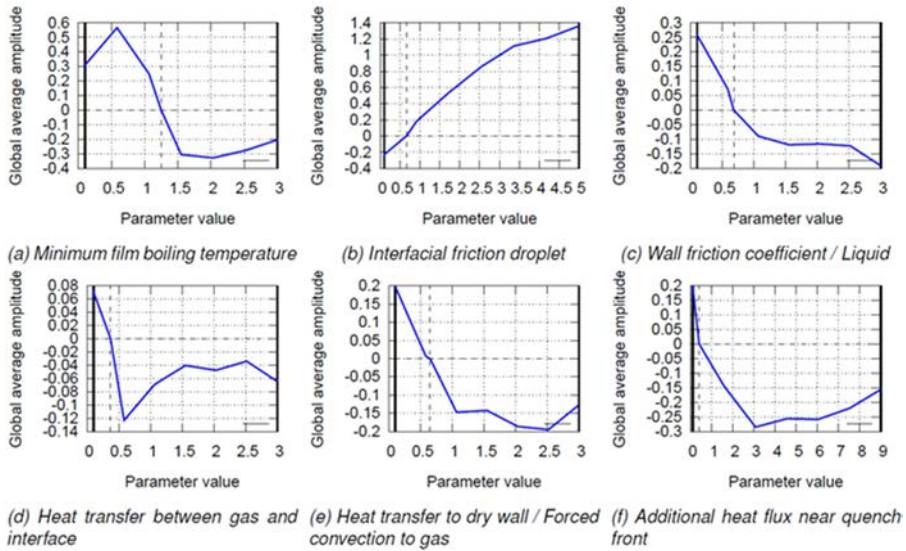


Figure 2. FFTBM analysis results for the different input parameters with nominal values defined with the following CIRCE analysis. The black vertical lines define the ranges of the variation.

CIRCE analysis

The workflow of the CIRCE method as described in [Alku, 2013] is as follows:

1. Select uncertain input parameters
2. Run sensitivity and best-estimate runs
3. Choose output points
4. Derive all the $\frac{\partial R_j}{\partial \alpha_i}$ (per j output points and i input parameters)
5. Create CIRCE input file and run CIRCE
6. Check the residuals and remove unfit output points, if required
7. Run sensitivity calculations to determine that hypothesis of linearity is met and whether linear or log-linear formulation is better
8. Transform the bias results, b_i , to input parameter distributions, p_i
9. Check that new best-estimate runs with biases produce better results
10. Check that for example 93 randomly varied runs envelop about 95 % of experimental output points (BEPU analysis)

The application of the CIRCE method for the quantification of the uncertainties was performed in a somewhat different manner compared to the PREMIUM analysis. Because the quenching phase was excluded from the analysis, as large amount of data points as possible were used to provide the input for CIRCE. The original idea was to use all available data points, but because the CIRCE program only allowed 500 points every second data point from each experimental curve was used.

The data points at 0 seconds, which was the initial state of the model, were also excluded. Choosing between the different points for example based on the formation of the derivatives used by CIRCE could be arbitrary and thus the idea was to use as much information as possible.

This on the other hand caused some practical issues, because there were 373 data points to analyze from the 15 experiments. Consequently the same time frame around each point and the same parameter increments were used for all points, which in turn caused some of the derivatives to be badly formed. I.e. the best-estimate run values would not be in between the positive and negative increment run values. The time frame was chosen as ± 1.3 seconds and the increments as approximately $\pm 10\%$ of the calibrated best-estimate value at each iteration.

Another difference to the previous CIRCE analysis was that at each iteration new derivatives were calculated; with each iteration all experiments were calculated 13 times to provide positive and negative increment runs and the calibrated best-estimate run. Also, with each iteration the CIRCE analysis was performed with all data points and based on the analysis of the residuals some points were removed. In a total of 11 iterations 65 different points were removed of which 39 only appeared once, 17 appeared two to five times and 9 appeared seven or more times. On average 16 points were removed in each iteration constituting 4.3% of all points.

Because the derivatives were calculated for each point with each iteration, the removal of different points in different iterations does not cause problems. In essence each previous iteration served as a hint of where to look for a better set of best-estimate values and the results of each iteration stood up on their own. Furthermore due to the nature of the simulations -- where a small difference in an input parameter may cause random behavior -- different data points may suffer from this erratic behavior and be unusable with each iteration. This of course begs the question of whether the CIRCE method works with the VEERA experimental data in general. Figure 3 presents the results of the iterations.

The CIRCE results show a partial convergence in the course of the iterations; most mean values hover around their average and the standard deviations also, although the standard deviations fluctuate more. Four of the parameters converge at values close to the ones determined in PREMIUM (which can be seen in the figure at point 12 on the x-axis) while two parameters were defined values in PREMIUM which were several times as large as the ones defined this time. The trial iteration from x-axis point 12 to 13 also proves that the values reached in PREMIUM are not a local optimum which could be reached with the VEERA experimental data.

The two parameters differing from previous results, *interfacial friction droplet* and *additional heat flux near quench front*, are also parameters, which affect the VEERA simulations mainly in the quenching phase. Because quenching times could not be included in the analysis, like they were in PREMIUM, a difference in the results can be expected.

The final values for both mean values and standard deviations were defined through averaging over the last five iterations. In the case of the mean values more

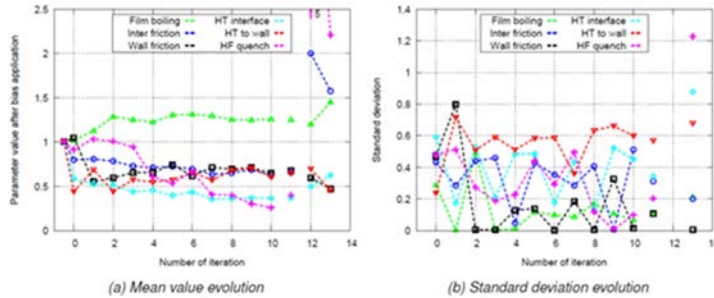


Figure 3. Results of the CIRCE iterations, where at point -0.5 on the x-axis are the nominal values and at 0 the original CIRCE application results. At point 10 are the results of the last CIRCE application and at 11 the final chosen calibrated mean/best-estimate and standard deviation values for the parameters. Another CIRCE application was performed using the calibrated values from the PREMIUM benchmark as the starting values for the parameters, which is shown at point 12, and the result of which at point 13.

focus is put on the last values in case convergence is evident. The ranges of variation were chosen at 2-sigma distance of the mean values either on a linear or logarithmic scale depending on which one would produce larger distance. The final results of the CIRCE iterations are listed in numerical form in Table 1.

The PDF types in the final PDF formulation are based on sensitivity runs. A visual comparison of the results in logarithmic and linear scale was performed and the one behaving more linearly was chosen. During the CIRCE iterations parameter wall friction coefficient / liquid was considered as following a log-normal distribution, but after defining the final ranges it was deemed to follow a normal distribution. Because of the iterative procedure and re-defining the derivatives with each iteration, this does not pose any problems.

Table 1. Final results of the CIRCE iteration to define the input parameter probability distribution functions. The mean values are the same as the calibrated best-estimate (CBE) values on a linear scale, while they are reported according to the PDF type. Similarly the standard deviations are reported in their respective scales, whereas the minimum and maximum values are on a linear scale for all parameters.

	Minimum film boiling temperature	Interfacial friction droplet	Wall friction coefficient / Liquid	Heat transfer between gas and interface	Heat transfer to dry wall / Forced convection to gas	Additional heat flux near quench front
PDF	normal	log-normal	normal	log-normal	normal	normal
CBE	1.25	0.66	0.68	0.37	0.65	0.4
Mean	1.25	-0.42	0.68	-0.99	0.65	0.4
Stdev	0.11	0.31	0.11	0.35	0.57	0.2
Min	1	0.05	0.45	0.05	0.05	0.05
Max	1.55	1.3	0.9	1.1	2	0.8

The ranges of the parameters' sensitivity runs were chosen to be the same as the final ranges of the PDFs, except for parameter additional heat flux near quench front for which the whole range of variation was used. This is due to the final range being so small compared to the variation range for the FFTBM application -- which is where the data is from -- that only one point would have fit inside the range allowing no conclusions of the linearity of the parameter. Thus the larger range, which clearly shows linear-scale variation, was selected. Since on such a large range the parameter acts consistently linearly, it can be assumed that it does so also on a smaller part of the range.

To check how well the quantification of the input parameters' uncertainty was accomplished BEPU analysis was performed. The 15 experiments used in the quantification were each simulated 93 times with randomly selected parameter values according to the defined PDFs to provide 95 %/95 % uncertainty bounds. Figure 4 presents the bounding limits for all the 373 data points used in the analysis highlighting the 65 points that were removed in different stages of the iterations.

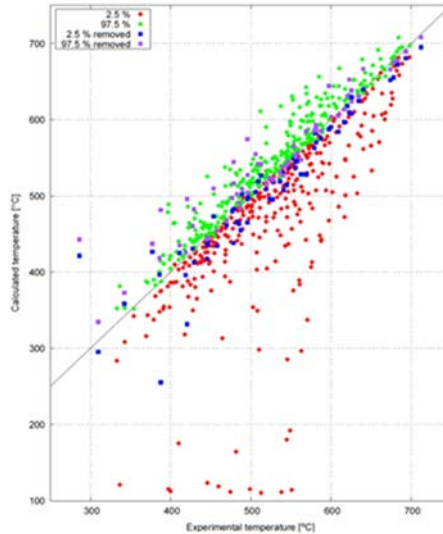


Figure 4. The 2.5 % and 97.5 % uncertainty limits for all the 373 data points used in the CIRCE analysis in relation to the experimental values.

The bounds portrayed in Figure 4 cover the experimental values for the most part. 23 of the lower limits, the 2.5 % values, are above the experimental values, while 66 of the higher limits are below the experimental values. Taking into account the 65 points, which were removed at some CIRCE iteration, the numbers are lowered to 7 and 38 respectively, constituting approximately 10 % of all of the points.

According to the BEPU analysis definition 95 % of the data points should be covered, but only 90 % are covered, although also by definition the certainty of covering the 95 % is 95 % leaving room for random error. Still, most likely the PDF definitions are not perfectly formed, nor should they be expected to be, since the application of CIRCE did not follow the instructions to the point. As such the PDFs are acceptable and although more work could be performed to refine them so that the BEPU results would cover all 95 % of the experimental points it is not deemed appropriate for the purposes of this study.

Summary and conclusions

The purpose of the work was to evaluate the current means by which the uncertainties of the constitutive equations of APROS could be quantified. If possible, the work was supposed to contribute to the task of actually quantifying the uncertainties, which could then be used in BEPU studies with APROS by all its users. In this form the uncertainties would be a part of APROS validation and verification providing a standard tool for analyses with APROS.

Yet several issues arose during the quantification process. The most important problems related to the rapid quenching of the cladding, which could not be duplicated with the simulations and caused the quenching phase to be dismissed in the quantification analyses.

The quantification of the uncertainties was started with a FFTBM analysis performed in a similar manner as in the PREMIUM benchmark. The results of the analysis were not usable. No better results were reached even when another attempt was made by setting the best-estimate parameter values to the ones defined by the CIRCE analysis, which was the process that was used for the final quantification of the parameter uncertainties in PREMIUM.

The CIRCE method was applied in a partly different manner compared to the instructions set by CEA: a very large amount of experimental points was used and with each iteration the derivatives were calculated again, instead of only the calibrated best-estimate run. Due to an automatized way of defining the derivatives some of them were badly formed, but the idea was that they would turn to noise in the CIRCE process, while the proper information would define the results.

Considering that the CIRCE iterations behaved fairly well the assumptions made about the process seem to have been at least not harmful to the successful application of the methodology. The parameters more or less converged during the iterations with four out of six converging to values close to the ones in PREMIUM. The other two were ones that have most of their impact on rewetting, which was not taken into account in the analyses.

The misgivings of FFTBM and CIRCE imply that not only is more work required to widen the basis for the quantification of the uncertainties, but also more research to advance the methodologies is necessary to reduce the amount of expert judgment required. In fact a proposition has already been presented to this effect within the SAFIR2018 USVA project plan.

References

- IAEA, 2008. Best estimate safety analysis for nuclear power plants: uncertainty evaluation. Safety reports series 52. STI/PUB/1306. Vienna: International Atomic Energy Agency. ISBN: 978-92-0-108907-6.
- Prošek, A. & Mavko, B. 2003. Review of Best Estimate Plus Uncertainty Methods of Thermal-Hydraulic Safety Analysis. International Conference: Nuclear Energy for New Europe 2003. Nuclear Society of Slovenia.
- Bucalossi, A. & al., 2010. Comparison Between Best-Estimate-Plus-Uncertainty Methods and Conservative Tools for Nuclear Power Plant Licensing. Nuclear Technology 172.1, 29-47.
- Glaeser, H., 2008. GRS Method for Uncertainty and Sensitivity Evaluation of Code Results and Applications. Science and Technology of Nuclear Installations (Feb. 2008). Article ID 798901.
- de Crécy, A. & Skorek, T., 2011. PREMIUM — Benchmark on the quantification of the uncertainty of the physical models in the system thermal-hydraulic codes. Barcelona: Workshop on Best-estimate Methods and Uncertainty Evaluations.
- Skorek, T., 2012. Description of FEBA Test Facility and FEBA/SEFLEX Experimental Program. GRS.
- Deruaz, R., Clement, P. & Veteau, J., 1985. Study of Two-dimensional Effects in the Core of a Light Water Reactor During the ECCS Phase Following a Loss of Coolant Accident. Commission of the European Communities.
- Alku, T., 2013. Quantification of APROS' physical model uncertainties in the context of the PREMIUM benchmark. MSc. thesis. Aalto University.
- Puustinen, M., Tuunanen, J. & Raussi, P., 1994. VEERA facility for studies of nuclear safety in VVER type reactors. Espoo: VTT.
- Alku, T., 2012. Identification of Influential Uncertain Parameters of PREMIUM Benchmark. VTT-R-08026-12. VTT.

22. Thermal hydraulics and fuel integrity in spent fuel dry cask interim storage facility (SPEFU)

22.1 SPEFU summary report

Risto Huhtanen, Asko Arkoma

VTT Technical Research Centre of Finland Ltd
P.O. Box 1000, FI-02044 Espoo

Abstract

The objective is to develop and validate a method for the analysis of spent fuel dry cask interim storage facility. A simplified 3D CFD-model is developed, where all the fuel rods and cooling fins are not modeled in detail. The peak cladding temperature of the fuel rods is calculated and used in studying the integrity of the fuel cladding during the interim storage. The phenomena affecting cladding integrity are reviewed and models appropriate for the interim storage conditions are developed. The issues of greatest safety significance are foreseen to be the cladding creep and the behavior of hydrides.

Introduction

The interim storage can be either water cooled or air cooled. In Finland the present facilities are water cooled storages with active cooling loop. Another possibility under consideration is an air cooled storage where cooling is driven by natural convection. This solution contains no active components, which is an advantage in exceptional situations. In Fukushima, the fuel storage pools in the power plant lost their cooling due to lack of electric power. In time that led to gradual loss of cooling water when water was evaporating.

Fuel behaviour during dry storage is actively investigated, especially now that in many countries interim storage times are foreseen to be extended to 100 years. The fuel behaviour models include irradiation integrally, and as such are not necessarily applicable to the interim storage conditions. The possible damage mechanisms

include creep rupture, as well as hydride-induced effects. The hydrides also reduce the ductility of the fuel cladding, possibly creating challenges during the fuel handling phase.

The fuel rods or even the casks with cooling fins cannot be modelled in detail in CFD analysis of the whole storage room because the numerical mesh would be extremely large. Therefore, some modelling assumptions and their validation are needed.

The behaviour of spent fuel cladding in dry cask storage

The objective of this subtask of the project was to study the integrity of nuclear fuel cladding in interim dry cask storage. The two phenomena postulated to be the risks for cladding integrity in dry storage, i.e. cladding creep (creep rupture) and hydride-induced failure, were investigated, and reported in two VTT Research reports (Arkoma, 2014 and 2015). The first mentioned involves modelling of cladding creep, and the second one is a literature study of hydride phenomena in dry storage.

Creep is permanent deformation mechanism that occurs at stresses below the yield stress. Creep is dependent on time and activated by temperature. Beside the temperature, stress and cladding alloy material characteristics like microstructure and chemical composition affect the creep rate.

The hydride effects include hydrogen precipitation to hydrides, dissolution, hydrogen migration, hydride re-orientation from circumferential orientation to detrimental radial orientation, loss of cladding ductility, delayed hydride cracking (DHC), and the influence of hydrides and hydrogen on cladding creep. Hydride effects are experimentally studied using most often artificially hydrided fresh cladding samples, and varying the hydride concentration, orientation, temperature and stress. The test types include ring-compression, ring-tensile and pressure tests.

Creep rupture is considered to be the dominant postulated cladding failure mode during dry storage, but nevertheless, hydride-induced failures cannot be excluded. Especially during handling and transportation of dry storage casks after several decades of dry storage, the embrittlement of the cladding by the hydrides has to be considered as the embrittled cladding may fracture in a cask drop accident.

Modelling of creep in dry storage

A fuel behaviour code should be able to model the behaviour of a fuel rod during all the stages of operation: irradiation, water pool cooling (~5 years), one day of drying, and finally the dry storage. Usually fuel behaviour codes are applied to model steady-state and transient conditions, and therefore in order to model dry storage, some models need to be updated.

In order to model the cladding creep, the goal was to extend the creep model of a single rod fuel performance code ENIGMA used at VTT to the interim dry cask storage conditions. For that, a literature search was made in order to find suitable models. Two dry storage creep models were found from open literature and those

were implemented into ENIGMA. The models are based on the same experimental database of Zircaloy-4 cladding alloy and have been developed by EDF/CEA and CIEMAT.

Preliminary testing of the laws was done with a U.S. PWR case from the International Fuel Performance Experiments (IFPE) database. Also, comparisons were done against the results published by CIEMAT. Parametric study of rod internal pressures was done, and the influence of internal pressure on cladding creep hoop strain was that way investigated.

At the moment, the results produced by the two creep models show too high creep values during the dry storage to be realistic, and that will still require further analysis of the creep laws and their implementation. Compared with the usually applied limit of 1% hoop strain during the dry storage, the obtained calculation results are higher as seen in Fig. 1.

Similar dry storage assessments have been made at UK National Nuclear Laboratory (NNL) with their version of ENIGMA (Rossiter, 2011. Nuclear Engineering And Technology, Vol. 43 No. 6, pp. 489-498). The EDF/CEA model has been implemented at NNL, but direct comparison is difficult as different steady-state creep formalism is used than commonly applied with VTT-ENIGMA.

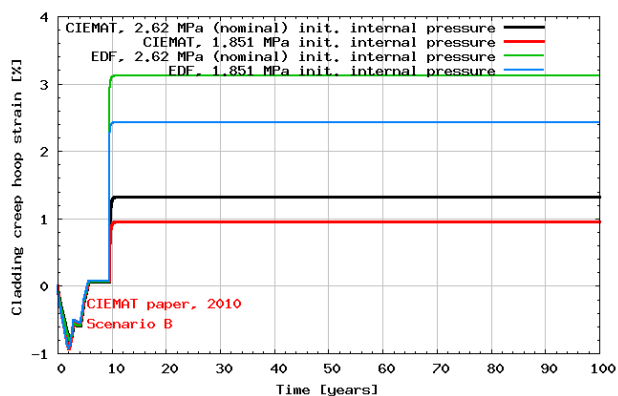


Figure 1. Cladding creep hoop strain calculated with ENIGMA using the steady-state power history found in an article by CIEMAT (L.E. Herranz, F. Fera, 2010. Progress in Nuclear Energy, Vol. 52, Issue 7, pp. 634-639). The increase in creep due to dry storage is 0.5% according to Herranz and Fera, calculated with FRAPCON code, while with VTT-ENIGMA, the increase is 1.3% when applying the CIEMAT creep model.

The effects of hydrides on cladding integrity in dry storage

Open literature was searched in order to gather and summarize information on the effects of hydrides on cladding integrity in dry storage. Results from both experimental research and computational analyses are elaborated, and the current state-of-the-art of research in this field has been brought out.

In nuclear reactor, hydrogen is formed due to oxidation of zirconium cladding and through radiolysis, and the generated hydrogen diffuses into the cladding. The solubility of hydrogen in zirconium alloy varies with temperature. When the concentration of hydrogen exceeds the solubility limit in a given temperature, insoluble zirconium hydrides ZrH_x are formed.

Finite element modelling (FEM) codes are used in the modelling of hydride effects such as the enhanced crack propagation in the cladding. Phenomena like that cannot be modelled with the simulation tools traditionally employed in the field of fuel behaviour modelling at VTT, i.e. 1.5-dimensional codes ENIGMA and FRAPCON, and therefore this subtask of the project was limited to a literature survey.

Based on the gathered references, it can be said that hydrides are widely investigated, as well as the hydride phenomena during dry storage. Also during the recent years, the research has been active. However, the laboratory experiments are more related to short-timescale changes in the cladding due to hydrides, not the long term evolution as in real dry storage conditions. The most popular research subject among the articles gone through seems to be the hydride re-orientation, and how various parameters affect this phenomenon. Also the other popular subject, loss of ductility due to hydrides, is closely related to radial hydrides. Radially oriented hydrides make the cladding more susceptible to failure compared to circumferentially oriented hydrides as the cladding is then more vulnerable to tensile hoop stress caused by the rod internal pressure. Thermal cycling and tensile stress can cause the hydrides to re-orient during the operation and dry storage.

Fewer research results may be found from studies with real irradiated fuel rods dry stored for a long time. At least two such studies are done, reported by Sasahara and Matsumura (Nuclear Engineering and Design, Vol. 238, pp. 1250-1259, 2008), and Einziger et al. (Nuclear Technology, Vol. 144, pp. 186-200). In both studies, no significant re-orientation of hydrides into radial direction was discovered. In the second mentioned study, the estimated maximum value for creep was only 0.1%. However, both studies were done in non-prototypical conditions and/or with low burnup fuel.

As the hydride effects depend on the cladding alloy composition and manufacturing process, and because the set-up in each study is different (the fraction of radially oriented hydrides, total hydrogen concentration in the cladding, temperature and stress range, cool-down rate etc.), the experimental information on hydride effects is quite scattered.

Heat transfer from fuel rods to the cask body

In order to ensure fuel rod integrity in dry storage the temperature of the fuel rod cladding has to be kept below creep limit of the material. The work done during year 2013 concerns heat transfer from a single fuel assembly, reported in (Huhtanen 2014). The essential heat transfer mechanisms are estimated with accurate modelling of a case known from the experiments. In the accurate modelling the amount of computational work is impractically large, especially when more fuel assemblies are

included to the simulation. In the experimental case heat transfer takes place mostly by radiation (75 %).

A proper simplification method is sought for modelling the heat transfer of the fuel rod bundle. In the suggested method reduction of computational cells is about 94%. The detailed rod bundle is modelled with solid block where the local heat conduction depends on local temperature. The modified heat conductivity is calculated from the geometrical parameters of the rod bundle. The method is described in detail in (Manteufel 1991).

The accurate simulation has got 1.38 million cells in the computational grid. The amount of cells in the coarse grid is only 4% of that. The temperature field in one cross section is shown in Fig. 2. Total height of the rod assembly is about 4 m.

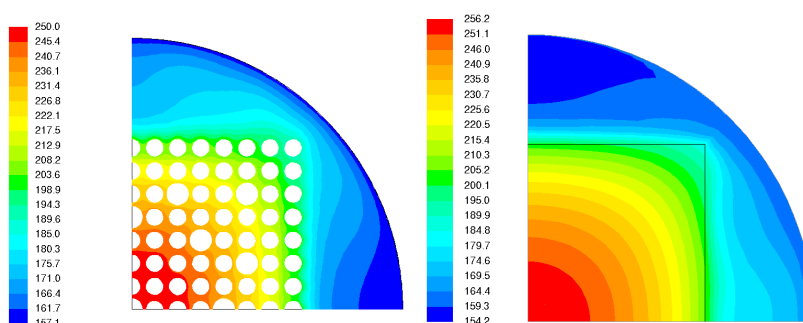


Figure 2. Accurate simulation results (left) for temperature [°C] in a cross section and solid model results (right) with a coarse grid. Level is 3 m in the rod bundle.

Estimated temperature peak value by solid modelling is found to give fairly good agreement with the experimental values given in (Lombardo & al. 1986). Also the trends in sensitivity analysis are of right order of magnitude. There are differences in temperature distribution along the rod, because flow and convective heat transfer inside the rod bundle is not included. The simulated and experimental temperature values along a line are shown in Fig. 3.

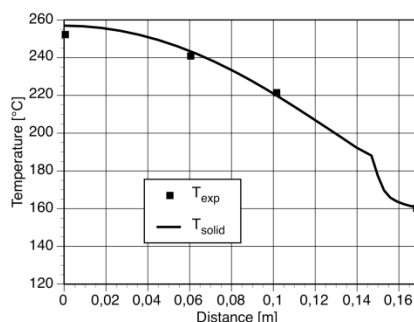


Figure 3. Temperature profile in a coarse grid solid model simulation along 45° diagonal on height 2.89 m in the rod bundle compared to the experimental values.

Heat transfer from cask to the environment

The simulation of cooling of a spent fuel cask with cooling fins has been performed with a fine grid and two optional coarse grids, reported in (Huhtanen 2015). The fine grid simulation has been used as a reference when searching for computational work for the task. Savings are necessary when simulating a large store with several fuel casks. In this simple one cask simulation with fine grid the amount of computational cells was 3.5 millions when two symmetry axes were used for defining the simulation domain. If the amount of casks is 100 or other high number, this kind of symmetry assumptions cannot be made.

The geometry of the cask is shown in Fig. 4. The cask is a single object on a surface with free space around. A 90° sector has been used in the simulations. The cask is same as was used in the original experiments (Lombardo & al. 1986).

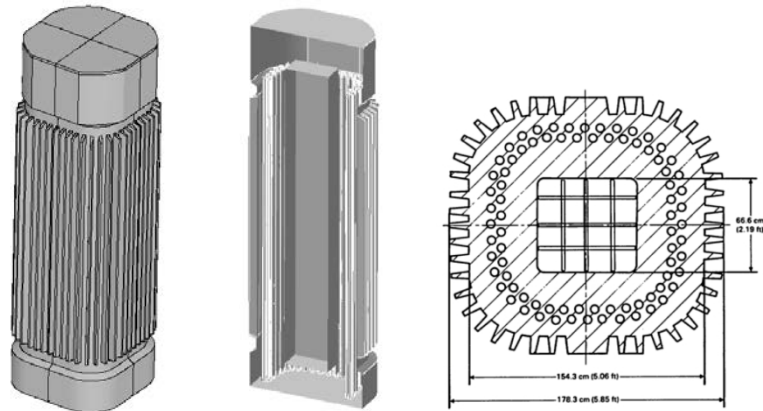


Figure 4. The modelled geometry and two cross sections of the cask.

The proposed method of using modified thermal conductivity for the air in the cooling fin domain takes into account the effect of the conducting cooling fins without the need to include all geometrical details into the model. In this example the number of computational cells was 92% lower than in the fine grid case. This will be reflected to the computational work needed to solve the problem. The simplified method can be used for solving the problem without compromising the accuracy too much.

For a new geometry it is necessary to make one fine grid simulation for a single cask and set the model parameter for a coarse grid. Fig.5 shows the surface temperature of the cask and radiation and convective heat transfer distributions on the surface. The total share of radiation is 44% in the case considered. The ratio will change over time when heat production of the fuel rods changes.

In the simplified modelling the modified conductivity is set so that the inner surface temperature of the cask is same as in the accurate simulation. This temperature defines heat transfer from fuel rod assemblies to the cask body. Using the simplified model the calculated temperature profiles are compared to the accurate profiles in

Fig. 6. The share of radiation heat transfer is 42%, slightly lower than in the accurate simulation. The influence of absorber rods are seen in the temperature profile in Fig. 6 around distance 0.6 m. The absorbers act also as thermal insulators and affect the local temperature gradient. In the coarse grid simulation the local features are not so well captured due to lower resolution. However, the general profile of temperature is very good in the simplified model.

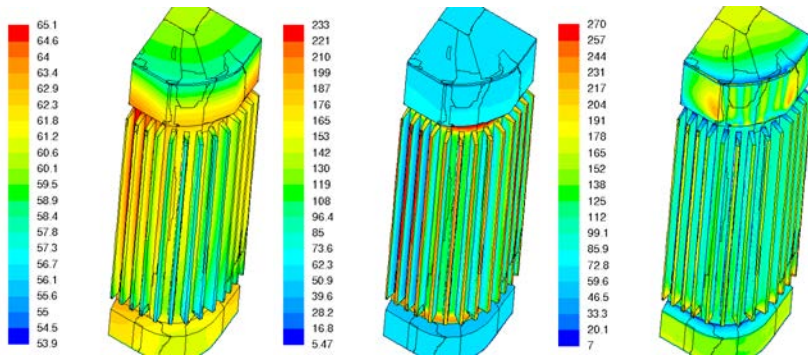


Figure 5. Surface temperature [°C] (left), net radiation heat transfer [W/m²] (mid) and convective heat transfer [W/m²] (right). Calculated with the fine grid.

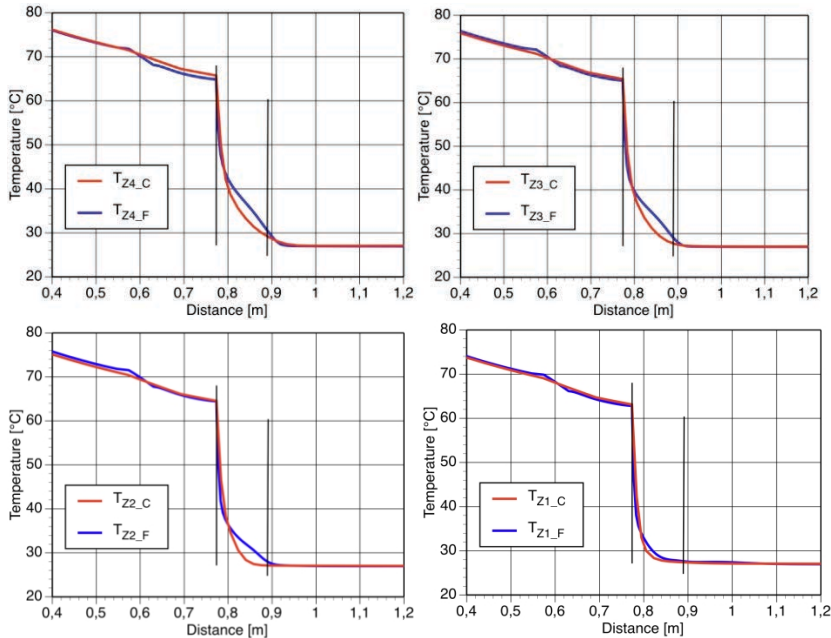


Figure 6. Temperature profile along the line through the solid block and gas on height levels 1...4 m. The subscript F denotes fine grid data and C coarse grid data. The vertical lines denote the area of cooling fin slot.

The flow field around the cask is demonstrated with iso-surfaces of temperature in fine grid and coarse grid case in Fig 7. The flow fields are similar, although more details are seen in the fine grid case. The fins guide flow along the cask. Omission of this guidance does not have essential effect on the flow field of the coarse grid in this case, but may have some influence in a crossflow.

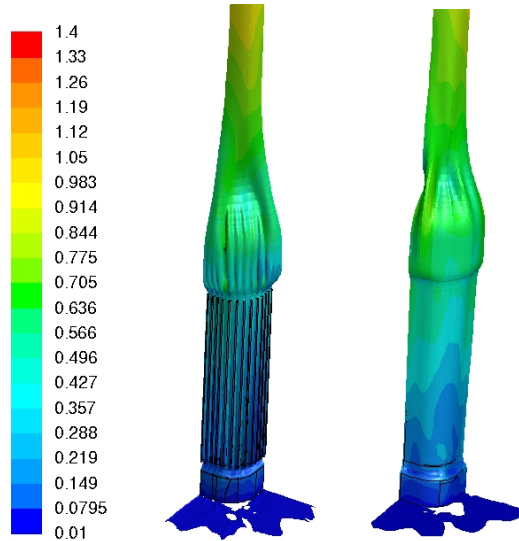


Figure 7. Flow velocity [m/s] on temperature iso-surface 30 °C in accurate (left) and simplified simulation.

References

- Arkoma, A., 2014. Long term behaviour of spent fuel in dry cask storage: Modelling of cladding creep. Espoo: VTT. Research report VTT-R-00812-14, 14 p. + app. 15 p.
- Arkoma, A., 2015. Long term behaviour of spent fuel in dry cask storage: The effects of hydrides. Espoo: VTT. Research report VTT-R-00379-15, 14 p.
- Huhtanen, R. 2014. CFD-modelling of a single assembly spent fuel. Espoo. VTT Research Report VTT-R-00685-14. 24 p.
- Manteufel, R. D. 1991. Heat transfer in an enclosed rod array. Thesis. Massachusetts Institute of Technology, 1991. 539 p.
- Huhtanen, R. 2015. Modelling of multi-assembly cask with fins. Espoo. VTT Research Report VTT-R-00592-15. 23 p. + app. 2p.
- Lombardo, N.J., Cuta, J.M., Michener, T.E., Rector, D.R. and Wheeler, C.L. 1986. COBRA-SFS: A thermal hydraulic analysis computer code, vol. III: validation assessments, Report PNL-6049, vol. III, UC-85, 1986

23. Core debris coolability and environmental consequence analysis (COOLOCE-E)

23.1 COOLOCE-E summary report

Eveliina Takasuo, Veikko Taivassalo, Jukka Rossi, Mikko Ilvonen, Tuomo Kinnunen,
Taru Lehtikuusi, Stefan Holmström, Pekka H. Pankakoski, Ville Hovi

VTT Technical Research Centre of Finland Ltd
P.O. Box 1000, FI-02044 Espoo

Abstract

The COOLOCE-E project focused on two specific topics in the research area of severe accidents: the coolability of ex-vessel core debris and the assessment of the environmental consequences of radioactive releases. The main objective of the project was to assess the coolability of porous debris beds considered representative of realistic debris beds. This consisted of experimental activities with the COOLOCE facility and the verification and validation of the analytical tools and methods commonly applied to model two-phase flow and predict dryout in the debris bed. As the severe accident management strategy in both Finnish and Swedish BWRs relies on cooling the core debris in a deep water pool, collaborative experimental and analytical efforts by VTT and KTH have been performed aiming for comprehensive understanding of the yet unresolved, high-priority issues in this research field. In the environmental consequence assessment ARANO and VALMA atmospheric dispersion simulation codes have been applied in predicting radiation doses caused by releases of radioactive materials. The objectives of the work were to assess the performance of the two codes against the measured data from the Fukushima accident and to study the applicability of the codes for predicting radiation doses at distances beyond 20 km from the power plant. This is necessary for answering the question of what countermeasures should be prepared outside the traditional emergency planning zone.

Experimental activities

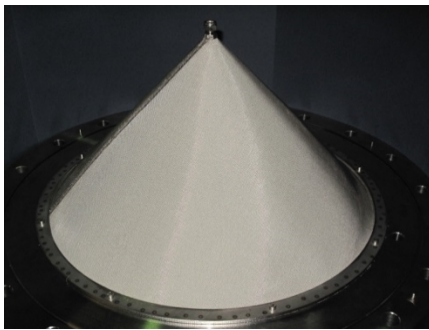
The COOLOCE test facility is a laboratory-scale facility at VTT specifically designed to investigate the coolability of porous particle beds of different shapes and flow modes. Different types of multi-dimensional flooding modes (achieved through different bed geometries) and their effect on the coolability have been examined. The flooding mode determines how the water infiltrates into the pores of the debris bed and it may play a key role in whether the debris bed is coolable or local dryout and, eventually, re-melting can occur.

The COOLOCE experiments were started in 2010-2011 with the main objective of comparing the dryout power of a conical (heap-like) particle bed configuration to that of a cylindrical (evenly distributed) configuration (Takasuo et al. 2012a). In 2012, experiments were conducted with irregular gravel as the simulant material (COOLOCE-8) and initially subcooled pool (COOLOCE-9) (Takasuo et al. 2012b).

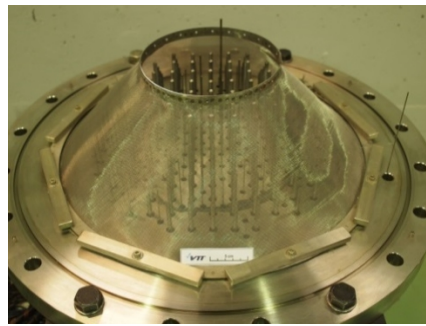
In 2013 and 2014, other debris bed shape variations were investigated. These included a cylindrical bed with impermeable top that represented agglomerated particles, a conical bed on a cylindrical base and truncated cone (Takasuo et al. 2013a-c, 2015). The test beds are shown in Figure 1. The resistance heater arrangement is shown in the photo of the truncated cone test bed (Figure 1(b)), the other beds are filled with the particle material, ceramic beads.

The debris bed shape variations extensively cover the flooding modes which are possible in realistic conditions. The dryout power and coolability was measured for these flooding modes which produced useful data for simulation code validation and new information about the relative coolability of the different debris bed shapes (see the COOLOCE-E Special article). It was also shown that the debris bed height is a key issue in dryout power.

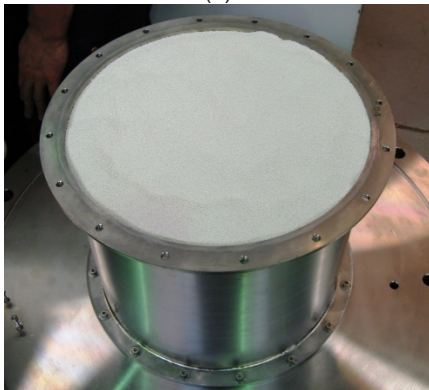
The research at VTT focuses on finding out the coolability limits in certain, well-defined representative conditions. It is, however, important to note that the debris bed configuration as well as its coolability depends on the melt discharge, and is determined by processes which include many uncertainties starting from the uncertainties inherent in the in-vessel accident progression. New data on the key physical phenomena of the debris bed formation which defines the spatial configuration, porosity, particle morphology and size distribution of the bed was produced by KTH (Royal Institute of Technology) in the APRI-8 project in Sweden. Joint efforts to reduce the uncertainties in coolability were conducted by VTT and KTH within the DECOSE project financed by NKS. The project facilitated information exchange and co-operation between the organizations so that the experimental and analytical activities in both APRI-8 and SAFIR2014 projects were combined to benefit both participants, end-users and the scientific community.



(a)



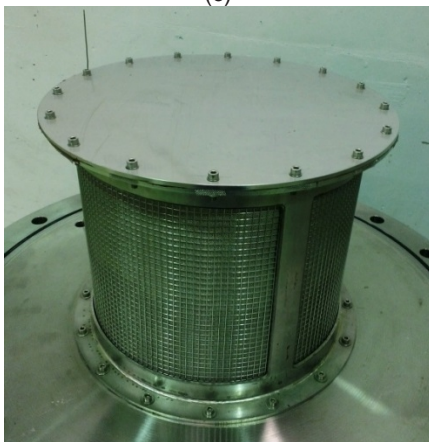
(b)



(c)



(d)



(e)



(f)

Figure 1. The COOLOCE test beds: (a) conical, (b), truncated cone, (c), cylindrical, (d) cylindrical with open walls, (e) cylindrical with impermeable top and (f) cone on a cylindrical base.

Modelling of debris bed coolability

The validation of simulation codes against experiments is a crucial part of the coolability research. Reactor scale experiments are non-existent which means that the reactor scenarios have to be analysed using simulation codes. The comparison of simulations and experiments reveal how well the simulations and the applied models are capable of reproducing the real-world dryout behaviour. The modelling is based on solving the two-phase flow conservation equations, namely, the mass, momentum and energy conservation for the gas and liquid phases. The closure models for the frictional forces and heat transfer are well-known models found in the literature.

The main computational tool used at VTT for analysing the particle bed coolability is the MEWA 2D severe accident code developed by the IKE institute of Stuttgart University (Rahman, 2013). Another approach is based on a full CFD model which facilitates the 3D modelling of the flow in the debris bed (Takasuo & Taivassalo, 2014, Takasuo et al. 2012b). This approach has been developed at VTT by incorporating the porous media models into the in-house code PORFLO and into the CFD code Fluent (the latter as user-defined functions).

All the experiments were modelled using MEWA, and direct comparisons between the experimental and simulated dryout power were made. The CFD approach was used for in-depth assessment of the dryout behaviour and the effects of the selection of physical and numerical models. Based on this work, the best practices for debris bed coolability simulations can be derived. For results, see the Special article and its list of references.

Environmental consequences of radioactive releases

The assessment of the consequences of radioactive releases, particularly those of severe accidents, was included in the COOLOCE-E project in 2012 and 2014 and consisted of two separate tasks. The first task in 2012 was to assess the performance of two environmental dispersion calculation codes used in Finland against a real and highly topical issue, the accident at Fukushima Dai-ichi, and to introduce a new researcher into the topic. Information about the Fukushima accident source term, radionuclide air concentrations and depositions and external radiation dose rates were acquired from public literature. Meteorological data during the accident required as input for the calculations was acquired via the Finnish Meteorological Institute.

Based on the collected information, atmospheric dispersion simulations were run using two codes dedicated for estimating the consequences of radioactive releases, ROSA and VALMA. The results were compared to the measurements of the dose rates, concentrations and deposited amounts of certain nuclides in the vicinity of the plant site, and to estimates given by other reported simulations (Ilvonen et al. 2013). ROSA and VALMA are based on the Lagrangian principles of dispersion modelling and calculate the trajectories of the pollutant particles in the atmosphere. ROSA is

based on the level 3 PSA calculation code ARANO developed at VTT and it is best suited for calculating short-range, short-duration releases, utilizing weather data for a given point. VALMA is a more advanced code that accounts for the meteorological conditions in a more detailed manner than ROSA, e.g. by replacing ROSA's linear central trajectories by freely winding ones. Both codes are used in Finland as a part of emergency preparedness for abnormal radiation situations: VALMA is used by STUK (Radiation and Nuclear Safety Authority) and ROSA by the utility company TVO.

The objective of the second task in 2014 was to clarify what technical possibilities are practically available for calculating probability distributions of radiation doses from different exposure pathways at distances beyond 20 km from the power plant. The codes selected for this task were ARANO and VALMA. The examined range extended to 300 km from the site of the release. This work was also motivated by the Fukushima accident, and the new recommendations developed by IAEA that consider emergency planning outside the traditional protection and emergency planning zones (IAEA, 2014).

Protection zones and countermeasures

The protection zones around a nuclear power plant are divided to a protection zone (< 5 km from the NPP), emergency preparedness planning zone (5 - 20 km), extended emergency planning zone (20 - 100 km) and ingestion and commodities planning zone (100 - 300 km). The Finnish YVL Guide gives deterministic specification that in the case of a severe accident resulting in a radioactive release, there shall not be need for evacuation beyond the protection zone and no need for sheltering beyond the preparedness planning zone. The two zones beyond 20 km from the NPP are the new zones for which the possible need of countermeasures is considered.

In the early phase of the accident, the dose criteria for population protection measures are given, based on which dose rates for operational intervention levels are consequently defined. These dose rate levels are for

- sheltering 0.1 mSv/h,
- moderate sheltering 0.01 mSv/h
- ingestion of iodine tablets 0.1 mSv/h,
- access control 0.1 mSv/h

If operational intervention level is exceeded or it is anticipated to be exceeded, protection measure is generally necessary. In the intermediate phase of the accident, the objective of the population protection measures is that the dose due to the radiation incident does not exceed the maximum level dose of 20 mSv during the first year, when taking into account all routes of exposures at early phase and intermediate phase, as well as the protection measures to reduce the impact of exposures. If the dose caused by exposure during the first year is expected to be

- greater than 10 mSv , protective measures shall be adopted to reduce the exposure of the population
- 1-10 mSv, protective measures are usually justified
- less than 1 mSv, protective measures can be adopted to reduce the exposure, especially when they are easy and reasonably practicable

Possible countermeasures in the intermediate phase are e.g. prolongation of sheltering, relocation of population, access control, decontamination of inhabitants, dwellings and ground and control or prohibition of foodstuff. Based on the new IAEA recommendations, it should be investigated whether in the case of a severe accident release, there would be need for countermeasures outside the preparedness zone of 20 km. Weather conditions in which radioactive material could spread outside emergency planning zone causing high doses are possible. Deterministic effects are not expected at longer distances but countermeasures could reduce the risk of stochastic effects.

ARANO and VALMA calculations

The aim of the study was to find out if the existing calculation models ARANO and VALMA are able to calculate radiation doses outside the emergency preparedness planning zone, i.e. at 20 - 300 km distances, and what modifications and improvements in the models should be done (Rossi & Ilvonen, 2015). ARANO is a local scale model unable to consider changing weather conditions during dispersion and therefore probably inaccurate at longer distances. VALMA can consider changing weather conditions and therefore it is more accurate at longer distances but the drawbacks are that the calculation time may be long and currently the model does not include dose by ingestion.

ARANO calculation results in a severe accident release are presented in Figure 2 and Figure 3. Figure 2 shows the radiation dose as a function of distance for the 95% fractile and Figure 3 shows the dose distribution at 50 km from the power plant with two different assumptions of rain. The radionuclide inventory of Olkiluoto 3 was used as a basis for the source term estimation and it was assumed that the iodine-131 release from the reactor is 1000 TBq, the cesium-137 release is 100 TBq and the noble gas release is 1% (Case 1).

Example of a VALMA calculation is shown in Figure 4 which shows the total dose rate in south-west Finland after one week of an assumed radioactive release at the Olkiluoto NPP. Here, a larger release was considered: 100% of noble gases, 20% of iodine and 20% of cesium and rubidium (Case 3).

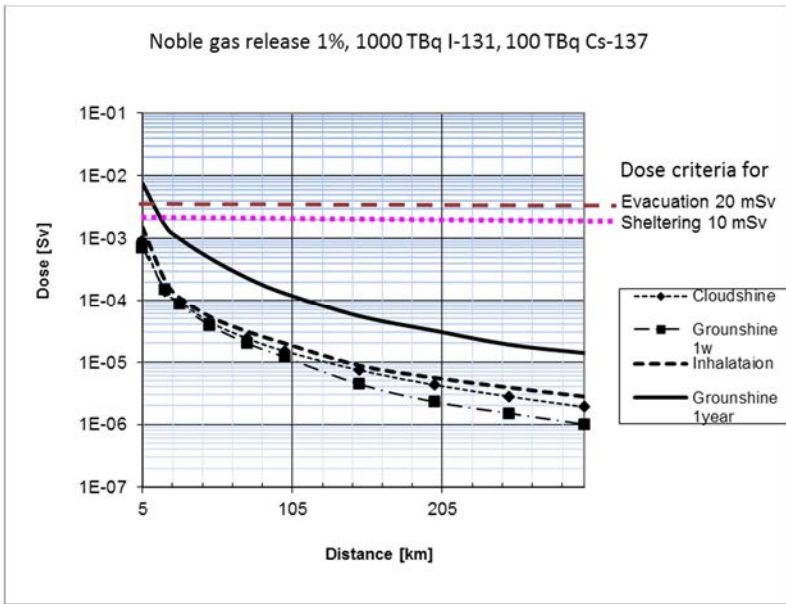


Figure 2. The dose components 95% fractile as a function of distance from the power plant calculated with ARANO (Case 1, small release). One year integration time of external radiation from the ground is added.

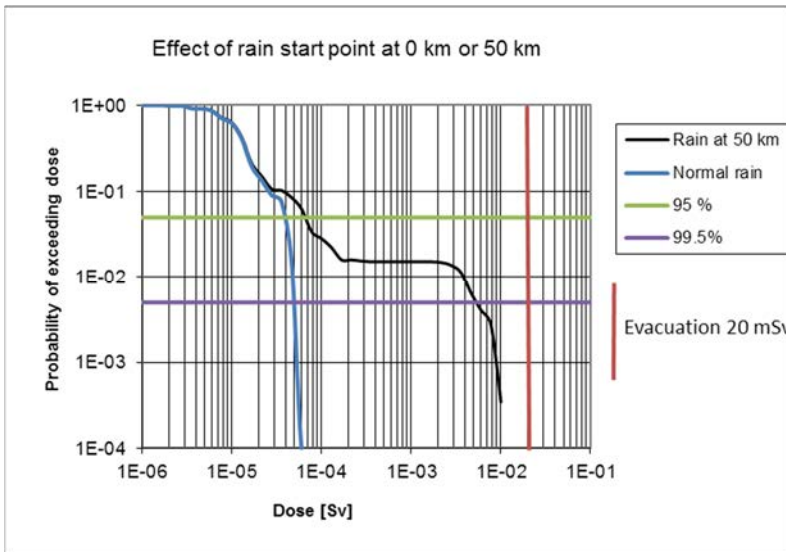


Figure 3. Groundshine dose distribution at the distance of 50 km calculated with ARANO (Case 1, small release). Effect of rain starting at the power plant or only at 50 km from the power plant. One week integration time of external radiation from the ground.

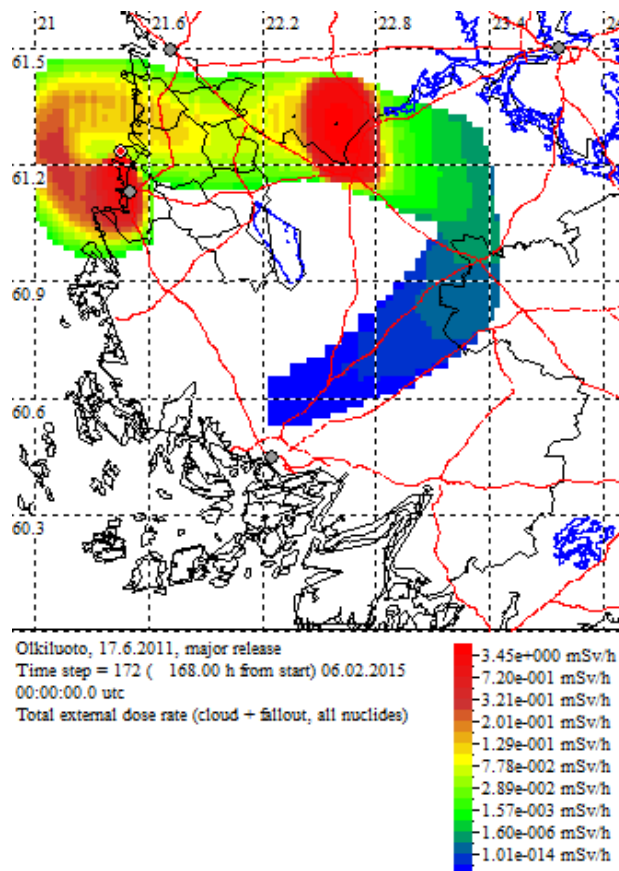


Figure 4. VALMA-predicted external dose rate one week after the start of an assumed release (Case 3, large release). Yellow color (middle / median of the scale) corresponds to appr. 0.1 mSv/h. Red circle = Olkiluoto, grey = Rauma, Pori etc. Side of a dotted rectangle is appr. 35 km.

The results suggest that the codes are, in principle, applicable to long-distance calculations. However, the accuracy of the predictions cannot yet be clearly judged due to the lack of comparisons to measurement data. Main sources of uncertainties are related to the weather conditions and the source term. Furthermore, NWP (numerical weather prediction) based weather data which uses a 3D flow field should be used for best results.

It was found that typical VALMA simulations are remarkably more time-consuming than the ARANO simulations as expected. ARANO is capable of calculating larger data sets faster than VALMA but a significant defect at long distances may be the

assumption of constant weather conditions all the dispersion time. VALMA, on the other hand, is capable of calculating results in changing weather conditions. Weather data can be based either on one point (e.g. a meteorological mast) or on the particle trajectories of a numerical weather prediction model. In these cases calculation time for large number of cases induces problems and it is necessary to reduce the amount of trajectories. Finally, it should be noted that results of the present study are quite preliminary and the work will continue in 2015 with a more focused and extended dose calculations at longer distances.

Main results and applications

The research combined an experimental programme of thermal hydraulic experiments investigating core debris coolability to analytical work and modelling of the coolability problem by using 2D and 3D two-phase flow simulation codes. The main outcome of the experiments was new data about the effect of the debris bed shape on coolability that can be utilized in simulation code validation. From nuclear safety perspective, the main applications of project results are the BWRs at Olkiluoto in which the severe accident management strategy includes the flooding of the lower drywell of the containment, and thus cool the solidified corium in a deep water pool (ex-vessel).

The simulations performed during the project have produced significantly increased understanding of the capabilities of the models and codes to predict coolability in complex flow conditions associated to realistic debris bed shapes and developed a high level of expertise in this type of analyses. Joint activities with the Swedish research projects on BWR corium coolability have increased the level of cooperation and information exchange on a topic which is commonly important in both Finland and Sweden.

The capability for fast and reliable radiation dose rate calculations for emergency preparedness purposes is important at all nuclear power plant sites in Finland. The efforts made in the COOLOCE-E project to prepare for the validation and improvement of the atmospheric dispersion calculation form a basis for future work in the frame of SAFIR2018. The aim is to comprehensively estimate the consequences of the radioactive releases in long-distance and to maintain expertise on this topic by transfer of knowledge.

References

- IAEA 2014. Preparedness and Response for a Nuclear or Radiological Emergency. General Safety Requirements Part 7 No. GSR Part 7. Draft DS457. Rev. 6.0, 16 April 2014.

- Ilvonen, M., Rossi, J., Takasuo, E. 2013. Fukushima atmospheric dispersion and dose assessment simulations with ROSA and VALMA. Research Report VTT-R- VTT-R-01377-13. 52 p.
- Rahman, S. 2013. Coolability of Corium Debris under Severe Accident Conditions in Light Water Reactors. Doctoral thesis, Insitut für Kernenergetik und Energiesysteme, Universität Stuttgart, IKE 2-155. ISSN-0173-6892.
- Rossi, J., Ilvonen, M. 2015. Dose estimates from severe accidents beyond emergency planning zone. Research Report VTT-R-00432-15. 45 p.
- Takasuo, E., Holmström, S., Kinnunen, T., Pankakoski, P.H. 2012a. The COOLOCE experiments investigating the dryout power in debris beds of heap-like and cylindrical geometries. Nuclear Engineering and Design 250 (2012), p. 687-700.
- Takasuo, E., Kinnunen, T., Holmström, S. 2012b. COOLOCE particle bed coolability experiments with a cylindrical test bed: Test series 8-9. Research Report VTT-R-07224-12. 44 p.
- Takasuo, E. , Kinnunen, T., Lehtikuusi, T., Holmström, S. 2013a. COOLOCE coolability experiments with a cylindrical debris bed and lateral flooding: COOLOCE-10. Research Report VTT-R-0463-13. 16 p.
- Takasuo, E. , Kinnunen, T., Lehtikuusi, T., Holmström, S. 2013b. COOLOCE debris bed coolability experiments with an agglomerate simulant: Test series 11. Research Report VTT-R-03316-13. 22 p.
- Takasuo, E. , Kinnunen, T., Lehtikuusi, T. 2013c. COOLOCE-12 debris bed coolability experiment: Cone on a cylindrical base. Research Report VTT-R-07967-13. 18 p.
- Takasuo, E., Taivassalo, V., Kinnunen, T., Lehtikuusi, T. 2015. Coolability analyses of heap-shaped debris bed. Research Report VTT-R-00367-15. 55 p +1 appendix.
- Takasuo, E., Hovi, V., Ilvonen, M. Applications and Development of the PORFLO 3D Code in Nuclear Power Plant Thermal Hydraulics. 2012b. 20th International Conference on Nuclear Engineering , Anaheim, California, USA, July 30 – August 3, 2012 (ICONE20-54161).
- Takasuo, E., Taivassalo, V., Hovi, V. 2014. A study on the coolability of debris bed geometry variations using 2D and 3D models. Research Report VTT-R-00676-14. Espoo, 2014. 66 p.

23.2 Coolability of realistically shaped debris beds

Eveliina Takasuo, Veikko Taivassalo, Tuomo Kinnunen, Taru Lehtikuusi, Stefan Holmström, Pekka H. Pankakoski, Ville Hovi, Mikko Ilvonen

VTT Technical Research Centre of Finland Ltd
P.O. Box 1000, FI-02044 Espoo

Abstract

The coolability of porous debris beds has been investigated experimentally with the COOLOCE test facility and analytically by using 2D and 3D simulation models. The main objective of the experiments was to examine the relative coolability of debris beds with different shapes and, consequently, different flooding modes. Dryout powers and heat fluxes have been measured for six test bed geometries. The experiments have been modelled by using two-phase flow simulation codes with models suitable for fluid flow and heat transfer in porous media.

Introduction

At the Finnish BWRs in Olkiluoto, the flooding of the lower drywell of the containment is an important part of the severe accident management strategy. In the course of a core melt accident, corium is discharged from the reactor pressure vessel into a deep water pool in the lower drywell of the containment. Corium is fragmented and it is expected to form a porous debris bed from which decay heat must be removed in order to prevent re-melting of the material. Boiling and water infiltration into the particle bed interior play key roles in the heat removal. VTT has conducted an experimental programme of ex-vessel debris coolability using the COOLOCE test facility (Takasuo et al. 2012a). Along with the experimental studies, analytical activities aiming for the validation and development of simulation codes have been performed (Takasuo et al. 2012b, Takasuo et al. 2012c, Takasuo & Taivassalo, 2014). The objective of the experiments is to measure the heat flux which results in local dryout (loss of coolant) within the porous bed. Then, the critical heat fluxes, or power densities, may be compared to realistic values of residual power in accident scenarios.

A debris bed which is formed in a realistic accident scenario is the result of jet fragmentation, solidification and the settlement of the solidified particles into a water-filled cavity. As a result, the geometry and porosity of the debris bed and the size and shape of the particles that compose the bed can vary significantly. It is not possible to exactly predict the debris bed properties. The COOLOCE test facility design makes it possible to change between different types of test beds geometries, so that the effect of the particle bed shape can be examined. The debris bed shape is important because it determines which types of flooding modes are possible. The

flooding mode, which determines which type of two-phase flow is present in the debris bed, may have a crucial effect on the coolability.

The COOLOCE experiments consisted of 13 test series in which dryout power was measured for six different debris bed shapes in the pressure range of 1-7 bar. In addition to the geometry comparison experiments, experiments for comparing two different particle simulant materials have been made.

Simulations of the experiments using dedicated severe accident codes and other suitable codes, e.g. computational fluid dynamics (CFD), are an integral part of the project. The availability of simulation codes capable of assessing coolability in reactor scenarios has to be maintained and verified based on latest knowledge of what type of debris configurations are expected in reactor scenarios. The main computational tool used in the COOLOCE-E project for analysing the particle bed coolability is the MEWA 2D code developed by the IKE institute of Stuttgart University (Bürger et al. 2006). Another approach in use at VTT is based on a full CFD model which facilitates 3D modelling of the flow in the debris bed (Takasuo & Taivassalo, 2014).

All the COOLOCE experiments are modelled with the simulation codes for the purposes of code development, verification and validation. The analytical work includes direct comparisons of the experimental and simulation results and in-depth investigation of the performance of the different codes and models by code-to-code comparisons (flow fields, temperatures, grid effects etc.).

Spatial distribution of the debris bed

The starting point of the experiments was the comparison of an evenly-distributed, cylindrical debris bed and a conical debris bed. Other shape (geometry) variations are modifications of these two basic set-ups. They include a cylindrical bed which allows flooding through all the surfaces, a cylindrical bed with a cake simulant that represents particle agglomeration, a combination of the conical and cylindrical geometries and a truncated cone. Sketches of the six debris bed shapes are illustrated in Figure 1.

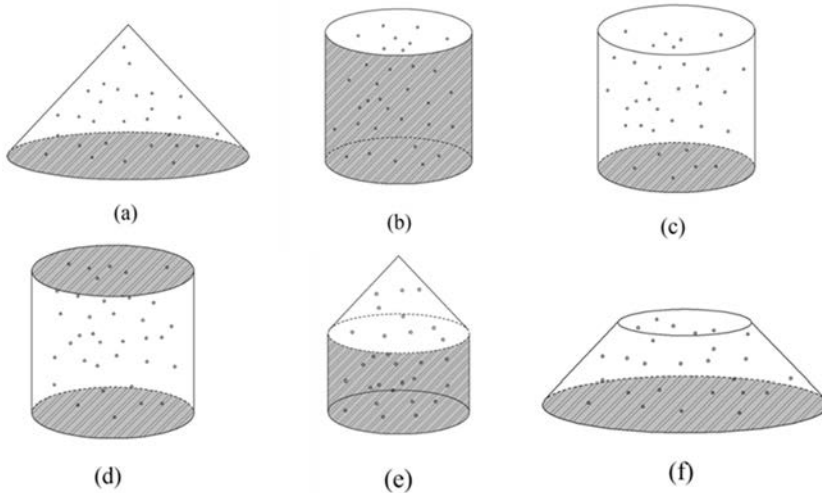


Figure 1. The debris bed geometries in the COOLOCE experiments: (a) conical, (b) top-flooded cylinder, (c) fully flooded cylinder, (d) cylinder with lateral flooding only, (e) cone on a cylindrical base and (f) truncated cone.

In all the geometries with the exception of the cylinder with closed walls (Figure 1(b)), i.e. the top-flooded cylinder, the water infiltration into the debris bed is governed by 3D and 2D flow phenomena which have not been taken into account in the traditional assessment of dryout heat flux by critical heat flux correlations and 1D models. Also, the more advanced 2D models that have been applied to debris bed coolability in recent years have not been validated against realistically shaped debris beds since experimental data of this type was practically non-existent.

The test facility

The test bed is installed into a custom-tailored pressure vessel with the design pressure of 8 bar and filled with demineralized water during the experiments. The heat generation of the debris particles – which in a realistic material would be caused by the radioactive decay of the fission products – is simulated by resistance heating. Dryout power measurements can be performed in the pressure range of 1-7 bar which is a representative range of the containment pressures for the Nordic boiling water reactors.

The main components of the COOLOCE test facility are the pressure vessel which contains the particle bed section with its heating arrangement, the feed water system and the steam removal system. The test vessel has a volume of 270 dm³ with the outer diameter of 613 mm. The pressure vessel is equipped with sight glasses that have been used for visual observations of boiling in the fluid volume (by a video recorder). The conical and cylindrical test beds are 500 mm and 310 mm in

diameter, respectively, and the height of the test beds is 270 mm, with the exception of the truncated cone (Figure 1(f)) which is 160 mm high. The total maximum power of the facility is around 50 kW, depending on the test bed. The test facility is shown in Figure 2 and a list of the experiments with the main specifications of each set-up is presented in Table 1.



Figure 2. The COOLOCE test facility. (1) feed water pre-heater, (2) feed water control valve, (3) connection box (power input), (4) pressure vessel, condenser and scale (steam removal), (6) video monitoring, (7) pressure gauges.

Table 1. Summary of the COOLOCE experiments.

Experiment	Test bed	Flow configuration	Particle material	Pressure [bar]
COOLOCE-1-2	Conical	Multi-dimensional	Spherical beads	1.6-2
COOLOCE-3-5	Cylindrical	Top flooding		1-7
COOLOCE-6-7	Conical	Multi-dimensional		1-3
COOLOCE-8	Cylindrical	Top flooding	Irregular gravel	1-7
COOLOCE-9		Top flooding*		1
COOLOCE-10		Lateral and top flooding	Spherical beads	1.3-3
COOLOCE-11	Lateral flooding only	1-7		
COOLOCE-12	Cone on a cylindrical base	Multi-dimensional through conical part		1.0-4.0
COOLOCE-13	Truncated cone	Multi-dimensional	1.3**	

* Initially subcooled water pool, saturated pool in all other experiments

**Pressure range varies in the tests because in some experiments the power required to reach dryout was greater than the maximum output of the facility

The debris simulant material was small, ceramic beads in all the geometry comparison experiments. In the experiments that investigated the effect of particle material, irregularly shaped and sized gravel particles were used (the same material as in the previous STYX experiments at VTT (Takasuo et al. 2010)). The scope of this paper is limited to the main topic of the COOLOCE activities, the debris bed shape comparisons. The results and discussion on different particle materials and the effective particle diameters can be found in Chickhi et al. (2014).

Experimental results – Conical and cylindrical beds

The experiments COOLOCE-1-7 clarify the relative coolability of the conical and cylindrical debris beds. The measurements directly show that if the conical and cylindrical beds are equal in height, the coolability of the cone is better by 50-60% compared to the top-flooded cylinder due to lateral flooding. However, if it is assumed that the debris beds are of equal in diameter and in volume, the coolability of a conical debris bed is reduced by 47-51% compared to the cylindrical bed.

In this case the cone is three times higher than the cylinder (because the volume of the cone is 1/3 of that of the cylinder). The greater height of the cone explains the poorer coolability: In a homogeneously heated debris bed, the heat flux in the bed increases with increasing height according to the following relation

$$HF = \frac{P}{V_{bed}} h \quad (1)$$

where HF is heat flux (kW/m^2), P is power (W), V_{bed} is the bed volume (m^3) and h is the bed height (m).

On the other hand, dryout is formed when the mass flux of steam is large enough to fully replace the water in the pore volume. Then, for the taller conical bed, there is more height “available” for the formation of dryout than in the flatter cylindrical bed. A total power (in kW) which causes dryout in a tall conical bed may not cause dryout in a flat-shaped cylindrical bed because the heat flux at the top of the cylinder is smaller by the same ratio as the height difference. In general, the multi-dimensional flooding tends to increase the dryout power and coolability compared to top flooding only but, according to the experiments, this is not adequate to compensate the effect of the increased height of the debris bed.

Because in a realistic scenario the debris can spread throughout the floor of the lower drywell and the debris mass (and heating power) can be assumed constant in this context, it is important to consider the actual distribution of the particles and the resulting bed height. The top-flooded cylinder is not the most conservative case.

Experimental results – Effect of flooding mode

The effect of the flooding mode on the debris bed coolability is seen by comparisons of the heat fluxes at the top boundary of the test bed. The heat fluxes are calculated

from the measured dryout power according to Eq. (1). Figure 3 presents the heat fluxes for all six COOLOCE test beds and all the different pressure levels. The accuracy of the measurement is shown in the bar chart: “DHF” denotes the dryout heat flux and “CHF” is the maximum coolable heat flux.

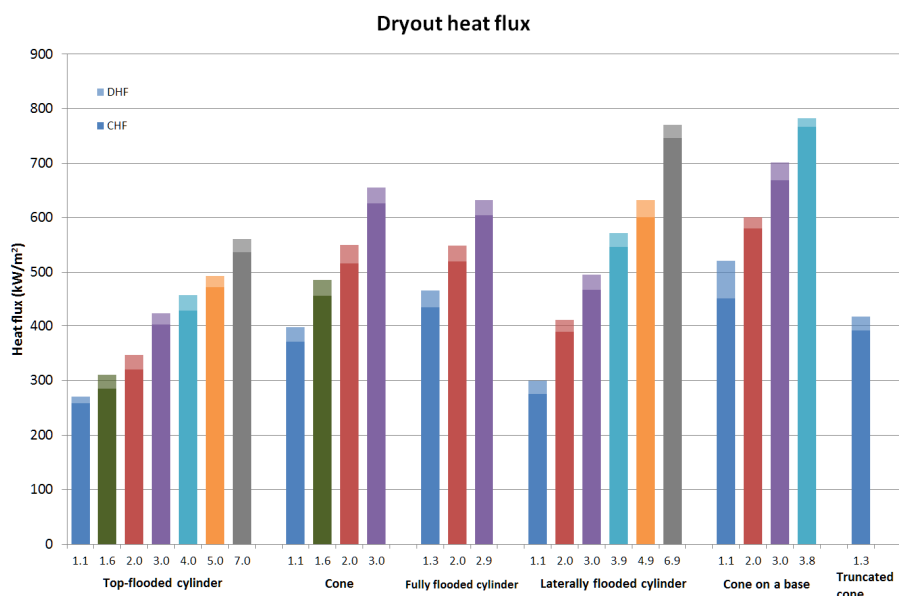


Figure 3. Dryout heat flux at the top boundary of the debris bed in the COOLOCE experiments. The light blue zone is the one-sided error margin of the measurement (difference between the maximum coolable heat flux CHF and the dryout heat flux DHF).

The heat flux varies between 260 –770 kW/m². The largest heat fluxes were obtained for the cone on a cylindrical base, the fully flooded cylinder and the fully conical bed, and also for the truncated cone. Common to these geometries is that some form of multi-dimensional infiltration of water is present: water can flood the bed through lateral surfaces to replace steam which exits upwards through the top of the bed.

Lower dryout heat flux is seen for the top-flooded cylinder and the cylinder with lateral flooding only. In the case of top-flooded cylinder, this is explained by the fact that the two phases have to flow in counter-current mode: water can infiltrate only through the top surface against the upwards flowing steam. In the case of the laterally flooded cylinder which has a solid top plate, both water and steam have to infiltrate and exit through the open lateral surface. The top plate forces the steam to escape through the side of the bed, instead of the top surface, which makes the top part below the plate vulnerable to dryout.

Even though these two flooding modes seem in principle different, according to the experimental results the modes are equally efficient (or inefficient) in removing

the heat generated by the test bed because the dryout heat fluxes are rather close to each other: 300 kW/m^2 for the laterally flooded cylinder and 270 kW/m^2 for the top-flooded cylinder. Compared to these values, the dryout heat flux measured for the cone is 33-47% greater and, for the fully flooded cylinder, 56-73% greater.

Debris bed coolability simulations

The multi-dimensional modelling of the debris bed dryout behaviour is based on solving the two-phase flow conservation equations, namely, the mass, momentum and energy conservation for the gas and liquid phases. The closure models for the frictional forces and heat transfer are well-known models found in the literature. The frictional forces within the porous medium are based on the two-phase extension of the Ergun's equation (Ergun, 1952). The models can be categorized as classical models without the explicit consideration of the gas-liquid drag and models with the gas-liquid drag force.

The objectives of the MEWA 2D simulations are to predict the dryout power and the dryout zone location for direct comparisons of the experimental and simulation results and to elucidate the flow field in the debris bed by means of 2D models. The goal of the CFD modelling is to complement the MEWA approach so that the effects of possible non-homogeneity of the debris bed can be taken into account. In general, the simulations aim for a more mechanistic, CFD type approach to the problem of internally heated porous bed in a water pool. The models for friction and heat transfer in porous media have been implemented as user-defined functions in the commercial CFD solver Fluent. The same models are also available in the in-house code PORFLO (Takasuo et al. 2012c).

In most cases, the Fluent results were qualitatively similar to the MEWA results. The agreement between simulation results and experiments varied from very good to reasonable in the cases of the top-flooded cylinder (Figure 1(b)) and the variations of the conical bed (Figure 1(a, e, f)). It was shown that the dryout power is mainly dependent on the height of the bed because the flooding modes are almost equally effective in removing the heat from the debris.

In the cases of the cylindrical test beds with full flooding (Figure 1(c)) and lateral flooding only (Figure 1(d)) the models commonly used to predict dryout had difficulties in capturing the flow behaviour, and the different drag force models yielded somewhat inconsistent results. In these cases, the role of lateral flooding is significant compared to the gravity and buoyancy controlled (co- and counter-current) flows in vertical direction. The inconsistency between the experiments and the models is not surprising taking into account that the applied models are originally developed based on experiments in either top- or bottom flooded beds in which the flow is effectively one-dimensional.

Another important result of the modelling work is that the steam flow can maintain post-dryout steady-states in which the temperature increase is not drastic enough to pose a risk of re-melting of the solid if the flooding mode allows this. It was proposed to use the increase of solid temperature as an alternative criterion for dryout, instead of the formation of the first dry zone which can be overly conservative for the heap-

like debris beds. Examples of the simulations are illustrated in Figure 4 and Figure 5 which show the void fraction distributions in the case of the latest experiment, truncated cone.

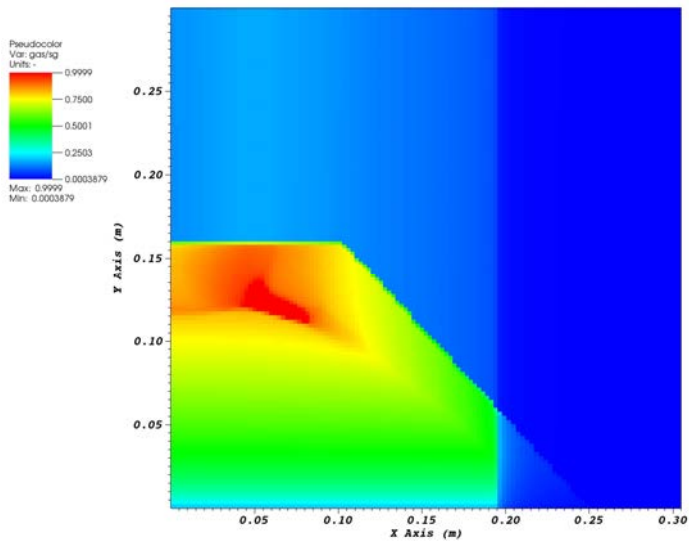


Figure 4. Void fraction distribution in dryout conditions (quasi-steady state), 38 kW power, calculated for a partially heated bed with the modified Tung & Dhir model.

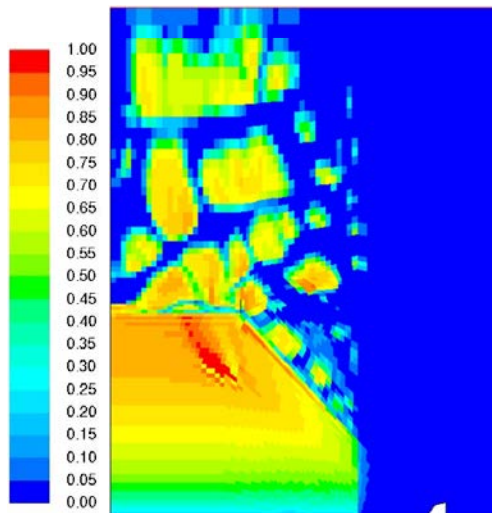


Figure 5. Instantaneous void fraction distribution for a partially heated bed in dryout conditions (quasi-steady state), 42 kW power, computed with Fluent using the 2nd order discretization and 1 ms time step and applying the Reed model.

Summary and conclusions

The research combines an experimental programme of thermal hydraulic experiments investigating core debris coolability to analytical work and modelling of the coolability problem by using 2D and 3D two-phase flow simulation codes. The main objective was to examine the effect of the debris bed shape on coolability and to produce data for simulation code validation.

Dryout power has been measured for six debris bed geometries with the COOLOCE facility: conical, cylindrical with top flooding, cylindrical with lateral flooding, cylindrical with an agglomerate simulant, conical on a cylindrical base and truncated cone. The geometries which allow multi-dimensional flooding generally have greater dryout power compared to geometries in which the water infiltration into the debris bed is limited by closed walls. On the other hand, it is emphasised that the coolability is strongly dependent on the height of the debris bed and, according to the experiments and the simulations, the effect of the bed height is often greater than the effect of the flooding mode.

All the experiments have been modelled with the MEWA code which solves heat transfer and fluid flow in the debris bed based on well-known porous media models. For most geometries, the agreement between simulations and experimental results ranges from very good to reasonable. In general, the simulation models yield better results if the role of lateral flooding is not very strong. In addition to MEWA, a full CFD model has also been applied. This has improved the general understanding of the flow phenomena in the debris bed-pool system and, thus, the formation of dryout in a manner that would be difficult to achieve only by comparisons of dryout power.

References

- Bürger, M., Buck, M., Schmidt, W., Widmann, W. Validation and application of the WABE code: Investigations of constitutive laws and 2D effects on debris coolability. *Nuclear Engineering and Design* 236 (2006), p. 2164-2188.
- Chikhi, N., Coindreau, O., Li, L.X., Ma, W.M., Taivassalo, V., Takasuo, E., Leininger, S., Kulenovic, R., Laurien, E. 2014. Evaluation of an Effective Diameter to Study Quenching and Dry-out of Complex Debris Bed. *Annals of Nuclear Energy*, Volume 74 (2014), p. 24-41.
- Ergun, S. 1952. Fluid flow through packed columns. *Chemical Engineering Progress* 48, 89-94.
- Takasuo, E., Holmström, S., Kinnunen, T., Pankakoski, P.H., Hosio, E., Lindholm, I. 2010. The effect of lateral flooding on the coolability of irregular core debris beds. *Nuclear Engineering and Design* 250 (2010), p. 687-700.
- Takasuo, E., Holmström, S., Kinnunen, T., Pankakoski, P.H. 2012a. The COOLOCE experiments investigating the dryout power in debris beds of heap-like and

cylindrical geometries. Nuclear Engineering and Design 250 (2012), p. 687-700.

Takasuo, E., Hovi, V., Ilvonen, M., Holmström, S. 2012b. Modeling of Dryout in Core Debris Beds of Conical and Cylindrical Geometries. Proceedings of the 20th International Conference on Nuclear Engineering, Anaheim, California, USA, July 30 – August 3, 2012. ICONE20-54159.

Takasuo, E., Hovi, V., Ilvonen, M. Applications and Development of the PORFLO 3D Code in Nuclear Power Plant Thermal Hydraulics. 2012c. 20th International Conference on Nuclear Engineering , Anaheim, California, USA, July 30 – August 3, 2012 (ICONE20-54161).

Takasuo, E., Taivassalo, V., Hovi, V. A study on the coolability of debris bed geometry variations using 2D and 3D models. Research Report VTT-R-00676-14. Espoo, 2014.66 p.

24. Chemistry of fission products (FISKES)

24.1 FISKES summary report

Kekki Tommi, Penttilä Karri, Nieminen Anna, Lavonen Tiina

VTT Technical Research Centre of Finland Ltd
P.O. Box 1000, FI-02044, VTT, Finland

Abstract

FISKES project investigated the chemistry of fission products inside a NPP containment after severe accident. Pool chemistry is very important part of behaviour of fission products in containment. ChemPool is a new program to be used with MELCOR to calculate the equilibrium composition and the pH values of the pools. It has been tested with BWR and PWR accident cases. Latest work has been done to make ChemPool compatible with ASTEC. The production of nitric acid during high dose rates was calculated which was also studied experimentally in this project. The iodine behaviour in the BWR containment with and without post-accident pH control was studied using ASTEC code. The project followed and participated in the work of international OECD/NEA BIP2 project. In addition, a lot of inactive chemicals are coming into water in structures and also some buffering chemicals are added into water during accident scenarios. The effects of these chemicals to pool chemistry was studied using literature study. Based on the information of literature review, laboratory experiments were done to investigate the formation of precipitations, colloids and gels in containment pool environment especially found in the Finnish LWRs. In the third goal was to calculate the transient 2D temperature profile for the Core Catcher with different decay heat values and then to calculate mass fraction of liquid in corium in concrete mixture at the solved temperature.

Introduction

In the event of a severe accident, some fission products could be released from the fuel and become in the reactor containment. Volatile iodine will be adsorbed at and desorbed from surfaces above the sump area. From a safety perspective, painted surfaces are among the most important especially for those plants with small sump volumes but with very large containment painted surface areas; their action on iodine behaviour is two-fold: they act as a sink for I_2 and as a source for volatile organic iodine. Radiation plays a strongly enhancing role, as it induces fast radiochemical reactions between iodine and the paints or paint components. The project followed and participated in the work of international OECD/NEA BIP2 project.

Nitric acid formation with irradiation has previously been studied in ORNL by Behm et al, (1992) NUREG/CR-5950. However, very little further studies have been performed although NUREG/CR-5950 formulas are applied in plant evaluation and pool pH estimation. The previous study by ORNL does not address HNO_3 production in all severe accident conditions. Consideration of additional HNO_3 formation contributes to estimation of pool pH and thus should be evaluated in connection with iodine source term.

Pool chemistry is very important part of behaviour of fission products in containment. A lot of inactive chemicals are coming into water in structures and also some buffering chemicals are added into water during accident scenarios. The effects of these chemicals to pool chemistry is important to estimate.

From the beginning of core melting up to the control of the accident by stopping and cooling the corium, the knowledge of corium physical properties versus temperature is essential to predict possible scenarios with a view to managing the accident. Viscosity plays a major role in many phenomena such as core melt down, discharge from reactor pressure vessel, interaction with structural materials and spreading in a core catcher.

This summary report introduces the main results of the FISKES project.

The formation of nitric acid inside a NPP containment after severe accident

In severe accident scenario the water vaporized by the melting core flows through compartments where it condenses again. Hydrochloric acid can be formed from organic materials containing chlorine. Cesium hydroxide and cesium iodine are formed from released fission products. Controlling the pH in the containment is important as in acidic conditions radioactive iodine could be formed and released into atmosphere. Injected buffer solutions can be used to keep the pH neutral or alkaline in the pools. Currently MELCOR code is not able to consider aqueous species and how they affect the pH in the pools. ChemPool is a new program to be used with MELCOR to calculate the equilibrium composition and the pH values of the pools. After MELCOR simulation the results from MELCOR are exported to external data-file containing the temperatures, the pressures and the compositions of the pools at

each time steps. The estimated formation rates of acids and dissolved salts from fission products are then coupled with these and the equilibrium compositions and the pH values of the pools are calculated with ChemPool. Internally ChemPool uses thermodynamic programming library, ChemApp®, for calculating the equilibrium composition of a thermodynamic system (gas, aqueous water and solids like fission products) by minimizing the Gibbs energy of the system. ChemPool is an easy to use tool for adding simulation of pH chemistry to a MELCOR simulation.

The formation of nitric acid is estimated inside a NPP containment after severe accident using Olkiluoto 1 and 2 BWR as an example plant. Firstly, the selected severe accident progression and some boundary conditions were calculated with the MELCOR 1.8.6 code. The investigated accident scenario was an extreme LOCA and station blackout. The big break was in the BWR main steam line. Accident sequence was followed until core debris melted a hole in the reactor cavity. Secondly, radioactivity and doses of the most significant radioisotopes in the containment gas phase and water pools were calculated using ORIGEN2 code. Finally, the nitric acid formation and the amount of HCl released were calculated and pHs of water pools were calculated using a new developed ChemPool program. ChemPool simulation was now extended to 28 days.

The total formation of HNO₃ in Wetwell was 24.315 kg and in Pedestal 9.704 kg after 2400000 s. Total formation of HNO₃ counting all compartments was 34.184 kg which is almost five times more than after 100800 s. Still in pedestal most of the acid came from the cables as HCl: 3222.6 moles of HCl compared to 542.5 moles of HNO₃. Due to this the pH dropped rapidly to 2.4 in Pedestal. In Wetwell the formation of nitric acid was small and the pH of Wetwell pool stayed alkaline due to CsOH. In the second simulation 600 kg of NaOH was added to Wetwell between 1200 s and 1500 s. This time the pH in Pedestal dropped from 10.6 to 9.6 at the time of HCl formation (14730 s). After that pH remained between 8.8 and 9.6. Figure 1. In these results only the formation of nitric acid in water phases was calculated using NUREG/CR-5950 formulas. This formation is very small and it is calculated that the dissolved nitrogen in water phase will be enough and do not limit this reaction.

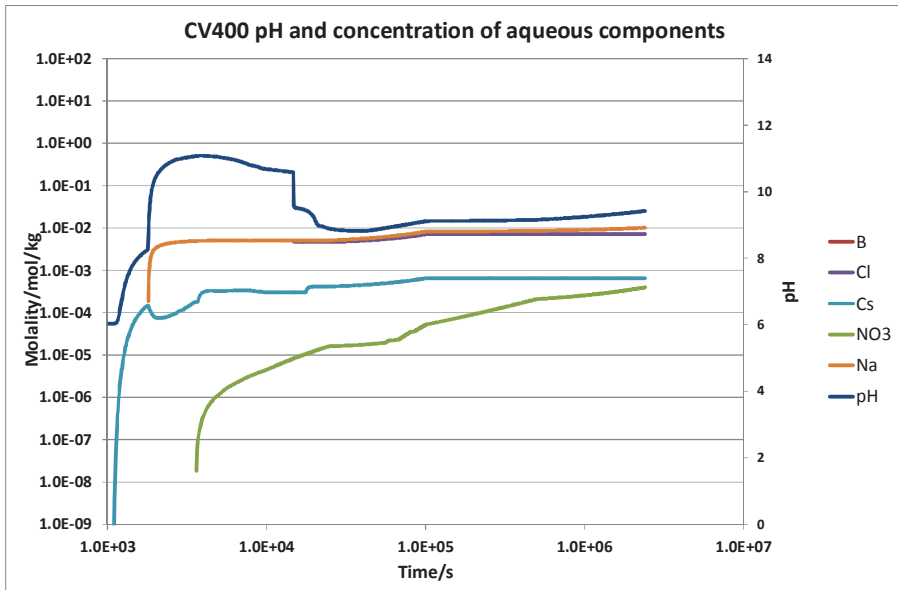


Figure 1. Chlorium (HCl), cesium (CsOH), nitrate (HNO₃), sodium (NaOH) and pH in Pedestal with addition of 600 kg NaOH to Wetwell.

To get more data of the nitric acid formation the experimental work has been done. Tests were performed with a small amount of distilled water and air irradiated in a closed vessel. The measurements have been carried out at VTT's aged gammacell that does not allow measurements at dose rates expected in containment during severe accidents. The first scoping measurements have been carried out also using Beta radiation (Kärkelä 2015). The chemical yield (G-value) for a species during the radiolysis of water may vary as a function of several factors in an irradiation system (Kekki 2015).

Latest work has been done to make ChemPool compatible with ASTEC. The idea is that ChemPool can be used with ASTEC in a similar way as with MELCOR. MELCOR input file structure (MELGEN file) is very different from ASTEC structure, but it contains same definitions for the containment specific parameters that ChemPool needs. ASTEC input file is hierarchical: it is divided into structures and substructures (structures inside structures) each containing definitions for a specific part of the containment (ZONE, WALL, CONNECTION, MATERIAL) or for a specific chemical component existing inside the containment (COMPONENT, AEROSOL). ASTEC structures are equivalent to MELCOR packages (CVH - control volume hydrodynamics, FL - flow paths, ...). ASTEC is also able store the values of selected variables to set of files during its simulation like MELCOR. These values like atmospheric pressures, water temperatures and masses in containment's pools and flow rate of water between the pools are then used by ChemPool during its own pH simulations. ChemPool does not calculate the hydrodynamics of the pools but relies on calcula-

tions done by the selected severe accident analysis program. ChemPool itself contains additional definitions for the chemicals affecting the pH like hydrochloric acid, nitric acid and variety of buffers.

ChemPool's own input file (CHEMPOOL.DAT) contains now new a parameter that tells which SA analysis program (ASTEC or MELCOR (default)) is to be used. Then ChemPool opens either ASTEC or MELCOR input file and reads control volume/zone, flow path (connections) and other needed parameters to initialize the containment geometry and flow network. Then at each time step, it reads the values of variables (like atmospheric pressures, temperatures and water masses of the pools) from the result files generated by the selected SA analysis program and updates the masses of the additional chemicals in the pools and calculates their pH values.

Code for reading ASTEC input files has been implemented but ChemPool has not yet been tested with results (files) generated by ASTEC (Penttilä 2015).

Analysing iodine behaviour in the containment with ASTEC

The objective of the study was to analyse iodine behaviour in the Nordic BWR containment in a previously defined accident scenario with and without post-accident pH control. The chosen tool for the analyses was ASTEC since it is known to have better models for iodine chemistry than for example MELCOR. With current ASTEC version V2.0R3p2 it is not possible to model accurately a BWR core. As a result it was decided to only model the containment and to use previous MELCOR results as boundary conditions.

The notably small difference in airborne masses as well as in deposited aerosol masses was not expected. However, since the rupture venting line opened relatively early in the analysed accident scenario, the airborne masses were actually just the masses of the products passing by the containment and then it is reasonable that the differences remained small. It is assumed, that in an accident scenario in which the rupture venting line would not open, more clear interaction between the aqueous and gaseous phase would be resulted as well as steady-state concentrations for gaseous species.

In the liquid phase obvious difference in the iodine behaviour was observed when the NaOH was added to the wetwell pool. When the pH reached 7, there was no more conversion of non-volatile iodine species to I_2 as illustrated in Figure 2. Whereas the behaviour of organic iodide was not dependent on the pool pH in the liquid phase as seen from Figure 3.

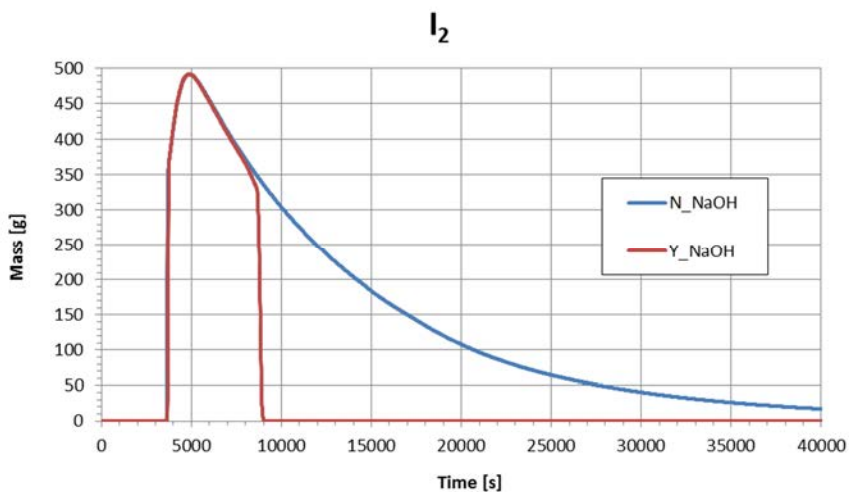


Figure 2. The mass of I_2 in liquid phase without pH control (N_NaOH) and when NaOH is added to the wetwell pool (Y_NaOH).

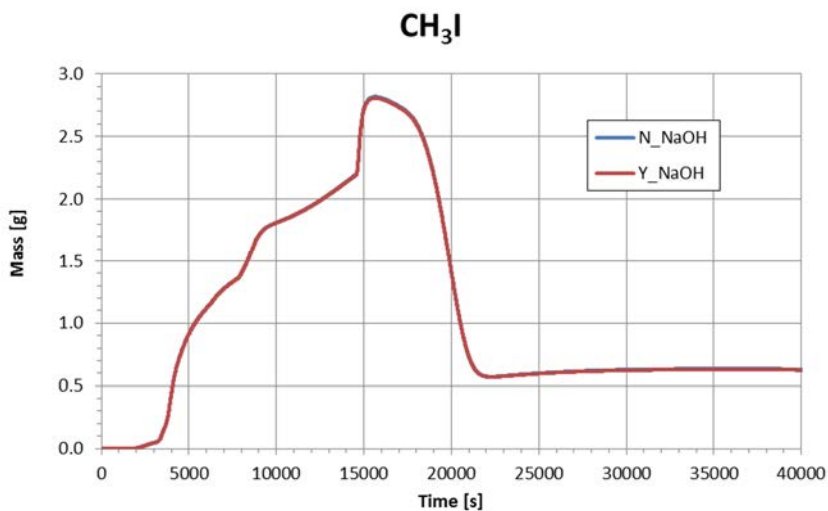


Figure 3. The mass of CH_3I in liquid phase without pH control (N_NaOH) and when NaOH is added to the wetwell pool (Y_NaOH).

According to the results can be concluded that there is a clear difference for iodine behaviour in the aqueous phase when the pool pH is above and below 7 excluding organic iodides. Even though this is just a result of single computational analysis, it must be noted, that the models in ASTEC are continuously updated to

achieve the state-of-the-art level in dealing with the different phenomena related especially to fission product behaviour under severe accident conditions (Nieminen 2015).

Chemical effects in the sump water pool during post-LOCA conditions

Pool chemistry is very important part of behaviour of fission products in containment. A lot of inactive chemicals are coming into water from containment structures and also some buffering chemicals are added into water during accident scenarios. The goal of this work was to investigate the chemical effects, which take place in the containment pool environment, so that chemical effect information can be utilised in the ChemPool modelling.

Based on the information found from literature the most important features that effect on the precipitation during post-LOCA conditions are pH of the solution, insulation materials, pH buffer and corrosion of metal alloys, such as Al and Zn. Also temperature evolution during LOCA may have some effects on the chemical effects. Chemical effects that may occur during post-LOCA environment depend highly on plant specific conditions and therefore the evaluation of chemical effects must be done for each plant design and conditions separately. In the case of Finnish PWR, in addition to all previously described phenomena also the use of KOH in the sump water should also be considered. Reference for such studies with KOH as an additive in sump water cannot be found due to the fact that it is not used as an additive in PWR's very often, at least not in countries where information could be found easily (Lavonen 2014).

Based on the information of this literature review, laboratory experiments were done to investigate the formation of precipitations, colloids and gels in containment pool environment especially found in the Finnish LWRs. Simple approach was selected for the tests and test setup is presented in Figure 4.



Figure 4. Test setup of the chemical effect tests.

Four parallel tests were conducted in order to simulate the conditions in different times of the loading period of the reactor. First three steps of the experiment include normal chemicals added to the primary cooling water during the normal use of PWR, in the case of Loss-of-coolant accident and the emergency cooling and ice condenser, which activate for example after LOCA. Steps four and five were conducted to simulate the chemical effects of the containment building materials. Most problematic elements when considering precipitation are Al, Si and Ca. Therefore, these elements were selected for the chemical effect tests to simulate the effects of the materials of the containment building. Results confirmed that without drastic pH shift during the emergency cooling, visible precipitation will not form when KOH is used as pH buffer. However, if large amounts of coolant are lost due to evaporation and compounds become significantly concentrated precipitation effects could occur (Lavonen 2015).

Transient 2D heat conduction model for the Core Catcher

A core melt accident could occur if all emergency measures fail to transfer the decay heat power out of the fuel after reactor shutdown. Such a situation could only be developed if the initiating event, for example a large leak of cooling water or a total loss of electricity, is combined with a major loss of plant safety systems. In the EPR, core melt accident mitigation strategy is based on spreading of the melt over a large area in a so-called core catcher, which is a lateral spreading compartment, separated from the reactor pit by a melt discharge channel. Its target is to increase the surface area of the melt, which makes cooling more effective.

In earlier SAFIR project a simple steady state heat conduction model was implemented to solve temperatures in a 2D cross-sectional area of the core catcher (Penttilä 2013). The goal of this study was to make a transient 2D heat conduction model for the Core Catcher and to calculate its temperatures and liquid mass fractions as function of time.

Four cases were calculated and compared against each other in order to do sensitivity analysis for model parameters like convection coefficient between pool and the cooling water and the thermal conductivities of the materials in the pool.

Case 1 used low convection heat transfer coefficient (1000 W/m²·K) and normal thermal conductivities (5 W/m·K, 20 W/m·K, 1 W/m·K) for the materials (oxidic, metallic and concrete layers) in the spreading pool. The metallic layer was placed on top of the oxidic layer.

Case 2 used medium (10000 W/m²·K) convection heat transfer coefficient but the cooling was not much more efficient as the resistance to conduction within the spreading pool is higher than the resistance to convection across the cooling water boundary layer ($Bi \gg 1$).

Case 3 used the oxidic layer on top of the metallic layer. The oxidic layer behaved more or less the same way as in case 1 but the metallic layer cooled clearly slower.

Case 4 used low thermal conductivities (2.5 W/m·K, 10 W/m·K, 0.5 W/m·K) for the materials (oxidic, metallic and concrete layers) in the spreading pool. This time the oxidic layer cooled clearly slower than in case 1.

All other cases solidified completely by ~30000 s except case 4 where the oxidic phase solidified completely by ~155500 s (Penttilä 2014).

Acknowledgements

The project group acknowledges the representatives of the Reference Group 5 who have contributed to the successful accomplishment of FISKES project by providing case studies, giving comments and reviewing reports.

References

- Beahm e. V., et al., 1992, Iodine Evolution and pH control. NUREG/CR-5950, Oak Ridge National Laboratory. 1992
- Kekki, T., Lipponen, M., 2015, The formation of nitric acid under radiation field. VTT Research Report, VTT-R-00598-15. Espoo, 2015
- Kärkelä, T., Gouëlo, M., Kekki, T., Kotiluoto, P., Auvinen, A., 2015, Formation of HNO₃, O₃ and IO_x particles by beta radiation. VTT Research Report, VTT-R-00641-15. Espoo, 2015.

- Lavonen T., 2014, Chemical effects in the sump water pool during post-LOCA conditions – literature review. VTT Research Report, VTT-R-01126-14. Espoo, 2014.
- Lavonen T., 2015, Chemical effects in the sump water pool during post-LOCA conditions – laboratory experiments. VTT Research Report, VTT-R-00114-15. Espoo, 2015.
- Nieminen, A., 2015, The effect of post-accident pH control to iodine behaviour in the containment. VTT Research Report, VTT-R-06022-14. Espoo, 2015
- Penttilä, K., Könönen, N., Rossi, J., 2014, The formation of nitric acid inside a PWR containment after severe accident Ver. 2. VTT Research Report, VTT-R-01072-14. Espoo, 2014.
- Penttilä, K., Könönen, N., Rossi, J., 2014, The formation of nitric acid inside a BWR containment after severe accident Ver. 2. VTT Research Report, VTT-R-01071-14. Espoo, 2014.
- Penttilä, K., 2013, Molten corium concrete interactions – Core Catcher transient 2D model. VTT Research Report, VTT-R-01817-13. Espoo, 2013.
- Penttilä, K., 2014, Molten corium concrete interactions – Transient Core Catcher 2D model. VTT Research Report, VTT-R-01172-14. Espoo, 2014.
- Penttilä, K., 2015, Using ChemPool with MELCOR and ASTEC. VTT Research Report, VTT-R-00561-15. Espoo, 2015.

25. Thermal hydraulics of severe accidents (TERMOSAN)

25.1 TERMOSAN summary report

Tuomo Sevón, Anna Nieminen, Veikko Taivassalo, Karri Penttilä

VTT Technical Research Centre of Finland Ltd
P.O. Box 1000, FI-02044 Espoo

Abstract

The objective of the TERMOSAN project was to improve modeling capabilities on severe accident thermal hydraulics. MELCOR is Finland's main severe accident analysis tool, and its license fee was paid by this project. Passive containment cooling system experiments, made by Lappeenranta University of Technology, were calculated with ASTEC and MELCOR codes. The international OECD THAI-2 research program was participated in the frame of this project. In the THAI-2 program, hydrogen combustion experiments during spray operation were calculated with Fluent. In-vessel melt retention in VVER-440 reactor was investigated with ChemSheet and ASTEC codes. The Fukushima accident was calculated with MELCOR.

Introduction

The target of severe accident management is to keep the containment intact and to reduce the amount of radioactive materials released to the environment. The thermal-hydraulic phenomena in severe accidents are very complex due to the high temperatures and exotic materials that are involved. Modeling them requires experimental research and development of computational models. In addition to research on the phenomena, it is essential to maintain and improve the competence to perform simulations with severe accident analysis computer codes.

MELCOR Code License

MELCOR is an integral severe accident analysis code, developed by Sandia National Laboratories. In the frame of the TERMOSAN project, Finland participates in U.S.NRC CSARP (Co-operative Severe Accident Research Program) and pays its participation fee. The TERMOSAN project provides license for latest versions of MELCOR and the right to participate in the annual CSARP/MCAP meeting for all Finnish nuclear energy organizations.

Modeling of Passive Containment Cooling Systems

Lappeenranta University of Technology has started a new experimental program on passive containment cooling systems. The tests concentrate on horizontal-tube condensers, similar to those used in the ABWR design, and investigate also aerosol deposition in the condensers and the effect of deposited aerosols on the heat transfer. Condensation in a horizontal tube is difficult to model because cylindrical symmetry is lost and the condensate film becomes thicker at the bottom than at the top of the tube.

The experiments were made in the PCCS project, and the experiments were calculated with the ASTEC and MELCOR codes in the TERMOSAN project. The target is to develop modeling practices that can be used in safety analyses of reactors equipped with horizontal-tube PCCS and to gain a better understanding of the accuracy of PCCS models that can be achieved with the integral severe accident codes.

The MELCOR work was started by calculating very simple Purdue University experiments (Wu 2005) on steady-state condensation in a straight horizontal tube. With MELCOR's default heat transfer parameters, 28 % average underestimation was the best result that could be achieved using optimized nodalization. When the condensate film Reynolds number limits were changed to values commonly used in heat transfer literature, the results improved significantly, and average underestimation of 14 % was reached (figure 1). (Sevón 2014)

In the more complicated experiments at Lappeenranta University of Technology, steam was injected into a vessel that represents the drywell in a BWR containment. From there the steam flowed into three horizontal u-shaped tubes, immersed in a water pool. Part of the steam condensed, and the condensate flowed to drywell 2 vessel. Non-condensable gases and uncondensed steam flowed to the wetwell. The model development was started by calculating the PCC-06 experiment (Vihavainen et al. 2014) in the Lappeenranta facility with MELCOR (Sevón 2014) and ASTEC (Nieminen 2015). MELCOR nodalization of the test facility is shown in figure 2. The condenser tubes were modeled as six parts.

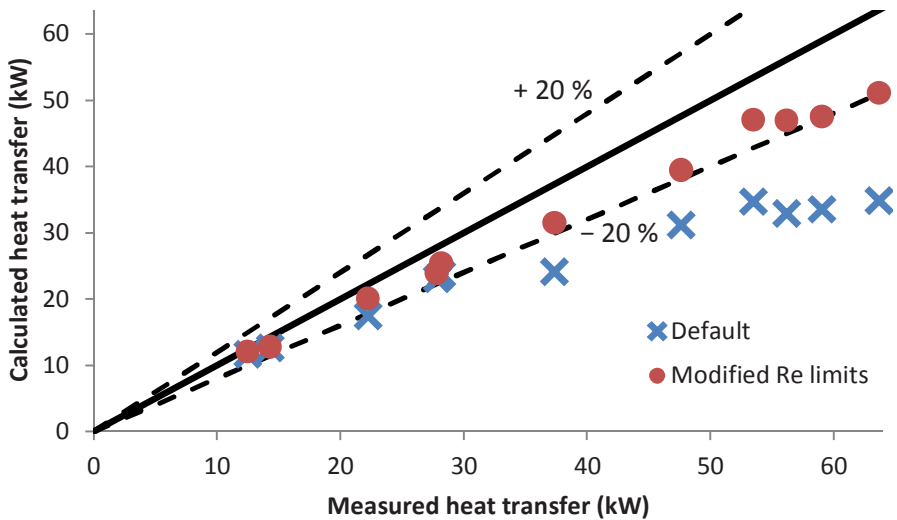


Figure 1. Purdue University condensation experiments calculated with MELCOR (Sevón 2014).

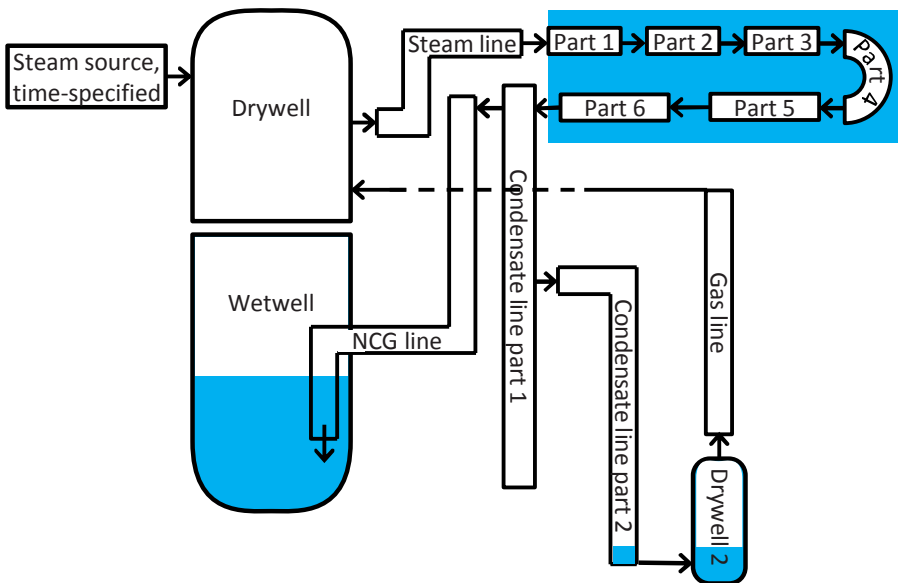


Figure 2. Nodalization of Lappeenranta University of Technology PCCS test facility, used in MELCOR model.

Both MELCOR and ASTEC significantly underestimated condensation in the PCC-06 experiment. MELCOR with default heat transfer parameters underestimated the integral condensation by 52 %. With the modified condensate film Reynolds number limits the MELCOR results improved, but the condensation was still under-

estimated by 42 %. This result is much poorer than in the simple Purdue University experiments. The reason could be the U-shape of the tubes or the larger flow rates used in the PCC-06 test. ASTEC underestimated the integral condensation by over 50 %.

Calculated pressure in the PCC-06 experiment is compared with the measurement in figure 3. Both codes overestimate the pressure in the beginning. After 600 s the ASTEC result is below the measurement, while MELCOR overestimates the pressure for the whole test duration. Reason for the poor results with both codes is unknown. LUT has made several experiments in the same facility. The work should be continued by calculating other experiments in different conditions in order to find out if the poor calculation results are specific to PCC-06 test conditions.

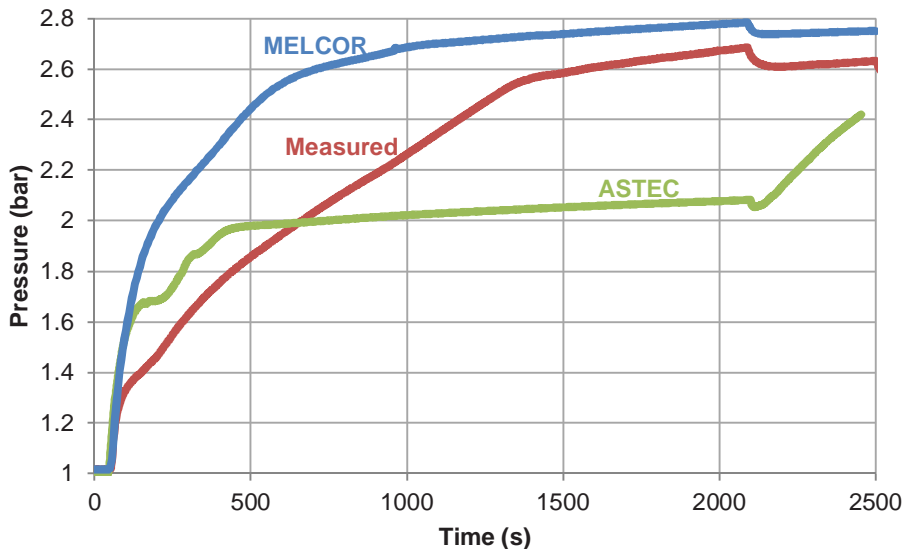


Figure 3. Drywell pressure in PCC-06 experiment. Comparison of measurement and MELCOR and ASTEC calculations.

Behavior of Hydrogen and Iodine: OECD THAI-2

THAI-2 was an international experimental research program for investigating iodine issues and hydrogen behavior. The program was coordinated by OECD NEA, and it was finished in 2014. Finland participated the program in the frame of the TERMOSAN project. Two experiments were made on interaction between gaseous iodine and aerosol particles and one experiment on gaseous iodine release from a flashing jet. Ten experiments were made on the behavior of hydrogen recombiners, and they concentrated on the effect of low oxygen concentration. Two types of recombiners were used: AREVA and NIS. Six experiments were made on the effect of containment spray operation on hydrogen deflagration.

The deflagration experiments during spray operation were calculated with Fluent in the TERMOSAN project (Taivassalo 2014). For comparison, experiments in the same facility under the same conditions but without spray were calculated with the same model. Figure 4 shows the calculated flame propagation in one of the experiments. It is seen that the spray in the center of the vessel slows down the flame propagation.

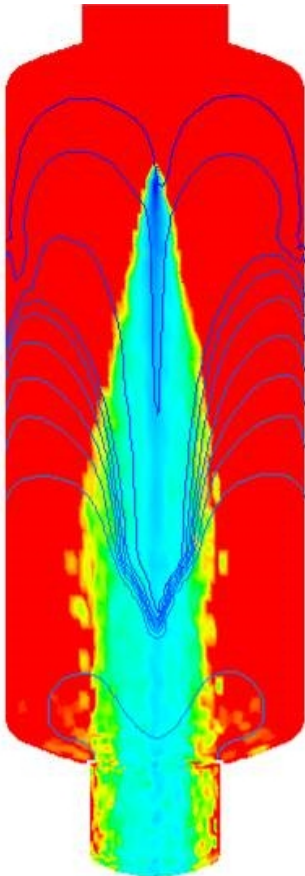


Figure 4. Influence of the spray on the flame propagation in the CFD-based modelling of the THAI-2 HD-31 test. Colored contours represent the water droplet concentration and blue isolines flame propagation.

In-Vessel Melt Retention

Severe accident management strategy of the Loviisa plant is based on retention of the molten corium in the reactor pressure vessel by external cooling of the vessel wall. The heat flux through the wall depends on the layering configuration of the melt. In the TERMOSAN project methods were developed for modeling a three-layer

melt pool, where an oxide layer is sandwiched between heavy and light metal layers. This configuration has the potential to cause a very thin upper metallic layer and large heat flux to the vessel wall due to the focusing effect. Chemical equilibrium of the melt pool was calculated with the ChemSheet code (Penttilä 2013). These results were used as a starting point for ASTEC calculations (figure 5). The heat flux to the water did not exceed the critical heat flux in the calculated case (Nieminen 2014).

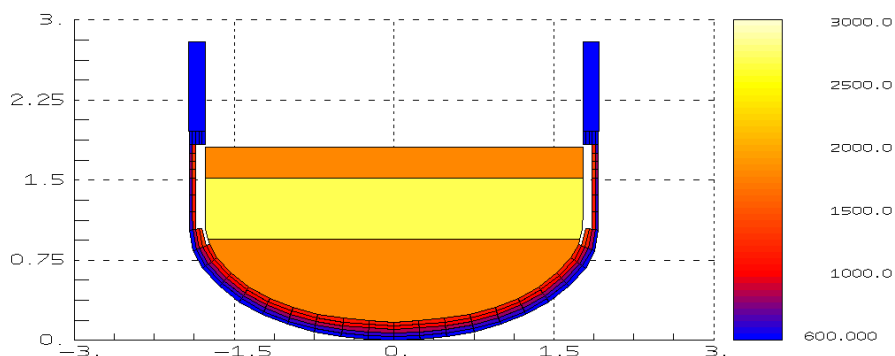


Figure 5. Temperature profile in VVER-440 reactor lower head during in-vessel melt retention, calculated with ASTEC (Nieminen 2014).

Fukushima Accident Analysis

MELCOR models of accidents at Fukushima units 1, 2, and 3 were developed. The results are presented in a special article in this report.

Conclusions

The TERMOSAN project has improved Finnish expertise in modeling of severe accidents. An important part of the project is paying Finland's annual MELCOR license fee and providing the code license for VTT, STUK, power companies, and universities.

Development of modeling techniques for a horizontal passive containment cooling system, similar to the ABWR design, was started. Good results were obtained for simple steady-state experiments with a straight condenser tube, but first attempts to calculate more complicated time-dependent experiments with u-shaped tubes gave poor results. More work is needed before the passive system can be reliably modeled in accident analyses.

Experiments on iodine issues and hydrogen behavior were performed in the international OECD THAI-2 research program, and CFD-based modeling techniques were developed for calculating the effect of containment spray on hydrogen deflagrations.

Success of the in-vessel melt retention strategy in Loviisa may depend on the layering configuration of the melt in the reactor lower plenum and its effect on the heat transfer. Chemical equilibrium in the melt pool was calculated in the TERMOSAN project, and Fortum has used the results in a Master's Thesis (Laato 2013). One of the first applications of the ASTEC code in Finland was modeling of a three-layer melt pool in the VVER-440 reactor lower head.

MELCOR models of the Fukushima unit 1, 2, and 3 accidents were developed in the TERMOSAN project, starting from scratch. Important insights to the progression of the Fukushima accident and the phenomena that took place have been obtained, and the modeling expertise will be utilized in Finnish reactor license reviews.

References

- Laato, T. 2013. Stratification and heat transfer of molten corium pool at Loviisa nuclear power plant. Master's thesis, Aalto University School of Science.
- Nieminen, A. 2014. ASTEC application to VVER-440 in-vessel retention. Research report VTT-R-01112-14.
- Nieminen, A. 2015. Modelling of PCC-06 experiment with ASTEC: version 2. Research report VTT-R-00283-15.
- Penttilä, K. 2013. ChemSheet calculations for in-vessel melt retention modeling. Research report VTT-R-02739-13.
- Sevón, T. 2014. Modeling of horizontal passive containment cooling system with MELCOR. Research report VTT-R-05175-14.
- Taivassalo, V. 2014. CFD modelling of hydrogen combustion during spray operation – applicability of the $k\epsilon$ model in OECD THAI-2 test HD-30. Research report VTT-R-00915-14.
- Vihavainen, J., Laine, J., Purhonen, H., Partanen, H., Räsänen, A., Puustinen, M. & Telkkä, J. 2014. Passive Containment Cooling System (PCCS) experiments. Lappeenranta University of Technology. (PCCS 2/2013.)
- Wu, T. 2005. Horizontal in-tube condensation in the presence of a noncondensable gas. Ph.D. thesis, Purdue University.

25.2 Fukushima Accident Analysis

Tuomo Sevón

VTT Technical Research Centre of Finland
P.O. Box 1000, FI-02044 Espoo

Abstract

Models of the accidents at Fukushima units 1, 2, and 3 have been developed with the MELCOR code in the TERMOSAN project. Measured pressures in the reactors and containments could be reproduced quite well. This required some assumptions about leaks starting after all electric power had been lost and tuning of models for turbine-driven cooling systems. According to the calculations, at units 1 and 3 molten fuel has probably been discharged to the containment from broken reactor pressure vessel, while at unit 2 all the fuel is probably still inside the reactor. The radioactive release to the environment was the largest from unit 3, according to these calculations, because the containment venting was made soon after core damage started, when there were a lot of cesium particles in the air, and the venting system was not equipped with filters. Calculated timing of the release corresponds quite well to timing of measured peaks of radiation dose at the plant area.

Introduction

A severe accident occurred at Fukushima Daiichi nuclear power plant Units 1, 2, and 3 in 2011. The events started with an earthquake at 14:46 Japanese time on March 11. The fission reactions were automatically stopped by inserting the control rods. Connection to the electricity grid was lost because power lines collapsed in the earthquake, but power was supplied by emergency diesel generators, and safety systems were working as designed.

About 50 min later a tsunami inundated the site. The emergency diesel generators and much of the emergency power distribution systems were located in the basement of the turbine building, in a room that was not water-tight. Therefore the electricity systems were submerged by the tsunami. This caused a total loss of AC power for all the three units and, in addition, loss of DC power at units 1 and 2.

The accidents at all three units have been calculated with MELCOR 2.1 in the TERMOSAN project. The objectives of the work are: 1) improving expertise in severe accident modeling, using data from a real, full-scale reactor accident; 2) gaining a better understanding of the events in the Fukushima reactors; 3) getting insights into the capabilities and weaknesses of the MELCOR code in simulating severe accidents.

Information for developing the calculation models were collected from publicly available documents. The most important data source was the Fukushima information portal (<https://fdada.info/>) and the links to the investigation reports

provided there. Much plant data was found in TEPCO publications. Missing pieces of plant data were taken mainly from the Peach Bottom plant in the United States (GE 1978). While similar to the Fukushima plant, Peach Bottom is larger: its electric power is 1112 MW, compared with 460 MW at Fukushima unit 1 and 784 MW at units 2 and 3. Therefore the Peach Bottom data could not be used directly, but it required some scaling, which inevitably increases uncertainties.

Unit 1

Unit 1 core melted before units 2 and 3. From the earthquake until the tsunami, the reactor was cooled by a passive Isolation Condenser (IC) system. IC was temporarily stopped at the time of the station blackout, and it was not possible to restart it without DC power. Thus, the reactor lost all of its cooling only 48 min after the earthquake. The MELCOR calculation (Sevón 2015a) was started at this time. It was not necessary to model the IC system because the interesting part of the accident begins after the loss of cooling and the conditions at this time were measured, so that they can be used as initial conditions in the calculation.

Water level in the reactor is presented in figure 1. The core started to uncover at 2 h 42 min after the earthquake, and all water in the RPV has evaporated at 8 h 39 min.

Pressure in the containment drywell is presented in figure 2. It is necessary to assume some leak from the reactor coolant system to the containment drywell – otherwise the containment pressure would be underestimated. In this calculation it was assumed that the recirculation pump seal starts leaking at 5 h, but it is possible that the leak was in some other location.

The measured pressure peak at 12 h is not reproduced by the calculation. Probably the RPV failed at 12 h, while in the calculation it fails at 14 h 6 min. At 24 h the pressure decreased because the operators performed wetwell venting. Starting and stopping of the water injection to the reactor with the fire engine has a large effect on the calculated pressure but has no effect on the measured pressure. At 50 h the measured pressure started decreasing unexpectedly, and increase of containment leak area was assumed at this time.

A hydrogen explosion occurred in the reactor building at 24 h 50 min. The calculated hydrogen concentration at this time was very high, 21 %.

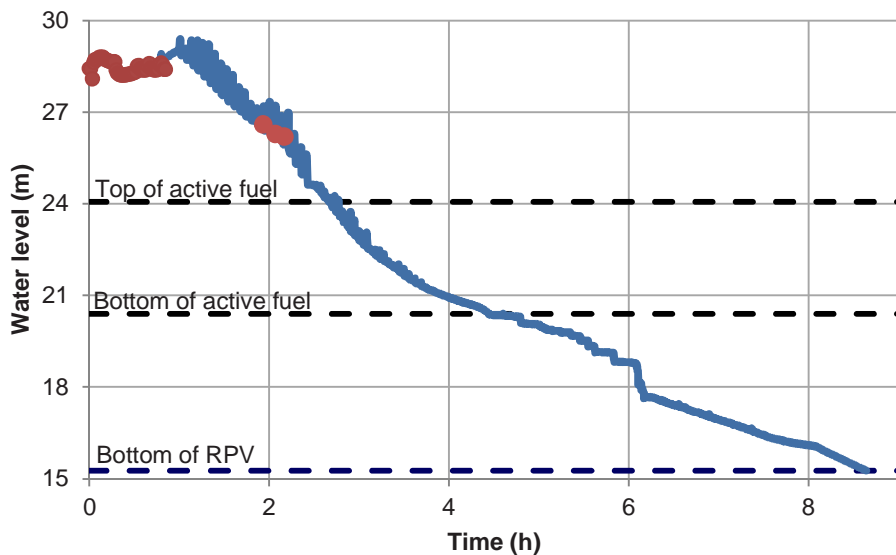


Figure 1. Water level in unit 1 reactor. Red circles are measurement data, and blue line is the calculation result.

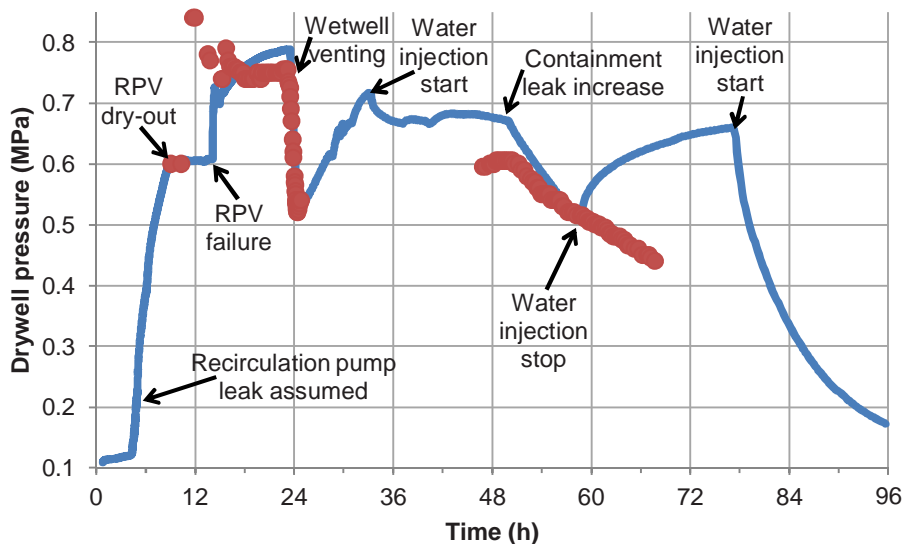


Figure 2. Pressure in unit 1 containment. Red circles are measurement data, and blue line is the calculation result.

Unit 2

Unit 2 survived the longest time of the three reactors before its core melted. The RCIC (Reactor Core Isolation Cooling) system provided cooling for the reactor for as

long as 66 h, even though the operators were not able to control system in the absence of DC power. The RCIC turbine is driven by steam coming from the steam line. The exhaust steam is discharged to the wetwell. The turbine drives a pump that delivers water to the reactor.

Water level in the reactor, calculated with MELCOR (Sevón 2013), is presented in figure 3. The core started to uncover at 74 h 44 min after the earthquake. Seawater injection with fire engines started at 77 h 8 min, but the injection rate was small because pressure in the reactor was high, and it took 17 h to reflood the core. The water injection rate is not accurately known, so this result is uncertain. It is estimated that the RPV did not fail at unit 2, and all the fuel is still inside the reactor, but about 13 % of it has relocated from the core to the bottom of the RPV.

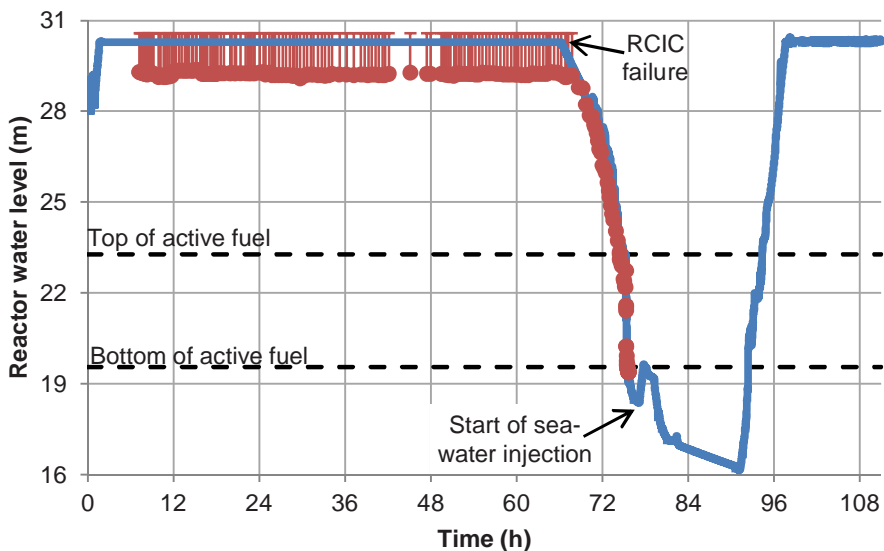


Figure 3. Water level in unit 2 reactor. Red circles are measurement data (with error bars because measurement range was exceeded), and blue line is the calculation result.

Pressure in the containment drywell is presented in figure 4. The pressure increased slower than expected. This could be caused by leakage from the containment, but then the pressure increase after 80 h would be difficult to explain. The slow increase of containment pressure was probably caused by flooding of the reactor building basement by water from the tsunami. The water cooled the outer surface of the containment wetwell, which is made of steel, and removed heat from the containment. This is supported by worker reports that they observed water flooding the lowest floor of the reactor building during the accident. In the model the flooding rate was adjusted so that the measured containment pressure is reproduced.

The operators attempted opening the containment venting valves, but it was not successful at unit 2. After 90 h the containment pressure decreased. This was probably caused by a major leak from the containment.

Unit 2 was the only one of the three units that did not suffer a hydrogen explosion in the reactor building. The calculated hydrogen concentration in the reactor building exceeded the flammability limit, but the steam concentration was much above 55 %, and this prevents combustion. Most of the steam in the reactor building originated from boiling seawater in the flooded basement of the building. A blowout panel in the reactor building wall opened during the accident, but it was probably not important in preventing the explosion.

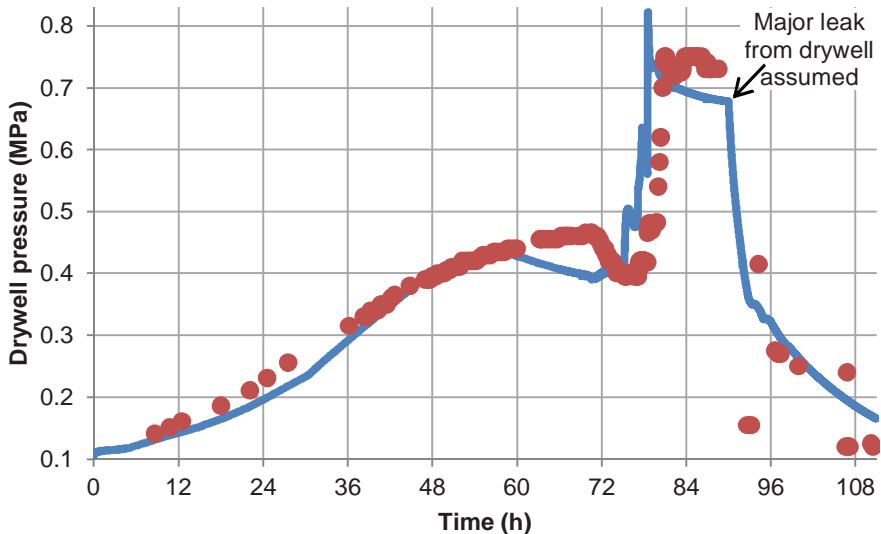


Figure 4. Pressure in unit 2 containment. Red circles are measurement data, and blue line is the calculation result.

Unit 3

DC power from batteries was available at unit 3 but not at units 1 and 2. As a result, the unit 3 operators were able to control the valves of the RCIC and HPCI (High Pressure Coolant Injection) systems and monitor the pressure and water level in the reactor. HPCI system is similar to RCIC (see discussion at Unit 2 section), but its capacity is larger. The reactor was cooled by the RCIC system until 20 h 50 min. Then the HPCI system was started, and it operated until 35 h 56 min, even though its water injection rate was probably insufficient at the end of this period, due to the low pressure in the reactor.

Water level in the reactor, calculated with MELCOR (Sevón 2015b), is presented in figure 5. Core uncover started at 36 h 9 min after the earthquake. Water injection with fire engines started at 42 h 39 min, and it took 8 h to reflood the core. The water injection rate is not accurately known, so this result is uncertain. The RPV lower head is calculated to fail at 53 h 16 min because the debris in the lower head was not in a coolable configuration and the temperature continued increasing despite the water injection. This result is highly uncertain, and even small changes to the model

could cause the RPV not to fail in the calculation. TEPCO has not been able to verify whether the RPV has actually failed or not. At the end of the calculation, 30 % of the fuel was still inside the reactor and 70 % had been discharged to the containment.

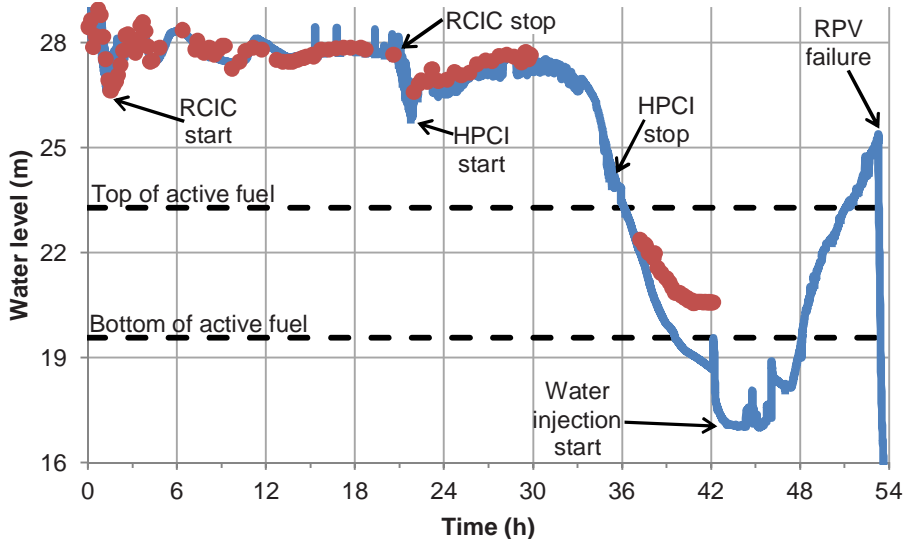


Figure 5. Water level in unit 3 reactor. Red circles are measurement data, and blue line is the calculation result.

Pressure in the reactor is presented in figure 6. The good match between the calculation and measurement during the first 36 h is the result of manual adjustment of the RCIC and HPCI flow rates so that the measured pressure is reproduced. At 42 h 9 min the reactor pressure dropped, even though the operators had not opened a safety relief valve. It was assumed that the steam line failed at this time.

Pressure in the containment is presented in figure 7. The pressure increase accelerated after 6 h. In the model it was assumed that the recirculation pump seal started leaking to the containment drywell at this time. For comparison, the figure shows the pressure without the leakage with the green line. With this assumption the containment pressure would be significantly underestimated.

The wetwell spray was started at 21 h 20 min using a diesel-driven fire pump. This reduced the containment pressure. The calculation overestimates the pressure during this period. It can be caused by uncertainties in the spray model or by a very simplified wetwell stratification model that was used. After 42 h the wetwell venting valve was opened and closed several times, and this is seen as periods of increasing and decreasing pressure.

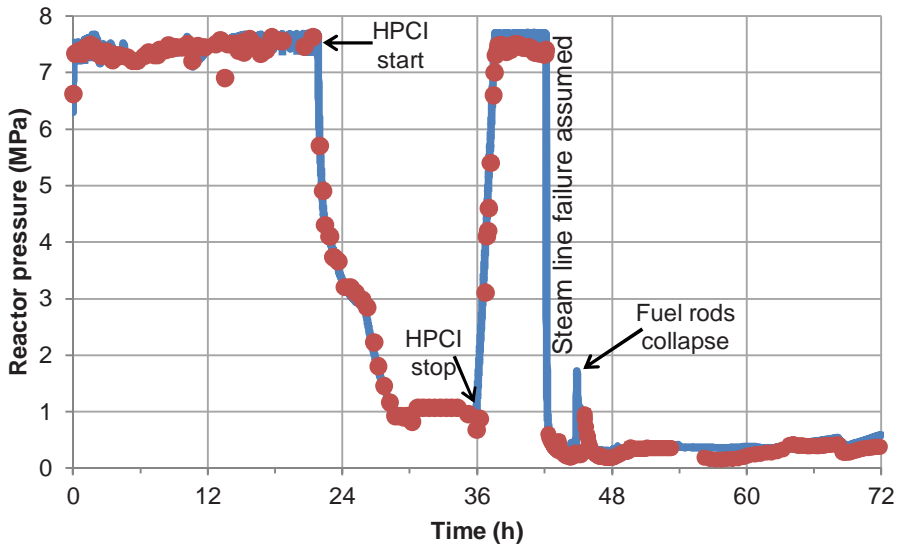


Figure 6. Pressure in unit 3 reactor. Red circles are measurement data, and blue line is the calculation result.

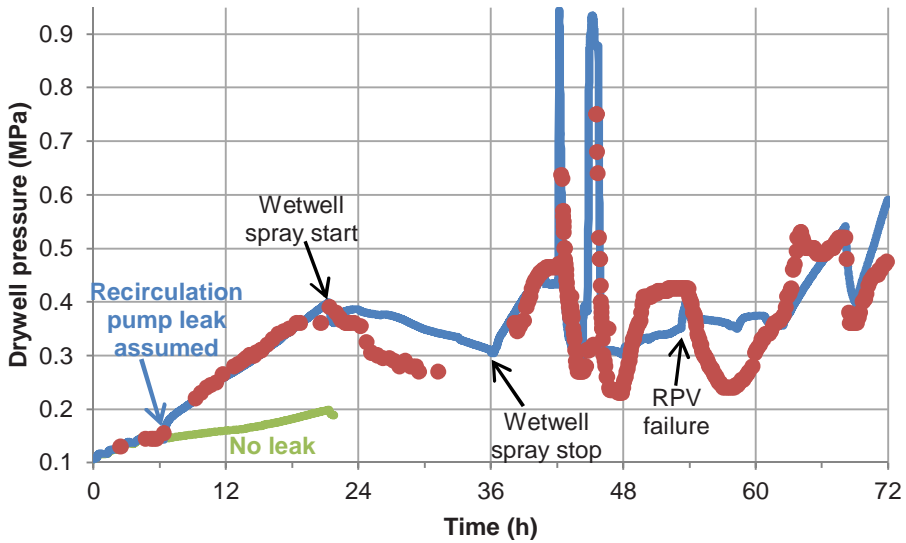


Figure 7. Pressure in unit 3 containment. Red circles are measurement data, and blue line is the calculation result. The green line shows the calculated pressure without a recirculation pump leak.

A hydrogen explosion occurred in the reactor building at 68 h 15 min. The calculated hydrogen concentration at this time was 4.4 %. This cannot cause an explosion, so the calculation underestimates the hydrogen concentration in the reactor

building. This can be caused by underestimation of hydrogen generation or underestimation of containment leakage, or there may have been leaks in the containment venting lines, or the hydrogen concentration may have been non-homogenous, while the MELCOR model calculates only the average concentration.

Radioactive releases

The noble gas inventory of all three reactors was almost completely released to the environment during the accident. Cesium is the most important element regarding long-term consequences. The calculated cesium release is 0.05 % of core inventory at unit 1, 0.08 % at unit 2, and 0.95 % at unit 3. The unit 3 release was the largest because the containment venting was made at an early phase, only 3 h after the start of core damage, when there was still a lot of cesium in the wetwell atmosphere. At unit 2 venting was attempted but did not succeed, and major leak from the drywell started 13 h after the start of core damage, when most of the cesium aerosols had already deposited. At unit 1 the time between the start of core damage and containment venting was almost 20 h. This long time for deposition caused the lowest cesium release of all three units. The explosions in the reactor buildings did not cause large radioactive releases to the atmosphere. There are still large uncertainties in the calculated releases, and they will be updated when more information about the accident becomes available.

Figure 8 shows the measured radiation dose rate in the power plant area during the accident (TEPCO 2011) and noble gas release rate from all three units, calculated with MELCOR by VTT. The purpose of the figure is to compare the timing of calculated releases with the timing of measured dose rates. Noble gas release was used instead of other fission products because noble gases cause most of the external doses in the plant area during the accident.

From figure 8 it is seen that timing of the calculated release rate corresponds quite well to the timing of the measured dose rate. The dose rate at the site before any release from the cores is about 0.04 $\mu\text{Sv/h}$. The dose rate increases rapidly after 13 h, when the unit 1 RPV had probably failed, containment pressure peaked and its leak rate increased. At 24 h there is a major peak in both measurement and calculation because the unit 1 wetwell venting was performed.

At 30 h there is a peak in the measured dose rate, but this peak could not be explained. It must come from unit 1 because cores of units 2 and 3 had not yet uncovered at that time. The peak does not correspond to any recorded event at unit 1. The unit 3 venting from 42 to 48 h caused a large peak in the measured dose rate and in the calculated release.

After 72 h both the measured dose rate and the calculated release rate were small for about six hours, and then started increasing because releases from unit 2 started. At 90 h there is a large peak both in the measurement and in the calculation. It was caused by a major leak from unit 2 containment. The highest dose rate, 11.93 mSv/h, was measured at this time.

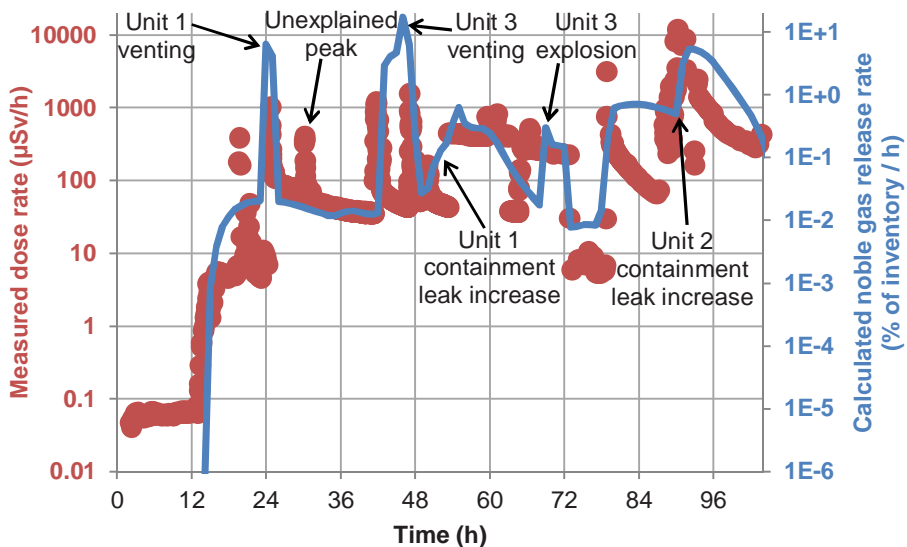


Figure 8. Measured dose rate at the power plant area (red circles), and calculated total noble gas release rate from units 1, 2, and 3 (blue line).

Recent investigations of the containments

TEPCO (2014) has published recent investigation results of the situation of the containments. Below is a summary of the investigations.

By injecting nitrogen to the wetwell of unit 1, TEPCO has estimated that the wetwell is almost full of water. In robot investigations they have found small water leaks from the drywell to the basement of the reactor building and from an expansion joint of a vacuum breaker tube on the top of the wetwell. There is no information whether the leaks started during the accident or at a later time. TEPCO has also inserted a camera to the unit 1 drywell. They found out that there was about 2.8 m of water on the drywell floor. Core debris was not visible, but the camera could see only small part of the drywell floor. Dose rate in the drywell was 5–11 Sv/h.

TEPCO has investigated the outer surface of the unit 2 wetwell by robots and ultrasound devices. They found out that the water level inside and outside the wetwell is about the same. Hence, there is probably a leak below the water level. They could not find the location of the leak, but they think that the suction line of the RCIC pump that is connected to the wetwell may be leaking. There is no information whether the leak started during the accident or at a later time. TEPCO has also inserted a camera to the unit 2 drywell. They found out that there was about 60 cm of water on the drywell floor. Core debris was not visible, but the camera was able to see only small part of the drywell floor. Dose rate in the drywell was 45–80 Sv/h.

Based on pressure measurements in unit 3 wetwell and drywell, TEPCO thinks that the current water level is about 7 m above the drywell floor and that the wetwell is full of water. Water is leaking from the drywell to the first floor of the reactor

building through a main steam line penetration, and this is consistent with the high water level in the drywell. There is probably no large leak in the wetwell (otherwise the water level would not stay so high). Despite nitrogen injection to the drywell, the oxygen concentration is about 8 % (compared to nearly zero in units 1 and 2). It is not possible to pressurize unit 3 drywell by injecting more nitrogen, while unit 1 and 2 drywells are several kPa above atmospheric pressure. Hence, there are probably large gas-phase leaks in unit 3 drywell. It is unknown whether these leaks started during the accident or at a later time. TEPCO has not been able to insert a camera into unit 3 drywell because high dose rates in the reactor building prevent access.

Summary and conclusions

MELCOR models of Fukushima unit 1, 2, and 3 accidents were developed. According to the calculations, at units 1 and 3 molten fuel has probably been discharged to the containment from broken reactor pressure vessel, while at unit 2 all the fuel is probably still inside the reactor. These results cannot yet be verified because TEPCO has not been able to insert a camera to the reactors.

The radioactive release to the environment was the largest from unit 3, according to these calculations, because the containment venting was made soon after core damage started, when there were a lot of cesium particles in the air, and the venting system was not equipped with filters. Calculated timing of the release corresponds quite well to the timing of measured peaks of radiation dose at the plant area. At 30 h there is an unexplained peak in the measured dose rate. The peak does not correspond to any recorded event in the accident progression.

Starting from scratch and developing models of three real full-scale accidents has significantly improved VTT's expertise in severe accident modeling. Comparing results with measured pressure data helps in developing better modeling practices. The effect of temperature stratification of the water pool in the wetwell has a large effect on containment pressure, but its modeling is difficult, and experimental data from large-scale facilities with annular geometry have not been found for validating stratification models. Behavior of safety systems in conditions for which they have not been designed, for example under two-phase flow, is challenging to predict. It is expected that visual inspections of the reactors will generate much new information that can be used for improving severe accident calculation models in the future.

References

- GE, 1978. Core design and operating data for cycles 1 and 2 of Peach Bottom 2. General Electric. (EPRI NP-563.)
<http://www.osti.gov/bridge/servlets/purl/6561294/6561294.pdf>
- Sevón, T. 2013. MELCOR modeling of Fukushima Unit 2 Accident. 22nd International Conference Nuclear Energy for New Europe (NENE), Bled, Slovenia, September 9–12, 2013.
- Sevón, T. 2015a. Fukushima Unit 1 Accident Modeling with MELCOR, Version 2. Research report VTT-R-00390-15.
- Sevón, T. 2015b. A MELCOR model of Fukushima Daiichi Unit 3 accident. Nuclear Engineering and Design 284, 80–90.
- TEPCO. 2011. Results of Monitoring at Fukushima Daiichi Nuclear Power Station. Tokyo Electric Power Company. http://www.tepco.co.jp/en/press/corp-com/release/betu11_e/images/110528e14.pdf
- TEPCO. 2014. Status of investigation on estimating situation of cores and containment vessels. Tokyo Electric Power Company.
http://www.tepco.co.jp/en/press/corp-com/release/betu14_e/images/140806e0106.pdf

26. Transport and chemistry of fission products (TRAFI)

26.1 TRAFI summary report

Teemu Kärkelä, Jarmo Kalilainen, Mélanie Gouëlle,
Pekka Rantanen, Ari Auvinen

VTT Technical Research Centre of Finland Ltd
P.O. Box 1000, FI-02044 VTT, Finland

Abstract

The aim in TRAFI project during 2011-2014 was to investigate the transport and chemistry of gaseous and particulate fission products in severe accident conditions. The main focus was on the behaviour of iodine and ruthenium which are highly radiotoxic and the mitigation of their possible source term is of utmost importance. A specific focus was on phenomena taking place in a primary circuit and containment building, which are poorly known and thus they are not considered in the current severe accident analysis codes. In order to be able to mitigate the FP releases or to estimate the possible source term with SA analysis codes accurately, the behaviour of fission products needs to be understood in detail.

Introduction

In Fukushima Daiichi nuclear plant cooling of the reactor cores at units 1, 2 and 3 was lost due station black out. Since the cooling could not be restored in time, fuel damage took place in all three reactors and fission products were partly released from the core. As expected in a such severe accident, the highest contribution to the source term to the environment was from iodine isotopes. In case of the Chernobyl accident, a high release of fission products to the environment took place and FPs were spread e.g. across the continent of Europe. In this accident, a fall-out of radioactive FPs containing also ruthenium was detected as far away as in Finland [Pöylänen, 1997].

Traditionally, it has been assumed that in a severe accident most iodine would be released from the fuel. Release to the containment would take place mostly as aerosol particles with gaseous fraction of about 5%. Along with iodine, low-volatile ruthenium is released from the fuel in oxidizing conditions. The most important volatile forms of ruthenium are RuO_3 and RuO_4 . Currently, the fraction of ruthenium which can be transported to the containment atmosphere in gaseous form is not well-known. VTT's previous studies [Kärkelä, 2014] indicated that the gaseous fraction can be significantly higher than what is expected based on thermodynamic equilibrium calculations. However, most ruthenium would be transported mainly as RuO_2 aerosol as a consequence of a reactive condensation of RuO_3 at ca. 1000 K.

Phébus FP program provided an opportunity to test e.g. iodine chemistry with realistic configurations and chemical environment. In Phébus FP tests iodine was indeed mostly released to the model containment as aerosol particles with gaseous iodine species making up few percent of the overall release. The release rate of iodine as well as aerosol sedimentation were also consistent with current severe accident modelling. Contrary to the expectations, gaseous iodine depleted from the atmosphere much faster than expected in the early phase of the tests. More alarmingly, a steady-state concentration of iodine in containment atmosphere was reached in all Phébus FP tests. The sump pH did not seem to influence the iodine partition in the gas phase. In addition, iodine concentration in the gas phase increased when the sump was condensing and decreased when it was evaporating. One would expect exactly opposite behaviour, if the source of the iodine is from the sump. In addition, silver iodide precipitated in the sump, when AIC control rod was applied in the tests. With B_4C control rod most iodine released in the model containment was in gaseous form.

Based on the results from Phébus FP program a number of hypothesis on iodine behaviour were formulated [Lee, 2008]. It was suggested that:

- 1) Either the painted surface or the steel walls acted as the source of the persistent gas phase iodine species in the tests.
- 2) Radiolytic processes destroyed gas phase molecular iodine and organic iodide to form iodine oxide or iodine nitroxide particles. These particles further coagulated and settled or were removed by other natural processes.
- 3) The source of gaseous iodine from the circuit was either chemical reactions in the gas stream or on the surfaces of the tube walls.

TRAFI –project was launched in SAFIR2014 program in order to test the hypothesized mechanisms. Only by mechanistic understanding of iodine behaviour the consequences of a severe accident can efficiently be mitigated.

Primary circuit chemistry of iodine and ruthenium

Iodine chemistry

It was assumed that chemical reactions either in the gas phase or on primary circuit surfaces may modify the amount, composition and timing of fission product release to the containment. The gas phase reactions of iodine are studied at IRSN within ISTP and OECD STEM programs. At VTT the work has concentrated on quantifying the effect of surface reactions on gaseous iodine release from the circuit in various steam-argon-hydrogen atmospheres. The possible influence of surface reactions on iodine speciation has a direct effect on nuclear safety. At the moment, they are not considered at all in the analysis of severe accidents.

Primary circuit experiments done in TRAFI project featured also silver, cadmium and caesium hydroxide precursors in addition to caesium iodide, molybdenum and boron used in the previous experiments within CHEMPC project. Silver could be present at severe accident conditions since it is one of the widely used control rod materials. Previous studies have also indicated that silver could play a major role in transport of iodine during severe nuclear accidents [Girault, 2006]. As cadmium is also one of the components used in control rod materials, its impact on the trapping of iodine needs to be investigated. In CHEMPC project boron was found to be able to trap caesium and thus a high release of gaseous iodine was detected. Also, previous experiments [Kalilainen, 2011] showed that when CsI reacted with molybdenum species, gaseous iodine would be released at lower temperatures than 650 °C. For this reason, some tests were conducted at lower temperatures, such as 400 °C or 550 °C. Caesium hydroxide was used to increase the molar fraction of caesium in the precursor and to examine its effect on the formation of gaseous iodine.

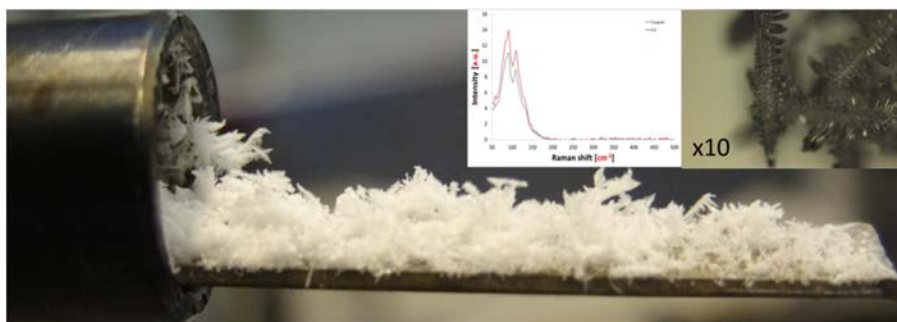


Figure 1. Deposits observed on a stainless steel coupon (thermal gradient from 650°C to 550°C) after the vapourisation of Cd and CsI at 650°C under Ar/H₂O/H₂ atmosphere. Raman analysis verified that the deposition was composed of CsI.

As a main outcome of the experiments, iodine was observed to be released from the precursor mixtures in a gaseous form even at low temperatures. Thus it verified the hypothesis formulated on the basis of Phébus FP program that fission product deposits on the primary circuit surfaces can act as a source of volatile iodine. The importance of this source becomes even more significant in a late phase of accident

when the thermal–hydraulic conditions of primary circuit are varying. A more detailed description of the experiments is presented as part of TRAFI special article in these proceedings.

Ruthenium chemistry

Most of experiments on the transport of ruthenium through a reactor coolant system have been conducted in a flow of pure air and/or steam with Ru oxides [Kärkelä, 2014]. The focus in TRAFI project was to find out the effect of other components, such as aerosols and air radiolysis products, on the transport of gaseous and particulate ruthenium species through a model RCS in air ingress conditions. Thus this study gave a possibility to study the speciation of ruthenium in more realistic conditions. The work was conducted with VTT’s Ru transport facility in collaboration with Chalmers University of Technology within SAFIR2014 and Nordic Research on Nuclear Safety NKS-R (ATR activity) programs. The experimental matrix is presented in Table 1.

Table 1. Matrix of Ru transport experiments (air atmosphere; 1500 K).

Exp.	T (K)	precursor	additive precursor concentration	comments	humidity
1	1500	RuO ₂	-	-	dry
2	1500	RuO ₂	-	-	humid
3	1500	RuO ₂	-	-	humid
4	1500	RuO ₂ +AgNO ₃	4 wt.% of AgNO ₃ solution	-	humid
5	1500	RuO ₂ +AgNO ₃	4 wt.% of AgNO ₃ solution	-	humid
6	1500	RuO ₂ +CsI	4 wt.% of CsI solution	-	humid
7	1500	RuO ₂ +NO ₂	O ₂ /N ₂ /NO ₂ ~21%/~79%/75 ppm(V)	no air feed	humid
8	1500	RuO ₂ +SiO ₂	4 wt.% of SiO ₂ solution	monodisperse 0.5 µm SiO ₂	humid
9	1500	RuO ₂ +Ag	4 wt.% of Ag solution	0.5-1 µm Ag	humid

All experiments were conducted at 1500 K with air as the carrier gas which was mixed with steam, AgNO₃, Ag particles, CsI particles, SiO₂ particles, or air was replaced with NO₂ gas mixed with N₂ and O₂ gases. The source of ruthenium (RuO₂ powder) was located in a ceramic crucible, which was placed inside the furnace. Ru oxides were vaporised from the powder when it was heated to the furnace set-point. The first results showed that the transport of gaseous RuO₄ downstream from the furnace increased when Ag particles, generated from AgNO₃–water droplets, were fed to flow of Ru oxides. However, the detailed study of AgNO₃-Ru system revealed that actually NO₃⁻, which decomposes to NO₂ + ½ O₂ and eventually to NO + O₂ when heated, was responsible for the enhanced transport of RuO₄. This was verified

with an experiment where only NO_2 gas was fed to the flow of Ru oxides. On the other hand, when only pure Ag particles (diameter 0.5-1.0 μm) were fed, the transport of RuO_4 decreased significantly (see Figure 2). Most likely, gaseous RuO_4 had reactively condensed on the surface of Ag particles as RuO_2 . The feed of CsI particles seemed to increase the transport of gaseous Ru even more than the feed of NO_2 (see Figure 2). In these experiments, the observed transport of gaseous Ru seemed to be several orders of magnitude higher than in the previous experiments [Kärkelä, 2014] with only pure Ru oxides in the air atmosphere. These new findings on ruthenium chemistry (NOx-Ru and CsI-Ru systems) will be investigated in detail in CATFIS project (SAFIR2018 programme).



Figure 2. Gaseous ruthenium collected in two sequential traps of NaOH solution (Experiments 6 and 9). Regardless of the fed aerosol compound, the experimental conditions and sampling times were similar in both experiments. The feed of Ag particles (a) to the flow of Ru oxides at 1500 K decreased the transport of gaseous Ru, whereas the feed of CsI particles (b) increased the Ru transport significantly.

Containment chemistry of iodine

One of the most surprising results of the Phébus FP program was the observed fast destruction of gaseous iodine within the containment atmosphere. It was assumed that radiolytical processes may lead to formation of iodine oxide particles. This has been studied in the previous CHEMPC project (SAFIR2010) by exposing gaseous organic iodine to gamma radiation. Several complementary tests were also conducted where inorganic and organic iodine were exposed to ozone and UV (c-type) radiation [Kärkelä, 2009; Holm, 2010]. The focus in TRAFI has been on the radiolytical oxidation of iodine by beta radiation, which causes the highest fraction of absorbed dose in the gas phase of containment [Bosland, 2010]. Another task has been to find out the speciation of iodine oxide and caesium iodide particles on various containment materials (paints, metals) after reacting with the surface and the desorption of

iodine from iodine oxide and caesium iodide deposits on the surfaces. This latter task has been studied in collaboration with Chalmers University of Technology within SAFIR2014 and Nordic Research on Nuclear Safety (NKS-R) programs. The basic studies on iodine oxidation at VTT have already lead to a new filtration system, which can be applied to trap both gaseous elemental iodine as well as organic iodides. The efficiency of the system is currently evaluated in EU PASSAM project, which aims at demonstrating the ability of innovative systems to achieve larger source term attenuation.

Oxidation of gaseous iodine

The first experiments on the radiolytical oxidation of gaseous iodine by beta radiation were conducted within a new BESSEL (Beta irradiation vESSEL) test facility – built at VTT. The reaction chamber was made of glass and a source of beta radiation (P-32, activity 5 mCi) was placed at the bottom. The residence time of the gaseous sample in the radiation field, the composition of the gas flow and the temperature of the facility could be adjusted. In the experiments, gaseous molecular iodine (I_2) and methyl iodide (CH_3I) were exposed to beta radiation in various mixtures of oxygen and nitrogen. The results of the experiments at 20 °C revealed that as an outcome of radiolytical oxidation the nucleation of particles took place in both cases and the diameter of particles was very small, ca. 10-50 nm. However, particles seemed to react with the humidity of air and dissolve very rapidly. A more detailed description of the experiments is presented as part of TRAFI special article in these proceedings.

Behaviour of IOx and CsI deposits in the containment building

In order to validate the source of gaseous iodine in the containment, samples were prepared for iodine desorption studies. If iodine is assumed to form iodine oxide particles within the containment atmosphere or if a high fraction of iodine is assumed to be transported from the primary circuit to the containment atmosphere as caesium iodide particles, representative samples should be prepared by depositing the said particles on the substrates. A set-up to produce iodine oxide and caesium iodide particles and to deposit them on surface samples (15mm x 15 mm x 0.25-1 mm) was designed and built at VTT. The surfaces exposed to IOx or CsI particles were painted (Teknopox Aqua V A) with various heat and gamma irradiation pre-treatments, stainless steel (316), copper, zinc and aluminium. The IOx particles for deposition on the surface materials were synthesized by the reaction of ozone and gaseous elemental iodine at 120 °C. At this temperature, the formation of I_2O_5 is more likely especially as both other oxides I_2O_4 and I_4O_9 decompose to I_2O_5 and I_2 . When I_2O_4 and I_4O_9 particles react with humidity they form HIO_3 and I_2 . After exposure to humid air, I_2O_5 is rapidly converted to its partially hydrated form $I_2O_5 \cdot HIO_3$, also defined as HI_3O_8 . The same product is formed when HIO_3 is partially dehydrated. The observed decomposition reaction was faster than reported in the literature and is assumed to be caused by a smaller diameter of the iodine oxide particles. CsI particles were generated by spraying droplets of CsI solution with an atomizer and then drying the produced droplets in the gas phase at 120 °C.

With Raman and XPS analyses no chemical reactions of iodine oxides with the stainless steel surface and painted surfaces could be identified. According to the recorded Raman spectra the form of iodine seemed to be partially hydrated $I_2O_5 \cdot HIO_3$ on steel and painted surfaces. In addition, both Raman and XPS analysis found molecular iodine (I_2), which is likely to be formed due to decomposition of I_2O_4 and I_4O_9 particles on the surfaces. There was no obvious reaction with the aluminium surface detectable with SEM-EDX analysis. On copper and zinc samples the peaks of solid HIO_3 and molecular iodine were detected in the Raman spectra. The results of the XPS analyses also suggested reactions between the iodine oxide deposit and the surface on both samples. This may relate to the fact that zinc forms water soluble iodide (ZnI_2). In contrast copper forms water insoluble iodide (CuI). The reaction seemed to be more extensive on the zinc surface, for which no chemical form of oxidised iodine could be identified with XPS. The XPS spectrum of CsI was observed on all metal and painted samples on which CsI particles were deposited. Solid CsI particles were observed on the studied metal surfaces with SEM. However, on painted samples no CsI particles were observed. It is very likely that the particles on painted samples were mostly dissolved. Some CsI was most likely dissolved also on metal surfaces as iodine was observed outside the area with caesium iodide deposit. According to XPS analyses, this iodine may have reacted with the oxidized metal surfaces to form metal iodates. Only traces of oxidised iodine were detected on painted surfaces.

The desorption of iodine from I-131 labelled iodine oxide and caesium iodide deposits on paint and metal surfaces was observed to take place when the samples were exposed to heat, humidity or gamma irradiation. Humidity was shown to be the major factor for the reevaporation. The release rate of iodine in case of paint seemed to be the highest from heat treated surface and the lowest from fresh paint in which the concentration of solvents was still high. In case of metal surfaces, copper seemed to react with iodine and to bound it quite efficiently, especially in the occurrence of CsI deposits. The highest release rate of iodine was from deposits on stainless steel surface. The release of iodine to the gas phase seemed to be higher from CsI deposits than from IO_x deposits, except on copper and fresh paint surfaces.

Turbulent deposition of fission products

The deposition of fission products on the walls was significantly higher than expected in Phébus FP program. One hypothesis to explain the high deposition was that turbulent flow might have increased the fraction of wall deposition within the model containment. The phenomenon of particle deposition in a cubic cavity with turbulent natural convective flow has been investigated at Paul Scherrer Institut (PSI) using Direct Numerical Simulations (DNS) [Puragliesi, 2010] and Large Eddy Simulations (LES) [Bosshard, 2012]. Similar turbulent natural convection flows will develop in real containment building due to temperature gradients. These models are validated against experiments carried out in TRAFI –project. The main aim of

this investigation is to experimentally determine the fluid motion, temperature fields, and particle motion inside a differentially heated cavity. Special emphasis is to enable validation of models used in LES, as well as enable comparison with earlier computational work using DNS. A detailed description of this work is presented in a PhD thesis of Jarmo Kalilainen.

Differentially heated cavity with Aerosol in turbulent NATural convection (DIANA) facility was constructed for measurements of particle deposition on a turbulent natural convection. DIANA facility is a cubic with heated and cooled vertical walls with constant temperatures and top, bottom and lateral walls with close to adiabatic boundary conditions. DIANA facility was designed to allow measurements using $Ra = 10^9$, which was also used in the simulation works [Puragliesi, 2010; Bosshard, 2012]. The flow field measurements as well as inside gas temperature measurements were conducted with Particle Image Velocimeter (PIV). Also in this work, on-line aerosol devices were used for particle concentration measurements together with PIV, e.g. Tapered Element Oscillating Microbalance (TEOM) for mass concentration analysis. The deposition of monodisperse amorphous silica oxide (SiO_2) particles was investigated with two particle diameters, $d_p = 1 \mu m$ and $d_p = 2.5 \mu m$ and density $\rho_p = 2000 \text{ kg/m}^3$.

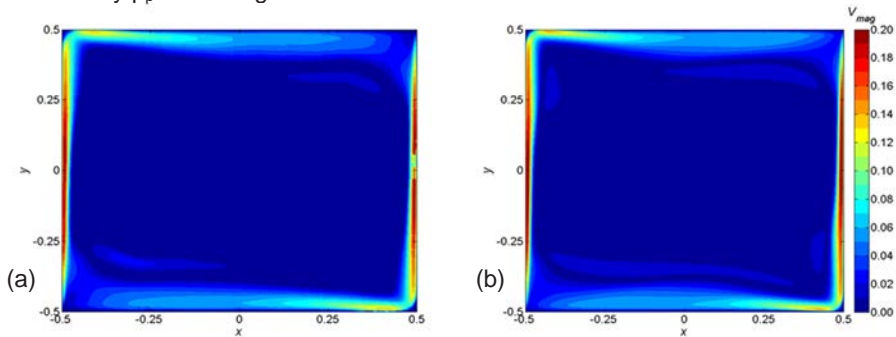


Figure 3. (a) Flow and temperature data measurements (b) in validation of Large Eddy Simulation (LES) model of the DIANA cavity. V_{mag} is the dimensionless velocity magnitude.

Particle deposition was investigated using a Lagrangian Particle Tracking (LPT) method. The particle tracking was carried out using a Large Eddy Simulation (LES) of the DIANA cavity, which was found to produce the flow and temperature fields that matched reasonably well with the measurements (see Figure 3). The LPT work, as well as the previous LES, was conducted using Ansys FLUENT software. In the particle tracking study, particles with a diameter of $d_p = 2.5 \mu m$ and density $\rho_p = 2000 \text{ kg/m}^3$ were used. At the beginning of the calculation, 10^5 motionless particles were uniformly distributed to the cavity atmosphere. The time-step used in the particle calculation was $\Delta t_p = 1.8E-5 \text{ s}$. The particles hitting the cavity walls were assumed to be trapped and the placement and time of the deposition was monitored. Approximate 1700 s of simulation was conducted. No LPT simulations were conducted using $d_p = 1 \mu m$ particles. This is due to considerable increase in computing time

that would have been required in order to achieve an estimate for the deposition rate equally representative than when using $d_p = 2.5 \mu\text{m}$ particles.

The results showed that the deposition rate, dependent of the particle size, was almost uniform everywhere in the cavity atmosphere. Only at the close vicinity of the bottom wall ($y = 0.41-0.42$) the deposition rate was found to be smaller compared to the rest of the cavity. This indicates that at the bottom, particles stay airborne longer than in rest of the cavity atmosphere, possibly partially trapped in the flow circulation near the floor. Elsewhere in the cavity the turbulent flow causes the particles to stay approximately uniformly distributed, thus producing identical deposition rates. With $d_p = 1 \mu\text{m}$ particles, thermophoresis was seen to have a potential effect on the deposition, causing approximately 10 % of the particles to be found from the cold wall sample slides. No similar behaviour was observed in the experiments using $d_p = 2.5 \mu\text{m}$ particle.

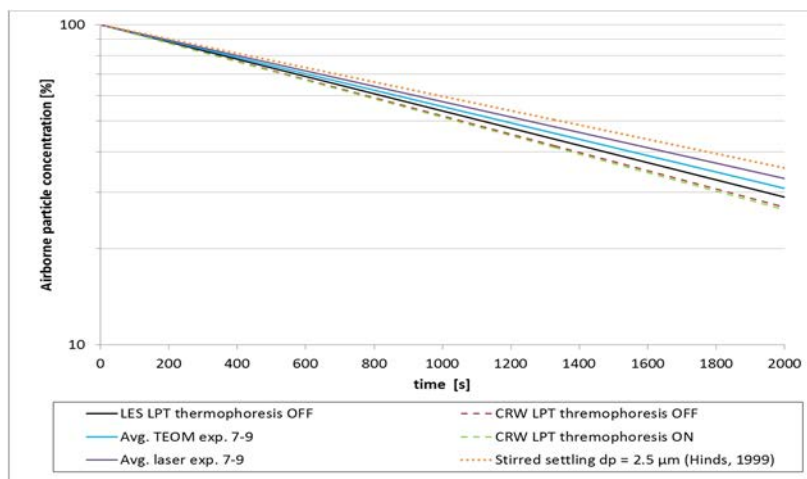


Figure 4. The LES model is used in Lagrangian Particle Tracking (LPT) simulation – computed deposition rates of $2.5 \mu\text{m}$ particles compared to the measurement data.

The simulation data obtained from the particle tracking calculation using the $d_p = 2.5 \mu\text{m}$ particles coincided well with the measurement (Figure 4). It showed that the particles follow the flow quit rigorously and are mostly deposited from the bottom boundary layer due to gravitational settling. For this reason, $d_p = 2.5 \mu\text{m}$ particle behaviour was also seen to be well described by the stirred settling model where uniformly distributed particles are deposited to the cavity floor due to sedimentation. However, with $d_p = 1 \mu\text{m}$ particles the measurement data matches the stirred settling calculation poorly. Since no additional phenomenon influencing the deposition rate (e.g. electrical forces) was detected in the experimental work, supplementary particle tracking computations will be needed to determine validity of the measurements with the $d_p = 1 \mu\text{m}$ particles. Due to this observed difference in the deposition rate of $1 \mu\text{m}$ particles when compared with $2.5 \mu\text{m}$ particles, a complementary test with $0.5 \mu\text{m}$ particles is also planned to be conducted in CATFIS project (SAFIR2018).

Acknowledgement

The financial support of VTT Technical Research Centre of Finland, The Finnish Research Programme on Nuclear Power Plant Safety (SAFIR2014), Nordic Nuclear Safety Research Programme (NKS-R) and Severe Accident Research NETWORK of excellence (SARNET) is acknowledged.

References

- Bosland, L. Cantrel, L. & Girault, N. 2010. Evaluation of the dose rate inhomogeneities in PHEBUS containment during FPT1 and FPT3 tests, 31th CCIC meeting.
- Bosshard, C. 2012. Large Eddy Simulation of Particle Dynamics Inside a Differentially Heated Cavity. Ph.D Thesis, Eo: 5297, Ecole Polytechnique Federale de Lausanne, Lausanne.
- Girault, N., Dickinson, S., Funke, F., Auvinen, A., Herranz, L. & Krausmann, E. 2006. Iodine behaviour under LWR accident condition: Lessons learnt from analyses of the two Phebus FP tests. Nuclear Engineering and Design 236(12), 1293-1208.
- Holm, J., Kärkelä, T., Auvinen, A., Glänneskog, H. & Ekberg, C. 2010. Experimental study on iodine chemistry (EXSI) – Containment experiments with methyl iodide, NKS-220.
- Kalilainen, J., Kärkelä, T., Rantanen, P., Forsman, J., Auvinen, A. & Tapper, U. 2011. "Primary circuit chemistry of iodine", SAFIR2010, The Finnish Research Programme on Nuclear Power Plant Safety 2007-2010, Final report, 312-320.
- Kärkelä, T., Holm, J., Auvinen, A., Ekberg, C., Glänneskog, H., Tapper, U. & Ziliacus, R. 2009. Gas phase oxidation of elemental iodine in containment conditions, 17th International Conference on Nuclear Engineering, ICONE17. Brussels, 12 - 16 July 2009. ASME. Vol. 2, 719 – 727.
- Kärkelä, T., Vér, N., Haste, T., Davidovich, N., Pyykönen, J. & Cantrel, L. 2014. Transport of ruthenium in primary circuit conditions during a severe NPP accident. Ann. Nucl. En. 74, 173-183.
- Lee, R. Y. & Salay, M. 2008. Findings on iodine behaviour in design basis and severe accidents, Presented to the Advisory Committee on Reactor Safeguards 8.5.2008, U.S.NRC
- Puragliesi, R. 2010. Numerical Investigation of Particle-Laden Thermally Driven Turbulent Flows in Enclosure. Ph.D. Thesis, Eo: 4600, Ecole Polytechnique Federale de Lausanne, Lausanne.
- Pöllänen, R., Valkama I. & Toivonen, H. 1997. Transport of radioactive particles from the Chernobyl accident. Atmospheric Environment 31(21), 3575-3590.

26.2 Recent findings on iodine behaviour in a severe accident

Teemu Kärkelä, Mélanie Gouëlle, Jarmo Kalilainen
Pekka Rantanen, Tommi Kekki, Ari Auvinen

VTT Technical Research Centre of Finland Ltd
P.O. Box 1000, FI-02044 VTT, Finland

Abstract

Radiotoxic iodine is one of the most hazardous fission products, which is generated during the normal operation of a nuclear power plant and iodine is accumulated in the fuel. It is assumed that most of iodine would be released from the fuel in a severe accident. In order to mitigate the possible iodine source term, its behaviour in accident conditions should be understood in detail. Recent work at VTT has focused on iodine behaviour in the primary circuit and more specifically on the effect of fission product deposits on the formation of gaseous iodine. Another aim has been to study the radiolytical oxidation of gaseous inorganic and organic iodine when exposed to containment conditions, e.g. beta radiation. These studies have given new information on iodine speciation, which has already led to a development of new filtration system. It can be applied to trap both gaseous and particulate iodine.

Introduction

In Fukushima Daiichi nuclear plant cooling of the reactor cores at units 1, 2 and 3 was lost due to station black out. Since the cooling could not be restored in time, fuel damage took place in all three reactors and fission products were partly released from the core. As expected in a such severe accident, the highest contribution to the source term to the environment was from iodine isotopes.

Traditionally, it has been assumed that in a severe accident most iodine would be released from the fuel. Release to the containment would take place mostly as aerosol particles with gaseous fraction of about 5%. Particulate iodine is expected to be removed from the gas phase of the containment by engineered safety systems as well as by natural aerosol processes like settling and diffusiophoresis. Particulate and gaseous iodine would finally end up in sump waters and remain there if alkaline conditions are maintained. However, most iodides (except AgI, TlI and CuI) are very water soluble. Unfortunately, iodine water chemistry is also very complicated as it can assume several different oxidation states. In case of acidification of the water from nitric acid formation and other radiolytic processes, molecular iodine would partition back to the atmosphere. It might also form volatile organic iodides. Rate of

release from water would increase as the sump temperature would approach the boiling point.

Phébus FP program provided opportunity to test these expectations in iodine chemistry with realistic configurations and chemical environment. In Phébus FP tests iodine was indeed mostly released to the model containment as aerosol particles with gaseous iodine species making up few percent of the overall release. The release rate of iodine as well as aerosol sedimentation were also consistent with current severe accident modelling. Contrary to the expectations, gaseous iodine depleted from the atmosphere much faster than expected in the early phase of the tests. More alarmingly, a steady-state concentration of iodine in containment atmosphere was reached in all Phébus FP tests. The sump pH did not seem to influence the iodine partition in the gas phase. In addition, iodine concentration in the gas phase increased when the sump was condensing and decreased when it was evaporating. One would expect exactly opposite behaviour, if the source of the iodine is from the sump. In addition, silver iodide precipitated in the sump, when AIC control rod was applied in the tests. With B₄C control rod most iodine released into the model containment was in gaseous form.

Based on the results from Phébus FP program a number of hypothesis on iodine behaviour were formulated [Lee, 2008]. It was suggested that:

- 1) Either the painted surface or the steel walls acted as the source of the persistent gas phase iodine species in the tests.
- 2) Radiolytic processes destroyed gas phase molecular iodine and organic iodide to form iodine oxide or iodine nitroxide particles. These particles further coagulated and settled or were removed by other natural processes.
- 3) The source of gaseous iodine from the circuit was either chemical reactions in the gas stream or on the surfaces of the tube walls.

The focus in the recent work of VTT has been to test the hypothesized mechanisms. Only by mechanistic understanding of iodine behaviour the consequences of a severe accident can efficiently be mitigated.

Primary circuit chemistry of iodine

After fission products have been released from the overheated and molten fuel, they are transported through the reactor coolant system and FPs will reach areas at lower temperature. As a consequence, vapour condensation and particle nucleation processes takes place in the gas flow. If vapour condensation takes place close to the surfaces of primary circuit, a layer of condensate can be formed on it. Particles in the gas flow may also deposit on the circuit surfaces together with control rod and structural materials. The release of gaseous iodine from precursor mixtures simulating deposits in primary circuit conditions have been investigated with EXSI-PC facility [Kärkelä, 2009a; Kalilainen, 2011; Kalilainen, 2012; Kalilainen, 2014; Gouëlle, 2014; Gouëlle, 2015a]. A list of the recently conducted experiments is present in Table 1.

Table 1. Recently conducted experiments on primary circuit chemistry of iodine.

Precursors	Temperature [°C]	Crucible material	Atmosphere*
CsI	650	Al ₂ O ₃	A, B and C
CsI	650	AISI 304	A, B and C
CsI	550	Al ₂ O ₃	A, B and C
CsI	400	Al ₂ O ₃	A, B and C
CsI + MoO ₃	650	Al ₂ O ₃	A, B and C
CsI + Mo	650	Al ₂ O ₃	A, B and C
CsI + Mo	650	AISI 304	A, B and C
CsI + Ag	650	Al ₂ O ₃	A, B and C
CsI + Ag	400	Al ₂ O ₃	A, B and C
AgI	650	AISI 304	A, B and C
AgI	400	AISI 304	A, B and C
CsI + Ag + MoO ₃	400	Al ₂ O ₃	A, B and C
CsI + B ₂ O ₃	650	AISI 304	A, B and C
CsI + B ₂ O ₃	650	Al ₂ O ₃	A, B and C
CsI + B ₂ O ₃	400	AISI 304	A, B and C
CsI + Cd	650	Al ₂ O ₃	A and C
Cd	650	Al ₂ O ₃	A and C
CsI + Cd	400	Al ₂ O ₃	A, B and C
Cd	400	Al ₂ O ₃	A, B and C
CsI + CsOH	650	Al ₂ O ₃	A and C

* The composition of atmosphere is explained in Table 2.

The crucible containing the precursors was heated up to 400 °C, 550 °C or 650 °C in the reaction furnace. The furnace tube used in the experiments was made of alumina or stainless steel (AISI 304), which was pre-oxidized before the experiment. The reaction product particles were collected on PTFE filters with 5 µm pore size, and the gaseous reaction products were trapped in two consecutive bubbling bottles (0.2 M NaOH and 0.02 M Na₂S₂O₃ water solution), which located downstream the aerosol filters. Additional toluene trap was used in some experiments. The elemental composition of both samples was analyzed with Inductively Coupled Plasma Mass Spectrometer (ICP-MS). Experiments included three different gaseous atmosphere conditions, with different fractions of steam, argon and hydrogen, shown in Table 2.

Table 2. Gas flow rates (NTP conditions: 0 °C and 1013 mbar) and volume fractions (at 100 °C and 1013 mbar) fed to the reaction furnace.

		Condition		
		A	B	C
Argon	Flow rate [l/min, NTP]	3.3	3.2	2.9
	Gas vol-%	86.7	83.9	76.1
Steam	Mass flow rate [g/min]	0.3	0.3	0.3
	Gas vol-%	13.3	13.5	13.4
Hydrogen	Flow rate [l/min, NTP]	0	0.1	0.4
	Gas vol-%	0	2.6	10.5

In experiments with only CsI precursor, the overall release of iodine decreased significantly when temperature was decreased to 400 °C. As a consequence, the transport of iodine containing particles (CsI) was very low. Nevertheless, a small amount of gaseous iodine was observed to be released from the precursor even at 400 °C. In that specific case, the fraction of gaseous iodine was higher than the fraction of aerosols. The addition of Ag to CsI precursor at 650 °C resulted in the similar release of CsI aerosol as with pure CsI precursor, whereas the transport of gaseous iodine decreased. Some amount of silver was found on filter in aerosol form, probably as AgI, which could explain the observed decrease in gaseous iodine transport. At 400 °C reaction temperature, the release of gaseous iodine was much higher compared to the experiment at 650 °C and almost no iodine containing aerosol particles were formed, see Figure 1. Most likely, the lower reaction temperature reduced significantly the vaporization of Cs, I and Ag compounds. Similar behaviour was observed when CsI precursor, mixed with additional MoO₃, was heated to 400 °C. Addition of metallic Mo seemed to increase the release of gaseous iodine as well.

The formation of vitreous caesium borate compound was noticed, when a mixture of CsI and B₂O₃ was heated to 650 °C. This could be a potential cause of blockages in the circuit. Such a boron-rich partial blockage was observed in the rising line before the steam generator inlet in Phébus FPT3 test. Also as a result of boron trapping most of caesium in the crucible, a high fraction of gaseous iodine was transported to the bubbling bottle. The release of gaseous iodine remained high even at 400 °C. The transport of cadmium was significantly increased by the presence of caesium iodide, whereas CsI aerosol transport was decreased only slightly. 10 to 60 times more cadmium reached the sampling lines than in the experiment with only cadmium. As it was observed, most of cadmium was condensed on the facility's surfaces before the sampling lines in the cadmium experiment. Thus, it is highly probable that the vaporised cadmium had condensed on caesium iodide particles and transported to the filter. A fraction of cadmium was transported as cadmium hydroxide Cd(OH)₂, that was verified by XRD. Addition of Cd to CsI precursor seemed to result in a higher transport of gaseous iodine, but the formation of Cd-I compound was not detected.

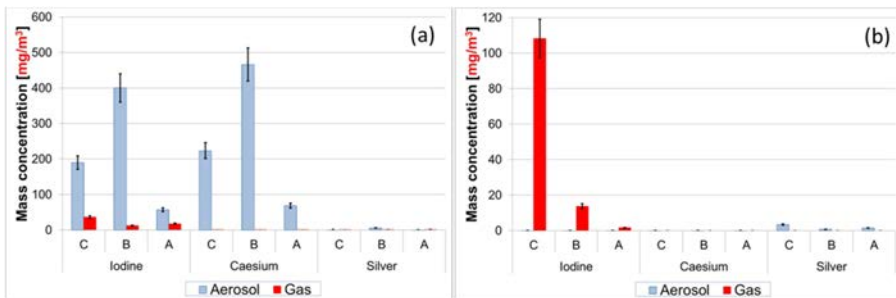


Figure 1. Iodine, caesium and silver mass concentrations, transported in gaseous and particulate forms, in the experiments at (a) 650 °C and (b) 400 °C. Conditions were in order from C to A. [Kalilainen, 2012]

The amount of gaseous iodine was barely detectable when the initial Cs/I molar ratio was higher than 1 (addition of CsOH to CsI precursor), see Figure 2. The effect of the atmospheric composition was noticed as well; when hydrogen was present in the carrier gas (condition C), the amount of aerosols (caesium and iodine) released from the crucible was significantly decreased.

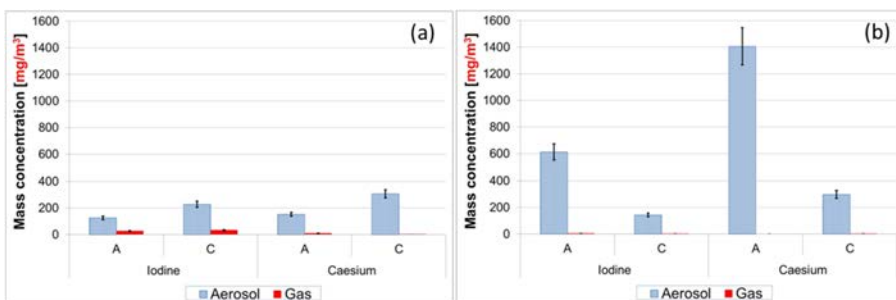


Figure 2. Iodine and caesium mass concentrations (aerosol and gas) at 650 °C with caesium to iodine molar ratio of (a) 1.0 and (b) 1.6. Conditions A and C only. [Gouëlle, 2015a]

Containment chemistry of iodine

Volatile iodine can form several compounds with other fission products, control rod and structural materials in the primary circuit. Therefore, e.g. in case of a tube break, iodine can be transported to the containment atmosphere both in gaseous and particulate forms. It is very likely that iodine at least partly deposits on painted walls of a reactor containment building during a severe accident. In such a case, molecular iodine can be released from these deposits back to the gas phase. Furthermore, iodine may also react with painted surfaces to form organic iodine species. These

organic species are another possible source of volatile iodine, which may increase the fraction of iodine in the gas phase. Therefore, it is important to study the transport of iodine in containment conditions. This is being investigated in collaboration between VTT and Chalmers University of Technology (Sweden). Another question is, whether these iodine compounds are transported as gaseous molecules or as aerosol particles resulting from reactions with air radiolysis products. To answer this last question several experiments were conducted in co-operation with Chalmers University of Technology [Kärkelä, 2009b; Kärkelä, 2010]. In experiments molecular iodine and methyl iodide were fed into the VTT's EXSI-CONT facility in an air mixture. In some experiments the flow contained also humidity. The reactions took place in a quartz tube heated either to 50 °C, 90 °C or 120 °C. UV-light was used as a source of radiation to produce ozone from oxygen. A separate generator was also applied to reach higher ozone concentrations. VTT has carried out further studies on the radiolytical oxidation of I₂ and CH₃I by beta radiation in oxygen at 20 °C with a new BESSEL facility [Kärkelä, 2015a; Kärkelä 2015b].

As a result of CH₃I experiments with EXSI-CONT, there was a clear trend in the formation of gaseous reaction product species. The main gaseous reaction products were methanol and formaldehyde. Especially at elevated temperature other reaction products, such as formic acid and methyl formate, became important as well. Increasing amount of reaction product species were detected while the concentration of ozone was increased. The measured gaseous reaction product species in experiments at 50 °C to 120 °C are presented in Figure 3. Similarly, the mass concentration of aerosols increased as well, thus aerosol nucleation was enhanced. Also, increase in temperature seemed to increase the aerosol mass concentration. This is probably partly due to more efficient decomposition of gaseous CH₃I and subsequent aerosol formation with ozone. The formation of gaseous reaction products was efficient in this study, even though the residence time of the flow inside the facility was only approx. 7 seconds. It seemed that thermal decomposition reactions further enhanced the formation of reaction products.

In the beta irradiation experiments with BESSEL facility, it was found out that the concentration of formed particles (ca. 10 nm to 50 nm in diameter) decreased very slowly with increasing irradiation time, see Figure 4. It seemed that an equilibrium was reached between gas phase iodine compounds and iodine species deposited on wall surfaces. At that equilibrium the rate of new particle formation was low. When the facility was purged with oxygen, a new formation of particles was observed in every CH₃I experiment. It suggested that the radiolysis reaction products were limiting the particle formation. Oxygen, a precursor of ozone when irradiated, was also needed for the nucleation to take place, since the new particle formation was not observed without irradiation or when the atmosphere was pure nitrogen. The formed particles were highly water soluble and volatile. These findings could also partially explain the constant concentration of iodine, which was observed in the gas phase of containment at the end of every Phébus FP test.

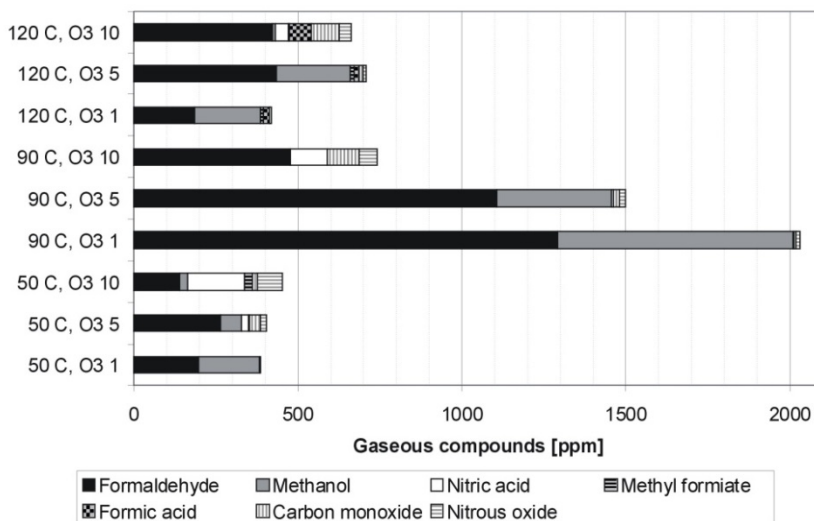


Figure 3. The gaseous reaction products (in ppm) from the oxidation of methyl iodide with ozone. The temperature of EXSI-CONT facility and the power setting of ozone generator are presented on vertical axis. [Kärkelä, 2010]

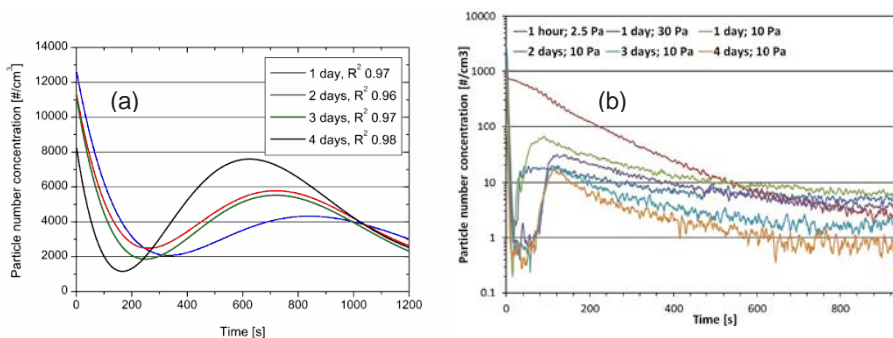


Figure 4. The number concentration of the formed aerosols after the exposure of gaseous (a) CH_3I [Kärkelä, 2015a] and (b) I_2 [Kärkelä, 2015b] precursors to beta radiation in oxygen atmosphere at 20 °C. The irradiation period ranged from 1 hour to 4 days. The initial vapour pressure of CH_3I was approx. 4 kPa, whereas the vapour pressure of molecular iodine ranged from 2.5 Pa to 30 Pa.

Filtration of gaseous and particulate iodine

In the containment atmosphere, part of gaseous iodine compounds is radiolytically decomposed mainly by gamma rays and beta particles originating from fission products. As a result of radiolytical oxidation, gaseous iodine can be transformed to e.g. iodine oxide particles. Due to the high contribution of radiotoxic iodine to the possible source term, the retention of iodine containing compounds and thus the prevention

of their release to the environment is of primary importance. Currently, VTT is studying the filtration of both gaseous and particulate iodine with a new filtration system. This technique can be used to filter e.g. other FP aerosols as well. The efficiency of the system is being evaluated in EU PASSAM project, which aims at demonstrating the ability of innovative systems to achieve larger source term attenuation.

The basic studies on iodine oxidation at VTT have produced a significant amount of data and knowledge on the behaviour of iodine in a severe accident. The knowledge is being used to enhance the filtration efficiency of the wet electrostatic precipitator (WESP) technique. The conventional ESP technique can be used to filter gaseous pollutants when the gas flow is pre-treated before the filtration unit. The water droplets fed into the system adsorb gaseous impurities. The effect can be enhanced by injecting additives with the water. The gaseous compounds can also be oxidized to form solid particles which are filtered with the ESP technique. Both proposed methods are being studied now for the decontamination of gaseous species in containment conditions. Gaseous iodine is oxidized with additional ozone and water droplets are fed to the gas flow just before the filtration unit of WESP.

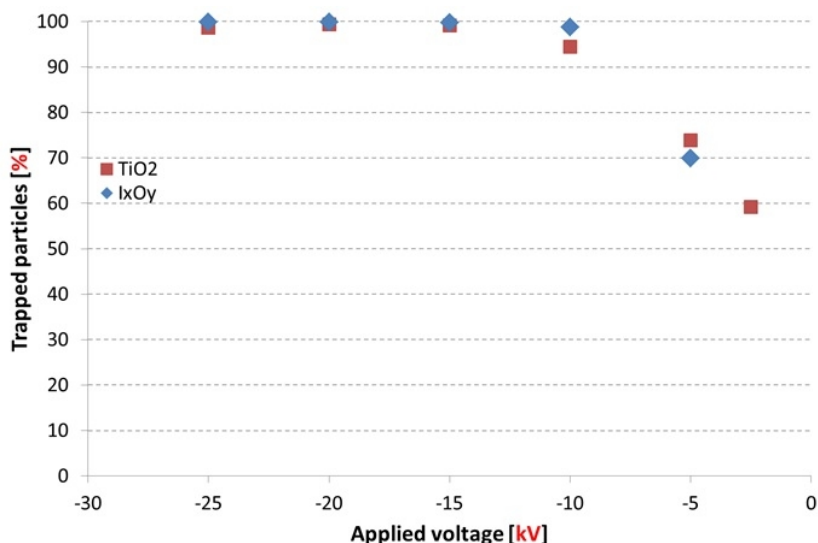


Figure 5. Evolution of the fraction of trapped TiO₂ and I_xO_y particles with the WESP filter as a function of the applied electric voltage between the electrodes. [Gouëlle, 2015b]

The first experiments were carried out with TiO₂ and I_xO_y aerosols, see Figure 5. The applied electric voltage between the electrodes, the residence time of particles inside the ESP chamber and the injection of water droplets before the ESP chamber were varied in the experiments. The injection of water droplets significantly increased the trapping efficiency of TiO₂ particles for applied electric voltage less than 15 kV (negative). In the iodine experiments, a gas flow containing elemental iodine (2.2 l/min, 16 ppm) was mixed with ozone (3 l/min, > 1000 ppm) in order to oxidize

all gaseous iodine to iodine oxide particles. The gas flow was further diluted and the total flow rate through the WESP was 86 l/min (20 s residence time). As a result of the first filtration experiments, close to 100 % of the formed I_xO_y particles was filtered with the WESP when the applied electric voltage was in a range from -10 kV to -25 kV.

Summary and conclusions

Phébus FP program raised a number of questions that could not be answered by the current severe accident analysis tools. Based on the experimental observations several hypothesis e.g. on iodine behaviour in the primary circuit as well as within the containment were formulated. These hypothesis must be experimentally tested and not just parameterized.

Some of these hypotheses have been experimentally verified by VTT. One of the uncertainties was the effect of reactions on primary circuit surfaces on the fraction and timing of iodine release into the containment atmosphere. In the experiments, a difference in the release of iodine in the primary circuit conditions at 400 °C, 550 °C and 650 °C temperatures was detected. Iodine seemed to be released almost completely in gaseous form at lower temperature despite the used precursor mixtures. This surprising observation suggests that the FP deposits on the surfaces of primary circuit may act as a source of volatile iodine for a long period since the beginning of severe accident. However, an excess amount of Cs to I seemed to reduce the formation of gaseous iodine at 650 °C. Results on the radiolytical oxidation of gaseous molecular and organic iodine by beta radiation, and complementary experiments with ozone and UV radiation, verified the formation of aerosol particles, which was one of the formulated hypothesis after Phébus FP experiments. The diameter of nucleated particles ranged from ca. 10 nm to 50 nm. These very small particles were highly water soluble and volatile.

Recent studies by VTT have produced new information on the chemistry and transport of iodine in severe accident conditions. These results are needed e.g. in order to explain the observed behaviour of iodine in the experiments of Phébus FP program. However, the most important impact of these results will be on the development of severe accident analysis codes. Previously, the lack of information has prevented to taking into consideration the FP deposits on primary circuit surfaces and iodine oxide particles both in the containment gas phase and on the containment surfaces as a short and long term source of volatile iodine. The new information on the iodine chemistry developed have been utilized e.g. in the development of electric filtration technique for gaseous and particulate iodine species. The efficiency of this Finnish innovation is currently evaluated in EU PASSAM project.

References

Gouëlle, M., Kalilainen, J., Rantanen, P., Kärkelä, T. & Auvinen, A. 2014. Experimental study on the behaviour of CsI on primary circuit surfaces and ef-

- fects of cadmium on iodine transport during a severe nuclear accident. VTT-R-00630-14.
- Gouëlle, M., Kalilainen, J., Kärkelä, T. & Auvinen, A. 2015a. Experimental Study on the Behaviour of CsI on Primary Circuit Surfaces: Effects of Cadmium and Caesium Hydroxide on Iodine Transport during a Severe Nuclear Accident. VTT-R-00424-15.
- Gouëlle, M., Kärkelä, T., Hokkinen, J. & Auvinen, A. 2015b. Presentation in the 5th management team meeting of EU PASSAM project.
- Kalilainen, J., Kärkelä, T., Rantanen, P., Forsman, J., Auvinen, A. & Tapper, U. 2011. Part "Primary circuit chemistry of iodine," SAFIR2010, The Finnish Research Programme on Nuclear Power Plant Safety 2007-2010, Final report, 312-320.
- Kalilainen, J., Rantanen, P., Kärkelä, T., Lipponen, M., Auvinen, A. & Jokiniemi, J. 2012. Effects of molybdenum and silver on iodine transport in primary circuit on severe nuclear accidents. VTT-R-00425-12.
- Kalilainen, J., Kärkelä, T., Zilliacus, R., Tapper, U., Auvinen, A. & Jokiniemi, J. 2014. Chemical reactions of fission product deposits and iodine transport in primary circuit conditions. *Nuclear Engineering and Design* 267, 140-147.
- Kärkelä, T. & Auvinen, A. 2009a. Experimental study on iodine chemistry (EXSI) – Facility for primary circuit experiments. VTT-R-02791-09.
- Kärkelä, T., Holm, J., Auvinen, A., Ekberg, C., Glänneskog, H., Tapper, U. & Zilliacus, R. 2009b. Gas phase oxidation of elemental iodine in containment conditions. In *Proc. ICONE17, Brussels*, 2, 719 – 727.
- Kärkelä, T., Holm, J., Auvinen, A., Zilliacus, R., Kajolinna, T., Tapper, U., Glänneskog, H. & Ekberg, C. 2010. Gas phase reactions of organic iodine in containment conditions. In *Proc. ICAPP2010, San Diego*, 2, 1084 – 1091.
- Kärkelä, T., Auvinen, A., Kekki, T., Kotiluoto, P., Lyyränen, J. & Jokiniemi, J.K. 2015a. Radiolytical oxidation of gaseous iodine by beta radiation. Submitted to *Radiochimica Acta*.
- Kärkelä, T., Gouëlle, M., Kekki, T., Kotiluoto, P. & Auvinen, A. 2015b. Formation of HNO₃, O₃ and IOx particles in air/oxygen/I₂ atmospheres by beta radiation. VTT report.
- Lee, R. Y. & Salay, M. 2008. Findings on iodine behaviour in design basis and severe accidents, Presented to the Advisory Committee on Reactor Safeguards 8.5.2008, U.S.NRC

27. Reactor vessel failures, vapour explosions and spent fuel pool accidents (VESPA)

27.1 VESPA summary report

Anna Nieminen, Kari Ikonen, Magnus Strandberg, Mikko Patalainen

VTT Technical Research Centre of Finland Ltd
P.O. Box 1000, FI-02044 Espoo,

Abstract

VESPA project had three main objectives: (1) to investigate the applicability of a commercial code Abaqus for modelling reactor pressure vessel lower head deformations, (2) to develop expertise to evaluate steam explosion loads for PWR and BWR containment and (3) to gain in-depth understanding of the phenomenology related to possible spent fuel pool accidents evaluating also the applicability of integral severe accident code to model related phenomena. All these objectives were fulfilled during the project on adequate degree.

Introduction

This project brings together three different fields of nuclear safety research: structural integrity, steam explosions and Spent Fuel Pool (SFP) accidents. In order to analyse containment loadings that are determined by the discharging core melt, the timing and the place of reactor vessel rupture have to be defined accurately. Preserving of knowledge of steam explosions is important still today, since the risk of steam explosions during a severe nuclear accident cannot be excluded in our current nuclear power plants. The accident at the Fukushima Dai-ichi Nuclear Power Plant has highlighted the vulnerability of nuclear fuels that are in SFPs due to the potential loss of sufficient cooling. Even though the progress of this type of accident is relatively slow, the time scales and needed mitigation measures are not that widely studied. Also the related phenomena differ from reactor applications.

Benchmarking Abaqus code against PASULA code in simulating high temperature pressure vessel failures

The first objective of the project was to investigate the applicability of a commercial code Abaqus for modelling reactor pressure vessel lower head deformations at high temperatures. This is done by comparing the simulation results with suitable experimental data as well as with results obtained with the specific code PASULA developed at VTT (Ikonen, 2001) especially for this purpose.

The first selected benchmark case was widely studied Sandia OLHF-1 experiment (Humphries et al., 2000). Compared to previous approach, the creep models were improved by fitting the creep parameters against available test data and by carrying out sensitivity studies. The results were compared to results obtained with PASULA and also to the results of international benchmark (Patalainen, 2013). A comparison between vertical displacement estimations can be seen in Figure 1.

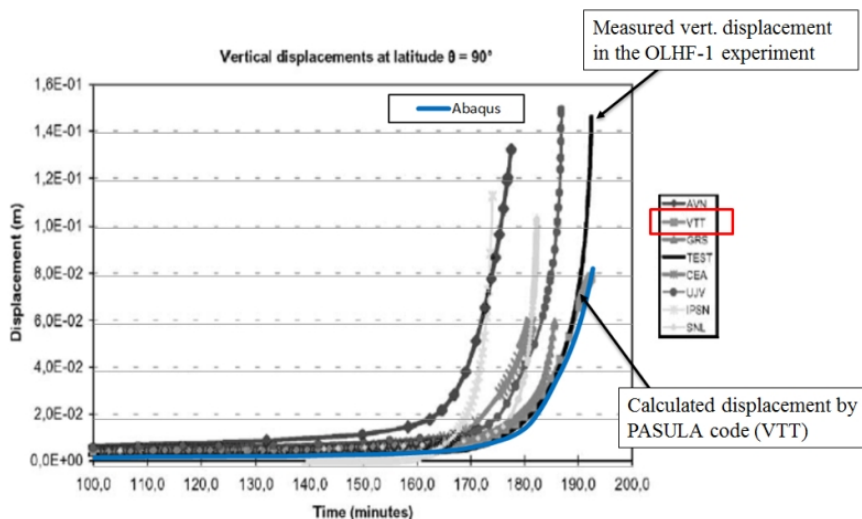


Figure 1. Estimated vertical displacement at the bottom of the vessel by the OLHF-1 benchmark participants and the result obtained with Abaqus.

In the OLHF-1 experiment 1:5 scaled pressure vessel wall was circumferentially heated using electrical heaters and the pressure was maintained high to understand the mechanical behavior under extreme conditions. More prototypic conditions were analysed in EC FOREVER-C2 experiment (Nourgaliev et al., 1999), that was selected for the second benchmark case (Patalainen, 2014). In the experiment 1:10 scaled pressure vessel was filled with oxide melt that was heated to maintain adequate temperature level. The pressure was lower than in OLHF-1 experiment and the melt was in natural convection. Temperature distributions produced by Abaqus of both experiments can be compared from Figure 2 (a) and (b).

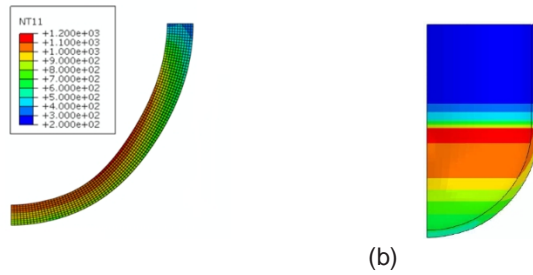


Figure 2. (a) Temperature distribution (°C) prior the rupture in simulation of OLHF-1 experiment. (b) Temperature distribution in 3D section model of EC FOREVER-C2 simulation after reaching the steady state.

In the case of EC FOREVER-C2, comparing the simulation results to the experiment was challenging since the loading data utilized in the computation was not equivalent with the experimental conditions. The mechanical loading was applied as a pressure loading that was a design value since there was no available data from the experiment. Temperature load was interpolated from CFD analysis because the thermocouples inside the vessel worked only for 15 minutes. However, the same loading data was utilized in earlier PASULA calculations be compared.

In Figure 3 (a) is presented the vertical displacement and in Figure 3 (b) the radial displacement produced by Abaqus and by PASULA. Vertical displacement results are nearly identical and also the radial displacements are in very good agreement. The total maximum displacement in the FOREVER-C2 experiment was about 20 mm. The maximum total displacement estimated by Abaqus was 21 mm.

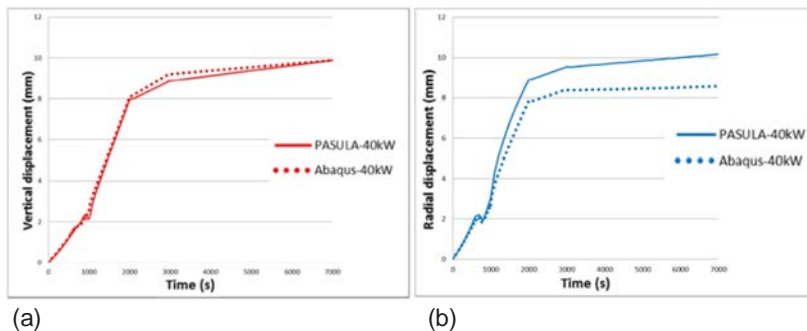


Figure 3. (a) Vertical and (b) radial displacement obtained by Abaqus 3D section model from the bottom of the vessel at $\theta = 18^\circ$ and comparison to PASULA results.

In both benchmark cases the Abaqus and PASULA results were in a good agreement with each other and also with available test data. This proves that both of these tools can be utilised in analysing vessel deformations and possible failure under severe accident circumstances. However, it was also found out that experimental material test data have an essential role in achieving good results.

Analysing steam explosions with MC3D

The second objective of the project was to become acquainted with phenomena related to steam explosions and to learn to use MC3D. Steam explosions are Fuel Coolant Interactions (FCI) that might occur when high temperature molten material fragments into water. This causes rapid transfer of thermal energy, which leads to a major pressure increase. Steam explosions are usually split into three stages: pre-mixing, triggering and propagation. In Table 1 (Strandberg, 2014) is presented how different initial conditions are assumed to effect explosion probability and strength.

Table 1. A quick overlook of the different premixing parameters and their effect on the explosion probability and strength.

Property		Explosion probability	Explosion strength
Amount of melt	↑	↑	↑
Melt temperature	↑	↑	↑
Melt density	↓	↑	↑
Hydrogen production	↑	↑	↓
Void fraction	↑	↑	↓
Ambient pressure (< 0.8 MPa)	↑	↑	↑
Ambient pressure (> 0.8 MPa)	↑	↓	↑
Coolant temperature	↓	↓	↑

MC3D is a multidimensional Eulerian code developed by IRSN and CEA to simulate multiphase and multi-constituent flows for nuclear safety applications. MC3D utilises two different FCI codes. One of the codes is for the premixing stage and the other for the explosion stage into which is incorporated also the triggering stage. Then the simulation is split into two parts, in the first part the fragmentation of the melt jet, the vapour build-up and the heat transfer is simulated. The second part, which can be started at a time chosen by the user, handles the rapid fragmentation of the melt drops and the heat transfer from the molten drops to the coolant.

In Figure 4 is an illustration of the result of premixing stage calculation for purely oxidic TROI-TS4 experiment (Hong et al., 2009) with MC3D. Whereas, in Figure 5 is the result of the explosion stage i.e. the pressure at the test vessel wall (Strandberg, 2014). The simulated pressure is compared with the value measured in the experiment. In the experiment the steam explosion was triggered externally and in the simulation the explosion was triggered at the same moment.

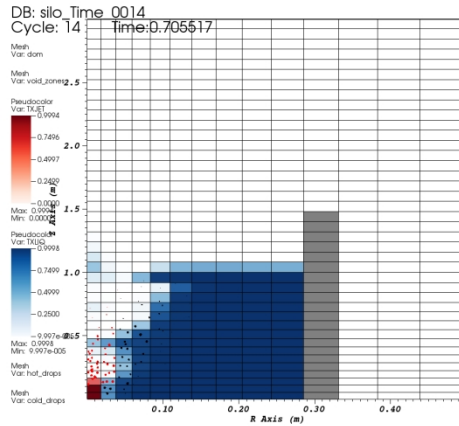


Figure 4. Snapshot showing the premixing conditions at a time just before the triggering. The red part of the mesh represents the melt fraction in that part, and the blue color water fraction. The hot (molten) drops are represented by red dots and the cold (solidified) drops by black dots.

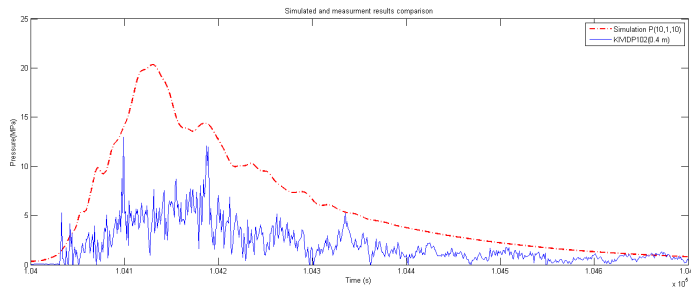


Figure 5. Comparison of the pressures in the middle of the test vessel wall; the red dashed line is the value from the MC3D simulation and the blue line is the measured value in the TROI-TS4 experiment.

A sensitivity study has been performed (Strandberg, 2015) for some of the parameters presented in Table 1 and for some user defined simulation values to evaluate the usability of MC3D for reactor applications. As starting point in these analyses was used TROI TS-5 experiment (Hong et al., 2011) that had also metals in the melt. It can be assumed that partly oxidised melt will produce hydrogen during the premixing increasing void build-up and then making the explosion weaker.

In Figure 6 is presented the effect of different melt temperatures to the pressure load explosion induces to structures. In this case with partly metallic melt the differences remained small. In Figure 7 is presented the effect of trigger time to the pressure peaks. The trigger time affects not only the explosion strength but also if explosion occurs or not. Also the effect of ambient pressure was analysed but in that case differences were not noticed.

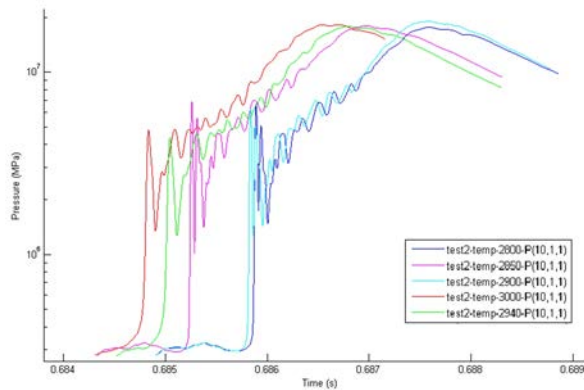


Figure 6. The effect of different melt temperatures to the pressure impulse.

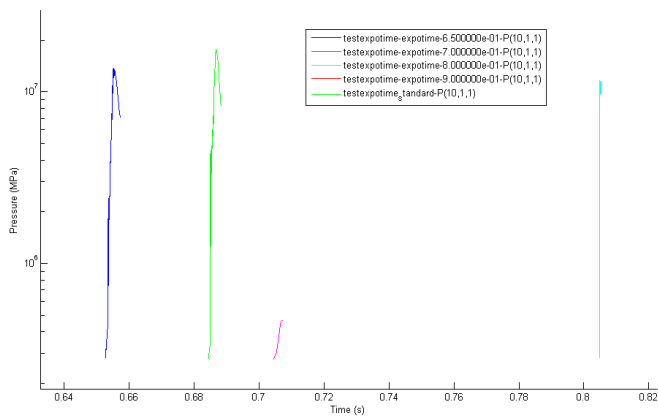


Figure 7. The effect of trigger time to the pressure peaks. At trigger time $t = 0.9$ s no explosion occurred.

The amount of uncertainties related to steam explosions is large and based on current worldwide research, it cannot be confirmed in which conditions the explosion is triggered. To be able to analyse the possibility of steam explosion to occur, specific know-how is needed not only of the phenomenon but also of specialised codes. First steps towards this goal have been taken.

Development of PANAMA computing model for simulating heating of water-cooled interim spent fuel storage in loss of coolant

The third objective of the project was to analyse thoroughly phenomena related to SFP accidents. Firstly was studied in a detailed way the heat-up of the water-cooled spent fuel interim storage in a case that cooling of water pool fails. It has been found

out that the most severe case occurs in a situation, when water boils slowly away from the pool. In this case the fuel has time to heat-up significantly, before water level descends below the racks and cooling ventilation beneath becomes possible. Numerical CFD type calculation methods and a computer program called PANAMA (Polttoainealtaiden ANALyysi ja MALLinnus) were developed for this slow boil-off case.

On the basis of the performed studies it has been found that most attention should be paid on phenomena occurring on the level of the upper end of fuel elements. Heat removal from this interface has an essential effect on the evolution of the maximum temperature in the fuel. From the numerical CFD point of view next phenomena make the modelling very complicated: (1) water level between fuel rods descends continuously, (2) hot vapour flows vertically between the fuel rods and with varying velocity out from the fuel elements, (3) multidimensional heat conduction and vapour flow above fuel elements transport heat to upper direction and (4) thermal radiation emitted from hot end of fuel elements absorbs to varying vapour depth. All these phenomena have been programmed into PANAMA. Some details are discussed in (Ikonen, 2014) and (Ikonen, 2015).

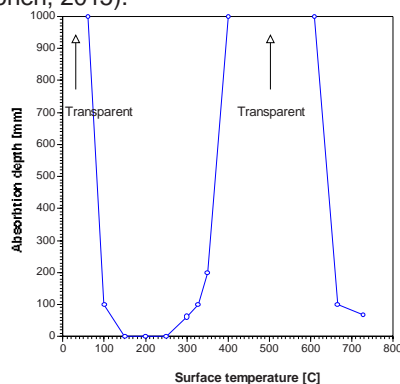


Figure 8. Absorption depth as a function of surface temperature.

At high temperature heat is transferred significantly from hot surfaces by thermal radiation. Thermal radiation is absorbed to water vapour above the interface. The absorption depth depends on the local temperature of the emitting surface. In some surface temperatures vapour is practically transparent as shown in Figure 8 and heat is more efficiently transferred to concrete structures.

The effect of varying absorption depth to the maximum fuel temperature evolution was analysed with PANAMA, but no significant difference was observed compared to previous analyses when this phenomenon was not taken into account. The water level decrease with three different decay heat levels is illustrated in Figure 9 (a) and evolution in maximum fuel temperature in Figure 9 (b).

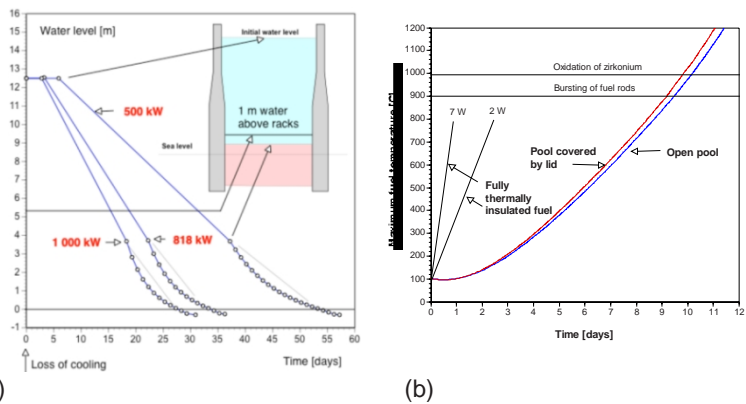


Figure 9 (a) Water level decrease vs. time. (b) Maximum fuel rod temperature evolution. Time starts from the moment when the fuel racks start to uncover.

Steam flow velocities between the fuel racks start from zero when the rods start to uncover. Flow pattern above the fuel changes continuously forming large eddies that can be seen in performed transient analyses. Figure 10 demonstrates some flow patterns. There is actually no stationary state in the heat-up of spent fuel storage. In transient natural circulation analyses very short time steps are needed in CFD type analysis.

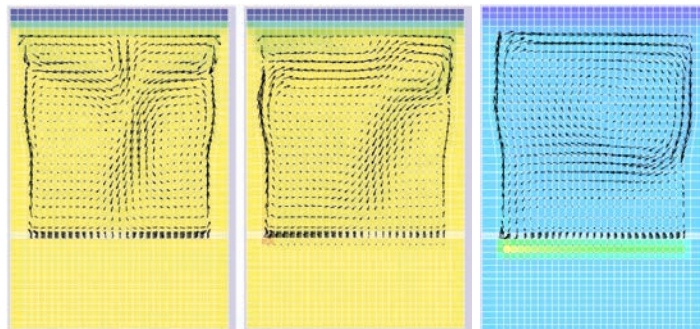


Figure 10. Demonstration of continuously changing flow pattern in case of a lid above pool.

Assessment of MELCOR code for fuel pool accidents

Secondly coolant losses in SFPs were analysed with integral code MELCOR (Nieminen, 2014). The selected case study for MELCOR calculations was a loss of cooling in the SFP in VVER-440 ice-condenser containment. The objective was to study the effect of an accident scenario and the effect of a lid on top of the pool. Boil-off and leak scenarios were analysed both lid on and off in a situation when the fuel is just recently inserted to the pool i.e. the decay heat level is relatively high.

The water level behaviour is illustrated in Figure 11 in the boil-off case with a lid on top of the pool. In Figure 12 is depicted the air flow in the core region in the cases with and without the lid. According to the results, there is plenty of time to react to loss of cooling in SFP if there is no leak. However, even a relatively small leak at the bottom of the pool causes this type of accident to proceed very fast.

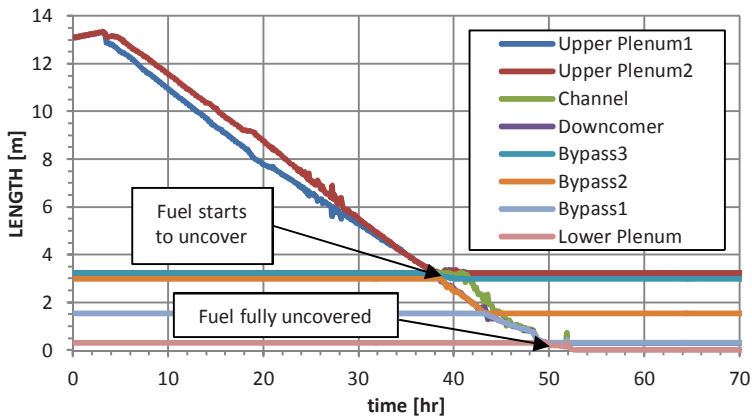


Figure 11. Water level in different control volumes in the boil-off scenario with a lid on top of the pool. Fuel starts to uncover after 37 hours from the loss of cooling and is fully uncovered after 49 hours and 50 minutes.

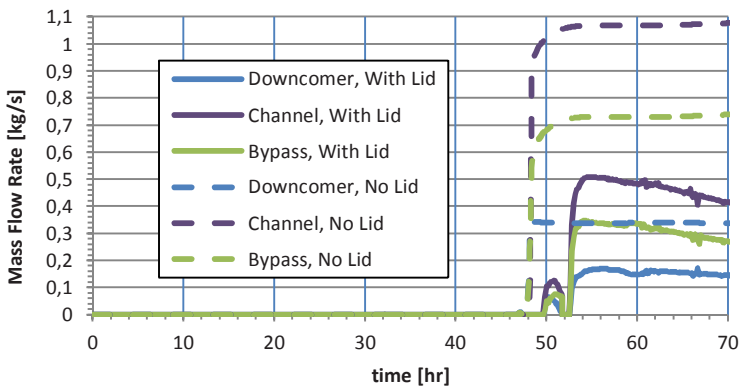


Figure 12. The effect of lid to the air flow in the core region. Air flow is directed downwards in downcomer and in bypass and upwards in the channel.

A lid on top of the pool seems to delay the accident progress, since it acts as an additional condensing surface returning part of the coolant. When there is still water in the pool, air is not able to flow down to the pool due to strong steam flow upwards. After the boiling phase, air appears to be able to cool down the structures in the pool and as expected, a lid limits the air flow. The results were very similar to those obtained with PANAMA.

References

- Hong, S.W, Kim, J. H., Min, B. T., Hong, S. H. & Ha, K. S. 2009. Troi ts-4 test data report – draft. OECD/SERENA-2009-TRXX . 59 p.
- Hong, S.W, Kim, J. H., Min, B. T., Hong, S. H. & Ha, K. S. 2011. Troi ts-5 test data report. OECD/SERENA-2010-TR08. 61 p.
- Humphries, L.L., Chu, T.Y. & Bentz, J.H. 2000. Data report for OLHF-1 Experiment, Sandia National Laboratories.
- Ikonen, K. 2001. Large inelastic deformation analysis of steel pressure vessels at high temperature. Doctoral Thesis. VTT Publications 437. ISBN 951-38-5856-1. 141 p. + app. 15 p.
- Ikonen, K. 2014. Development of PANAMA computing methods for analysing heating of interim spent fuel storage. Research Report VTT-R-000615-14. 22 p. + app. 6 p.
- Ikonen, K. 2015. Heating of water-cooled interim spent fuel storages in loss of coolant. Research Report VTT-R-00276-15. 18 p.
- Nieminen, A. 2014. MELCOR analysis of Spent Fuel Pool Accidents in VVER-440 Icecondenser Containment. Research Report VTT-R-01086-14. 19 p.
- Nourgaliev R.R et al., 1999. Failure Of Reactor Vessel Retention FOREVER-C2 test and analysis. Research Report. Division of Nuclear Power Safety, Royal Institute of Technology. Stockholm, Sweden.
- Patalainen, M. 2013. SAFIR 2014 – VESPA 2013 Axisymmetric high temperature failure simulation of a pressure vessel in the OLHF-1 experiment. Research Report VTT-R-08366-13. 33 p.
- Patalainen, M. 2014. SAFIR 2014 – VESPA 2014 High temperature failure simulation of a pressure vessel in the EC FOREVER-C2 experiment. Research Report VTT-R-04316-14. 23 p.
- Strandberg, M. 2014. Introduction to Steam Explosion Phenomena. Research Report VTT-R-03242-14. 27 p.
- Strandberg, M. 2015. Analysing Steam Explosions with MC3D. Research Report VTT-R-00489-15. 24 p. + app. 2 p.

28. Passive Containment Cooling System tests (PCCS)

28.1 PCCS summary report

Juhani Vihavainen¹, Teemu Kärkelä²

¹Lappeenranta University of Technology
P.O. Box 20, FI-53850 Lappeenranta

²VTT Technical Research Centre of Finland Ltd
P.O. Box 1000, FI-02044 Espoo

Abstract

The PCCS project consisted of thermal hydraulic and aerosol behaviour experiments during 2013 and 2014 at facilities of Lappeenranta University of Technology (LUT) attached with aerosol measurement systems provided by VTT. In 2013, basic thermal hydraulic tests with the PCCS model, which is connected to the drywell and wetwell compartments of PPOOLEX facility, acting as a host facility, were conducted. Aerosol measurement systems were prepared and installed during 2014. Aerosol systems were designed and manufactured by VTT containing systems for producing and measuring the aerosols. The experiments were conducted with three of five heat exchange tubes of the PCCS. The facility was proven to be capable for this purpose. The designed measurement setup was successful in analysing the gas and particle phase at inlet and outlet of the PCCS with satisfactory precision.

Introduction

The main goal of the PCCS project was to provide experimental data on the behavior of Passive Containment Cooling System (PCCS) condenser used in ABWRs for the development and validation of computer codes. The first part of the experiments which were carried out in 2013 (thermal hydraulic tests) serves the validation of

system codes (APROS, TRACE) and thermal hydraulic models of severe accident codes (MELCOR, ASTEC). The second part of experiments, which were carried out in 2014, the actual aerosol tests, serves mostly the development and validation of severe accident codes. There has not been data available on the behavior of aerosols (deposition, condensation, retention etc.) in horizontal PCCS. Flow conditions, which effect on the aerosol behavior, differ significantly in horizontal PCCS from those with vertical tubes.

PCCS TEST RIG

The PCCS test rig at Lappeenranta University of Technology (LUT) is integrated with the PPOOLEX test facility modelling the drywell and wetwell compartments of BWR containment, Figure 1.

Steam needed in the experiments was produced with the nearby PACTEL test facility. The operation phase of the combination of the test facilities (PCCS model, PPOOLEX, PACTEL), is remote-controlled from the control room with the help of the process control system. Suitable initial conditions were created by injecting steam from the PACTEL steam generators into the containment model of PPOOLEX. When the desired conditions were established, the operation of the PCCS model was initiated by opening a valve in a DN80 pipeline to the PCCS model. Because the PCCS is designed to operate passively, no control procedures are needed for the PCCS system itself.

The PCCS model at LUT consists of five horizontal U-tube shaped heat exchange tubes installed inside a secondary side liquid pool see Figure 2. The pool is in atmospheric pressure and covered by a lid with an exit pipe out of the laboratory and with viewing windows for video cameras. The heat exchange tubes can be disassembled into three pieces and the PCCS model can also be operated in single tube configuration. The experiments were conducted with three of five heat exchange tubes. On both sides of the heat exchange tubes in the secondary side pool there is a vertical flow controller made of polycarbonate plate.

Condensation water and non-condensables are separated from each other by gravity in the outlet chamber. In the first two experiments the condensate was drained from the outlet chamber into the lower part of the PPOOLEX wet well through a DN25 line by gravity. Correspondingly, non-condensables were led from the outlet chamber into the wet well through a DN50 line.

The facility was modified during 2013 by adding an extra tank simulating the lower dry well to ensure the correct operation of system in different test conditions. This tank was named drywell 2 (DW2). Its purpose is to gather condensate drain. The collapsed level is measured, thus the condensation mass can be defined.

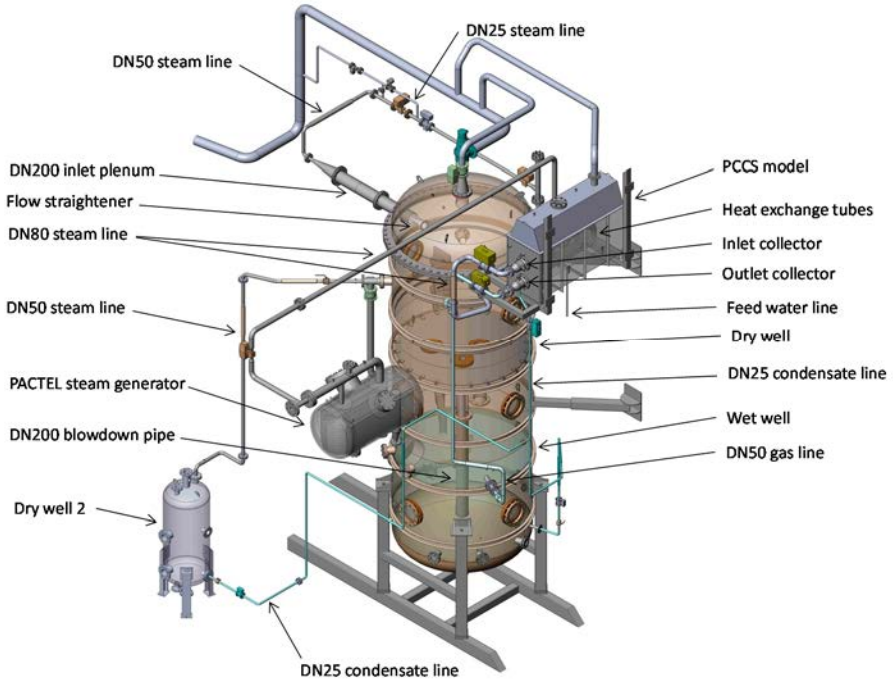
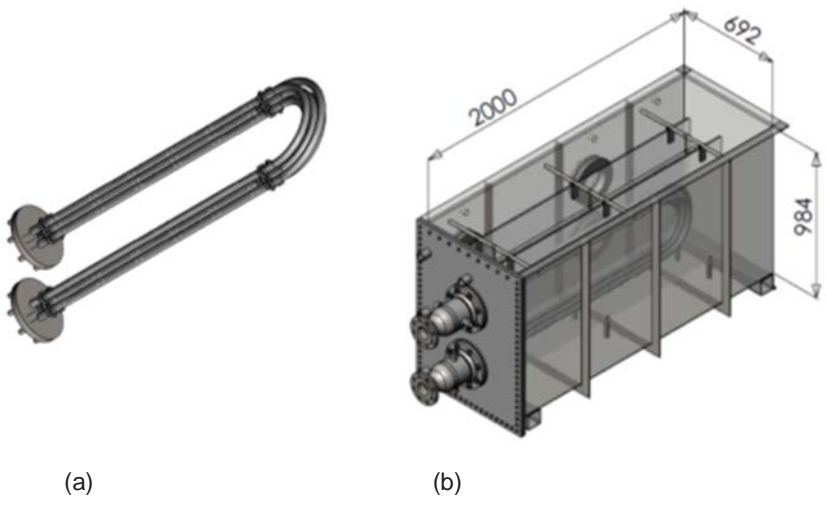


Figure 1. PCCS system integrated with the PPOOLEX test rig.



(a)

(b)

Figure 2. PCCS model with heat exchanger tubes (a) and pool (b).

Test programs

During year 2013 six experiments (labeled PCC-01 to PCC-06) were carried out. The main purpose of these first experiments was to test the thermal hydraulic behavior and operation capability of the PCCS as integrated to the PPOOLEX and thus define operation limits and characteristics of the system for actual aerosol tests. In the first experiment PCC-01 general behavior was studied. The steam flow into PPOOLEX upper drywell was increased stepwise upwards and then decreased back in one step. In the second experiment PCC-02 the steam flow was changed in shorter steps upwards and downwards. After the first two tests a second drywell (DW2) was attached to the main facility. This arrangement ensured that the condensed water could be gathered separately and measured. It also ensured the correct operation of system in different test conditions. The PCC-03 was carried out with almost similar parameters as the experiment PCC-02. For the PCC-04 test and all tests afterwards a cone shaped flow straightener was installed inside the inlet plenum of PPOOLEX upper drywell. Also PCC-04 was run with similar stepwise procedure in order to see if this flow straightener device had any effect compared to the results of previous experiments. For PCC-05 experiment two of five the heat exchange tubes were blocked. In PCC-06 experiment the blowdown pipe was plugged and steam flow rate was kept almost constant.

Table 2. PCC-01-PCC-06 experiments in 2013.

Experiment	Steam flow	Steam flow (min.max) [g/s]	DW2	Remarks
PCC-01	Stepwise	~150-380	No	System testing
PCC-02	Stepwise	100-430	No	Similar steps in steam flow upwards and downwards
PCC-03	Stepwise	~100-410	Yes	Similar steps in steam flow upwards and downwards
PCC-04	Stepwise	~100-410	Yes	Flow redirecting device added
PCC-05	Stepwise	~100-410	Yes	3/5 heat ex. pipes in use
PCC-06	Constant	150	Yes	3/5 heat ex. pipes in use; blowdown pipe plugged

During year 2014 four experiments (labeled from PCC-07 to PCC-10) were carried out. The main purpose of these experiments was to test the aerosol systems integrated to the PCCS. The experiments contained different sequences forming separate reference and aerosol injection periods (see Table 3). In all experiments 3/5 heat exchanger tubes were in use and the blowdown pipe was blocked (similar set-up as PCC-06). Different steam flow rates were used in experiments. The experiments PCC-07 and PCC-08 were carried out in order to test the aerosol equipment installation and the operation procedures together with PCCS test facility. No aero-

sols were injected in these experiments. In PCC-09 aerosols were injected for the first time. The aerosol material used in the experiments was carbon black. In PCC-09 some obscurities appeared in air injection. Thus, another experiment, PCC-10, was carried out with almost similar procedure than the PCC-09 (see Table 2). The experiment were terminated due to limitation in aerosol measurement system was not qualified for system pressure exceeding 3 bar.

These experiments contained two types of procedures:

- 1) Clean experiments sequences without aerosol feed in order to define the dilution ration for both sampling legs as function of the pressure. All clean experiments were conducted with steam feed. In some experiments also air was fed to the steam flow prior to PCCS from the same location as the aerosol feed in aerosol experiments.
- 2) In aerosol experiments sequences carbon black particles were fed with an auxiliary air flow from the fluidized bed aerosol generator to the steam feed.

Table 3. PCC-07 - PCC-10 experiments in 2014.

Experiment	Steam flow rate (min.max) [g/s]	Remarks
PCC-07	90-150	Aerosol equipment installed but no aerosol injected
PCC-08	90-150	Additional air feed to PCCS, test rehearsal
PCC-09	90-150	Aerosol injection. Reference state included, intermediate ventilation between reference and aerosol injection sequences.
PCC-10	90-150	Similar procedure to PCC-09. Termination criteria met for aerosol equipment; 3 bar system pressure exceeded.

Table 4. Seven different experiment sequences with the aerosol sampling system were conducted (included in experiments PCC-07, PCC-08 and PCC-10).

Test [#]	Experiment	Time [s]	Steam [g/s]	Air [N l/min]	Carbon black [Y/N]
1	PCC-07	6200-8000	50	0	N
2	PCC-07	8000-9800	90	0	N
3	PCC-07	9800-11600	130	0	N
4	PCC-08	4000-5500	90	90	N
5	PCC-08	1240-4000	130	90	N
6	PCC-10	15000-16860	90	240	Y
7	PCC-10	10980-12360	130	240	Y

Results of thermal hydraulic tests

One of the main objectives of the first experiments in 2013 was to define characteristics and operation limits of the PCCS facility. Hence, stepwise steam flow increment and decrement was used. To estimate the maximum heat removal capacity of the PCCS different approaches could be introduced. With these methods theoretical maximum power was estimated.

Temperature measurements in the blowdown pipe give indicate clearly the maximum heat removal capacity of the PCCS. When temperatures in the blowdown pipe start to rise for the first time, the steam starts to flow through blowdown pipe. The timing indicates the corresponding steam mass flow rate for maximum capacity of the PCCS. Figure 3 shows that in PCC-03 experiment the first reaction of the blowdown pipe is observed, when steam flow is increased from 150 g/s to over 200 g/s. Next increment in steam flow finally set the blowdown pipe in full operation.

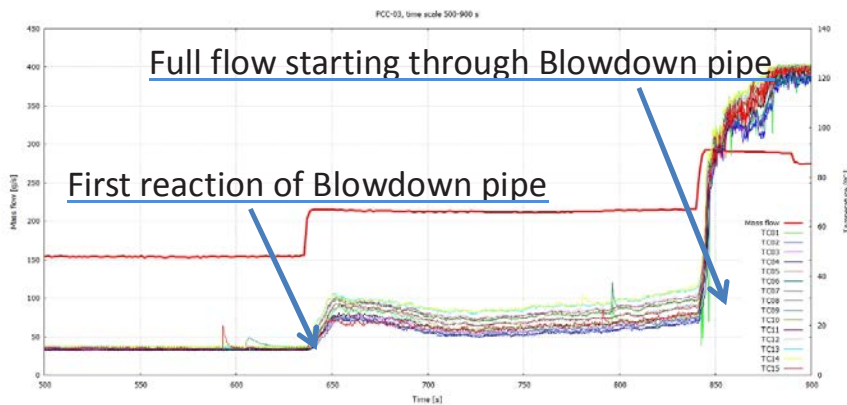


Figure 3. Steam mass flow rate (red line) and temperatures in the blowdown pipe in experiment PCCS-03.

Figure 4 shows the flow measurements of steam injection, in condensation line and in non-condensable line in experiment PCC-06. This experiment carried out with two, almost constant steam flow rates. The blowdown pipe was plugged and 3 of 5 heat exchanger tubes were in use.

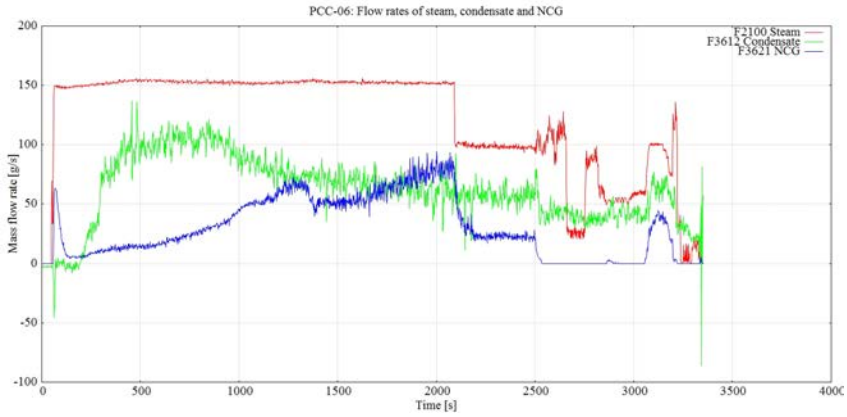


Figure 4. Steam (red), condensate (green) and Noncondensable (NCG, blue) flows in experiment PCC-06.

Results of aerosol tests

The total number concentration and the total mass concentration of particles are presented in table 4 for the aerosol experiments with two different steam mass flow rates. The measured number concentration is one or two orders of magnitude larger than the background aerosol concentration and thus the aerosol feed rate was sufficient for the study.

Table 4. The total number concentration of particles in aerosol experiments corrected to dry gas volume flow. BOA_cb_H130_A240 refers to PCC-10 experiment when steam mass flow rate was 130 g/s and air flow rate 240 l/min.

		BOA_cb_H90_A240	BOA_cb_H130_A240
Background concentration inlet	#/cm ³	2.7·10 ³	2.7·10 ³
Background concentration outlet	#/cm ³	4.4·10 ³	4.4·10 ³
Inlet concentration in dry gas	#/cm ³	6.1·10 ⁵	8.9·10 ⁴
Outlet concentration in dry gas	#/cm ³	2.2·10 ⁵	1.4·10 ⁴
Particle losses number basis	%	64	84
Particle mass flow at inlet	g/h	43	152
Particle mass flow at outlet	g/h	30	68
Particle losses mass basis	%	30	55

An example of the particle number size distributions at the PCCS inlet and outlet are presented in two graphs in Figure 5. Data is corrected with the primary dilution ratio, which were calculated as a function of time. The distributions were not corrected with humidity. Therefore, the absolute concentration appears to be larger at the PCCS outlet.

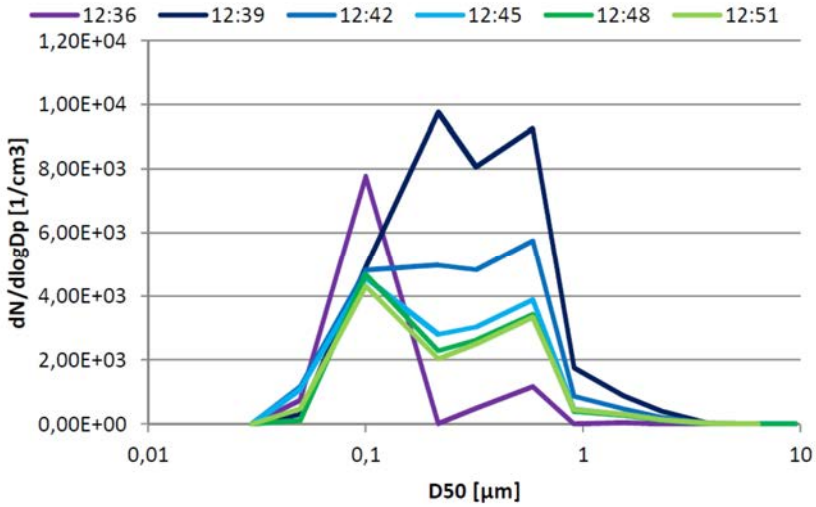
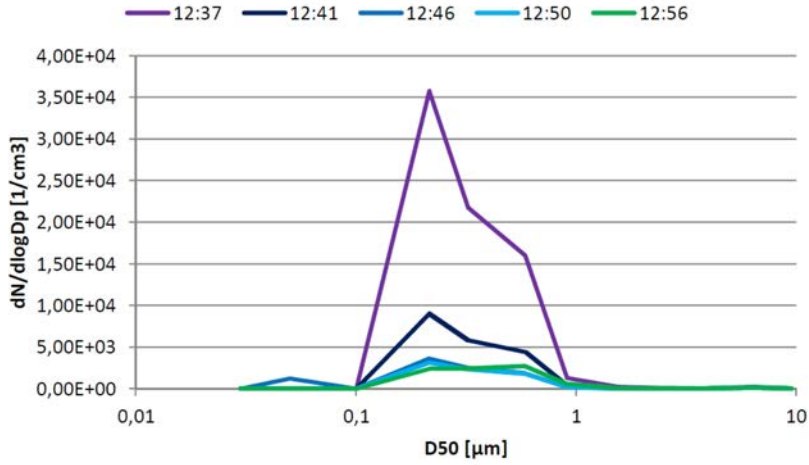


Figure 5. Particle number size distribution at the PCCS inlet (upper graph) and outlet (lower graph) in experiment PCC-10. Steam flow rate was 130 g/s and air flow rate 240 l/min. Data is corrected with the primary dilution ratio as a function of time (no humidity correction).

Conclusions

Six thermal hydraulic experiments and four aerosol behaviour experiments at PCCS-facility have been carried out during 2013-2014. The main objective of the experiments was to check the functionality of the aerosol measurement system attached to the PCCS facility as well as perform the actual aerosol experiments at LUT. The aerosol injection and sampling systems were provided by VTT. The experiments were conducted with three of five heat exchange tubes. The aerosol was clearly separable from background aerosol and the behaviour of particles in the PCCS and their effect on heat exchange can be analysed with the presented method.

References

- Forsman, J., Rantanen, P., Measurement setup and experiments on the particle behaviour in PCCS, VTT Research Report VTT-R-04018-14. 2014.
- Puustinen, M., Partanen, H., Räsänen, A., Purhonen, H., PPOOLEX Facility Description. Lappeenranta University of Technology. 2007. Technical Report POOLEX 3/2006.
- Tuunanen, J., Kouhia, J., Purhonen, H., Riikonen, V., Puustinen, M., Semken, R. S., Partanen, H., Saure, I., Pylkkö, H., General Description of the PACTEL Test Facility. Espoo: VTT. 1998. VTT Research Notes 1929. ISBN 951-38-5338-1.
- Purhonen, H., Passive Containment Cooling System Experiments: Preliminary Design of the PCCS Test Facility. Research Report EXCOP 3/2011.
- Yonamoto, T. Kondo, M. Nakamura, H., 2005. "Summary of the research project on horizontal heat exchanger for PCCS", JAERI. IAEA's Second Research Coordination Meeting on the CRP on Natural Circulation Phenomena, Modelling, and Reliability of Passive Safety Systems that Utilize Natural Circulation Oregon State University, Corvallis, Oregon, USA, Aug. 29 - Sep.2, 2005.

29. Environmental influence on cracking susceptibility and ageing of nuclear materials (ENVIS)

29.1 ENVIS summary

Ulla Ehrnstén¹, Juha-Matti Autio¹, Matias Ahonen¹, Pekka Moilanen¹, Mykola Ivanchenko¹, Santtu Huotilainen¹, Pertti Aaltonen¹, Aki Toivonen¹, Hannu Hänninen², Roman Mouginot², Teemu Sarikka², Antti Forsström², Tapio Saukkonen², Risto Ilola²

¹VTT Technical Research Centre of Finland Ltd
P.O. Box 1000, FI-02044 Espoo

²Aalto University, School of Engineering
P.O. Box 11000, FI-00076 AALTO

Abstract

The objective of the joint VTT – Aalto ENVIS project is to support safe operation of NPP's through increased understanding of the influence of light water reactor environments on the ageing and environmentally-assisted cracking (EAC) susceptibility of nuclear reactor materials. To meet these goals, several tasks are pursued dealing with thermal ageing, determination of low temperature crack propagation of Ni-based weld metals, characterisation of irradiated stainless steels and of austenitic nuclear components, investigating EAC initiation susceptibility in nuclear materials, designing new equipment for fuel clad biaxial creep testing etc. International co-operation is important as a tool to bring the latest knowledge to Finland and benchmark the scientific level of our research. Knowledge transfer and continuous education will secure uninterrupted availability of high-quality expertise for ageing management.

The ENVIS project comprises of totally twelve topics, and only selected main results from the ENVIS project are briefly presented in this article.

Introduction

The objective of the joint VTT – Aalto ENVIS project is to support safe operation of NPP's through increased understanding of the influence of light water reactor environments on the ageing and environmentally-assisted cracking (EAC) susceptibility of nuclear reactor materials. To meet the goals, several tasks are pursued. Crack initiation and its precursors are investigated using super-slow strain rate tests in simulated NPP environments followed by detailed characterisation of the test specimens showing that it is the strain gradient rather than the level of residual strain, which is important for SCC crack initiation [Ehrnstén, 2015]. Mock-ups and nuclear components are characterised to increase the knowledge of the characteristics of such material conditions. Understanding irradiation-assisted cracking (IASCC) is increased through characterisation of irradiated stainless steel materials including field samples. The effect of environment on the fracture behaviour is measured for nickel-based materials in hydrogenated water [Ahonen et al. 2014] (see also separate report in this volume). The role of thermal ageing of lean duplex stainless steels and of stainless steel weld metals are investigated showing that also stainless steel weld metals suffer from thermal ageing [Ehrnstén et al. 2012, Lucas et al. 2015]. Fuel clad research capabilities are improved by development of testing capabilities for biaxial creep testing, enabling investigations on irradiation creep. Knowledge transfer to the young generation is performed through everyday mentoring, teaching, updating the digital report archive, and by giving the project personnel possibilities to learn by doing [Hänninen & Kiesi (ed.), 2012]. Two MSc works has been performed within the ENVIS project; one on dissimilar metal welds [Mouginot, 2012] and one on the role of dynamic strain ageing on the fatigue behaviour of stainless steels [Apajalahti, 2013, Apajalahti et al. 2015]. The PhD work on low temperature crack propagation in Ni-base weld metals is also ready for review. The latest international knowledge is brought to Finland through active participation in international projects such as the EPRI 690 expert group and networks, e.g., the International Co-operative Group on Environmentally Assisted Cracking, and by delivering detailed travel reports. Participation in the NEA-CODAP (Component Operational Experience, Degradation and Ageing Programme) gives the Finnish NPP parties (regulator and licensees) access to an event and knowledge base, and to topical reports on selected important issues such as flow assisted corrosion [CODAP, 2013]. Participation in the activities of the Nugenia association has included development of an accelerated crack initiation technique [Toivonen 2013, Ehrnstén, 2014] and work towards a unified corrosion fatigue assessment methodology in Europe [Ehrnstén&Karlsen 2014, Solin 2013].

The ENVIS project comprises of totally twelve topics with sub-topics, and reporting all results is beyond the target of this volume. Selected main results from the ENVIS project are briefly presented in this article and the reader is referred to the SAFIR 2014 Interim Report [Simola, 2013], and to the public ENVIS reports and publications for further information.

Characterisation of NPP components and mock-ups

During the ENVIS project three different samples from nuclear components, which had been in operation were characterised to get a deep insight in factors affecting stress corrosion cracking. Two cases are summarised below, while the results from the third case, i.e., a sensitised Type 304 stainless steel pipe section are found in [Autio&Ehrnstén 2015]. Additionally, the results from mock-ups on dissimilar metal welds are summarised below.

Detailed investigations were performed on a BWR main steam gate valve piston made of Stellite 6 after 30 years of operation. The complicated Co-based microstructure is metastable and could therefore change due to thermal ageing resulting in formation of brittle phases. The investigations revealed no changes of the properties due to thermal ageing. However, selective oxidation, which is also a time dependent phenomenon, was observed, and this has obviously affected crack initiation, Figure 1. The results suggest that more failures of Stellite 6 components can be foreseen after long operation times. It is therefore recommended that similar cases are characterised instead of just replacing them, to confirm the observations, and to develop a proactive ageing management program for this material [Aaltonen 2013 a and b, Aaltonen et al. 2013].

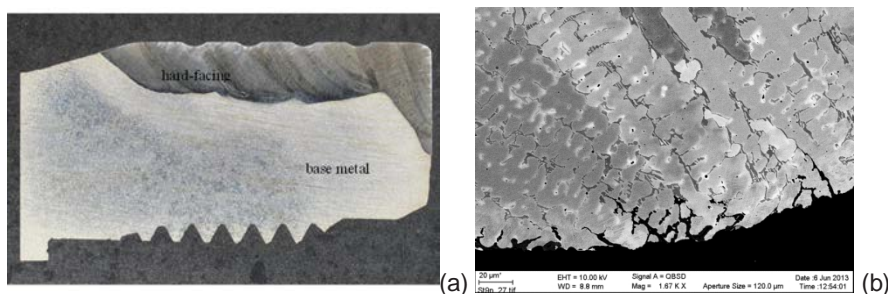


Figure 1. The welded Stellite 6 hard facing on the steam gate valve piston (a) had suffered from selective oxidation (b), increasing crack initiation susceptibility due to thermal stresses.

The second sample, made of Type 316L stainless steel, had been removed from a boiling water reactor (BWR) steam dryer inner roof plate, which had suffered from intergranular stress corrosion cracking (IGSCC) after only a few (1-2) years of operation. A non-homogeneous microstructure, with some α' -martensite in the mid-thickness of the plate as a consequence of deformation, was confirmed by SEM EBSD. Macro-segregation bands were observed with consequent fluctuations in the composition of especially Ni and Cr, Figure 2 a and b. Corresponding hardness difference over the bands was measured with a nano-hardness tester, Figure 2 c. Also very high surface hardness, obviously from surface grinding during manufacturing, was measured on both sides of the 6 mm thick plate. The non-homogeneous, macro-segregated microstructure is a result from continuous casting, which does not include upset forging as a manufacturing step. The non-homogeneous material and

the high surface hardness are both material characteristics which have increased this material's susceptibility to IGSCC. High residual stresses from welding, which were also very likely in this case, have also increased the IGSCC susceptibility of the plate. The thickness of the deformed layer with high hardness was so thin, that it would not be detected using conventional techniques, e.g. Rockwell C hardness, typically used for quality assurance during manufacturing [Autio&Ehrnstén 2014, Autio et al. 2014].

The material fulfilled all set requirements, but had characteristics increasing the EAC susceptibility. To mitigate the risk for IGSCC, due diligence must be taken at all steps of manufacturing and assembly. To ensure safe and economic nuclear power plant operation for 60 years and above, it is of utmost importance that nuclear materials fulfil stringent requirements and that assembly is performed using qualified methods.

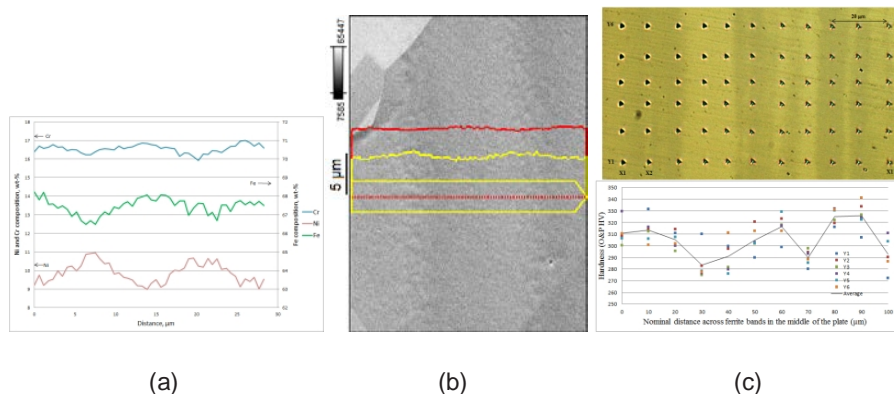


Figure 2. Image a) shows fluctuation in the composition over the macrosegregation bands (b), where Ni is marked as a yellow line and Cr as a red line. Fluctuations were also observed in nano-hardness values (c).

Dissimilar metal welds (DMW) between low-alloy steels (LAS), stainless steels (SS) and nickel-base alloys are key elements in the design and performance of conventional and nuclear power plants. However, they have often been related to the premature failure of components. Especially, the metallurgical changes occurring during post-weld heat treatment (PWHT) at the interface of ferritic/austenitic DMWs can affect greatly the mechanical properties. In modern PWRs, the substitution of filler metals Alloy 82 and 182 by Alloy 52 and 152 with higher chromium content, and new design using narrow-gap welding without any buttering layer, are made to improve the performance of the welds without reducing their structural integrity. However, metallurgical changes during PWHT can still lead to concerns for the long-time behaviour.

A narrow-gap weld dissimilar metal mock-up (NG-DMW), representing a typical modern PWR RPV nozzle (SA 508 clad with AISI 309L/308L) welded to a safe-end (Type 304) with Alloy 52 weld metal, was characterised in both as-welded and

heat-treated condition. It was compared to other samples, e.g. those provided by EPRI (Electric Power Research Institute) representing interfaces between Alloys 52, 52M and 152 and LAS. Characterisation of the interfaces and transition zones was done with optical and electron microscopy, micro- and nano-indentation tests.

All samples showed carbon depletion of the LAS near the fusion line, resulting from carbon migration to the weld metal and leading to lower hardness. The results showed that PWHT of the Alloy 52 mock-up weld resulted in increased carbon depletion and hardness drop in the LAS side, and the formation of a hard layer close to the fusion line inside the Alloy 52 weld metal, Figure 3. Inside the the weld metal, a planar growth zone free of precipitates and Type II boundaries are observed very close to the fusion line. A similar hardness peak was found in the Alloy 52M weld metals, due either to the featureless zone or to precipitates, but not in Alloy 152. When compared to the other weld metals, higher hardness was found in Alloy 152, followed by Alloy 52 and 52M, respectively. Alloy 152 showed different behaviour than Alloy 52 concerning carbon migration at the interface, with a reduced carbon-depleted zone (CDZ) and no hardness peak [Hänninen et al. 2012, Mougnot 2012, Mougnot&Hänninen 2013, Mougnot et al 2014a, Hänninen et al. 2012]. These microstructural features will also have an effect on the mechanical properties, which change within short distances [Nevasmaa et al. 2013]. More research is still needed to verify the ageing behaviour of this type of NGW and to develop further structural integrity assessment methods.

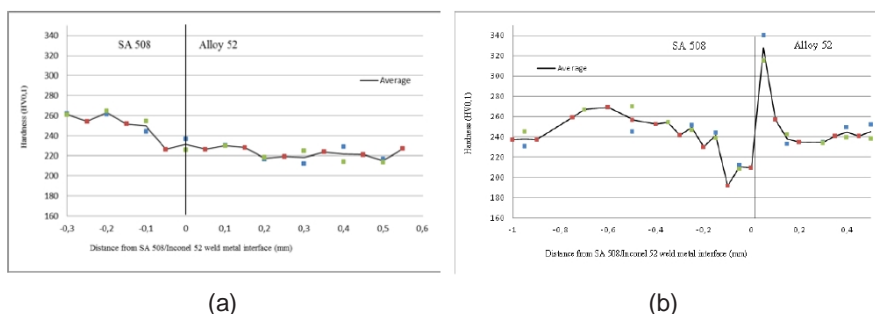


Figure 3. Comparison between microhardness (HV0.1) profiles across the SA 508/Alloy 52 interface of as-welded (a) and PWHT (b) NG-DMW.

Effect of irradiation on stainless steel microstructures

Irradiation changes the properties of stainless steels, which is the most common structural material used for reactor internals. The yield and ultimate tensile strength increase, while the elongation to fracture and fracture toughness decrease. These changes are due to the changes in the microstructure, i.e., radiation induced grain boundary segregation (RIS) and formation of irradiation induced defects. Both irradiated stainless steel materials, used in the OECD Halden project for e.g. crack growth rate experiments, and post-irradiation annealed materials have been characterised in the ENVIS project to add to the understanding of irradiation induced stress

corrosion cracking, IASCC [Ivanchenko 2014, Ivanchenko et al. 2014, Karlsen 2011 a and b, Karlsen et al. 2014, Pakarinen 2012b, c and d].

Additionally, a core basket bolt from a VVER-plant, with observed IASCC after a relatively low dose of 2.7 dpa, was investigated in ENVIS, and the results confirmed that IASCC, as other forms of SCC, is a combination of material, environment and stress [Ehrnstén, Kytömäki & Hietanen 2011, Ehrnstén et al. 2013, Keinänen 2013, Pakarinen 2012a, Simola, 2013].

The effect of post-irradiation annealing (PIA) on radiation-induced segregation (RIS) at the grain boundaries of 7.7 dpa AISI 304 stainless steel was examined using analytical transmission electron microscopy (ATEM). The grain boundary profiles and the irradiation damage were analysed in the as-irradiated state and after PIA of 6 h at 500 °C and after 25 h at 500°C and 550°C. As a main conclusion from the TEM examinations, the effects of PIA were found to be relatively small after only 6 hours, while after 25 h of PIA at both 500 and 550°C, RIS was almost recovered and only marginal deviation in chemical composition was found near the GBs. The as-irradiated state showed extreme RIS values of Si 4.9 wt%, Cr 14.7 wt%, Ni 23.4 wt%, and P 1.4 wt%, while upon PIA for 6 h the extreme values for RIS were Si 3.9 wt%, Cr 16.0 wt%, Ni 21 wt%, and P 0.9 wt%. After 6 h annealing at 500°C dislocation loops start to grow, while dislocation density remains of the same order of magnitude. After annealing for 25 h at 500°C the average size of dislocation loops remains nearly the same, while dislocation density was reduced almost by one fold. In the areas where dislocation density was found to be the lowest some features, which can most likely be attributed to stacking fault tetrahedra (SFT) were found.

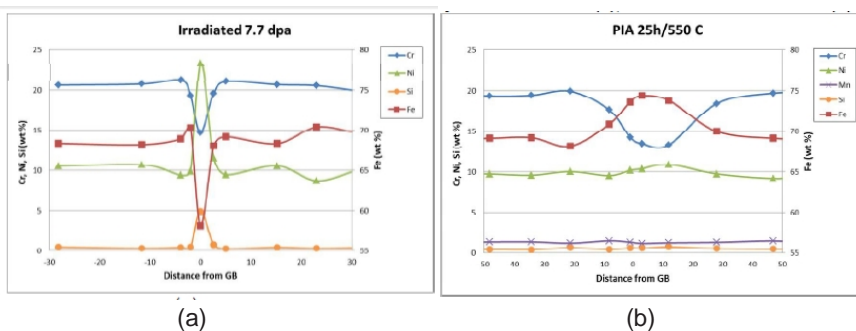


Figure 4. Examples of EDS profiles at a grain boundary in as-irradiated condition and after PIA at 550°C/25h.

Annealing at even higher temperature (550°C) affected the average size of the dislocation loops, making them almost twice as large as well as resulting in a very broad distribution of dislocation loop sizes. Density of dislocations is also reduced by one fold in comparison to the as-irradiated condition and leads to formation of SFT's, which were consistently found in the specimen. None of the applied PIA treatments had caused formation of voids.

Development of new equipment for biaxial creep testing of fuel clad materials

The Crebello equipment was developed for biaxial creep testing of fuel clad materials [Moilanen, 2014]. The possibility to either move or copy the equipment to the Centre for Nuclear Safety (CNS) for testing or irradiated materials was taken into consideration in the design. Such measurements would give new data for life time assessment on irradiation creep [Tähtinen&Huotilainen, 2012]. The pneumatic loading technology provides important benefits and has already successfully been applied for material testing in different environments. Pneumatic servo-controlled material testing system has earlier been used to perform fracture toughness, corrosion fatigue, tensile and electrochemical measurements in gas, high temperature aqueous, hydrogen and irradiation environments [Huotilainen, 2014]. The main advantages of the pneumatic testing system are the sensitivity and the possibility to separate the material testing equipment and the control system by long (> 30 m) pressure tubes without decreasing the test load accuracy.

The loading frame is equipped with two pneumatic loading units, i.e., Alloy 625 bellows. These bellows can perform well controlled and adjustable axial push/pull load for the specimen during the test. Axial strain and hoop strain are measured with the mechanical extensometers which are placed on the tubular specimen body, Figure 5. The maximum operational temperature for the selected extensometers is 540°C, but extensometers are available for even higher temperatures. The main test load control, i.e., pressure control for the bellows is performed with the PLC (Programmable Logic Control) system. Different feedback signals for the PLC control can be used, i.e., pressure, bellows displacement, axial or/and hoop strain and tube specimen internal pressure or a combination of these signals. Tube pressurising by argon gas is done by a special compressor which is equipped with its own pressure controlling (PLC) system. The bellows controlling PLC and the compressor controlling the PLC are connected together, to fulfil the main safety requirements for the high pressure tube creep tests. The maximum pressure for the pressure control of the tube is 690 bars.

The equipment was designed, manufactured and tested for functionality in the ENVIS project and has already been employed in other projects. The accuracy is very good, Figure 6, and performed long-term tests of several months, have further proven the reliability and accuracy of the equipment.

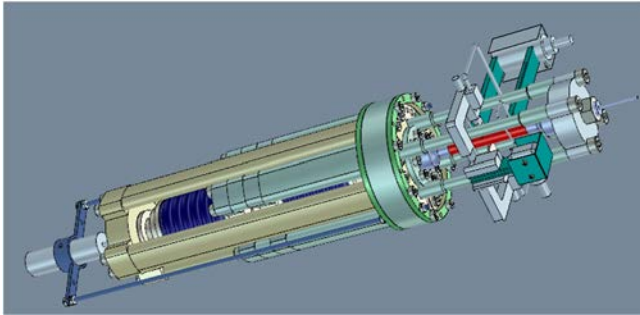


Figure 5. 3D drawing of the Crebello main parts. The specimen has been coloured red.

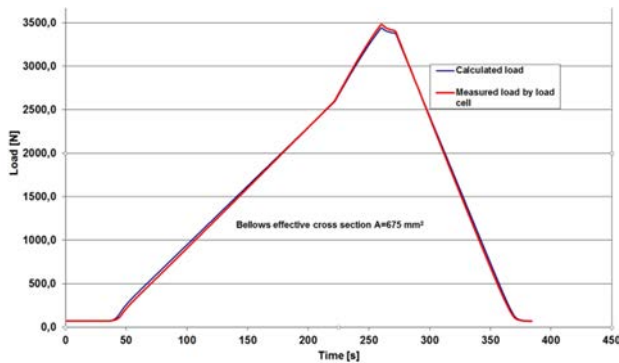


Figure 6. The load and the pressure of the pneumatic loading unit as a function of time.

Acknowledgement

The funding of the ENVIS project by VYR (Finnish Nuclear Waste Fund), VTT (Technical Research Centre of Finland), SSM (Swedish Radiation Safety Authority), Aalto University, Fortum Oyj and OECD Halden project as well as the licensees positive attitude towards letting the project use materials from their plants and the profound support from the SAFIR 2014 Support Group 6, is highly appreciated. The project team is acknowledged for their devoted work and eagerness to learn.

References

- Aaltonen, P. 2013a. Ageing degradation of a hard-facing alloy after long-term exposure to BWR conditions. VTT Research Report VTT-R-00216-13, 18.2.2013.28p.
- Aaltonen, P. 2013b. Ageing degradation of hard-facing alloy after long-time exposure to BWR conditions II. Research Report VTT-R-06904-13, 22.11.2013. 29p.
- Aaltonen, P. et al. 2013. Ageing degradation of hard-facing alloy after long-time exposure to BWR conditions. 16th International Conference on Environmental Degradation of Materials in Nuclear Power Systems – Water Reactors, NACE, August 11 – 15, 2013, Asheville, NC, USA.
- Ahonen, M. et al. 2013. Low temperature crack propagation (LTCP) susceptibility of nickel-based alloy 182, 152 and 52 weld metals in PWR primary water. 16th International Conference on Environmental Degradation of Materials in Nuclear Power Systems – Water Reactors, NACE, August 11 – 15, 2013, Asheville, NC, USA.
- Apajalahti, H. 2013. Effect of Non-monotonic Cyclic Loading under Dynamic Strain Ageing Conditions on Mechanical Properties of Austenitic Stainless Steels. MSc Thesis, Aalto University 2013. 111p.
- Apajalahti, H. et al. 2015. Effects of cyclic loading under dynamic strain aging conditions on mechanical properties of AISI 304L austenitic stainless steel. Submitted to Materials Science and Engineering A.
- Autio, J-M. & Ehrnstén, U. 2014 Microstructural characterisation of a Type 316L material removed from a BWR steam dryer. VTT-R 00500-14, 30.01.2014. 31p.
- Autio J-M. et al. 2014. Investigations of a Type 316L steam dryer plate material suffering from IGSCC after few years in BWR's. Proceedings of the International Symposium Fontevraud 8, 2014, SFEN Technical Section, Paper 76-T03.
- Autio, J-M & Ehrnstén, U. 2015. DL-EPR measurements on a sensitised Type 304 stainless steel pipe section. VTT-R-05905-14, 8.1.2015. 20p.
- CODAP Topical report: Flow accelerated corrosion (FAC) of carbon steel & low alloy steel piping in commercial nuclear power plants. NEA/CSNI/R (2013) NN.
- Ehrnstén, U. & Aaltonen, P. 2012. Literature report on thermal ageing of selected nuclear materials. VTT-R-00431-12, 5.3.2012. 51p.

- Ehrnstén, U., Kytömäki, O. & Hietanen, O. 2011. Investigation on core basket bolts from a VVER 440 power plant. 15th Symposium on Environmental Degradation of Materials in Nuclear Power Systems - Water Reactors. 7-12.8.2001. Colorado Springs, CO, USA.
- Ehrnstén U. et al. 2013 Investigations on a core basket bolt from a VVER 440 power plant. *Engineering Failure Analysis* 33 (2013) 55 – 65.
- Ehrnstén, U. 2014. Status report on project MICRIN, Mitigation of Crack Initiation. VTT Research Report VTT-R-05439-14, 24.11.2014. 7p.
- Ehrnstén, U. & Karlsen, W. 2014. From INCEFA to INCEFA PLUS - a summary report on in-kind contributions for corrosion fatigue EU-project preparation. VTT Research Report VTT-R-05440-14, 24.11.2014, 24p.
- Ehrnstén, U. 2015. Super slow rate strain rate testing in simulated LWR conditions. VTT Research Report VTT-R-06114-14, 15.1.2015. 38p.
- Lucas, T. et al. 2015. Effects of thermal aging on materials properties, stress corrosion cracking and fracture toughness of AISI 316L weld metal. Submitted to *Journal of Nuclear Materials*.
- Huutilainen, S. 2014. Melodie glove box development. VTT Research Report VTT-R-06111-14. 19.12.2014, 19p.
- Hänninen, H. Kiesi, T. (ed). 2012. Materials science and technology – nuclear material, advanced course. Postgraduate seminar on engineering materials, seminar papers, Kon-67.5100, September 5-6, 2012.. Aalto University, Department of Engineering Design and Production.
- Hänninen H. et al. 2012. Characterization of dissimilar metal welds and their typical microstructural features. Presentation at the EPRI MRP Alloy 690/52/152 Expert Panel meeting, 29 – 30 November 2012, Tampa, Florida, USA.
- Ivanchenko, M. 2014. TEM examination of the effect of post-irradiation annealing on 7.7 dpa AISI 304L stainless steel. VTT Research Report VTT-R-05957-14, 19.12.2014. 17p.
- Ivanchenko, M. et al. 2014. TEM examination of the effect of post-irradiation annealing on 7.7 dpa AISI 304L stainless steel. Enlarged Halden Programme Group Meeting, 2014.
- Karlsen, W. 2011a. Grain boundary segregation in a 24 dpa 304 stainless steel after post-irradiation annealing. VTT Research Report VTT-R-03033-11, 23.8.2011. 27 p.

- Karlsen, W. 2011b. Grain Boundary Segregation in a 24 dpa 304 Stainless Steel After Post-Irradiation Annealing. Enlarged Halden Programme Group Meeting 2011. 3-7.10.2011, Sandefjord, Norway.
- Karlsen, W. 2012. The role of non-monotonic loading in EAC - a literature review. VTT Research Report VTT-R-00867-12, 17.2.2012. 71p.
- Karlsen, W. et al. 2014. TEM Examination of the Effect of Post-Irradiation Annealing on 7.7 dpa AISI 304L Stainless Steel. Proceedings of the International Symposium Fontevraud 8, 2014, SFEN Technical Section, Paper 70-T02.
- Keinänen, H. 2013. Stress analysis of core basket bolt. VTT-R-00443-13, 22.1.2013. 13p.
- Moilanen, P. & Ehrnstén, U. 2014. The biaxial creep testing device. VTT Research Report VTT-R-01863-14, 6.8.2014. 23p.
- Mouginot, R. 2012. Microstructures of nickel-base alloy dissimilar metal welds. Aalto University, School of Engineering, Department of Engineering Design and Production, Engineering Materials, Master thesis Kon-67, 5.12.2012. 186 p.
- Mouginot, R. & Hänninen, H. 2013. Microstructures of nickel-base alloy dissimilar metal welds. Aalto ST 5/2013, 2013. 178 p.
- Mouginot, R. et al. 2014a Characterization of a Ni-base NG-DMW weld of modern PWR. Proceedings of the International Symposium Fontevraud 8, 2014, SFEN Technical Section, Paper 189-T05.
- Mouginot, R. et al. 2014b. Thermal ageing and ordering of Alloy 690. Aalto University work report, 18.12.14. 28p.
- Nevasmaa, P. et al. 2013. Fracture mechanical characterization of ferrite – austenite dissimilar metal welds (DMWs) for high temperature service in view of metallurgical mis-match. International Conference on Fast Tools for Condition and Life Assessment of Power Plants. Baltica IX, June 11- 13, 2013.
- Pakarinen, J. 2012a. ATEM characterization of a failed core basket bolt removed from Loviisa NPP Unit, VTT-R-00647-12, 27.3.2012. 19p.
- Pakarinen, J. 2012b. TEM examination of the effect of post-irradiation annealing on 7.7 dpa AISI 304 stainless steel. VTT-R-05228-12, 4.10.2012. 9p.
- Pakarinen, J. 2012c ATEM characterization of a failed core basket bolt removed from Loviisa NPP Unit 1 – part II. VTT-R-05230-12, 6.10.2012. 22p.
- Pakarinen, J. 2012d. ATEM characterization of a slice from a 15 dpa AISI 316 stainless steel baffle bolt. VTT-R-05229-12, 8.10.2012. Pakarinen, J. et al.

2013. Microstructural characterization of irradiated baffle bolts removed from a Finnish VVER and a French PWR. 16th International Conference on Environmental Degradation of Materials in Nuclear Power Systems – Water Reactors, NACE, August 11 – 15, 2013, Asheville, NC, USA.

Simola, K. (ed.). 2013. SAFIR2014 The Finnish research Programme on Nuclear Power plant safety 2011-2014, Interim report. VTT Technology 80. Pp. 268 – 282.

Solin, J. 2014. Effects of temperature, time and environment in fatigue of stainless steel. VTT-R-00633-14, 30.1.2014. 48 p.

Toivonen, A. 2013. BWR SCC test acceleration by testing in SCW. Research Report VTT-R-07971-13, 15.11.2013. 37 p.

Tähtinen, S. & Huotilainen, S. 2012. Review on Irradiation Creep. VTT Research Report VTT-R-02354-12. 29p.

29.2 Low Temperature Crack Propagation (LTCP) Susceptibility of Nickel-Based Alloy 182, 82, 152 and 52 Weld Metals

Matias Ahonen¹, Ulla Ehrnsten¹, Tapio Saukkonen², Olga Todoshchenko² and Hannu Hänninen²

¹VTT Technical Research Centre of Finland Ltd
P.O. Box 1000, FI-02044 Espoo

²Aalto University
School of Engineering
P. O. Box 14200, FI-00076 Aalto, Finland

Abstract

The effect of microstructure on the Low Temperature Crack Propagation (LTCP) susceptibility of nickel-based Alloy 182, 152 and 52 weld metals was studied comparing the obtained results from J-R tests, thermal desorption spectroscopy (TDS) and scanning electron microscope (SEM) fractography. The single edge bend (SE(B)) specimens were tested in hydrogenated (100, 30 and 5 cm³ H₂/kg H₂O) low temperature (55 °C) water with and without exposure to high temperature hydrogenated PWR water (24 h or 30 days at 300 °C) prior to loading at 55 °C. The obtained J-R test results show that Alloy 182 is the most susceptible nickel-based weld metal to LTCP, whereas Alloy 52 retains its high fracture resistance in hydrogenated water with moderate hydrogen content. The results obtained for all-weld metal Alloy 52

showed, however, a clear reduction of fracture resistance when tested at a high hydrogen content ($100 \text{ cm}^3 \text{ H}_2/\text{kg H}_2\text{O}$), whereas narrow gap mock-up dissimilar metal weld (DMW) Alloy 52 showed to be less susceptible to LTCP in the corresponding environment. Hydrogen content measurements show that bulk hydrogen concentrations of Alloy 182 and 152 weld metal samples decrease during the high temperature water exposure, even when exposed to water containing $30 \text{ cm}^3 \text{ H}_2/\text{kg H}_2\text{O}$. Also the fracture resistance values of Alloys 182 and 152 are improved after high temperature water exposure. Microstructural characterisation of fracture surfaces was performed using SEM and energy-dispersive X-ray spectroscopy (EDS). A clear relation between the low fracture resistance values and intergranular/interdendritic type of fracture was observed. The effect of grain boundary carbides and their trapping properties are discussed based on obtained SEM/EDS and TDS results and a model was applied in order to determine the activation energies for hydrogen desorption of Alloys 182 and 52.

Introduction

This report summarizes the results of the research on low temperature crack propagation phenomenon performed within the ENVIS project. Some earlier data has also been included in the graphs showing the average values for fracture resistance of nickel-based weld metals. This report also presents some essential results that will be included in the upcoming doctoral thesis by the first author. The experimental procedures and the test results are presented in more detail in scientific publications [1-4] and in VTT Research Reports [5-8].

Low temperature crack propagation (LTCP) is widely considered as a hydrogen-induced embrittlement phenomenon that has been observed in laboratory conditions for various nickel-based alloys at the temperature range of ~ 50 to $150 \text{ }^\circ\text{C}$ in hydrogenated water. A sharp pre-crack as well as high load and slow loading rate are required for LTCP to initiate [9,10]. However, it has been shown that the environment causes a substantial reduction in initiation toughness of Alloy 82H due to a hydrogen-induced transgranular fracture mechanism [10]. Although LTCP could have severe safety implication, e.g. for dissimilar metal welds (DMW) no LTCP incidents have been reported in open literature to date.

Low temperature stress corrosion cracking (SCC), later named as LTCP, was first reported to occur in Alloy X-750 fasteners by Grove and Petzold [11]. The LTCP behaviour of solid-solution strengthened Alloys 600 and 690 and their weld metals has been extensively studied over the past 15 years by Mills and Brown. Their results have later been confirmed by several other researchers. Mills et al. [9] observed that LTCP is a hydrogen-induced phenomenon. Their findings demonstrate that the change in fracture mechanism from ductile dimple to more brittle intergranular (or interdendritic) cracking occurs regardless of the source of hydrogen.

Hydrogen trapping may have a crucial effect on LTCP behaviour of nickel-based alloys where various types of inclusions and carbides are present [12]. Different material defects can act as either hydrogen traps or hydrogen repellers [13]. Hydro-

gen traps can be divided in two categories: attractive traps and physical traps. Attractive traps are regions of the lattice where hydrogen atoms are subjected to an attractive force of various origins such as electronic force, tensile stress field, thermal gradient or chemical potential gradient. A physical discontinuity may create a location where it is more energetically favourable for hydrogen to stay [13]. Yonezawa et al. [14] observed that coherency of the carbides is important considering the IGSCC susceptibility of Alloy X-750 since only the material with incoherent carbides showed IGSCC susceptibility in hydrogenated (up to 40 cm³ H₂/kg H₂O) high temperature simulated PWR water. The incoherent precipitates trap more hydrogen and thus the precipitation conditions on grain boundaries dominate IGSCC susceptibility.

Materials and Methods

Two types of materials have been used to manufacture the SE(B) test specimens for fracture toughness, J-R testing, i.e., all-weld metal blocks and dissimilar metal weld mock-ups. All-weld metal blocks were fabricated by welding Alloy 182, 82, 152 and 52 weld metals on crossed steel bars. In DMW mock-ups the studied weld metals consist of Alloys 182, 152 and 52. The test materials are described in more detail in [5].

The fracture toughness tests were performed using pneumatic servo-controlled loading device and the crack growth was measured using potential drop (PD) method. The J-R curves were calculated according to the standard test method for measurement of fracture toughness, ASTM E 1820 – 01. Since the specimens manufactured from an inhomogeneous material do not always meet all the requirements of the standard, the results obtained from the fracture toughness testing are reported as fracture resistance J_Q instead of fracture toughness J_{IC} , which is, according to the ASTM 1820 – 01 standard, a size-independent value of fracture toughness. An in-house “Cracklength” software was used to determine the actual crack lengths after the tests.

The water temperature in the autoclave tests was 55 °C, and in some tests pre-exposure for 30 days or 24 hours to high temperature water (300 °C) was employed prior to loading of the specimens at 55 °C. The applied loading rate was 0.1 mm/h in all tests. 30 days pre-exposures were conducted with hydrogen contents 5 and 30 cm³ H₂/kg H₂O and 24 hours pre-exposure with 100 cm³ H₂/kg H₂O. In all the pre-exposure tests the autoclave was cooled from 300 to 55 °C as fast as possible (in about 11 h), which simulates the procedures of operating plants rather well. The specimens were loaded immediately when the target temperature 55 °C was reached. Boric acid H₃BO₃ (200 ppm) and lithium hydroxide LiOH (2.1 ppm) was added in the water in all the tests.

Thermal desorption spectra (TDS) measurements were carried out with a thermal desorption apparatus designed and assembled at Aalto University. TDS curves were determined for samples manufactured from DMW Alloys 182, 152 and 52. Measurements were first performed for materials in as-welded condition and after pre-exposure to hydrogenated high temperature (300 °C) water. The applied hydrogen

contents in pre-exposures were 5 and 30 cm³ H₂/kg H₂O. TDS curves were also determined for Alloy 182 and 52 DMW samples after material specific post-weld heat treatments (PWHT). The bulk hydrogen measurements for DMW samples of Alloys 182, 152 and 52 were performed using hydrogen measurement system of Leybold-Heraeus.

Overview of the J-R test results

Clear and systematic reduction of fracture resistance due to hydrogen was observed in the J-R tests conducted on nickel-based Alloy 182, 82, 152 and 52 weld metals as illustrated in Figure 1. Alloy 182 exhibits the lowest average J_Q values in hydrogenated water (30 and 100 cm³ H₂/kg H₂O). Addition of 30 cm³ H₂/kg H₂O hydrogen lowers the fracture resistance of Alloys 152 and 82, although not dramatically. Alloy 52 does not show a measurable reduction of fracture resistance when tested with 30 cm³ H₂/kg H₂O hydrogen. When tested with higher hydrogen content (100 cm³ H₂/kg H₂O) hydrogen has a clear effect in some Alloy 52 specimens while some specimens retain high fracture resistance and show no signs of LTCP.

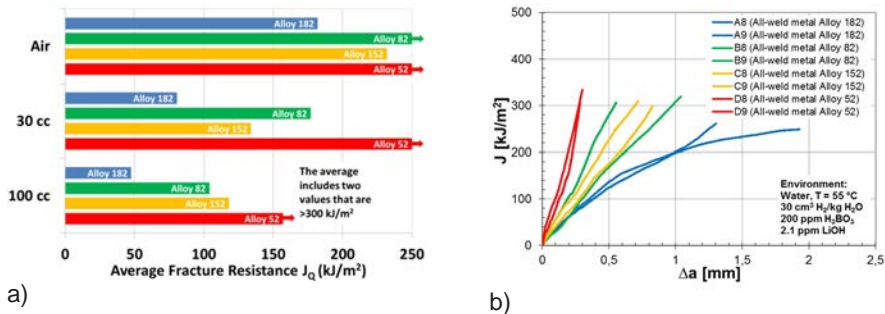


Figure 1. In a) average fracture resistance (J_Q) values for as-welded Alloys 182, 82, 152 and 52 tested in room temperature air and in 55 °C water (200 ppm H₃BO₃ and 2.1 ppm LiOH) with hydrogen contents of 30 and 100 cm³ H₂/kg H₂O. The J-R curves obtained for all-weld metal specimens from the tests with 30 cm³ H₂/kg H₂O are presented in b).

The effect of pre-exposure on fracture resistance

The J-R –test results obtained for Alloys 182 and 152 after pre-exposure in 300 °C hydrogenated water are consistently higher than those obtained in the same test environment without pre-exposure as shown in Figure 2.

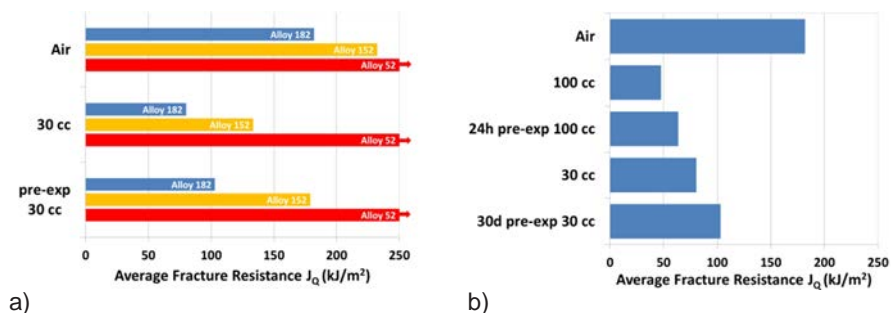


Figure 2. The average J_Q results for Alloys 182, 152 and 52 obtained in air and in low temperature water with 30 cm³ H₂/kg H₂O with and without pre-exposure to high temperature water presented in a). The results obtained for Alloy 182 in air and in low temperature water with 100 and 30 cm³ H₂/kg H₂O shown in b).

The results for Alloys 182, 152 and 52 tested in air and in low temperature water with 30 cm³ H₂/kg H₂O (= cc in the figures) with and without pre-exposure to high temperature water are presented in a). The results obtained in air and in low temperature water with 100 and 30 cm³ H₂/kg H₂O for Alloy 182 are presented in b). Alloy 52 does not show measurable susceptibility to LTCP with hydrogen content 30 cm³ H₂/kg H₂O, neither with nor without pre-exposure to high temperature water.

The effect of post-weld heat treatment on fracture resistance

The J-R –test results obtained for Alloys 182 and 52 after PWHT (Figure 3) are somewhat similar to the results obtained for as-welded (AW) specimens (Figure 1). The fracture resistance was not significantly affected by the PWHT, although the obtained average J_Q values for PWHT specimens were slightly below the ones obtained for the as-welded DMW specimens. However, although Alloy 182 shows slightly lower J_Q values in PWHT condition, the J_{1mm} and tearing resistance $T_{0.5mm}$ values after PWHT are slightly higher than those obtained for AW specimens when tested in hydrogenated low temperature water (30 and 100 cm³ H₂/kg H₂O), as shown in Figure 3 b).

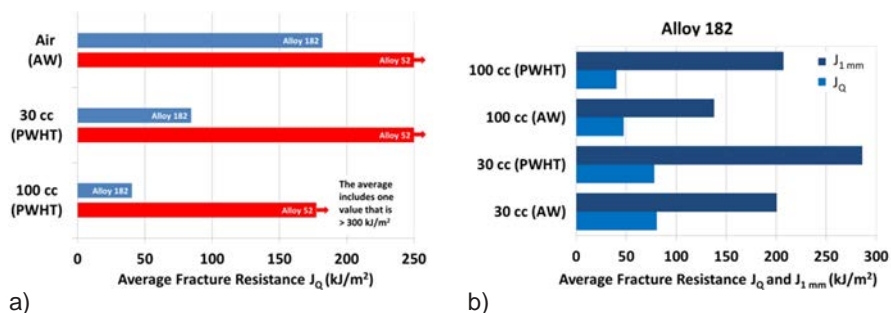


Figure 3. J-R test results for PWHT specimens of DMW Alloy 182 and 52 in a). Comparison of J_Q (light blue) and J_{1mm} (dark blue) values obtained for AW and PWHT DMW Alloy 182 in b).

Hydrogen content measurements

Results from the hydrogen desorption measurements are presented in detail in [1]. The studied materials were DMW Alloys 182, 152 and 52. The main observation was that pre-exposure decreases the hydrogen content of Alloy 182 and 152 weld metals. In the case of Alloy 52 the pre-exposure slightly increases the hydrogen content of the material. The as-welded hydrogen content of Alloy 52 was significantly lower than that of Alloys 182 and 152. The hydrogen content measurements indicate that the equilibrium hydrogen content of Alloy 52 in 300 °C hydrogenated water (30 cm³ H₂/kg H₂O) is higher than the as-welded hydrogen content of the material and thus the hydrogen content increases due to pre-exposure. The hydrogen desorption measurements were also applied in determining the activation energies of hydrogen desorption from different trapping sites of Alloys 182 and 52 (Figure 4). The activation energies were determined according to the model by Lee et al. [15]. According to the results it appears that hydrogen trapping in Alloy 182 is a) dominated by a single type of trap whereas in Alloy 52, b) there are two different trapping sites that both exhibit a lower activation energy for hydrogen desorption than that of Alloy 182.

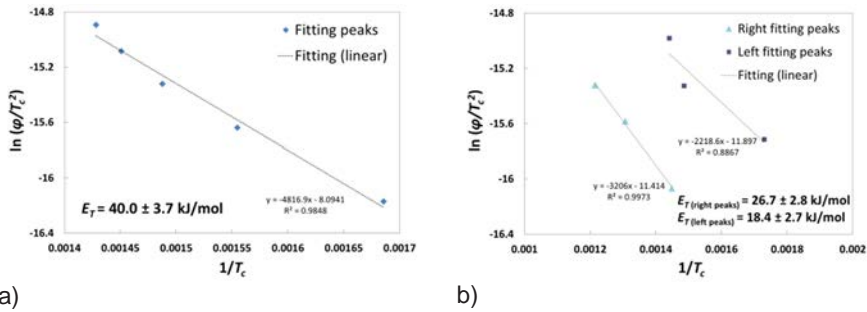


Figure 4. Determination of the activation energies and their 95% confidence intervals for hydrogen desorption from the ramped TDS results for as-welded DMW Alloy 182 in a) and PWHT + 30 cc pre-exposed DMW Alloy 52 in b).

Cracking path of Alloy 52

SEM images of the intergranular/interdendritic (IG/ID) fracture surfaces of Alloy 52 show that the IG/ID cracking deviates from one specimen half to another resulting in a carbide-rich fracture surface layer on the both mating halves of the specimen (Figure 5).

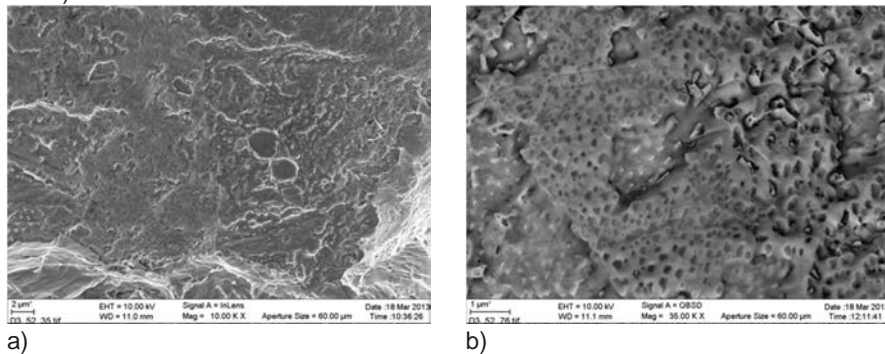


Figure 5. Fracture surface structure of Alloy 52 specimen tested in low temperature water with 100 cm³ H₂/kg H₂O. A moderate magnification SEM image reveals the fracture surface structure, in a). A higher magnification SEM image in b) illustrates a high density of carbides in the structure and signs of plastic deformation on the areas where the carbides have been detached and left on the mating half of the specimen.

The carbides are mostly Cr-rich M₂₃C₆ -type carbides. A 3D SEM analysis (Figure 6) shows that the surface layer thickness is in the same range with the largest observed carbide size (about 300 nm). According to Kekkonen et al. [16], M₂₃C₆ carbide growth causes a formation of a de-alloyed zone in Type 304 type austenitic stainless steels due to grain boundary migration and chromium depletion (Figure 7).

This kind of a zone would explain the complex appearance of the cracking path if the crack propagation alternates between the two boundaries of the de-alloyed zone.

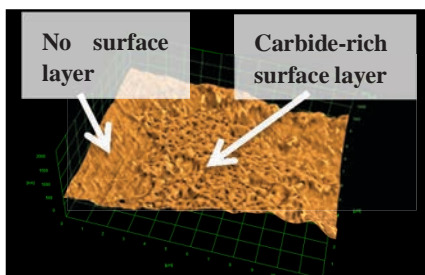


Figure 6. A 3D SEM image of an area of the fracture surface of all-weld metal Alloy 52 showing areas with and without carbide-rich surface layer.

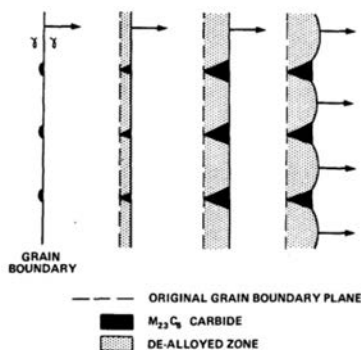


Figure 7. A schematic presentation of the various stages of $M_{23}C_6$ carbide growth in AISI 304 stainless steel during grain boundary migration [16].

Discussion

The fracture resistance of nickel-based Alloy 182/82 and Alloy 152/52 weld metals decreases in hydrogenated low-temperature water, as has been previously reported by a few researchers but most extensively by Mills and Brown. Even low hydrogen contents ($5 \text{ cm}^3 \text{ H}_2/\text{kg H}_2\text{O}$) are sufficient to cause intergranular/interdendritic cracking and decrease the fracture resistance of Alloy 182 [17]. The results of this study confirm the degrading effect of hydrogen on fracture resistance of nickel-based weld metals. It has also been shown in this study that higher hydrogen content results in lower J_Q values. All the studied nickel-based weld metals showed a similar trend, regarding the effect of hydrogen content of the water, but to a different extent. Thus, a general observation is that fracture resistance of all the studied nickel-based alloys is decreased by hydrogenated low temperature water, although in the case of Alloy 52 large hydrogen contents are needed in order to induce LTCP. Alloy 182 exhibits the highest susceptibility to LTCP whereas higher chromium Alloys 152 and 52 exhibit higher fracture resistance values in general. However, when tested with $100 \text{ cm}^3 \text{ H}_2/\text{kg H}_2\text{O}$, all-weld metal Alloy 52 specimens showed extensive IG cracking and J_Q values that were similar to those of Alloy 182.

The effect of pre-exposure at the reactor operation temperature to the LTCP susceptibility has not been extensively studied thus far. Herms et al. [17] reported that pre-exposure at $320 \text{ }^\circ\text{C}$ for 250 or 1000 h did not have a significant effect on the LTCP behavior of Alloys 182 and 152 at low hydrogen contents ($3\text{-}5 \text{ cm}^3 \text{ H}_2/\text{kg H}_2\text{O}$). In the present study low hydrogen content ($5 \text{ cm}^3 \text{ H}_2/\text{kg H}_2\text{O}$) pre-exposure (30 days,

about 720 h) was studied for DMW specimens of Alloy 152, and the attained results were somewhat similar with or without the pre-exposure, although there was a slight increase in the average fracture resistance values due to the pre-exposure. Pre-exposure was studied with a moderate hydrogen content ($30 \text{ cm}^3 \text{ H}_2/\text{kg H}_2\text{O}$) for DMW specimens of Alloys 182, 152 and 52 and the results obtained with and without pre-exposure are compared in Figure 2. Alloys 182 and 152 showed a slight increase of the fracture resistance due to high temperature pre-exposure. DMW material NGW Alloy 52 was also studied in the same environments with Alloys 182 and 152 but no effects of the environment could be measured due to the limitations of the test equipment.

When all the attained results for the different pre-exposures (24 h and 30 days at $300 \text{ }^\circ\text{C}$) with different hydrogen contents of the water are compared with the results obtained without pre-exposure, a clear trend can be observed. It seems that at least for Alloys 182 and 152 the high temperature water pre-exposure increases the fracture resistance of the material regardless of the hydrogen content of the environment. This result indicates that the hydrogen content of the water and the amount of trapped hydrogen in the material both play important roles in the reduction of the fracture resistance.

The effect of Post-Weld Heat Treatment (PWHT) was studied for DMW specimens of Alloys 182 and 52. Hydrogen contents of 30 and $100 \text{ cm}^3 \text{ H}_2/\text{kg H}_2\text{O}$ were applied. The fracture toughness behaviour of the different materials has been evaluated in this study mainly by comparing fracture resistance J_Q values. However, J_Q (or J_{IC}) is a parameter that is very sensitive to the pre-crack tip location relative to the microstructure and also to possible crack propagation measurement inaccuracy. Therefore, J_{1mm} , i.e. the value of J-integral at Δa of 1 mm, is sometimes used for DMW materials and basically it can be used for any kind of structural materials to describe the fracture resistance of a specimen because the dJ/da of the J-R curve typically decreases with increasing Δa . When comparing the J_Q values of Alloy 182 in AW and PWHT conditions, the AW samples exhibit somewhat lower susceptibility to hydrogen-induced LTCP in both applied environments, although the difference in J_Q between AW and PWHT material state is marginal. On the contrary, PWHT specimens of Alloy 182 exhibit higher fracture resistance when J_{1mm} values are considered. This is due to a higher tearing resistance of PWHT specimens and also due to slightly different shape of the J-R curve observed for AW and PWHT specimens, which may be related to the different mechanism of fracture observed at some areas in the SEM study (TG vs. IG/ID). When the fracture occurs partly with a transgranular mechanism, as in the case of DMW Alloy 182, the energy required for initiation of the stable crack growth is not significantly different than when the fracture occurs with an intergranular mechanism. However, in specimens where TG fracture occurs alongside with IG/ID fracture the tearing resistance is higher than in specimens that exhibit fully IG/ID fracture in the J-R test.

References

1. Ahonen, M., Ehrnstén, U. & Hänninen, H. The Effect of Microstructure on Low Temperature Crack Propagation (LTCP) Susceptibility of Nickel-Based Alloy 182, 152 and 52 Weld Metals in PWR Primary Water. International Symposium Frontevraud 8. 2014. France: SFEN, French Nuclear Energy Society. 14 p.
2. Ahonen, M., Ehrnstén, U., Saukkonen, T., Todoshchenko, O. & Hänninen, H. Low Temperature Crack Propagation (LTCP) Susceptibility of Nickel-Based Alloy 182, 152 and 52 Weld Metals in PWR Primary Water. Proceedings of the 16th International Conference on Environmental Degradation of Materials in Nuclear Power Systems - Water Reactors. USA: Omnipress, 2013. 19 p.
3. Ahonen, M., Ehrnstén, U. & Hänninen, H. Low Temperature Crack Propagation of Nickel-Based Weld Metals in Hydrogenated PWR Primary Water. International Symposium Frontevraud 7. 2010. France: SFEN, French Nuclear Energy Society. 11 p.
4. Ahonen, M., Ehrnstén, U. & Hänninen, H. Effect of Hydrogenated Low Temperature Water on Fracture Toughness of Nickel Based Weld Metals. Baltica VIII. Life Management and Maintenance for Power Plants. Vol. 1. Auerkari, Pertti & Veivo, Juha (eds.). VTT Symposium 264. VTT. Espoo (2010), pp. 372 – 383.
5. Ahonen, M. Collation of LTCP Test Results Obtained in Years 2008-2013. Espoo: VTT Technical Research Centre of Finland, 2014. VTT Research Report VTT-R-00352-14. 24 p.
6. Ahonen, M. Collation of LTCP Test Results Obtained in Years 2008-2012. Espoo: VTT Technical Research Centre of Finland, 2013. VTT Research Report VTT-R-00491-13. 22 p.
7. Ahonen, M. Effect of Hydrogenated Low Temperature Water on Fracture Toughness of Nickel Based Weld Metals. Espoo: VTT Technical Research Centre of Finland, 2009. VTT Research Report VTT-R-00474-10. 41 p.
8. Ahonen, M. Ympäristön ja muodonmuutosnopeuden vaikutus austeniittisten materiaalien murtumisvastuskäyttäytymiseen. Espoo: Valtion teknillinen tutkimuskeskus, 2008. VTT Tutkimusraportti VTT-R-06182-08. 64 p.
9. Mills, W.J., Lebo, M.R. & J.J. Kearns. Hydrogen Embrittlement, Grain Boundary Segregation, and Stress Corrosion Cracking of Alloy X-750 in Low- and High-Temperature Water. Metallurgical and Materials Transactions A, 30 A (1999) 6, pp.1579 - 1596.

10. Brown, C.M. & Mills, W.J. Effect of Defect Acuity on the Fracture Behavior of Alloy 82H Welds in Low Temperature Water. Proceedings of the 13th International Symposium on Environmental Degradation of Materials in Nuclear Power Systems - Water Reactors. Canada: CNS-SNC, 2007.
11. Grove, C.A. & Petzold, L.D. Mechanisms of Stress-Corrosion Cracking of Alloy X-750 in High-Purity Water. *Journal of Materials for Energy Systems*, 7 (1985) 2, pp. 147 - 162.
12. Mills, W.J. & Brown, C.M. Fracture Toughness of Alloy 600 and EN82H Weld in Air and Water. *Metallurgical and Materials Transactions A*, 32A (2001) 5, pp. 1161 - 1174.
13. Pressoyre, G.M. Hydrogen Traps, Repellers, and Obstacles in Steel; Consequences on Hydrogen Diffusion, Solubility, and Embrittlement. *Metallurgical Transactions A*, 14 A (1983), pp. 2189 – 2193.
14. Yonezawa, T., Yamaguchi, Y. & Iijima, Y. Electron Micro Autoradiographic Observations of Tritium Distribution on Alloy X750. Proceedings of the 6th International Conference on Environmental Degradation of Materials in Nuclear Power Systems – Water Reactors. USA: The Minerals & Materials Society, 1993.
15. Lee, H. G. & Lee, J.-Y. Hydrogen Trapping by TiC Particles in Iron. *Acta Metallurgica et Materialia*, Vol. 32 (1984) 1, pp. 131-136.
16. Kekkonen, T., Aaltonen, P. & Hänninen, H. Metallurgical Effects on the Corrosion Resistance of a Low Temperature Sensitized Welded AISI Type 304 Stainless Steel. *Corrosion Science*, 25 (1985) 8/9, pp. 821 – 836.
17. Herms, E., Raquet, O., De Curières, I. & Joly, P. LTCP of Alloy 182/152 Tested in PWR Primary Water. Proceedings of the 14th International Symposium on Environmental Degradation of Materials in Nuclear Power Systems - Water Reactors. USA: ANS, 2009.

30. Fracture assessment of reactor circuit (FAR)

30.1 FAR summary report

Tom Anderson¹, Päivi Karjalainen-Roikonen¹, Kalle Kaunisto¹, Heikki Keinänen¹,
Juha Kuutti¹, Sebastian Lindqvist¹, Mikko Patalainen¹, Tapio Planman¹,
Pekka Nevasmaa¹, Qais Saifi¹, Kim Wallin¹

¹VTT Technical Research Centre of Finland Ltd
P.O. Box 1000, FI-02044 Espoo

Abstract

The objective of the FAR project was to develop and to validate numerical and experimental methods for reliable reactor circuit structural integrity assessment. Numerical fracture mechanical assessment methods, Leak Before Break (LBB) approach, irregular and shallow-shaped cracks with low constraint stress state and transferability and dissimilar metal welds (DMW) assessment and characterization methods were studied in the project. This report summarizes the results of the project.

Introduction

For fracture risk assessment of nuclear components it is essential to know loads, operational conditions, material properties and their changes due to ageing or environment as well as fracture mechanisms. Both experimental material data and validated numerical assessment methods are needed for qualitative assessment of fracture risk. New material and structural solutions such as narrow gap welds set specific requirements for structural analysis and development of numerical and fracture mechanical testing methods.

Recent development in fracture assessment methods has been in the field of numerical modelling. Numerical tools are often required in assessing crack growth in complex cases such as leak before break analyses or unsymmetrical crack criticality analyses. A recently developed method for modelling crack growth is the extended

finite element method (XFEM). An objective of FAR project was to develop and evaluate numerical structural integrity assessment methods and to evaluate and further develop advanced methods - such as XFEM - for nuclear structural integrity assessment.

Leak before break (LBB) approach is based on the assumption that a crack in a wall of a pressurised component will be detected via leakage before the crack becomes critical. Use of LBB approach requires fracture mechanical evaluation methods (simple and numerical), knowledge of material properties (stress/strain, fracture toughness) and fluid mechanics (leak size, leak rate) and leak detection systems. The LBB approach stems from operating experiences showing extremely low probability of breaks in primary circuit piping. LBB is already included in nuclear safety authority codes in many countries. In Finland it is included in the design of new plants and is a part of Finnish nuclear safety YVL codes. Recent development of LBB is based on R6 and has been developed in European non-nuclear projects (e.g. FITNET). Applicability and limitations of LBB approach concerning effect of ageing on material fracture properties, different crack shapes, tearing instability and welded structures (narrow gap welds, dissimilar metal welds, DMW) as well as special loading cases is not yet established. An objective of FAR project was to study applicability and limitations of leak-before-break (LBB) approach such as limiting factors, requirements for material input data, tearing instability, effect of ageing, special features of LBB for narrow gap welds and dissimilar metal welds (DMW).

Low constraint i.e. lower stress triaxiality which prevails in a tip of a shallow crack is less severe for fracture than the stress caused by a deep crack. Fracture mechanical input data for structural analysis is usually based on deep crack fracture toughness. This leads to extra safety margins in structural assessment. For more realistic integrity assessment of a structure with irregular shape or shallow cracks further development of numerical and experimental methods is required. An objective of FAR project was to evaluate growth and criticality of real cracks with shallow or irregular shapes. Low-constraint fracture mechanical testing methods, transferability to structures and advanced numerical methods were applied and studied.

For dissimilar metal welds (DMW) research is needed especially for a successful control of the metallurgical properties across the near-interface zone. It is noteworthy that the potential flaws forming typically on the DMW joint interfaces are difficult to detect using common NDE techniques. New welding methods, e.g. narrow gap welding, particularly require mastery of the correlations between the mixing of the base material, the alloying element gradients, the microstructures formed and degradation and failure phenomena. Chemical composition and material properties may vary greatly within a narrow zone close to the weld fusion line, which makes it difficult to determine the relevant zone-specific material properties experimentally. In practise, this requires the use of miniature specimen techniques. An objective of FAR project was to develop structural integrity assessment methods for dissimilar metal weld based on realistic failure criteria of DMWs, and develop methods for identifying the critical zones for fracture and determining their fracture toughness and mechanical strength reliably.

Main objectives

The objective of the 4-year project was to develop and to validate numerical and experimental methods for reliable reactor circuit structural integrity assessment. Numerical structural integrity assessment methods such as XFEM are evaluated and further developed for nuclear purposes. The applicability and limitations of the LBB approach are studied. Limiting factors, requirements for material input data, tearing instability, effect of ageing, special features of LBB for dissimilar metal welds are considered. Experimental and analytical methods for LBB will be developed. One objective was to evaluate growth and criticality of real cracks with shallow or irregular shape in structures; low-constraint fracture mechanical testing methods, transferability to structures and advanced numerical methods will be developed. One objective was to develop structural integrity assessment procedure for dissimilar metal weld (DMW) based on realistic failure criteria of DMWs, and develop practice with which the zones that are most critical for fracture can be identified and their fracture toughness and mechanical strength can be determined reliably

The following sections discuss each of these aspects related to the fracture assessment of a reactor circuit.

Evaluation of XFEM for nuclear applications

A short summary of the XFEM related studies and findings performed in the FAR project are presented in [1]. During the project XFEM was studied for its applicability to nuclear related fracture mechanical cases. The discussion applies mostly to XFEM implementation in Abaqus.

The extended finite element method is an extension of the conventional finite element method that includes discontinuous element shape functions and additional degrees of freedom to incorporate the effects of cracks. The description of the crack geometry is obtained using the level set method that is suitable for tracking the movement of lines and boundaries in three dimensional spaces. The discontinuity location is defined using two signed distance functions for describing the crack surface and its boundaries. The values for these two functions for each node of the enriched elements are required to describe crack geometry as shown in Figure 1.

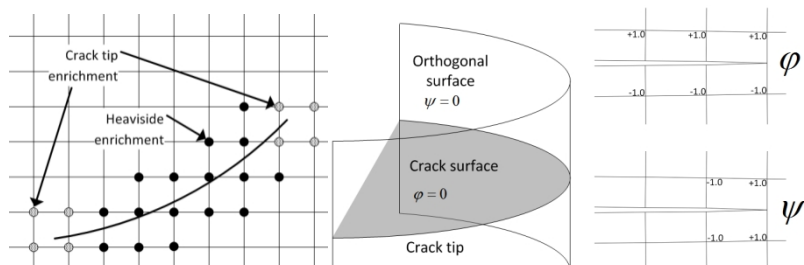


Figure 1. Definition of distance function nodal values for modelling the discontinuity within a finite element mesh.

Using XFEM with Abaqus studies of static cracks in regular components can be performed with relative ease. A coarse mesh is adequate for capturing the global stiffness effects and stress field caused by the discontinuity. Accurate evaluation of stress intensity factors or J-integrals requires a highly refined mesh around the crack and the results can still be far from the accuracy achieved with traditional FE-analyses (Figure 2a). The accuracy of the stress intensity factor and J-integral evaluation performed by Abaqus using internal contour integral routines has been found to be inaccurate in all studies within this project. The XFEM analyses were started with Abaqus version 6.10 and the most recent analyses were performed with version 6.14.

Most of the important aspects relevant in NPP component analyses can be applied together with XFEM. Most notable of these features is the possibility to include residual stress fields, temperature loads and different material models. Some plastic models are not supported in all XFEM analyses. Modelling of crack growth is fairly straightforward with XFEM as the internal degrees defining the discontinuity can be updated during the simulation (Figure 2b). A crack growth model such as ductile tearing law or Paris law for fatigue has to be specified. The drawback in Abaqus is the lack of crack tip singularity functions needed in evaluating crack criticality parameters in sharp cracks for crack growth analyses. XFEM cracks can cross material boundaries and penetrate several materials without any extra effort. In some studies inclusion of multiple materials induced numerical errors not present in single-material cases. One application where XFEM has advantage over traditional XFEM is crack growth studies over material boundaries where crack path is not known beforehand and several sensitivity studies are required if the crack is modelled using element boundaries.

As accurate contour integral results require dense mesh in the crack location submodels can be applied to reduce the size of the model. The size of the submodel with respect to crack size has certain limits to obtain matching stiffness between the global model and submodel. XFEM is well adopted for parametric analyses. Cracks of several sizes or locations can be analysed with a single mesh, boundary condition and load combination just by changing the crack definition values in the analysis input file.

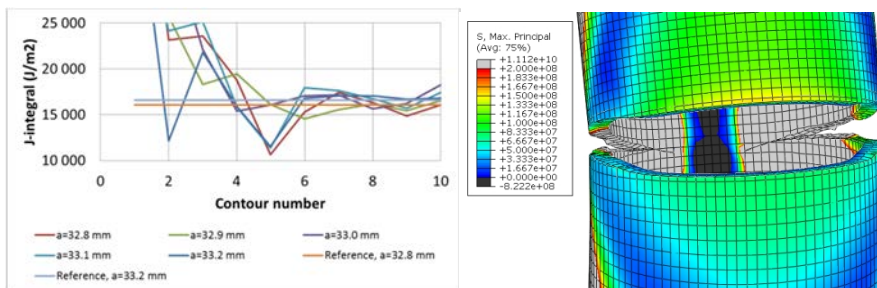


Figure 2. (a) Contour integrals for J-integral evaluation. (b) Example of crack growth simulated with XFEM.

XFEM has been widely applied in literature. In works where XFEM is applied as an analysis tool most authors have programmed the implementation in in-house codes instead of applying third-party tools. Only a few authors have published research utilizing the XFEM implementation in Abaqus but the focus of these works has been in other topics than the results obtained with XFEM.

Leak before break studies

LBB procedure development

The YVL guidelines for LBB specified in (YVL E.4-7), is based on a Break Preclusion principle. A more stringent leak before break (LBB) assessment criteria specified in the "TÜVIS Grundlagen" have been compared against the latest state of the art LBB assessment procedures available in report [2]. It was found that the TÜV criteria contain several unjustified demands that lead to highly over-conservative results in the case of LBB. The unjustified demands include for example: Prevention of leak as a primary safety criterion is in contradiction with the whole principle of LBB. Use of safety factors intended for global plastic collapse, are over-conservative with respect to local plastic collapse of a small ligament. The numerical values of the ASME safety factors are not realistic for elastic-plastic stress analysis of flawed piping.

Based on the state of the art knowledge of ductile tearing assessment and LBB, a new procedure with new rules for safety factor definitions has been proposed [2]. The procedure follows basically the state of the art, European consensus, FITNET assessment procedure and the safety factor rules are based on the latest research funded and approved by the US NRC. When using the new procedure, the resulting safety is at least comparable to the safety intended by the original ASME safety factors, but the application is specific for LBB and undue over-conservatism is avoided. The new procedure is in line with the YVL guidelines.

The YVL guideline E.4 contains a requirement that the potential for fast fracture in the upper shelf region must be considered for SC1 pressure equipment. Potential for fast fracture was discussed in [3]. Fast fracture in the upper shelf area occurs either by tearing instability (or plastic collapse) or brittle fracture. In the latter case the material has not been in the factual upper shelf temperature zone. The probability of brittle fracture is affected, besides by the crack driving force, by changes in constraint, the loading rate and the increased sampling due to crack propagation. Crack propagation, per se can lead to constraint changes and it also affects the effective strain rate at the crack tip. Especially in the case of LBB where a surface crack transforms instantaneously to a through-wall crack the increase in local strain rate, combined with constraint change and ductile crack extension, can be sufficient to cause a transition from ductile fracture to brittle fracture. This and other similar events require the development and verification of an advanced Master Curve procedure to account for combined, constraint, ductile tearing and loading rate effects on the brittle fracture probability. Also, a methodology to assess ductile crack growth

under different temperature transients and constraint conditions is needed to be able to reliably assess the potential for fast fracture occurring in the upper shelf area.

LBB case study

Leak before break (LBB) sensitivity analyses of a dissimilar weld of a steam generator primary collector was carried out in work [4] (Figure 3). During operation the collector is subjected to both thermal and mechanical loads. A three dimensional FE model was generated for fracture mechanics assessment as a part of the leak before break assessment. As a part of the LBB investigation the J-integrals were computed using different loading or material parameters. The main goal was to find out which parameter, whether loading or material related, has the most effect on the crack opening and the J-integrals.

The J-integral results indicated that raising the secondary pressure increased the J-integrals. Increase or decrease of the primary pressure had nearly no effect on the J-integrals. Also increase of the operating temperature increased the J-integral values. The increase of J-integral values was significant especially in the middle and the outer end of the crack tip. The results from the material parameter sensitivity analyses showed that the most significant effect on the J-integrals was obtained by increasing the materials thermal expansion properties. The crack opening displacement results indicated that the largest axial crack opening displacements were obtained in the case of decreased secondary pressure. Also decrease of the primary pressure caused increase of axial crack opening displacement. The crack opening displacements were remained lower than 1 mm in every case. The equivalent plastic strain results indicated that the plastic strains remained lower than 1% in the structure, excluding the crack vicinity and the risk of plastic collapse remains low even if the normal operating load was multiplied several times.

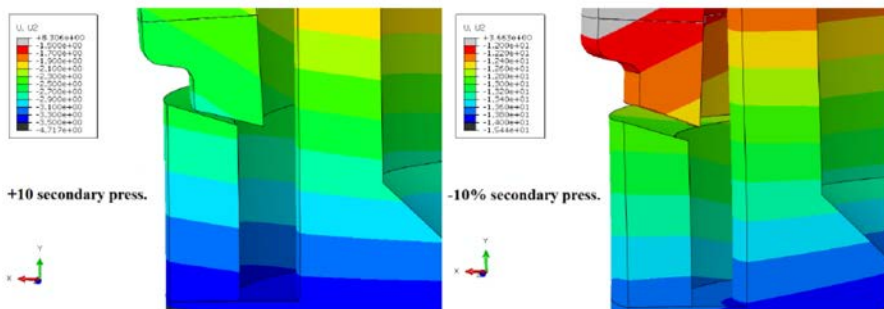


Figure 3. Crack opening displacements from steam generator collector case study.

Fracture model results with different assumed through-wall cracks indicated that J-integrals obtained from the analyses were relative low by a magnitude. Based on experience of similar materials the obtained crack driving forces does not exceed the material fracture toughness. It was also observed that the crack loading direction was not purely axial but also sliding between crack surfaces was obtained. This could result to a crack closure in the best case scenario and more over limit the leak

rate. Based on the obtained results, the component is at risk of breaking before leak if material fracture toughness is less than about 20 kJ/m^2 . The possibility of plastic collapse was observed to be negligible as well.

In connection to LBB behaviour the instability of long cracks was experimentally studied. In the tests fracture resistance specimens with different slenderness were utilized to study whether the slenderness affects the tearing resistance. It was found that the fracture resistance seems not to decrease as a function of slenderness or crack growth. No crack growth was observed. Limit load decrease was observed with high strength steels but this is not relevant for nuclear materials. An example of obtained growth path and results are shown in Figure 4.

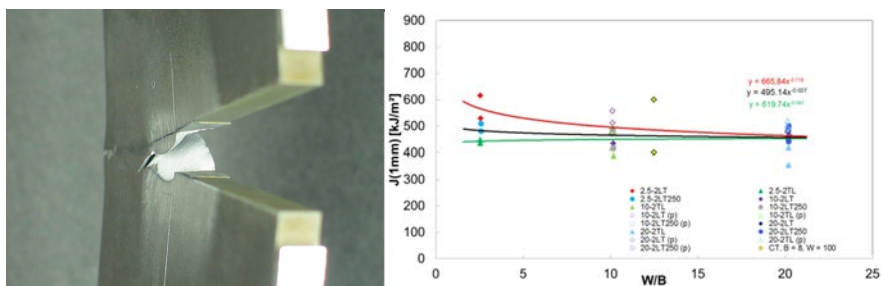


Figure 4. Observed crack path and J1mm values for specimens with different slenderness.

Low constraint

The Unified Curve and the Master Curve are two popular cleavage fracture toughness assessment engineering methods. The methods are very similar. They basically differ only in the assumed fracture toughness temperature dependence. The standard Master Curve approximates the temperature dependence as being fixed, whereas the Unified Curve assumes that the shape changes as a function of transition temperature. The shape difference becomes significant only for highly brittle steels. Previous comparisons of the two methods have applied a procedure that may cause a bias on the comparison when assessing censored data sets. In the work by Kim Wallin [5], a fully objective comparison using the censored likelihood, have been made for 50 large data sets with transition temperatures in the range $+8 \text{ }^\circ\text{C} \dots +179 \text{ }^\circ\text{C}$. The standard Master Curve shows overall a trend of higher likelihood than the Unified Curve. In the work is also shown that, because of shortages connected to the use of the Prometey probabilistic cleavage fracture model, the Unified Curve cannot be considered universally applicable.

The national round robin concerning fracture toughness (T_0) and fracture resistance (JR) was organized [6]. The round robin will be performed in 2015. Material for the round robin has been chosen as structural steel Laser 420 MC. Round robin participants are VTT hot cell, VTT research hall and SSAB Raahe. SSAB Raahe was responsible for test specimen manufacturing. Test specimens will be ready in 2014 but actual Round Robin takes place in 2015. 60 specimens for T_0 tests and 36

specimens for JR-tests are manufactured. Short report on Round Robin definition was prepared. In future, every partner makes the analysis of their data and performs reporting according to the ASTM E1820 and E1921 standards. The results will be summarised as a summary report.

DMW

Presently, no standards are available to assess the structural integrity of DMW components. Moreover, there are no standards for materials testing of DMWs either. Ensuring safe service of a DMW component therefore requires complete strength and fracture toughness based information from all microstructural zones of a DMW as input data for structural integrity assessment. An essential prerequisite of such assessment is that local fracture resistance and crack growth behaviour of a DMW are experimentally investigated and underlying characteristics understood. As it comes to fracture toughness, this requires detailed post-test specimen sectioning with associated metallographic and fractographic investigation, which can reveal the true fracture path during the entire crack initiation and propagation history.

The aim of the research reported in [7] was to experimentally determine the fracture toughness properties of a Ni base DMW mock-up obtained from KAIST in terms of fracture resistance (J-R) curves using small-scale ($5 \times 10 \times 55 \text{ mm}^3$) pre-fatigued 3-point bend SE(B) specimens (Figure 5).

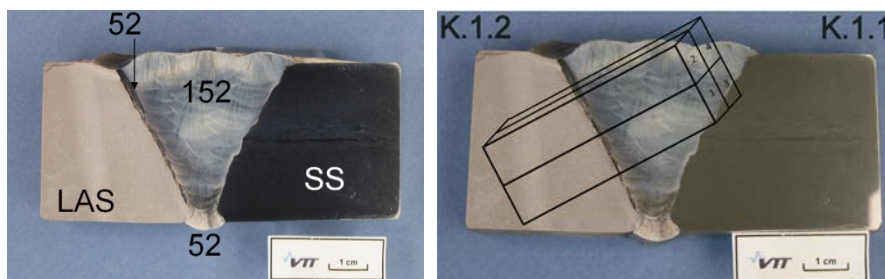


Figure 5. Extraction of 5 mm x 10 mm x 50 mm SE(B) specimens for fracture resistance tests from KAIST DMW mock up.

The fracture resistance tests were performed at room temperature according to the standard ASTM E1820-13 “Standards Test Method for Measurement of Fracture Toughness” in order to define J value at the onset of ductile tearing, since this is an important parameter in the case of LBB assessment. Due to limited amount of available DMW material, testing was focused on the near-interface region (NIZ) of the ferritic RPV steel and the Ni base Alloy 52 buttering layer. The results demonstrated, the J integral values for the onset of ductile tearing were not fully reached, and as no actual crack growth took place only crack blunting occurred during the tests. All the fracture resistance test results (J-R curves) showed essentially ductile fracture behaviour (Figure 6).

This was confirmed by the post-test fractographic investigation of the specimen fracture surfaces (Figure 7); all the specimens exhibited fully ductile fracture surface appearance. The results demonstrated that the fracture toughness associated with the onset of ductile fracture is above 80–100 kJ/m².

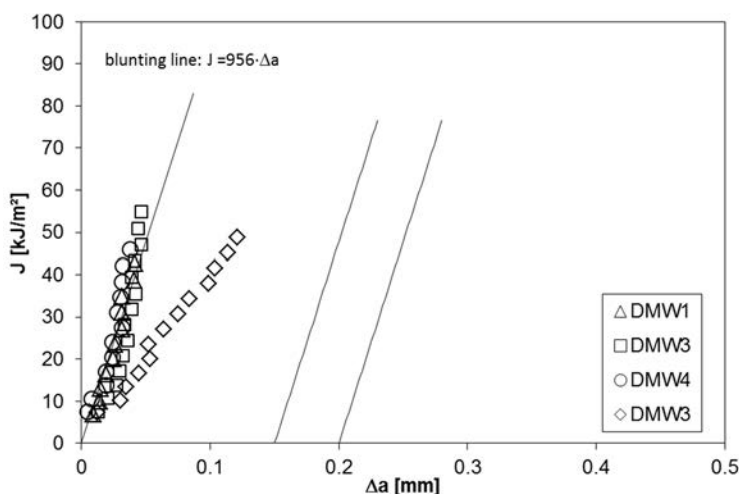


Figure 6. Fracture resistance curves for the NIZ of the LAS–Alloy 52 of KAIST DMW showing blunting without reaching J value for the onset of ductile tearing. Specimen DMW3 had weld defect causing different blunting behaviour. SE(B) specimens 5x10x50 with 20 % side grooves were used in the tests.

The observed crack path in all the specimens was found relatively straight without any sudden crack deviations from its original location i.e. the NIZ into the neighbouring weld microstructural zones during growth, which is often encountered in the case of DMWs. One cannot, however, rule out the possibility that a very limited amount of crack growth in a specimen has hindered any crack path deflections that otherwise might have occurred in later stages of crack propagation.



Figure 7. Fracture surfaces of fracture toughness test specimens DMW1...DMW4 for NIZ LAS/Alloy 52 of KAIST DMW show blunting. Weld defect can be seen on the fracture surface of specimen DMW 3. Nominal thickness was 5 mm, and width 10 mm.

Conclusions

The objective of the FAR project was to develop and to validate numerical and experimental methods for reliable reactor circuit structural integrity assessment. Numerical fracture mechanical assessment methods, Leak Before Break (LBB) approach, irregular and shallow-shaped cracks with low constraint stress state and transferability and dissimilar metal welds (DMW) assessment and characterization methods were studied in the project.

In the project the applicability and limitations of the XFEM method in Abaqus was studied. Leak before break approach was studied and applied as a case study and an updated procedure proposed. Instability of long cracks was studied in connection to LBB behaviour. A national round robin on JR and T_0 determination was organized. A comparison between Master Curve and Unified Curve was made. Brittle fracture low constraint tests with surface crack specimens (SENT, SENB, deep crack) were performed and analysed. Fracture mechanical testing of nickel-based dissimilar metal weld specimens was performed. Near interface zone DMW material characterization techniques were developed and applied in the project.

References

1. Kuutti, J. and Kaunisto, K., 2014. "Applicability of Abaqus XFEM implementation in NPP cases". VTT Research Report VTT-R-05745-14.
2. Wallin, K., 2014. "Evaluation of rules for LBB assessment". VTT Research Report VTT-R-00815-14.
3. Wallin, K., 2014. "Potential for a fast fracture occurring in the upper shelf area". VTT Research Report VTT-R-04898-14.
4. Patalainen, M., 2014. "SAFIR2014 – Pipe break analysis: Leak before break sensitivity studies of a steam generator primary collector". VTT Research Report VTT-R-04969-14.
5. Wallin, Kim, "Objective comparison of the Unified Curve and Master Curve methods" (2014). International Journal of Pressure Vessels and Piping. DOI: 10.1016/j.ijpvp.2014.07.008
6. Karjalainen-Roikonen, P., 2014. "Round Robin plan on fracture toughness and fracture resistance for structural steel Laser 420 MC". VTT Research Report VTT-R-00097-15.
7. Karjalainen-Roikonen, P., Nevasmaa, P., Lindqvist, S., 2014. "Fracture mechanical tests on Ni- base dissimilar metal (DMW) welds". VTT Research Report VTT-R-00063-15.

31. Monitoring of the structural integrity of materials and components in reactor circuit (MAKOMON)

31.1 MAKOMON summary report

Tarja Jäppinen, Jonne Haapalainen, Esa Leskelä, Ari Koskinen, Antti Tuhti,
Kari Lahdenperä & Stefan Sandlin

VTT Technical Research Centre of Finland Ltd
Kemistintie 3, P.O. Box 1000, FI-02044 Espoo

Abstract

Monitoring of the structural integrity of the primary circuit components in nuclear power plant is an important part of in-service inspections. The development of the non-destructive testing techniques towards more reliable and efficient inspections promotes the safety of nuclear power plants. That is also the objective of the SAFIR2014 MAKOMON project. Main NDT methods used in the MAKOMON project are ultrasonic applications and ultrasonic simulation, eddy current and radiography.

In MAKOMON the aim was to test different artificial fatigue defects with several ultrasonic inspection techniques and to find the possible differences in reflector properties on indications. The results of the tests were also used to verify the ultrasonic modelling. Another task was to develop and test an eddy current technique capable to locate the magnetite piles within the SG tubing. The measurements were conducted in a simple mock-up that had tubes representing the SG tubing using eddy current bobbin probes.

The results of the project are shortly presented in this article. More detailed analysis can be found in the VTT research reports.

Introduction

Non-destructive testing (NDT) techniques are used to inspect the condition of the structures of the primary circuit components during the operation of nuclear power plants (NPP). The development of the NDT techniques towards more reliable and efficient in-service inspections (ISI) promotes the safety of the nuclear power plants. Also the development of the inspection techniques that can be applied to primary circuit components where the access is restricted can increase the reliability of ISI. The in-service inspections are normally performed during the outage with a tight time schedule.

The objective of the SAFIR2014 MAKOMON project was to develop more reliable and more efficient ways to use NDT techniques for monitoring the structural integrity of the primary circuit components. The main NDT -methods used in the MAKOMON project are different ultrasonic applications and ultrasonic simulation, eddy current and radiography.

MAKOMON project during years 2011-2014 consisted of three main subtasks. One task compared the indications received from different types of defects in ultrasonic evaluation. The comparison of the indications was done between mechanical and thermal fatigue cracks and EDM notches.

The second main task in the MAKOMON project was ultrasonic simulation. The simulation can be used to optimize the inspection techniques, and to see the restrictions of the inspection. Another aim in the simulations was to gain data to calculate probability-of-detection (POD) curves from simulated defects.

The third main task develops of eddy current method to detect the magnetite piles in the steam generation (SG) tubing. It is an area of interest that have continued in this project. Magnetite on the SG tubing is well detected and the existence of the magnetite can be measured up to certain limit.

One year lasting tasks of new ultrasonic methods were introduced during the MAKOMON project. Nonlinear ultrasound [Sandlin, 2011] and laser ultrasound [Haapalainen & Sandlin, 2012] have been reviewed for new possibilities of detecting early stages of material degradation. The potentials for digital X-ray detectors in nuclear environment have been studied in the project. X-ray tomography equipment is introduced in the project.

NDE applications for detecting cracks in primary circuit components

Artificial defects are typically used as a reference when the performance of an NDT procedure is demonstrated. Defects are also needed for certification and training of the inspectors. The renewed NPP safety regulator guides (YVL) also emphasise that it is important for the inspections to be able to define the reference defect.

According to the performed studies in the MAKOMON the indication of the ultrasonic reflection varies with the type of the defect. To be able to tell the severity of the detected defects it is highly important to know the exact type of the defects of

the reference samples and their correspondence to actual defects. This work started in 2012 in the MAKOMON project [Koskinen, 2012].

One of the main objectives in the MAKOMON project research was to produce new data of artificial reflectors for the needs of qualification as well as inspection. Results can also be directly used for estimating and improving the reliability of ISI. The aim of the study was to test different sizes of artificial fatigue defects and to find the possible differences in reflector properties on indications.

Specimens used in the test were welded austenitic stainless steel plates where four different defects were produced in the heat affected zone. The defects were a thermal fatigue (TF) crack, two mechanical fatigue (MF) cracks and one EDM notch.

The produced defects have been inspected with conventional ultrasonic testing (UT) and phased array (PA) techniques (Figure 1). Moreover scanning acoustic microscope (SAM) and time of flight diffraction (TOFD) were used to get a wider perspective to differences of the similar defects of the different manufacturers.

Typically defect detection and especially sizing the height of the defect is considered challenging in ultrasonic inspection done from the opposite side of a defect when the sound beam must penetrate through the weld material distorting and attenuating the sound waves. This study showed that mechanical fatigue cracks were not possible to reliably size by height through weld but in most of the cases both TF crack and EDM notch could. That may be a consequence of the branching shape of the TF crack and wider opening of both TF crack (surface area) and EDM notch. This indicates that the defect type chosen may have a significant influence in the evaluation of the performance of the technique in that case.

The length of a MF crack was most accurately measured. Conventional UT performed better in sizing the crack length than phased array ultrasound.

In the crack manufacturing the target was to get two similar MF cracks. Yet the sizes of the MF cracks were different from each other. Also there was a difference in length/height ratio of the two MF cracks. This needs to be taken into account when relying on the reference defects.

The results of the ultrasonic examination with the results of the destructive examination conducted for the cracks within the project ENVIS are presented in the research report [Leskelä et.al. 2014] and in the special article in this SAFIR2014 final report.



Figure 1. Scanning of the test plate with phased array ultrasonic technique.

X-ray tomography examination

Specimens with one thermal fatigue crack and two mechanical fatigue cracks were examined with digital X-ray tomography system at BAM (Federal Institute for Materials Research and Testing) in Germany. The tomography examination gave valuable information of the cracks for further evaluation of the ultrasonic indications.

The results of the tomographic x-ray imaging showed that it can be a good method for sizing fatigue defects. The length and the height measurements of the tomographic imaging (Table 1.) do not vary much from the measurements made from the fracture surface of the crack. The length of the TF crack differs more from the destructive results than the lengths of MF cracks. TF crack has branches in both ends and the branching is not fully visible in tomographic x-ray imaging (Figure 2). This can effect on the accuracy of the length measurement.

X-ray tomography is a potential method for NDT inspections of crack like defects in austenitic stainless steels and welds. As seen in Figure 2 the shape of the crack is not entirely representative, especially the crack tip area seems to be more or less incomplete compared to destructive analysis. Verifying the full potential of the method would need more research with different types and sizes of defects as well as different materials and material thicknesses. X-ray tomography is relatively slow inspection method and therefore the use of the method requires careful planning in advance. The best option for in-service inspections with x-ray tomography would be to use the method to verify and size the indications found with other NDT methods.

Table 1. Dimensions of the crack measured using x-ray tomography.

Sample	Maximum length measured from tomographic x-ray imaging (mm)	Difference to length measured from fracture surface (mm)	Maximum height measured from tomographic x-ray imaging (mm)	Difference to height measured from fracture surface (mm)
MF A	13.0	-0.1	6.3	0.1
MF B	14.5	0.2	5.0	0.0
TF	12.5	-1.0	5.2	0.0

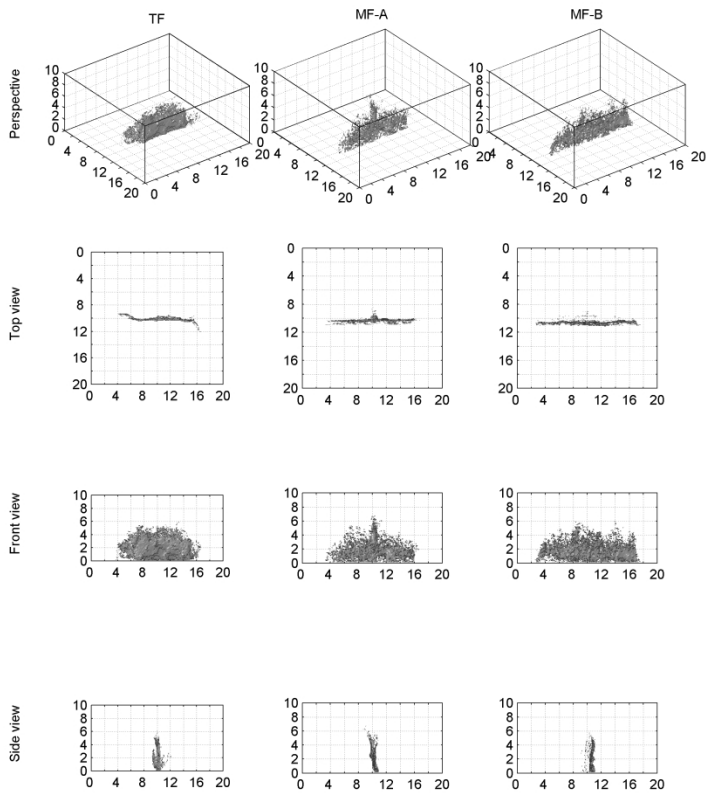


Figure 2. Tomographic x-ray imaging visualised in different views. On the left thermal fatigue crack in the middle and on the right two mechanical fatigue cracks.

Ultrasonic Simulation and POD

Simulation on NDE field can give new ways to approach e.g. ultrasonic responses on different types of reflectors. In the MAKOMON project the ultrasonic simulation program CIVA have been used for calculating ultrasonic response from a known reflector. In order to use simulation tool as an aid for ISI, every aspect of simulation (e.g. material, transducers, defects) should represent the real-life inspection. The results of the simulation were compared with experimental results of the TF and MF cracks in order to verify the simulation procedure. The comparison shows that i.e. simulations underestimate the amplitude difference between TF and MF crack.

The probability of detection (POD) curves are important information describing the performance of a non-destructive examination system. To produce such curves with statistically confidence a large number of tests is required. Experimental tests using real samples and defects are often very expensive and it would be desirable to widen the test results applying simulations. Simulation provides a fast way of determining the POD -curves.

The simulation in MAKOMON shows the capability of CIVA to simulate defects that represent ISI defects. The defect geometry affects the inspection results greatly, which can be also confirmed by comparing the results to measurement data.

During the MAKOMON project comparison between measurements and simulations are done to find out the limitations of the simulations. The crack morphology is verified with destructive testing.

Detecting of Magnetite mapping in steam generator

In MAKOMON the task was to further develop and test a technique capable to size the magnetite piles within the SG tubing. The measurements were conducted in a simple mock-up that had tubes representing the SG tubing using eddy current method and standard bobbin probes. The measurements were conducted with either a single probe technique or a novel two-probe technique. In two-probe technique two similar probes were located in the adjacent parallel tubes. One probe was transmitting and another was receiving the eddy current signal. The tests were conducted with absolute technique and using several frequencies, between 10 and 200 kHz.

During the project years several test series were conducted with different size of magnetite pile on the tubing in the mock-up (Figure 3). The results showed that the existence of the magnetite pile was detected best with low frequencies (10 - 50 kHz). The amplitudes of the indications due to magnetite pile were increasing when the height of the pile was growing.

The results of one of the test series is presented in Figure 4. The amplitude of the magnetite pile indication increases when the height of the magnetite pile grows. The amplitude increases up to pile level of 24 mm with all applied test frequencies with a single probe technique.



Figure 3. A part of steam generator tubing in a mock up. The two lowest tubes are submerged into the black magnetite pile.

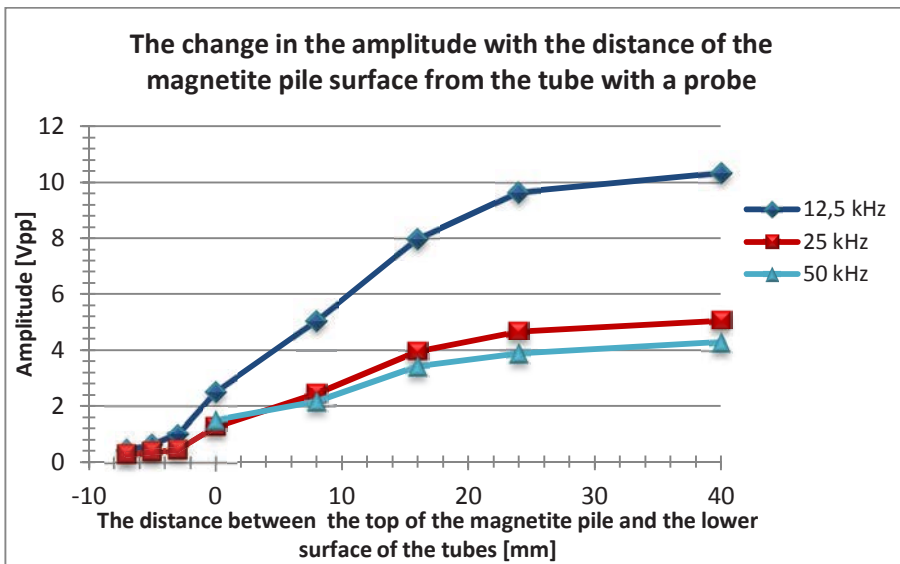


Figure 4. Test series to detect the existence of the magnetite pile. The amplitude of the magnetite pile indication versus the distance between the upper level of the pile and the lower surface of the tubes where the probes are located. The positive distance indicates that the surface of the magnetite pile is above the lower surface of the tube. Respectively the negative distance indicates the upper surface of the magnetite pile is below the lower surface of the tube. Amplitude of the indication due to a 1.3 mm through-wall hole was 1.0 V (12.5 kHz).

The relative permeability of the magnetite pile was determined comparing the results achieved by modelling with CIVA ET module and the results achieved with actual measurements of the lift off indication of the magnetite pile. The relative permeability of the studied lightly compacted magnetite pile was about 3 (2.7 when the ET frequency was 10 kHz and 3 when frequency was 50 kHz). The exact value of the relative permeability of the magnetite pile depends strongly on the compactness of the pile.

Conclusions

The development of the NDT techniques towards more reliable and efficient in-service inspections promotes the safety of the nuclear power plant. The objectives of the SAFIR2014 MAKOMON project was to develop more reliable and more efficient ways to use NDT techniques for monitoring the structural integrity of the primary circuit components. The main NDT -methods used in the MAKOMON project are different ultrasonic applications and ultrasonic simulation, eddy current and radiography.

One of the main objectives in the MAKOMON project research was to produce new inspection data on artificial reflectors for the needs of qualification as well as inspection. The aim of the study is to test different artificial fatigue defects with several ultrasonic inspection techniques and to find the possible differences in reflector properties on indications. The defects in this study were mechanical fatigue cracks, a thermal fatigue crack and EDM notch.

The results of the crack height and lengths measurements combined with destructive testing gave valuable information of these artificial reflectors. The results were also used to verify the ultrasonic modelling.

One objective of MAKOMON was to develop and test an eddy current technique capable to locate the magnetite piles within the SG tubing. The measurements were conducted in a simple mock-up that had tubes representing the SG tubing using eddy current bobbin probes. The results of the measurements showed that the extension of the magnetite pile can be mapped. A technique with a single probe is found more reliable. Therefore the research work will continue with an improved single probe technique.

The NDT related research work on primary circuit component with addition of the concrete integrity NDT is continuing in the SAFIR2018 programme in the project WANDA.

Acknowledgement

The MAKOMON project has been financed by VYR, VTT, Fortum and Fennovoima. The project personnel are grateful of the financial support and co-operation to the power companies.

References

- Koskinen, A., Haapalainen, J., Virkkunen, I. & Kemppainen, M. Differences in Ultrasonic Indications – Thermal Fatigue Cracks and EDM Notches. 18th World Conference on Nondestructive Testing, 16-20 April 2012, Durban, South Africa.
- Koskinen, A. 2012. Ultrasonic reflectors in ultrasonic inspections for primary circuit components – work report, VTT Research Report VTT-R-00538-12. 13 p.
- Leskelä, E, Koskinen, A., Haapalainen, J., Ehrnsten, Ulla & Autio, J-M. 2014. Comparison of artificial flaws in austenitic steel welds with NDE methods, VTT Research Report VTT-R-05649-14. 50 p.
- Haapalainen, J. 2012. Digital Radiography in Power Generation Industry, VTT Research Report VTT-R-00965-12. 29 p.
- Haapalainen, J. & Leskelä, E. Probability of Detection Simulations for Ultrasonic Pulse-echo Testing. 18th World Conference on Nondestructive Testing, 16-20 April 2012, Durban, South Africa.
- Haapalainen, J. 2012. Ultrasonic simulation and simulation verification in demanding inspection applications, VTT Research Report VTT-R-01326-12. 8 p.
- Haapalainen, J. 2013. Ultrasound simulation of fatigue flaws. VTT Research Report, VTT-R-00674-14. 10 pp.
- Sandlin, S. 2011. Evolving ultrasonic NDE techniques for detecting fatigue damage and partially closed cracks, VTT Research Report VTT-R-08878-11. 45 p.
- Haapalainen, J & Sandlin, S. 2012. The Possibilities of Laser Ultrasonic Material Inspection in the Nuclear Industry, VTT Research Report VTT-R-00845-13. 21 p.
- Jäppinen, T., Lahdenperä, K. & Ala-Kleme, S. Locating Magnetite on the Steam Generator Tubes with Eddy Current. 18th World Conference on Nondestructive Testing, 16-20 April 2012, Durban, South Africa.
- Jäppinen, T. & Lahdenperä, K., Sizing magnetite piles in steam generator tubing with two-probe eddy current technique, 10th international conference on Non Destructive Evaluation in relation to structural integrity for nuclear and pressurized components, 1st -3rd October, 2013, Cannes France.
- Jäppinen, T. & Lahdenperä K. 2014. Magnetite Measurements on Steam Generator Tubing with Eddy Current Techniques, VTT report VTT-R-00209-15. 16p.

31.2 Comparison of Artificial flaws in Austenitic Steel Welds with NDE Methods

Ari Koskinen, Esa Leskelä

VTT Technical Research Centre of Finland Ltd
P.O. Box 1000, FI-02044 Espoo

Abstract

Qualification of non-destructive examination (NDE) procedures for in-service inspections (ISI) of nuclear power plant (NPP) components is performed using different types of artificial flaws. The assessment of the reliability of a procedure requires representative flaws compared to the real service-induced flaws.

Fatigue cracks can nowadays be produced artificially as thermal fatigue or mechanical fatigue cracks. Thermal fatigue crack production is very well controlled in matter of size and opening. That kind of cracks are very realistic option compared to the real service-induced cracks. Mechanical fatigue crack production is well known and widely used method and can produce very realistic cracks as well. The aim of the study is to get a wider perspective to the differences in similar type of flaws from different manufacturers.

Ultrasonic indications are highly dependent on defect characteristics like roughness, crack opening, tilt and branching. This work studies the influence of different reflector properties on flaw indications. Two kinds of artificially produced cracks from different manufactures and one EDM (electric discharge machining) reference notch were made in welded austenitic stainless steel test blocks. Flaws were examined using conventional ultrasonic testing (UT), phased array ultrasonic testing (PAUT) and digital radiography. The flaws were sized with different techniques and those results are compared to the true state flaw dimensions as determined by destructive analysis.

Introduction

Qualification of non-destructive examination (NDE) procedures for in-service inspections (ISI) of nuclear power plant (NPP) components is performed using different types of artificial flaws. The assessment of the reliability of a procedure requires representative flaws compared to the real service-induced flaws.

Fatigue cracks can nowadays be produced artificially as thermal fatigue or mechanical fatigue cracks. Thermal fatigue crack production is very well controlled in matter of size and opening. That kind of cracks are very realistic option compared to the real service-induced cracks. Mechanical fatigue crack production is well-known and widely used method and can produce very realistic cracks as well.

Ultrasonic indications are highly dependent on defect characteristics like roughness, crack opening, tilt and branching as well as any additional disturbances of the

material caused for example by the flaw manufacturing process. This work studies the influence of different reflector properties on flaw indications. The aim of the study is to get a wider perspective to the differences of two different type of fatigue cracks from different manufacturers [1].

Goal

The goal of the study was to compare NDE indications of different kinds of artificial flaws. Another objective was to evaluate the accuracy of various ultrasonic techniques – both conventional ultrasonic testing (UT) and phased array ultrasonic testing (PAUT) – in flaw sizing. Also the effect of flaw type on sizing accuracy was compared. The crack characterization and sizing accuracy with digital radiography was also studied.

The goal of destructive examination was to measure the dimensions of the flaws, to characterise the fracture surface as well as the crack path in the materials. Another objective was to evaluate how well the characteristics of the flaws mimic real cracks in NPP primary system piping.

Test samples

Two different fatigue samples were studied. Both samples were made of austenitic stainless steel 316L (ASTM) plate with a thickness of 25 mm. Samples were butt welded of two pieces and both weld face and root sides were ground to allow full scanning access and to exclude geometrical indications. The cracks were produced on the weld root side along the fusion line (Figure 1 a) to simulate inside surface breaking service-induced stress corrosion cracks (SCC). One of the samples contained one thermal fatigue (TF) crack and EDM (electric discharge machining) reference notch and the other contained two mechanical fatigue (MF) cracks [2].

Liquid penetrant indications of both thermal and mechanical fatigue cracks are shown in Figure 1 b and c. The branching shape of the TF crack is well visible whereas the shape of the MF crack seems to be rather smooth. The dimensions of the cracks in both samples were targeted to be 15 mm in length and 5 mm in height. The true dimensions were determined by destructive investigation as a part of SAFIR2014 ENVIS project [3].

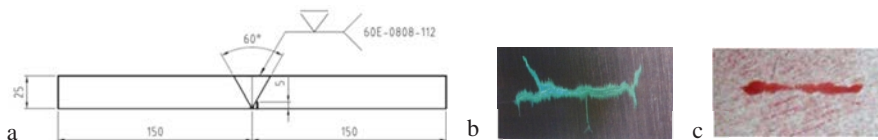


Figure 1. a) Schematic picture of the sample and liquid penetrant indications of b) thermal fatigue crack and c) mechanical fatigue crack.

Methods

Destructive examination

The three plate samples, named MF A, MF B and TF were received for destructive examinations after thorough NDE investigations which are presented in detail in the following chapters. First, the locations of the defects in the plates were identified and then about 30 x 80 mm sized samples were cut out, containing the defects.

The surfaces with the cracks were investigated using scanning electron microscopy (SEM), and the length was measured from the SEM-pictures in the two cases, where the cracks were visible on the surfaces. The cracks were then opened and the sizes (length and height) were measured from stereo microscope pictures. One of each fracture surface was investigated using SEM, and the typical features were documented.

A cross-section was prepared from each flaw by cutting a slice across the crack. As the crack was opened, the cut was performed separately from each half at the same location. This will, however, never result in a perfect match of the two fracture surfaces. If the cutting would have been performed before opening of the flaws, the dimensions would have been less accurate, and this was considered more important. The cross-sections were investigated in polished and etched condition using an optical microscope.

Ultrasonic examination

The ultrasonic inspections were performed on the two test blocks containing flaws. Scanning was performed from the outer surface of the blocks from both sides of the weld. PAUT and conventional UT were both used with multiple setups. With conventional UT eight different setups and with PAUT six different setups were used for height sizing for each flaw. In length sizing with conventional UT 12 setups and with PAUT eight setups were used for each flaw including mode conversion technique (MC). The PAUT TRS (transmit-receive shear wave) and TRL (transmit-receive longitudinal wave) techniques are included in a procedure qualified through the Performance Demonstration Initiative (PDI) program administered by Electric Power Research Institute (EPRI). The procedure which is later referred as 'PDI technique' is not qualified for height sizing but only for length sizing.

X-ray tomography examination

Digital radiography was used to gather more information on the crack size, tilting, possible branching etc. [4] Digital radiography examinations were done at Federal Institute of Material Research and Testing (BAM), Division 8.3, Radiological Methods in Berlin. The used methods included Vidisco RayzorX flat panel detector and TomoCAR which is equipment for x-ray tomography. TomoCAR results are included in this article.

The TomoCAR equipment has an ENIQ certification for detecting cracks in the tube with 25 mm wall thickness, the total penetration thickness 50 mm. The certified crack opening is min. 100 μm and the tolerance in crack height sizing is ± 1 mm. In the equipment the X-ray tube moves along a straight bar over the examined specimen taking 400 images. The Cadmium telluride detector is made by AJAT Finland. The size of the detector is 100 mm x 25 mm with 0.1 mm pixel size. Tomographic data was processed and analysed using Analytical RT Inspection Simulation Tool (aRtist) [5].

Flaw sizing in ultrasonic examination

Height sizing was primarily based on crack tip diffraction method: height of a flaw is the distance between flaw base and the maximum amplitude of tip diffraction signal. In the case that this signal was not detected or clearly separated, the estimation of height was based on 6 dB maximum amplitude drop sizing method: height is the distance between flaw base and the position where the flaw amplitude decreases 50 % (6 dB drop) of the maximum amplitude of the flaw.

Length sizing was done according to full amplitude drop technique: length of a flaw is the distance between two end points where the flaw signal drops on the average noise level of the surrounding area.

According to ASME Code, Section XI, Appendix VIII acceptance criterion, to pass a typical weld qualification examination, the maximum difference between indicated and true state values for flaw height and length is 3.18 mm and 19.05 mm, respectively [6].

Evaluation of sizing performance of ultrasonic examination

Some statistical analysis of flaw length and height characterization was done to make conclusions concerning flaw sizing capability and to compare the flaws and UT techniques. The statistical analysis presented in this article is limited to calculations of the root mean square error (RMSE). Also measurement error, mean error and standard deviation were calculated [1], but are not presented in this article. RMSE is computed according to the formula shown below:

$$RMSE = \sqrt{\frac{1}{n} \sum_{i=1}^n (M_i - T_i)^2} \quad (1)$$

Results

In the destructive analyses the study included the surface examination, dimensioning, fracture surface examination and 3D-profiling (in Figure 2), followed by the results from the microscopical analyses. In this article a short conclusion of the de-

structive results is presented. The dimensions of the cracks were determined after opening from stereomicroscope pictures and the results are presented in Table 1. As can be seen from the table, there is a difference between the length measurements from the surface and from the fracture surface. The measurements from the fracture surfaces are considered more accurate. The height measurements are projections, and do not take the inclination into account.

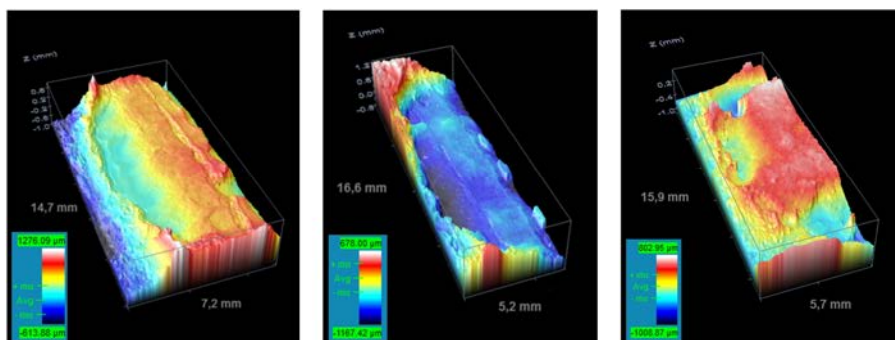


Figure 2. 3D-profilometric picture of the fracture surface in samples. From the left MF A, MF B and TF.

Table 1. Summary of dimensions for samples MF A, MF B and TF.

Sample	Length measured from surface (mm)	Maximum length measured from fracture surface (mm)	Maximum height measured from fracture surface (mm)	Length/height
MF A	(14.5)	13.1	6.2	2.11
MF B	-	14.3	5.0	2.86
TF	(12.8)	13.5	5.2	2.60

Height sizing results

It can be seen on the left hand side in Figure 3 that most of the techniques tend to undersize crack MF A except the conventional UT techniques with longitudinal wave (LW) mode which oversized the crack. The height sizing error was smallest with shear wave SW55 PAUT technique and the both PDI techniques.

All conventional UT techniques oversized crack MF B. PAUT techniques with lower frequencies (1.5–2.25 MHz) slightly undersized and PAUT techniques with higher frequency (5 MHz) slightly oversized the crack. The errors were smallest with MWK45-4 conventional UT and SW45 PAUT techniques. The both PDI techniques slightly undersized the crack.

It can also be seen on the right hand side in Figure 3 that most of the conventional UT techniques oversized TF crack but all the PAUT techniques undersized the crack. Error was smallest with TRL 45-2 technique.

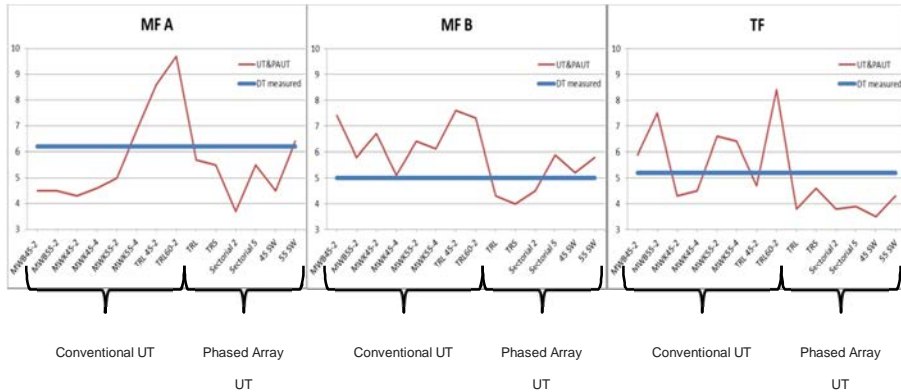


Figure 3. Comparison of the ultrasonic measurement height from the near side and destructively measured height.

Only PAUT was performed for EDM notch. All the techniques were able to height size the notch both from near side (sounding from defect side) and far side (sounding through the weld). Half of the techniques undersized the notch when scanned from near side and all the techniques except TRS technique undersized the flaw when scanned from far side of the weld. The maximum error was -1.5 mm with SW45 technique.

Reliable flaw height sizing of mechanical fatigue cracks was not possible from far side This was due to the strong structural noise and metallurgical indication on the crack tip area. Half of the techniques were able to height size the thermal fatigue crack also from far side.

In the study all test techniques fulfilled the RMSE requirement of 3.2 mm in height sizing. The lowest RMS values were calculated for MWK 45-4, MWK 55-4, SW 55, TRL and TRS techniques. The highest RMSE value was calculated for TRL 60-2 technique.

The highest RMSE value with both conventional UT and PAUT was calculated for crack MF A. The lowest RMSE value with conventional UT was calculated for TF crack and with PAUT for crack MF B. There was a clear difference between the two mechanical fatigue cracks with both conventional UT and PAUT. All RMSE values were lower with PAUT than with conventional UT and unexpectedly the far side RMSE values were lower than the near side RMSE values.

Results showed lower RMSE values for PAUT than with conventional UT and highest RMSE values for crack MF A. It was also seen that the combined RMSE values were lowest for EDM notch and highest for crack MF A. There was a difference between the two mechanical fatigue cracks. The combined RMSE value for height sizing in this study was approximately 1.4 mm.

Length sizing results

According to results the greatest flaw undersizing for crack MF A occurred with conventional UT techniques MWB55-2 and MWK55-2 together with the PAUT TRS technique when scanned from far side as can be seen on the left hand side in Figure 4. The TRL70-2 undersized the crack both from near and far side. Techniques MWB45-2, MWB70-2, MWK70-2, Sectorial 2 and 70SW oversized the crack in near side scanning.

As can be seen in the middle of Figure 4, with crack MF B the TRL70-2, TRS and sectorial 2 techniques undersized the crack when scanned from far side. Techniques MWB45-2, Sectorial 2, 45SW and 55SW oversized the crack in near side scanning. Comparison of length measurement results of MF A and MF B indicated the difference between the results of two similarly targeted mechanical fatigue cracks. The common observation was that all undersizing was done when scanned from far side with one exception (TRL70-2) and all oversizing was done when scanned from near side.

The results of length sizing of crack TF showed that all PAUT techniques except TRL and MC well oversized the crack when scanned from far side as can be seen on the right hand side in Figure 5. That was likely a consequence of noise due to weld metal causing difficulties to define the actual end points of a flaw indication. Despite of that, only two conventional techniques, MWK55-2 and MWK55-4, oversized the crack. Several techniques undersized the crack in near side inspection and TRL technique in both scanning directions. The results differ from those of mechanical fatigue cracks.

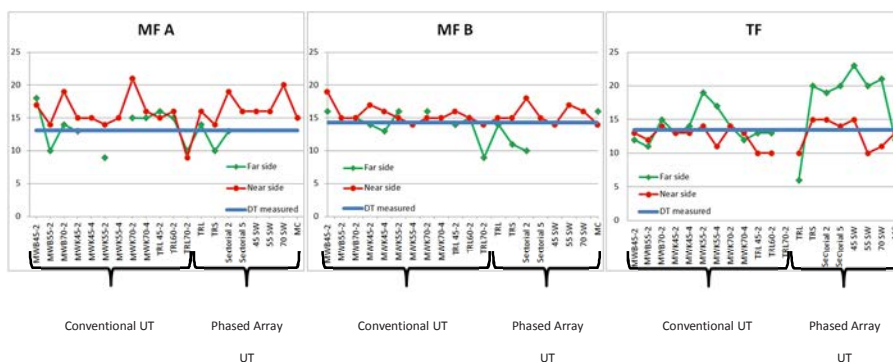


Figure 4. Comparison of the ultrasonic measurement length and destructively measured length.

Results showed that all PAUT techniques used in the inspection of EDM notch oversized the flaw except 55SW and MC techniques.

It was also seen that the highest RMSE values with conventional UT were calculated for techniques MWK55-2 from far side and MWK70-2 from near side. All PAUT

RMSE values were rather high. The highest values were calculated for TRS and Sectorial 2 techniques from both scanning directions ranging from 4.0 mm to 5.0 mm. Also the RMSE of 70SW from near side and with TRL from far side were among the highest values. A combination of near and far side inspection results indicated the higher RMSE of PAUT (except MC) compared to those of conventional UT.

Clearly higher RMSE was seen for crack MF A than for other cracks with conventional UT. With PAUT, the RMSE for crack TF scanned from far side and EDM notch scanned from near side were clearly higher than the others.

Comparison of conventional UT and PAUT showed that RMSE of TF crack and EDM notch with PAUT procedure were clearly the highest and there was no difference between the techniques with crack MF A.

The highest length sizing RMSE values were measured for TF crack when scanned through the weld (4.7 mm) and for EDM notch in both scanning directions (far side 4.0 mm and near side 5.5 mm). The RMSE of crack MF A was clearly higher when scanned from near side. Combination of near and far side inspection data showed that there was a difference between the two mechanical fatigue cracks and the highest RMSE was measured for EDM notch and secondly highest for TF crack. Results indicated that the length RMSE values of the studied flaws were higher in far side inspection with PAUT. With conventional UT, there was only a minor difference between near and far side inspection. The combined RMSE value of all length sizing data in this study was 3.3 mm.

X-ray tomography results

The results of tomographic x-ray imaging are presented in more detail in VTT research report VTT-R-05649-14 [1]. The length and the height measurements of the tomographic imaging are shown in Table 2. According to these results tomographic imaging seems to be good method for sizing fatigue flaws. The TF length measure differs more from the destructive results than MF A and MF B lengths. It can be concluded that the true branching of the both ends of the TF crack is not fully visible in tomographic x-ray imaging and this can affect on the accuracy of the length measurement done using tomographic results. It seems that tomographic imaging results are showing the shape of the flaws quite nicely near the surface area. Although the height measurement is relatively accurate, the shape of the flaw tip does not represent the actual flaw shape described in the destructive results.

Table 2. Dimensions measured using x-ray tomography.

Sample	Maximum length measured from tomographic x-ray imaging (mm)	Difference to length measured from fracture surface (mm)	Maximum height measured from tomographic x-ray imaging (mm)	Difference to height measured from fracture surface (mm)
MF A	13.0	-0.1	6.3	0.1
MF B	14.5	0.2	5.0	0.0
TF	12.5	-1.0	5.2	0.0

Summary and conclusions

In this study two kinds of artificial cracks from different manufactures and one reference notch were made in austenitic stainless steel test blocks. Flaws were examined using conventional UT, PAUT, computed x-ray tomography and digital radiography. The flaws were sized with different techniques and those results were compared to the true state flaw dimensions as determined by destructive analysis.

Typically flaw detection and especially flaw height sizing is considered challenging in ultrasonic inspection done from far side as the sound beam must penetrate through the weld material distorting and attenuating the sound waves. This study showed that mechanical fatigue cracks were not possible to reliably height size from far side but in most of the cases both TF crack and EDM notch could be height sized also from far side. That may be a consequence of the branching shape of the TF crack and wider opening of both TF crack (surface area) and EDM notch. This indicates the flaw type chosen may have a significant influence in the evaluation of the performance of the technique in that case.

To draw some conclusions of the performance of the techniques, RMSE values were compared. According to RMSE, EDM notch was height sized most accurately. PAUT performed better in height sizing than conventional UT and far side access was better than near side access. With conventional UT, TF crack was height sized most accurately and with PAUT, crack MF B was height sized most accurately. This study indicated slight height undersizing for PAUT techniques. Still, all PAUT techniques fulfilled the requirement of sizing accuracy stated by ASME.

Best performing conventional UT techniques for height sizing were techniques utilizing composite probes and angles of 45 and 55 degrees. The poorest conventional UT techniques for height sizing were the techniques utilizing longitudinal waves. Best performing PAUT technique for height sizing was SW55. This indicates that rather high frequency can be used for austenitic weld inspection with thickness of at least 25 mm. However, both side access is required to ensure the detection. The poorest PAUT technique for height sizing were Sectorial 2 and SW45 techniques both undersizing the flaws. Comparison between SW45 and SW55 – both utilizing 5 MHz frequency with linear scanning – indicates that a higher angle performs better in height sizing.

Crack MF B was length sized most accurately. Conventional UT performed better in length sizing than PAUT and near side access was slightly better than far side

access. With conventional UT, both MF B and TF crack were length sized with smallest error and with PAUT, crack MF B was length sized most accurately.

Conventional UT techniques MWK45-2 and MWK45-4 were both performing best in length sizing. The poorest conventional UT techniques for length sizing were MWB45-2, MWK70-2 and TRL70-2. PAUT technique performing best in length sizing was MC technique utilizing inside creeping wave. The poorest PAUT technique for length sizing were 45SW and 70SW both oversizing the flaws.

The size of the two mechanical fatigue cracks differed from each other. Also there was a difference in length/height ratio of the two similarly targeted flaws. All the flaws were reliably detected with all techniques when scanned from near side and with all techniques with frequency of 4 MHz or lower when scanned from far side.

X-ray tomography seems to be very accurate NDT method for length and height measurements of fatigue cracks with the setup and samples used in this research. There is some deviation in thermal fatigue crack length measurement but this is probably due to branching of the thermal fatigue crack is not fully visible with x-ray tomography. As a conclusion, x-ray tomography is a potential method for NDT inspections of crack like defects in austenitic stainless steels and welds. As seen in the x-ray tomography results section, the shape of the flaw is not entirely representative, especially the flaw tip area seems to be more or less incomplete compared to destructive analysis. Verifying the full potential of the method would need more research with different types and sizes of flaws as well as different materials and material thicknesses. X-ray tomography is relatively slow inspection method and therefore the use of the method requires careful planning in advance. The best option for in-service inspections with x-ray tomography would be the use of the method for verification and sizing the indications detected with other NDT methods.

The destructive investigations revealed that the cracks, in the investigated cross-sections, located in the weld metals, close to the fusion line. The cracks were unbranched and in two cross-sections, i.e., from samples MF A and MF B, small weld pores were observed. The cracks resembles fatigue cracks, although typical fatigue (corrosion fatigue and mechanical fatigue) are even straighter than these flaws. Intergranular stress-corrosion cracks in sensitized austenitic stainless steels are typically only slightly branched and the resemblance to the flaws is thus good. Also intergranular stress corrosion cracks in non-sensitized stainless steels are unbranched and resemble those of the flaws. They locate very close to the fusion line, within the few first grains from the fusion line. Transgranular stress corrosion cracks are, however, typically much more branched than the flaws.

In the future, more data from flaws of different sizes is needed to extend the knowledge of different reflector properties and the performance of different techniques. Also real geometries (pipe) shall be used. The presence of weld cap can also be studied by limiting the scanning area. As flaw manufacturing is expensive, destructive testing cannot be always done so data and knowledge gathered from this study is very important for future research work.

References

1. Leskelä, E.; Koskinen, A.; Haapalainen, J.; Ehrnsten, U.; Autio, J.-M. 2014. Comparison of artificial flaws in austenitic steel welds with NDE methods, VTT. 51 p. Research Report ; VTT-R-05649-14
2. Jäppinen, T.; Koskinen, A.; Leskelä, E.; Tuhti, A.; Haapalainen, J.; Sandlin, S. 2013. Monitoring of the structural integrity of materials and components in reactor circuit (MAKOMON). In: SAFIR2014. The Finnish Research Programme on Nuclear Power Plant Safety 2011-2014. Interim Report. Simola, Kaisa (ed.). VTT Technology 80. VTT, pp. 292 – 301 <http://www.vtt.fi/inf/pdf/technology/2013/T80.pdf>
3. Ehrnsten, U.; Pakarinen, J.; Karlsen, W.; Hänninen, H.; Mougnot, R.; Soinila, E.; Ahonen, M.; Autio, J.-M., Aaltonen, P.; Saukkonen, T. 2013. Environmental influence on cracking susceptibility and ageing of nuclear materials (ENVIS). In: SAFIR2014. The Finnish Research Programme on Nuclear Power Plant Safety 2011-2014. Interim Report. Simola, Kaisa (ed.). VTT Technology 80. VTT, pp. 268 – 282 <http://www.vtt.fi/inf/pdf/technology/2013/T80.pdf>
4. Koskinen, A.; Leskelä, E. 2013. Differences in indications of different artificially produced flaws in non-destructive examination. The 10th International Conference on NDE in Relation to Structural Integrity for Nuclear and Pressurized Components, Cannes, France, 1 – 3 October 2013. COFREND (Confédération Française pour les Essais Non Destructifs)
5. Leskelä, E. and Koskinen, A. Comparison of mechanical and thermal fatigue cracks by ultrasonic examination. VTT, Espoo 2014. 65 p. Research Report; VTT-R-00626-14
6. ASME. 2004. "Rules for Inservice Inspection of Nuclear Power Plant Components, Section XI." In ASME Boiler and Pressure Vessel Code – An International Code. American Society of Mechanical Engineers, New York.

32. RI-ISI analyses and inspection reliability of piping systems (RAIPSYS)

32.1 RAIPSYS summary report

Otso Cronvall¹, Jouni Alhainen¹, Kalle Kaunisto¹, Ilkka Männistö², Taneli Silvonen²,
Tero Tyrväinen²; Ari Vepsä¹

¹VTT Technical Research Centre of Finland Ltd
Kemistintie 3, P.O. Box 1000, FI-02044 Espoo

²VTT Technical Research Centre of Finland Ltd
Vuorimiehentie 3, P.O. Box 1000, FI-02044 Espoo

Abstract

The overall objective of the RAIPSYS project is to support the implementation of risk informed in-service inspection (RI-ISI) at Finnish nuclear power plants (NPPs) by studying and further developing relevant issues related to RI-ISI. The main objectives were the development of structural reliability methods for quantification of piping leak and break probabilities, further development of methods for evaluating inspection capability, further development of RI-ISI analysis methods, as well as strengthening inter-disciplinary readiness to combine structural integrity, non-destructive testing (NDT) and probabilistic safety analysis (PSA) expertise in Finland. The project has contributed to international activities, including the participation in the work of the Task Group on Risk (TGR) of the European Network for inspection and Qualification (ENIQ).

Introduction

RI-ISI aims at rational in-service inspection management by taking into account the results of plant specific risk analyses in defining the inspection programme and focusing the inspections efforts to the most risk-significant locations. Ideally the optimisation of ISI can lead to improved safety and availability, reduced radiation doses and reduced inspection costs.

From a technical perspective, a typical RI-ISI process consists of the following main steps [1]:

- definition of RI-ISI scope, collection and analysis of the required input data,
- identification and evaluation of piping failure consequences,
- identification and evaluation of piping failure potential,
- risk ranking,
- definition of the new inspection programme.

Typically, before implementing the RI-ISI program, the results of the RI-ISI analysis are required to be submitted to the national regulatory body for approval.

Even though RI-ISI has been widely applied in the US, European utilities and safety authorities think that several issues need further research. Furthermore, the US RI-ISI approaches cannot always be adopted as such since they have been originally developed to the US regulatory environment, and do not comply as such with national regulations and different standards in many European countries.

In Finland, the use of risk-informed methodology in planning new ISI programmes is a regulatory requirement, and both domestic utilities are developing RI-ISI programmes for the existing plants. The ISI programme for the new EPR unit will also consider risk insights.

The results of the first two project years are summarised in SAFIR2014 interim report [2], which is freely available, e.g. in the Internet. Thus, the emphasis of this final summary report is on the results of the latter two project years.

The structure of this document is such that it is divided into three main parts, those being Assessment of piping failure potential, Screening criteria and load application methods for probabilistic piping degradation analyses and RI-ISI methodologies, all of which cover several related research topics.

Assessment of piping failure potential

There are alternative ways to assess the probability of failure, ranging from purely qualitative assessment to quantification with either statistical analysis of service data or structural reliability models. The disadvantage of a qualitative approach is that the relative importance/severity of the degradation potential is not addressed, and quantitative comparison of e.g. alternative inspection strategies cannot be done. In RAIPSYS project, methods and tools for quantification of piping failure probabilities are developed. This requires applications for computation of leak and break probabilities due to relevant degradation mechanisms. This is carried out by further devel-

oping structural reliability approaches and probabilistic fracture mechanics (PFM) procedures.

In particular, the PFM procedures allow taking into account in a realistic quantitative way piping component geometry, material properties, loads and inspection strategies. Rather than considering the computed probability of failure (POF) results to represent some form of true or absolute value, they much better serve in quantifying relative POF differences between the piping components. The accuracy of the POF results can be improved by using statistical estimates based on both plant specific and global databases in order to provide anchoring/calibrating points for single POF results, in relation to which they could be improved in other locations as well. Quantitative approaches can also be used to conduct sensitivity studies, for instance to assess the impact of inspection capability and interval on the POF results.

Probabilistic analysis methods for estimating pipe component failures

Research work on structural reliability analysis methods at VTT has resulted in further development of a PFM tool. This tool is an expanded version of fracture mechanistic analysis code VTTBESIT, developed by the Fraunhofer-Institut für Werkstoffmechanik (IWM), Germany and by VTT. VTTBESIT code allows quick computation of the Mode I stress intensity factor (SIF) values along the crack front and, based on this, simulation of the crack growth. VTTBESIT was developed further by improving the crack growth computation procedure.

The results of the first two project years, 2011-2012, are briefly summarised in the following, for more detailed descriptions see ref. [2].

The accuracy of VTTBESIT was improved by developing and implementing a more accurate crack growth increment computation procedure [3]. This procedure takes into account the crack growth potential in all computation points along the crack front, whereas the earlier procedures considered it only in one or two crack front points.

VTTBESIT code uses Latin hypercube simulation (LHS) in the probabilistic crack growth simulations. In order to investigate possible computationally more efficient probabilistic methods, a case study concerning importance sampling (IS) was performed. This sampling method is a variance reduction method that can be used to enhance the plain Monte Carlo simulation (MCS) method. According to the analysis results, if the procedure is to be repeated often, and if less conservative assumptions are used for lower transfer probabilities, the IS is a useful alternative probabilistic simulation procedure [3].

A study on the estimation of crack initiation and leak frequencies concerning NPP piping components by using NPP piping degradation databases was performed [5]. The OECD Pipe Failure Database OPDE on NPP piping component degradation and failures was used for this purpose. However, OPDE does not contain any piping component or weld population data. As for the performed computations, the applied

procedure for crack growth was based on discrete Markov model. The used procedure was also programmed. It was concluded that the applied approach for computation of flaw initiation and leak frequencies is feasible for practical analysis purposes. However, without piping component or weld population data the usefulness of the obtained results is somewhat limited.

To expand the probabilistic analysis capabilities, the convolution integral method for computation of pipe break probabilities was implemented [4]. This method can be used both for deterministic and probabilistic crack growth analyses. The method combines crack initiation probability and growth probabilities. This method was also programmed. The method has some advantages over the discrete Markov chain method used in the previous RI-ISI analysis studies at VTT. In the Markov models the probability distributions are characteristically exponential. The convolution method does not have any assumptions about the form of the probability distributions, and consequently these distributions can be arbitrary. The method allows the use of multiple probability distributions and thus an arbitrary number of degradation states can be modelled. Thus, the convolution method is feasible for computation of pipe break probabilities, and is also promising from the viewpoint of further development.

The results of the latter two project years, 2013-2014, are summarised in the following.

In 2013, the discrete Markov model was developed further. Complicated pipe leak and break probabilities cannot be modelled accurately with the stationary Markov chain approach, and consequently the non-stationary Markov chain approach was implemented [6]. The non-stationary Markov chain method calculates separate degradation matrices for given time intervals, whereas the stationary Markov chain considers the whole NPP time in operation as a homogeneous process, by using a single degradation matrix for this time span. This analysis tool takes now better into account the different ageing phases of NPP systems, which can e.g. follow the bath tube curve. The purpose was also to apply this analysis tool to representative domestic NPP piping components. Three pipe welds were analysed with the stationary and non-stationary Markov chain approaches. Two non-stationary time interval options used in the computations were: 1) 0 – 10, 10 – 40, 40 – 60 years, and 2) 0 – 20, 20 – 40, 40 – 60 years. An example of obtained analysis results is presented in Figure 1 in the following for Medium size pipe. The outer diameter and wall thickness of the considered pipe cross-section are 170 mm and 11.0 mm, respectively, and the considered degradation mechanism is stress corrosion cracking (SCC).

In addition to implementing the non-stationary Markov chain method, also new probability of detection (POD) function was incorporated to the Markov analysis application of VTT [6]. The POD function provide the connection between inspections and quantitative RI-ISI analyses. If a crack is detected in the yearly inspections, the piping component in question is either repaired or replaced with a new one. Both of these actions return the pipe component to intact flawless state. The implemented POD function has been developed by the Fraunhofer institute (IZPF).

In 2014, the convolution integral based procedure for computation of NPP piping component degradation/failure probabilities was developed further [7]. This simple but efficient procedure was already implemented during 2012, and it applies also to

computation of small probabilities. The further development included taking into account the effect of inspections and considering more degradation states. Through these developments the procedure became more accurate and now provides more results.

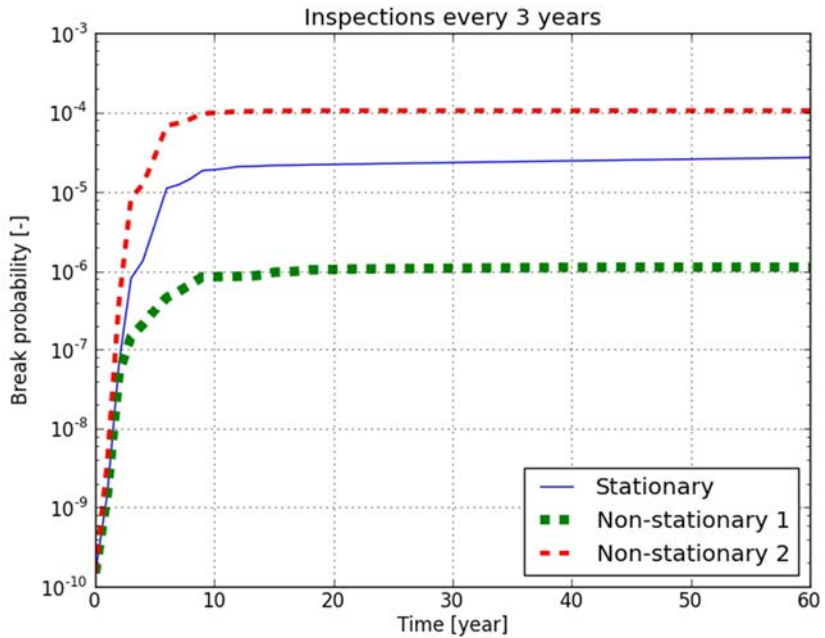


Figure 1. For inspection interval of three years, probability of failure results over 60 years computed with stationary and non-stationary Markov models for Medium size BWR primary circuit pipe weld [6].

In addition to further developing the convolution integral based procedure, a probability distribution was created for the initial size of thermal fatigue induced cracks [7]. This distribution was based on the data of 63 artificially evoked thermal fatigue induced cracks, as produced by Trueflaw Ltd company. Their maximum size is 3 mm and they have undergone at maximum 60000 loading cycles worth of growth before detection. A second order polynomial cumulative probability function was found to give better fit for the data than normal or lognormal distributions, which are commonly used for probability distribution functions of a variable with a natural scatter. Sampling for the initial crack size is then carried out by first assigning a random number between 0 and 1 for the cumulative probability and then solving the resulting second order equation for the initial crack size. The creation of this probability distribution included a number of uncertainties and deficiencies which give reason to take the results with certain caution.

Screening criteria and load application methods for probabilistic piping degradation analyses

As NPP piping component failure probabilities are usually very low, calculation of them can be tedious and require pipe component specifically several or even hundreds of thousands of deterministic simulations, using each time different sets of input values, as sampled from their corresponding density functions. It would considerably decrease the computational work, if part of the analysis cases could be screened out before the computations, as based only on the associated input data. This would require threshold data on the parameters that start and propagate the growth of flaws, such as cracks.

The main characteristics of cyclic loading are the frequency of occurrence and the amplitude. Both of these can remain constant or vary, the latter option describing much more realistically actual cyclic loading conditions than the former. There are several cases of cyclic loading with locally highly varying frequency of occurrence and amplitude. This is typical in such NPP piping Tees, where turbulent mixing of two water flows having different temperatures occurs. Such high-cycle loading conditions with substantially varying temperatures call for probabilistic more realistic method for application of loading, instead of applying such conservative application methods where some severe constant frequency of occurrence and amplitude are assumed.

Screening criteria for probabilistic piping degradation analyses

NPP piping components and their welds are inspected periodically to detect the possible flaws, such as cracks. As inspection of all components and welds is not feasible, the inspections are focused on sites with the highest risk. Deciding upon which components should be inspected and when, calls for RI-ISI analyses, which in turn can include calculation of failure probabilities for the piping components.

The SIF and SIF range threshold values can be used as screening criteria for the onset of SCC and fatigue induced crack growth, respectively. The main result of the study carried out in 2013 [8] is a collection of threshold data concerning these degradation mechanisms. The SIF and SIF range values describe the intensity of the loading and loading range at the crack front, respectively. When these values are below some specified threshold values, the crack growth should not start and the cases with such input data can be excluded from the computational analyses. Since austenitic stainless steel is the main material type of NPP piping components, the study is concentrated mainly on its several grades in different environments and temperatures.

Concerning SIF threshold data associated with the onset of SCC, the values found in the literature ranged from 5.8 MPa \sqrt{m} for 316N weld material in 108 °C to 27.5 MPa \sqrt{m} for mill annealed 316LN also in 108 °C. It was deemed, based on these data, that suitable threshold values and thus screening criteria are 6.0 MPa \sqrt{m} , assuming sensitized material, and 9.0 MPa \sqrt{m} , assuming annealed material. Con-

cerning SIF range threshold data associated with the onset of fatigue induced crack growth, for many stainless steels the values found in literature are between approximately $5 \text{ MPa}\sqrt{\text{m}}$ and $12 \text{ MPa}\sqrt{\text{m}}$. This threshold data is dependent on stress ratio, R .

To test how much the use of the threshold data decreases the computational work, two sets of fracture mechanics based analyses were carried out too, one concerning SCC and the other concerning fatigue induced crack growth. Different load magnitudes were applied in the computational analyses. Three different but small initial crack postulates were used in the analyses. According to the analysis results, depending on the load magnitude, either all or none of the cases exceed the associated threshold value.

Load application methods for probabilistic piping degradation analyses

In 2014 a study was carried out on collection, review and development of cyclic loading methods applicable to probabilistic fatigue induced crack growth analyses [9]. All considered approaches are applicable to NPP piping components. The scope of this study mainly concerns thermal high-cycle loading. The covered documents are codes and rules of a number of countries using nuclear energy, as well as fitness-for-service procedures and scientific literature. The developed new straightforward method for application of cyclic loading was compared to a corresponding existing one in a computational example concerning fatigue induced crack growth in a representative NPP piping Tee. To get a more distinctive model response, exaggerated loading was used.

The fatigue loading application methods in all covered national codes, such as U.S. ASME code Article NB-3000 [10], do not consider the chronological order of the load cycles. Instead, the computation of the cumulative fatigue usage factor is a simple algebraic sum covering all considered load cycles. In addition, the load cycles are to be conservatively summed up in the most severe order. These fatigue dimensioning procedures contain also other conservative features, through incorporation of safety factors and conservative definition of the fatigue strength curves. Thus, these conservative methods are not suitable for application of thermal high-cycle loading.

Some of the covered fitness-for-service procedures contain application methods for thermal high-cycle loading. The time history sequences description in the FITNET procedure [11] considers the chronological order of the load cycles, whereas the histogram description and the power or energy density spectrum description do not. In case of power or energy density spectrum approach, if the load cycles are picked randomly, which would correspond to loading conditions in NPP piping mixing points, it would make this method applicable to associated variable amplitude fatigue analyses. The time history sequences description appears suitable as such for application of cyclic thermal variable amplitude loading.

Altogether 5 levels for application of thermal cyclic loading in NPP Tees are presented in the extended THERFAT approach [12]. The Level 1 method is a simple screening criterion. The application of thermal loading in Level 2 and 3 methods uses sinusoidal shape for the thermal fluctuation against time and conservatively determined constant temperature range. The more advanced Level 4 and 5 methods use the power spectral density (PSD) procedure for application of thermal loading. The use of this procedure requires detailed input data, from actual measurements and/or from computational fluid dynamics (CFD) analysis results. Thus, the feasibility of this procedure for application of cyclic thermal variable amplitude loading involving crack growth up to pipe leak/break is good in terms of correspondence with reality but limited due to large amount of required detailed input data.

As for developments involving VTT this far, Hannink and Timperi [13] developed a method for application of thermal loading at NPP piping mixing points that delivers continuous and time dependent thermal loads from discrete data. On the other hand, it is limited to consider only one surface point. The approach is based on reproducing the fluid-temperature statistics from actual measurements or CFD simulations at locations near wall.

A more robust but still realistic method for application of the cyclic thermal loading in the NPP mixing points was developed in the VTT study [9]. The method uses sinusoidal shape for the thermal fluctuation against time and conservatively determined temperature range. To produce a discrete approximation of the load cycle duration range obtained in Step 4, five (or more) representative fluctuation frequencies are selected. The assembly of a long enough loading sequence is carried out by adding to consecutive order representative load cycles (as corresponding representative fluctuation frequencies) randomly, but when the load cycle causing the most severe stress range is picked, it is added twice in a row.

The developed new method for application of cyclic thermal loading is compared to THERFAT Level 2 method in a computational example concerning fatigue induced crack growth in a typical Tee in a BWR unit. The analysis results show that the VTT approach is considerably less over conservative than the THERFAT Level 2 method. Both as a function of time and of load cycles, the crack growth rate through wall is more than twice faster with the Level 2 method than with the VTT approach. However, at least for application of high-cycle thermal loading in NPP piping mixing points, the new VTT method still appears too conservative as compared to actual BWR operation experience. On the other hand, at least a part this conservatism originates from the applied fracture mechanics procedure.

RI-ISI methodologies

The research work on RI-ISI methodologies concerns issues related to risk ranking, selection of inspection sites and acceptance criteria of a RI-ISI program. As the main criterion for the acceptance of a RI-ISI program is that the risk will not increase when replacing the earlier ISI program with the risk informed equivalent, one research subject is the robust quantification of the change in risk. Another issue is to provide

both development and application guidance concerning quantitative RI-ISI methodology. The international co-operation and connections concern mainly participation to activities of ENIQ.

Effect of initial flaw and load assumptions on risk estimate changes

This study, spanning altogether three years, concerns the effect of initial flaw and load assumptions on risk estimate changes [14, 15, 16]. In addition, the effect of inspections is also taken into account. The performed degradation potential and risk analyses concern a representative selection of NPP piping welds. Worldwide several initial flaw distribution assumptions for NPP pipe welds have been published. The main load component concerning welds is most often the welding process induced residual stresses (WRSs), and also for them several distribution assumptions have been published. Of the degradation mechanisms encountered in the NPP environments, the WRSs affect especially SCC. To describe the accuracy of the NDT to find cracks, applicable probability of detection (POD) functions were used.

The scope of the most recent computational analyses covers:

- one representative BWR pipe weld cross-section size with the weld material similar to austenitic stainless steel, see Table 1,
- SCC as the considered degradation mechanism, with the considered flaw postulate being a semi-elliptic circumferentially oriented crack opening to inner surface,
- operational BWR conditions as the considered process loads, with pressure of 70 bar and temperature of 286 °C,
- three sets of probability density distributions for sizes of initial cracks, one of which has been developed within this study, see Table 1,
- one distribution for the WRSs, see Table 1,
- inspection intervals of 3 and 10 years as well as the case of no inspections.

In the VTT application for degradation potential and risk analyses, the crack growth through the pipe wall is quantified with discrete degradation states. This approach allows the use of Markov process simulations to calculate the leak and failure probabilities for piping components. The transition probabilities are assessed using the results from the PFM simulations, which are performed with the probabilistic VTT-BESIT code. In the VTTBESIT simulations the sizes of the initial cracks are taken randomly from the respective probability density functions, while all other input data

variables are considered as deterministic. VTTBESIT results are used to construct a degradation matrix for the Markov process, in which crack growth leads into more degraded states, while inspections and subsequent repairs/replacements lead into less degraded states. For transition probabilities into less degraded states, POD functions are used. They are applied in the computations in the form of inspection matrices.

The results of the first two project years, 2011-2012, are summarised in ref. [2], and are thus not repeated here. The results of the latter two project years, 2013-2014, are summarised in the following. The analysis results are taken mainly from VTT ref. [15].

Table 1. Input data used in performed leak and break probability analyses.

Pipe size	Outer diameter [mm]	Wall thickness [mm]	Reference
FRESH	323.85	17.45	[17]
Initial crack sizes by	Cause for crack initiation	Median crack depth [mm]	Reference
Simonen & Khaleel	fabrication	1.4 ... 2.7 (*)	[18]
NURBIT distribution	SCC	1.0	[19]
VTT distribution	SCC	0.5	[14]
Axial WRSs by/from	Maximum value [MPa]	Minimum value [MPa]	Reference
FRESH project results	300	-100	[17]
POD from	Scope	NDT quality options	Reference
NUREG/CR-3869	intergranular SCC, austenitic stainless steels and ferritic steels	advanced, good, poor	[20]
CCDP value	No. of degradation states	Time in operation [years]	Reference
0.00001	10	60	[14]

(*) depends on wall thickness.

In the legend of Figure 2 below, the following abbreviations are used:

- "Ins 3y" is inspection interval of 3 years, "Ins 10y" is inspection interval of 10 years, and "No Ins" is no inspections,
- "FRESH" is WRSs according to FRESH project results,

- "NURBIT ic" is initial SCC induced cracks according to NURBIT code, and "VTT ic" is initial SCC induced cracks developed within this research project.

A set of leak probability results is shown in Figure 2. To summarise, the effect of initial flaw and load assumptions as well as inspections on leak and break probabilities is remarkable. At the start and early phase of operation the initial crack sizes dominate the leak and break probability results. In general, the highest leak and break probability values were obtained with fabrication cracks, while the lowest leak and break probability values were achieved with SCC induced initial cracks developed within this study. Towards the end of operation the effect of initial crack sizes to leak and break probabilities decreases remarkably, while the effect of loads increases considerably. The inspections have a significant effect on the break probability results, as can be seen from the shapes of the green and black result curves. The break probabilities for analysis cases without inspections are after 20 and 60 years from 1 to 4.5 decades higher than for the cases with 3 year inspection interval.

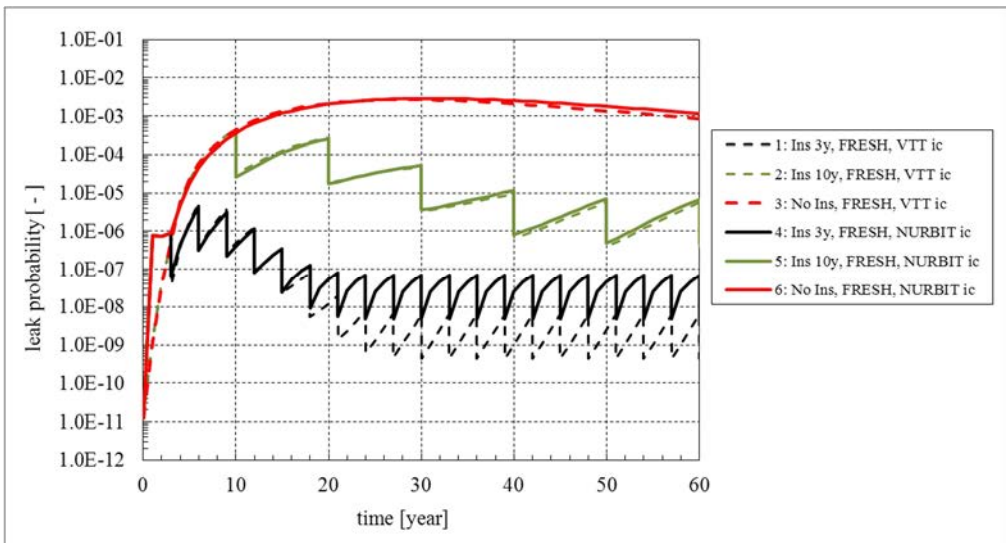


Figure 2. Leak probability results for FRESH weld cross-section [15].

ENIQ Task Group Risk activities

VTT has actively participated in the work of the Task Group Risk (TGR) of ENIQ. The TGR works towards developing European best practices for RI-ISI methodologies. The participation to TGR work includes contributing to ENIQ consensus documents, position/discussion documents and technical reports as well as participating

the ENIQ TGR meetings. ENIQ activities have included also the follow-up of development of and adaptation to ENIQ, as in 2012 it has become a part of the NUGENIA Association. This far the main reporting contribution by VTT has been to ENIQ TGR discussion document: RI-ISI – Lessons Learned from Application to European Nuclear Power Plants. Through ENIQ TGR activities VTT also participated in preparation and submitting of the REDUCE EU research project proposal in November 2014. The acronym REDUCE stands for "Justification of risk reduction through in-service inspection".

Scientific and academic publications

Scientific journal article: Assessment of Initial Cracks for RI-ISI Analysis Purposes [21]. The article concerns quantitative assessment of initial cracks. Two developed approaches to recursively calculate estimates for the sizes of the initial cracks are described. The application example presents the impact of different initial crack sizes on POF results.

Scientific journal article: A study on the effect of flaw detection probability assumptions on risk reduction achieved by non-destructive inspection [22]. The article summarises the results of a study on the effect of piping inspection reliability assumptions on failure probability using structural reliability models. The main interest was to investigate whether it is justifiable to use a simplified POD curve. Further, the study compared various structural reliability calculation approaches for a set of analysis cases. The results indicate that the use of a simplified POD could be justifiable in RI-ISI applications.

Scientific VTT publication: Structural lifetime, reliability and risk analysis approaches for power plant components and systems [23]. The publication begins with an overview of power plant environments and a description of the various degradation mechanisms affecting the power plant systems and components. Then, deterministic structural analysis methods are described. Several probabilistic analysis procedures and risk analysis methods are presented. The modelling methods for various degradation (or ageing) mechanisms are described. As for the analysis applications, a wide selection of probabilistic system/component degradation and risk analysis software tools is presented. The computational application concerns probabilistic failure and lifetime analyses to a representative set of NPP piping components with probabilistic analysis codes VTTBESIT and PIFRAP. The publication ends with a summary and suggestions for future research.

Licentiate in technology thesis: Structural lifetime, reliability and risk analysis approaches for power plant components and systems [24]. The above mentioned scientific VTT publication is based on this thesis.

References

1. Chapman O., J., V., Gandossi, L., Mengolini, A., Simola, K., Eyre, T. and Walker, A., E. (Editors). European Framework Document for Risk Informed In-Service Inspection, ENIQ Report No. 23, JRC-Petten, EUR 21581 EN, 2005.
2. SAFIR2014 - The Finnish Research Programme on Nuclear Power Plant Safety 2011–2014 Interim Report. Editor: Simola, K., Report VTT TECHNOLOGY 80, VTT Technical Research Centre of Finland (VTT), Finland, 2013. 452 p.
3. Cronvall, O., Vepsä, A. Further development and validation of probabilistic analysis application VTTBESIT. Research Report VTT-R-01837-12, Technical Research Centre of Finland (VTT), Espoo, Finland, March 2012. 49+7 p.
4. Alhainen, J., Kaunisto, K., Vepsä, A. Further development and validation of probabilistic analysis application VTTBESIT: the work carried out in 2012. VTT Research Report VTT-R-08803-12, Technical Research Centre of Finland (VTT), Espoo, Finland, 2013. 39 p.
5. Kaunisto, K., Männistö, I. Estimation of crack initiation and leak frequencies using NPP piping degradation databases. Research Report VTT-R-00078-12, Technical Research Centre of Finland (VTT), Espoo, Finland, March 2012. 25 p.
6. Kaunisto, K. Probabilistic modelling of piping degradation with non-stationary Markov chains. VTT Research Report VTT-R-00757-14, Technical Research Centre of Finland (VTT), Espoo, Finland, February 2014. 28 p.
7. Kaunisto, K., Vepsä, A. Development of initial fatigue crack size distribution and probabilistic NPP piping degradation computation procedure. VTT Research Report VTT-R-00059-15, Technical Research Centre of Finland (VTT), Espoo, Finland, January 2015. 44 p.
8. Vepsä, A., Silvonen, T. Usage of stress intensity factor thresholds as screening criteria in probabilistic fracture mechanics computations. VTT Research Report VTT-R-00546-14, Technical Research Centre of Finland (VTT), Espoo, Finland, February 2014. 45 p.
9. Cronvall, O. Literature study and methodology development for cyclic loading application to probabilistic fatigue analyses. VTT Research Report VTT-R-00213-15, Technical Research Centre of Finland (VTT), Espoo, Finland, January 2015. 48 p.

10. ASME Boiler and Pressure Vessel Code Section III, Division 1, Article NB-3000, Paragraph NB-3200. 2013 Edition.
11. FITNET Fitness-for-Service PROCEDURE, Revision MK8. Editor(s) Koçak, M. et al. European Fitness-for-Service Thematic Network – FITNET. Germany, January 2008.
12. Paffumi, E., Radu, V., Nilsson, K.-F. Thermal fatigue striping damage assessment from simple screening criterion to spectrum loading approach. *International Journal of Fatigue* 53 (2013) 92–104.
13. Hannink, M. H. C., Timperi, A. Simplified methods to assess thermal fatigue due to turbulent mixing. In: 19th International Conference on Nuclear Engineering (ICONE19), 2011, Chiba, Japan.
14. Cronvall, O., Kaunisto, K. Second phase of a study - Effect of initial flaw and load assumptions on risk estimate changes. VTT Research Report VTT-R-08805-12, Technical Research Centre of Finland (VTT), Espoo, Finland, 2013. 60 p.
15. Cronvall, O. Third phase of a study - Effect of initial flaw and load assumptions on risk estimate changes. Research Report VTT-R-01044-14, Technical Research Centre of Finland (VTT), Espoo, Finland, February 2014. 31 p.
16. Tyrväinen, T. Summary on effect of initial flaw and load assumptions on risk estimate changes. Research Report VTT-R-00020-15, Technical Research Centre of Finland (VTT), Espoo, Finland, January 2015. 24 p.
17. Keinänen, H., Chauhan, C. Computation of Welding Residual Stresses in a Multi-Pass Welded Mock-up Pipe. Research Report VTT-R-08364-12, Technical Research Centre of Finland (VTT), Espoo, Finland, December 2012. 22+3 p.
18. Khaleel, M., A., Simonen, F., A. Effects of alternative inspection strategies on piping reliability. *Nuclear Engineering and Design* 197 (2000) 115–140.
19. Brickstad, B. The Use of Risk Based Methods for Establishing ISI-Priorities for Piping Components at Oskarshamn 1 Nuclear Power Station. SAQ/FoU-Report 99/5, SAQ Control AB, Sweden, 1999. 83 p.
20. Simonen, F., A., Woo, H., H. Analyses of the Impact of Inservice Inspection Using a Piping Reliability Model. NUREG/CR-3869, Topical Report. U.S. Nuclear Regulatory Commission (USNRC), July 1984. 59 p.

21. Cronvall, O., Männistö, I., Alhainen, J. On Assessment of Initial Cracks for RI-ISI Analysis Purposes. *Journal of Materials Science and Engineering B* 1 (2011) 296-307.
22. Cronvall, O., Simola, K., Männistö, I., Gunnars, J., Alverlind, L., Dillström, P., Gandossi, L. A study on the effect of flaw detection probability assumptions on risk reduction achieved by non-destructive inspection. *Reliability Engineering & System Safety* 105 (2012) 90–96.
23. Cronvall, O. Structural lifetime, reliability and risk analysis approaches for power plant components and systems. VTT Publication P775. 264 p.
24. Cronvall, O. Structural lifetime, reliability and risk analysis approaches for power plant components and systems. Aalto University School of Science and Technology, December 2011. 193 p.

32.2 Effect of initial flaw and load assumptions on risk estimate changes

Otso Cronvall¹, Jouni Alhainen¹, Kalle Kaunisto¹, Ilkka Männistö², Tero Tyrväinen²

¹VTT Technical Research Centre of Finland Ltd
Kemistintie 3, P.O. Box 1000, FI-02044 Espoo

²VTT Technical Research Centre of Finland Ltd
Vuorimiehentie 3, P.O. Box 1000, FI-02044 Espoo

Abstract

This document concerns the effect of initial flaw and load assumptions on nuclear power plant (NPP) piping failure potential and risk estimate changes. In addition, the effect of inspections is also taken into account. These issues concern in particular quantitative risk informed in-service inspection (RI-ISI) analyses of NPP piping systems. This document presents the results from a three year study. The issues in question were examined through computational analyses, while at the same time further developing the applied analysis procedures and applications. The analyses concern pipe leak/break probability and risk computations performed with probabilistic VTTBESIT code and Markov process based application for a set of representative NPP piping welds, covering a wide range of initial flaw and load assumptions. The considered degradation mechanism is stress corrosion cracking (SCC). The new developments include new size estimates for SCC induced initial cracks as well as extension and improvement of the Markov application. The sizes initial flaws have a considerable effect on the leak/break probability and risk results. On the other hand,

towards the end of time in operation, the effect of initial crack sizes to leak/break probability and risk results decreases remarkably, while the effect of loads increases considerably. The magnitude of the loading has the biggest effect on the pipe break probability results. The loading is clearly governed by the weld residual stresses (WRSs). The effect of inspections on the results is very beneficial, as the leak/break probability and risk values decrease. However, soon they start to climb up again. It is deemed that the applied analysis tools are feasible to quantitative RI-ISI analyses, providing useful analysis results for risk informed decision making.

Introduction

The RI-ISI analyses aim at rational in-service inspection management by taking into account the results of plant specific risk analyses in defining the inspection programme and focusing the inspections efforts to the most risk significant locations. Ideally, the optimisation of ISI can lead to improved safety and availability, reduced radiation doses and reduced inspection costs.

Concerning NPP piping component welds, initial flaw and load assumptions have major impact on both leak/break probability and risk results. Worldwide several initial flaw distribution assumptions for NPP pipe welds have been published. The main load component concerning welds is most often the WRSs, and also for them several recommendations have been published. Often the WRS recommendations for NPP pipe welds are such that on both axial and hoop directions the stresses are of the scale of material yield strength in tension in and near the inner surface, and remaining so through wall in the hoop direction, but turning to compression towards the outer surface in the axial direction. Of the degradation mechanisms encountered in the NPP environments, the WRSs affect especially SCC.

The leak/break probability and consequently the risk of NPP piping components can be considerably decreased by performing inspections with non-destructive testing (NDT) techniques. The more accurate the NDT technique, the smaller the cracks that can be found. When a crack is detected before it has grown through wall, which would lead to leak or break, the weld and associated component(s) can be safely repaired or replaced with new ones. The probability of detection (POD) functions are commonly used to describe the accuracy/reliability of NDT, and they often include also the quality of the NDT team. The POD functions typically express the POD in relation to crack depth through component wall. Worldwide several material and degradation mechanism specific POD functions applicable to NPP components have been published.

Concerning the initial flaw and load assumptions as well as inspections it needs to be clarified:

- what quantitative impact these assumptions have on NPP piping component leak/break probability and risk assessment results,
- which assumptions appear unrealistic/overly conservative,

- which assumptions could be recommendable to be applied,
- what effects inspection interval has on leak/break probability and risk assessment results.

This document comprises the results from three VTT research reports, see refs. [25, 26, 27].

The structure of this document is as follows. The probabilistic VTTBESIT code and Markov process based analysis tool developed by VTT are briefly described next, including the further development of the latter. A summary of the used input data are presented then, including the development of new size estimates for SCC induced initial cracks. This is followed with a description of the performed NPP piping component leak/break probability and risk analyses. The most significant analysis results are presented next. The document ends with a summary and conclusions.

Applied probabilistic analysis tools

As necessary input data, the Markov process application needs the crack growth simulation results obtained with the probabilistic VTTBESIT code [28, 29, 30, 31, 32]. The capabilities of the probabilistic VTTBESIT and Markov application are briefly described in detail in the following.

In both deterministic and probabilistic versions of VTTBESIT, the fracture mechanics parameter driving the crack growth is the mode I stress intensity factor, K_I [31]. The computation of the K_I values is performed along the crack front at 30 ° intervals with the code part developed by IWM. It is based on the weight and influence function methods. Solutions are provided for "infinite" and semi-elliptical crack cases in plates and hollow cylinders. The crack growth computation part and probabilistic capabilities have been developed by VTT. The material and geometry data for the computations are given through a graphical interface. The same data can also be given in a text file format. The loading data, in form of stress distributions through the component wall, are given in a separate file. For the computations, initial crack postulates are needed. The code user can either choose those from a provided library of postulates/distributions or insert some specified crack size. Two crack growth models are provided in the analysis code: Paris-Erdogan equation for fatigue induced crack growth [34] and rate equation for SCC [35, 36]. Thus, besides K_I values, VTTBESIT results include also the dimensions of the growing crack as a function of load cycles in case of fatigue, and as a function time in case of SCC. The analysis code writes the results in a separate file.

The analysis flow of the probabilistic VTTBESIT is as follows [25]:

- reading of the deterministic input data,

- random picking of certain input data parameters from the specified distributions; 1) SCC; probability distributions for initial crack depth and length, 2) fatigue induced crack growth; probability distributions for initial crack depth, length, and frequency of load cycles,
- crack growth analysis; the magnitude of crack growth in each time step is calculated from the respective crack growth equation \Rightarrow the ending criterion of the analysis is that crack depth reaches the opposite pipe surface,
- for each analysed piping component, at least 5000 separate simulations with Latin hypercube simulation (LHS) procedure are computed,
- the degradation state to which the crack has grown is computed for each year of the assumed time in operation and for each simulation \Rightarrow these results are used in the ensuing probabilistic Markov process based degradation potential analyses.

The applied discrete time Markov procedure for degradation potential analyses is summarised by the following four steps [33]:

1. Crack growth simulations with probabilistic VTTBESIT provide most of the needed input data.
2. Construction of degradation matrix transition probabilities from VTTBESIT simulation results and database analysis of crack initiation frequencies.
3. Model for inspection quality, as based on applicable POD functions, which are in turn used to construct inspection matrix transition probabilities.
4. Markov model to calculate pipe leak/break probabilities and risks for chosen inspection programs.

The Markov model uses either 8 or 10 degradation states, as depending on the wall thickness of a piping component. This enables the simulation of all possible inspection programs, including the possibility of detecting a flaw and not repairing it. The consequence measure used in the risk computations is the conditional core damage probability (CCDP).

In 2013, the Markov process application was developed further. Complicated pipe leak and break probabilities cannot be computed accurately with the stationary Markov chain approach, and consequently the non-stationary Markov chain approach was implemented [6]. The non-stationary Markov chain method calculates separate degradation matrices for given time intervals, whereas the stationary Markov chain considers the whole NPP time in operation as a homogeneous process, by using a

single degradation matrix for this time span. This analysis tool takes now better into account the different ageing phases of NPP systems, which can e.g. follow the bath tube curve.

Performed analyses and necessary input data

The performed leak/break probability and risk analyses concern a representative selection of NPP piping welds. To describe the accuracy of the NDT to find cracks, applicable probability of detection (POD) functions were used.

The scope of the computational analyses covers:

- four representative BWR pipe weld cross-section sizes with the weld material similar to austenitic stainless steel, see Table 1,
- SCC as the considered degradation mechanism, with the considered flaw postulate being a semi-elliptic circumferentially oriented crack opening to inner surface,
- operational BWR conditions as the considered process loads, with pressure of 70 bar and temperature of 286 °C,
- three sets of probability density distributions for sizes of initial cracks, one of which has been developed within this study, see Table 1,
- three distributions for the WRSs as well as the case of no WRSs, see Table 1,
- inspection intervals of 3 and 10 years as well as the case of no inspections.

Table 1. Input data used in performed leak/break probability and risk analyses.

Pipe size	Outer diameter [mm]	Wall thickness [mm]	Reference
Small	60	4.0	[14]
Medium	170	11.0	[14]
Large	310	26.0	[14]
FRESH	323.85	17.45	[17]
Initial crack sizes by	Cause for crack initiation	Mean crack depth [mm]	Reference
Simonen & Khaleel	fabrication	1.4 ... 2.7 (*)	[18]
NURBIT distribution	SCC	1.0	[19]
VTT distribution	SCC	0.5	[14]
Axial WRSs by/from	Maximum value [MPa]	Minimum value [MPa]	Reference
ASME recommendations	200, 210, 210 (**)	-200, -210, -210 (**)	[41]
R6 Method, Rev. 4	320, 320, 320 (**)	30, 30, 120 (**)	[42]
SSM handbook	200, 260, 50 (**)	-200, -170, -50 (**)	[43]
FRESH project results	300 (***)	-100 (***)	[17]
POD from	Scope	NDT quality options	Reference
NUREG/CR-3869	intergranular SCC, austenitic stainless steels and ferritic steels	advanced, good, poor	[20]
CCDP value	No. of degradation states	Time in operation [years]	Reference
0.00001	8 or 10	60	[14]

(*) depends on wall thickness,

(**) for Small, Medium and Large pipe weld cross-sections, respectively,

(***) for FRESH pipe weld cross-section.

The assessment of depth and length of SCC induced initial circumferential cracks developed within this study is described in the following. This treatment is based on the same flaw data as was used for the assessment of the corresponding initial cracks included in the NURBIT code, see ref. [19]. These data consist of 98 detected SCC cases, ca. 90 % of which are circumferentially oriented cracks opening to inner pipe surface. A recursive method based on fracture mechanics and statistical curve fitting was used to assess the probabilistic distributions for depth and length of cracks initiating due to SCC during plant operation. The first step in the applied approach is to convert the size data concerning detected grown SCC induced cracks to dimensionless form in relation to pipe wall thickness and inner circumference. Then, with recursive fracture mechanics based analyses, the thus obtained data is

matched with the assumed initial size criteria, corresponding here to respective K_I threshold values for SCC initiated cracks. Finally, the thus obtained data is converted to probabilistic form and suitable reliability distribution functions are fitted to them. The fitted probabilistic density function for estimated initial crack depths is a linear function with mean value of 0.48 mm. Whereas the fitted probabilistic density function for estimated initial crack lengths is an exponential function with mean value of approximately 6.5 % of the inner cross-section circumference.

The pipe break probability results after 1, 5, 20 and 60 years in operation for the Medium and FRESH project [17] weld cross-sections are presented in Figures 1 to 3. The results for the Medium weld cross-section are presented first, then those for the FRESH project [1] weld cross-section. In all analysis cases the quality of the inspections is good, as according to NUREG/CR-3869 report [20].

In the legends of the result figures, the following abbreviations are used:

- "Fabr. ic" is fabrication induced cracks [18], "NURBIT ic" is initial SCC induced cracks according to NURBIT code [19], "VTT ic" and is initial SCC induced cracks developed within this project [25],
- "ASME" is WRSs according to ASME recommendations [41], "R6" is WRSs according to R6 Method, Rev. 4 [42], "SSM" is WRSs according to SSM handbook [43], and "FRESH" is WRSs according to FRESH project results [17],
- "Ins 3y" is inspection interval of 3 years, "Ins 10y" is inspection interval of 10 years, and "none" is no inspections.

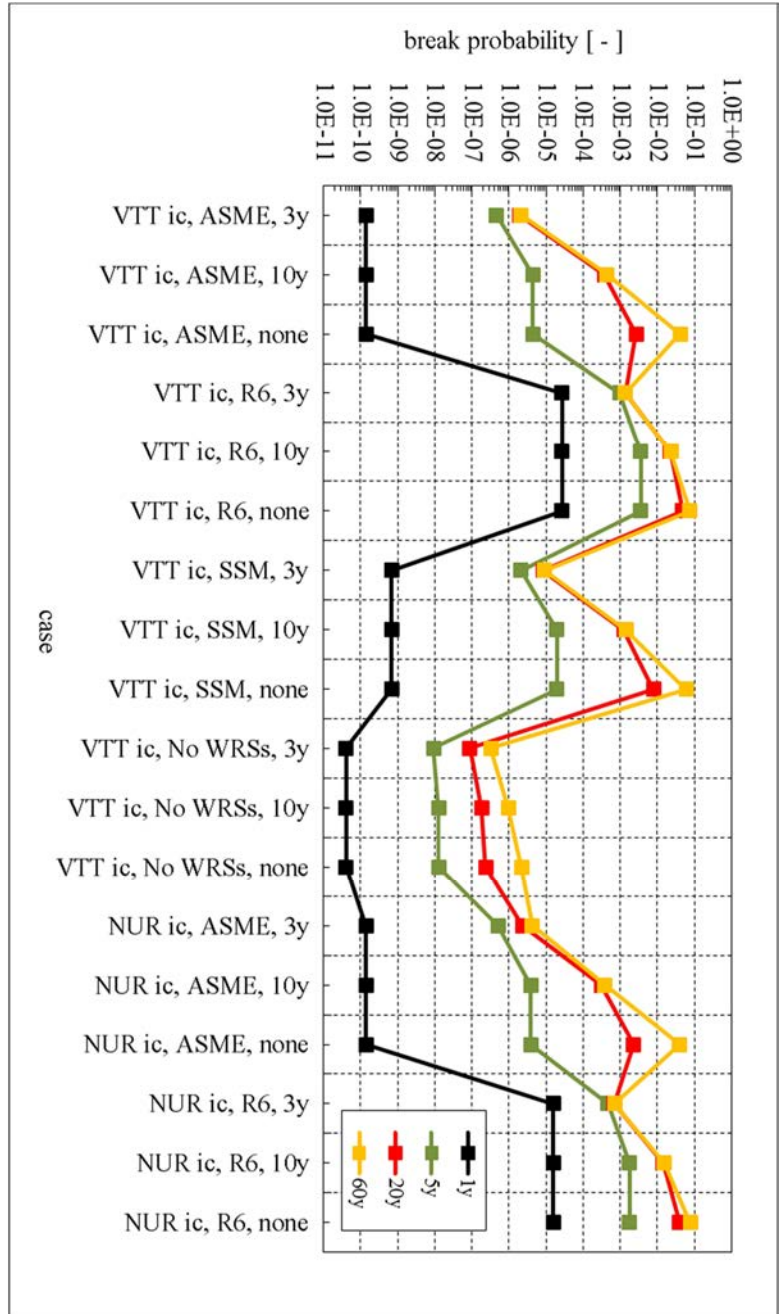


Figure 1. Comparison of pipe break probabilities after 1, 5, 20 and 60 years in operation for Medium weld cross-section, Cases 1-17 [26].

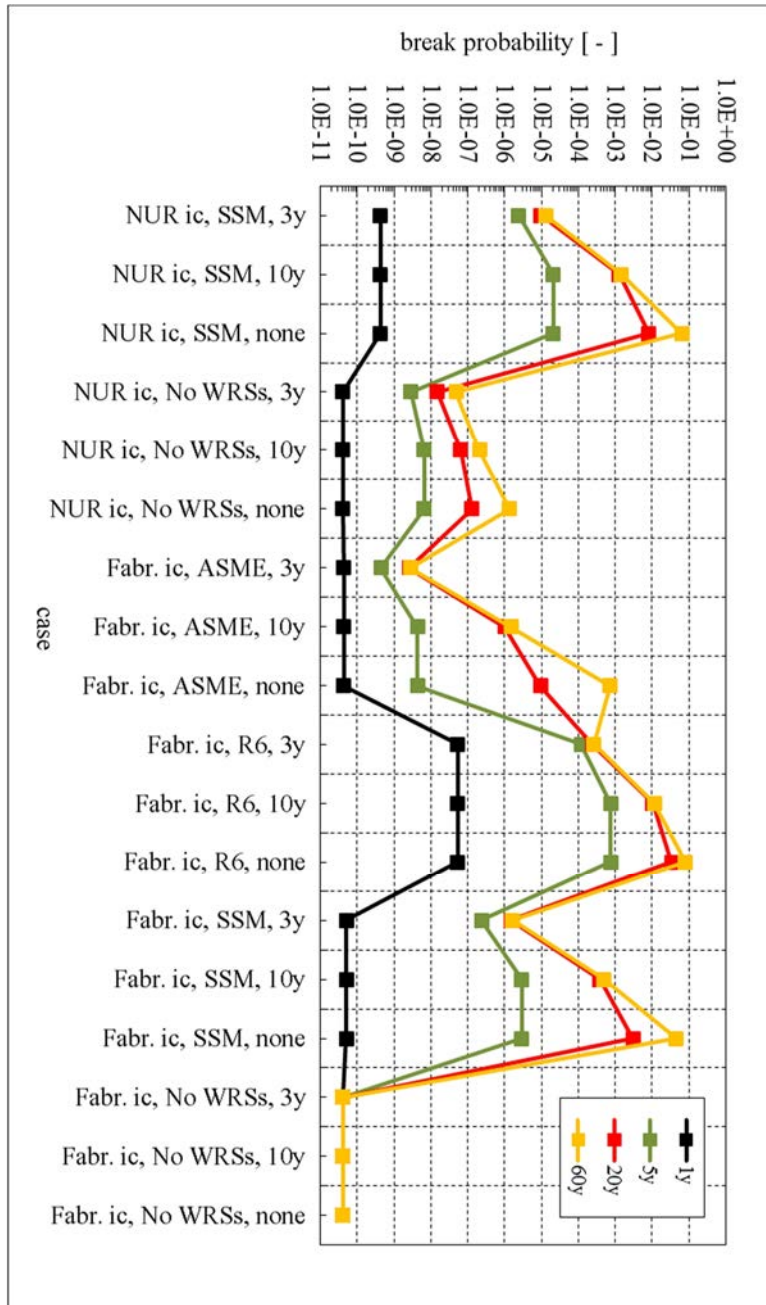


Figure 2. Comparison of pipe break probabilities after 1, 5, 20 and 60 years in operation for Medium weld cross-section, analysis Cases 18-34 [26].

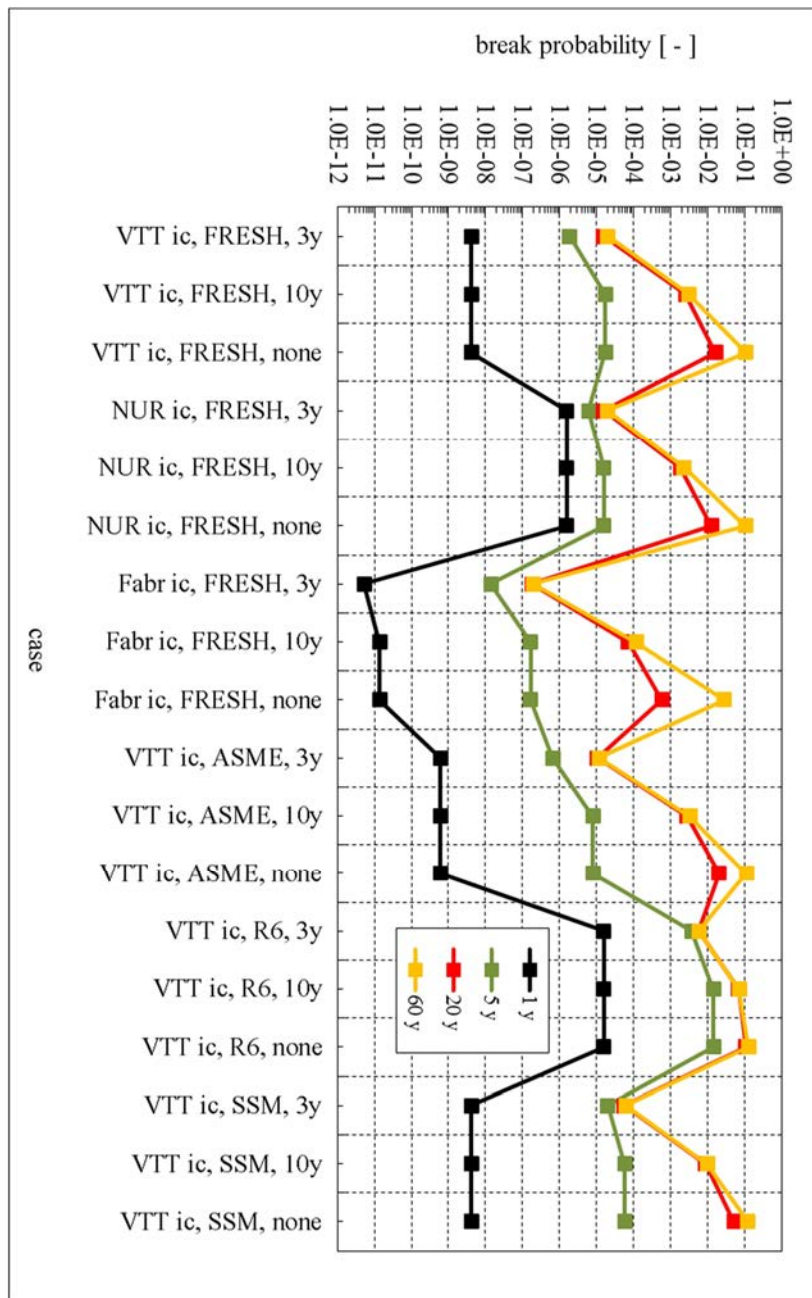


Figure 3. Comparison of pipe break probabilities after 1, 5, 20 and 60 years in operation for FRESH weld cross-section, analysis Cases 35-53 [27].

Summary and conclusions

All varied input data parameters, namely weld cross-section size, initial flaw and load assumptions as well as inspection intervals have a remarkable effect on the resulting leak and break probabilities as well as on the risk values. The discussion on the results here is limited to concern the pipe break probabilities, thus leak probability and risk results are not considered. This is because of the two flawed states, leak and break, the latter is more severe one, whereas the risk result curves only repeat with an offset those concerning break probability, due to having used the same CCDP value in all risk computations.

The pipe weld cross-section size clearly has an effect on the resulting break probabilities. For Small weld cross-section with 4.0 mm thick wall, the break probabilities are generally from 3 to 8 decades higher after one year in operation than for the other two weld cross-sections. The break probabilities after one year in operation for the Medium weld cross-section with 11.0 mm thick wall and Large weld cross-section with 26.0 mm thick wall are almost matching. The maximum break probability values after 20 and 60 years in operation are almost matching for all three considered pipe weld cross-sections, being of the scale of $1.0E-01$. However, in general the break probability values after 20 and 60 years are much lower for Medium and Large cross-sections than for Small cross-section.

The assumptions concerning initial flaw sizes have a considerable effect on the failure probability results. The fabrication induced cracks [18] provide the initial flaw state for all analysis cases, whereas for the cases with SCC induced initial cracks developed by VTT [25] and with those in the NURBIT code [19], additional SCC flaws initiate during operation as according to the associated probabilistic density functions and initiation frequency. The break probabilities after one year in operation are the smallest for the cases with fabrication induced cracks alone, whereas these probabilities are from 1 to 3 decades higher for the cases with the SCC induced initial cracks developed by VTT and with those in the NURBIT code. The effect of the initial flaw sizes to break probabilities is most pronounced in the early phase of the time in operation. As for the maximum break probability values after 20 and 60 years in operation, they are almost matching for all three used assumptions for initial crack sizes, thus reflecting their decreased effect.

The magnitude of the loading has the biggest effect on the break probability results. The loading is clearly governed by the WRSs. Of the considered four sets of WRS distributions, those given in the R6 Method, Rev. 4 [42] are by far the most severe. This is strongly reflected in the analysis results, as for the cases with the R6 Method, Rev. 4 [42] WRSs, the break probabilities after one year are from 1 to 6 decades higher than for all other cases with WRSs, whereas for break probabilities after 20 and 60 years this difference varies from 1 to 11 decades. However, for Medium weld cross-section all cases with WRSs and without inspections show almost matching break probabilities after 20 and 60 years. For all cases with no WRSs, the resulting break probability values are extremely low.

When comparing the analysis cases with FRESH WRSs [17] to those with WRSs from the ASME recommendations [9, 10], the R6 Method, Rev. 4 [42] and the SSM handbook [43], the break probabilities after one year in operation are the smallest for the cases with FRESH WRSs and fabrication cracks only. Whereas after 60 years the smallest break probabilities are for analysis cases with FRESH and ASME WRSs and fabrication cracks only. In general, for analysis cases with FRESH WRSs the break probabilities are from 0 to 3 decades lower than for those with the other three WRS distributions.

The inspections have a significant effect on the break probability results. For analysis cases with WRSs, comparing the break probabilities without inspections after 20 and 60 years to those with 3 year inspection interval, they are from 0.5 to 1.5 decades higher for Small weld cross-section, from 2 to 4.5 decades higher for Medium weld cross-section, and from 1 to 2.5 decades higher for Large weld cross-section, respectively.

Recommendations concerning initial flaw and load assumptions to be used in quantitative RI-ISI analyses are presented in the following.

The fabrication induced cracks provide the initial flaw state for all analysis cases, whereas for the cases with SCC induced initial cracks developed by VTT [25] and with those in the NURBIT [19] code, additional SCC flaws initiate during operation as according to the associated probabilistic density functions and initiation frequency. For the sizes of fabrication induced cracks, it is recommended to use the definitions developed by Khaleel and Simonen [18]. As for the estimates for sizes of SCC induced initial cracks, those provided by VTT [25] and those in the NURBIT code [19] have been developed using similar recursive approach. Of them those provided by VTT give a wider scope of probabilistic variation than those in the NURBIT code, as in the former case the probabilistic density functions are provided both for the initial crack depth and length, whereas according to the NURBIT code the depth of the initial cracks is fixed to 1.0 mm and a probabilistic density function is given only for the length of initial cracks. This fixed value for the crack depth can be considered as unnecessary conservatism. The median depth for the SCC induced initial cracks provided by VTT [25] is 0.48 mm, being in relative terms much less than the fixed crack depth in the NURBIT code [19]. Thus, it is recommended that for the sizes of SCC induced initial cracks in the NPP piping welds, those developed by VTT [25] are used.

The WRSs should be self-balancing, meaning that when other loads are removed and WRSs act alone, they should balance themselves across the cross-section in the axial pipe component direction. The R6 Method, Rev. 4 [42] axial WRSs for welds joining NPP pipes of austenitic stainless steel remain on the tensile side through the wall, thus being not self-balancing, which is unrealistic. Due to that, and because the magnitude of these WRSs is of the scale of material ultimate strength for almost half of the wall thickness and considerably higher than yield strength elsewhere, they are deemed as overly conservative, and thus it is not recommendable to use them. On the other hand, the ASME recommendations [41] and SSM handbook [43] do provide self-balancing axial WRSs across the wall and cross-section for welds joining NPP pipes of austenitic stainless steel, exceeding the yield

strength only at and near the inner surface, and being in no point near the ultimate strength. Of the WRS recommendations, those which are published more recently are also backed by more experimental data and more accurate finite element (FE) simulation results. The ASME recommendations [41] have been published 30 years ago, whereas the WRSs given in the SSM handbook [43] have originally been published almost 20 years ago. The ASME recommendations [41] provide one of the very first published sets of WRS recommendations, but due to relatively small amount of associated background data the presented WRS distributions are in some cases very simple and probably not very accurate. However, the WRS recommendations in the SSM handbook [43] are based on much greater amount of both experimental data and FE simulation results. Thus, the SSM handbook [43] WRSs for welds joining NPP pipes of austenitic stainless steel are recommended to be used. Another more recently published collection of WRS distributions, namely that in the SINTAP procedure [45], is recommended to be used too. The SINTAP WRS recommendations are backed by more experimental data and FE simulation results than those in the SSM handbook [43], and are also self-balancing in the axial direction for welds joining NPP pipes of austenitic stainless steel.

As a final conclusion, the presented computational analysis examples show that the used procedure, with probabilistic VTTBESIT code and Markov process based programmed analysis tool, is applicable for quantitative RI-ISI analyses. There are also some suggestions concerning further development of the VTT RI-ISI analysis procedure.

References

25. Cronvall, O., Männistö, I., Alhainen, J. First phase of a study - Effect of initial flaw and load assumptions on risk estimate changes, Rev. 1. VTT Research Report VTT-R-08024-12, Technical Research Centre of Finland (VTT), Espoo, Finland, November 2012. 50 p.
26. Cronvall, O., Kaunisto, K. Second phase of a study - Effect of initial flaw and load assumptions on risk estimate changes. VTT Research Report VTT-R-08805-12, Technical Research Centre of Finland (VTT), Espoo, Finland, 2013. 60 p.
27. Cronvall, O. Third phase of a study - Effect of initial flaw and load assumptions on risk estimate changes. Research Report VTT-R-01044-14, Technical Research Centre of Finland (VTT), Espoo, Finland, February 2014. 31 p.
28. Varfolomeyev, I. et al. BESIF 1.0: Stress Intensity Factors for Surface Cracks under 2D Stress Gradients. IWM-Report T 14/96, Fraunhofer-Institut für Werkstoffmechanik (IWM), July 1996. 42 p.
29. Busch, M. et al. KI-Factors and Polynomial Influence Functions for Axial and Circumferential Surface Cracks in Cylinders. IWM-Report T 18/94, Fraunhofer-Institut für Werkstoffmechanik (IWM), October 1994. 41 p.
30. Busch, M. et al. Polynomial Influence Functions for Surface Cracks in Pressure Vessel Components. IWM-Report Z 11/95, Fraunhofer-Institut für Werkstoffmechanik (IWM), January 1995. 88 p.
31. Vepsä, A. Verification of the stress intensity factors calculated with the VTTBESIT software. Research Report TUO72-044578, Technical Research Centre of Finland (VTT), Espoo, Finland, October 2004. 40+2 p.
32. Männistö, I., Cronvall, O. Combining discrete-time Markov processes and probabilistic fracture mechanics in RI-ISI risk estimates. International Journal of Pressure Vessels and Piping 86 (2009) 732–737.
33. Cronvall, O., Männistö, I., Simola, K., Development and testing of VTT approach to risk-informed in-service inspection methodology, Research Notes 2382, Technical Research Centre of Finland (VTT), Espoo, 2007, 43 p.
34. Paris, P., C., Erdogan, F. A Critical Analysis of Crack Propagation Laws. Journal of Basic Engineering, Vol. 85, 1960, pp. 528 - 534.

35. Hazelton, W.S., Koo, W.H. Technical Report on Material Selection and Processing Guidelines for BWR Coolant Pressure Boundary Piping. Springfield. U.S. Nuclear Regulatory Commission (NRC), Office of Nuclear Reactor Regulation, NUREG-0313-Rev2-F, Final Report. U.S., Jan 1988. 25 p.
36. Congleton, J., Craig, I., H. "Corrosion Fatigue" in Corrosion Processes, Parkins, R., N., Ed., Applied Science Publishers, 1982.
37. Kaunisto, K. Probabilistic modelling of piping degradation with non-stationary Markov chains. VTT Research Report VTT-R-00757-14, Technical Research Centre of Finland (VTT), Espoo, Finland, February 2014. 28 p.
38. Keinänen, H., Chauhan, C. Computation of Welding Residual Stresses in a Multi-Pass Welded Mock-up Pipe. Research Report VTT-R-08364-12, Technical Research Centre of Finland (VTT), Espoo, Finland, December 2012. 22+3 p.
39. Khaleel, M., A., Simonen, F., A. Effects of alternative inspection strategies on piping reliability. Nuclear Engineering and Design 197 (2000) 115–140.
40. Brickstad, B. The Use of Risk Based Methods for Establishing ISI-Priorities for Piping Components at Oskarshamn 1 Nuclear Power Station. SAQ/FoU-Report 99/5, SAQ Control AB, Sweden, 1999. 83 p.
41. Section XI Task Group for Piping Flaw Evaluation, ASME Code. Evaluation of Flaws in Austenitic Steel Piping. Journal of Pressure Vessel Technology, Vol. 108, 1986. Pp. 352-366.
42. R6 Method; Assessment of the Integrity of Structures containing Defects, Revision 4. 2004 update of 2001 edition. British Energy (BE).
43. Dillström, P. et al. 2008. A Combined Deterministic and Probabilistic Procedure for Safety Assessment of Components with Cracks – Handbook. SSM Research Report 2008:01, Swedish Radiation Safety Authority (Strålsäkerhetsmyndigheten, SSM). Stockholm, Sweden, 2008. 27+196 p.
44. Simonen, F., A., Woo, H., H. Analyses of the Impact of Inservice Inspection Using a Piping Reliability Model. NUREG/CR-3869, Topical Report. U.S. Nuclear Regulatory Commission (USNRC), July 1984. 59 p.
45. SINTAP - Structural Integrity Assessment Procedures for European Industry; Final Procedure: November 1999. Project funded by the European Union (EU) under the Brite-Euram Programme: Project No. BE95-1426, Contract No. BRPR-CT95-0024.

33. Advanced surveillance technique and embrittlement modelling (SURVIVE)

33.1 SURVIVE summary report

Matti Valo, Petteri Lappalainen, Anssi Laukkanen, Tapio Planman, Kim Wallin,
Jari Lydman, Tuomo Lyytikäinen, Marko Paasila

VTT Technical Research Centre of Finland Ltd
P.O. Box 1000, FI-02044 Espoo

Abstract

The main topics in the SURVIVE2014 sub-project were validation of small specimen test techniques in irradiated material testing the focus being on specimen reconstitution technique and applicability of small fracture toughness specimens within the frame of Master Curve. The subject named multiscale modelling focusses on development of cleavage fracture model for a real polycrystalline material. The third area was identification of microstructural changes occurring during material irradiation and annealing in order to gain deeper understanding on mechanical property changes. Only some key results of each topic are shown as an example of activities in the sub-project.

Introduction

SURVIVE2014 is a sub-project of SAFIR2014, where techniques and analyses essential for irradiated material testing and data interpretation are developed. Three categories of works are included in the project, namely issues in 1) small specimen test techniques, 2) multiscale modelling concentrating on modelling of fracture in multi-crystalline material and 3) understanding of microstructure of pressure vessel steels in various irradiation-annealing conditions. The project has enabled participation in the IGRDM (International Group for Radiation Damage Mechanisms) activities including Kim Wallin's role as the Technical Area Co-ordinator of sub-task Micro-mechanics.

Small specimen test techniques

Embrittlement of pressure vessel materials is monitored by specimens irradiated in surveillance capsules, where small specimen size is either a necessity or an advantage. Due to technical and scientific development the focus of test techniques has moved from the indirect Charpy-V test towards direct measurement of cleavage initiation fracture toughness K_{JC} and data analysis based on Master Curve concept. Welds of several pressure vessels have been anneal and hence data on annealing and re-irradiation behaviour is required. Without specimen reconstitution technique the new data based on already tested material could not have been created. The reconstituted specimen data shall meet all requirements of relevant standards and hence proper validation of the technique is required. In some applications only semi-quantitative data is needed, i.e. when the effect of annealing parameters or the effect of impurity elements on toughness is studied. With miniature Charpy-V test data can be created cheaply and with small amount of material but the data is only semi-quantitative.

Co-operation with foreign partners was preferred in order to benefit in costs and time of completion. VTT participated in the NIST (USA) arranged round robin on miniature Charpy-V testing (KLST-specimen), where data was created and statistical analysis was performed. Data analysis is presented in two publications [1,2]. CRIEPI arranged a round robin test on "Master Curve reference temperature evaluation utilizing Miniature C(T) specimen" aiming to validate the use of a very small size CT specimen of dimensions $B=4\text{mm}$, $W=8\text{mm}$. The miniature CT-specimens can be prepared from tested Charpy-V specimen halves and thus enables supplementing Charpy-V surveillance data with fracture toughness data. The round robin data is discussed in publications [3-4]. The miniature specimen reproduces well the T_0 values measured with larger specimens. As additional work based on CRIEPI CT-specimens the role of rotation point assumptions made in data processing was analysed and the data was published [5]. The load point displacement cannot easily be measured from specimen load line due to small specimen dimensions and hence rotation point assumptions are used. The deviation was noticed to be small between the two conventionally used assumptions. Further the location of cleavage fracture initiation points on specimen fracture surfaces was identified with SEM as an additional work [6]. Distribution of the initiation sites is shown in Figure 1 indicating that side-grooving is important in promoting triaxiality in the specimen. Fracture toughness data measured by Areva and VTT with same material in varying neutron doses were compared and the data falls excellently on one transition curve [7]. As co-operation with ORNL Master Curve T_0 was measured by VTT with Charpy-size specimens in order to compare the data with a larger data base measured with various specimen sizes and geometries. The data is under processing.

Specimen reconstitution is a widely used technique, where non-active end studs are welded into the centre insert representing the original material cut from a original parent specimen. The concerns about reconstitution are annealing of the irradiated material by the weld heat pulse, non-ideal specimen geometry due to misalignment of the joint parts in the weld jig or due to non-uniform heat transient and subsequent

thermal contraction, limited deformation capability of the reconstituted specimen compared to initial specimen due to hard weld joints, residual stresses of the weld, which may affect prefatiguing of the specimen and strength of the reconstitution weld seam exposed to fast cooling and possibly martensite formation. Reconstituted specimens shall meet all requirements defined in respective mechanical test standards and the deformation field in the reconstituted specimen shall be identical to the field in the original specimen as well as the material properties within this volume shall not be altered by the weld heat pulse. Rather extensive tests with the new EB-welding technique were performed and reported [8]. Weld heat pulse was also simulated and the results were compared with the measured temperature values [9]. The measured heat pulse in the reconstituted specimen characterised in Figure 2 and the axial extension of deformation is a Charpy-V specimen is shown in Figure 3.

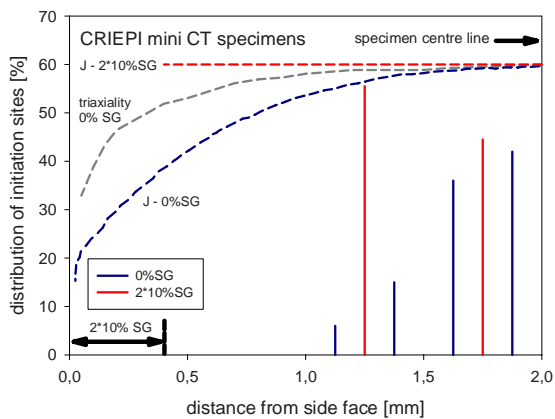


Figure 1. Distribution of cleavage initiation sites on fracture surface in miniature CT-specimens used in CRIEPI round robin [6]. $X=0$ is the specimen side face and $X=2$ is centre of the specimen. Blue colour indicates the distribution of initiation sites and the calculated J-value over the later distance of non-side-grooved specimens and red colour the same parameters in side-grooved specimens. Fracture initiation is concentrated quite in the specimen centre in non-side grooved specimens as in the side-grooved specimens the distribution seems to be more even. More data is required with side-grooved specimens.

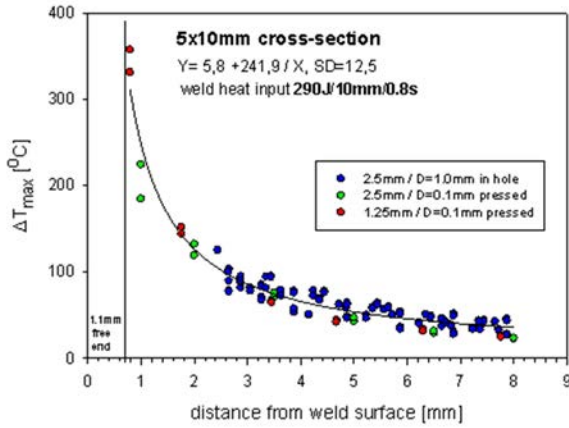


Figure 2. The maximum temperature measured in a reconstituted specimen as a function of distance from the weld surface [8]. Simulation of heat transient

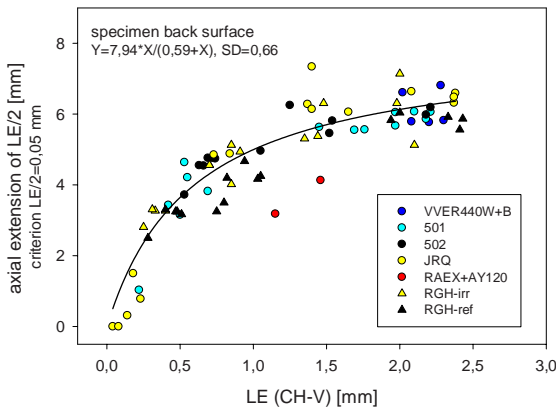


Figure 3. Extent of specimen deformation in tested Charpy-V specimens along the specimen axis [8]. Lateral expansion from the Charpy-V test is shown on x-axis and extent of deformation on specimen axial direction is given on y-axis. The extent of deformation is measured from the V-notch location and the criterion for extension of $LE/2=0.05\text{mm}$ is applied. On upper shelf the deformation extends up to 6 mm from the V-notch and the value starts to fall down quickly at Charpy-V lateral expansion value of approximately 0.5mm. Specimen deformation shall be included within the centre section in a reconstituted specimen.

Multiscale modelling

The current fracture initiation models do not consider plasticity in polycrystalline structures and multiscale modelling task aims to improve the situation. Crystal plas-

tivity analyses with a dislocation dynamics based constitutive model were carried out for “Eurocurve Material A”. The crystal plasticity model was applied to a selected lath containing aggregate mesh over three differing states of imposed constraint in order to derive triaxial stress states ranging from those of uniaxial tensile tests to those indicative of near crack-tip plane strain conditions. The aggregate in question loosely mimics the microstructural morphology present in lower bainitic pressure vessel steels. The findings demonstrate the effects of temperature and crack-tip constraint on the distribution of stress and strain fields within the polycrystal aggregate, and are to be utilized further in the hierarchical multiscale modeling chain in development of cleavage fracture models, especially the micromechanically informed WST cleavage initiation model. Findings and trends within the results are discussed and the results are found indicative and in line with expectations for the differing temperatures and states of constraint. The modelling work is documented in reports [10-12], Example of stress distributions in a multicrystalline model is shown in Figure 4.

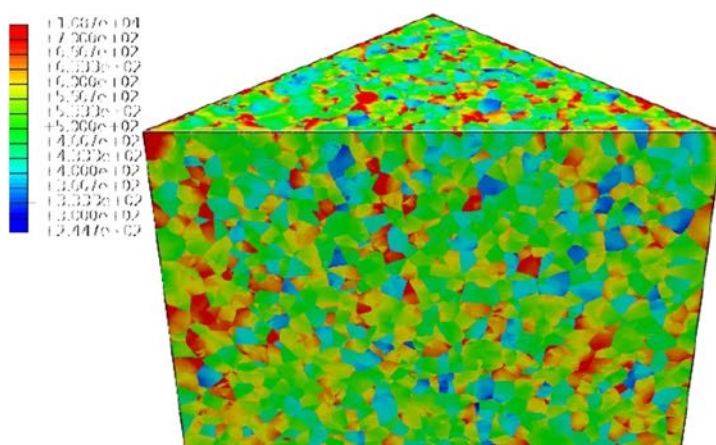


Figure 4. The calculated distribution of von Mises stresses in a 10k grain model indicating large local variation of stresses within a multicrystalline array [10]. Stress values increase from blue to red.

Irradiation induced microstructure

The formations created in the irradiated pressure vessel materials by fast neutrons are nanoscale precipitations or segregations. Powerful characterisation tools for these formations are Small Angle Neutron Scattering (SANS) and Atom Probe Tomography (APT), which techniques are not available in Finland. Hence co-operation with foreign partners has been essential. Much information is available on microstructure of high copper steels, where the principal cause for hardening is the formation of iron rich copper, manganese, nickel and silicon containing precipitates. The focus of our work has been in old VVER440 pressure vessel welds available in Loviisa. In these steels high phosphorus content is responsible for most of the em-

embrittlement according to the trend curve derived from mechanical test data. Because Loviisa-1 pressure vessel weld has been annealed, understanding of microstructural changes occurring in annealing and re-irradiation are of interest. Physical bases of the hardening mechanism due to phosphorus impurity has not yet been revealed. The microstructural changes of weld 501, which is a typical high phosphorus weld and which was used as surveillance material for Loviisa-1 annealing, has been studied.

Earlier SANS measurements revealed that small precipitates develop during irradiation and they disappear in annealing. During reirradiation the small size precipitates evolve again and the amount of large size formations increase slightly [13]. The behaviour is described in Figure 5. APT characterisation of the same samples was performed and it reveals that the formations are iron rich copper, manganese, nickel and silicon containing precipitates, which have also small amount of phosphorus [14,15]. Composition of the formations in various irradiation-annealing conditions is shown in Figure 6. Size distribution of the formations agrees well with SANS data. Phosphorus is found in the irradiated condition on all surfaces, in dislocations and in copper rich precipitates. In the annealed condition all phosphorus is dissolved in the iron matrix. The formations were also characterised by resistivity measurements in order to identify various stages of dissolution or growth of the precipitates. Resistivity data receives its signal from lattice distortions. The dissolved impurities deform the lattice and increase the resistivity compared to the situation, where the impurities are localized in relatively few precipitates. Annealing response measured by resistivity [16] is shown in Figure 7.

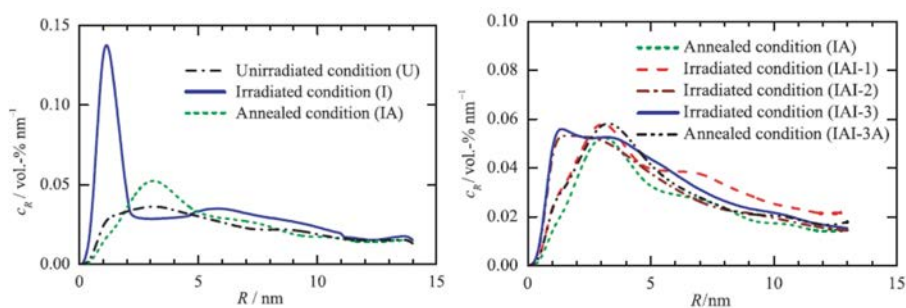


Figure 5. Size distribution of irradiation induced formations in weld 501 in various irradiation-annealing conditions from SANS data [13].

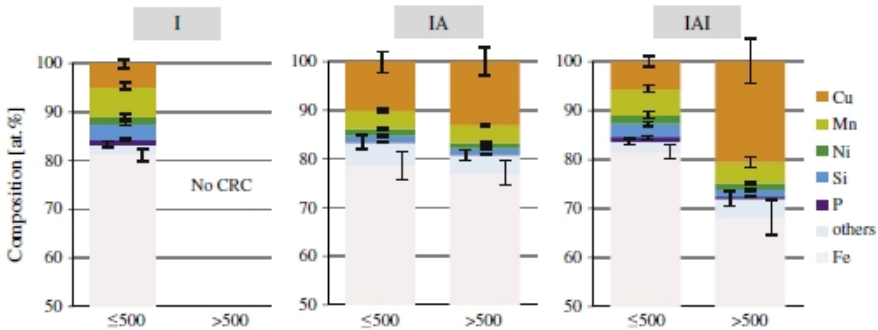


Fig. 7. Average solute atom concentration in CRCs with less than 500 and more than 500 atoms.

Figure 6. Composition of irradiation induced formations in weld 501 in various irradiation-annealing conditions [14]. No phosphorus is found in precipitates in the annealed condition. The data is measured by APT.

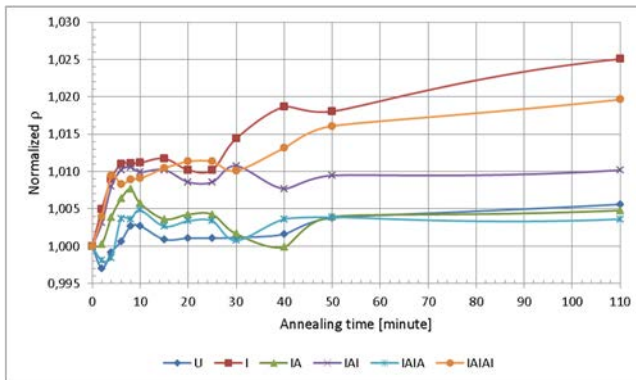


Figure 7. Annealing response of weld 501 in varying irradiation-annealing conditions measured by resistivity [16]. Within 5 minutes resistivity of irradiated conditions (I, IA, IAIA) increase suddenly and clearly and thereafter at the annealing time of approximately 25 minutes resistivity starts to increase again but slowly. Proper interpretation of the phenomena would require information on the annealing response of hardness. The first increase of resistivity is tentatively related to dissolution of small copper rich precipitates and the slow increase later on to dissolution of larger precipitates.

As a separate work the melting points of irradiation temperature monitoring alloys prepared were determined by differential scanning calorimetry and the data is reported [17].

Acknowledgement

The works were financed by the State Nuclear Waste Research Fund (VYR), VTT Technical Research Centre of Finland, Strålsäkerhetsmyndighet SSM, Sweden and Fortum Ltd. We are grateful to Helmholtz Zentrum Dresden-Rossendorf for SANS work and to Tohoku University for atom probe and positron annihilation works.

References

1. Enrico Lucon, Chris McCowan, Ray Santoyo, Jolene Splett, NIST Special Publication 260-180, Standard Reference Materials, Certification Report for SRM 2216, 2218, 2219: KLST (Miniaturized) Charpy V-Notch Impact Specimens. National Institute of Standards and Technology, Boulder, CO 80305-3328, July 2013. (includes VTT data)
2. E.Lucon / NIST, Certified KLST Miniaturized Charpy Specimens for the Indirect Verification of Small Scale Charpy Machines, *presented in ASTM 6th Symposium on Small specimen Test Techniques (2014), accepted for publication in J of ASTM International.*
3. M.Valo, T.Planman, K.Wallin, CRIEPI Mini-CT Master Curve Round-robin Tests, VTT Data 2013, VTT-R-08526-13.
4. M.Yamamoto, K.Onizava, K.Yoshimoto, T.Ogava, Y.Mabuchi, M.Valo, M. Lambrecht, H-W,Viehrig, N.Miura, N.Soneda, International Round Robin Tests on Master Curve Reference Temperature Evaluation Utilizing Miniature C(T) Specimens, *accepted for publication in Journal of ASTM International, presented in ASTM 6th Symposium on Small specimen Test Techniques 2014.*
5. M.Valo, T.Planman and K.Wallin, Rotation Point and K_{Jc} estimations for miniature CT-specimens based on off-load line displacement, *presented in ASTM 6th Symposium on Small specimen Test Techniques, accepted for publication in Journal of ASTM International.*
6. M.Valo, U.Ehrnsten, T.Planman, P.Lappalainen, K.Wallin, Supplementary tests with CRIEPI mini CT-specimens, VTT-R-05628-14.
7. J.May, J.Rouden, P.Efsing, M.Valo, H.Hein, Extended mechanical testing of RPV surveillance materials using reconstitution technique for small sized specimens to assist Long Term Operation, *presented in ASTM 6th Symposium on Small specimen Test Techniques 2014, accepted for publication in Journal of ASTM International.*

8. M.Valo, P.Lappalainen, J.Lydman, T.Lyytikäinen, Physical bases of specimen reconstitution,VTT-R-00508-12.
9. Veli-Matti Pulkkanen, Petteri Lappalainen, Matti Valo, Modelling Heat Transfer in Electron Beam Welding, VTT-R-00368-15.
10. Anssi Laukkanen, Library and wrapper for synthetic microstructures of polycrystalline and composite materials, VTT-R-00214-12.
11. Anssi Laukkanen, Crystal plasticity analyses of tessalated and lath containing aggregates of pressure vessel steels, VTT-R-02166-13
12. Anssi Laukkanen, Crystal plasticity analysis of cleavage fracture initiating stress-strain fields, VTT-R-00746-14
13. Ulbricht, F. Bergner, J. Böhmert, M. Valo, M.-H. Mathon, A. Heinemann, "SANS response of VVER440-type weld material after neutron irradiation, post-irradiation annealing and reirradiation," Philosophical Magazine, Vol.87, No 12, 21 April 2007, 1855-1870.
14. Kuramoto, T. Toyama, Y. Nagai, K. Inoue, Y. Nozawa, M. Hasegawa, M. Valo, "Microstructural changes in a Russian-type reactor weld material after neutron irradiation, post irradiation annealing and re-irradiation studied by atom probe tomography and positron annihilation spectroscopy" Acta Materialia, 61 (2013) 5236–5246.
15. T. Toyama, A. Kuramoto, Y. Nagai, K. Inoue, Y. Nozawa, Y. Shimizu, Y. Matsu-kawa, M. Hasegawa, M. Valo, "Effects of post-irradiation annealing and re-irradiation on microstructure in surveillance test specimens of the Loviisa-1 reactor studied by atom probe tomography and positron annihilation" Journal of Nuclear Materials 449 (2014) 207-212.
16. M.Valo, P.Lappalainen, Electrical resistivity response to annealing of VVER440 weld material in irradiated, post-irradiation annealed and re-irradiated conditions, VTT-R-00163-15.
17. Petteri Lappalainen, Riku Talja, Matti Valo, Validation of melting temperatures of temperature monitoring alloys, VTT-R-00162-15, VTT

34. Water chemistry and plant operating reliability (WAPA)

34.1 WAPA summary report

Timo Saario¹, Konsta Sipilä¹, Essi Velin¹

¹VTT Technical Research Centre of Finland Ltd
P.O. Box 1000, FI-02044 Espoo

Abstract

Both experimental and modelling tools were developed and used to quantify the effect of water chemistry (lithium hydroxide and boric acid) in simulated Hot Functional Test (HFT) conditions on the stability and protective ability of the passive film formed on Alloy 690 as the main PWR steam generator material. A HFT water chemistry with low to intermediate LiOH ($0.5 < [\text{Li}] < 1$ wppm) concentration and boron addition as H_3BO_3 seems to produce films that exhibit enhanced resistance against corrosion and thus lower activity build-up during power operation.

Effect of water chemistry on magnetite deposition was studied using zeta potential measurements as the main experimental approach. At the steam generator operating temperatures the zeta potential of magnetite was found to be close to zero irrespective of the amine used for pH control (ammonia, ethanolamine or morpholine). In addition, a model for magnetite deposition was developed which takes into account the numerous variables affecting the process and is able to address both deposition and re-entrainment of magnetite particles as well as consolidation of the formed deposit.

Introduction

Corrosion products released from component surfaces of a nuclear power plant primary loop can be carried with the coolant flow to the core, then deposit on the fuel elements and become activated. These activated corrosion products may again be released, transported by the coolant flow and subsequently deposited onto other component surfaces in the primary loop causing an increase in the local radiation levels, i.e. activity build-up. The dominating source term of the process in Pressurised Water Reactors (PWRs) is the corrosion product release rate from steam generator tubing surface comprising about 70% of the total surface area exposed to the coolant.

In case of a new PWR plant the first passivation treatment during the Hot Functional Test (HFT) period is crucial in creating a surface film with as low as possible corrosion product release rate. The tubing material selected for steam generators in modern PWRs is mainly Alloy 690. In early years passivation was performed in pure water, and starting from 1980's in water with 0.5–2 wppm of Li (added as LiOH) with or without 30–40 cm³ kg⁻¹ of dissolved H₂. In recent years, the addition of zinc has been shown to result in a clear radiation source reduction effect during the first years of power operation. However, at the moment, there is no consensus on the optimal concentration of LiOH to be used during HFT. In addition, the possible benefit from adding boric acid in the HFT passivation treatment is somewhat unclear.

A major factor influencing the lifetime and reliability of the steam generator and some other components in the PWR secondary circuit is degradation caused by magnetite (Fe₃O₄) deposition. Magnetite is formed mainly from corrosion of carbon steel tubing and other carbon steel components. Magnetite particles originating from the corrosion process are transported with the flow through the feed water line and deposit e.g. in the flow holes/crevices between the steam generator tubes and tube support plate as well as on the tube sheet creating flow and corrosion problems.

Main objectives

The main objectives of the work carried out within the WAPA project were 1) to determine the optimal concentration of lithium and the possible beneficial effect of boric acid to be used in passivation of PWR primary circuit before loading in the first fuel, 2) to develop in situ techniques for determining the effect of alternative water chemistries on deposition of magnetite particles onto steam generator surfaces and 3) to develop the basis of a deterministic model for magnetite deposition.

Optimisation of water chemistry for Alloy 690 passivation

Samples were manufactured from Alloy 690 tubes (UNS N06690, courtesy of EPRI NDE Centre, nominal composition in wt%: Cr 30.3, Fe 9.4, Si 0.3, Mn 0.3, Cu 0.04, C 0.02, P 0.011, S 0.0002, balance Ni), the material being in an annealed condition, and were used as-received to preserve the original microstructure. The measurements were performed at 292 ± 1 °C in a flow-through cell connected to a recirculation loop (flow rate $0.4 \text{ cm}^3 \text{ s}^{-1}$). The temperature corresponds to the maximum temperature achievable in an EPR –type PWR before loading in the first fuel. The water chemistries (0.5-2.0 ppm Li as LiOH, 0-1200 wppm B as H_3BO_3) were prepared from analytically pure chemicals and de-ionized water. A hydrogen overpressure of 1.5 bar was maintained in the feed water tank ensuring a concentration of 30 cm^3 (STP) kg^{-1} (1.3 mmol l^{-1}) of dissolved H_2 .

Samples were exposed for 100 hrs and changes in the oxide layer growing on the surface were monitored in situ using electrochemical impedance spectroscopy (EIS). Impedance spectra were obtained with a Solartron 1287/1260 system controlled by ZPlot software (Scribner) roughly at every three hours till the end of exposure at open circuit. For the simulation and fitting of impedance spectra to the transfer function derived from the kinetic model, a Microcal Origin-based software routine was employed. XPS spectra were registered using an ESCALAB Mk II (VG Scientific) electron spectrometer. To obtain depth profiles, Ar ion milling was used.

As an example of the EIS spectra measured, Figure 1 shows a comparison for three concentrations of Li, 0.5, 1 and 2 ppm [Betova et al. 2012]. Polarization resistance, which is inversely proportional to corrosion rate and can be used as a measure for corrosion resistance, is equal to the impedance magnitude at the frequency level of 1.7 mHz. Thus the data in Figure 1 indicates that the corrosion rate increases when Li concentration increases. A total of three time constants could be detected in the phase angle vs. frequency curves by preliminary deconvolution of the impedance spectra. Following previous interpretations of impedance spectra in high-temperature electrolytes [Bojinov 2007], the highest frequency time constant (above 100 Hz) is associated with the electronic properties of the inner, continuous layer of the oxide film, the medium frequency time constant (between 5 and 50 Hz) most probably reflects the ion and electron transfer processes at the oxide/electrolyte interface, and the lowest-frequency time constant (around and below 1 Hz) is assigned to the transport of point defects in the inner layer of oxide.

To quantitatively interpret the data, the Mixed Conduction Model (MCM) [Betova 2009] was used. The solid lines in Figure 1 represent the best fit of the MCM. From the model, the oxidation rate at the metal-oxide interface was extracted and recalculated as corrosion penetration, as shown in Figure 2 [Betova et al. 2014]. The boron concentrations studied were chosen to keep the high temperature pH constant, i.e. so that at each lithium concentration the $\text{pH}_{292\text{C}} = 6.9$.

The main conclusion that can be drawn from both experimental and calculation results is that increasing LiOH concentration in the simulated HFT water leads to higher dissolution rates, higher metal oxidation and transport rates through the oxide, or in other words, the formed oxide is found to be the more defective, the higher

the concentration of Li in the electrolyte is. On the other hand, boron added as H_3BO_3 was found to have a beneficial effect that counter-acts the corrosion accelerating influence of Li. On the basis of our experiments and their interpretation, HFT water chemistry with low to intermediate Li contents ($0.5 < [Li] < 1.0$ ppm) and boron addition seems to produce films that exhibit better electrochemical stability and thus better corrosion resistance.

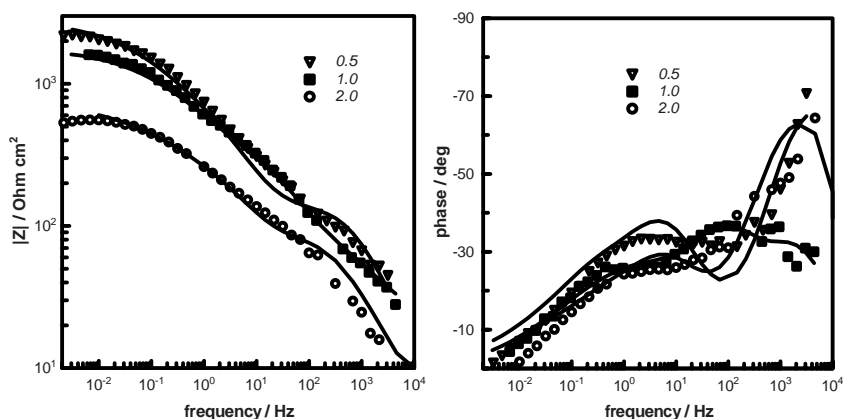


Figure 1. Electrochemical impedance spectra of Alloy 690 at 292°C as depending of increasing Li content (ppm) in electrolyte without boric acid. Left – impedance magnitude vs. frequency, right – phase angle vs. frequency. Points – experimental data, solid lines – best-fit calculations according to the MCM.

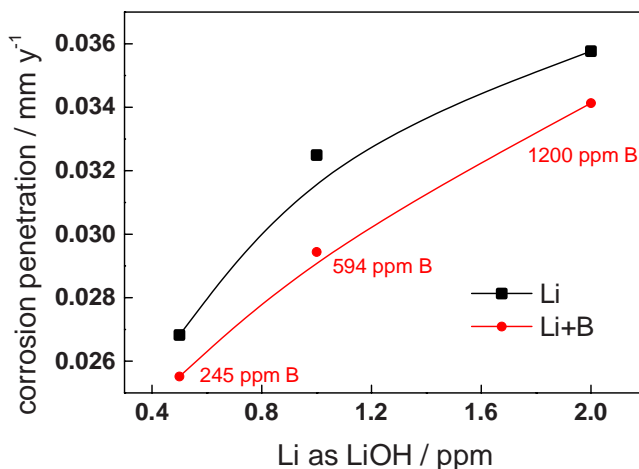


Figure 2. Corrosion penetration estimated from the oxidation rate constant k_1 as depending on the water chemistry conditions during HFT. Alloy 690, $T = 292^\circ\text{C}$, exposure time 100 hrs.

Magnetite deposition into steam generator

The function of the steam generator (SG) in an indirect cycle nuclear-power plant (NPP) is to generate steam from the nuclear heat produced by fission reactions in the core during operation at power, and to act as a heat sink to remove decay-heat from fission products during both normal reactor shut down and for a post-accident scenario in the event that reactor-core cooling has been impaired. Situated at the boundary between the nuclear (radioactive primary coolant system) and conventional (non-radioactive secondary coolant system) sides of the plant, the SG plays two safety-critical roles:

- Provides a barrier to prevent the release of radioactivity from the primary reactor coolant to the secondary coolant where it can be released to the environment;
- Removes heat from the primary coolant to the secondary coolant to maintain a safety margin during power operation and some post-accident scenarios.

Thus, the integrity of the SG and its internal components is vital for assuring both the safety and the performance of the NPP.

Soluble iron (Fe^{2+} -ions) and magnetite (Fe_3O_4) particles are formed in the secondary circuit mainly as a result of the corrosion of carbon steel tubing and other carbon steel components. Magnetite particles are transported with the flow and deposit e.g. in the SG tube support plate and re-heater cassette area creating flow, thermo-hydraulic and corrosion problems. Recent tube failures in some Electricité de France (EdF) plants were caused by high-cycle fatigue related to flow redistribution and tube lock up in the tube-support structure of the SG [Bodineau & Sollier 2008]. Current corrosion problems caused by magnetite deposition include also denting and stress corrosion cracking of SG lower level tubing both in Spanish and Romanian utilities [Fernández-Saavedra et al. 2014] and localised corrosion of SG lower level tubing in WWER plants.

Within the WAPA project the basis has been laid of a model for magnetite deposition [Bojinov & Saario 2013] under PWR secondary side conditions and the model has been verified using available experimental data. A sensitivity study of the model showed that the two most important parameters affecting the deposition are the Hamaker constant and the zeta potential of magnetite [Bojinov & Saario 2014]. Applications of such a model includes evaluation of the possibilities of minimising magnetite formation and deposition onto steam generator and other secondary side surfaces through an optimization of the water chemistry and hydrodynamics (hydrazine injection, different amines, use of dispersants etc.).

Figure 3 shows the scheme of the magnetite deposition process according to the proposed model. Under isothermal conditions three mechanisms are assumed to progressively dominate transport of Fe_3O_4 particles in turbulent flow as the particle size increases: diffusion, inertia and impaction. In the presence of heat transfer and temperature gradients, the transport rates based on isothermal conditions must be modified, taking into account two additional mechanisms that come into play: thermophoresis and thermoelectric effect. After reaching the substrate surface attach-

ment of particles is governed by the interplay between electrostatic and van der Waals interactions. Growth of adsorbed particles into a solid layer (consolidation) is thought to be affected by Fe^{2+} -ions, which “glue” the particles together. In the model, also the possibility of magnetite particle re-entrainment (before consolidation) is taken into account.

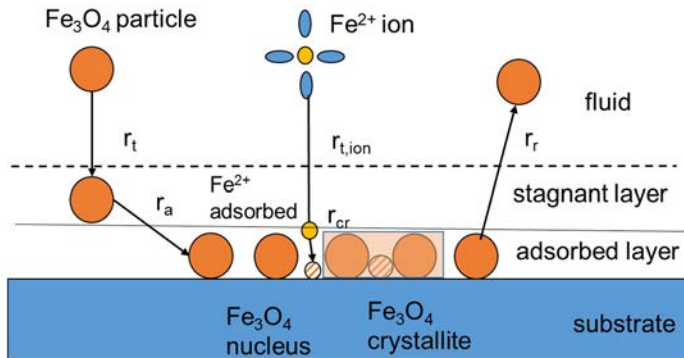


Figure 3. Scheme of the magnetite deposition process according to the proposed model.

Summarizing, the following model equation is used for the deposition:

$$\frac{m_d(t)}{m_p} = \frac{k_a}{k_d [1 - \alpha(t)] \left[1 - e^{-k_d [1 - \alpha(t)] t} \right]}$$

where $m_d(t)$ is the deposited mass as a function of time (kg m^{-2}) and m_p is the mass concentration of particles in the liquid phase (kg m^{-3}), rate constants of deposition k_d and detachment k_a , and the fraction of consolidated (recrystallized) deposit $\alpha(t)$.

The model can be used e.g. to find out the relative importance of different variables on magnetite deposition. Figure 4 shows as an example the effect of surface energy (Hamaker constant, a material property that represents the strength of van der Waals interactions between macroscopic bodies) on the predicted deposition rate, when compared to experimentally determined data. It is clear that even 1% change in the surface energy influences dramatically the deposition behaviour. In case of changing the surface charge (zeta potential), the influence was also found to be quite large.

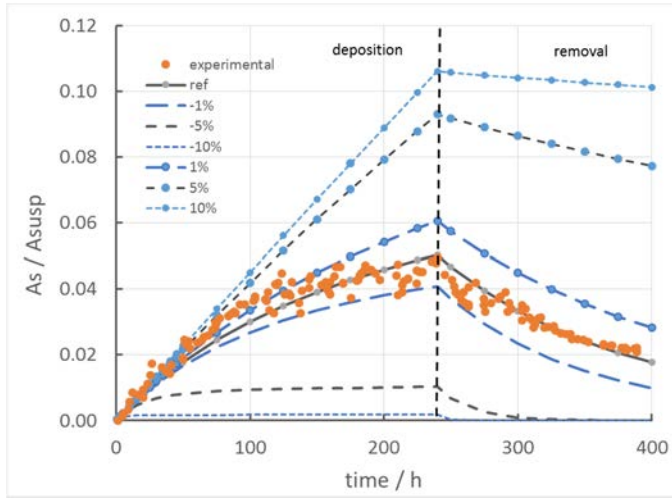


Figure 4. Effect of changing the Hamaker constant AH by $\pm 1, 5$ and 10% on the predictions of the model. The surface activity of ^{59}Fe (A_s) was normalized by the activity of the same nuclide in the suspension (A_{susp}) to provide a measure of deposition coverage.

A new experimental arrangement was developed within two consecutive MSc-thesis works to enable zeta potential measurements at high temperatures using a method based on streaming potential measurements [Väisänen, 2012, Velin, 2013], Figure 5. In streaming potential phenomenon, the pressure gradient which is formed through a column of magnetite particles, induces a potential difference over the column which can be measured with electrochemical measurement devices. When the relation of the potential difference and the pressure gradient over the ends of the column is multiplied with certain constants that represent the properties of the solution and the column, the zeta potential is achieved as

$$\zeta = \frac{\Delta E}{\Delta P} \frac{4\eta l}{\epsilon_{rs}\epsilon_0 a^2 R}, \quad (1)$$

Here ΔE is the potential difference, ΔP is the pressure gradient, η is the viscosity of the solution, l is the length of the magnetite column, $\epsilon_{rs}\epsilon_0$ is the absolute permittivity of the solution, a is the radius of the magnetite column and R is the inverse of the conductivity of the flow path.

In magnetite zeta potential measurements the zeta potential of magnetite particles was measured in a temperature range of $T=25-250^\circ\text{C}$ in ammonia, ethanolamine, and morpholine solutions. The pH was 9.2, corresponding to the pH used in PWR secondary side in a plant with copper containing components. The zeta potential at room temperature varied from -36 mV in case of morpholine, -25 mV in case of ammonia, and -16 mV in case of ethanolamine [Velin et al., 2014]. The magnitude of

zeta potential decreased as a function of temperature in all cases and approached zero at $T = 250^{\circ}\text{C}$, i.e. close to operating temperature of SGs. This suggests that other forces than surface charge, e.g. thermohydraulic phenomena dominate the deposition of magnetite particles at high temperatures.

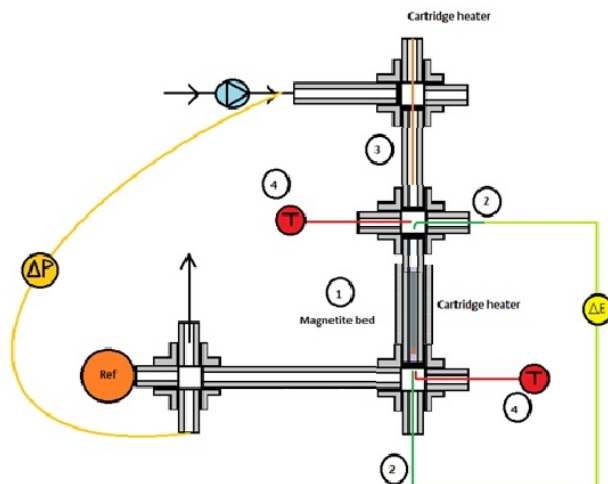


Figure 5. The arrangement of zeta potential test loop: 1-Magnetite bed, 2-Platinum electrodes, 3-Cartridge heater, 4-Thermocouples

Conclusions

Based on the work performed within the WAPA-project the following conclusions can be made.

- In situ electrochemical tools, combined with application of the Mixed Conduction Model (MCM) for high temperature oxide films provide a reliable methodology to estimate the effect of chemical variables on the corrosion resistance of central NPP components
- The optimal concentration of Li for prepassivation of PWR primary circuit with Alloy 690 steam generator tubing is $0.5 < [\text{Li}] < 1.0$ ppm; the higher the Li concentration, the higher the corrosion rate of Alloy 690. Addition of boric acid is beneficial irrespective of the Li concentration applied.
- The model for magnetite deposition shows promising capability in predicting the effect of different variables affecting deposition.
- The possibilities of affecting magnetite deposition into SGs through the use of advanced amines are limited as the zeta potential of magnetite close to the operating temperatures of SGs ($T = 250^{\circ}\text{C}$) was shown to be close to zero irrespective of the amine used (ammonia, ethanolamine or morpholine).

References

- Betova, I., Bojinov, M., Kinnunen, P., Lungren, K. & Saario, T. 2009. Influence of Zn on the oxide layer on AISI 316L(NG) stainless steel in simulated pressurised water reactor coolant. *Electrochim. Acta* 54 (2009) 1056-1069.
- Betova, I., Bojinov, M., Karastoyanov, V., Kinnunen, P. & Saario, T. 2012. Effect of water chemistry on the oxide film on Alloy 690 during simulated hot functional testing of a pressurised water reactor. *Corrosion Science* 58 (2012) 20–32.
- Betova, I., Bojinov, M., Karastoyanov, V., Kinnunen, P. & Saario, T. 2014. Optimisation of the water chemistry used during hot functional testing of a pressurised water reactor regarding the passivation of Alloy 690 steam generator tubing. *International Symposium on Material Service Performance in Nuclear Power Plants-2014*. November 12-15, 2014, Shanghai, China.
- Bodineau, H. & Sollier, T. 2008, Tube support plate clogging up of French PWR steam generators, EUROSAFE, Paris, 2008.
- Bojinov, M., Galtayries, A., Kinnunen, P., Machet, A. & Marcus, P. 2007. Estimation of the parameters of oxide film growth on nickel-based alloys in high-temperature water electrolytes. *Electrochim. Acta* 52 (2007) 7475-7483.
- Bojinov, M. & Saario, T. 2014, Modelling magnetite deposition on secondary circuit surfaces – foundation and boundary conditions. VTT Research Reports VTT-R-00627-14, 44 p.
- Bojinov, M. & Saario, T. 2015, Deposition model for magnetite on secondary circuit surfaces – a sensitivity study. VTT Research Reports VTT-R-00034-15, 31 p.
- Fernández-Saavedra, R., Fernández-Díaz, M., Gómez-Mancebo, M, de Diego, G., Quejido-Cabezas, A. & Gómez-Briceño, D. 2014, Hard sludge and denting in the secondary side of PWR steam generators. *Nuclear Plant Chemistry Conference 2014*, Sapporo, Japan.
- Velin, E., Saario, T., Sipilä, K. & Väisänen, S. 2014. Streaming potential technique in determining zeta potential of magnetite in PWR secondary side water treated with ammonia or morpholine. *Nuclear Plant Chemistry Conference 2014*, Sapporo, Japan.
- Velin, E. 2013, The effect of temperature on the zeta potential of magnetite particles in ammonia, morpholine and ethanolamine solutions. MSc-thesis, Aalto University, School of Chemical Technology.

Väisänen, S. 2012. Zeta Potential of Magnetite under PWR Secondary Circuit Conditions. MSc-thesis, Tampere University of Technology.

35. Fatigue affected by residual stresses, environmental and thermal fluctuations (FRESH)

35.1 FRESH summary report

Heikki Keinänen, Juha Kuutti, Otso Cronvall, Qais Saifi, Antti Timperi

VTT Technical Research Centre of Finland Ltd
P.O. Box 1000, FI-02044 Espoo

Abstract

The FRESH project aims at expanding and deepening understanding of fatigue behaviour experienced by NPP pressure boundary components under realistic loads and environment. The following topics were studied during the first year of the project:

- stresses in a weld prior and after to NPP operation (weld residual stresses);
- sensitivity of the Fen-factor to variation in the loads;
- determination of the realistic loads caused by turbulent mixing;
- clarification of stress component categorization for numerical fatigue analyses;
- and weld overlay as a repair method.

Introduction

The FRESH project aims at expanding and deepening understanding of fatigue behaviour experienced by nuclear power plant (NPP) pressure boundary components under realistic loads and environment. The project was organised in four sub-projects, and the specific goals of each subproject are described below.

Existing experimental data was utilised to produce thermal fatigue and crack growth data with the help of numerical analyses.

Residual stresses and the influence of operational loads on residual stresses were studied in several components, a mock-up of a pipe containing multiple butt-welds, RPV nozzle and RPV cladding.

Categorisation of stresses was performed in two parts, which were theoretical and numerical comparison of nuclear codes and analysis procedures.

Turbulent mixing of hot and cold water may lead to thermal fatigue and crack growth in piping and components of NPPs. Computational Fluid Dynamics (CFD) and structural calculations of thermal mixing were performed for a T-junction having approximately same conditions as in the FATHER experiment [1].

Main objectives

The main objectives of the 4-year project were

- Determination of the realistic stresses in a weld prior to and during NPP operation;
- determination of the realistic loads caused by turbulent mixing and NPP environment, and
- clarification of stress component categorization for numerical fatigue analyses.

Thermal fatigue simulation

The numerical simulations related to the thermal fatigue experiments started in 2013 in the FRESH project were improved and extended in project year 2014 [2]. The simulation models were updated to utilize symmetric boundary conditions to reduce the computational effort. All models now use quadratic tetrahedron elements to obtain consistency in the results between the models. Based on a review of available cyclic plastic models in Ansys and their popularity in scientific literature, the Voce model for isotropic hardening and the Chaboche model for kinematic hardening were selected to be utilized in the thermal fatigue simulations. The parameters for the models were obtained from a NRC welding residual stress round robin simulation exercise for piping material SS316, nozzle material A508 and weld material A182 for the current temperature range of 20°C – 350°C.

The selected simulation approach was verified by simulating heat transfer and resulting stress field in a solid disk and comparing the results with an analytical solution. The elastic simulated stress and strain results were in good agreement with the analytically calculated stresses and strains. When including plastic material properties in the analysis, the most significant changes in the stress and strain distributions occurred in the location of the peak stress and strain value.

Two separate representative thermal fatigue experiments were simulated to obtain the differences between the previous elastic solution and current plastic solution in the stress and strain amplitudes caused by thermal loading. The studied example cases were plate without weld and pipe with weld. Both cases were simulated with both elastic and cyclic-plastic material properties. The resulting stress and strain histories from the heating area were compared as well as their through-thickness

distributions. Specimen temperature time histories and an example stress contour are shown in Figure 1.

The results showed total strain amplitude differences up to 17% for the last simulated loading cycle. Inclusion of plastic properties increased the mean stress values from compression to nearly zero. The recorded stress histories showed large tensile stresses on the heating area surface but the stress state transformed to compressive stresses in the through-thickness direction. Tensile stress amplitudes of 500 MPa were obtained in the heating area centroid. These results are visualized in Figure 2 and Figure 3.

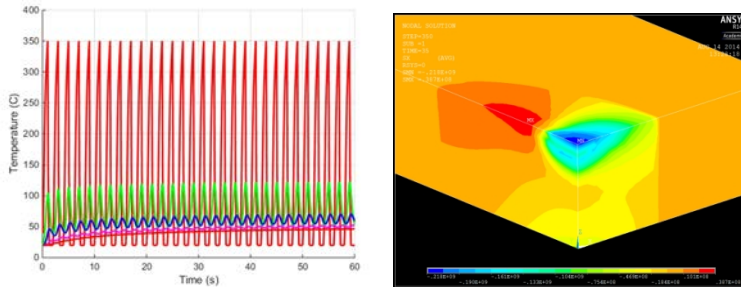


Figure 1. Example plots of specimen temperature histories and stress contours in a thermal fatigue simulation.

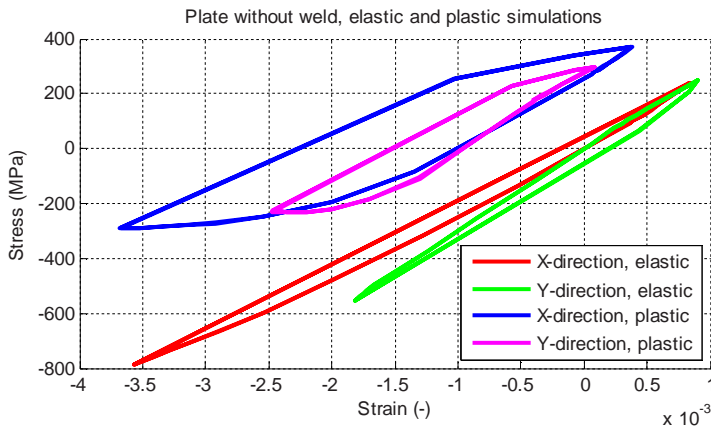


Figure 2. Simulated stress-strain plots from an elastic and corresponding elastic-plastic analysis.

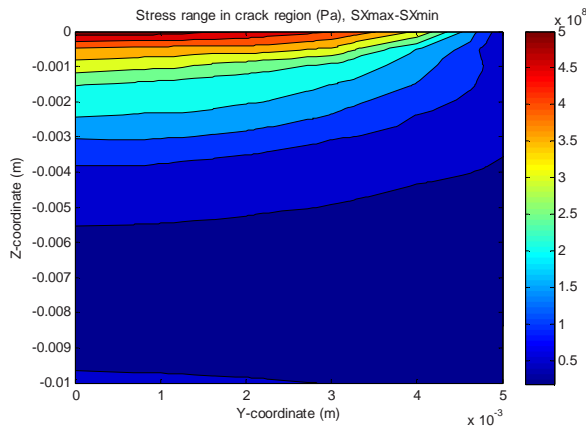


Figure 3. Through-thickness cack opening stress distribution in the specimen heating area.

Weld residual stresses

During 2012 a literature survey was performed on the issue. The knowledge acquired was be utilized to simulate stresses in butt welded pipe, RPV nozzle weld overlay (Figure 4) and RPV cladding [3,4,5]. The change of stresses due to operational loading and post weld heat treatment was also studied.

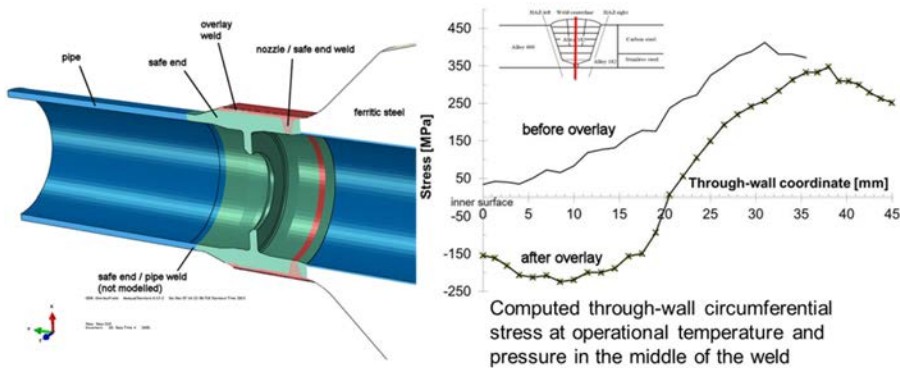


Figure 4. Residual stresses in an overlay welded nozzle.

In the case of butt welded pipe larger tensile stresses were obtained with the axisymmetric model in the weld area near the inner surface. This is most probably partly due to thermal results and partly due to the lack of capability of the axisymmetric model to model the movement of welding torch in the circumferential direction and deformations in front of and behind the torch.

In the case of overlay welding three dimensional predicts smaller stress decrease due to weld overlay than the axisymmetric model. In the case of the butt welded pipe

and RPV nozzle the stresses were slightly relaxed due to pressure test and operational loading.

The computational results show that the post weld heat treatment reduces RPV cladding stresses especially in the base material beneath the cladding. The cladding stresses are also reduced due to pressure test and operational loading. In the operational loading (pressure and temperature) highest stresses occur in the base material underneath the cladding. The value of tensile hoop stress is approximately 200 MPa.

The results show the suitability of computational methods for plant safety assessment applications.

Plastic strain correction factor

The third subproject aims mainly to assess the level of conservatism in the existing plastic strain correction factor definition in ASME code. This study is divided into two parts, which are theoretical and numerical comparison of nuclear codes and analysis procedures.

In the context of the commonly applied fitness-for-service codes, i.e. the ASME Code, safety standard KTA 3201.2 and RCC-M code, the K_e factor is part of the fatigue design procedure. This is an important issue from the viewpoint of computational fatigue life of NPP piping components. Unfortunately, the K_e factor definitions according to these codes are often overly conservative, e.g. those in the ASME code. Thus, more realistic but still to a reasonable extent conservative K_e definitions are needed. A review of both conservative and more realistic K_e definition procedures was carried out, see ref. [6].

The second part of the study [7] began with comparing two plastic strain correction factor procedures, as taken from: ASME Section III, NB-3200 [8] and ASME Section VIII, Division 2 [9]. A safe-end and connecting pipe from an existing boiling water reactor (BWR) NPP were chosen as analysis targets. The heat transfer and stress/strain analyses were performed with FE code Abaqus. The FE analyses were performed for two more severe load sequences as composed of cyclic loads with constant amplitude. Within the scope of the performed analyses, it is concluded that the considered plastic strain correction factor procedures give quite corresponding results in terms of alternating stress intensities, which in turn are needed in NPP piping system fatigue analyses. It is often deemed that the ASME III, NB-3200 procedure is always conservative, and in several cases overly so. However, for the cases with less severe load cycle sequence, the ASME VIII, Division 2 procedure gave higher alternating stress intensity values, but being still close to those obtained with the ASME III, NB-3200 procedure.

In the further computational analyses [10], a structure operating in Olkiluoto 1 NPP unit was chosen as an analysis target to calculate plastic strain correction values. The examined structure consists of an elbow and a reducer. The reference stresses and strains were computed with FE analyses code. Two separate transient sequentially coupled FE analyses were performed. The sequentially coupled FE analysis

consists of thermal and structural parts. The loads applied to the structure were merely realistic or factor from real loadings.

Firstly, from the sequentially coupled FE analysis with linear-elastic material properties, reference stresses at the desired cross-section path were obtained to calculate plastic strain correction factor and alternating stress values according to the ASME III, NB-3000. Subsequently, without changing boundary conditions and loadings of the model, a sequentially coupled FE analysis with elastic-plastic analysis of the structural part was performed. Elastic-plastic material properties were provided and isotropic hardening theory was implemented to perform FE elastic-plastic analysis. Total elastic-plastic strain range value was obtained at the desired location of the structure, where at the same location strain range was obtained from linear-elastic analysis as well. By dividing elastic-plastic strain range value to the linear-elastic strain range value, a reference plastic strain correction factor value was obtained at the desired cross-section path.

Reference plastic strain correction factor value was used to detect the level of conservatism in plastic strain correction factor value obtained according to ASME NB-3200 [8] and linear-elastic FE analysis. For a result example, see Figure 5 below. Based on result comparisons, conclusions were drawn and recommendations were provided on procedure selection. All the FE analyses were performed with ANSYS 14.5 code, where post-processing of results for calculating plastic strain correction factor were carried out with Matlab R2014a.

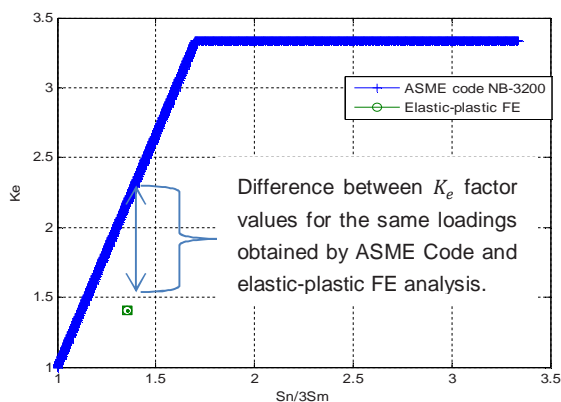


Figure 5. Plot of Plastic strain correction factor (K_e) results from ASME code and K_e value from elastic-plastic and linear-elastic FE results.

Crack growth caused by thermal mixing

The CFD and FEM calculations were performed by using the Star-CCM+ 8.06 and Abaqus 6.11 codes. The Smagorinsky turbulence model and wall functions were used for Large-Eddy Simulation (LES) of the temperature fluctuations. The transient thermal loads were interpolated to the structural model of the T-junction by a script created in Star-CCM+. Corresponding crack growth calculations using straight pipe

models with simplified sinusoidal and turbulent thermal loads were also performed to study the effect of model geometry and load simplification.

Instantaneous temperature and temperature variance in the T-junction are shown in Figure 6. The cold flow from the vertical branch stays close to the bottom of the horizontal main pipe due to the low cold flow rate; the situation is also affected by buoyancy where the heavier cold flow tends to stay at the bottom. The highest temperature variance in the T-junction is about 3400 K^2 , i.e. the Root-Mean-Squared (RMS) value normalized by the total temperature difference of 160 K is about 0.364 . For comparison, the corresponding normalized RMS value for a sinusoidal signal is $1/\sqrt{8} \approx 0.354$, and thus the maximum value in the T-junction is close to that of the sinusoidal signal. Near the wall, the corresponding maximum value is about 0.235 , which is 66% of the sinusoidal signal value. Ref. [12] proposes to use 80% amplitude in the sinusoidal (SIN) method to reduce the over-conservatism of the thermal fatigue assessment. The proposed value of 80% is somewhat reasonable compared to the maximum of 66% at wall in the LES. The mean Heat Transfer Coefficient (HTC) at the location of highest wall fluctuations is about $27 \text{ kW/m}^2\text{K}$, i.e. 1.8 times the Colburn correlation for fully developed pipe flow. Studies performed in the project and in [13,14] indicate too low values of the peak wall heat fluxes for LES with wall functions. However, since otherwise the results with wall functions have been generally fairly good, they are used here for obtaining close-to-realistic thermal mixing loads for comparative crack growth studies where the same HTC is assumed in each case.

The largest cracks observed in the experiment were about 1 mm deep, and hence a crack with depth 1 mm and having aspect ratio 32 was modelled at the location of maximum wall RMS temperature. Examples of instantaneous stresses in the T-junction are presented in Figure 7. The Stress Intensity Factor (SIF) and the corresponding SIF cycles obtained from rainflow counting are plotted in Figure 8.

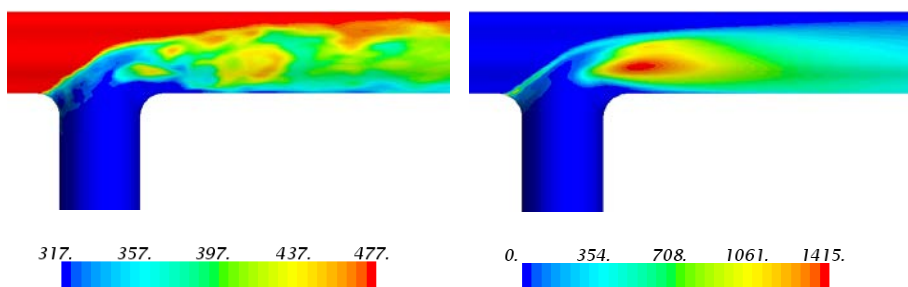


Figure 6. Instantaneous temperature (left) and temperature variance (right) at the wall of the T-junction (units K and K^2).

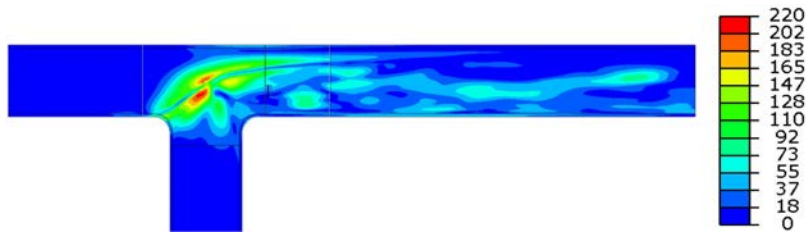


Figure 7. Instantaneous von Mises stress field (MPa) at the T-junction inner surface.

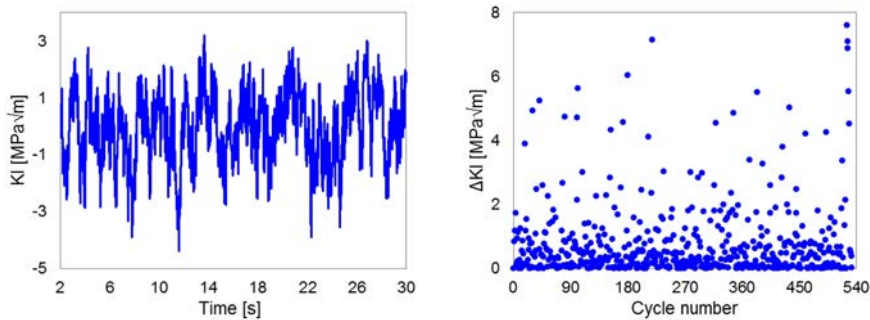


Figure 8. SIF signal and corresponding SIF cycles for crack in the T-junction.

Conclusions

The numerical simulations related to the thermal fatigue experiments started earlier were improved and extended. The simulation models were updated to utilize symmetric boundary conditions to reduce the computational effort. The selected simulation approach was verified by simulating heat transfer and resulting stress field in a solid disk and comparing the results with an analytical solution. The elastic simulated stress and strain results were in good agreement with the analytically calculated stresses and strains. When including plastic material properties in the analysis, the most significant changes in the stress and strain distributions occurred in the location of the peak stress and strain value. Inclusion of plastic properties increased the mean stress values from compression to nearly zero. The recorded stress histories showed large tensile stresses on the heating area surface but the stress state transformed to compressive stresses in the through-thickness direction.

Numerical computation of residual stresses were performed for several cases and the effect of post weld heat treatment, overlay welding and operational loading was estimated. The main results of the analysis are the residual stress field caused by welding and the effect of loading on the WRS state. The comparison of axisymmetric and three dimensional computations have also been performed. The results show the suitability of computational methods for plant safety assessment applications.

FE analyses of a real NPP structure from Olkiluoto 1 were done to compute plastic strain correction values. Due to insufficient amount of loadings, the external load-

ings of the structure have been multiplied by a factor to obtain stresses beyond yield point. Thus, by exceeding yield point plastic strain correction factor values above 1 were computed. Level of conservatism in plastic strain correction factor according to the ASME code was detected by comparison to reference plastic strain correction factor. Nearly realistic reference plastic strain correction value, which was obtained from FE elastic-plastic and linear-elastic analyses, suggests that K_e obtained by ASME code NB-3200 to be sufficiently conservative in this particular case. Thus, it is encouraged to consider the use of other nuclear codes as well.

Thermal mixing in a T-junction was studied by CFD and FEM calculations. LES has been found sufficiently accurate in the bulk of the flow [11]. However, further development and validation work is needed for near-wall regions, since wall-resolved LES has too high computational demand for many practical cases while LES with wall functions indicate too low HTC. Sinusoidal thermal loads having different spatial extents yielded similar crack growth rates, i.e. the load distribution was of minor importance. In addition, a straight pipe model with uniform load but signal taken from LES showed similar results as the T-junction simulation, indicating that the load signal is more important than the structural model geometry or load distribution. Using the worst-case frequency in the SIN method resulted in over-conservatism, since the frequency content of the actual thermal load depends on flow conditions. The SIN method was only slightly conservative, however, if the frequency was set based on the actual frequency content, the HTC was estimated accurately and the 80% amplitude was applied.

References

1. Courtin, S., Le Duff, J.A., Tacchini, B., Fissolo, A., Vincent, L., Stephan, J.M. and Tampigny, R., 2011. High cycle thermal fatigue father experiment: non destructive and metallographic examinations. Proceedings of the 21st International Conference on Structural Mechanics in Reactor Technology (SMiRT 21), New Delhi, India, November 6 - 11, 2011, SMiRT21-099.
2. Kuutti, J., 2014. Plasticity effects in thermal fatigue simulations. VTT Research Report VTT-R-03748-14. 40 p.
3. Keinänen, H., Chauhan, M., 2012. Computation of welding residual stresses in a multi-pass welded mock-up pipe. Research Report VTT-R-08364-12. 22+3 p.
4. Keinänen, H. Simulation of weld overlay., 2014 Research Report VTT-R-00485-14. 35+10p.
5. Keinänen, H. Computation of cladding welding stresses, 2014. Research Report VTT-R-06020-14. 19+3p.
6. Cronvall, O. NPP piping Stress component treatment - Part 1 - Theoretical comparison of nuclear codes and analysis procedures. Research Report VTT-R-08651-12, Technical Research Centre of Finland (VTT), Espoo, Finland, January 2013. 32 p.
7. Cronvall, O. NPP piping stress component treatment - Part 2 - Numerical comparison of nuclear codes and analysis procedures. Research Report VTT-00799-14, Technical Research Centre of Finland (VTT), Espoo, Finland, March 2014. 47 p.
8. ASME Boiler and Pressure Vessel Code, Section III, Division 1, Article NB-3000 Design, 2010 Edition.
9. ASME Boiler and Pressure Vessel Code. Section VIII, Division 2, Part 5, Design by analysis requirements. Rules for construction of pressure vessels, 2013.
10. Saifi, Q. Numerical comparison of plastic strain correction factor against elastic-plastic FE analysis. Research Report VTT-R-00060-15, Technical Research Centre of Finland (VTT), Espoo, Finland, March 2014. 21 p.
11. Timperi, A., 2014. Conjugate heat transfer LES of thermal mixing in a T-junction. Nuclear Engineering and Design, Vol. 273, pp. 483 – 496

12. Dahlberg, M., Nilsson, K.-F., Taylor, N., Faigy, C., Wilke, U., Chapuliot, S., Kalkhof, D., Bretherton, I., Church, M., Solin, J., Catalano, J., 2007. Development of a European procedure for assessment of high cycle thermal fatigue in light water reactors: final report of the NESC-thermal fatigue project. EUR 22763 EN, European Communities.
13. Pasutto, T., Péniguel, C., Sakiz, M., 2009. Chained computations using an unsteady 3D approach for the determination of thermal fatigue in a T-junction of a PWR nuclear plant. In: 20th International Conference on Structural Mechanics in Reactor Technology Espoo, Finland, August 9–14, 2009, Paper 3-2494
14. Jayaraju, S.T., Komen, E.M.J. and Baglietto, E., 2010. Suitability of wall-functions in large eddy simulation for thermal fatigue in a T-junction. Nuclear Engineering and Design, Vol. 240, pp. 2544 - 2554.

35.2 Welding stress analyses

Heikki Keinänen

VTT Technical Research Centre of Finland Ltd
P.O. Box 1000, FI-02044 Espoo

Abstract

Numerical computation of residual stresses has been performed for several cases [1,2,3] and the effect of post weld heat treatment, overlay welding and operational loading has been estimated. The main results of the analysis are the residual stress field caused by welding and the effect of loading on the WRS state. The comparison of axisymmetric and three dimensional computations have also been performed. The results show the suitability of computational methods for plant safety assessment applications.

Introduction

The welding computations were performed as specifically tailored finite element (Abaqus [4]) analyses modelling the studied welding process pass-by-pass basis. Thermal and mechanical analyses were performed separately. The non-linear characteristics of the material including temperature dependency and plasticity were taken into account. In one studied case post weld heat treatment and time dependency of material properties (creep) was modelled. The effect of operational conditions (pressure, temperature) on the simulated residual stresses was computed.

The material properties included the material parameters for combined isotropic/kinematic hardening material model of Abaqus [4]. The combined isotropic/kinematic hardening material model was first introduced by Armstrong and

Frederick [5] and later expanded by Chaboche [6]. The model is suitable to simulate cyclic loading conditions, such as occurs in multi-pass welding.

An anneal temperature of 1000...1400 °C was utilised in the mechanical analysis. The anneal procedure simulates the relaxation of stresses and plastic strains.

In-house codes were used to generate some of the input data, see Figure 1. Reduced integration hybrid finite elements were used in order to avoid volumetric locking. In most analyses (except in those where solution mapping was utilised) small strains and displacements were assumed. In the mechanical analysis, soft double elements (two sets of similar elements on top of each other) were used in the areas which were not yet active in the computation to track the accumulated deformation of the nodes, which are not yet active in the model.

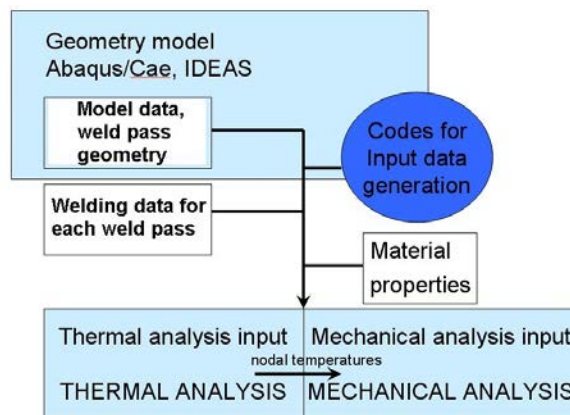


Figure 1. Flow chart of the analysis procedure.

In the thermal analysis the given welding data was utilised. Pass by pass modelling was performed adding the corresponding elements to the model utilising 'model change, add'- option of Abaqus code [4]. Pass lumping was performed in most of the analyses.

The heat input was modelled using uniform internal heat generation and an exponential time function. The length of the time function was chosen so that the length of the heat input area was approximately achieved. In addition, the initial temperature of 1400 °C of the weld material was modelled. The amount of the heat input Q [J/s], was obtained using the welding parameter and thermal efficiency. Concerning surface heat losses convection was modelled. No heat losses from weld pool were modelled. Radiation was not modelled.

Butt welded mock-up pipe

A mock-up containing multiple butt-welds was manufactured and residual stresses were measured from the mock-up pipe [1]. The pipe outer diameter was 323.85 mm and wall thickness was 17.45 mm. The length of the mock-up was 400 mm consist-

ing of two pipes of 200 mm length which were welded together. The pipe materials were austenitic steel SA 376 TP 304 and weld material AISI 318L. The properties of Eshete 1250 [7], which is a fully austenitic chromium-nickel steel, having a rather similar chemical composition as AISI 304 steel, were utilised in this computation.

The welding was performed by nine passes. The first three passes were welded using gas tungsten arc (TIG) welding and the rest of the passes were welded using manual metal arc welding. Figure 2 compares the real welding process sequence to the modelled sequence. Welding voltage was 13.5-22 V, welding current 77-100 A, torch speed 0.33-1.6 mm/s and interpass temperature 23-88°C. Heat input into the model was calculated based on voltage, current and thermal efficiency. Torch speed controls the welding rate.

Figure 3 shows the finite element model. One quarter of the whole circumference was modelled. The element side length varied between 0.6...2.2 mm in the weld area. Figure 4 shows computed temperatures during the welding of bead 4. The molten (grey) area is visible in the Figure.

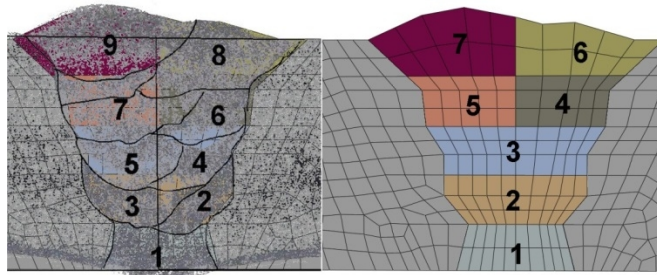


Figure 2. Real welding process sequence (left figure), and the sequence in the three dimensional FE analysis (right figure).

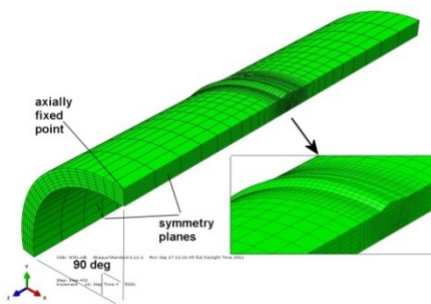


Figure 3. The finite element model. Figure shows also symmetry planes and axially fixed point.

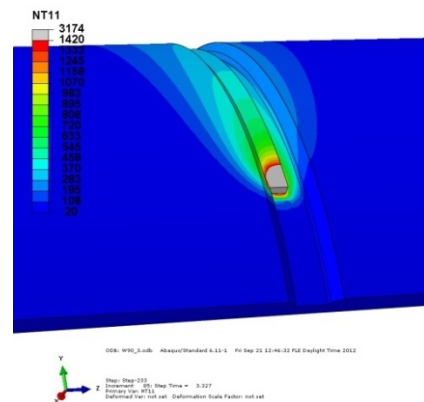


Figure 4. Computed temperatures during the welding of bead 4.

For comparison, computations were performed also with an axisymmetric model. Figure 5 shows computed axial and circumferential (hoop) residual stress (MPa) after welding at the middle of the weld (after welding at room temperature at the middle of the circumference).

The computed axial stresses are rather similar between axisymmetric and three dimensional model. Differences exist, however, in the computed circumferential (hoop) stresses. Larger tensile stresses were obtained with the axisymmetric model in the weld area near the inner surface. This is due the lack of capability of the axisymmetric model to model the movement of welding torch in the circumferential direction and deformations in front of and behind the torch.

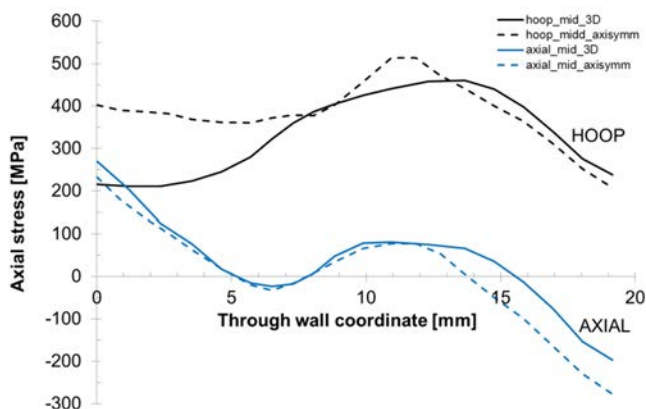


Figure 5. Computed axial and circumferential (hoop) residual stress (MPa) after welding at the middle of the weld and at the middle of the circumference. Three dimensional and axisymmetric results are shown. Inner surface corresponds to coordinate value of 0 mm.

Overlay welded nozzle

The study considered the welding residual stresses after simulated weld overlay and operational loads of a RPV feed water inlet nozzle. Comparison was performed between two and three dimensional modelling.

The reactor pressure vessel and nozzle material in the analysis was ferritic SA 105 with TP316 cladding. The safe-end and weld materials in the analysis were Inconel 82. The material properties were obtained from references [8] and [9]. Figure 6 shows stress strain curves for the materials at room temperature (constant strain amplitude 0.01).

Three dimensional modelling was performed for the overlay welding using symmetric model generation procedure of Abaqus code [4]. A 90 degree three dimensional model was utilised. Welding voltage was 16 - 25 V, welding current 50 - 110 A, torch speed 1 - 2 mm/s and interpass temperature 150°C.

The analysis procedure was rather complex including welding, machining and operational loading phases. In the analysis the heat treatments and the welding of the buttering were not modelled. The basic analysis load steps were:

- Structure is stress free at heat treatment at 575°C, cool down of structure to 20°C;
- Welding of the nozzle/safe-end weld and machining of the safe-end and weld cap removal;
- Pressure test and service loading after welding;
- Overlay welding, and service loading after overlay welding.

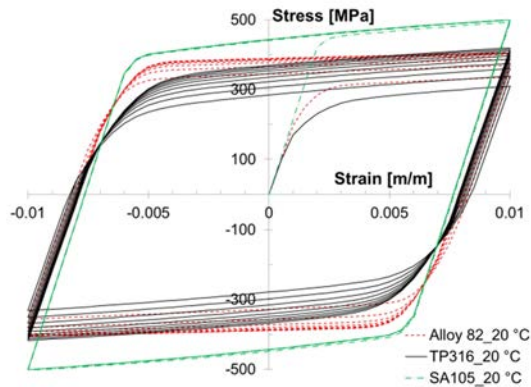


Figure 6. Stress strain curves for the materials at room temperature (constant strain amplitude 0.01).

The computed hoop stress after overlay welding varied around the circumference, Figure 7. The stress variation is larger near the inner surface. The stress state in the middle of the circumference differs from the stress state at the welding start (0°) and welding end location (90°). The reasons for the difference are thermal effects (no heat conduction on the cutting surfaces) and boundary conditions on the cutting surfaces. Figure 8 shows computed trough wall hoop stress in the middle of the weld after nozzle/safe-end welding (w1) and after overlay welding (w2) at room temperature (20 °C). The results are presented at circumferential location of 45° and 69° from start of welding. The results show that the decrease of the circumferential stress due to overlay welding is small at depths larger than half of the wall thickness from inner surface.

The stresses were slightly relaxed due to pressure test and operational loading. The operational loading, pressure and temperature, causes clear non-permanent change in the stresses. Table 1 shows computed hoop and axial stress at operational loading before and after overlay welding. The results are shown in the middle of the nozzle/safe-end weld at three circumferential locations and at five locations in the wall. The overlay welding reduces circumferential stresses especially near the inside surface. Three dimensional model predicts, however, smaller stress decrease than the axisymmetric model. The results show that the decrease of the circumferen-

tial stress due to overlay welding is small at depths larger than half of the wall thickness from inner surface.

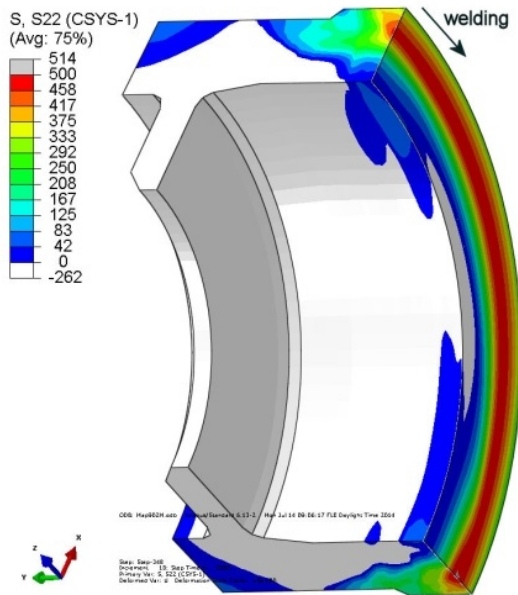


Figure 7. Procedure for generating three dimensional model from axisymmetric model and its results.

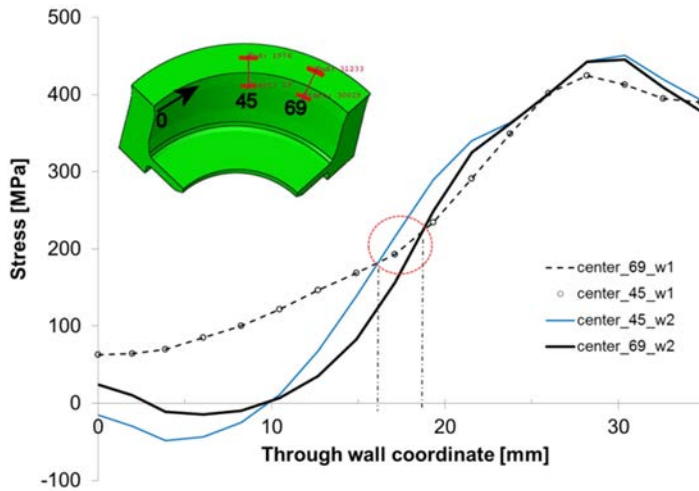


Figure 8. Computed trough wall hoop stress in the middle of the weld after nozzle/safe-end welding (w1) and overlay welding (w2) at room temperature (20 °C). The results are presented at circumferential location of 45° and 69°. The location in the wall where overlay welding starts to decrease stresses is shown.

Table 1. Computed hoop and axial stress at operational loading before and after overlay welding. The results are shown in the middle of the nozzle/safe-end weld at three circumferential locations and at five locations in the wall (0t = inside surface, 1t = outside surface).

t	Hoop [MPa]			Axial [MPa]			
	0°	45°	90°	0°	45°	90°	
0	41	41	41	-37	-38	-37	<i>before overlay welding</i>
	-4	-56	11	23	64	45	<i>after overlay welding</i>
¼	89	89	89	-132	-132	-131	<i>before overlay welding</i>
	19	-59	-22	-147	-160	-149	<i>after overlay welding</i>
½	184	184	184	-30	-30	-29	<i>before overlay welding</i>
	172	151	158	-11	-86	-102	<i>after overlay welding</i>
¾	353	353	353	206	206	206	<i>before overlay welding</i>
	297	302	325	140	114	99	<i>after overlay welding</i>
1	362	362	362	181	181	181	<i>before overlay welding</i>
	331	325	327	186	194	170	<i>after overlay welding</i>

Residual stresses in RPV cladding

The stresses due to welding of RPV cladding and change of stresses due to post weld heat treatment and operational loading were computed in this study. The geometry of the modelled RPV wall is presented in the Figure 9. Due to axisymmetric modelling a plane of the wall was modelled. The base material in the computation was SA 105 and cladding material TP316.

The time independent material properties for the analysis were taken from references [8,9]. These properties include the material parameters for combined isotropic/kinematic hardening material model of Abaqus [4]. For the time dependent material behaviour (post weld heat treatment) Norton strain hardening creep is adopted as following creep constitutive equations in the analysis [10]:

$$\dot{\epsilon}^{cr} = 2.82 \cdot 10^{-17} \cdot \bar{\sigma}^{5.24} \quad (\text{SA105, originally for SA533B-1 in [10]}) \quad (1)$$

$$\dot{\epsilon}^{cr} = 1.49 \cdot 10^{-28} \cdot \bar{\sigma}^{9.88} \quad (\text{TP316, originally for 309L SS in [10]}) \quad (2)$$

where $\dot{\epsilon}^{cr}$ is the equivalent creep strain rate [1/s], and $\bar{\sigma}$ is the Mises equivalent stress [MPa]. These equations are given in for temperature of 615°C, which is almost equal to the post weld heat treatment temperature utilised in this analysis, 620°C. The heating and cooling phases were assumed be rapid, thus creep during these phases were not taken into account.

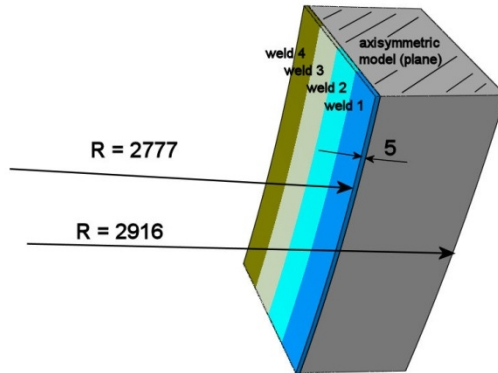


Figure 9. The overall geometry of the modelled RPV wall.

The welding current was 420 A, welding voltage 29 V, torch speed 5 mm/s and interpass temperature 150°C. The analysis included welding of the cladding passes, post weld heat treatment, pressure testing and operational loading.

Figure 10 show the computed hoop stress after welding and after post weld heat treatment at room temperature (20 °C).

The computational results show that the post weld heat treatment reduces stresses especially in the base material beneath the cladding. The cladding stresses are reduced after pressure test and operational loading. It is usually assumed that structure is stress free at operational temperature. The results show, that although the stresses in the cladding are near zero there is tensile stress of approximately 50 MPa in the base material beneath the cladding.

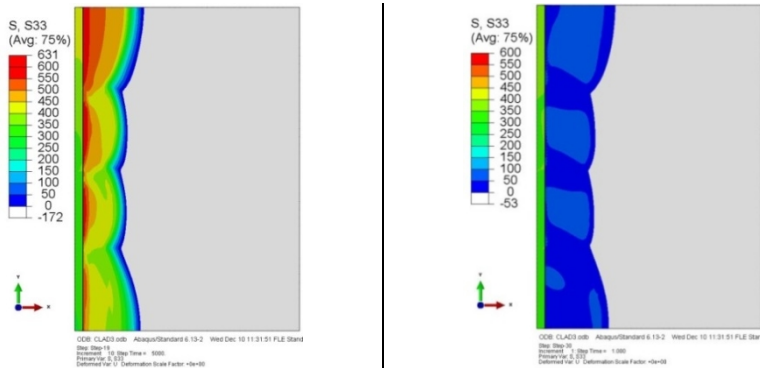


Figure 10. Computed hoop stress [MPa] after welding at room temperature (20 °C) (left), and computed hoop stress [MPa] after post weld heat treatment at room temperature (20 °C) (right).

Figure 11 shows computed through wall axial and hoop stress [MPa] along line L1 at operational load (pressure and temperature). The computed axial and hoop stress

according to an analytic formula (without thermal and residual stresses) is also shown. The results show that highest tensile stresses occur in the base material underneath the cladding.

In the operational loading (pressure and temperature) the highest stresses occur in the base material underneath the cladding. The value of tensile hoop stress is approximately 200 MPa.

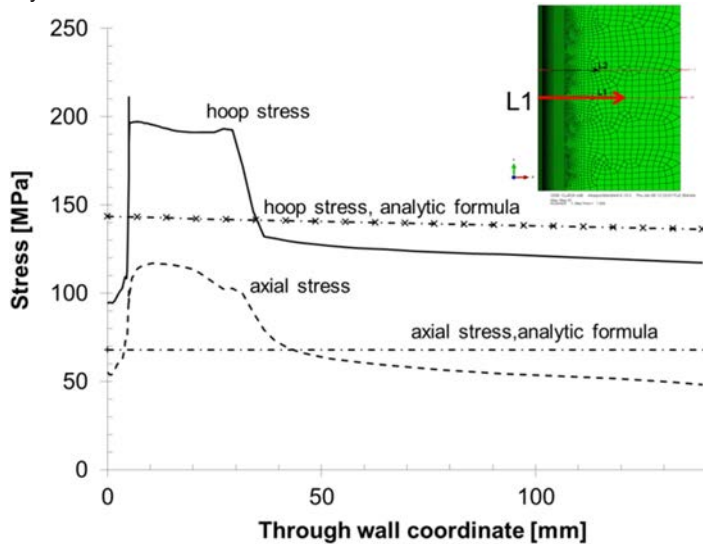


Figure 11. Computed through wall axial and hoop stress [MPa] along line L1 at operational load (pressure and temperature). The computed axial and hoop stress according to an analytic formula (without thermal and residual stresses) is also shown.

Summary and conclusions

Numerical computation of residual stresses has been performed for several cases and the effect of post weld heat treatment, overlay welding and operational loading has been estimated.

Although axisymmetric and three dimensional results were generally similar, differences were observed especially in the critical areas. In the case of butt welded pipe larger tensile stresses were obtained with the axisymmetric model in the weld area near the inner surface. This is most probably partly due to thermal results and partly due to the lack of capability of the axisymmetric model to model the movement of welding torch in the circumferential direction and deformations in front of and behind the torch.

In the case of overlay welding three dimensional predicts smaller stress decrease due to weld overlay than the axisymmetric model. In all the case of the butt welded pipe and RPV nozzle the stresses were slightly relaxed due to pressure test and

operational loading. The operational loading, pressure and temperature, causes clear non-permanent change in the stresses.

The computational results show that the post weld heat treatment reduces RPV cladding stresses especially in the base material beneath the cladding. The cladding stresses are also reduced due to pressure test and operational loading. In the operational loading (pressure and temperature) highest stresses occur in the base material underneath the cladding. The value of tensile hoop stress is approximately 200 MPa. The results show the suitability of computational methods for plant safety assessment applications.

References

1. Keinänen, H., Chauhan, M. Computation of welding residual stresses in a multi-pass welded mock-up pipe. Research Report VTT-R-08364-12. 22+3 p.
2. Keinänen, H. Simulation of weld overlay. Research Report VTT-R-00485-14. 35+10p.
3. Keinänen, H. Computation of cladding welding stresses. Research Report VTT-R-06020-14. 19+3p.
4. Abaqus Theory Manual, version 6.13-1. Dassault Systemes, 2013.
5. Armstrong, P.J. & Frederick, C.O. A mathematical representation of the multiaxial Bauschinger effect, C.E.G.B. Report RD/B/ N731, Berkeley Nuclear Laboratories, Berkeley, UK, 1966.
6. Chaboche J. L. 1989. Int. J. of Plasticity 5 247.
7. Keinänen, H. 2012. STYLE WP2.2 Weld Repair Simulations. Research Report VTT-R-05566-12. 45 p.
8. International Weld Residual Stress Round Robin Problem Statement, Version 1.0, December 14, 2009. US Nuclear Regulatory Commission, Office of Nuclear Regulatory Research, Division of Engineering, Component Integrity Branch.
9. Crooker, P. & Rathbun, H. 2011. Weld Residual Stress Finite Element Analysis Validation. Introduction and Overview. June 14-15, 2011, Rockville, MD, USA.
10. Katsuyama, J., Udagawa, M., Nishikawa, H., Nakamura, M. & Onizawa, K. 2010. Evaluation of weld residual stress near the cladding and J-weld in reactor pressure vessel head for the assessment of PWSCC behaviour. E-Journal of Advanced Maintenance, Vol 2 (2010), 50-64.

36. Heavy fouling and corrosion risks in the cooling water systems of NPPs and methods for their mitigation (RICO)

36.1 RICO summary report

Johanna Lukin, Pauliina Rajala, Timo Saario, Essi Velin, Saija Väisänen

VTT Technical Research Centre of Finland Ltd
P.O. Box 1000, FI-02044 Espoo

Abstract

Numerous chemical shipments are transferred on Baltic Sea and possibility of a chemical spill caused by some accident is therefore present. Since nuclear power plants (NPPs) in Finland take their cooling water from Baltic Sea a large chemical spill in the proximity of the plant could possibly be harmful to the materials of the cooling water systems or decrease the heat transfer capacity of the plant.

In this project, it was first surveyed which are the most common and possibly harmful chemicals transported on Baltic Sea and what would be their concentration when they reach the cooling water systems of a nuclear power plant. The selected chemicals (ethanol, phosphoric acid, sodium hydroxide, phenol and rape seed oil) and concentrations with safety factors (0.1 ppm, 1 ppm, 10 ppm) were used in a series of corrosion, fouling and heat transfer experiments performed on cooling water system material titanium. It was also studied, whether these chemicals have an effect on the microbiologically induced corrosion of titanium.

It was found out that because nuclear power plants are situated rather far away from shipping routes the concentrations of chemicals would be rather low when a spill reaches a nuclear power plant. When these concentrations are used, the corrosion rates in titanium are very low, under 200 nm/year after three days of exposure, while the corrosion rate in brackish water without chemicals was around 100 nm/year after three days. No effect on heat transfer could be detected. These results were gained in abiotic artificial brackish water. When microbes from Baltic Sea were added to the measurement solution, all measured corrosion rates were under 100

nm/year and all chemicals decreased the corrosion rate of titanium when compared to the result without chemicals.

Introduction

Cooling water systems are essential for nuclear power plants to operate safely. Their integrity, however, can be compromised by material deterioration caused by fouling and corrosion of surfaces. Fouling increases the rate of corrosion and may decrease the heat transfer rate. Fouling and corrosion affect the cooling water systems even in normal operation when the cooling water is taken from natural waters. Different kind of macrofouling species, like mussels and barnacles, can enhance corrosion. Similarly, chemical spills from tanker accidents happening nearby can increase the rate of corrosion.

Large amounts of different chemicals are transferred in Baltic Sea. In 2010, around 290 million tons of oil and oil products, at least 11 million tons of liquid chemicals and 4 million tons of other liquid bulks were transported in Baltic Sea. Baltic Sea is a challenging environment because of its shallowness, narrow navigation routes and ice cover in winter. During the years from 1989 to 2010 there have been 1400 accidents in Baltic Sea. During that time 28 tanker accidents have happened which caused some kind of environmental pollution. Even though the risk of chemical spill is small, it must be taken into consideration, because all Finnish nuclear power plants take their cooling water from Baltic Sea.

In addition to macrofouling species and chemicals, also micro-organisms can harm materials by fouling or increasing corrosion rate. Microbiologically influenced corrosion is caused by different archaea, bacteria and unicellular eukaryotes. For example, sulphate reducing bacteria are known to harm titanium, which is commonly used as a condenser material in nuclear power plants. These bacteria use sulphate as the terminal electron acceptor and produce thus HS^- and finally hydrogen sulphide (H_2S).

Main objectives

Main objectives in this project were 1) to determine the most probable chemical spills on Baltic Sea which could be harmful for the water uptake of NPPs, 2) to study the effects of certain chemicals on corrosion and heat transfer of titanium in artificial brackish water simulating the cooling water condenser of a nuclear power plant, and 3) to compare whether the addition of microbes from Baltic Sea affects to the corrosion rates of titanium and to measure how the amount of microbes changes when these chemicals are added compared to pure brackish water.

Selection of chemicals and preliminary assessment of risks of these chemicals for water in-take of a nuclear power plant

In spring 2013 an expert panel was organized with a purpose of identifying potentially hazardous chemicals for cooling water systems of NPPs. The chemicals were selected based on their potential to cause corrosion in the water intake systems of power plants or to reduce heat transfer efficiency of the system. Also their toxic effects on mussels and other organisms was briefly evaluated. Another important selection criteria was the commonness of those chemicals in transports over Baltic Sea. Chemicals with very high volatility, poor solubility to water and low density were excluded from further analysis. The selected chemicals to be studied in RICO project were ethanol (representative of alcohols), sodium hydroxide (base), phosphoric acid (acid), phenol (aromatic alcohol, also viscous and hazardous chemical) and rape-seed oil (oil product).

Based on this chemical selection a preliminary risk evaluation was performed at the Finnish Environment Institute (SYKE), where the chemical properties and toxicity of chemicals and risks concerning the maritime transport of these chemicals were evaluated. Also an alert exercise was carried out by the Finnish Environment Institute (SYKE) where a chemical carrier grounded resulting in an outflow of 50 tons oil and 200 m³ of phenol. Based on such modelling exercises the concentrations of the spilled chemicals in the laboratory and pilot-plant scale experiments were chosen to be 0.1, 1 and 10 mg/l.

Abiotic experiments on the effect of spilled chemicals on corrosion and heat transfer in the cooling water cycles of NPPs

The effect of previously mentioned chemicals (ethanol, sodium hydroxide, phosphoric acid, phenol and rape seed oil) on the corrosion and heat transfer rate of titanium (sea water heat exchanger material) was measured in a series of experiments. These studies were conducted with a laboratory system (Figure 1) which can be used for online electrochemical measurements to study corrosion rate (electrochemical impedance spectroscopy, linear polarisation resistance) as well as for monitoring the inflow and outflow temperatures to determine heat transfer rate with a maximum sample temperature of $T = 80^{\circ}\text{C}$. The experiment period was selected to be 72 h, as this is the time needed for the NPP to shutdown in case of an alert for potentially risky chemical spill in the nearby sea area.

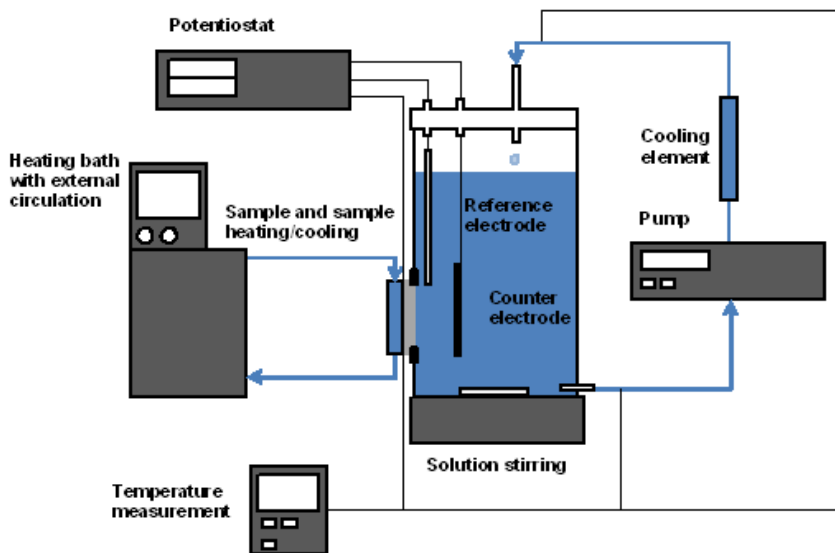


Figure 1. A schematic diagram of the laboratory equipment

The experiments were conducted in artificial brackish water corresponding to the water of Baltic Sea. During the experiment period artificial brackish water was circulated through the system. Experiments were conducted with concentrations of 0.1, 1.0 and 10 mg/l of selected chemicals. The titanium samples attached to the measurement cell were in contact with the test solution during the whole experiment and they were heated to the temperature of around 80°C with an external heating bath. High sample temperature was believed to accelerate corrosion (the actual maximum temperature of the condenser is about 40°C). The temperature of the measurement solution increased a few degrees while it was flowing through the measurement cell but remained still at room temperature. Electrochemical impedance spectrometry (EIS) and linear polarization resistance (LPR) measurements were conducted for titanium samples with a purpose of estimating the thickness of the deposit and the corrosion rate of the sample. After the experiments, the samples were dried in a desiccator for several days, photographed and weighed. The elemental composition of the precipitate formed on the samples was studied with SEM/EDS.

While exposed to the artificial brackish water, samples were covered by white calcium carbonate deposits. The experiments showed a decreasing corrosion rate as a function of exposure time for the chemicals studied. All corrosion rates were under 200 nm/year after three days (Figure 2). The differences in heat transfer rates were so small that no definite conclusions could be made on the effects of the chemicals.

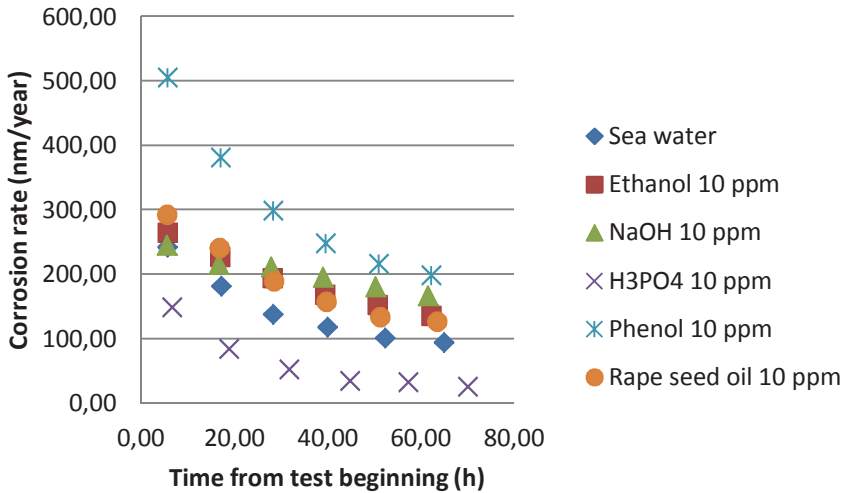


Figure 2. Corrosion rates of titanium samples in abiotic measurements

The effect of spilled chemicals on microbiologically induced corrosion in the cooling water systems of NPPs

Series of microbiological analyses and electrochemical measurements were conducted to monitor how the microbial population responds to addition of different chemicals in simulated cooling water cycle environment and how it changes the corrosion rate of titanium. The test solution was laboratory-made brackish water simulating Baltic Sea water. The inoculant of micro-organisms used in these experiments was collected from Baltic Sea. Studied chemicals and their concentrations were same as in abiotic measurements.

In the beginning of the experiment the baseline sample of the biomass was collected on sterile CA-filters. The artificial brackish water with inoculant was cycled through the measurement cell for three days and during that time the electrochemical impedance spectroscopy (EIS) and linear polarization resistance (LPR) measurements were conducted. Two sample temperatures (T_{plate}) were used, $T_{plate}=80^{\circ}\text{C}$ and $T_{plate}=40^{\circ}\text{C}$, lower corresponding to the highest temperature of water in the secondary side of condenser. Higher temperature was selected because it is comparable to the previous abiotic measurements and because it accelerates corrosion. The temperature of the test solution remained at room temperature.

After the measurements, the samples were dried in a desiccator, photographed and weighed. Several samples were selected for SEM pictures and EDS analysis. Also biomass from 1000 ml water was collected on CA-filters to see the microbial response to simulated cooling water cycle conditions with or without the added chemicals. As a proxy for bacterial biomass, quantitative PCR (qPCR) was used to

determine the amount of 16S rRNA gene copies in each sample. The amount of sulfate reducing microbes was determined on base of copies of β -subunit of dissimilatory sulfite reductase (*dsrB*) gene.

Whereas abiotic water with chemicals produced white precipitate containing mainly calcium carbonate, adding of microbes resulted in a much thinner layer consisting of organic substances and significantly less of calcium carbonate. All measured corrosion rates were small, less than 100 nm/year after three days (Figure 3), and were lower than previous measurements without microbes. Therefore it seems likely that chemical spill assumed in this project does not create a threat to cooling water systems of nuclear power plant. Smallest corrosion rates were achieved with addition of rape seed oil or sodium hydroxide.

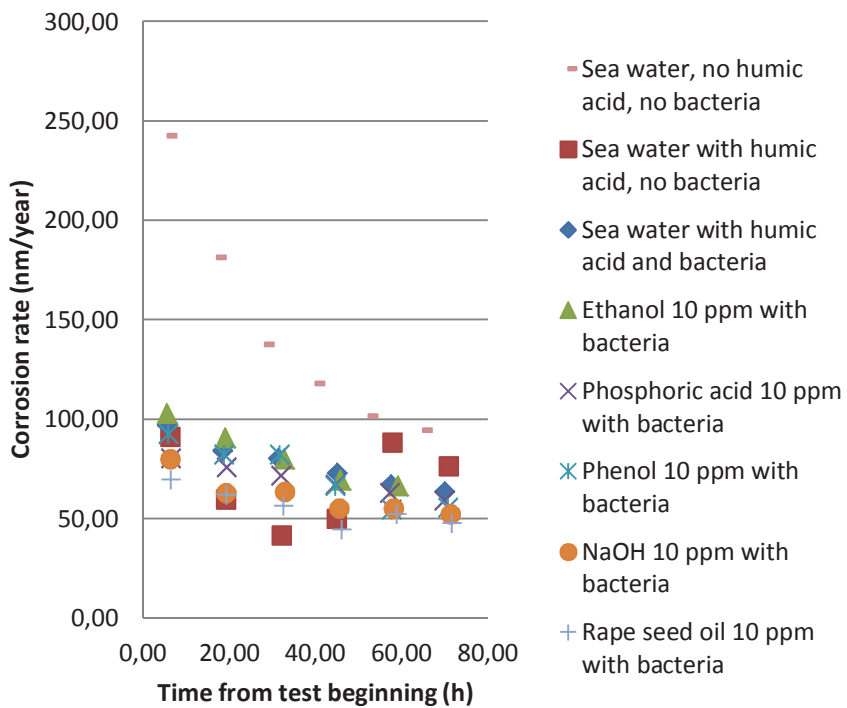


Figure 3. Corrosion rates of titanium samples for biotic measurements compared to abiotic results in artificial brackish water without microbes

The amount of bacteria according to 16S rRNA gene copies increased during the experiment at $T_{plate}=80^{\circ}\text{C}$ compared to baseline sample (Figure 4), suggesting that the conditions in flow cell were favourable for microbes from sea water. Also the amount of sulphate reducing bacteria increased during the experiments performed at $T_{plate}=80^{\circ}\text{C}$. Sulphate reducing bacteria had strongest response to phosphoric acid. When the experiments were repeated at $T_{plate}=40^{\circ}\text{C}$ the number of bacteria and sulphate reducing bacteria decreased during the experiment. This could be due to the nutrient poor conditions in flow cell when the high temperature is not accelerating the release of organic matter. When phosphoric acid was added to the experiment the amount of detected bacteria increased. This demonstrates that the naturally occurring microbes in Baltic Sea water have the ability to adapt to the high temperatures of heat exchange units. No clear correlation could be detected between corrosion rate and microbial community. The results suggest that temperature is more important factor than microbes when considering the performance of titanium.

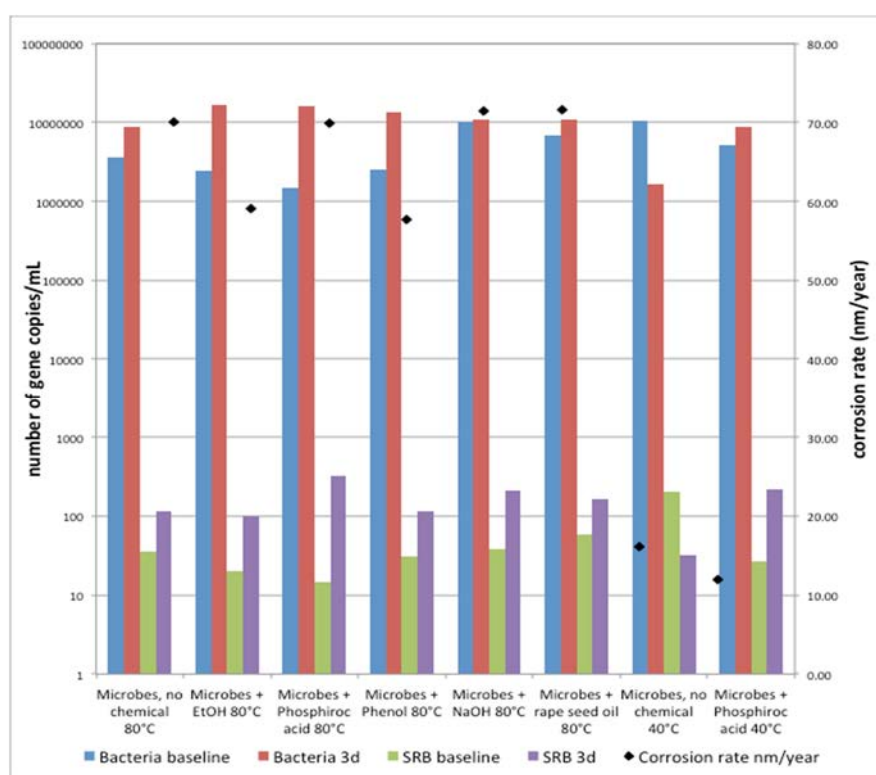


Figure 4. Corrosion rates of titanium samples compared to the amount of microbes

Conclusions

Following conclusions can be made from the results of RICO project:

- Studied chemicals (ethanol, sodium hydroxide, phosphoric acid, phenol and rape seed oil) are not harmful for titanium parts of cooling systems of nuclear power plants with concentrations estimated to be released from a tanker accident in Baltic Sea. All corrosion rates were in order of hundreds of nanometers per year and decreased over time.
- No clear correlation could be detected between the corrosion rate and type or extent of the microbial community in the biotic experiments.

References

- Holma, E., Heikkilä, A., Helminen, R. & Kajander, S. 2011. Baltic Port List 2011 – Annual cargo statistics of ports in the Baltic Sea Region. Centre for Maritime Studies, University of Turku, Finland.
- Posti, A. & Häkkinen, J. 2012. Survey of transportation of liquid bulk chemicals in the Baltic Sea. Publications from the Centre for Maritime Studies University of Turku, A 60.
- HELCOM. 2012. Report on shipping accidents in the Baltic Sea during 2011. Helsinki Commission, Response Group.
http://www.helcom.fi/shipping/accidents/en_GB/accidents/
- Häkkinen, J., Posti, A. & Rytönen, J. 2013. The Preliminary Assessment of Risks of Chemical Spills for the Water In-Take of the Nuclear Power Plant in Finland. Finnish Environment Institute, Helsinki, Finland. 68 p.
- Lukin, J., Saario, T. & Väisänen, S. 2014. Laboratory studies on the effect of spilled chemicals on corrosion and heat transfer in the cooling water cycles of NPPs. VTT Technical Research Centre of Finland. Research Report VTT-R-00850-14. 38 p. + app. 8 p.
- Velin, E., Väisänen, S., Lukin, J. & Saario, T. 2014. Effects of Spilled Chemicals on Fouling, Heat Transfer and Corrosion in the Cooling Water Systems of NPPs. Nuclear Plant Chemistry Conference 2014 Sapporo. October 26-31 2014, Royton Sapporo Hotel, Japan.
- Lukin, J., Rajala, P., Saario, T., Velin, E. & Väisänen, S. 2014. The effect of spilled chemicals on MIC in the cooling water systems of NPPs. VTT Technical Research Centre of Finland. Research Report VTT-R-06181-14. 26 p. + app. 19 p.

37. Impact 2014 (IMPACT2014) and Structural mechanics analysis of soft and hard impacts (SMASH)

37.1 IMPACT2014 summary report

Ari Vepsä, Seppo Aatola, Kim Calonius, Ilkka Hakola, Matti Halonen

VTT Technical Research Centre of Finland Ltd
P.O. Box 1000, FI-02044 Espoo

Abstract

Deliberate crash of a large passenger aircraft against nuclear power plant civil structures poses one improbable but possible threat for the safety of the plant. In Finland, for example, such a crash has been taken as one of the design basis accidents when licensing new plants. Resistance against such a crash is verified with numerical models and/or simpler semi-empirical or analytical formulas. These predictive methods have to be validated against suitable experimental data before they can be trustfully used. The problem is that such a data is very scarcely publicly available. This is the main reason why IMPACT 2014 project continued in the footsteps of its predecessors IMPACT 2006 and IMPACT 2010 to study the phenomena arising in an aircraft impact against a concrete structure and to produce vast amount of experimental data to be used in the validation of predictive models. During the project, total of 59 impact tests were carried out: 22 tests with so-called force-plate setup and 37 tests with 32 different reinforced concrete structures. Some of the structures were tested either twice or thrice in order to study how their behaviour changes when the structure gets damaged. In addition to “traditional” test types of bending and punching, two new types of tests were introduced in the project: combined bending and punching behaviour tests and vibration propagation and damping tests. In addition to impact tests, two static four point bending tests were carried out with reinforced concrete slabs.

Introduction

The topic of impact research on reinforced concrete structures has been included into SAFIR2006, SAFIR 2010 and SAFIR 2014 programmes. The main motivation for the study comes from a threat that a large passenger aircraft is deliberately crashed against civil structures of a nuclear power plant (NPP). The 9/11 terrorist attacks showed that this type of events are possible although improbable.

Collapse of a NPP reactor building due to such a crash may lead to radioactive leaks. Due to the devastating consequences of such a leak, more attention has been paid worldwide on mitigation of the consequences of a possible deliberate aircraft crash against civil structures of NPP after the 9/11 tragedy. For example, in Finland the Government Decree on the Safety of Nuclear Power Plants (717/2013), Section 17 stipulates that "*The design of a nuclear power plant shall take account of external hazards that may challenge safety functions. ... The design shall also consider unlawful actions with the aim of damaging the plant and a large commercial aircraft crash.*" (Finnish Council of State, 2013)) On this basis, the Finnish Radiation and Nuclear Safety Authority (STUK) has included crashworthiness of NPP as one of the design basis in its new regulatory guides issued in 2013 (2013).

Crashworthiness of these structures is demonstrated with numerical computation models and/or empirical-, semi-empirical or analytical formulas. The phenomena arising in these crashes are numerous and complicated. In addition, reinforced and, in some cases, also pre-stressed concrete, the material of which the NPP civil structures are commonly made, is not the easiest one to model. Consequently, modelling of these impacts is by no means an easy task and calls for considerable skills from the modeller(s) as well as reliable modelling tools and models. Experimental data obtained from tests in which similar phenomena arise is invaluable for education of the modeller(s) as well as for validation of the modelling tools and methods. Due to the expense of these types of tests, there is very little publicly available data that can be used for the aforementioned purposes. IMPACT 2014, as its predecessors, have tried to satisfy this need of validation data.). An overview of what has been done so far within the testing projects can be found in the work by Kärnä et al. (2004), Calonius et al. (2006, 2009, 2011), Hakola et al. (2013) and Vepsä (2013, 2014). Examples of the usage of the obtained test results in validation of the numerical models can be found for example in the work by Heckötter & Vepsä (2013), Saarenheimo et al. (2007, 2009) and Heckötter & Sievers (2009).

Multiple phenomena arise in an aircraft crash against reinforced concrete structures. These different aspects have been studied mainly in separate tests of different types. These different test types that have been executed within IMPACT 2014 and its predecessors can be divided as follows:

- soft impact bending behaviour tests,
- hard impact punching behaviour tests,
- combined bending and punching tests,
- vibration propagation and damping tests and
- water filled projectile tests.

The main objective of the research is to measure the response of a structure for an impact by a soft or hard flying projectile, simulating the fuselage or other parts of an aircraft. In this context, the terms soft and hard projectile mean that they are much more and correspondingly much less deformable the structure against which they are impacted. The responses to be measured may include for example displacements, accelerations, strains on the reinforcement as well as on the concrete

surface and support forces and they are defined case-specifically. In addition to the measured quantities, the impacts are documented with two high speed video cameras each taking 1000 frames per second (FPS). Majority of the tests have been designed in collaboration with the partners and all the test have been executed by VTT with its Impact test-bed. This test bed has been described for example in the work by Hakola et al. (2013).

Bending behaviour tests

When impacting the target, the fuselage of an aircraft causes causes mainly mass flow type of loading which results global response of the structure. This global response manifests itself in large deflections of the impacted surface and consequently large strains on the reinforcement. In an extreme case, the strains on the reinforcement become large enough so that the reinforcement breaks and the structure loses its load bearing capacity at and near these locations. This type of response behaviour has been studied in what are referred to as bending behaviour tests. Subgroup of this test type includes tests where the impacting projectiles are filled with water to simulate fuel tanks and the fuel inside them as well as tests where the used projectiles include wings. Soft impact bending behaviour tests that have been carried out previously have been discussed for example in the work by Tarallo et al. (2007).

In these bending behaviour tests, 150 mm thick simply supported reinforced concrete walls with spand width of 2 metres in both directions are impacted with projectiles which are usually made of stainless steel pipe with an inner diameter of 250 mm, a wall thickness of 2 mm and weight of 50 kg. This type of projectile is referred to as “soft” meaning that it is much more deformable than the structure that it collides against. In some cases, the projectiles were filled with water with mass of roughly 26 kg so that the total mass still remained roughly at 50 kg.

Nine bending behaviour tests were carried out within IMPACT 2014. Six of these were carried out with an empty projectile, two with a water filled projectile and one with an empty aluminium projectile with wings weighing 42 kg. The main objective of these tests was to measure the displacements and strains on the bending reinforcement. These variables can then be used for validating the predictive models. Other measured variables included the horizontal support forces, the strains on the front surface of the target and the permanent deformations of the target after the test.

As an example of the obtained results, the graph in Figure 1 shows both the maximum as well as the permanent displacement 400 mm away from the centre point, which acts also as the target point, both in vertical as well as horizontal direction. The graph includes the results from four of the bending behaviour tests (TF15-TF18) carried out within IMPACT 2014 with various impact velocities. In addition, the results of four similar tests (TF11-TF14), carried out within the previous project, are included in the graph for the sake of comparison. Four of the tests (TF13, TF14, TF16 and TF18) were carried out with water filled projectiles and the rest with hollow

projectiles with the same weight and roughly the same impact velocities. Second order best-fit curves have been added into the graph for each data set.

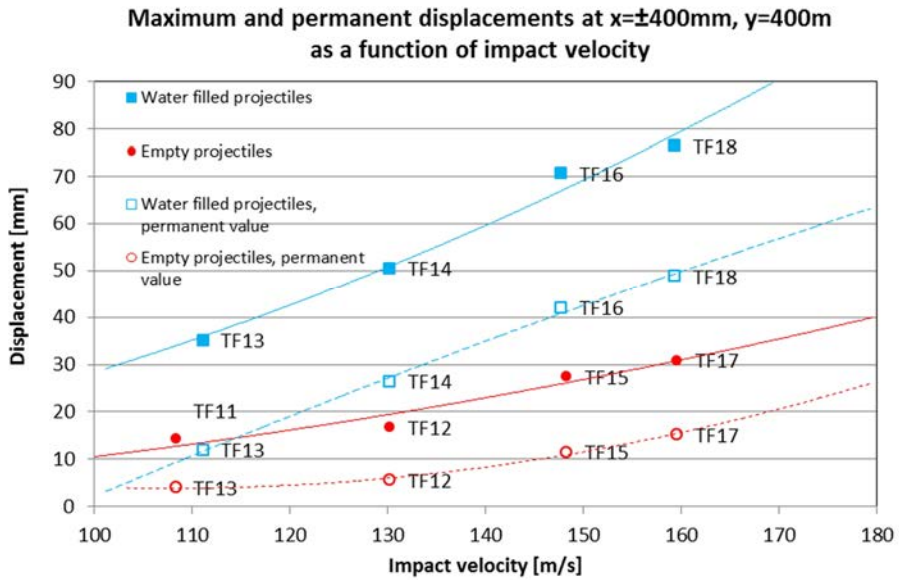


Figure 1. The maximum (solid markers) and the permanent (hollow markers) displacements as a function of the impact velocity measured in the bending behaviour tests with water filled (boxes) and hollow (dots) projectiles.

The water filling of the projectiles seems to magnify the maximum displacements 2.5 – 3 times compared to the ones obtained with hollow projectiles. The corresponding magnifying effect on the permanent values is 3.0 – 4.7 times. The small differences between the measured values and the predictive fitted curves can be explained mainly by differences in the Young's modulus between the different batches of concrete used for casting of the walls.

Punching behaviour tests

When impacting against a reinforced concrete target, hard parts of an aircraft, like the rotors of the motors and the landing gear, cause mainly local response of the structure meaning that these parts try penetrate inside and through it. In an extreme case, the hard parts perforate through the structure and continue their travel hitting and destroying the obstacles that lie in their path. In the process, they cause concrete particles to become deattached at the back surface of the structure. This type of response behaviour has been studied in what are referred to as punching behaviour tests. The punching behaviour tests carried out within the IMPACT-projects have been discussed for example in the work by Orbovic et al. (2011) and Oliveira et al. (2011).

In the punching behaviour tests, 250 mm thick simply supported reinforced concrete walls with span width of 2 metres in both directions are impacted with projectiles which are made of a thick steel tube with an outer diameter of 168.3 mm and a wall thickness of 12.5 mm, a solid steel dome in the front and lightweight concrete cast inside in order to reach target weight of 47.5 kg. This type of projectile is referred to as “hard” meaning that it is much less deformable than the structure that it impacts against. Both the longitudinal as well as the shear reinforcement of the tested walls have been varied in the tests. In addition, some of the tested walls have included prestressing bars both without and with prestressing of roughly 10 MPa and with or without grouting. Some of the tested walls have also included a thin steel liner at the back surface. The strength of concrete has been varied both naturally as well as intentionally with the unconfined cylindrical compression strength varying between 38.9-79.0 MPa.

The main purpose of the punching behaviour tests is to validate the existing semi-empirical formulas for predicting the “just perforation” velocity of different types of targets. This “just perforation” velocity is the impact velocity that the projectile must have in order to perforate through the target with no exit velocity. The target can be considered as perforated when there are no obstacles left that resist the movement of the projectile. The main problem with this type of formulas is that they are commonly based on some specific test series and thus valid only within the assumptions used in that series. For example, their validity commonly ends at concrete compressive strength of 40 MPa and extrapolation to higher strengths may not necessarily give conservative estimates for the “just perforation” velocity.

Eighteen punching behaviour tests were carried out within IMPACT 2014. The main variables that were measured in these tests were the residual or exit velocity of the projectile in cases it went through the wall and the penetration depth in cases it didn't. From these values one can estimate the “just perforation” velocity for the specific target wall configuration in question. Another important output variable is the area and the amount of concrete that becomes loose at the back surface of the wall during the impact.

As an example of the results, the graph in Figure 2 shows the distance to perforation (negative values of the vertical axis) and the residual velocity of the projectile (positive values) as a function of impact velocity for the slabs with (series T10, C12 and T12) and without (series A) shear reinforcement. Tests A1R, AT1, ATL21, P1 and P6 have been carried out within IMPACT 2014 while tests A21, A1, AT and AT2 were carried out during the previous IMPACT-projects. The tests in the negative vertical axis are those where perforation didn't happen while those in the positive axis resulted perforation. For each individual test, the cylindrical compressive strength of concrete is expressed after the code of the test.

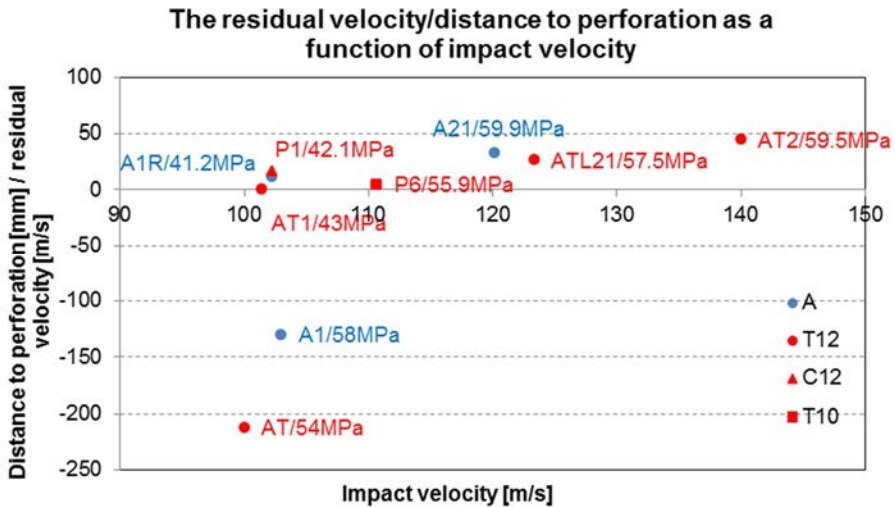


Figure 2. The distance to perforation (negative values of the vertical axis) and the residual velocity of the projectile (positive values) as a function of the impact velocity for the slabs with (series T10, C12 and T12) and without (series A) shear reinforcement.

Tests A1R and A1 as well as tests AT and AT1 were otherwise identical except the concrete compressive strength which was 11-17 MPa lower in tests AT1 and A1R than in tests AT and A1. As a result, the damage caused for the wall was much higher resulting perforation of these walls whereas in tests AT and A1 perforation wasn't achieved. Walls used in test series A and T12 were otherwise identical, except that in series T12, shear reinforcement was used in a form of T-headed bars with diameter of 12 mm and spacing of 90 mm in both directions. Based on the results, this type of shear reinforcement seems to improve the punching resistance of the walls little but not much. They have a bigger reducing effect on the amount of concrete that comes loose at the backside of the wall during the test. Test P1 was otherwise identical to AT1 as well as A1R, except shear reinforcement was used in a form of hooked stirrups. Based on the results, hooked stirrups may even decrease the punching resistance when compared to a wall without shear reinforcement. The remaining test P6 was carried out with T-headed bars with diameter of 10 mm.

Combined bending and punching behaviour tests

Combined bending and punching test is a totally new test type carried out in the project. It includes both global bending as well as local shear type response of the target. The purpose of these tests was to vary and study the effect of the parameters that affect the relation between these two response types. This type of tests have been discussed for example in the work by Borgerhoff et al. (2013).

The geometry and supporting of the target used in these combined bending and punching tests was the same than those used in the punching behaviour tests. The longitudinal reinforcement was also the same than what was used in most of the punching behaviour tests. The amount of shear reinforcement is one the main parameters that affects the shear response and as such it was one of the main parameters varied in the tests. The projectiles used in the tests were “softer” than those used in the bending behaviour tests and “harder” than those used in the punching behaviour tests, being more “soft” than “hard”.

Four combined bending and punching tests were carried out within the project. The main variables that were measured in the combined bending and punching tests were the same than in the bending behaviour tests. In case that the projectile goes through the target, the residual velocity of the projectile is estimated in a manner similar to the punching behaviour tests.

Vibration propagation and damping tests

Another new test type introduced in the project was vibration propagation and damping test. The objective of this test type was to emulate the propagation of vibration which happens in a postulated real case when an aircraft impacts against the NPP reactor building and the resulting vibrations propagate from the impact point via the base slab to the interior of the structure causing in a worst case malfunction of the critical equipment inside the building.

Two series of vibration propagation and damping tests were carried out within the project. Both of the tested structures had a front wall, a floor and a rear wall, the latter including also almost triangular side walls. Both of the targets were tested thrice with the same “soft” projectile type than what is used in the bending behaviour tests. The main purpose of multiple tests was to study how the response of the structure changes when it gets damaged. The response was measured with strain gauges on the reinforcement, displacement sensors and accelerometers. The structures were also subjected to modal testing before and after the individual impact tests. The first of these series is discussed in detail in the following special article (Vepsä et al., 2015).

Conclusions

IMPACT 2014 project continued the work paved by the previous impact testing projects providing valuable measurement data and information regarding the phenomena arising in an impact of an aircraft against large reinforcement concrete structures like the NPP reactor building. Traditional test types of bending and punching tests were continued and totally new test types of combined bending and punching tests as well as vibration propagation and damping tests were introduced. These new test types complemented the existing knowledge with information regarding the relation between the global bending and the local shear and punching damages of the tested wall as well as how the vibration propagates from the hit point to the far-her parts of

a structure and how it gets damped in the process. The obtained results are invaluable in validating the predictive methods used when assessing such a case.

Acknowledgement

The authors would like to acknowledge the project funding by VYR, VTT and the partners. The authors would also like to acknowledge the work by the project team, the SAFIR 2014 steering group and the combined IMPACT 2014 and SMASH ad hoc group.

References

- Borgerhoff, M., Schneeberger, C., Stangenberg, F. and Zinn, R., 2013, "Conclusions from combined bending and punching tests for aircraft impact design", in Transactions of the 22nd conference of Structural Mechanics in Reactor Technology (SMiRT 22), San Francisco, California, USA, August 18-23, 2013.
- Calonius, K., Hakola, I., Hostikka, S., Kankkunen, A., Lastunen, A., Saarenheimo, A., Silde, A., Tuomala, M., 2006, "Wall Response to Soft Impact (WARSI)", In: Rätty, H. and Puska, E. K. (ed.). VTT Research notes 2363: "SAFIR - The Finnish Research Programme on Nuclear Power Plant Safety 2003-2006 – Final Report". VTT Technical Research Centre of Finland, Espoo, ISBN 951-38-6886-9. pp. 207 - 224.
<http://www.vtt.fi/inf/pdf/tiedotteet/2006/T2363.pdf>
- Calonius, K., Hakola, I., Hostikka, S., Kuutti, J., Lastunen, A., Martikainen, H., Saarenheimo, A., Silde, A., Tuomala, M. and Kankkunen, A., 2009, "IMPACT2010 (IMPACT) and Structures Under Soft Impact (SUSI) – IMPACT and SUSI Summary Report", In: Puska, E. K. VTT Research notes 2466: "SAFIR2010 - The Finnish Research Programme on Nuclear Power Plant Safety 2007-2010 - Interim Report". VTT Technical Research Centre of Finland, Espoo, ISBN 978-951-38-7266-3. pp. 446-473.
- Calonius, K., Hakola, I., Hostikka, S., Saarenheimo, A. and Vepsä, A., 2011, "IMPACT2010 (IMPACT) and Structures Under Soft Impact (SUSI) – IMPACT and SUSI Joint Report", In Puska, E. K. and Suolanen, V. (ed.). VTT Research notes 2571: "SAFIR2010, The Finnish Research Programme on Nuclear Power Plant Safety 2007-2010 – Final Report", VTT Technical Research Centre of Finland, Espoo, ISBN 978-951-38-7689-0. pp. 490-519.
<http://virtual.vtt.fi/virtual/safir2010/pdf/T2571.pdf>
- Finnish Council of State, 2013, Government Decree on the Safety of Nuclear Power Plants (717/2013), Section 17.

- Finnish radiation safety authority (STUK), 2013, "Regulatory Guide on Radiation Safety (YVL) A11: Security measures of nuclear power plants, Addendum B: Ydinvoimalaitoksen ja käytetyn polttoaineen varaston rakenteellinen kestävyys sekä tila- ja sijoitussuunnittelu lentokoneiden törmäystä vastaan", (available in Finnish only at this moment), issued on 15.11.2013.
- Hakola, I., Vepsä, A. and Halonen, M., 2012, "Impact Testing and Test Apparatus", Research report VTT-R-01184-12, VTT Technical Research Centre of Finland, Espoo, 29 p.
- Hakola, I., Saarenheimo, A., Vepsä, A., Calonius, K., Hostikka, S., Kuutti, J., Silde, A., Sikanen, T. and Tuomala, M., 2013, "IMPACT 2013 (IMPACT2014) and structural mechanics analyses of soft and hard impacts (SMASH)", In Simola, K. (ed.). VTT Research notes 2571: "SAFIR2014, The Finnish Research Programme on Nuclear Power Plant Safety 2011-2014 –Interim Report", VTT Technical Research Centre of Finland, Espoo, ISBN 978-951-38-7918-1. pp. 344-362.
<http://www.vtt.fi/inf/pdf/technology/2013/T80.pdf>
- Heckotter, C. and Sievers, J., 2009, "Simulation of an Impact Test with a Deformable Projectile on a Concrete Wall", in Transactions of the 20th International Conference on Structural Mechanics in Reactor Technology (SMiRT 20), Helsinki, Finland, August 2009, Paper # 2502.
- Heckötter, C. and Vepsä, A., 2013, "Experimental Investigation and Numerical Analyses of Reinforced Concrete Structures Subjected to External Projectile Impact", ETSON Award winning paper, EUROS SAFE forum, Cologne, November 4-5.
http://www.eurosafe-forum.org/userfiles/file/Eurosafe2013/etsonaward/Heckoetter_paper.pdf
- Kärnä, T., Saarenheimo, A. and Tuomala, M., 2004, "Impact Loaded Structures". In: Rätty, H. and Puska, E. K. (ed.). VTT Research notes 2274: "SAFIR - The Finnish Research Programme on Nuclear Power Plant Safety 2003-2006 – Interim Report". VTT Technical Research Centre of Finland, Espoo, ISBN 951-38-6515-0. pp. 113 - 123.
<http://www.vtt.fi/inf/pdf/tiedotteet/2004/T2272.pdf>
- Tarallo, F., Ciree, B. and Rambach, J.M., 2007, "Interpretation of Soft Impact Medium Velocity Tests on Concrete Slabs", in Transactions of the 19th conference of Structural Mechanics in Reactor Technology (SMiRT 19), Toronto, Canada, August 2007, Paper # J05/2.
- Oliveira, D., Saady, A., Lee, N. and Elgohary, M., 2011, "The effect of T-headed bar reinforcements on the impact response of concrete walls", in Transactions

of the 21st conference of Structural Mechanics in Reactor Technology (SMiRT 21), New Delhi, India, November 6-11, 2011, Paper ID# 69.

Orbovic, N. and Blahoianu, A., 2011, "Tests on concrete slabs under hard projectile impact to evaluate the influence of transverse reinforcement and prestressing on perforation velocity", Transactions of the 21st conference of Structural Mechanics in Reactor Technology (SMiRT 21), New Delhi, India, November 6-11, 2011, Paper ID# 162.

Saarenheimo, A., Tuomala, M., Calonius, K., Lastunen, A., Hyvarinen, J. and Myllymaki, J., 2007, "Numerical Studies on Impact Loaded Reinforced Concrete Walls", in Transactions of the 19th conference of Structural Mechanics in Reactor Technology (SMiRT 19), Toronto, Canada, August 2007, Paper # J05/3.

Saarenheimo, A., Calonius, K., Tuomala, M. and Hakola, I., 2009, "Numerical Studies on Shear Reinforced Impact Loaded Concrete Walls", in Transactions of the 20th International Conference on Structural Mechanics in Reactor Technology (SMiRT 20), Helsinki, Finland, August 2009, Paper # 1844.

Vepsä, A., 2013, "IMPACT2014: Work carried out in year 2012", VTT Research report VTT-R-01653-13, VTT Technical Research Centre of Finland, Espoo, 47 p.

Vepsä, A., 2014, "IMPACT2014: Work carried out in year 2013", VTT Research report VTT-R-00853-14, VTT Technical Research Centre of Finland, Espoo, 47 p. +App. A-C.

Vepsä, A., Saarenheimo, A., Aatola, S., Calonius, C., Hakola, I. and Halonen, M., 2015, "Testing and modelling of vibration propagation and damping in a 3D-structure impacted multiple times with a soft projectile". In: "SAFIR - The Finnish Research Programme on Nuclear Power Plant Safety 2010-2014 – Final Report", VTT Technical Research Centre of Finland, Espoo. (Not yet published)

37.2 SMASH summary report

Arja Saarenheimo¹, Kim Calonius¹, Topi Sikanen¹, Ari Silde¹; Markku Tuomala²

¹VTT Technical Research Centre of Finland
P.O. Box 1000, FI-02044 Espoo

²Tampere University of Technology

Abstract

IMPACT project has produced valuable test data since 2003. Methods have been developed and the applicability of the already existing methods to different cases has already been tested in earlier predecessor projects. Although extensive nonlinear models are often needed, much simpler models can be utilized for preliminary safety assessment. Simplified methods, such as semi-empirical equations and models comprising of only few, most essential degrees-of-freedom, can especially well be applied for parametrical studies and preliminary design.

Introduction

An aircraft impact on safety related structures, in spite of its low probability, has for a long time been recognized as a relevant loading case, especially in designing plants to areas with heavy air traffic. It is required (Government Decree 733/2008) that the nuclear plant design takes into account large airliner crashes, as well as fires and explosions. Structural analyses of these phenomena require nonlinear numerical analysis methods. In order for the results of these numerical analyses to be reliable, the applicability of used methods should be validated by means of experimental results and analytical methods.

The main objective of this project is to develop and take in use numerical methods and models for predicting response of reinforced concrete structures to severe dynamic loads such as impacts of projectiles. The structures may additionally be prestressed or covered with a steel liner. The aircrafts contain fuel which leads to a high risk of fire. The aim of the liquid research is a validated capability to simulate spreading of burning liquid and smoke as a result of an aircraft impact.

Different methods are applicable to different types of cases. A soft, deformable missile typically damages the target by bending mode. A hard, almost undeformable missile penetrates into a softer target and may eventually perforate it. An explosion creates high compressive stresses which can crush the target. Scabbing, i.e. loosening/delamination and falling (flying) of concrete fragments on the rear face of protective wall, occurs when the propagating compressive stress wave is reflected as tensile wave from the rear side of wall and the dynamic tensile strength is exceeded. The whole structure may collapse due to a very forceful explosion. Also induced vibrations in entire building due to impact need to be assessed in order to ensure the

functionality of critical equipment and components. Damping is an essential phenomenon in these studies.

Post calculations for selected IMPACT tests

Finite element (FE) analyses of selected tests conducted within IMPACT project have been carried out.

Shear punching tests

Shear punching test series of three tests was carried out by using as a target a two way simply supported concrete plate with a span of 2 m and a thickness of 25 cm. The amount of the shear reinforcement was varied. The mass of the used stainless steel missile is 50 kg. Two types of missiles were used and impact velocities were about 143 m/s and 166 m/s.

Bending and shear punching capacity of an impact loaded reinforced concrete wall was studied by applying different kinds of numerical methods and models. Also, the effect of the temporal shape of the loading function was studied. Numerical solutions were compared with the experimental results obtained in impact tests conducted at VTT. The capabilities of different types of calculation methods in assessing local shear deformation and possible shear punching cone formation were studied.

Hard missile impact tests

Local response to hard projectile impact is usually analysed in terms of spalling, penetration, scabbing and perforation. Many so called punching tests have been conducted in IMPACT project during the last few years. Concrete slabs with a thickness of 0.25 m are tested using rigid hard steel missiles. The name "punching test" means that bending of the slab is insignificant and the primary damage mode is punching which in this case includes both the forming of shear cone and penetration of the missile into the slab. The penetration starts with a tunneling phase. If the remaining capacity of the wall is low enough, the missile continues its flight and perforates the slab with a certain residual velocity. A simplified penetration model of Forrestal et al. was used in calculating the tests and making some sensitivity studies by varying e.g. reinforcement, concrete strength, assumed shear cone angle and impact velocity. This model is capable of predicting the penetration depth or, in case of perforation, the residual velocity of the missile fairly accurately in a simple case like this. Calculation formulas are derived in [Saarenheimo & al, 2013].

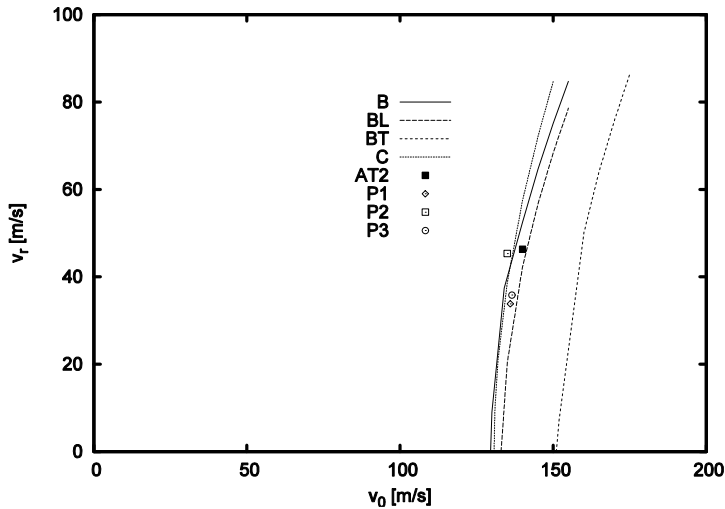


Figure 1. Projectile residual velocity as a function of impact velocity.

Projectile residual velocity as a function of impact velocity is presented in Figure 1. B is basic case, L with liner, T with T-bars, curve C is computed using the assumption that spalling depth is equal to projectile head length. AT (with T-bars), P1, P2 and P3 are test results.

The calculated residual velocity was 38.6 m/s for an impact velocity of 135 m/s in case B, which is close to the velocity observed in corresponding test P. In the second case, BL, a steel liner with a thickness of 1.5 mm is assumed on the rear side. The ultimate strength of liner is about 250 MPa. The liner would correspond to a reinforcement ratio of $\rho_{pl} = 0.6$. In case BT, the T-headed bars are included. They can be seen to have a great influence on the residual velocity. However, in tests this is not necessarily so. In Orbovic et al. (2009) it was concluded that the presence of T-bars may diminish the assumed shear cone angle in case of punching. E.g., assuming a cone angle of 50° will give a residual velocity of 21 m/s with the basic model and T-bars included. However, T-bars can reduce considerably the penetration depth when perforation does not occur.

Curve C in Figure 1 is calculated by assuming that the spalling phase ends when the missile head is penetrated into the slab. Assuming a slightly smaller cone angle of 57.6° will give about the same residual velocities as the basic model. In this case the penetration phase lasts for 0.47 ms and the maximum contact force is thereby higher, about 12.4 MN, while in the basic case the penetration lasts for 0.98 ms with the penetration of 0.097 m and the maximum contact force of 7.7 MN. The maximum plate deflection is about 12 mm, i.e. higher than that in test and also the frequency is higher. Changing the concrete compressive strength from 40 MPa to 70 MPa will change the residual velocity from 81 m/s to 8.1 m/s. This is probably more than would be obtained from tests.

The punching test is simulated with a detailed one quarter FE model. The main aim is to take in use the SPH (Smoothed Particle Hydrodynamics) feature and test its adequacy and reliability. The concrete is initially modelled with solid elements which are converted to SPH particles during the analysis by assumed criteria e.g. 15% max. principal strain. Concrete Damaged Plasticity material model can be used with SPH particles. Another way to simulate penetration is element erosion. Elements can be removed by means of a user subroutine. An erosion criteria (e.g. 20% plastic strain) needs to be defined.

When erosion and/or SPH are not defined, the simulations clearly overestimate spalling in the front surface. When both are defined, the spalling is fairly accurately reproduced in the simulations. The scabbing is simulated fairly realistically in each case, when compared to the test results. SPH method was found to work, but it needs a lot of further study and calibration of parameters. These preliminary results are somewhat promising and indicate that SPH may have some benefits in this kind of impact case compared to traditional FEM, but the computations are much more time-consuming and numerically unstable.

Figure 2 shows the actual front and back surfaces after the test (P1) considered here and a plot from a corresponding simulation. Figure 3 shows the deformed shape and equivalent plastic strain distribution at 0.8 ms, 1.8 ms and 9.3 ms after the start of the impact with velocity of 136 m/s in the simulation case, where both element erosion and SPH are used. Figure 4 shows the deformed shape and maximum principal strains at front and back surfaces well after the impact in the same case.

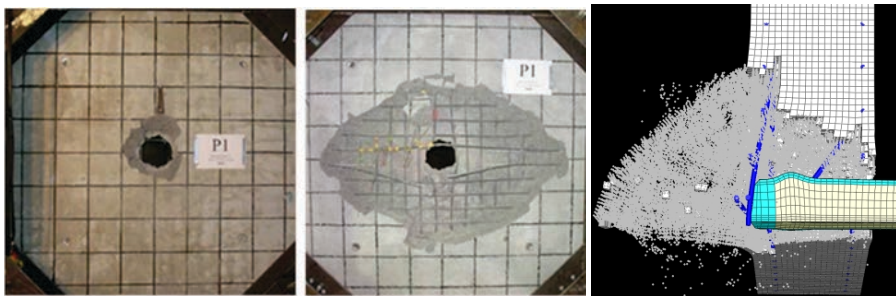


Figure 2. Front and back surfaces after impact test with velocity of 136 m/s and the deformed shape according to a FE analysis.

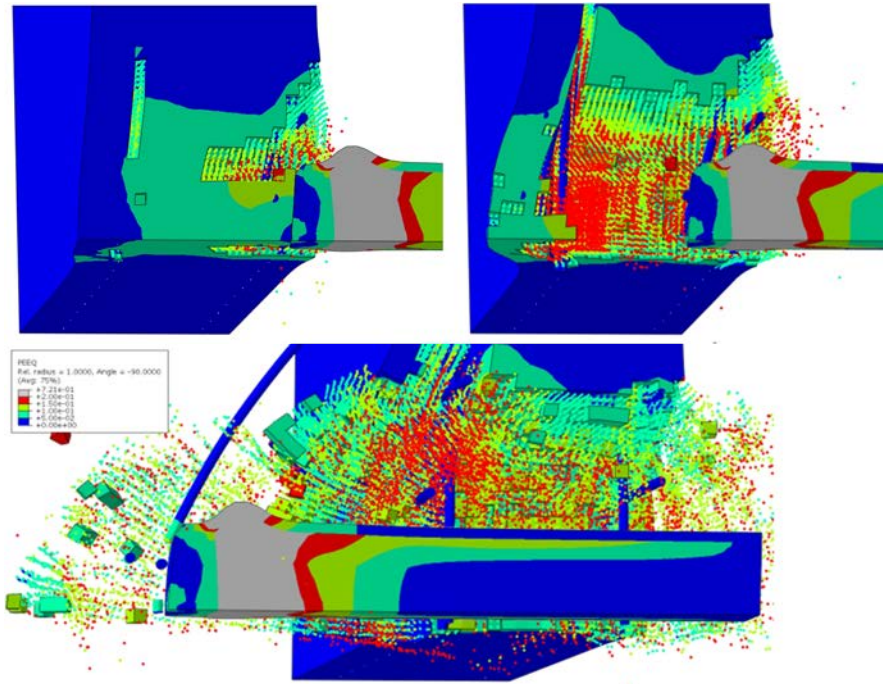


Figure 3. Deformed shape and equivalent plastic strain distribution at 0.8 ms, 1.8 ms and 9.3 ms after the start of the impact with velocity of 136 m/s.

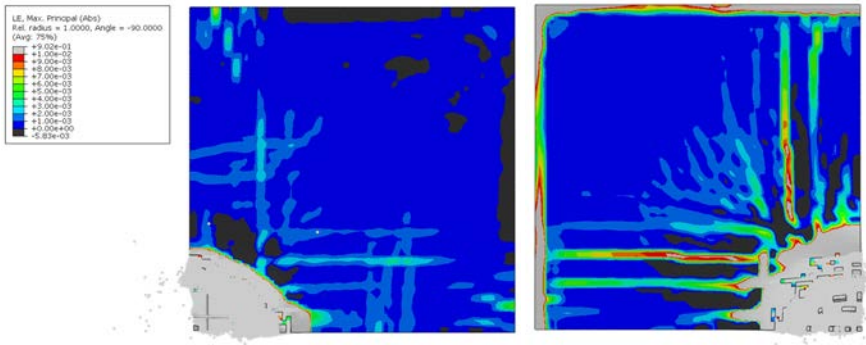


Figure 4. Deformed shape and maximum principal strains in front and back surfaces after an impact with velocity of 136 m/s.

Water filled missiles

There has been lately an increased interest in the numerical simulation of water-filled missiles or projectiles. The modern NPPs have to be designed to withstand an impact of a large passenger aircraft. Full fuel tanks comprise a substantial proportion of the total mass of the craft and thus contribute to the impact load.

Several tests have been carried out within IMPACT project in 2012, using missiles that are empty or filled with different amounts of water. Preliminary post-analyses on the dispersal and the hydrodynamic effect of the water have been carried out. The water was modelled in three different ways; as solid elements, as SPH particles or as material flow in Eulerian mesh. The steel pipe was modelled with shell elements and varying failure criteria. The main simulation results, the impact force, impulse, initial velocity of the water front and deformed shape of the missile, were all compared with the corresponding experimental values.

Figure 5 shows the simulated deformed shape and von Mises stress distribution in case where water is modelled with SPH (blue dots). The corresponding photograph from the test is on the right. Figure 6 shows a comparison of force-time functions obtained with different methods.

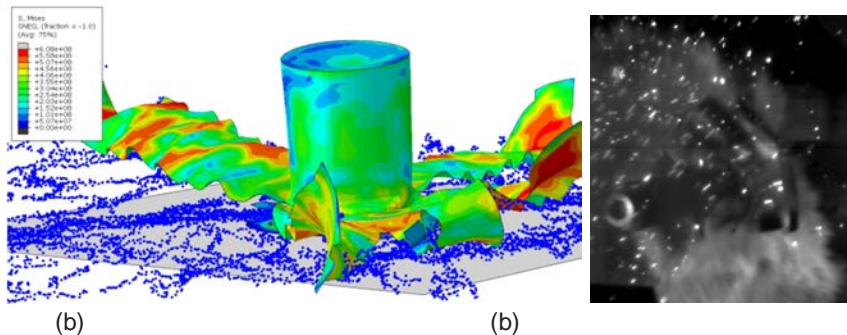


Figure 5. (a) Numerical result approx. 15 ms after impact. (b) Test approx. 8 ms after impact.

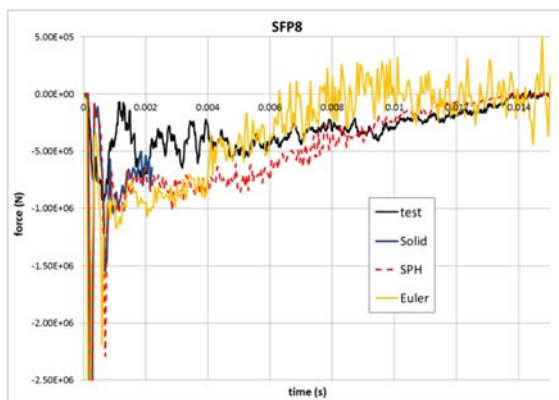


Figure 6. Comparison of force-time functions.

Liquid spreading

In the past programs, FDS has been used to calculate the impacts of fireballs generated by airplane impacts. CFD simulations require information on initial velocities of the droplets after impact as well as information on droplet size. The droplet data captured during impact experiments has been used to determine the initial data for simulations. The analysed data was also used to construct validation tests for simulations of liquid spreading.

The radial position of the water front and the spread direction were measured from the still figures taken from the high speed videos. The water front position was traced to 9 different angular directions from the impact target, measuring an exact location of the front using image analysis (Figure 7). The uncertainty of the water front position measurement is estimated to be ± 0.1 m or less. Since the frame rate of the videos was known, the momentary velocity of spray front could be estimated from the sequential still figures. The uncertainty of the velocity measurement is estimated to be ± 25 m/s or less. In the measurements of the impact tests so far, the nearest position where the liquid velocity could be reliably measured was about 0.2 m from the surface of impacted projectile.

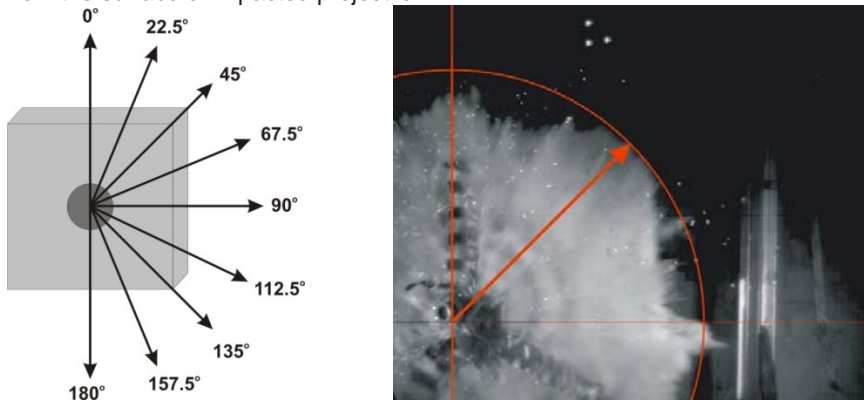


Figure 7. Angular directions where the water front position was measured (left) and an example from the test.

Figure 8b) shows measured velocities of the liquid front as a function of the distance from the projectile surface in three tests with different impact velocities. The velocities are presented as velocity ratios, determined by dividing the median velocity of liquid front (over all measuring directions) by the projectile impact velocity. The distance is normalized by the projectile diameter.

$$R^* = R_{front} / D_{missile} ; \quad V^* = V_{front} / V_{missile} \quad (1)$$

The results indicate that the front velocity decreases as the time and distance from the impact target increases. The deceleration of the front is strongest within the first 0.5 m distance from the projectile due to high drag forces and simultaneous liquid

atomization. The front decelerates to a level of projectile impact velocity (velocity ratio 1) within 1–1.5 m distance from the projectile. Some fluctuations in the front velocities are explained by the fact that the liquid spread occurs as sequential waves. If the leading front decelerates for some reason, following wave with higher velocity may pass it that is seen as a velocity jump in Figure 8b). In Figure 8a), each marker represents an average velocity from an individual test at a single distance. By linear extrapolation, the initial velocity of the liquid front becomes about 1.7 times the impact velocity.

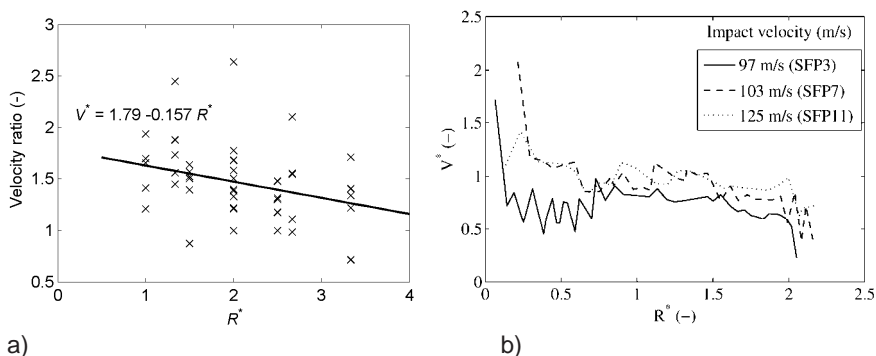


Figure 8. Normalized velocity as a function of normalized distance from the impact location.

The droplet size and speed data were used to construct validation simulations. In the simulations, droplets are released from a circular band with diameter equal to the missile diameter. The initial velocity is set to 1.7 times the impact velocity. Droplet size distribution is set to be that measured in the spray front. From the simulation results, distances of the droplets from the impact location were first determined. The spray front position was then defined as the maximum of distances for each time step. The spray front velocity was calculated from the distance data by finite differences.

Figure 9 shows comparisons of predicted and measured spray front velocities in three selected tests. The simulation results are in reasonable agreement with the median of the experimental data. In the simulations there is no significant difference in liquid front velocity in different directions.

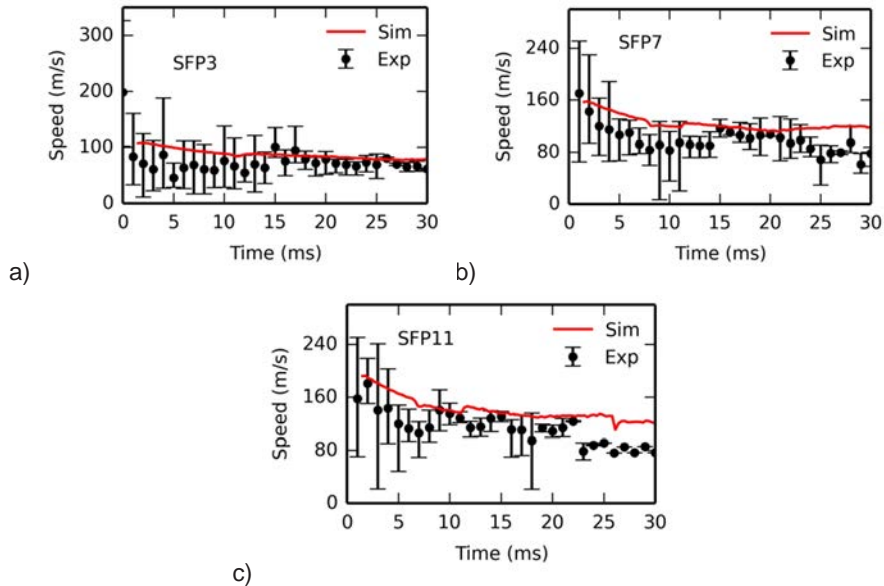


Figure 9. Predicted and experimentally determined liquid front velocity for three selected experiments. The errorbars in experimental values correspond to minimum and maximum velocities in different directions, while the black dot marks the median velocity.

Applications

Numerical methods and models for predicting response of reinforced concrete structures to severe dynamic loads such as impacts of projectiles

Conclusions

- No perfect method seems to exist for these types of analyses and thus different kinds of approaches are needed.
- Nonlinear analyses of reinforced concrete structures are sensitive for material parameters.
- Simple four-node shell element models without considering transverse shear deformation are capable of calculating the deflection behaviour of a reinforced concrete wall loaded by a deformable missile. In the case the wall collapses in bending mode, the maximum deflection can be predicted well.
- Bending and punching can be modelled by plate/shell elements with transverse shear deformation included. In detailed studies solid elements are needed.

- Simplified models are valuable when judging the reliability of both the test results and the more extensive numerical simulations.
- In cases of hard missile impact with simple geometry and boundary conditions, like the ones studied here, one-dimensional penetration model of Forrestal et al. [Forrestal et al, 1994] is capable of predicting the penetration depth or, in case of perforation, the residual velocity of the missile fairly fairly accurately.

Acknowledgement

The authors would like to acknowledge the project(s) funding by VYR, VTT and external partners. The authors would also like to acknowlge the work by the project teams, the SAFIR2014 reference group 7 and the compined IMPACT 2014 and SMASH ad hoc group

References

Abaqus/Explicit. Users Manual. Version 6.14.1. SIMULIA 2014

M.J. Forrestal, B.S. Altman, J.D. Cargile and S.J. Hanchak. "An empirical equation for penetration depth of ogive-nose projectiles into concrete targets", *International Journal of Impact Engineering*, **15**, pp. 395–405, (1994).

Arja Saarenheimo, Kim Calonius and Markku Tuomala. "Post analyses on impact loaded reinforced concrete slabs: penetration and combined bending and punching" Research Report VTT-R-08992-13. 91p.

37.3 Testing and modelling of vibration propagation and damping in a 3D-structure impacted multiple times with a soft projectile (IMPACT2014 and SMASH)

Ari Vepsä¹, Arja Saarenheimo¹, Seppo Aatola¹, Kim Calonius¹, Ilkka Hakola¹,
Matti Halonen¹ and Markku Tuomala²

¹VTT Technical Research Centre of Finland
P.O. Box 1000, FI-02044 Espoo

²TUT Technical University of Tampere
PO Box 527, FI-33101 Tampere

Abstract

Vibrations in an entire building induced by a highly dynamic impact need to be assessed in order to ensure the functionality of critical equipment and components of a nuclear power plant. Damping is an essential phenomenon in these studies. In standards, damping ratios are provided only for linear analyses and thus proper damping factor to be applied in nonlinear vibration studies is an open question. Non-linear material behaviour is absorbing energy and thus damping the vibrations. In a series of three vibration propagation tests, a structure having a front wall, a floor and a rear wall, each being 150 mm thick, was impacted with soft projectiles having mass of 50 kg and the impact velocity between 111.2 - 116.8 m/s. This paper discusses these tests and the preliminary numerical results obtained by using Abaqus/Explicit and an in-house finite element (FE) code. The main aim of the tests was to study how the vibration propagates from the hit point, how it gets damped and how these properties change when the structure is already damaged. The main aim of modelling was to carry out sensitivity analyses on the test set-up used in this test V0 in order to find out the essential phenomena to be considered in the numerical studies.

Introduction

The design of safety related structures of e.g. in nuclear power plants requires reliable analysis methods, which can be validated against the results of carefully conducted tests. The primary task of protecting walls is to keep possible flying projectiles and burning fuel outside the building housing vulnerable equipment or protecting them sufficiently against explosions generated by impacts or by explosives themselves. Damping is an important factor influencing the response of structures during impact and especially when studying the propagation of vibrations in concrete structures. Sensitive equipment vital for plant safety may be lost due to heavy vibrations.

Vibration propagation and damping test series V0

Test set-up

Vibration propagation and damping tests matrix V, which is a part of an experimental project conducted at VTT concerning impact loaded concrete structures, was initiated with a test series called V0. The tested structure and its supporting are shown in the drawings in Figure 1.

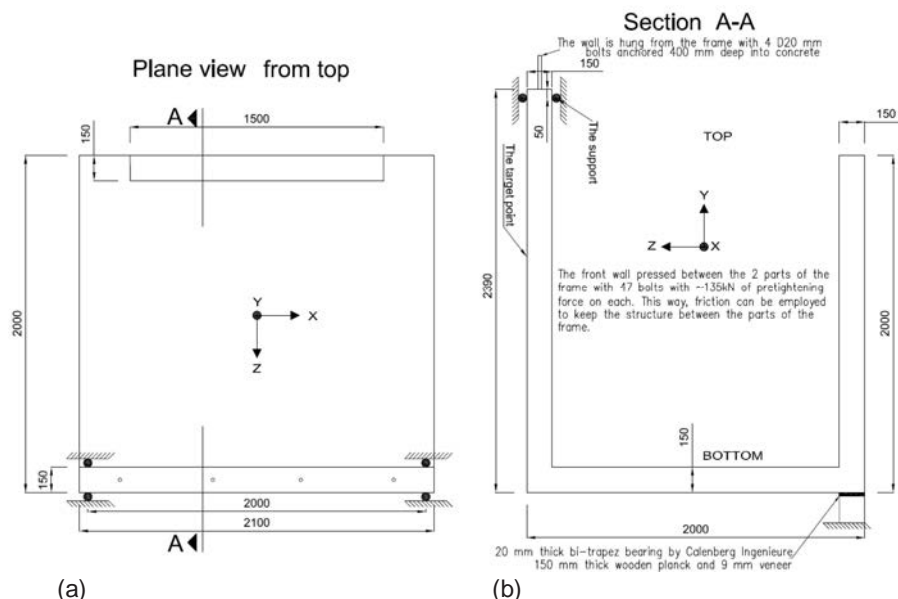


Figure 1. (a) The tested structure when viewed from top. (b) Section A-A of the tested structure.

The structure had a front wall, a floor and a rear wall, each 150 mm thick. This type of structure resembles very coarsely a NPP reactor building with an outer wall and a base slab and with the rear wall in the place of internal structures. The front wall was pressed between two halves of a steel test frame. The frame rested freely on wooden beams and was connected to solid bedrock with horizontal support pipes. At the back end of the floor slab, the structure rested freely on a 20 mm thick and 150 mm wide elastic bi-Trapez® bearing. In addition, the front wall was suspended from the top of the frame with steel rods anchored to the wall.

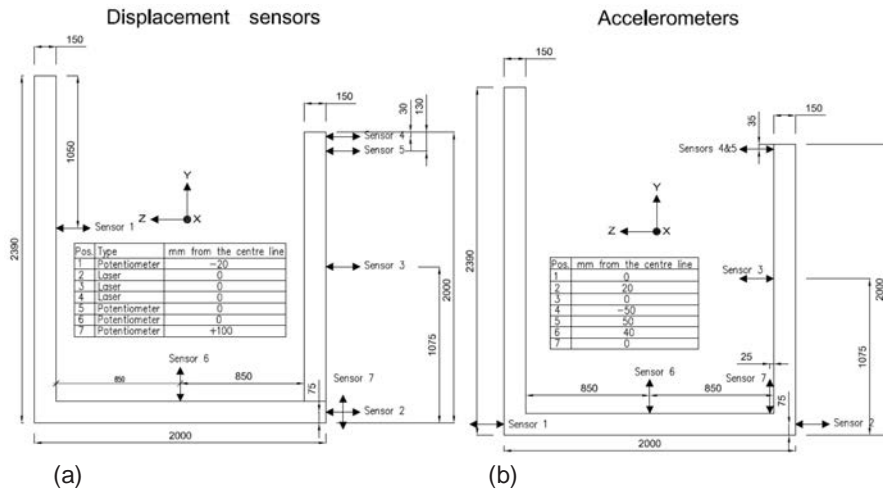


Figure 2. The type, location and measurement direction of the displacement sensors (a) and accelerometers (b) used in the tests.

Three similar impact tests were carried out with the structure. The projectile used in the tests was a soft one and made out of stainless steel pipe with an inner diameter of 250 mm, a wall thickness of 2 mm and weight of 50 kg. In this context, a soft projectile is considered to be much more deformable than the structure that it impacts against, resembling the fuselage of an aircraft. The realized impact velocities in these tests, V_{0A}, B and C, were 111.2, 113.6 and 116.8 m/s, respectively. The main purposes of the tests were to

- study how the vibration propagates from the hit point through the floor to the back wall and how it gets damped in the process,
- study how this vibration behaviour changes when the impact is repeated against already damaged structure and
- yield reliable measurement data for validation of the numerical model made of the structure.

The quantities which were measured during the tests were: strains at 10 selected locations on the reinforcement, displacements at 6 degrees of freedom (DOF), accelerations at 6 (DOF) and horizontal support forces acting on the support pipes. The locations and the measurement directions of the sensors are presented in Figure 2 for the displacement sensors (a) and accelerometers (b) and in Figure 3 (a) for the strain gauges on the reinforcement. Figure 3 (b) shows a photograph of the test set-up.

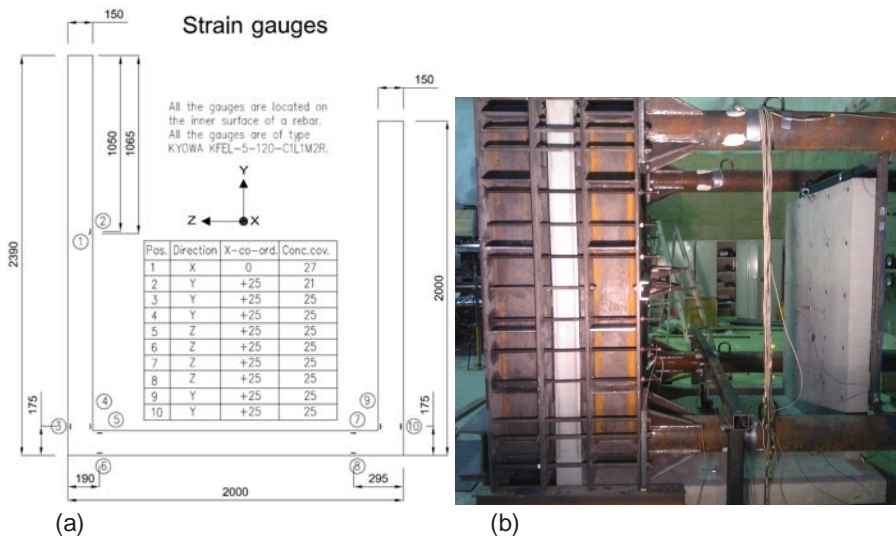


Figure 3. (a) The locations of the strain gauges on the reinforcement. (b) The test set-up.

In addition to the impact tests, modal tests and analyses were carried out for the structure at three different occasions: when intact before the first test, after the first test and finally after the last (third) test.

Test results

Nine natural vibration modes could be found in the modal tests which were the same for each measurement set. Despite being the same modes, their frequencies and damping changed from one set to another. These frequencies as well as the damping as percentage of the critical value are collected in Table 1 in case of each measurement set.

The natural frequencies decreased after each test with mode 2 making an exception. Mode 2 had a rise of 12 % in the frequency when the first and the last measurement sets are compared. Otherwise the frequencies decreased 5 – 28 % from the first measurement set to the last one with the average value being 10 % and the standard deviation being 11%. In a similar manner, in general, the damping values increased with modes 1 and 2 making exceptions as their damping decreased from measurement set 2 to 3. It is otherwise more difficult to draw a general rule for the change in damping than for the change in natural frequency as the increase of damping is really high (200-400 %) for some modes and only modest (5-70 %) for some others. On the average, the damping of the modes increased 139 % from measurement set 1 to 3 with the standard deviation being 133 %.

Table 1. The natural frequencies of vibration of the structure as well as the damping as percentage of the critical value measured before the tests, after the first test and after the third test.

Before the 1st test		After the 1st test		After the 3rd test	
Frequency [Hz]	Damping [%]	Frequency [Hz]	Damping [%]	Frequency [Hz]	Damping [%]
16.0	0.7	15.1	3.5	13.1	0.9
32.6	1.7	35.8	1.9	36.5	1.8
45.4	0.6	43.6	1.1	41.3	1.7
56.2	1.4	54.4	1.9	52.8	2.0
70.8	0.8	68.4	1.2	65.6	1.5
134.2	1.1	116.2	1.3	96.4	3.4
151.5	0.7	136.7	2.2	121.0	3.7
225.9	0.7	215.1	1.4	199.2	2.1
267.6	0.6	265.5	0.6	254.6	1.0

As an example of the accelerations, the ones measured at the top of the rear wall in the horizontal direction in tests A-C are shown in Figure 4 (a) and (b). Graph (b) shows only the duration of the actual impact. High frequency high amplitude accelerations were measured at each measurement location and in each test during this actual impact. After this, these high frequency components died out quickly.

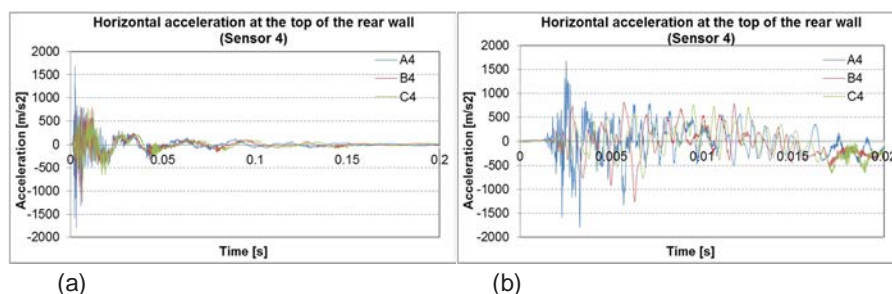


Figure 4. (a) The horizontal accelerations measured at the top of the rear wall. (b) The same data including only the duration of the actual impact.

The highest peak accelerations were measured at the bottom of the front wall with sensor 1, nearest to the hit point. These peaks were roughly three times as high as the highest peaks measured in the horizontal direction at the midpoint of the rear wall (sensor 3). In general, the maximum range of acceleration measured in different

tests but at the same locations decreased by 49 % on average from test A to test B and then by 19 % on average from test B to test C.

Figure 5 shows the frequency composition of the accelerations measured at the top of the rear wall in the horizontal direction in tests A-C in a form of an auto power spectrum (APS) in the range 0 – 150 Hz. For most of the locations, one or two clear frequency peaks could be identified from the data. These peaks were slightly lower than the natural frequencies of vibration identified in the modal tests and roughly at the same frequencies than those identified from the strain and displacement measurement data and they decreased by 15 % on average from test A to test B and by 12 % from test B to test C.

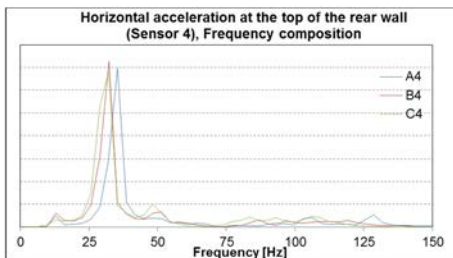


Figure 5. The frequency composition of the accelerations measured at the top of the rear wall.

As an example of the displacements, the horizontal ones measured at the top of the rear wall in tests A-C are shown in Figure 6 (a). Figure 6 (b) shows the frequency composition of these displacements in a form of an APS.

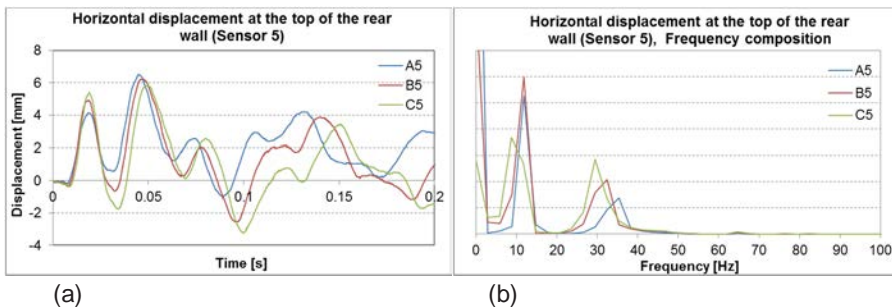


Figure 6. The time-history (a) and its frequency composition (b) of the horizontal displacements measured at the top of the rear wall.

The displacements were successfully measured at the floor as well as at the rear wall. The range of the measured displacements (i.e. maximum peak - to - peak values) in the horizontal direction varied from 1.97 mm, measured in the middle of the rear wall in test A, to 9.08 mm, measured at the top of the rear wall in test C. In the vertical direction, the range of values varied from 2.95 mm, measured at the bottom of the rear wall in test A, to 5.97 mm, measured at the same location in test C. The

range of values increased by 34 % on average from test A to test B and by 17 % from test B to test C. Especially the horizontal displacements took place clearly on two distinct frequencies, at 11-13 Hz and at 31-36 Hz which were roughly the same than those of the strain variation and acceleration. These frequencies decreased by 8-9 % from test A to test B and by 3-4 % from test B to test C

As an example of the strains on the reinforcement, the ones measured at the hit location in the lateral direction as well as the vertical ones measured in the front wall near the junction between the wall and the floor are shown in Figure 7 (a) and (b), respectively.

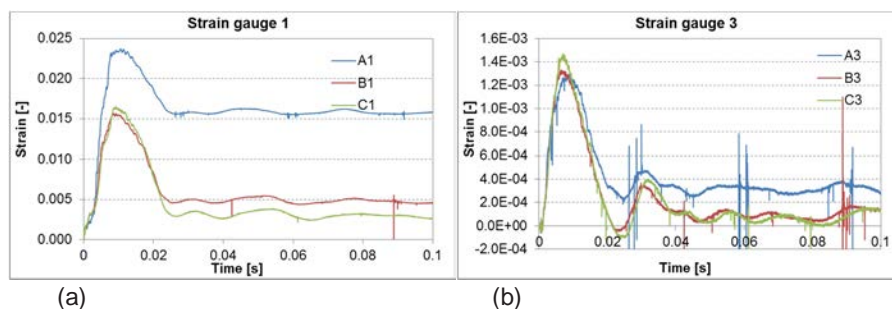


Figure 7. The strains measured on the lateral reinforcement at the hit location (a) and on the vertical reinforcement of the front wall near the junction to the floor (b).

Only the strains measured at the hit area exceeded the static yield limit of the re-bars. The strains at the junction between the front wall and the floor were roughly one decade lower and the strains at the junction between the floor and the rear wall two decades lower than those at the hit area. No clear tendency could be identified for the change of behaviour of the stresses between the consecutive tests. However, the additional permanent strains decreased from a test to the next. The elastic strain variation happened mainly at two frequencies which were slightly lower than the natural frequencies of vibration identified in the modal tests. These frequencies decreased by 6-9 % from a test to the next.

Numerical studies on vibration test V0A

Finite element analyses with Abaqus/Explicit

The main aim of this first study was to carry out sensitivity analyses on the test set-up used in Test V0 in order to find out the essential phenomena to be considered in the numerical studies. Two types of codes with also some differences in the applied methodology are used: Abaqus and an in-house finite element (FE) code. In this case, it is important to assess the effect of the test frame. This rather heavy steel frame affects the vibration behaviour of the whole test set-up. Also, the effect of the way to apply the loading is studied. There are two different types of approaches: loading function calculated with the Riera method and a so-called coupled approach

where also the missile is modelled with finite elements. The effect of structural damping is also tentatively studied. The study with Abaqus is considered here first [Saarenheimo et al., 2015].

Dynamic nonlinear simulations as well as some eigenmode analyses were conducted with Abaqus/Explicit version 6.14-1. The FE mesh consists mainly of linear four-noded shell elements. Beam or truss elements are used for some bolts and small steel beams. Element size for the missile, concrete structure and frame is on average 5 mm, 50 mm and 70 mm, respectively. Some nonlinear spring elements are used to model the supports such as the elastomer bearing under the back slab. Figure 8 shows the complete FE model.

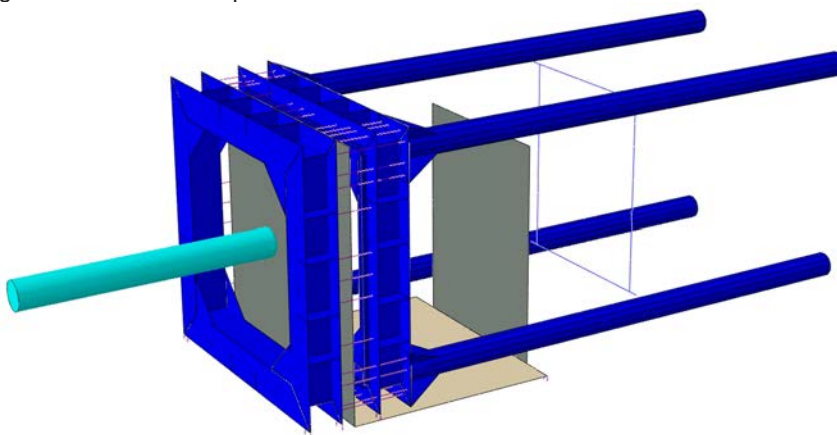


Figure 8. FE model.

Table 2. Elastic material properties.

material	Young's modulus	Poisson's coeff.	density
missile steel	210 GPa	0.3	7850 kg/m ³
frame steel	210 GPa	0.3	7850 kg/m ³
rebar steel	210 GPa	0.3	7850 kg/m ³
wall concrete	27.078 GPa	0.2	2242 kg/m ³
floor concrete	25.447 GPa	0.2	2236 kg/m ³

The mechanical properties of different materials used in the models are described below. All these properties are based on material testing. The elastic properties are listed in Table 2. The steel applied for the frame model is elastic, while the other materials also have plastic properties. Missile and rebar steel are elastic-plastic with von Mises yield surface. Concrete has Concrete Damaged Plasticity material model which includes tension stiffening and a damage law both in compression and tension. Rebar steel has rate dependency defined with Cowper-Symonds model with coefficient values of 40 and 5.

The impact load is given either by assigning an (geometrically) even transient pressure load to the impact location for 52 elements with an area of 0.13 m^2 or by simulating the missile and its impact explicitly. The impact velocity of the simulated missile is 110 m/s which is slightly lower than in the tests. Figure 9 shows the impact force as function of time calculated with Riera method [Riera, 1968] and FEM (Missile contact). It has been previously studied that both these curves correspond well to the measured force in separate force plate tests. Figure 10 shows the deformed missile after test V0A and in the simulation of an impact to a rigid plate of which force-time curve is shown in Figure 9.

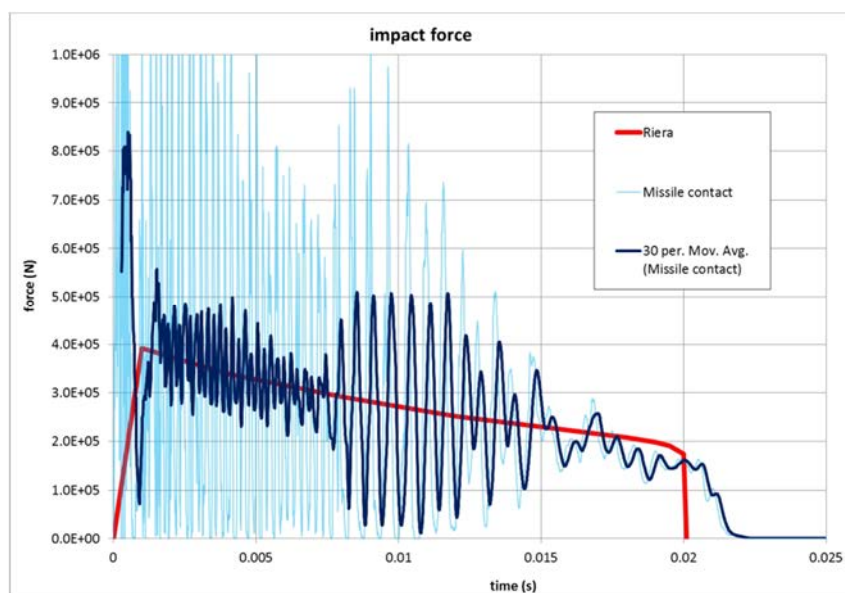


Figure 9. Impact force as function of time calculated with Riera method (Riera) and FEM (Missile contact).

During the test V0A (the first impact), permanent deformations occur mainly only at the impact hit point area. The rest of structure behaves mainly elastic. This is indicated in Figure 11 which shows simulated equivalent plastic strains in rebars after the impact. Outside the impact location, only minor damage in concrete is predicted by the FE calculation.

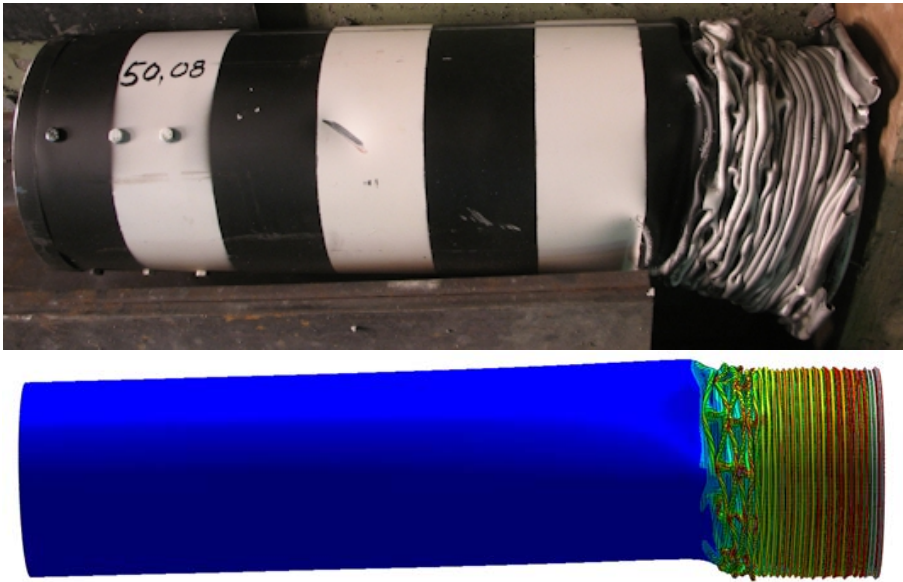


Figure 10. Deformed missile after test V0A and in the simulation of an impact to a rigid plate (force-time curve is shown in the previous figure).

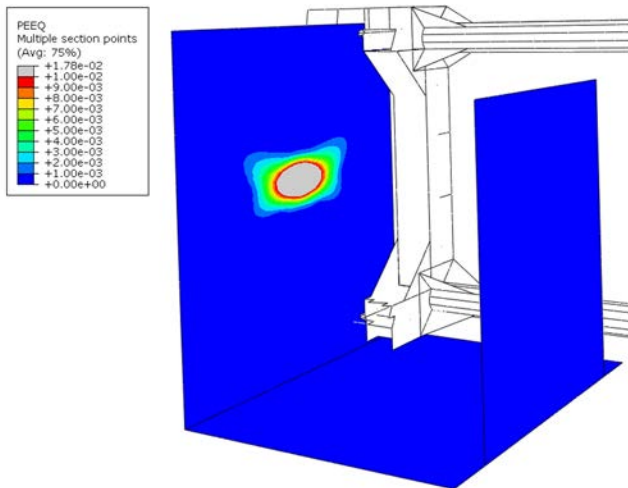


Figure 11. Equivalent plastic strain distribution in back surface rebars at 0.5 s with scale from 0 to 1 %.

Figure 12a shows the horizontal displacement of front slab centre in Abaqus cases with Riera load (R-F) or simulated missile (M-F). Figure 12b shows the corresponding results from the back slab top. Modelling the missile explicitly increases

the deflection of the impacted wall. However, this does not affect much the movement of the whole structure. Figure 13a shows the acceleration of back slab top in cases for the first 0.03 s. The acceleration values are much higher when the missile is modelled. Figure 13b shows the floor response spectra of back slab top up to 250 Hz. The differences begin to show after 100 Hz. Beyond that frequency also the measured values differ from the calculated ones. This is partly due to the fact, that in these calculation cases no structural damping was used.

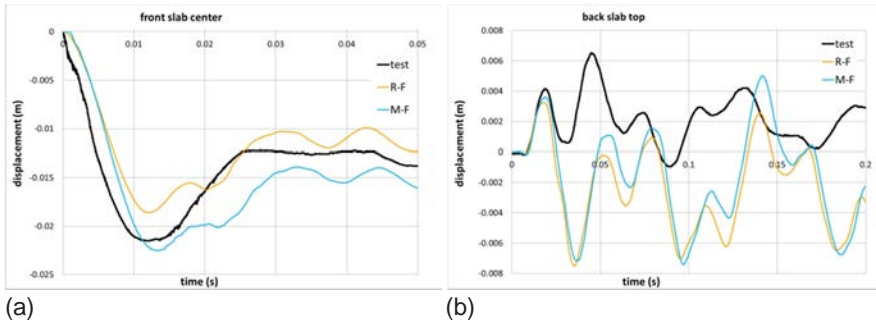


Figure 12. (a) Displacement of front slab centre and (b) back slab top in the test and in cases R-F and M-F.

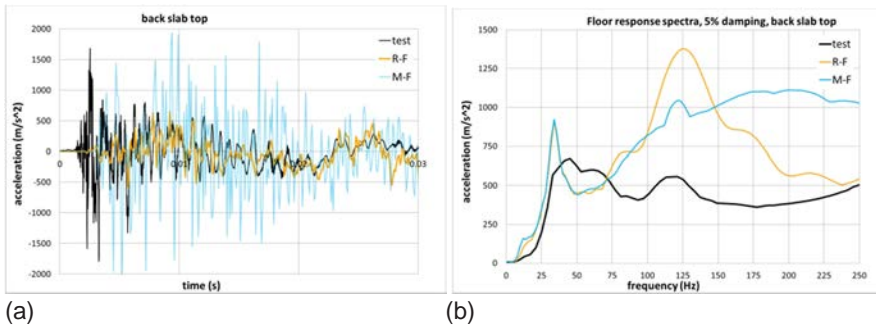


Figure 13. (a) Acceleration of back slab top and (b) floor response spectra of back slab top in the test and in cases R-F and M-F.

Finite element analyses with Reissner-Mindlin theory elements

A 24-degree-of-freedom (24 DOF) flat shell element is used in the computations of the vibration test. The element is constructed by combining a plate element and a membrane element and using a coordinate transformation from local to global coordinate system. The degrees of freedom of the shell element in local frame are: u , v , w , θ_x , θ_y and θ_z . Rotation corresponding to local θ_z is restrained except at shell junctions where two elements meet at an angle different from π .

The plate part of the element is constructed according to the Reissner-Mindlin theory. Linear polynomial interpolation is used for the deflection and the rotations. In computing the transverse shear strains covariant transverse shear strain assumption and interpolation is adopted [Bathe, 1985]. The von Karman definition of nonlinear Lagrangian strain is used in computing the membrane strains. Material nonlinearities are formulated in terms of stress resultants and curvatures in a similar fashion as e.g. in [Ibrahimbegovic, 1993] and [Koechlin, 2007]. The yield condition is defined in terms of bending moments and twist moment in a similar fashion as in [Ibrahimbegovic, 1993]. Separate yield condition is used for transverse shear forces. In reverse motion cracked state stiffness is assumed.

The moment-curvature relationship calculated with 6 mm bars is shown in Figure 14a. Curve 'simple' is obtained by utilizing the tensile strength of concrete and the yield stress of reinforcement and assuming that the rebars yield before concrete reaches its compression strength. The other curve is obtained by dividing the cross-section into 50 layers and using the equilibrium equations and integrating through the cross-section. Tension stiffening is taken into account so that the tensile stress goes to zero when the tensile strain is ten times the cracking strain. For simplicity, the curve 'simple' is used in computations by joining the point on the curvature line corresponding to tensile cracking to the point corresponding to steel yield by a straight line. Moment curvature relationship with 10 mm rebars is shown in Figure 14b. In the finite element model, rebars with a diameter of 10 mm are used in the front wall up to a height of 0.625m, in the entire floor slab and in the rear wall up to a height of 1.125 m.

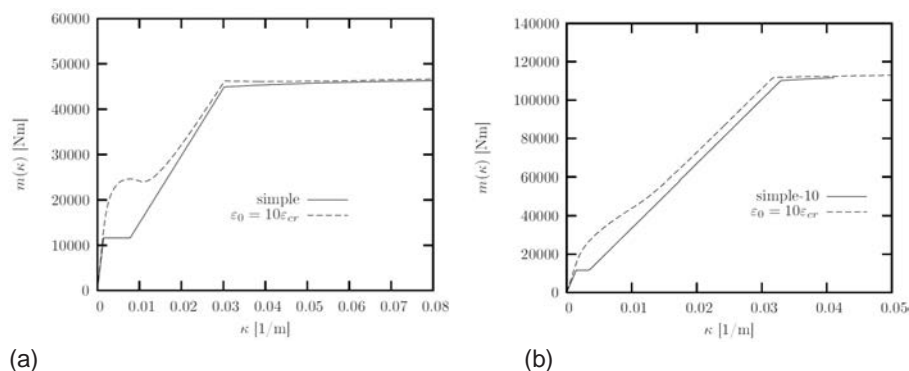


Figure 14. Moment curvature relationship for test plate V0A (a) with 6 mm bars and (b) with 10 mm bars.

Finite element mesh of front wall (impact wall) of specimen V0 is shown in Figure 15. The loaded area is also shown. Two finite element meshes are used with mesh 2 shown in Figure 15. In mesh 3 the element side length is divided by 2 from that used in mesh 2. Three Rayleigh damping values, named d1, d2 and d3, are considered. In case d1 the Rayleigh damping ratio is 0.05 at frequencies 45 and 5000 Hz,

while in case d2 the Rayleigh damping ratio is 0.03 at frequencies 30 and 200 Hz. In case d3 the Rayleigh damping ratio is 0.1 at frequencies 45 and 5000 Hz.

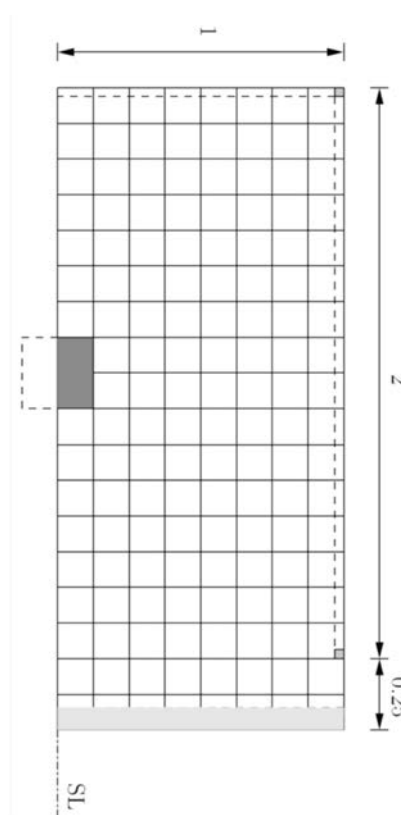


Figure 15. Finite element mesh of impact wall of specimen V0.

The load function is determined by the Riera method. The crushing force part of impact force is evaluated by an average visco-plastic folding model. The material parameter values for stainless steel are $p=5.13$ and $D=1522$ 1/s in the Cowper-Symonds one dimensional model. An average yield stress of 460 MPa is used. This loading curve is denoted with 'fvp3' is in Figure 16.

Load function obtained by taking into account the actual forming of folds is depicted also in Figure 16 and denoted with 'fold'. The final shape of folding model with a detail is shown in Figure 17.

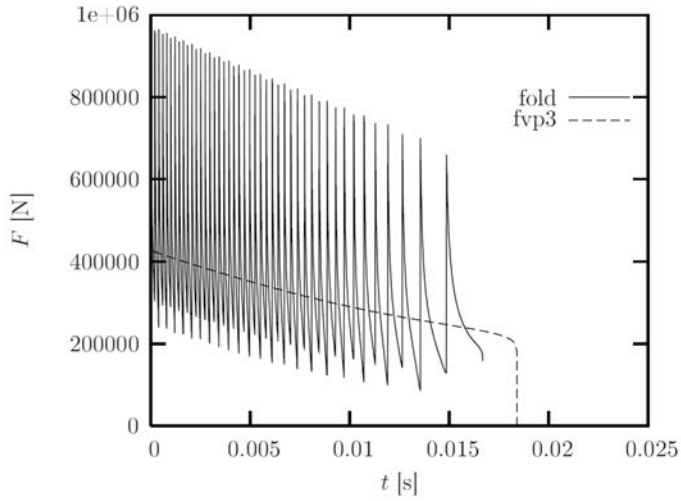


Figure 16. Folding viscoplastic model.

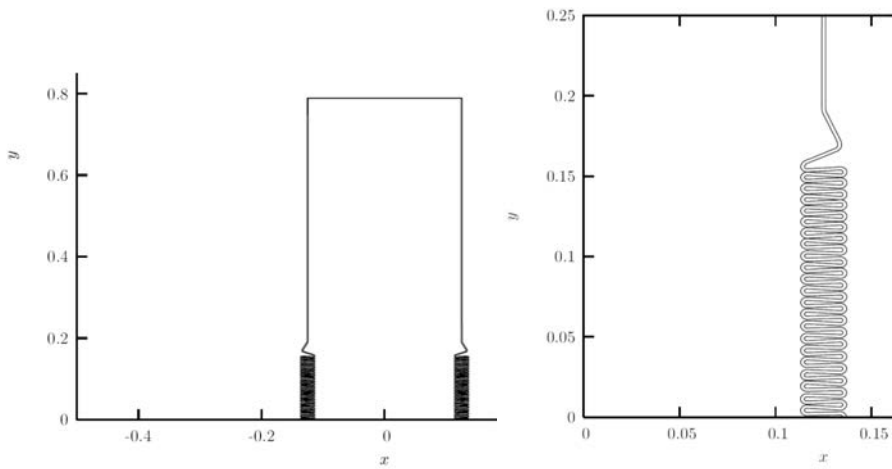


Figure 17. Final shape of folding viscoplastic model.

Floor response spectrum of acceleration history at top of rear wall at point 6 with damping ratio of 0.05 and structural damping d_1 , d_2 and d_3 are shown in Figure 18. Curve 2f-a6-d1 is obtained with the calculation model including the test frame. In Figure 19 the curve 2-a6-fold is obtained by using the actual folding model. The fluctuation of the force-time function clearly affects the vibration behaviour of the back wall.

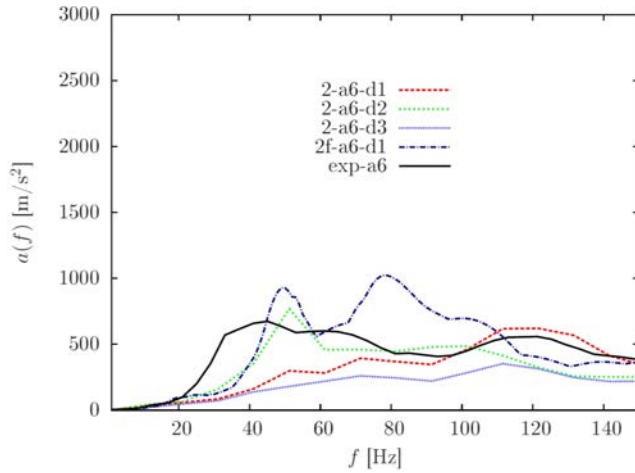


Figure 18. Floor response spectrum of acceleration history at top of rear wall at point 6 with damping ratio of 0.05 and structural damping d1, d2 and d3.

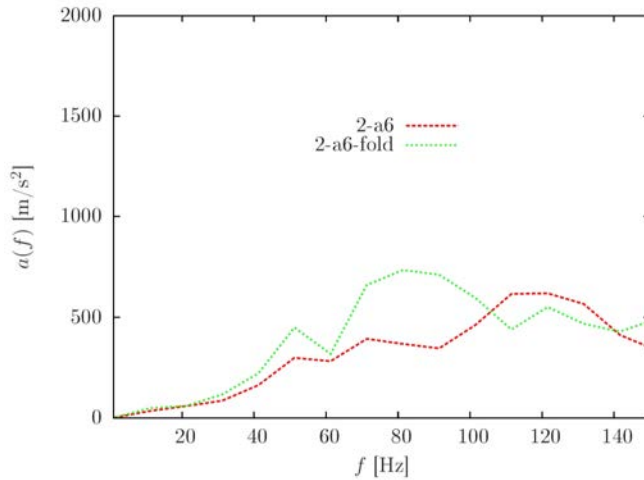


Figure 19. Floor response spectrum of acceleration history at top of rear wall at point 6 with damping ratio of 0.05 at 45 and 5000 Hz.

Summary and conclusions

In order to study vibration behaviour in reinforced concrete structure, a three-dimensional reinforced concrete test specimen with a front wall, a floor and a rear wall, each 150 mm thick, was impacted three times with a deformable steel projectile. Also modal tests and analyses were carried out. The response of the structure was measured with strain gauges on the reinforcement, displacement sensors and

accelerometers. The main aim of these tests were to study propagation of vibrations from the hit point through the floor to the back wall. Experimental data on damping behaviour in damaged reinforced concrete structure is needed in developing and validating numerical models and methods.

In summary, the damage caused for the structure by the tests was relatively mild and limited to the front wall where spalling of concrete took place at the hit area on the front surface and cracking as well as minor scabbing at the back surface just opposite to the hit area. In addition, crack could be observed also at the sides of the front wall near the location where the wall changes to the floor. The minority of the damage was mainly due to soft impacts with low velocities.

The change in response of the structure between the consecutive impacts depended on the type of quantity measured: the displacements increased somewhat from a test to the next one while the accelerations decreased in a similar manner. At the same time no clear behaviour could be identified for the reinforcement strains. In each case, the main frequencies at which the response occurred decreased slightly from a test to the next one with the frequencies being slightly lower than the ones identified in the modal FE analyses.

All in all, the test series was a successful start for testing of vibration propagation and damping properties of three-dimensional reinforced concrete structures under soft projectile impact. It gave a wealth of valuable data for validation of predictive models. It also gave valuable experience that can be used in future when designing similar tests.

So far, numerical studies have been carried out for the first vibration test V0A. The main aim of this first study was to carry out sensitivity analyses on the test set-up used in Test V0 in order to find out the essential phenomena to be considered in the numerical studies. Two types of calculation codes are used: Abaqus/Explicit and an in-house FE code.

Conclusion on analyses by Abaqus/Explicit

Assumed nonlinear material properties of concrete affect the bending behaviour of the wall. Nonlinear material behaviour is absorbing energy and damping the vibrations. In future studies the combination of nonlinear material modelling and structural damping should be studied more thoroughly in order to understand the effect of combined material and structural damping behaviour. In the codes and standards, damping ratios are provided only for linear studies and thus the proper damping factor for nonlinear vibration studies is an open question. Also, the vibration propagation through the structure should be studied in more detail. Measurement data exists now for several locations in the test structure.

As a general conclusion of a detailed FE modelling, all the additional characteristics bring the dynamic model behaviour for the most part closer to the real behaviour of the test structure. The essential phenomena need to be taken into account properly and carefully. Floor response spectra results obtained either using the loading function or by applying the missile model are rather similar below a frequency of 100 Hz. Until a frequency of 30 Hz, the simulated floor response spectra in both

cases agree well with the corresponding spectra obtained from the recorded acceleration results. Acceleration response peak at a frequency of 34 Hz seen in simulation results was not obtained by experimental measurements.

General conclusion on analyses with Reissner-Mindlin elements

Application of load was done in two alternative methods. In the first one, an average visco-plastic folding mechanism was adopted in the Riera formulation, while in the second one, the actual forming of folds was followed. This had only a small effect on the acceleration response spectra of most interesting component, the acceleration of the rear wall top middle point.

Acknowledgement

The authors would like to acknowledge the project(s) funding by VYR, VTT and external partners. The authors would also like to acknowledge the work by the project teams, the SAFIR2014 reference group 7 and the combined IMPACT 2014 and SMASH ad hoc group.

References

- Bathe K.-J. and Dvorkin E.N., 1985. A four-node plate bending element based on Mindlin/Reissner plate theory and mixed interpolation, *International Journal for Numerical Methods in Engineering*, Vol. 21, pp. 367-383.
- Ibrahimbegovic A. and Frey F., 1993. Stress resultant finite element analysis of reinforced concrete plates, *Engineering Computations*, Vol. 10, pp. 15-30.
- Jones, N. 1989. *Structural Impact*. Cambridge University Press, 1989.
- Koechlin P. and Potapov S., 2007. Global Constitutive Model for Reinforced Concrete Plates, *Journal of Engineering Mechanics*, Vol 133, pp. 257-266.
- Riera, J.D., 1968. On the stress analysis of structures subjected to aircraft impact forces, *Nuclear Engineering and Design*, Vol. 8, pp. 415–426.
- Saarenheimo, A., Calonius, K. and Tuomala, M. Numerical studies on vibration test V0. VTT Research Report VTT-R-00053-15. 83 p.

38. Ageing management of concrete structures in nuclear power plants (MANAGE)

38.1 MANAGE summary report

Miguel Ferreira¹, Mikko Tuomisto¹, Olli Stenlund¹,
Esko Sistonen² and Fahim Al-Neshawy²

¹VTT Technical Research Centre of Finland Ltd
P.O. Box 1000, FI-02044 Espoo

²Aalto University
P.O. Box 11000, FI-00076 AALTO

Abstract

Finnish nuclear power plants (NPP) are reaching their designed service life of approximately 40 years, therefore, the ageing management of the NPP, especially the concrete structures, has become an important issue. Based on international guidelines for ageing management systems, the physical ageing of structures, systems and components, and their obsolescence, needs to be managed by coordinating existing programmes, including maintenance, in-service inspection and surveillance, as well as operations, technical support programmes and external programmes such as research and development.

The MANAGE project has developed a platform for the systematic ageing management of concrete infrastructure. The MANAGE platform provides an essential tool for coordinating all activities relating to the understanding, control, monitoring and mitigation of ageing effects of the plant component or structure.

This MANAGE platform supports *applications tools related to the management of concrete structures*, based on a harmonised data system. The platform helps coordinate efforts in the acquisition of essential, up-to-date and proactive data on the condition and performance of concrete structures is secured. The MANAGE platform will provide systematic methods for planning, surveillance, inspection, monitoring, condition assessment, maintenance and repair of structures.

Introduction

Finlands first nuclear reactor came into operation in 1977. Within three years another three reactors were operational. Since these nuclear power plants (NPP) have been designed for a service life of approximately 40 years, they are reaching the end of their licensed operating service life. The ageing management of the NPP, especially the concrete structures, has become an important issue.

Based on the IAEA Safety Guide NS-G-2.12 [1] for ageing management systems addresses both physical ageing of structures, systems and components (SSC), and their obsolescence. Effective ageing management in practice is accomplished by coordinating existing programmes, including maintenance, in-service inspection and surveillance, as well as operations, technical support programmes (including analysis of any ageing mechanisms) and external programmes such as research and development. This requires the use of a systematic approach to managing ageing that provides a framework for coordinating all programmes and activities relating to the understanding, control, monitoring and mitigation of ageing effects of the plant component or structure [2].

According to STUK (Finnish Radiation and Nuclear Safety Authority) guideline YVL 1.0 [3], in "NPP design, the service life and the effect of their ageing on the safety of all safety significant structures, components and materials shall be assessed using sufficient safety margins. Furthermore, provision shall be made for the surveillance of their ageing and, if necessary, their replacement or repair." Furthermore, guideline YVL 1.4 [4] states that "a management system shall be planned and implemented to incorporate all the operations of an organisation, and it shall be continuously maintained and improved. The management system shall contain procedures to identify, assess and MANAGE safety risks relating to the operation of the nuclear facility."

It is especially important for the utilities to know the current condition state of their concrete structures. That is only possible by continuous inspection of structures and through an ageing management system which is able to store and treat the inspection reports in a systematic way. It should include predictive methods for evaluating the future performance of structures and to support the definition of a maintenance strategy for the prolonged life time of a plant. The utilities should be able to show the authorities a comprehensive ageing management programme with a description of how the design and qualification of the SSC, their operation and operating experience, in-service inspections and tests, and maintenance are integrated logically and systematically [5].

Therefore the NPP companies are interested in developing Ageing management systems to avoid premature degradation of NPP facilities and to be able to extend their operating service life. Massive concrete structures (i.e. foundations and containment structures) are not intended to be renewed and cannot be economically renovated. The final service life of NPP may be dependent on the service life of the concrete structures in the facilities.

In response to this need the "MANAGE project – Ageing Management of Concrete Structures in Nuclear Power Plants", funded by SAFIR 2014 (The Finnish

Research Programme on Nuclear. Power Plant Safety 2011 – 2014) [6], was initiated in 2011. MANAGE is a joint project with VTT Technical Research Centre of Finland and Aalto University.

The MANAGE ageing management platform

The premises of the MANAGE ageing management platform are based on those presented in the YVL Guides and in the IAEA Safety Guide NS-G-2.12. The main objective of the MANAGE project was to develop a platform for the ageing management of concrete infrastructure of existing Finnish NPP.

The platform provides access to the structural, material and environmental information and through the acquisition of essential, up-to-date and proactive data on the condition and performance of concrete structures, it assists the designers and engineers of a NPP in the planning, inspection, monitoring, condition assessment, maintenance and repair of structures. The implementation of an ageing management platform in practice helps guarantees a safe and uninterrupted use of the NPP for the whole intended lifetime. The ageing management platform helps provide useful information for the utilities and the authorities regarding the concrete structures ability to fulfil the serviceability and safety requirements during the whole licensed operating life.

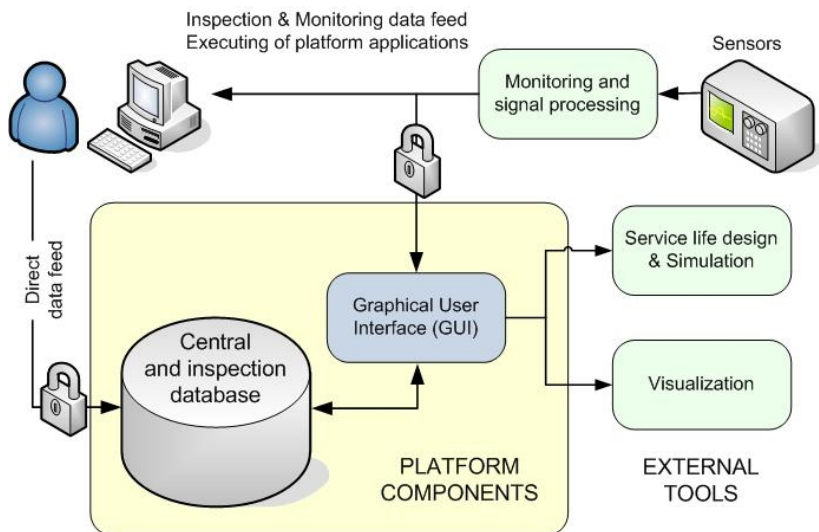


Figure 1. Schematic representation of the structure of the MANAGE platform and the user applications.

Structure. The development of the ageing management platform took into account the recommendation of the Finnish Regulatory guide YVL 1.1 [5] by providing in a systematic way the following information:

- new monitoring data on structures based on sensors and samples taken from structures;
- condition assessment and identification of potential risks related to degradation and performance of concrete structures over a long design period;
- improved timing of inspections and future repairs;
- structural safety and performance analyses with improved models;
- improved availability of data and visualisation, and
- electronic storage and treatment of inspection data.

Based on these recommendations the conceptual structure of the ageing Mngement platform was defined (Figure 1). Access to the platform is through the Graphic User Interface (GUI) which connects the user to the various applications and the central database. The platform consists of a harmonised central database and a group of analysing and planning tools which access the data from the database. The applications currently available are: i) ServiceMan – an independent service life management system [7], a visualization tool, and an inspection database. Direct access to monitoring data was not implemented at this stage.

The GUI & the central database

The GUI provides the user with access to the central database and the applications. The GUI features are organized by four access levels. Each access level has different screen pages providing various functionalities. The diagram in Figure 2 shows the layout of the platform screen pages. The application screens pages are accessed using navigation menu.

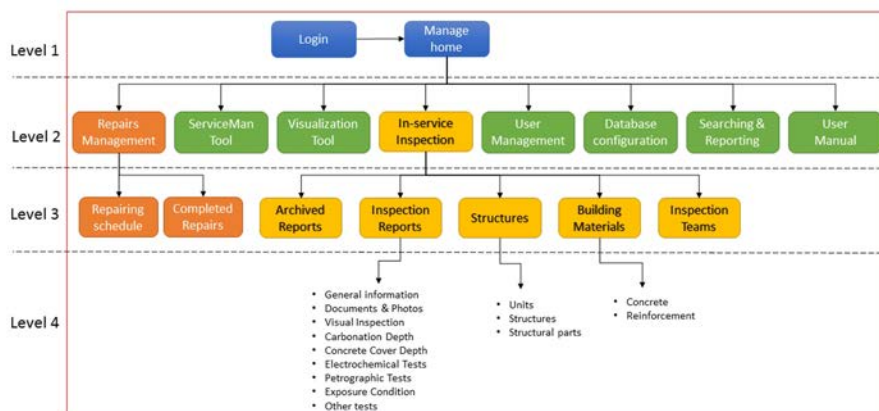


Figure 2. The access levels of the platform and their screen pages.

Users access to the GUI from server is by using a web browser. Web browser facilitates user access because there is no need to install additional applications to a user's computer. The GUI has been programmed by using Active Server Page (ASP.NET) and Visual Basic (VB.NET). Both ASP.NET and VB.NET are widely known technologies.

The central database is the core of the platform. It assembles and systematically organizes the information gathered from all applications [8, 9]. The goals and objectives of the central database are to (1) collect the essential and up-to-date data of the condition and the performance of the NPP concrete structures, (2) store and update these data effectively, (3) allow sophisticated search strategies, (4) produce detailed reports automatically for the condition and the performance of the NPP concrete structures and (5) enable data transfer to other software for further analysis: for example act as a data source for ServiceMan for the estimation of the service life of the NPP concrete structures.

The components of the platform's central database are organized into a series of sub databases relating to the ageing management system of the NPP concrete structures. These sub-databases are:

- User's management database for user's data and their authorized limits.
- Visualisation database for dealing with the geometrical input and out for the visualisation tool.
- Service life management database for the input and output data for the service life calculation application (ServiceMan).
- Structural database for storing information about the structural types and components of the NPPs concrete structures.
- Inspection database for the data gathered from the investigation and the diagnosis of the NPPs concrete structures.
- Monitoring database for monitoring and simulating the performance of the NPPs concrete structures

The authorized users of MANAGE platform come in two levels: the administrators, and end users. Administrators are responsible for managing the database system and have full access to modify the platform code and design. The end users are the persons that use the platform for querying, updating, generating reports, etc.

The ServiceMan application

ServiceMan is a service life management tool for life cycle planning of concrete structures in nuclear power plants. It is able to predict the degradation of concrete structures and to evaluate the timing of necessary maintenance and repair actions over the remaining licensed life time of the plant or longer (extended life time). The tool can also be used for planning, organizing and optimizing the maintenance strategy of concrete structures in NPPs. A detailed description of the ServiceMan tool is presented in [10].

The system was programmed based on Microsoft Excel. Macros, such as the user interface, were coded using Visual Basic for Applications. The actual service life management system includes the database and tool for service life management. The service life management tool includes prediction of degradation in structures, guarding of safety limits, timing of condition assessments, timing and specification of MR&R actions, and evaluation of life cycle costs and environmental impacts. In-service operations of the service life management system are condition assessment

for structures, maintenance, repair and rehabilitation (MR&R) actions, and, updating the degradation models.

An interface between ServiceMan's Excel sheet and the ageing management system's central database is done through the GUI. The application can read from and write to the database and make calculations using ServiceMan tool. Calculation results can also be stored back in the central database.

The Inspection database

The ageing management system's inspection database is part of the central database which includes all the NPP condition survey data. New inspection data is transferred to an electronic form then stored in the inspection database. The data consists of observations during both periodical inspections and special inspections. The design process of the inspection database is similar to the design of the central database. The structure of inspection database includes four main tables:

- Electronic documents and digital photos
- Visual investigation and diagnosis
- Non-destructive tests
- Destructive and laboratory tests

The components of the inspection database are organized into a series of database tables related to the ageing management of the nuclear power plants concrete structures as shown in Figure 3.

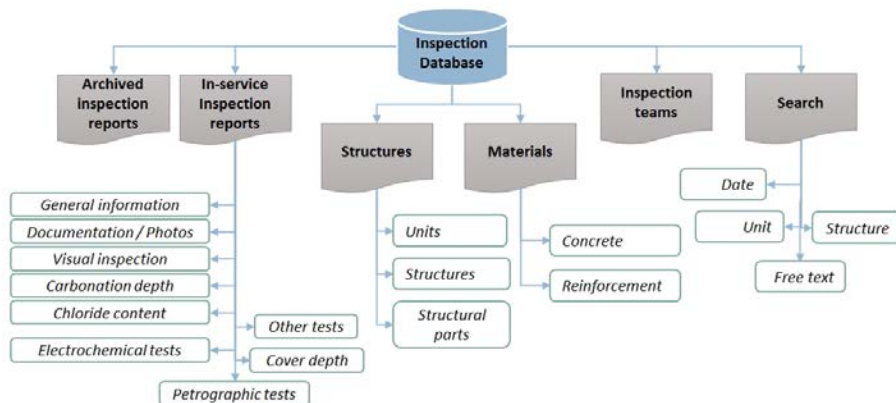


Figure 3. Conceptual design of the inspection database tables

The inspection home page, is working as a dashboard for the inspection database. It offers access to the sub-level inspection webpages which are: the archived in-service inspection reports; detailed inspection reports; NPP structures; building materials used in the NPP structures; and information about the inspection teams involved in the condition assessment of the NPP structures. The sub-level in-service inspection home pages are shown through Figure 4 to Figure 6. Condition inspection report search allows the platform user to enter one search criteria and view or print the matching report if there are any that match the searching criteria.

The report searching criteria are (i) date of the condition inspection report, (ii) free text search, (iii) in-spection report code name and (iv) research for units or structures of the nuclear power plants.

Figure 4. The archived inspection reports home page.

Figure 5. Print screen of the inspection report's general part.

MANAGE Version 1.05 10.12.2014 Welcome admin! [Log Out]

Manage-Home Archived Reports Inspection Reports NPP Structures **Concrete and Reinforcement** Inspection Teams

Concrete
 Reinforcement

Message: [Clear Message History](#)

Materials - form feed

CONCRETE No Yes

Concrete code (*) (*) Compulsory field

Date of casting

Structure(s) where concrete was used

Cement Information, if founded:
(Type, manufacturer, additions, cement composition, etc.)

Aggregate information, if founded: (fine /coarse aggregate, source of aggregates, grading, composition, etc.)

Cement content [kg]/m³-con Water to cement ratio [-]

Aggregate Content [kg]/m³-con Air content [%]

28 d compressive strength [MPa] 28 d tensile strength [MPa]

Hardened concrete density [kg/m³] Capillary porosity - if measured [%]

Concrete lab. / field testing result No file selected.

Figure 6. Concrete and reinforcement information webpage.

The Visualization application

The objective of the visualization application module is to propose an interactive system for visualization of data and documents related to the concrete structures of NPP. The proposed visualization environment is able to provide visual representations of the database content. It is also able to provide direct access to all the digital content, both in terms of physical access to the structural data files as well as in terms of searching and retrieving information.

The visualization interface can be used to import the geometrical data of the structures and report the in-service condition of these parts as attached notes to the geometry drawings. The application is currently using a simple procedure of visualization of all document types in their native format by external visualization software (e.g. AutoVue) that is able to interpret the data. Any kind of original (DWG, DXF, PDF, JPG, TIFF, etc.) can be stored in the central database and linked to the structure it represents. The platform interface will enable users to download process the drawing in an external application and then save the processing results and the original file in the MANAGE central database.

Visualization data is stored in a local Oracle database that consists of 4 tables. Vis-

ualization document data is stored in the first table and there are tables for possible unit, structure and module numbers also. Visualization document files are not stored in the database, just the path of the files. Each document is linked to only one unit, structure and module number. These numbers are stored in the Visualizations table. example of search screen for specific document is given in Figure 7.

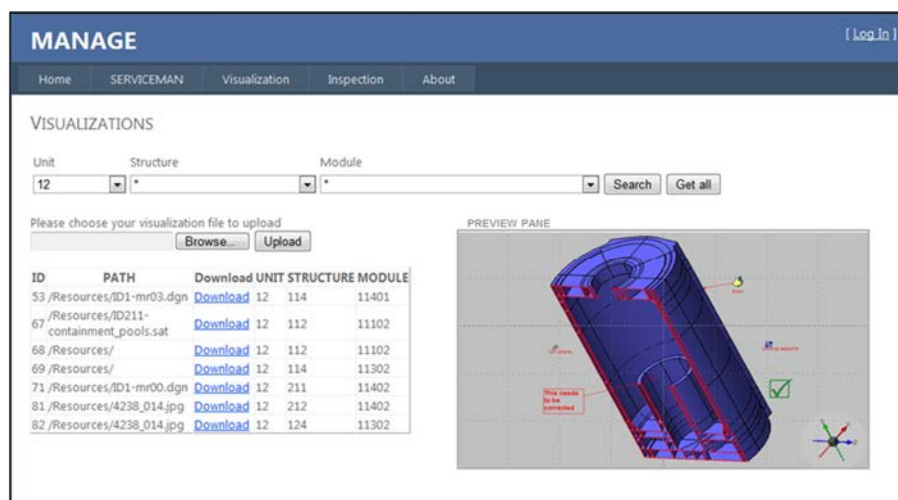


Figure 7. Screenshot of the GUI showing the Visualization interface

Complementary analyses & International Cooperation

Throughout the MANAGE project several complementary studies/analyses have been performed to provide additional support into the ageing management of NPP:

- Condition assessment of cooling water channels in Finnish Nuclear Power Plants (VTT-R-00342-11) – The objective was to evaluate the condition of cooling water channels in Olkiluoto 1 and Loviisa 1 NPP. The research was based on testing of concrete samples taken from the structures [11].
- Condition assessment of cooling water channels in Finnish Nuclear Power Plants – Based on sample tests in 2011 (VTT-R-08960-11) – Similar to [12] but with different locations for specimen extraction in the cooling water channels of Olkiluoto 2 and Loviisa 1 [12].
- Half-cell potential measurements in Loviisa 1 cooling water chambers (AALTO-R-001-12 2012) – The goal was to measure half-cell potential values of the reinforced concrete structures of the cooling water chambers in Loviisa 1 NPP to verify the state of corrosion of the reinforcement. The half-cell measurements were performed at the same positions in the cooling water chambers as with the condition assessment carried out in 2010 [13].
- Structural failure analysis of post-tensioned containment building of Olkiluoto 2 NPP (VTT-R-00327-11) – The main goal of this report is to conduct structural

failure analyses which help to evaluate the above mentioned probability. The intent is to calculate how possible tendon breaks affect the structural integrity of the whole containment building, and to be more precise, how the stress state of the containment wall changes and whether there is an underlying mechanism by which the degradation propagates further in the structure to concrete, adjacent tendons and liner. To evaluate damage in the concrete induced by tendon breaks and/or pressure tests, supplementary cracking analyses are also conducted [14].

- Condition assessment of pre-stressing tendons by NDT inspection techniques (Ramboll Report) – The aim is to verify the suitability of non destructive test methods (NDT), for example by Ultrasound MIRA 3D Tomographer system, for detection of voids in grouted pre-stressed structures tendon ducts. In addition, other NDT techniques were used for general evaluation of concrete structures: the Impact – Echo DOCTer system, the Surfer System, and the Impulse – Response s'MASH system. The structure chosen for the investigation task was the protective concrete structure of the containment structure of Olkiluoto 2 NPP [15].
- Condition assessment of the seawater system – Ancillary cooling water outlet tunnel at Olkiluoto 2. (VTT-R-07703-13) – The objective was to evaluate the condition of outlet tunnels of Olkiluoto 2 NPP. The research was based on in situ testing, and from of concrete samples taken from the structures. [16].

During the course of the MANAGE project, VTT was involved in the NUGENIA project ACCEPPT assessing the behaviour and ageing of pre-stressed concrete containment of NPP including steel liner and tendons, which focuses its research to the environmental and mechanical loads and their effects on the structural security of NPP concrete structures. VTT is also involved in the OECD/NEA/CSNI ASCET project on the assessment of structures subject to concrete degradation with focus on alkali-aggregate reaction (AAR). This is also done in cooperation the RILEM TC-ISR on the prognosis of deterioration and loss of serviceability in structures affected by AAR.

Conclusions

This report briefly presents an overview of the MANAGE ageing management platform developed and the complementary activities that took place within the project. The focus is on the inspection database and the application for durability service life and life cycle assessment. The platform provides access to structural, material and environmental information regarding NPP concrete infrastructure.

The ageing management system consists of the central database and a group of analysing and planning tools which access data from the database. The database together with the analysing and planning tools can be used during different phases in the lifetime of a NPP: design, operation, inspection, monitoring, maintenance and repair of structures.

The implementation of an ageing management system in practice assists in guaranteeing a safe and uninterrupted use of the NPP for the whole intended lifetime.

The purpose of the inspection database is to transfer the condition assessment data of NPP concrete infrastructure to an electronic form. The data consists of observations during both periodical inspections and special inspections. The inspection database allows for sophisticated data search strategies, produces detailed reports automatically for the condition and the performance of the NPP concrete structures and enables data transfer to other software for further analysis.

The ServiceMan tool for durability service life and life cycle assessment, can be used for systematic and proactive maintenance of concrete structures in nuclear power plants. The core process of the system is the combined condition, cost and environmental impact analysis. The application estimates the degradation of concrete structures with respect to different degradation types and also the timing of special inspections and MR&R actions for the remaining operating life of the plant.

Acknowledgement

The authors of this report would like to acknowledge the valuable contribution of their esteemed VTT colleague Erkki Vesikari (retired), who defined the concept and drove the initial development of the MANAGE project.

References

- [1] NS-G-2.12. Ageing Management for Nuclear Power Plants, IAEA Safety Guide, International Atomic Energy Agency, 2009.
- [2] E. Vesikari, M. Tuomisto, P. Hradil, K. Calonius, F. Al-Neshawy, E. Sistonen. Working plan for the Ageing Management System of concrete structures in Finnish Nuclear Power Plants. Research Report VTT-R-08738-11. 2011. 63p.
- [3] YVL 1.0. Safety criteria for design of nuclear power plants, Finnish Centre for Radiation and Nuclear Safety (STUK). 1996.
- [4] YVL 1.4. Management systems for nuclear facilities. Finnish Centre for Radiation and Nuclear Safety (STUK). 2008.
- [5] YVL 1.1. Regulatory control of safety at nuclear facilities, Finnish Centre for Radiation and Nuclear Safety (STUK). 2006.
- [6] SAFIR 2014 Framework Plan. National Nuclear Power Plant Safety Research 2011-2014. 2010. 102p.
- [7] E. Vesikari. Service life management system ServiceMan – User Manual. The Finnish Research Programme on Nuclear Power Plant Safety 2007 - 2010. Research Report VTT-R-00450-11. 41 p. (2011)
- [8] F. Al-Neshawy, E. Sistonen, J. Piironen, and S. Huovinen. Design of database

based on condition survey of concrete facades. CONSEC'07, Concrete under severe conditions: Environment and loading, Tours, France, June 4-6, 2007. pp. 1799 - 1806. (2007)

- [9] F. Al-Neshawy, E. Sistonen, J. Piironen, E. Vesikari and R.M. Ferreira. Development of database for the in-service inspection of the concrete structures of the Finnish Nuclear Power Plants, IABSE Workshop on Safety, Failures and Robustness of Large Structures. February 14-15, 2013. Tuusula, Finland.
- [10] E. Vesikari. Service life management system of concrete structures in nuclear power plants. VTT Technical research Centre of Finland. VTT Publications 648. 82 p. <http://www.vtt.fi/inf/pdf/publications/2007/P648.pdf> (2007).
- [11] E. Vesikari. Condition assessment of cooling water channels in Finnish Nuclear Power Plants. VTT Technical research Centre of Finland. VTT-R-00342-11. 2011. 51p.
- [12] E. Vesikari, R.M. Ferreira. Condition assessment of cooling water channels in Finnish Nuclear Power Plants – Based on sample tests in 2011. VTT Technical research Centre of Finland. VTT-R-08960-11. 2012. 44p.
- [13] J. Piironen, E. Sistonen. Corrosion Measurements in Loviisa 1 Cooling Water Chambers . Aalto University. Espoo: Research Report AALTO-R-001-12 2012. 26p.
- [14] K. Calonius, S.Fortino, M. Patalainen. Structural failure analysis of post-tensioned containment building of Olkiluoto 2 NPP. VTT Technical research Centre of Finland. VTT-R-00327-11. 2011. 83p.
- [15] G. Rapaport. Condition assessment of pre-stressing tendons by NDT inspection techniques. Ramboll Report. 44p.
- [16] Ferreira, M., Condition assessment of the seawater system – Ancillary cooling water outlet tunnel at Olkiluoto 2. VTT Technical Research Centre of Finland. VTT-R-07703-13. Espoo. 57p.

39. Seismic safety of nuclear power plants: targets for research and education (SESA)

39.1 SESA summary report

Ludovic Fülöp¹, Vilho Jussila¹, Marianne Malm², Timo Tiira³, Jouni Saari², Yue Li⁴,
Päivi Mäntyniemi³, Pekka Heikkinen³, Jari Puttonen⁵

¹ VTT Technical Research Centre of Finland Ltd
P.O. Box 1000, FI-02044 Espoo

² ÅF-Consult Ltd
Bertel Jungin aukio 9, FI-02600 Espoo, Finland

³ Institute of Seismology, University of Helsinki
P.O. Box 68, FI-00014, University of Helsinki, Finland

⁴ Dep. of Civil and Environmental Engineering, Michigan Technological University
1400 Townsend Drive, Houghton, USA

⁵ Aalto University
P.O. Box 11000, FI-00076 AALTO

Abstract

The paper summarises the main outcomes of the project carried out in the period 2011-2014. It is a continuation of the material published in the Interim Report of the SAFIR 2014 program (L. Fülöp et al., 2013), with a general shift from hazard prediction towards focus on qualification of systems, structures and components (SSC's). This shift resulted from the progress of the project. Still, some seismology related conclusions are refined compared to the previously published data, and this paper should be considered the definitive conclusion of the project.

The paper briefly presents topic areas studied in the project: (1) preliminary description of high quality near-field data recorded in 2012 from the Kouvola earth-

quake swarm, (2) a ground motion prediction equation (GMPE) proposal for mid magnitude earthquakes and recommendation of GMPE's to be used for high magnitude events, (3) results of a deaggregation study focused to north of Finland, (4) results of sensitivity modelling for a generic reactor building subjected to earthquake loads expected in Finland and (5) challenges concerning equipment qualification. Conclusions are given briefly after each topic, but the reader is directed to the project reports for in-depth understanding.

Introduction

Finland is one of the most stable continental regions. Earthquake events of higher magnitude are scarce and events of engineering significance non-existent. Because of the relative scarcity of instruments in the Finnish National Seismic Network, earthquakes are usually measured at a large hypocentre distance, hence leading to data significant for seismologist but less interesting for engineers.

Against this background of empirical data scarcity, the SESA project was started in 2011 with the goal to collect the data available in Fennoscandia, and analyse the data with the purpose of understanding its design significance for nuclear structures, systems and components (SSC's).

Within the first project year the Fukushima Daiichi nuclear disaster happened. Few lessons of that accident are directly relevant in Finland, but the scale of the tragedy reminded stakeholders of the potential destructiveness of low probability high consequence events. Hence, understanding of why projects like SESA are needed improved at all levels of decision making.

Within the project we focused on a very broad spectrum of topics related to seismic safety: (1) earthquake hazard assessment, (2) structural assessment and (3) equipment qualification procedures.

Data collection, analysis and interpretation

Data collection in the project included the systematization and interpretation of a large databank of recordings in order to develop empirical ground motion prediction equations (GMPE) from Fennoscandian data.

New data also became available, as the project team has also had the fortune to measure an earthquake swarm in Kouvola. The M_L 2.8 (01.12.2011) triggered swarm events were measured with four temporary stations installed in the source area, using broad-band sensors. The interpretation of the data from seismological point of view has been done by Smedberg et al. (2012a, 2012b). The interpretation from engineering point of view is ongoing. Temporary (distance from events 1-9 km) and permanent (distance from events 40-120 km) stations were measuring the swarm events in Kouvola. Highest magnitude measured was M_L 2.6 with 250Hz sampling rate. Majority of events $<1M_L$ at very shallow depth (~1-2km)

Data used for calibration of the GMPE was selected from over 38 000 3-channel seismograms of earthquakes. The number of earthquakes in the original data set

was 1550 and the waveform data has been registered at 40 seismic stations in Finland, Sweden, Norway, Russia, Estonia and Latvia. GMPE's were computed using a selected data set with a more restricted geographical distribution (Tiira and Heikkinen, 2014).

The magnitude used in the annual reports of earthquakes in Northern Europe by the Institute of Seismology is local magnitude defined by Uski and Tuppurainen (1996). This magnitude scale has been used for GMPE's. The same magnitude scale was used in studies made recently for utilities (Korja and Kosonen, 2014).

Empirical GMPE's were fitted for Finland using linear regression to the equation 1, adopted from Atkinson and Boore (2006).

$$\log(PGA) = c_1 + c_2M + c_3M^2 + (c_4 + c_5M)f_1 + (c_6 + c_7M) + (c_8 + c_9M)f_0 + c_{10}R_{ed} + c_{11}S \quad (2)$$

Where PGA is peak ground acceleration, M is the magnitude, R_{ed} distance to the fault, $f_0 = \max(\log(R_0/R_{ed}), 0)$, $f_1 = \min(\log R_{ed}, \log R_1)$, $f_2 = \max(\log(R_{ed}/R_2), 0)$, with $R_0 = 10$, $R_1 = 70$ and $R_2 = 140$. For hard rock sites $S=0$, for soil sites $S=1$.

This equation was also recommended for stable continental environments by Stewart et al. (2013). The coefficients were fitted using linear regression both for peak ground acceleration (PGA) and 5% damped acceleration response spectra at frequencies 10 and 20 Hz. The coefficients from Eq.1 are given in Table 1. Fitting was done using statistical program package R (www.r-project.org). The equations were fitted to empirical data using linear regression. The residual standard errors (sigma) are 0.327 (PGA), 0.317 (10Hz) and 0.314 (20Hz).

Predicting ground motions for earthquakes which have magnitudes above magnitude range of previous earthquakes in the study area is a complicated task. GMPE's fitted using earthquakes with small magnitude range are not reliable outside this magnitude range. The empirical model presented is only valid in the magnitude range of the database. For small magnitudes GMPE's fitted to equation 1 is recommended. For larger magnitudes ($M_w \sim 4 \dots 5$) the use of the average of GMPE's by Pezeshk et al., (2011), Atkinson and Boore, (2006, 2011) and Silva et al., (2002) is suggested.

Revisiting seismic hazard predictions

The earthquake hazard assessment work focused on identifying suitable software for hazard calculations having in mind the needs in Finland. Twelve software options were reviewed: CRISIS V6 (2007), EQRM V3.2 (2009), EXSIM (2005), EZ-FRISK V7.60, FRISK88M V1.8, MoCaHaz (2004), MRS V3.0, NSHMP (2008), OHAZ V2.1, OpenSHA (2009), SEISHAZ (2005), SEISRISK III M (1996). EZ-FRISK was chosen as software for analysis (Malm et al., 2013). Previous hazard calculations in Finland have been done using SEISRISK III and EZ-FRISK for example Saari et al. (2009) or Smedberg et al. (2011).

Table 1. Coefficients of equations estimating median horizontal ground motions on hard rock for 5% damped acceleration spectra at given frequencies and PGA. Updated from Tiira and Heikkinen (2014)

	PGA	10hz	20hz
C ₁	-2.2410048	-2.4516811	-2.4427721
C ₂	0.7021008	0.737952	0.7995751
C ₃	0.025966	0.0246379	0.03389
C ₄	-1.615146	-1.4460975	-1.3646644
C ₅	0.0631582	0.0459802	-0.0058337
C ₆	1.1490929	1.1136652	1.3288603
C ₇	-0.0426829	-0.0222339	-0.0844612
C ₈	-0.4600796	-0.2637734	-0.2182231
C ₉	-0.2529065	-0.2991514	-0.3476451
C ₁₀	-0.0049509	-0.0049316	-0.0051065
C ₁₁	0.3047806	0.2392695	0.2612056

The use of the old version of SEISRISK III program was criticized in reviews of the previous hazard prediction work (Saari et al., 2009). The difference between the SEISRISK III (Bender and Perkins, 1987) and SEISRISK IIIM, version modified by LaForge was investigated. It was found that no changes had been made in the computational procedures of the program. The changes made for the modified version were a more efficient and user friendly input file and an output file suitable for plotting. Hence, SEISRISK III is as valid as the SEISRISK III M in the seismic hazard calculations.

CRISIS2007 (Ordaz et al., 2007) was rejected because of unclarified input table entries, FRISK88M because price was considered too high for the purpose of the project. OpenSHA was dropped because it does not allow user defined attenuation functions. Only a preliminary check of EqHaz (Assatourians and Atkinson, 2012) was performed. OpenQuake seemed very promising but the program was not well documented and proper explanation of sample files was missing. The priority was to find a free program for hazard studies, but finally EZ-FRISK was taken into consideration. The program allows user defined faults and attenuation equations, area sources and seismic parameters. Also deaggregation calculations are possible.

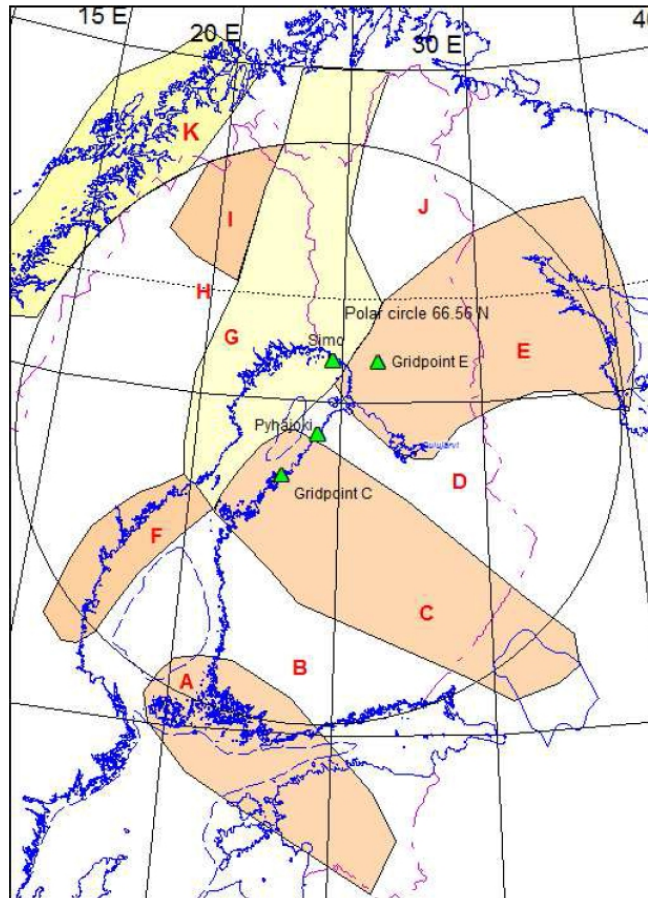


Figure 1. Seismic source areas used in the calculations; higher activity in the coloured areas. Capital letters A ... K refer to 11 seismic zones delineated (see Table 2). Calculated sites are marked with green triangles. The source areas used in 2013 and 2014 calculations were inside the 500 km circle around Pyhäjoki.

Further work concentrated on carrying out hazard calculations with focus on deaggregation calculations (Malm and Saari, 2014a, 2014b). The zoning (Figure 1) was identical to the one used in 2009 (Saari et al., 2009) and the attenuation relationship has been mostly based on the Saguenay and Newcastle earthquakes and used in Finland since 2000 (Varpasuo et al., 2000). The use of the 2013 version (Tiira and Heikkinen, 2014) of the attenuation equation based on earthquake data from the Fennoscandian shield was judged to be premature because work continued in that area and an updated version is expected in 2015.

The parameters of the seismic zones from Figure 1 are summarised in Table 2. Hazard and deaggregation was calculated for four sites (Pyhäjoki, Gridpoint C, Simo and Gridpoint E) for three frequencies (4 Hz, 10 Hz and peak ground accelera-

tion/PGA) and five amplitudes (0.01g, 0.05g, 0.1g, 0.2g and 0.4g). The locations of the four calculation points are given in Figure 1 and Table 2.

Table 2. Seismicity parameters a and b of the equation $\text{Log } N = a - b \cdot M$ and maximum magnitudes (M_{max}) of the seismic zones. Coordinates of the four sites calculated (Malm and Saari, 2014b)

	Seismic zone	b	a	M_{max}	Site	Coordinate
A	Åland Archipelago - Paldis - Pskov Zone	0.731	0.36	4.9	-	-
B	Southern Finland Quiet Zone	1.166	2.019	3.2	-	-
C	Southern Bothnian Bay - Ladoga Zone	0.782	1.41	4.6	Gridpoint C	63.910°N, 23.100°E
D	Central Finland Quiet Zone	0.976	2.222	3	Pyhäjoki	64.532°N, 24.261°E
E	Kuusamo Zone	0.736	1.725	5.2	Gridpoint E	65.640°N, 26.340°E
F	Swedish coast (Gulf of Bothnia)	0.843	1.786	4.2	-	-
G	Western Lapland Zone	0.92	2.434	4.9	Simo	65.639°N, 24.693°E
H	Northern Sweden Zone	0.911	1.795	4.1	-	-
I	Pärvie Zone	0.75	1.597	3.7	-	-
J	Eastern Lapland Zone	0.755	0.889	4.4	-	-
K	Northern Caledonides	0.867	2.187	5.8	-	-

In general terms, the results obtained in SESA are compatible with the ones from Saari et al. (2009) and Malm and Saari (2014a). The hazard curves have similar shapes, but the peak ground acceleration amplitudes were higher in the SESA calculations with EZ-FRISK. This was likely because the 2009 results were presented as the median values of all the logic tree branches and the new results are the mean values of the four different attenuation equations. No logic tree was adapted for the SESA calculations.

The frequencies for calculating deaggregation results were chosen to correspond to the PGA, 4Hz and 10Hz in the spectra. The 4Hz approximately correspond to the main frequency of the horizontal direction vibration of stiff concrete buildings in NPP's, e.g. a reactor building (Figure 3); while the 10Hz was chosen with the intention of covering the frequency region of highest spectral amplification in Finland (YVL 2.6, 2001). The range of 10Hz and frequencies above are also likely to affect components hosted in NPP structures.

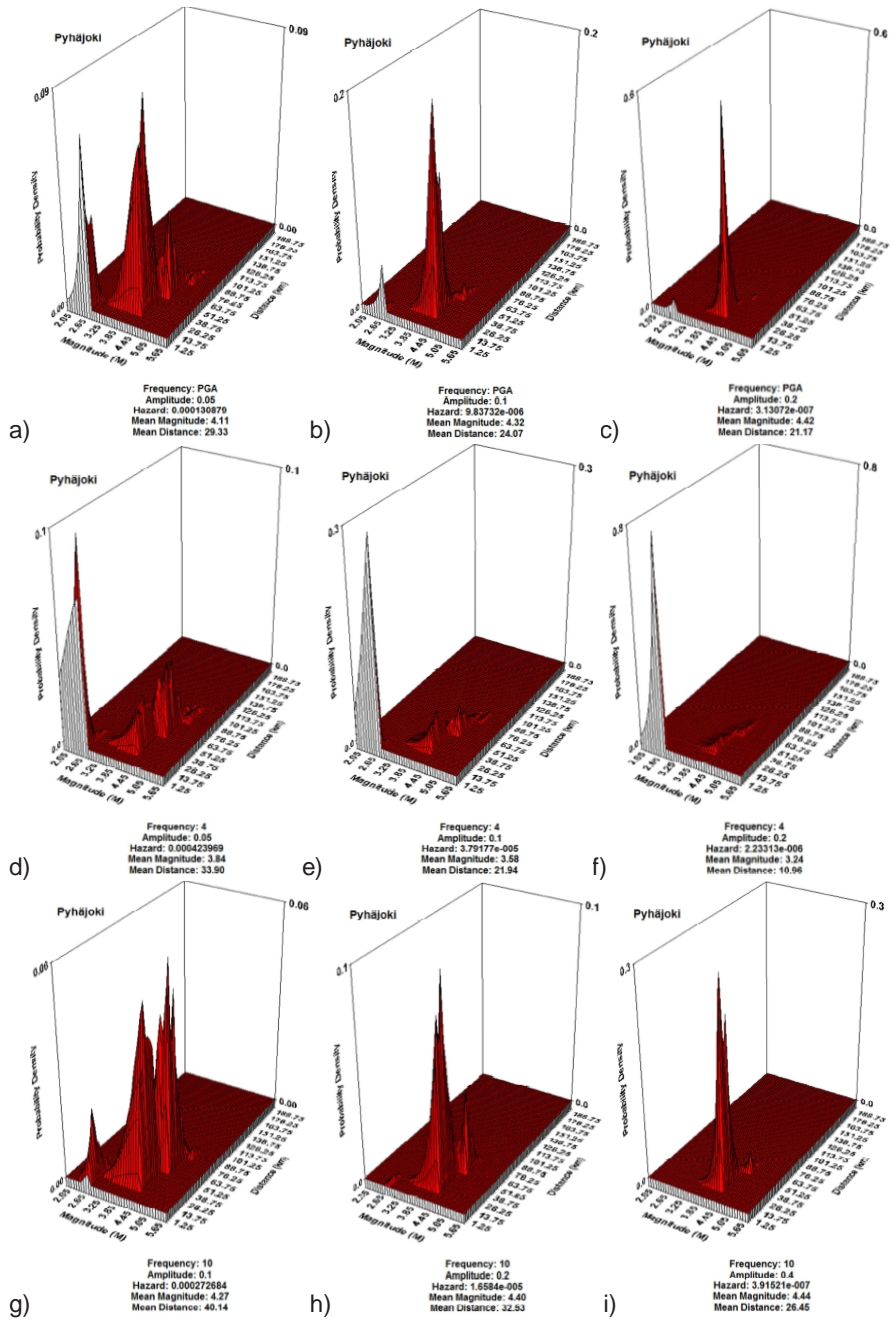


Figure 2. EZ-FRISK magnitude-distance deaggregation for Pyhäjoki, 5 % damping, average horizontal component of PGA amplitude (a) 0.05g, (b) 0.1g, (c) 0.2g; 4Hz spectral amplitude for (d) 0.05g, (e) 0.1g, (f) 0.2g; and 10Hz spectral amplitude for (g) 0.1g, (h) 0.2g and (i) 0.4g.

Given the shape of the spectra with soil condition in Finland the expect proportion is so that unit PGA correspond to pseudo-acceleration $PSA_{4Hz} \sim 1.1-1.4 * PGA$ and $PSA_{10Hz} \sim 2.1-2.4 * PGA$. The design load in southern Finland stands at $PGA = 0.1 * g$ (YVL 2.6, 2001). In Figure 2, selected results of the deaggregation study are presented for Pyhäjoki, with more detailed results being reported by Malm and Saari (Malm and Saari, 2014b). Horizontal X-axis shows the magnitude ($M = 2 \dots 6$), horizontal Y-axis the distance ($0 \dots 200$ km) and the vertical axis Z the probability density. Note that the probability density maximums (Z axis) are different for each graph.

Seismic design of NPP structures and vibration in structures

Once vibrations reach the buildings of an NPP, the focus is shifting to the evaluation of the response of buildings. There are two practical points of interest. It has to be studied if the stability of the buildings may be affected and the propagation of vibrations within the building needs to be understood, in order to qualify equipment (Fülöp, 2012). The overall aim is to show that no structures, systems and components (SSC) are affected by earthquake induced shaking.

In Finland there are two particularities related to buildings in NPP installations. Firstly, they are founded on hard rock sites so the effect of soil structure interaction (SSI) is eliminated. Secondly, the level of acceleration in terms of PGA and spectral acceleration ordinate corresponding to natural frequencies of NPP buildings is very low. Therefore, extensive damage to nuclear buildings is very unlikely.

Hence, our studies focused on vibration propagation within buildings and the uncertainties related to the vibrations arriving to the building floors. Because of the high shear wave velocity of the base-rock (>2500 m/s) and the stiff constructions used in NPP's, it is also possible that vibration of high and very high frequencies are propagated within the structures. This aspect has also been assessed.

The modelling of a generic reactor building (RB) was carried out by Jussila and Fülöp (2013, Jussila and Fülöp, 2014a) and Jussila et al., (2014). The basic FE model had: (a) plan dimensions 61x58m; (b) elevation 55.76m to edge of the dome; (c) outer walls 2m thick; (d) structure supported at base in vertical direction and horizontal direction; (e) total mass 222 425 tons, pressure vessel and two spent fuel storage tanks modeled; (f) prevailing mesh size ~ 0.67 m. The model had 151158 elements, 143144 shells with six degree of freedom nodes; 687 linear line elements; 144272 quadrilateral elements and 16 linear triangular elements (Figure 3).

Most plate elements were modeled with the "Shell/Continuum Shell Homogeneous" element type in ABAQUS, using 5 integration points on the thickness for all elastic models. Vertical and horizontal supports were concentrated only to the base nodes of the model, because re-fill soil provides little restraint to the walls during earthquake shaking.

The calculations have been carried out guided by provisions of YVL 2.6 (2001) and ASCE 4-98, (2000), with the aim of exploring loading scenarios expected in Finland. The extreme load combinations were defined according to KTA-GS 78 (KTA, 2005), including: permanent physical effects (G_k), effects due to prestressing

($P_k=0$ in this case), dominant temporary effects (Q_{k1}), other varying effects ($Q_{ki}, i>1$), extreme physical effects (A_d), effects due to earthquakes (A_{Ed}).

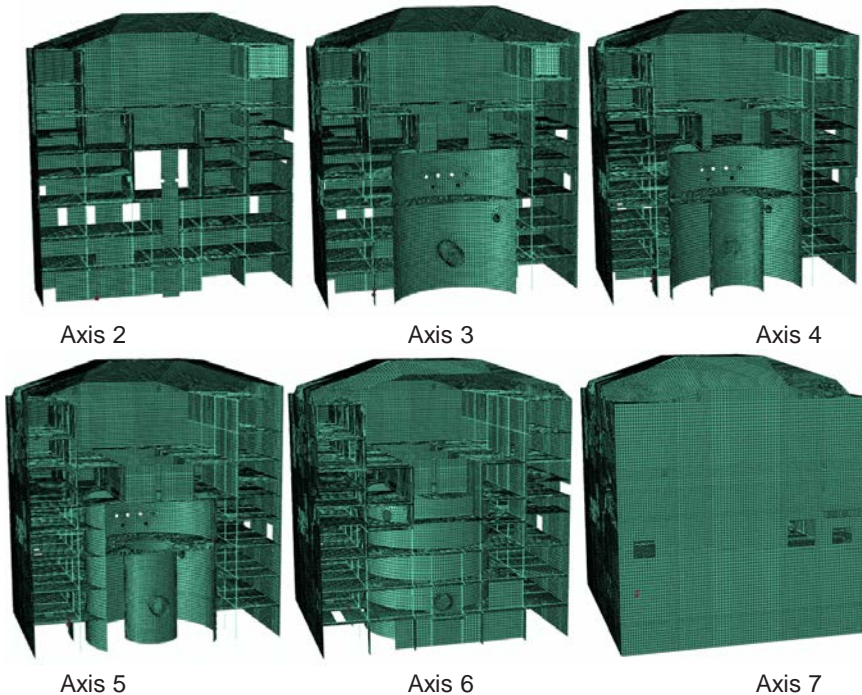


Figure 3. Internal structure of the RB highlighted by sections on the main axis in the Y direction

Regarding the design-basis earthquake in accordance with KTA 2201.1 (KTA, 2011), A_{Ed} was considered as nominal value based on the recommendation of YVL 2.6 (2001) response spectra and a spectra with much broader frequency content (Figure 4).

Three sets of 3D component accelerograms were generated for the spectra, respecting duration requirements for 6.5-7 magnitude earthquakes (ASCE 4-98, 2000). Total duration of records was 18.5s, with 1.5s rise time, 7s decay time and 10s duration of strong motion segment. The cross-correlation of the records was checked and was not exceeding the code required maximum value of 0.3 (ASCE 4-98, 2000).

Classical Rayleigh damping has been used for the elastic models. Two sets of damping factors α and β were calibrated: $\alpha=1.6$, $\beta=0.00020$ and $\alpha=1.55$, $\beta=0.00035$. These correspond to about 4% damping at the expected natural frequencies (3.5-4Hz) of the RB and about 2.5%-4% for 30Hz. The main objective was to assess if reduced damping on higher vibration modes has significant effect on the frequency content of vibration transmitted to components. We estimate that the upper limit of frequencies transported by the FEM mesh is ~ 277 Hz; but due to significant damping at higher frequencies the results are valid only up to 30Hz.

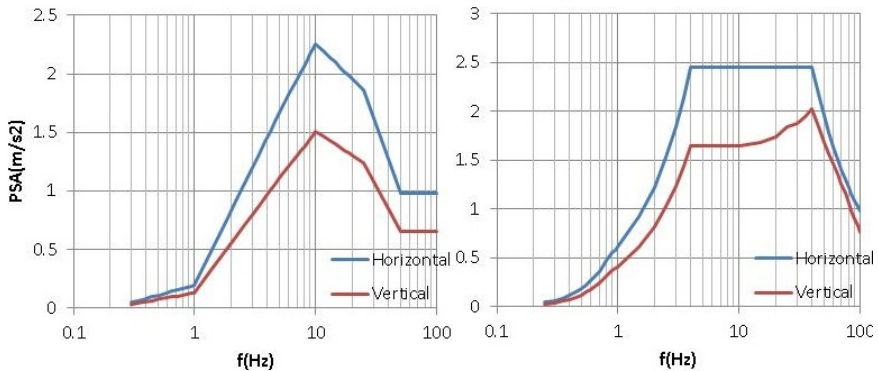


Figure 4. Spectra used as basic for the analysis of the generic RB. PGA of the horizontal shaking component was taken 0.1g (Jussila and Fülöp, 2013)

The same RB type studied in SESA, has been modelled independently by TVO, and the following comparative observations were noted. While the SESA model had 222 425 tons, TVO's model was about 13% heavier. Some additional structural elements were also present in TVO's model. The frequencies from the two models are summarized in Table 3. Based on the comparison it can be concluded that the models, while not identical, are reasonably close for general comparison of results.

Table 3. Summary of natural frequencies comparing VTT's and TVO's models (Jussila et al., 2014)

Mode No.	Direction	Frequency [Hz] - VTT	Frequency [Hz] - TVO
1	Y	3.20	3.94
2	X	3.59	4.11
3	Z	5.93	7.10
8	Torsion	5.50	5.78

For the evaluation of floor spectra, nodes on different floors, with different horizontal position relative to the external walls and to vertical supporting elements (i.e. walls, beam, and columns) have been monitored. At start nodes were selected based on engineering judgment, but later it was shown that this may not be sufficient to represent the floor loads accurately. In horizontal direction the concept of node eccentricity was introduced as follows: $e=1$ near the external walls and $e=0$ at centre of floor layout. As it can be seen in Figure 5.a, horizontal acceleration of the floor nodes strongly correlates with eccentricity. At the mid-span of any given floor, accelerations can be two times higher compared to near-wall locations. On the other hand, horizontal accelerations correlate less with the height (Figure 5.a & b). In vicinity of the external walls, accelerations are practically independent of the floor level. In mid-span nodes some dependency on height can be observed (Figure 5.b). The RB is a stiff wall and flexible floor system from the point of view of vibration transmission.

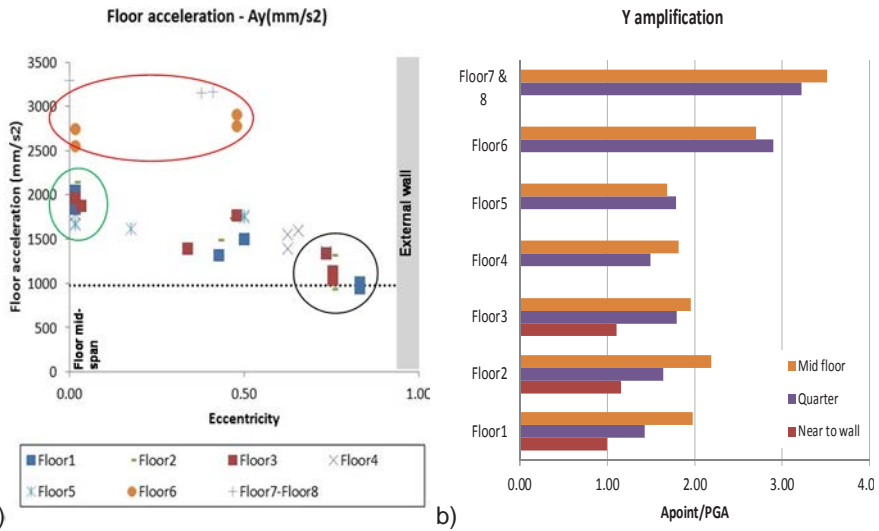


Figure 5. (a) Variation of the floor acceleration in horizontal direction as function of the eccentricity (e) and floor height and (b) in the vertical direction

The observed acceleration amplifications (A_{node}/PGA) are in line with previously obtained values, ranging between 1...3 (Figure 5.b). It can also be noticed that partial floors introduce significant flexibility in the system, amplifying accelerations. In the RB case, Floor 6, 7 and 8 span only half the width in the Y direction, resulting in significant amplification in these floors for Y direction shaking.

It became obvious that engineering judgment is insufficient to choose nodes in order to cover the possible amplifications of the floor vibration. It has been decided to automate the process, and carry out statistical analysis of the floor node responses. For each floor an approximate grid of 2m×2m has been used where output was generated. For the 4th floor this means 416 node outputs to be analyzed (Figure 6).

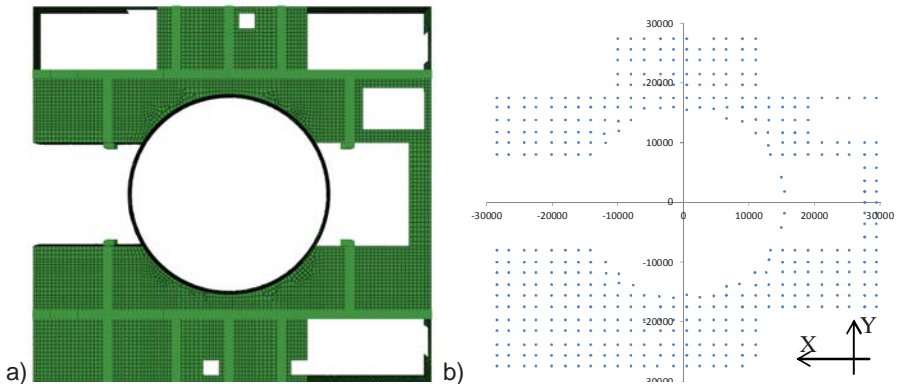


Figure 6. (1) Layout of 4th floor (b) and the set of 416 nodes where accelerations were monitored

First the acceleration outputs in 3 directions (X, Y, Z) were collected from the nodes, than the pseudo-acceleration (PSA) spectra were calculated from the 3x416 acceleration signals in 100 log10 spaced frequencies between 0.1 and 100Hz. Finally peak acceleration, the peak spectral response and the frequency at which it occurs were summarized in a file for all 3x416 signals.

A full map of the acceleration and PSA values for all nodes on the 4th floor is providing a better understanding of the acceleration concentrations (Table 4, Figure 7). It can be observed that, for horizontal accelerations, the main source of concentration are the flexible parts of the floors in the middle section of the building, while for the vertical components it is the middle spans of the floors.

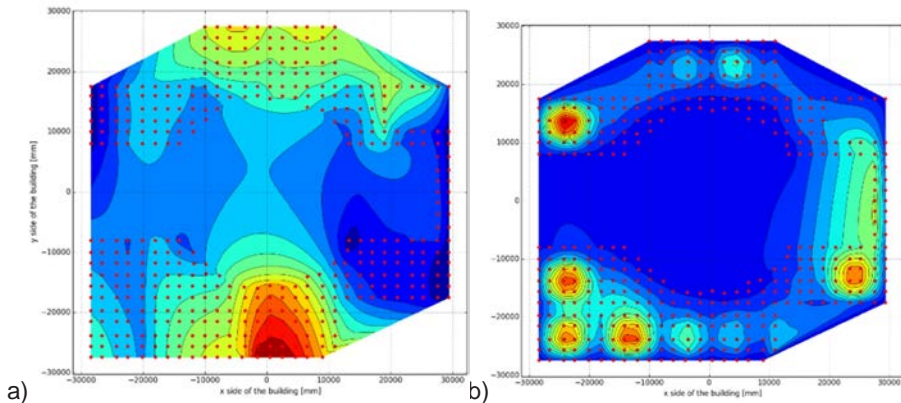


Figure 7. Distribution of accelerations and PSA's on the 4th floor (YVL-Set1-Damp2). Accelerations in the Y direction (a) and Z direction (b)

Table 4. Statistical parameters of the 4th floor accelerations (Jussila et al., 2014)

	Function parameters (General extreme value distribution)			Mean	ST Dev	C.O.V.	P(95%) ExtValDist	0.95x416= 396th value (P95%)
	k	σ	μ					
A _x	0.169	172.5	1359.1	1493	294	0.20	2024	2157
A _y	-0.1909	181.6	1517.5	1593	192	0.12	1929	1922
A _z	0.2313	744.8	1966.1	2614	1473	0.56	5147	5342
PSA _x	-0.0266	380.9	7824.8	8035	472	0.06	8913	8902
PSA _y	-0.05400	168.9	5413.5	5502	203	0.04	5877	5907
PSA _z	0.3139	4091.3	8897.2	13076	10468	0.80	28977	32392

Extending the study of the results to the full range of frequencies between 0.1 and 100Hz, we can obtain the pseudo-acceleration plots from the 416 nodes (Figure 8). Validity of the plots is limited up to 30Hz due to the choice of damping. It can be noticed that, at the 4th floor level the spectral peak corresponding to the natural (1st)

mode of vibration is the highest in the mean curve. The response corresponding to the natural frequency is also very homogeneous on the entire floor. However, there is uncertainty (variability) in the horizontal response in the frequency range above 5Hz, resulting in higher values of PSA if the 95 percentile curves are compared. The situation is different for vertical vibration, where the variability of responses is present o the full range of frequencies.

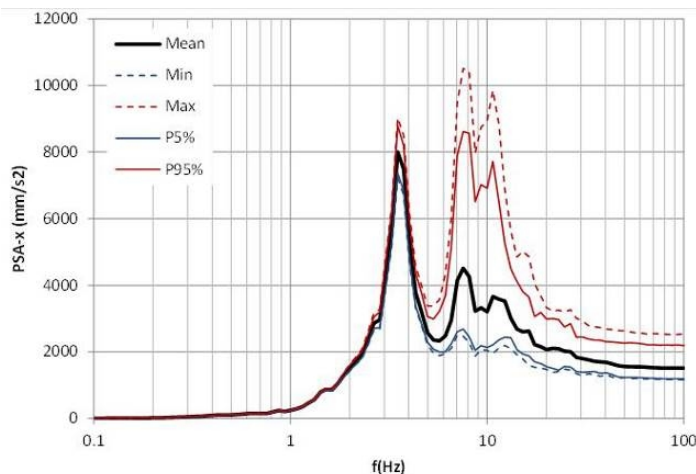


Figure 8. Results of the 416 node data on the full range of frequencies (X direction)

The study of the RG building has been extended to non-linear modeling in order to estimate the equivalent damping due to the micro cracking of the concrete in tension (Jussila and Fülöp, 2014a).

Qualification of complex components

Qualification of complex equipment has been explored concentrating on general provisions (Fülöp, 2013), qualification methods (Jussila and Fülöp, 2014b) and exploratory example of an emergency diesel generator (EDG) fuel tank (Jussila and Fülöp, 2014c).

Potential applicability of the results

The seismological work in SESA provided important update on understanding of seismic hazard. The collected database is an important asset the project will leave behind, giving the possibility to further refine the GMPE's developed. This is already happening; with new data inputs added to the database from Sweden. The practical use of the data and of the GMPE's is underway when estimating hazard of the Pyhäjoki site.

The deaggregation studies contributed to a better understanding the nature of the seismic activity contributing to the hazard in Finland. It appears that mid-magnitude

events ($M \sim 3 \dots 5$), hosted at near-site locations ($< 70 \text{ km}$) contribute most significantly to the seismic hazard.

Based on the extensive modeling of the generic building it can be concluded that horizontal direction floors spectra is controlled by fundamental frequency of the structure. Since reactor structures have fundamental frequency in the range of 3-5 Hz, the spectral amplitude in this range is very important. It is not the PGA which controls floor spectra amplitudes, and the low spectral amplification in the 3-5 Hz range in Finland is an important advantage. For higher frequency ranges of the floor spectra (6-20 Hz), the ground spectra shape plays a smaller role since a typical amplification on rock is close to 2-2.2.

Acknowledgements

The authors wish to express their gratitude to the active Ad-Hoc group of the SESA project. Challenging, stimulating, sometimes contradicting discussions took place in 17 meetings, with valuable contributions to steering SESA. The role of strengthening research networks on seismic safety studies in Finland resulted in several planned and ongoing projects. These contributions are gratefully acknowledged.

References

- ASCE 4-98 (2000). Seismic analysis of safety-related nuclear structures and commentary (Reston, Va: American Society of Civil Engineers).
- Assatourians, K., and Atkinson, G. (2012). EqHaz.
- Atkinson, G.M., and Boore, D.M. (2006). Earthquake Ground-Motion Prediction Equations for Eastern North America. *Bull. Seismol. Soc. Am.* 96, 2181–2205.
- Atkinson, G.M., and Boore, D.M. (2011). Modifications to Existing Ground-Motion Prediction Equations in Light of New Data. *Bull. Seismol. Soc. Am.* 101, 1121–1135.
- Bender, B., and Perkins, D.M. (1987). SEISRISK III: A Computer Program for Seismic Hazard Estimation (Washington: United States Government Printing Office).
- Fülöp, L. (2012). Seismic design of NPP's versus practice for ordinary structures (Espoo: VTT Technical Research Centre of Finland).
- Fülöp, L. (2013). Codes of practice guiding qualification of components in NPP (Espoo: VTT Technical Research Centre of Finland).

- Jussila, V., and Fülöp, L. (2013). Principles and practice of exploiting beyond elastic-response reserves in structures (Espoo: VTT Technical Research Centre of Finland).
- Jussila, V., and Fülöp, L. (2014a). Damping estimates based on the level of non-linear response in stiff concrete buildings (Espoo: VTT Technical Research Centre of Finland).
- Jussila, V., and Fülöp, L. (2014b). Variability of targets for component qualification with structural response (Espoo: VTT Technical Research Centre of Finland).
- Jussila, V., and Fülöp, L. (2014c). Seismic qualification of complex equipment by combined analysis and testing (Espoo: VTT Technical Research Centre of Finland).
- Jussila, V., Li, Y., and Fülöp, L. (2014). Sensitivity of NPP building structural response (Espoo: VTT Technical Research Centre of Finland).
- Korja, A., and Kosonen, E. (2014). Evaluating seismic hazard for the Hanhikivi nuclear power plant. Part 2. Seismotectonic framework and models in the northern part of the Fennoscandian Shield. (Helsinki: Institute of Seismology, University of Helsinki).
- KTA (2005). Recommendations regarding the application of KTA safety standards considering current structural engineering standards.
- KTA (2011). Design of Nuclear Power Plants against Seismic Events; Part 1: Principles (KTA-Geschaefsstelle c/o Bf).
- L. Danciu, M. Pagani, D. Monelli, and S. Wiemer (2010). GEM1 Hazard: Overview of PSHA Software (Pavia, Italy: GEM Foundation).
- L. Fülöp, I. Smedberg, T. Tiira, P. Mäntyniemi, P. Heikkinen, M. Malm, N. Leso, J. Saari, J. Puttonen, and V. Jussila (2013). Seismic safety of nuclear power plants: targets for research and education (SESA). In: SAFIR2014, The Finnish Research Programme on Nuclear Power Plant Safety 2011-2014, (Interim Report), Ed. K. Simola. VTT Technol. 80, 373–380.
- Malm, M., and Saari, J. (2014a). SESA, Subproject 1 - Earthquake Hazard Assessment, Progress Report 2013 (ÅF-Consult Ltd).
- Malm, M., and Saari, J. (2014b). SESA, Subproject 1 - Earthquake Hazard Assessment, Progress Report 2014 (ÅF-Consult Ltd).
- Malm, M., Leso, N., and Saari, J. (2013). SESA Subproject 1 - Earthquake Hazard Assessment, Progress Report 2012 (ÅF-Consult Ltd).

- Ordaz, M., Aguilar, A., and Arboleda, J. (2007). CRISIS2007 Help File.
- Pezeshk, S., Zandieh, A., and Tavakoli, B. (2011). Hybrid Empirical Ground-Motion Prediction Equations for Eastern North America Using NGA Models and Updated Seismological Parameters. *Bull. Seismol. Soc. Am.* 101, 1859–1870.
- Saari, J., Heikkinen, P., Varpasuo, P., Malm, M., Turunen, E., Karkkulainen, K., Valtonen, O., and Uski, M. (2009). Estimation of Seismic Hazard in Territory of Finland (ÅF-Consult).
- Silva, W., Gregor, N., and Darragh, R. (2002). Development of regional hard rock attenuation relations for central and eastern North America (El Cerrito: Pacific Engineering and Analysis).
- Smedberg, I., Malm, M., Saari, J., and Heikkinen, P. (2011). SESA Subproject 1 - Earthquake Hazard Assessment, Progress Report 2011 (Institute of Seismology, University of Helsinki & ÅF-Consult).
- Smedberg, I., Uski, M., Tiira, T., Komminaho, K., and Korja, A. (2012a). Intraplate earthquake swarm in Kouvola, south-eastern Finland. In *EGU General Assembly Conference Abstracts*, p. 8446.
- Smedberg, I., Uski, M., Tiira, T., Korja, A., and Komminaho, K. (2012b). Shallow swarm-type earthquakes in south-eastern Finland. In *The 43rd Nordic Seismology Seminar*, (Tallinn).
- Stewart, J., Douglas, J., Javanbarg, M.B., Di Alessandro, C., Bozorgnia, Y., Abrahamson, N.A., Boore, D.M., Campbell, K.W., Delavaud, E., Erdik, M., et al. (2013). GEM-PEER Task 3 Project: Selection of a Global Set of Ground Motion Prediction Equations (Pacific Earthquake Engineering Research Center).
- Tiira, T., and Heikkinen, P. (2014). SESA, Subproject 1 - Earthquake Hazard Assessment, Progress Report 2013 The SESA data bank and new empirical attenuation functions for Finland (Helsinki: Institute of Seismology, University of Helsinki).
- Uski, M., and Tuppurainen, A. (1996). A new local magnitude scale for the Finnish seismic network. *Tectonophysics* 261, 23–37.
- Varpasuo, P., Nikkari, Y., and Saari, J. (2000). Estimation of seismic hazard in territory of southern Finland (Fortum Engineering Ltd).
- YVL 2.6 (2001). Seismic events and nuclear power plants.

40. Extreme weather and nuclear power plants (EXWE)

40.1 EXWE summary report

Kirsti Jylhä, Hilikka Pellikka, Matti Kämäräinen, Milla Johansson, Seppo Saku, Pauli Jokinen, Kimmo Kahma, Ari Venäläinen, Hilppa Gregow

Finnish Meteorological Institute (FMI)
P.O. Box 503, FI-00101 Helsinki

Abstract

Very rare weather phenomena that trigger extreme sea level variations, abundant freezing rain or excess coastal snowfall, very cold spells or hot and humid episodes, need to be included in the risk calculations of the nuclear power plants. We studied the occurrence of these extreme events and their expected changes in the future by investigating quality controlled observations of the Finnish Meteorological Institute, archives of non-digitized data, reanalysed weather data sets as well as output from regional and global climate models. According to the results, climate change has more obvious impacts on extreme temperatures than on daily precipitation amounts from freezing rain in coastal areas or coastal (lake-effect) snowfall. Due to the complexity of studying these precipitation events, methodological progress was needed. This was true also for meteotsunamis that appear as sudden variations of sea level. None of the studied sites (Loviisa, Olkiluoto, Hanhikivi) seems to be particularly vulnerable to meteotsunamis.

Introduction

Exceptional weather and sea level phenomena may prevent normal operation at nuclear power plants and in some cases lead to a reactor trip. Adverse weather events may affect the safety of nuclear power plants also indirectly, e.g. by causing injuries and damages in the transport sector. Therefore, safety management over the life cycle of a nuclear power plant (NPP) requires evaluation of external events

triggered by rare weather and sea level conditions (YVL B.7, 2013). Estimates of probabilities of weather-related hazards are used as design basis and in the Probabilistic Risk Assessment (PRA) of NPPs (YVL A.7, 2013).

In the SAFIR2014 programme, extreme weather, climate and sea level events potentially posing risks to NPPs have been examined in the EXWE project, originally launched in 2007 within SAFIR2010. This summary and the accompanied special article (Jylhä *et al.*, 2015a, this volume) give the key findings of the project.

Main objectives

The primary objective of the project is to support the overall safety of nuclear power plants. New knowledge is acquired about the occurrence and probabilities of weather and sea level phenomena that affect the design principles of the power plants and might pose external threats to the plants. In SAFIR2014, special emphasis was put on occurrences and trends of freezing rain, intense coastal (lake-effect) snow, extreme temperatures, mean sea level scenarios and meteorological tsunami waves. Due to the complexity of the studied phenomena, methodological development work was required.

Development of methods for studying extreme events

Extreme weather phenomena that have never or only very seldom been detected in observations pose challenges for climate researchers. Extreme value analysis, discussed by Jylhä *et al.* (2015a), makes it possible to give best estimates and confidence intervals for probabilities of events that are more extreme than those actually observed. Besides relatively short observational time series, there are also other challenges. The network of weather stations is rather sparse and only covers land areas. The output data from climate models typically have relatively coarse spatial and temporal resolutions, and deficiencies in reproducing the current climate. Consequently, estimates of the occurrences of very rare phenomena, if derived from raw model output statistics, are likely to fail.

We developed or applied the following methods to alleviate these difficulties:

- Selecting criteria for distinguishing severe weather events primarily based on 3-hourly reported weather codes at manually operated FMI weather stations.
- Selecting and testing of predictors for the identification of hazardous weather cases in model runs.
- Statistical downscaling of output from coarse-resolution global climate models (CMIP5) to local scales using a bias correction method originally developed by Räisänen *et al.* (2012).
- Use of dynamically downscaled climate model data (regional climate models)
- Use of reanalysis data and millennium-long climate model simulations.

The selected criterion for a significant case of freezing rain was "at least four weather stations in Finland reporting moderate or heavy freezing rain during a day". For

significant lake-effect snow cases, the criteria were more complicated. The identified past significant cases in Finland were utilized to find optimal predictors of extreme weather events in reanalysis data sets. After selecting the combinations of predictors, these were applied to output from climate model experiments in order to find out how often the simulated meteorological situations favour formation of freezing rain or lake-effect snowfall. Using the results, approximate probability distributions of the occurrences of freezing rain and lake-effect snowfall could be constructed (for details, see Kämäräinen and Jokinen, 2015).

Freezing precipitation and lake-effect snowfall

Freezing precipitation is supercooled liquid rain falling and freezing on surfaces upon impact (Fig. 1a). The observed amounts of freezing precipitation in Finland are usually modest. The maximum, unverified record that presumably also included non-freezing precipitation is 22 mm in a day (Kauhava in 1968). About 30 mm or more of freezing rain may result in collapses of power lines but even smaller amounts of ice can affect the reliability of energy supply (Karttunen et al., 2013). In Europe several severe cases of freezing precipitation have occurred during the past ten years, e.g., in the Moscow district in 2010 (Mekhanoshin, 2012) and in Slovenia in 2014 (Markosek, 2014).

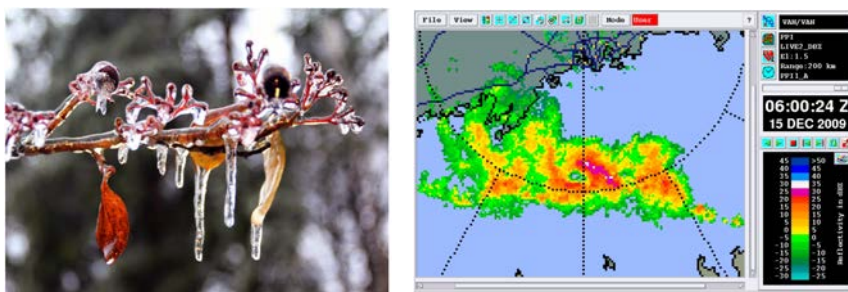


Figure 1. (a) Icicles on a tree branch after freezing rain in Kajaani on 24.-25.10.2014 (photo: J. Kämäräinen). (b) FMI Weather radar observations of a lake-effect snowfall case over the Gulf of Finland on 15.12.2009.

Using CORDEX regional climate model data and the filters discussed above, cumulative probability distributions of precipitation amounts due to freezing rain were constructed for Loviisa, Olkiluoto and Hanhikivi (Fig. 2). Because data from 13 models, two emission scenarios, 40x365 days and 25 grid cells for each NPP sites were put together, the analysed cases total to 10^7 , a large majority of them without identified freezing rain. Some freezing rain was identified in about 2% of all cases and more than 10 mm/d of freezing rain in about 0.1% of the cases.

The results suggest that very severe freezing rain events, exceeding 30 mm/d, will remain highly unlikely at the three sites, although their probabilities seem to

increase due to the projected changes in climate. Otherwise the distributions for the periods 1971-2010 and 2060-2099 differ very little. A possible explanation is that the effects of decreases in the number of below-zero days near the coast, changes in vertical temperature profiles and increases in the atmospheric moisture compensate each other.

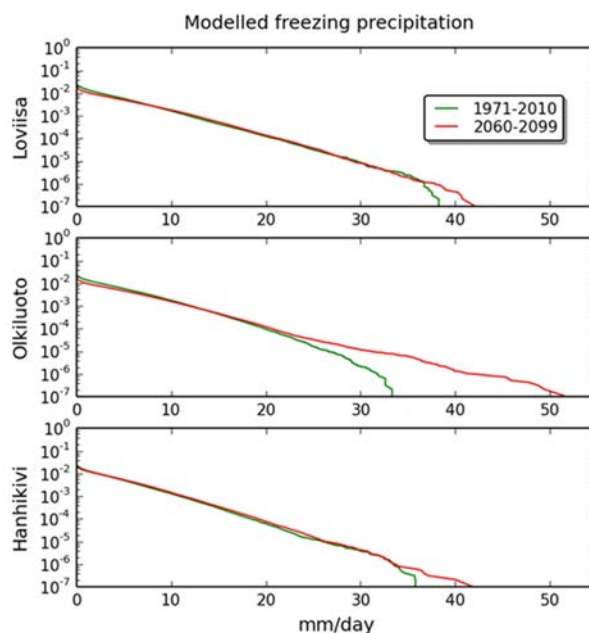


Figure 2. Estimated complementary cumulative distributions of daily precipitation amounts due to freezing rain at three coastal locations in Finland in the present-day and end-of-century climates. Note that the days with no identified freezing rain are included in the daily probability distributions of exceedance.

Intense coastal snowfall may occur if the air flowing over the Gulf of Finland or the Gulf of Bothnia is considerably colder than the ice-free sea water. The name of lake-effect snowfall originates from the North American Great Lakes region. With southerly or easterly wind directions snowbands generated over the Gulf of Finland can drift over the coasts of southern Finland (Fig. 1b). Respectively, with north-easterly or easterly winds the snowbands can drift over the coasts of Sweden. For example, in December 1998 in Gävle, Sweden, a metre of snow was recorded (Savijärvi, 2012). Snowbands generated over the Gulf of Finland contributed to multiple car accidents in the Helsinki region in February 2012 (Mazon et al., 2015).

By applying the predictors of lake-effect snow to gridded historical model data (ERA-Interim reanalysis), it was possible to construct a climatological map about the frequencies of lake-effect snowfall over the Baltic Sea. Based on it, lake-effect snowfall is more common over the warmer North Gotland Basin (west of Estonia) than over the colder Gulf of Finland and the Gulf of Bothnia. Less sea ice in the future (Luomaranta et al., 2014) could be expected to cause more opportunities to lake-

effect snowing also in the latter sea areas. However, forming of snowbands over the sea also requires outbreaks of cold air. The lengthening of the ice-free season in the future may not be sufficient to overcome the effect of reductions of cold air outbreaks in the warming climate. This is suggested by the fact that the estimated amounts of lake-effect snow in millimetres were slightly smaller for the end-of-century climate than for the present-day climate.

Extreme temperatures

The annual mean temperature in Finland has increased very likely over 2°C during 1847–2013. The warming has been particularly strong in November, December and January, but smaller in July, August and September (Mikkonen et al. 2014). The findings in EXWE for extreme temperatures are in consistency with these reported changes. Based on the longest available time series (75-165 years) at 30 locations in Finland, the annual minimum temperature has increased statistically significantly at half of the sites studied. The same is true at few stations for the annual maximum temperatures. However, the annual frequency of daily maximum temperatures higher than 23°C have increased statistically significantly at 10 out of 30 locations during the period 1961-2010. The increases in high summertime temperatures that persist for 7 days were statistically significant at 5 out of 8 stations. (Jylhä et al. 2015b)

In the future, spells of warm and hot weather are projected to get longer and more intense. For example, the annual maximum length of a hot spell during which temperature persists above 27°C has typically been about 3-5 hours in southern and central Finland in 1980-2009, and about 11 hours at the longest (Fig. 3). Based on scenario data on hourly basis (Ruosteenoja et al. 2013), around the year 2050 a typical length would be 8-9 hours and an extreme length a few hours more.

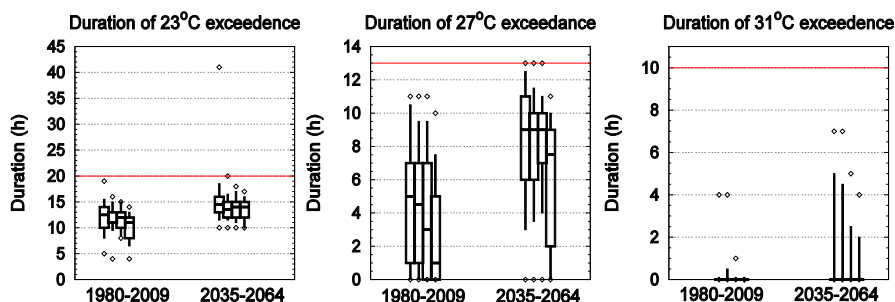


Figure 3. Annual maximum duration of spells with air temperature higher than 23°C (left), 27°C (middle) or 31°C at four sites in Finland (from left to right: Vantaa, Jokioinen, Jyväskylä, Sodankylä). The results for 1980-2009 are based on observations, while those for 2035-2064 on model projections, assuming the SRES A2 emissions scenario. In each column of values are shown (from bottom to top) the minimum, the 10th, 25th, 50th, 75th and 90th percentiles and the maximum during 30 years. The red horizontal lines show the observed durations in Joensuu on 29 July 2010.

In Joensuu on 29 July 2010 the air temperature was continuously higher than 31°C for ten hours (red lines in Fig. 3). According to the future scenarios, such a hot spell would not occur at the four study sites even decades ahead. This indicates how extraordinary the record-breaking temperatures were in 2010. It also tells about uncertainties related to the quantitative future estimates. The greatest uncertainty in short-term climate projections originates from natural variability of climate. In the long run, the main uncertainties are related to deficiencies of climate models and to the future evolution of greenhouse gas emissions.

Sea level rise and coastal flooding risks

The probability of extremely high sea levels can be expressed as a combination of two factors: the mean sea level and the short-term sea level variability. The sea level studies in EXWE have addressed these two issues, as well as methods for combining them, to yield estimates for the exceedance probabilities of high sea levels now and in the future.

Long-term changes in mean sea level on the Finnish coast are mainly regulated by two counteracting phenomena: global sea level rise and postglacial land uplift. Sea level rise is mainly caused by the thermal expansion of sea water and the melting of glacier ice in the warming climate. Regionally, sea level rise on the Finnish coast is expected to be somewhat lower than globally (approximately 80% of the global mean), particularly due to gravitational and crustal changes resulting from the melting of the Greenland ice sheet (Johansson et al. 2014).

According to a combination of several global sea level rise predictions, adjusted to take into account regional effects, the 5–95 % probability range of regional sea level rise in 2000–2100 is +24 to +126 cm in the Gulf of Finland, +24 to +122 cm in the Bothnian Sea, and +24 to +115 cm in the Bothnian Bay (Johansson et al. 2014). These ranges do not include land uplift. The largest source of uncertainty is the fate of the West Antarctic ice sheet (WAIS) in the warming climate. WAIS is mainly grounded below sea level, which allows positive feedback mechanisms if the ice sheet starts to retreat. The potential instability of WAIS may result in an additional sea level rise compared to the predictions given by IPCC (2013), even though this is considered unlikely. The WAIS instability has been taken into account in the EXWE scenarios by including an ensemble of sea level rise predictions, many of them higher than the IPCC estimate.

Changes in the wind climate are also expected to result in a small additional sea level rise on the Finnish coast. Johansson et al. (2014) showed that 84–89% of the year-to-year variations of annual mean sea levels on the Finnish coast are explained by variations in westerly wind conditions over the southern Baltic Sea. Westerly winds generally drive water from the North Sea into the Baltic Sea and towards the northeastern part of the Baltic Sea basin.

The net effect of regional sea level rise, postglacial land uplift and changes in the wind climate is estimated to result in relative sea level rise in the Gulf of Finland, while in the Gulf of Bothnia land uplift will probably still outweigh sea level rise during

the 21st century (Fig. 4). However, highest scenarios predict rising mean sea level everywhere on the Finnish coast, the upper limit being nearly 1 m above the present mean in the Gulf of Finland.

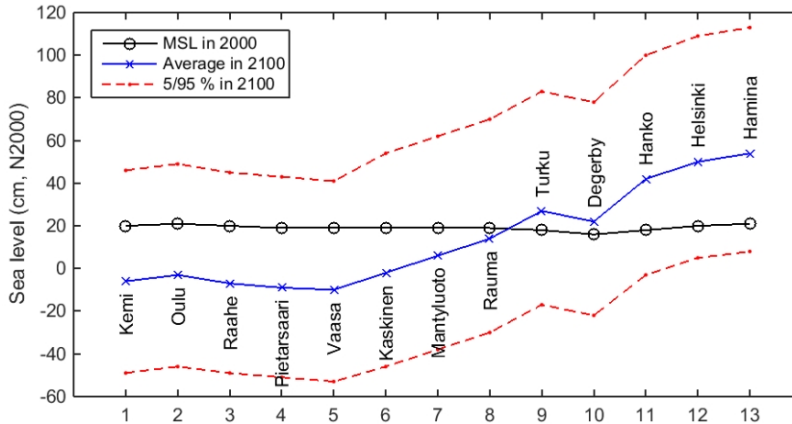


Figure 4. Scenarios for mean sea level at the Finnish tide gauge stations in 2100 compared to the estimated mean sea level (MSL) in 2000 (Johansson *et al.* 2014). The best estimate is marked with blue, uncertainty ranges with red.

Leinonen and Kahma (2013) analysed the success of global sea level rise scenarios published in the 1980s. Comparing the first 20–30 years of these scenarios with the observed sea level rise since 1980s gives some insight into how well the current scenarios might be able to predict future sea level rise. About 70% of the scenarios predicted faster sea level rise than what has been observed, and it is evident that the highest scenarios in the 1980s were gross overestimates.

Short-term sea level variability on the Finnish coast is mainly controlled by wind and air pressure variations. The probabilities of high sea levels have increased on the Finnish coast during the 20th century, the increase being most evident in winter-time (Johansson, 2014). At least part of these changes is related to wind conditions over the Danish Straits, which regulate the Baltic Sea water balance.

The new sea level scenarios, together with information on the short-term variability, allow refined estimates for the occurrence of high sea levels in the future. New estimates of flooding risks on the Finnish coast and recommendations for minimum building elevations for conventional buildings are given by Kahma *et al.* (2014).

Meteotsunamis

Meteotsunamis, or meteorological tsunamis, are a hazard whose existence on the Finnish coast was rediscovered after several eyewitness reports of such phenomena in 2010–2011. Meteotsunamis are tsunami waves generated by exceptionally rapid air pressure disturbances (e.g. thunderstorms) moving above the sea at a speed that

matches the tsunami wave speed in the sea. On the coastline, meteotsunamis appear as exceptionally rapid and strong sea level variations (up to 1 m in 5–15 minutes during the events reported by eyewitnesses; Pellikka *et al.* 2014a). The strongest known meteotsunamis in the world have been 5–6 m high, but such waves can only occur in certain places with a vulnerable coastal topography.

To investigate the frequency of meteotsunamis in Finland, and eventually to be able to estimate their probability, the research in EXWE has concentrated on identifying past meteotsunami events in sea level data. Before the 1980s, the only source of data with a sufficiently high time resolution are the original tide gauge charts, on which sea level variations have been plotted as a continuous curve. Dozens of small potential meteotsunamis were identified in the charts of the Hanko and Hamina tide gauges from the 1920s to 1979 (Fig. 5). Most of the cases were confirmed with air pressure data. There is no clear trend in their occurrence, rather decadal variability.

The detected meteotsunamis are small, generally 10–40 cm high (crest to trough). However, because their strength strongly depends on coastal topography, higher oscillations may have taken place even though they are not observed at the tide gauges. To study the vulnerability of NPP sites to meteotsunamis, refraction modeling has been carried out. The refraction model can be used to resolve the large-scale concentrations of wave energy caused by coastal bathymetry. Based on the results, none of the studied sites (Loviisa, Olkiluoto, Hanhikivi) are particularly vulnerable to meteotsunamis (Pellikka *et al.* 2014b), and the probability of a strong meteotsunami occurring there is very small. To bring the probability estimate on a firmer basis is a priority in future works.

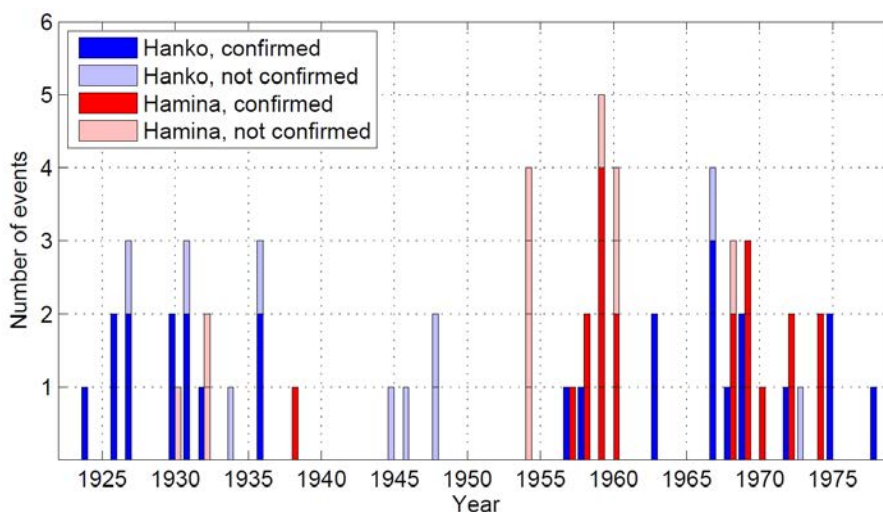


Figure 5. The number of potential meteotsunami events per year (in May–October) detected in the tide gauge charts of Hanko and Hamina. The events plotted with darker colours have been confirmed with air pressure data, the rest have not been confirmed due to lack of data.

Conclusions

- New methods need to be developed and adopted in order to assess probabilities of exceptional or unprecedented extreme weather and sea level phenomena.
- Hot spells are projected to get longer and more intense in the future.
- Very severe freezing rain and lake-effect events, based on the current results, will remain very unlikely at the Finnish NPPs sites, but more research is needed.
- Sea level rise predictions involve large uncertainties, and it is important to update the scenarios regularly based on the most recent knowledge. New, improved estimates of sea level rise and future flooding risks on the Finnish coast have been published.
- Meteotsunamis are much more common on the Finnish coast than has been previously known. They are predominantly small, however, and highest oscillations are restricted to topographically vulnerable places. None of the Finnish NPPs seem to be located in meteotsunami hotspots.

References

- IPCC, 2013: Summary for Policymakers. In: *Climate Change 2013: The Physical Science Basis. Contribution of Working Group I to the Fifth Assessment Report of the Intergovernmental Panel on Climate Change* [Stocker, T.F. & coauthors (eds.)]. Cambridge University Press, Cambridge, United Kingdom and New York, NY, USA.
- Johansson, M.M. 2014. Sea level changes on the Finnish coast and their relationship to atmospheric factors. *Finnish Meteorological Institute Contributions* 109, 132 p
- Johansson, M.M., Pellikka, H., Kahma, K.K. & Ruosteenoja, K., 2014. Global sea level rise scenarios adapted to the Finnish coast. *Journal of Marine Systems* 129, 35–46.
- Jylhä, K., Saku, S. & Venäläinen, A. 2015a. High specific enthalpy in the recent and projected future climate of Finland. Special report on the EXWE project, this volume.
- Jylhä K., Pellikka, H., Kämäräinen, M., Johansson, M., Saku, S., Jokinen, P., Kahma, K., Venäläinen, A. & Gregow, H (eds.) 2015b. Extreme weather and sea level events as potential external threats to nuclear power plant safety — Synthesis of the EXWE project outcomes in 2011-2014. EXWE project report. Finnish Meteorological Institute.
- Kahma, K., Pellikka, H., Leinonen, K., Leijala, U. & Johansson, M., 2014. Pitkän aikavälin tulvariskit ja alimmat suositeltavat rakentamiskorkeudet Suomen rannikolla. *Ilmatieteen laitos, Raportteja* 2014:6. 48 p.

- Karttunen, V. Halonen, M., Vanhanen, J., Raivio, T., Lunabba, J., Gregow, H., Saku, S., Jokinen, P., Lehtonen, I., Ruosteenoja, K., Pellikka, H., Vainio, J., Tanskanen, E., Peitso, P., Laitinen, T., Viljanen, A. & Hynönen, R. 2013. Äärevien sää- ja avaruussääilmiöiden vaikutus kriittisiin infrastruktuureihin. Huoltovarmuuskeskuksen raportteja. 2013.
- Kämäräinen, M. & Jokinen, P. 2015. Severe winter weather in Finland: Part II: Freezing rain and lake-effect snowfall. FMI, EXWE project report.
- Leinonen, K. and Kahma, K., 2013. 1980-luvulla tehtyjen merenpinnan noususkenaarioiden osuvuus. Finnish Meteorological Institute. EXWE report.
- Luomaranta, A., Ruosteenoja, K., Jylhä, K., Gregow H., Haapala J., & Laaksonen A. 2014. Multimodel estimates of the changes in the Baltic Sea ice cover during the present century. *Tellus A* 2014, 66, 22617.
- Markosek J. 2014. Severe freezing rain in Slovenia. A presentation in 20th WGCEF meeting, Geneva, 3 October 2014. Available at http://www.euroforecaster.org/presentations_2014/slo.pdf
- Mazon, J., S. Niemelä, D. Pino, H. Savijärvi & Vihma T. 2015. Snow bands over the Gulf of Finland in wintertime. *Tellus A* 67, 25102.
- Mekhanoshin, B., 2012: A severe ice storm in Russia leads to re-evaluation of ROW status and vegetation management practices. *T&D World Magazine*.
- Mikkonen, S., Laine, M., Mäkelä, H.M., Gregow, H., Tuomenvirta, H., Lahtinen, M. & Laaksonen A. 2014. Trends in the average temperature in Finland, 1847–2013. *Stoch Environ Res Risk Assess*. DOI 10.1007/s00477-014-0992-2
- Pellikka, H., Rauhala, J., Kahma, K.K., Stipa, T., Boman, H. & Kangas, A. 2014a. Recent observations of meteotsunamis on the Finnish coast. *Natural Hazards* 74, 197–215.
- Pellikka, H., Kahma, K., Boman, H., Karjalainen, A., Rauhala, J., Hohti, H., Pirinen, P., Tikka, K., Jokinen, H., Mäkelä, A., Gregow, H., Aalto, J. 2014b. Meteotsunamis on the Finnish coast. In: Jylhä *et al.* (2015b) (See above)
- YVL A.7, 2013: Regulatory Guides on nuclear safety (YVL): Probabilistic risk assessment and risk management of a nuclear power plant (A.7). <http://plus.edilex.fi/stuklex/en/lainsaadanto/saannosto/YVLA-7>
- YVL B.7, 2013: Regulatory Guides on nuclear safety (YVL): Provisions for internal and external hazards at a nuclear facility (B.7). <http://plus.edilex.fi/stuklex/en/lainsaadanto/saannosto/YVLB-7>

40.2 High specific enthalpy in the recent and projected future climate of Finland

Kirsti Jylhä, Seppo Saku and Ari Venäläinen

Finnish Meteorological Institute
P.O. Box 503, FI-00101 Helsinki

Abstract

Enthalpy of the air is a quantity typically considered when ventilation and cooling systems are designed. Based on air temperature, humidity and air pressure data recorded at three hour intervals during the past five decades, instantaneous values of enthalpy, as well as values above which enthalpy stays for 6 hours, 24 hours, 7 days or two weeks, were calculated at ten locations in southern and western Finland. For these five enthalpy indices, extreme value analysis was then carried out to assess recurrence levels that correspond to annual probabilities of 10^{-1} ... 10^{-3} , or to return periods of 10–1000 years. Values that are exceeded with an annual probability of 0.002 in the current climate conditions, on average ranged from 72 kJ kg^{-1} for the instantaneous enthalpy to 40 kJ kg^{-1} for the two-week enthalpy. Projections for changes in the enthalpy indices were made using model-based synthetic future weather data for temperature and humidity at four weather stations. According to these estimates, the return levels of enthalpy will increase by about 10 % by the middle of this century.

Introduction

The globally averaged temperature in 2014 was the highest among all years since record keeping began in 1880 (NOAA, 2015). Record warmth was spread around the world, including most of Europe. In Finland, 2014 was the second warmest year on record (FMI, 2015). Between May and August 2014, hot summer weather (temperatures exceeding $25 \text{ }^{\circ}\text{C}$) was recorded in some parts of the country in 50 days, which is 14 days more than the average. The daily maximum temperature was higher than $25 \text{ }^{\circ}\text{C}$ somewhere in Finland for 38 days without interruptions. With regard to individual weather stations, 26 consecutive days of hot temperatures were recorded at two stations in the Kuovola and Hattula regions (FMI, 2014). In the future, as the enhanced greenhouse effect proceeds, hot summer days will be increasingly common and periods of hot weather are getting longer (IPCC, 2013).

A long and exceptionally severe heat wave may pose external threats that need to be included in safety analysis of nuclear power plants. Besides affecting seawater temperature and thereby heat removal to the sea, hot and moist weather may impair the functioning of ventilation and cooling systems of electric and electronics equipment rooms. A thermodynamic quantity that is typically considered when ventilation

and cooling systems are designed is called the specific enthalpy. It increases with increasing air temperature and humidity, and slightly also depends on air pressure.

Knowledge about the persistence of high enthalpy values is of large importance for designing of the ventilation and cooling systems. Based on instantaneous measurements taken every three hours at five locations in Finland in 1956-2007, Venäläinen et al. (2009) considered five types of enthalpy extremes: the instantaneous highest value and the highest values that last at least six hours, 24 hours, one week or two weeks. The same five enthalpy indices were examined in the EXWE project by Jylhä et al. (2014). In order to have more observational data, the number of study locations was increased from five to ten. Jylhä et al. (2014) additionally constructed future climate change scenarios for enthalpy. This paper summarizes and somewhat extends that work. At first, data and methods are briefly described. Our results for probabilities of high enthalpy indices based on observations are then presented. We also assess the impacts of climate change on the occurrence of high enthalpy indices in the middle of this century.

Materials and methods

Moist air is a mixture of dry air and water vapour, the gas phase of water. Enthalpy of moist air is hence equal to the sum of dry air enthalpy and water vapour enthalpy (Rodrigues et al. 2010). The specific enthalpy (or in short: enthalpy) h (J kg^{-1}) of moist air can be calculated from

$$h = (c_{pd} + wc_{pv})T + wL \quad (1)$$

where T is temperature ($^{\circ}\text{C}$), w is the mixing ratio, c_{pd} is the heat capacity of dry air at constant pressure ($\text{J kg}^{-1} \text{K}^{-1}$), c_{pv} is the specific heat of water vapour at constant pressure ($\text{J kg}^{-1} \text{K}^{-1}$) and L is the latent heat of condensation ($\text{J kg}^{-1} \text{K}^{-1}$). Note that c_{pd} , c_{pv} and L slightly depend on the temperature. Here we adopted the values used by Sarkomaa et al. (2002).

Using the definitions of mixing ratio w and relative humidity RH (%), the equation of state of an ideal gas and an approximate dependence of the saturation water vapour pressure on temperature, (1) can be written as

$$h = c_{pd}T + g(p)f(T)F(T)RH \quad (2)$$

where p is air pressure and the functions g , f and F are as follows

$$g(p) = \frac{0.622 e_s(0)}{100 p}$$

$$f(T) = \exp\left(\frac{17.27T}{t+237.3}\right)$$

$$F(T) = c_{pv}T + L$$

The equation (2) indicates that the enthalpy is linearly dependent on RH and inversely dependent on p . The dependence on T is stronger and more complicated.

Two observational data sets were used in this study. The primary set consisted of synoptic weather observations of T , RH and p made in May–September 1961–2012 at intervals of three hours at ten measurement stations of the Finnish Meteorological Institute: Mariehamn, Vantaa, Hanko, Pori, Turku, Jokioinen, Utti, Kankaanpää, Kauhava and Oulu. Vantaa, Jokioinen, Jyväskylä and Sodankylä. The secondary observational data set consisted of hourly values for T and RH in 1980–2009 and climatological monthly mean air pressures at four stations: Vantaa, Jokioinen, Jyväskylä and Sodankylä. The hourly values were obtained by linearly interpolating the actual three-hourly observations.

The influence of human-induced climate change on the enthalpy indices by the middle of this century was assessed using synthetic future hourly data for T and RH . Potential changes in the air pressure were ignored. The data sets were produced by Ruosteenoja et al. (2013) using multi-model mean changes derived from 19 CMIP3 global climate models and the delta-change technique. The most important objectives of the procedure were 1) to minimize the influence of biases that commonly exist in climate model simulations; 2) to realistically describe temporal fluctuations of weather from day to day and hour to hour; and 3) to ensure that the statistical properties of the data sets are consistent with the climate model projections for changes in mean values and variability. The changes in enthalpy were calculated for the A2 SRES emission scenario that assumes no reductions in the increasing rate of greenhouse gas emissions into the atmosphere.

In this study we assessed values of the enthalpy indices that have the following annual probabilities of exceedance: 0.1, 0.01, 0.005 or 0.001. Ignoring any potential temporal changes, these correspond to return periods of 10, 100, 500 and 1000 years, respectively. For a 100-year period, the probability of at least one event exceeding the 100-year return level is 63%. The assessment was made with the aid of statistical distributions that were fitted to the data. This allowed us to estimate probabilities and related uncertainties for enthalpies that are higher and less likely to occur than those actually observed. Two widely used alternatives are the “sample block maxima” and the “peaks over threshold” (POT) methods. The block maxima asymptotically follow the generalized extreme value (GEV) distribution while events above a specified threshold asymptotically follow the generalized Pareto (GPD) distribution. Both distributions are characterized by shape, location and scale parameters; in this work they were regarded constant in time. We predominantly fitted the GPD distribution to the observed annual maxima of the enthalpy indices, defining the threshold separately for each station and enthalpy index. When the POT method is used to annual maxima, the emphasis is put on “real” extremes and the cases are evidently independent. The GEV distribution was in turn applied to assess future probabilities of extreme enthalpy indices. In the work, the functions `gev.fit` in the package `ismev` and `return.level` in the package `extRemes` in R were employed either through a graphical user interface or using R scripts.

Probabilities of high enthalpy indices based on observations

Based on air temperature, relative humidity and pressure data at ten weather stations in southern and western Finland in 1961–2012, the high enthalpy values persisting for two weeks are almost half smaller than the high transient values. This can be seen in Fig. 1 which shows for Pori, as an example, the five enthalpy indices as a function of annual probability of exceedance. The 95% confidence intervals, indicated by the vertical bars, partially overlap. Note that these confidence intervals are strongly asymmetric: the upper limit of the estimate deviates more notable from the best estimate than the lower limit does.

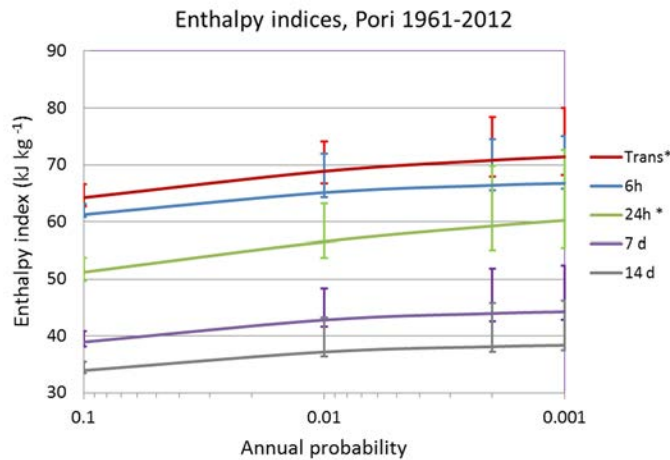


Figure 1. Return levels of the five enthalpy indices at Pori as a function of annual probability. The solid lines show the best estimates and the vertical bars indicate the 95% confidence intervals. An extreme value analysis based on the GEV distribution instead of GPD is indicated by an asterisk.

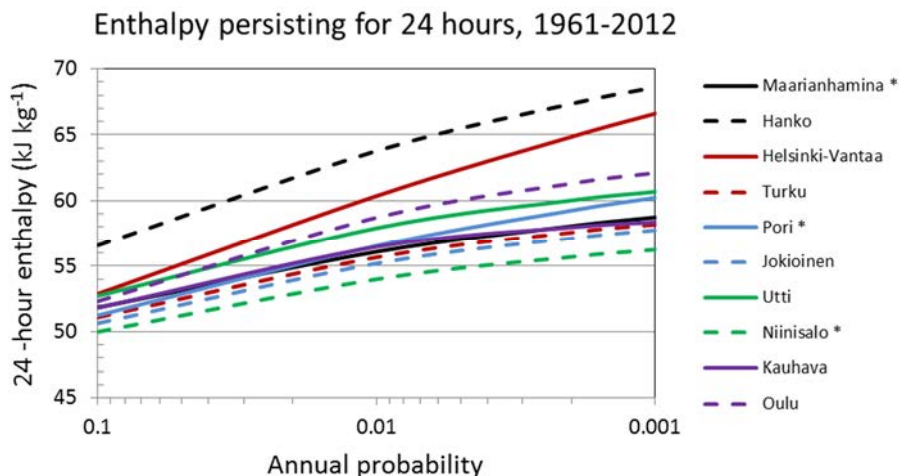


Figure 2. Best estimates for levels of enthalpy that are uninterruptedly exceeded for at least 24 hours. The results are shown for the ten study locations as a function of annual probability. An extreme value analysis based on the GEV distribution instead of GPD is indicated by an asterisk.

The best estimates and the 95 % confidence limits for the enthalpy indices, corresponding to the annual probabilities of 0.1, 0.01, 0.002 and 0.001, at the ten study locations are given by Jylhä et al. (2014), separately for each location and index. The scatter among the stations, in terms of coefficient of variation, was smallest (less than 2%) for the transient and 6-hour enthalpies having a 10-% chance of being exceeded during a year. Although the coefficient of variation appeared to increase with decreasing annual probability, for the 14-days enthalpies it was constantly 7%. The 24-hour enthalpies, shown in Fig. 2 for all the study locations, fall between the transient and 14-days enthalpies in terms of both of the absolute values and the relative differences between the locations. The highest 24-hour enthalpies can be found at Hanko and Vantaa, and the lowest at Niinisalo. Hanko also had the highest 7- and 14-days enthalpies but for the transient and 6-hour enthalpies there are no locations with consistently higher or lower values compared to the other sites.

Combining information about the best estimates and the 95% confidence intervals, Table 1 summarises the main observational-based results for the five enthalpy indices. The values are weighted averages of the best estimates at the ten weather stations in Finland. The larger the uncertainty in the extreme value analysis, the smaller the weight, and vice versa. More exactly, the weights are inverses of ratios between the 95% confidence intervals and the best estimates.

Based on Table 1, values that are exceeded with an annual probability of 0.002 in the current climate conditions, on average range from 72 kJ kg⁻¹ for the instantaneous enthalpy to 40 kJ kg⁻¹ for the two-week enthalpy.

Note that the values for maximum transient enthalpy may be slight underestimates due to the fact that air temperature and humidity were measured at intervals

of three hours only. Actual recordings of instantaneous daily maximum temperature would be available (see e.g., Saku et al. 2011) but long-term time series of relative humidity at the warmest moment of a day are missing.

Table 1. Five enthalpy indices tabulated as a function of their annual probabilities. The values are weighted averages of the best estimates at ten locations in Finland. The weights increased with increasing confidence in the extreme value analysis (see text for details).

Enthalpy index [kJ kg ⁻¹]	Annual probability			
	10 ⁻¹	10 ⁻²	2·10 ⁻³	10 ⁻³
Transient	64	70	72	73
6 hours	61	66	68	69
24 hours	52	57	59	60
7 days	40	44	46	47
14 days	35	39	40	40

Projected changes in air temperature and humidity by 2050

Based on the 19 CMIP3 climate models used in this study to examine enthalpy, the annual mean temperature in Finland is projected to increase at an average rate of about 0.3-0.4°C per decade within the next few decades. Around 2050, the target year of this study, the climatological (30-year averages of) monthly mean temperatures in May to September is estimated to exceed those in 1980-2009 by about 1.5 °C (Fig. 3, left). The summertime changes in relative humidity are small and even the sign of the change is uncertain (Fig. 3, right).

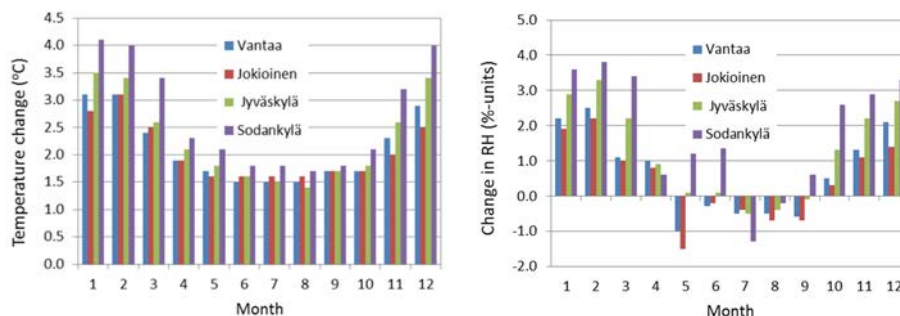


Figure 3. Projected 30-year mean changes in monthly (1: Jan, 12: Dec) mean temperature and relative humidity by 2050, relative to the mean of the reference period 1980-2009, at Vantaa, Jokioinen, Jyväskylä and Sodankylä under the A2 scenario.

Projected changes in the occurrence of high enthalpy

The enthalpy indices are likely to become higher in the future. This is first demonstrated by box-and-whisker plots of the observed and model-derived annual maxima of 6-hour and 14-day enthalpies at Jokioinen during three 30-year periods, a recent one (1980-2009) and two future time spans (Fig. 4). Considerable changes in the percentiles of the annual maxima can be expected already by the middle of this century.

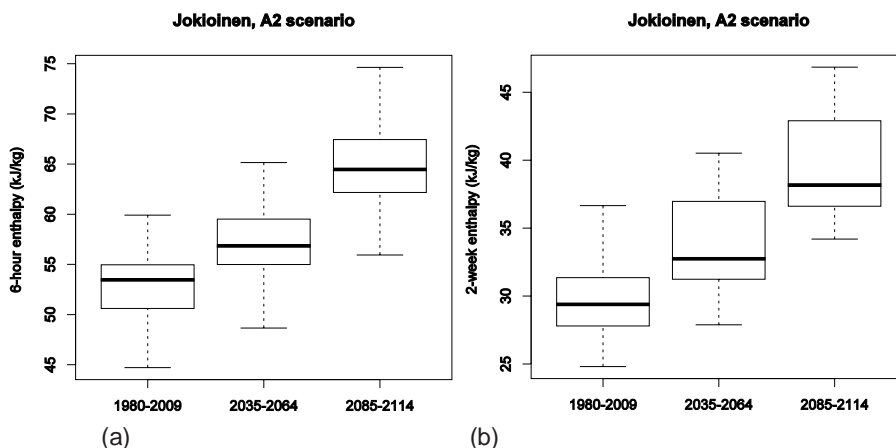


Figure 4. The box-and-whisker plots of annual maximum (a) 6-hour and (b) 2-week enthalpies at Jokioinen based on observations in 1980-2009 (left), and around the years 2050 (middle) and 2100 (right), based on model projections under the A2 scenario. Shown are the lowest maximum, the 25th, 50th and 75th percentiles, and the highest maximum. Note the different vertical scales.

Extreme value analyses for the observed past and projected future annual maxima of the enthalpy indices likewise indicate that high enthalpy values are likely to increase in time. An example is given in Fig 5 that shows the return level estimates of the 24-hour enthalpies at four locations during two 30-year periods, 1980-2009 and 2035-2064. The figure suggests that the annual probability of high 24-hour enthalpies at Sodankylä in the middle of this century (grey dashed line) will be slightly higher than the present-day probabilities at Jokioinen and Jyväskylä but still lower than those at Vantaa. Currently very rare enthalpy values, with an annual probability of 0.001, will clearly be more common around year 2050. This is because even a relatively small shift in the probability density function of a variable can result in substantial changes in the likelihood of extreme events.

Averaged over the four stations, the return levels would increase by about 10 % by the middle of this century (Table 2). The percentage changes seem to have a slight tendency to increase with increasing persistence of enthalpy, up to one week. However, the differences between the indices and the annual probabilities are very

small. Considerations of changes in enthalpy up to the end of this century might strengthen (or weaken) these deductions. At that time horizon, the signal-to-noise ratio in climate change projections becomes larger

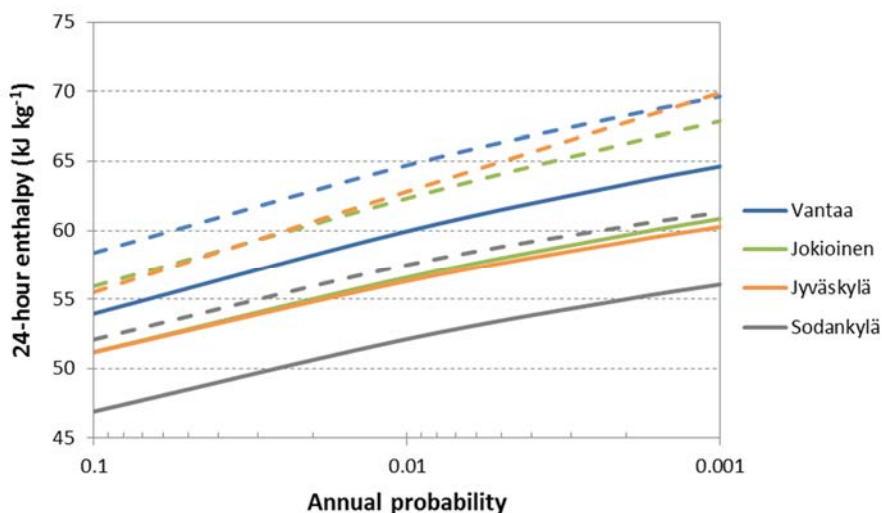


Figure 5. Current (solid line) and projected future (dashed line) return levels of 24-hour enthalpy at four locations as a function of annual probability. The projections are for the period 2035-2064 (around 2050) under the A2 scenario.

Table 1. Projected percentage increases in the five enthalpy indices as a function of annual probability. All values are averages over four locations (Vantaa, Jokioinen, Jyväskylä and Sodankylä).

Change in enthalpy index [%]	Annual probability			
	10^{-1}	10^{-2}	$2 \cdot 10^{-3}$	10^{-3}
Transient	8	9	9	10
6 hours	8	9	10	10
24 hours	9	10	11	11
7 days	10	11	11	11
14 days	12	11	10	10

Summary and conclusions

Enthalpy is a thermodynamic property of the air that is routinely considered when ventilation and cooling systems are designed. In this study, as part of the EXWE project under the SAFIR2014 programme, we examined the occurrence of high values of transient enthalpy and values persisting for 6 or 24 hours or for 7 or 14 days in the recent past and projected future climate. The following annual probabilities of occurrence were considered: 0.1, 0.01, 0.002 and 0.0001, corresponding to return periods of 10, 100, 500 and 1000 years.

The assessment of the return levels in the recent past climate conditions was based on air temperature, humidity and pressure data at ten locations in southern and western Finland in 1961-2012. The extrapolations from the 52-year period of observations to the recurrence periods of up to 1000 years were conducted by using the POT method. The General Pareto Distribution was fitted to the data of annual maxima exceeding a threshold that was defined separately for each station and enthalpy index.

According to weighted averages across the ten locations, values that are exceeded with an annual probability of 0.002 in the current climate conditions range from 72 kJ kg^{-1} for the instantaneous enthalpy to 40 kJ kg^{-1} for the two-weeks enthalpy.

The estimates of future changes in the enthalpy indices were based on synthetic future weather data. The data sets had been previously constructed using multi-model mean responses of temperature and humidity to global increases in greenhouse gas concentrations in the atmosphere. We considered here the SRES A2 scenario. In terms of greenhouse gas concentrations and magnitude of projected climate changes, in the middle of this century the A2 scenario is still close to two other widely used SRES scenarios (B1 and A1B).

According to the future estimates, the return levels of the enthalpy indices would increase by about 10 % by the middle of this century. Currently very rare enthalpy values, with an annual probability of 0.001, are expected to be clearly more common around year 2050.

Estimating extremes, with a small probability of occurrence, is a less robust exercise than studying average conditions. Because extreme episodes are very rare, the reliable assessment of their likelihood is difficult. Hence uncertainty is unavoidable in the assessment of extremes.

References

- FMI 2014. An exceptionally long heatwave. Press release archive. <http://en.ilmatieteenlaitos.fi/press-release/10014539>
- FMI 2015. 2014 was Finland's second warmest year on record. Press release archive. <http://en.ilmatieteenlaitos.fi/press-release/42503751>
- IPCC, 2013: Summary for Policymakers. In: Climate Change 2013: The Physical Science Basis. Contribution of Working Group I to the Fifth Assessment Report of the Intergovernmental Panel on Climate Change [Stocker, T.F., D. Qin, G.-K. Plattner, M. Tignor, S. K. Allen, J. Boschung, A. Nauels, Y. Xia, V. Bex & P.M. Midgley (eds.)]. Cambridge University Press, Cambridge, United Kingdom and New York, NY, USA.
- Jylhä, K., Saku, S. & Venäläinen, A. 2014. Return levels of enthalpy in Finland. EXWE project report. Finnish Meteorological Institute. Available upon request at climateservice@fmi.fi
- NOAA. 2015. National Climatic Data Center, State of the Climate: Global Analysis for December 2014, published online January 2015, retrieved on January 25, 2015 from <http://www.ncdc.noaa.gov/sotc/global/2014/12>.
- Rodrigues, V.C., da Silva, I.J.O., Vieira, F.M.C. & Nascimento, S.T. 2010. A correct enthalpy relationship as thermal comfort index for livestock. *Int J Biometeorol*. DOI 10.1007/s00484-010-0344-y.
- Ruosteenoja K., Jylhä, K., Mäkelä, H., Hyvönen, R., Pirinen, P. & Lehtonen I. 2013. Rakennusfysiikan testivuosiensa sääaineistot havaitussa ja arvioidussa tulevaisuuden ilmastossa - REFI-B -hankkeen tuloksia (Weather data for building physics test reference years in the observed and projected future climate - results from the REFI-B project). Finnish Meteorological Institute, Reports 2013:1. 48 p. (In Finnish with abstract in English and Swedish).
- Sarkomaa, P., Kaikko, J. & Vepsäläinen, A. 2002. Kostean ilman prosessien laskenta. Opetusmoniste 2002, Department of Energy Technology and Environmental Engineering, Lappeenranta University of Technology.
- Venäläinen, A., Saku, S., Jylhä, K., Nikulin, G., Kjellström, E. & Barring, L. 2009. Extreme temperatures and enthalpy in Finland and Sweden in a changing climate. NKS-194. NKS Secretariat, NKS-776, DK-4000 Roskilde, Denmark.

41. Risk assessment of large fire loads (LARGO)

41.1 LARGO summary report

Anna Matala¹, Topi Sikanen¹, Terhi Kling¹, Antti Paajanen¹, Simo Hostikka²

¹VTT Technical Research Centre of Finland Ltd
P.O. Box 1000, FI-02044 Espoo

²Aalto University, Espoo, Finland

Abstract

The fire risks at nuclear power plants can nowadays be assessed by numerical simulations. The simulation tools and methods are being continuously improved. Full scale validation of the models is a very significant part of this process. In LARGO project, tools and methodology for assessing the risks related to large fire loads were developed. The main areas of interest were the defence-in-depth evaluation in fire situations, the response of the plant systems, structures and components (SSC) as well as operating personnel to the fire situations, and the prediction of fire heat release rate from large fire loads.

Introduction

The most significant fire loads in nuclear power plants are oils and cables. The computational assessment of the fire consequences is currently possible with sufficient reliability for prescribed fires within the compartment of fire origin, but the prediction of fire spread is still a challenge. These models need further improvement and especially large scale validation to ensure their accuracy. The overall goal of this project was to develop tools and competence to evaluate and ensure the operation of the defence-in-depth principle in fire protection.

The main objectives of LARGO were:

- (1) Defense-in-depth evaluation for fires,
- (2) Response of plant components and personnel to fire,
- (3) Predictive simulation of large fire loads, and

(4) Participation and utilisation of OECD PRISME2 project

In the first task the performance of the structural barriers in fire was studied. This included numerical assessment of fire doors that are exposed to non-standard fire curves, participation in developing a tool that enables combination of fire (CFD) and structural (FEM) simulations, and a case study where heat and smoke spread to other buildings after a large fire was investigated. The second task concentrated on response to fire, from the point of view of the automation electronics and the fire brigade personnel. Third task was the actual model development and simulation of the large fire loads, meaning liquid pool fires and cable trays. Here CFD submodels were developed for the two-phase flows involving evaporatin surfaces and sub-grid scale particles. The last task was the participation and utilisation to OECD NEA PRISME2 project (2011–2016). This task covered the participation fee of Finland, preparations and presentations in the project meetings, and introducing the project results to the SAFIR2014 reference group 8.

The most significant results of LARGO 2011–2014 are summarised in this report.

Defence-in-depth for fires

Defence-in-depth (DID) is one of the main concepts used to reduce the risk of severe accidents in nuclear facilities (IAEA 1996). While the DID against large emissions of radioactive substances in case of core damage relies mostly on the use of physically nested systems and barriers, the DID against fires relies also on barriers and systems that are sequential in time. The levels of Fire-DID (U.S.NRC 1979) are:

1. Prevention of ignitions
2. Fire detection
3. Fire suppression by active systems and manually activated systems
4. Physical confinement of fire effects by barriers
5. Protection of sensitive equipment against fires

The evaluation of levels 2, 3, and 5 has been previously studied in the context of Fire-PRA methodologies. Step 1 is measured in terms of statistics and developed through the improvements in safety culture, work instructions, and electrical system designs, and based on the operational experiences because the theoretical framework for the actual ignition mechanisms is still very limited, and due to the wide range of possible ignition reasons and scenarios.

Despite – or possibly because of – the fact that the structural fire safety is the oldest and well-established form of fire protection, the development of the fourth step “Physical confinement of fire effects by barriers” has to large extent been neglected in the previous research programs. In this project we aimed at developing a general methodology for the evaluation of barrier failure probability and computational tools for the deterministic barrier performance analyses.

In the past Fire PRA studies, the conditional suppression and target failure (fire consequence) probabilities were determined using probabilistic (Monte Carlo) simulations with deterministic tools. In principle, the same method could be used to determine the conditional probability of barrier failures by combining the CFD fire simulation results with the thermo-mechanical simulations of the barrier element perfor-

mance. Possible barrier elements could be e.g. fire doors, dampers and penetration seals. This method would, however, be computationally too expensive due to the huge number of possible fire condition – barrier element combinations and relatively complex numerical problem in question. A simplified method was needed.

A similar problem was previously faced by the EDF engineers investigating the suitability of barrier elements with different fire classifications to the different locations of the EPR design (Gautier et al. 2010). This method was here extended to a probabilistic approach where a small number of realistic (natural) time-temperature curves is first prescribed and the barrier element performance is assessed against these curves in sufficiently detailed numerical or experimental method. In the application phase, the time-temperature realizations of the probabilistic fire simulations are compared against the prescribed set of curves. Barrier performance analyses are not needed during the probability calculation.

A contribution was made to the development of a multi-field simulation framework for fire-structure analysis. The framework is based on coupling existing simulation software, namely:

- Fire Dynamics Simulator (FDS), which is a widely used Computational Fluid Dynamics (CFD) tool for the simulation of fire phenomena. It is developed as an open-source project led by the National Institute of Standards and Technology (NIST).
- ABAQUS, which is a general purpose Finite Element Analysis (FEA) software, and a commercial product of Dassault Systèmes.

FDS is used to model the fire environment and the heat exposure to relevant structures, while ABAQUS is used to analyse their thermal and mechanical response. Thermal exposure to surfaces is extracted from the fire dynamics simulation and used as a time-dependent boundary condition in the subsequent thermal-mechanical analysis. The sequential coupling scheme is illustrated in Figure 1.

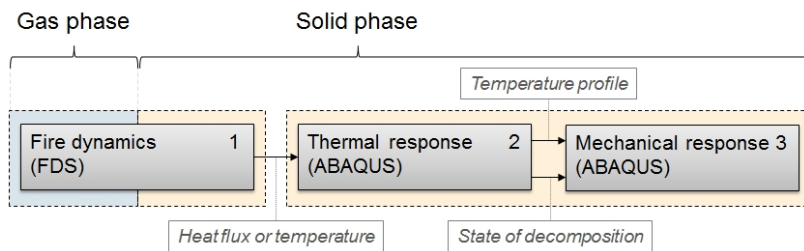


Figure 1. The multi-field simulation framework for fire-structure analysis.

To establish the coupling, an interoperability tool called FDS2FEM was developed. It was implemented as a command-line application for Linux and Windows operating systems.

Effects of a transformer fire occurring between the turbine hall and the diesel generator building was selected as a case study (Figure 2). The goal of the study was to explore the effects of the transformer fire on other transformers and nearby

buildings. Particular attention was paid to dispersion of smoke. Smoke from the transformer fire may cause arcing in the nearby electrical equipment. Smoke may also reach the air intakes of the diesel generator building possibly impeding the use of the generators. Predicted heat fluxes on the walls and on the ground around the burning transformer were recorded in order to assess the thermal stress on the structures and the conditions facing the fire fighters.

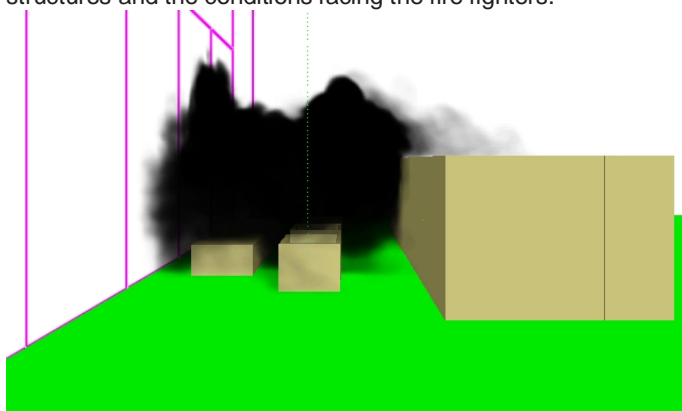


Figure 2. Smoke plume from transformer fire when 10 m/s wind is blowing from the direction of the turbine hall towards the diesel building.

From the simulation results it is clear that in addition to the lines above the burning transformer, also other power lines may be surrounded by heavy smoke. In the worst case scenario, strong wind from the direction of the turbine hall blows smoke over the diesel building and into the switchyard beyond, possibly affecting large number of equipment.

Heat fluxes on the walls and roof of the diesel building and on the walls of the turbine hall were found to be less than 5 kW/m^2 almost everywhere, regardless of the wind direction. Strong winds do tilt the fire plumes, but this mostly affects the distribution of the heat flux and has a smaller effect on the maximum values of the heat flux. For ignition of the building materials, significantly larger heat fluxes are needed. Generally heat fluxes in excess of 10 kW/m^2 are needed for ignition. The mechanical performance of the structures and the possible consequences of thermal expansion induced compressive stresses were not evaluated in the project.

Major assumption in the simulations is that the bunker around the transformer stays intact and the transformer oil mostly stays inside the bunker. Failure of a wall in the bunker would increase the heat fluxes to nearby objects and buildings significantly. This was noticed in the transformer fire experiments (Norta, 1995), where in some tests the front wall of the bunker was removed. Up to 10 fold increase in heat flux measurements was seen 5 meters from the bunker (increase from $2,8 \text{ kW/m}^2$ to 29 kW/m^2). Source of majority of the thermal radiation in a pool fire is the luminous band at the base of the plume. Since the base of the transformer fire is below the

edge of the bunker, the bunker walls block majority of the radiation. The bunker may also reduce air entrainment in to the fire thus possibly limiting the burning rate.

Response to fire

Sensitivity of digital automation on heat and smoke was studied exploiting theoretical and experimental results in the literature and VTT's own database. The overall goal of this task was to formulate chain of events that could be used in modelling. The modelling chain consists of five main steps:

1. Fire source and heat release rate assessment,
2. Soot yield, and the consequent soot production assessment,
3. Soot transport calculation, using e.g. CFD,
4. Soot deposition calculation, using e.g. CFD,
5. Assessment of the reduction in surface insulation resistance, and
6. Comparison against critical threshold value for the insulation resistance.

Current version of Fire Dynamics Simulator (FDS, McGrattan et al. 2014) has a soot deposition model that includes the effects of gravitation, diffusion and thermophoresis. It was not clear whether the model should also take into account electrophoresis. The results can be seen in Figure 3 which is based on the collected data and models from the literature. It shows that in the typical electrical fields in NPP the electrophoresis has many orders of magnitude weaker influence than the other mechanisms and hence can be ignored.

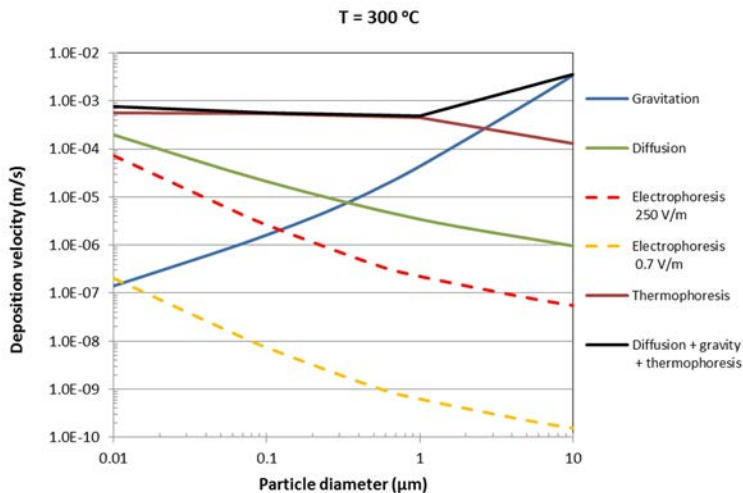


Figure 3. Mechanisms of soot deposition. Electric field strengths are literature values near electrical office equipment (250 V/m) or ambient in nuclear or electric power plants locations (0.7 V/m).

The prediction of an actual failure is far more complicated. The results showed that the failure mechanisms of soot are very complicated and depend on many fac-

tors. Humidity seems to increase the probability of malfunction, and visible water to accelerate the failure process even further. Some studies show that if the surface insulation resistance decreases below 1 MΩ, the failure probability increases substantially. However, failures may occur above this limit, and equipment may stay operational below it.

Regarding the human responses, in the SAFIR-projects an approach has been developed, which is called “stochastic operation time modelling” (SOTM). The model allows the user to estimate the development of available resources by considering the distributions of individual operation times, inter-organizational communication needs and possibilities for additional delays. It has been used in several applications to evaluate the performance of nuclear power plant fire services as well as other fire services. These experiences of the SOTM-approach have shown that the method is capable of revealing the bottlenecks of an organization’s response and the most error-prone operations. The method can also give quantitative information on the response.

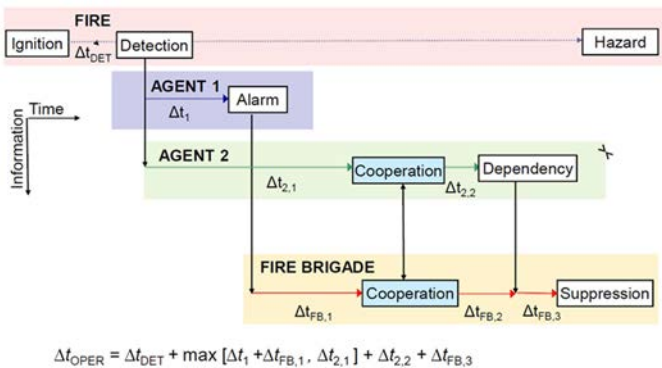


Figure 4. A timeline showing the actors, connections and time delays in a generic fire brigade response scenario.

As the stochastic operation time model approach has proven its usefulness, there was a strong motivation for finding ways to speed up the modelling process, increase the traceability and reduce the vulnerability of the calculations. One way of achieving these goals was to describe the rescue organization as an agent-based model and run a continuous-time simulation that follows the course of events step-by-step. In this approach, the intellectual burden was shifted from formulating an analytical expression to creating a working and general-enough program logic and a feasible user interface. In the LARGO-project a trial case of employing agent-based simulation to create a stochastic operation time model of a realistic fire-fighting scenario was carried out (Figure 4). The SOTM was implemented as a command-line operated C-program running a continuous-time simulation. The code is a feasible starting point for a more generic agent-based SOTM simulator.

Simulation of large fire loads

The objective of this task was to improve and validate the current models for simulating large fire loads, more specifically liquid pools and cables. Models were implemented to FDS version 6 (McGrattan et al. 2014). Model validation has been done comparing the simulation predictions to experimental results in large scale (OECD PRISME² and PRISME 2³, and NRC Christifire projects (McGrattan et al. 2012)).

Pool fires are an important class of industrial fire hazards due to the large amounts of flammable liquids present in most industrial facilities including Nuclear Power Plants (NPPs), and because the rapid development of the heat release rate in such fires poses a challenge to the safety systems. This topic has been discussed in more detail in the following article with title “Predicting the heat release rate of liquid pool fires using CFD”. Figure 5 shows comparisons of predicted burning rates with two empirical correlations.

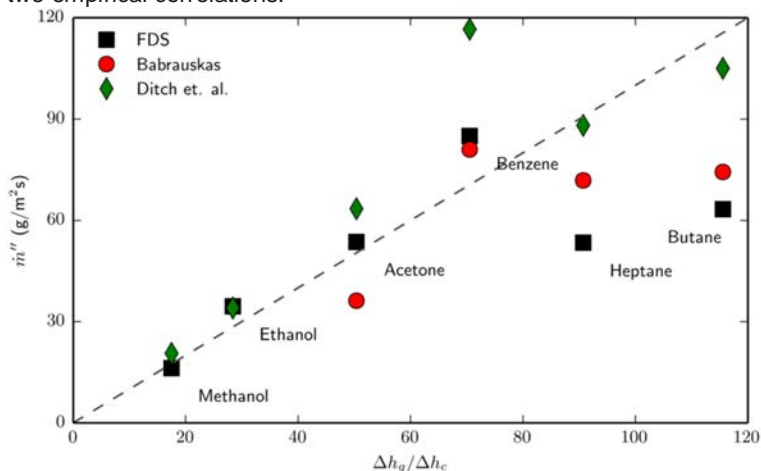


Figure 5. Comparison of predicted pool fire burning rates against empirical correlations.

Predicting flame spread in a cable tray is one of the main objectives in the NPP fire modelling. Modelling of these non-homogenous, non-rectangular, combustible objects is not simple in CFD. In addition, the composition of the sheath (and other components) may vary significantly between different products even for the same nominal polymer. The fire behaviour of a cable depends on the amount and type of additives, but the real composition is not usually declared by the manufacturer. Yet another challenge is to predict the fire behaviour of the cables that have spent decades in the NPP cable tunnels, possibly exposed to elevated temperatures and radiation.

² <https://www.oecd-neo.org/jointproj/prisme.html>

³ <https://www.oecd-neo.org/jointproj/prisme-2.html>

Real chemical compositions of PVC cable components were tracked using several different techniques, including Fourier transformed infra-red spectroscopy (FTIR), gas chromatography combined with mass spectrometry (GC-MS), X-rays and calcination. Although none of these methods provided directly the mass fractions of each component, it was possible to deduce that the cable sheath included only 46 w-% of PVC (the nominal polymer), 32 w-% of filler CaCO_3 , and the rest 22 % was most likely mainly phthalates (plasticizers). The fire behaviour of this kind of polymer blend has significantly different than pure PVC; pure PVC does not release combustible gases during the first reaction step, but the plasticizers do.

The polymer composition of a cable changes slowly during the decades of plant operation. Both heat and radiation accelerate the ageing of polymer, main mechanism being oxidation. Oxidation breaks the polymer chains and thus degrades material. This may lead to decrease of combustible material and thus reduce the flammability of the polymer blend. Also migration of plasticizers and additives may occur, further reducing the related fire risk. The flame spread rate of brand new and slightly older PVC cables were studied experimentally in the 2-m vertical flame spread apparatus at VTT (Mangs and Hostikka 2013). The results are shown in Figure 6. It can be observed that the flame spread rate is higher for the new cable at all initial temperatures. This confirms the theory that the ageing actually reduces the fire risks of a polymer. However, it is not clear how modern flame retardant cables age, because loss of flame retardant additives may actually increase the fire risk.

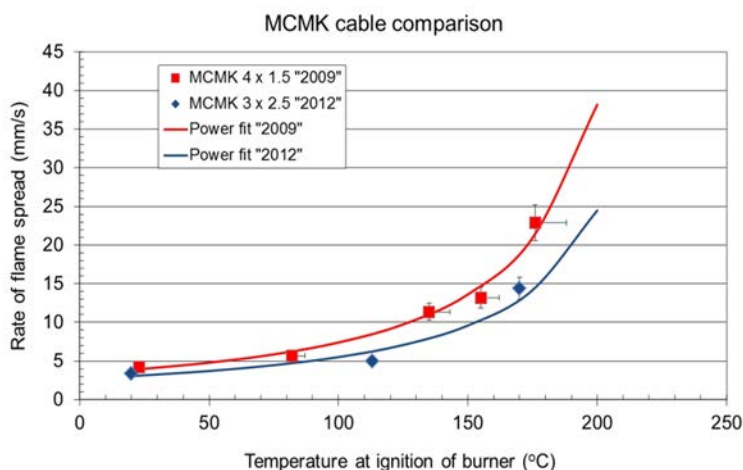


Figure 6. Rate of flame spread as a function of ambient temperature for MCMK cable samples.

Cable modelling has been studied widely in LARGO, from the model development to modelling real NPP cables, and the experimental validation of the models. Improvements in the cable modelling have been focused on developing a sub-grid-scale representation of cables instead of the traditional using grid-dependent, rec-

tangular obstacles. The new approach is implemented using Lagrangian particles, which enable different geometries for computing the heat conduction through the cable, including cylinders. The difference of these geometries is demonstrated in Figure 7, where the real cable mapping to Cartesian and Cylindrical models is presented. Although the cylindrical geometry is more realistic by means of heat conduction, several other challenges have been encountered, including the incoming radiation from different angles, radiation interaction between particles and the flow resistance of the particles.

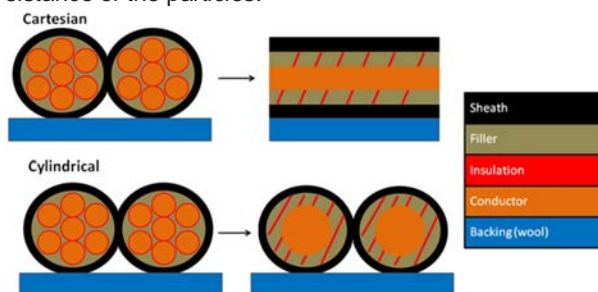


Figure 7. Cable geometry and layer structures in Cartesian and Cylindrical models of cone calorimeter samples.

In addition, some improvements have been also made to the pyrolysis modelling routine, to be able to simulate oxidative reactions, and swelling or shrinking surfaces. Especially the latter is significant mechanism in PVC pyrolysis, where the PVC chars and swells significantly, insulating the cable below from the heat until the char layer starts to crack and degrade. The insulative effect of swelling (or shrinking) layer is demonstrated in Figure 8.

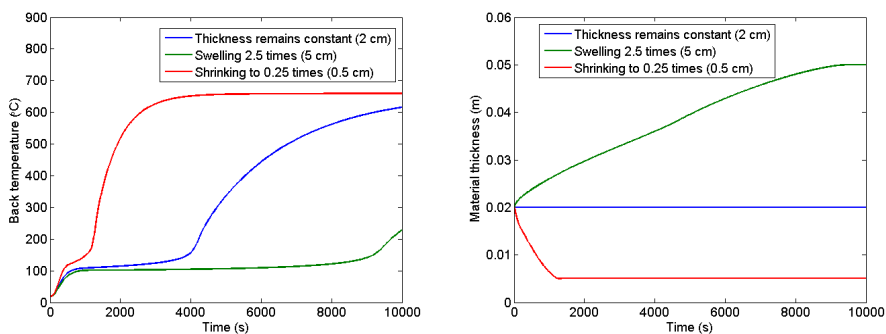


Figure 8. Effect of swelling or shrinking surface. a) Temperature at unexposed side. b) Material thickness.

Cable pyrolysis and combustion can be modelled using a set of parameters that are estimated from the small scale experimental methods. Several estimation meth-

ods have been studied and tested (Matala, 2013), and the methodology has been applied to many different cables.

Cable models have been used in predicting flame spread in larger scale set-ups. The simulation results have been compared to experimental results of Christifire (McGrattan et. al 2012), PRISME and PRISME 2 projects. The results show that although sometimes the predicted heat release rates are close to the experimental ones, this does not happen in general in every case. Part of the problem is the significant uncertainty that is related to the large scale experiments. In the simulations the challenge is in the different scales of the phenomena; predicting correctly the flame spread (or ignition) requires very accurate boundary conditions at the material surface (meaning very tight grid), which is not practical in large scale simulations. In general, it can be concluded that the experiments with large initial fire can be simulated more accurately than the others.

References

- Gautier, B., Mosse, M. and Eynard, O. (2010) EPRESSI Method – Justification of the Fire Partitioning Elements. Sixth International Seminar on Fire and Explosion Hazards, UK.
- IAEA (1996) Defence in depth in nuclear safety. INSAG-10. A report by the International Nuclear Safety Advisory Group. International Atomic Energy Agency. Vienna.
- Mangs, J. and Hostikka, S. 2013. Vertical flame spread on charring materials at different ambient temperatures. *Fire and Materials*, Vol 37 (3), pp. 230–245. DOI: 10.1002/fam.2127
- Matala, A. 2013. Methods and applications of pyrolysis modelling for polymeric materials. VTT Science 44.
- McGrattan, K., Lock, A, Marsh, N., Nyden, M, Bareham, S., Price, M., Morgan, A.B., Galaska, M. and Schenck, K. 2012. Cable Heat Release, Ignition, and Spread in Tray Installations During Fire (CHRISTIFIRE), Phase 1: Horizontal Trays (NUREG/CR-7010, Volume 1).
- McGrattan, K., Hostikka, S., McDermott, R., Floyd, J., Weinschenk, C., and Overholt, C. 2014. Fire Dynamics Simulator. Technical Reference Guide Volume 1: Mathematical Model. NIST Special Publication 1018. 6th edition.
- Norta, A. 1985. Muuntajan palokokeet Inkoossa. Koeselostus, LO1-K500-38.
- U.S.NRC. (1979) 10 CFR Appendix R to Part 50—Fire Protection Program for Nuclear Power Facilities Operating Prior to January 1.

41.2 Predicting the heat release rate of liquid pool fires using CFD

Topi Sikanen¹

¹VTT Technical Research Centre of Finland Ltd
P.O. Box 1000, FI-02044 Espoo

Abstract

In this paper a model for predicting the heat release rates of liquid pool fires is presented. The model accounts for the in-depth heat transfer by both radiation and convection. The in-depth radiation transport is solved by a one dimensional radiation transport model together with effective absorption coefficients determined from experimental data. Possibility of convective heat transfer in the liquid phase is studied using effective thermal conductivity. The model is implemented as a boundary condition in the Fire Dynamics Simulator. It is shown that the in-depth heat transfer has an effect on the dynamics of the fire. However for maximum burning rates, the most important parameters are found to be related to gas phase combustion. Overall, the predictions of maximum burning rates are found to be in agreement with experimental data.

Introduction

Pool fires are an important class of industrial fire hazards due to the large amounts of flammable liquids present in most industrial facilities including Nuclear Power Plants (NPPs), and because the rapid development of the heat release rate in such fires poses a challenge to the safety systems. Pool fires have been studied for decades. The focus of the research has usually been on the steady state behaviour and maximum burning rates of pool fires of various sizes. The results from such studies are often empirical correlations for the burning rate of a pool fire. A recent example is by Ditch et al. (2013) where the authors correlated the mass burning rate with the fuel heat of gasification and smoke point.

The fire analyses are usually performed using the Computational Fluid Dynamics (CFD) type of fire simulations. The most important boundary condition for these simulations is the fire source burning rate, or liquid evaporation rate in case of pool fire analyses. While many of the analyses can be performed by prescribing the pool burning rate using either experimental data or empirical correlations as sources of information, there are situations where the conditions of the fire scenario differ so much from any experimental study that a reliable prediction of the pool burning rate cannot be made in advance. For example, in nuclear power plant settings, pool fires are expected can be expected occur in enclosures, where combustion may be oxy-

gen limited. Heated walls of the compartment will also add to the radiation incident on the fuel surface.

On the other hand, the heat transfer within the pool itself can also be significantly different from the situation behind the empirical conditions. In experiments, steps are sometimes taken in to minimize in-depth radiation absorption and liquid convection. This is done in order to determine the steady state burning rate. The transient nature of fire analyses requires the knowledge on the time-dependent burning rate, not just the peak or steady state value. It is therefore necessary to develop sub-models for the CFD fire models that can predict the pool fire dynamics and burning rate during the simulation

In a pool fire the heat from the flame is transported to the liquid by thermal radiation and convection. Heat conduction takes place between the vessel and the liquid. For very small fires with pool diameter, the conduction through the vessel walls dominates. For slightly larger pool fires, convective transport is the most important. For large pool fires, radiative transport dominates. The exact diameters where these transitions between dominant heat transfer mechanisms occur are fuel dependent.

In the liquid phase the dominant modes of transport are convection and radiation. The convection can be driven by heat transfer from the walls, unsteady burning rate, uneven surface temperature and buoyancy. Very little experimental data exists on the importance of liquid side convection in determining the burning rates of pool fires.

Vali et al.(2013) found that there is a near constant temperature region directly below the surface of a pool fire. In this region, the heat transfer was found to be dominated by convection driven by heated pool walls. The importance of the initial temperature of the liquid fuel on pool fire dynamics has been previously noted by Hayasaka (1997) and investigated by Chen et al. (2011), who recorded the temperature gradient within the fuel. They found that the initial temperature did affect the peak burning rate but not significantly the steady state burning rate.

To investigate the heat transfer within the liquid, we must also consider the depth over which the radiation reaching the liquid surface is absorbed. Depending on the fuel, the thickness of absorption can vary significantly, which has a great influence on the method how the radiation should be taken into account in numerical modeling. In fuels which are optically very thick in the infrared region, the thermal radiation is absorbed within a very thin layer on the surface, and the the radiation can be taken into account as a boundary condition of the liquid's internal heat transfer problem. If the liquid is not optically thick the in-depth absorption must be taken into account as an internal source term of the heat conduction/convection problem. Additionally, the re-radiation of the fuel and vessel must be taken into account to ensure the conservation of energy in case of optically thin fuels and high temperatures.

Mathematical model

The simulation tool used in this work is the Fire Dynamics Simulator (FDS) (McGrattan et. al., 2014). FDS solves the Navier-Stokes equations in a form suitable for low-

Mach number thermally driven flows. Turbulence is treated by Large Eddy Simulation (LES). In this section, a description of the FDS liquid pyrolysis model is presented.

In FDS, liquids are considered to be semi-transparent solids. A one dimensional heat conduction equation is solved for each boundary cell

$$\begin{aligned} \rho c \frac{\partial}{\partial t} &= \frac{\partial}{\partial x} \lambda \frac{\partial T}{\partial x} + \dot{q}''' \\ -\lambda \frac{\partial T}{\partial x} \Big|_{x=0} &= h(T_g - T_s) - \Delta h_v \dot{m}'' \\ h &= \max \left[1.52 |T_g - T_s|^{\frac{1}{3}}, \frac{1}{1} 0.037 Re^{4/5} Pr^{1/3} \right] \end{aligned} \quad (3)$$

Here ρ , c , λ and T are respectively the fuel density, specific heat, thermal conductivity and temperature. The subscripts S and g refer to conditions at the fuel surface and in the first gas phase cell respectively. On the surface Δh_v and \dot{m}'' are the heat of vaporization and the evaporation mass flux, respectively.

The radiative transport can be described as volumetric heat-source term \dot{q}''' in Eq. (3). The FDS condensed phase model uses a “two-flux” model, where the radiative intensity is assumed to be constant in “forward” and “backward” hemispheres. The forward radiative heat flux into the fuel is

$$\frac{d\dot{q}^+}{dx} = \kappa(\sigma T^4 - \dot{q}^+) \quad (4)$$

A corresponding formula can be written for the backward flux \dot{q}^- . The heat source term in Equation 3 is the difference between the forward and backward fluxes

$$\dot{q}''' = \frac{d\dot{q}^+}{dx} - \frac{d\dot{q}^-}{dx} \quad (5)$$

Boundary condition at the fuel surface is given by

$$\dot{q}^+ \Big|_{x=0} = \dot{q}_{in}'' + (1 - \varepsilon) \dot{q}^- \quad (6)$$

where ε is the fuel emissivity and \dot{q}_{in}'' is the incoming radiative flux. The effect of the unresolved concentration boundary layer near the pool surface is taken in to account. In this model the mass flux is given by

$$\dot{m}'' = h_m \rho_{f,g} \log \left(\frac{X_G - 1}{X_S - 1} \right); X_S = \exp \left[-\frac{\Delta h_v W}{R} \left(\frac{1}{T_b} - \frac{1}{T_s} \right) \right] \quad (7)$$

Here $h_m = Sh \mu_g / Sc \Delta x$ is the mass transfer coefficient and $\rho_{f,g}$ and X_G are the density of the fuel vapour and the volume fraction of fuel vapour in the grid cell adjacent to the pool surface, W is the molar mass of the fuel gas and R is the universal gas constant. The Schmidt number Sc is 1 and the Sherwood number is given by

$$Sh = 0.037 Sc^{\frac{1}{3}} Re^{\frac{4}{5}}; Re = \max \left[5 \times 10^5, \frac{\rho u L}{\mu} \right]. \quad (8)$$

The Reynolds number is calculated based on conditions in the cell adjacent to the surface. Properties of liquids considered in this paper are listed in Table 1. In the above, L is some characteristic length that is set to 1 meter for calculations in this paper. Note that the Reynolds number is bounded from below. This ensures a non-zero mass flux from liquid fuels and thus circumvents the need to model the ignition process. The Reynolds number varies over time through the gas speed dependence, and so do the Sherwood and mass transfer numbers.

Table 1. Thermophysical properties of liquids considered.

	ρ^1	cp^2	λ^3	h_v^2	y_s^4	T_b^2
Acetone	791	2.13	0.2	501	0.014	56.3
Benzene	874	1.74	0.14	393	0.181	80.3
Butane	573	2.28	0.12	385	0.029	0
Ethanol	794	2.44	0.17	837	0.008	78.5
Heptane	675	2.24	0.14	317	0.037	98.5
Methanol	796	2.48	0.2	1099	0.001	64.8

¹Babrauskas (2002),²Linstrom and Mallard (2014),³Haynes (2015),
⁴Tewarson (2002)

Effective absorption coefficients

Absorption of thermal radiation in semitransparent media is highly dependent on the wavelength of the radiation and cannot be represented by a single number for all cases. The absorption coefficients in Table 1 are based on a curve fitting procedure. The procedure is as follows:

- Start with spectrally resolved absorption coefficients κ_λ for a liquid. Here λ is frequency.
- Assume incoming radiation follows blackbody spectrum with temperature 1450 K

$$E_{b,\lambda} = \frac{2hc^2}{\lambda^5} \frac{1}{\exp\left[\frac{hc}{k\lambda T}\right] - 1} \quad (9)$$

- Calculate transmitted fraction of radiation at distance S from the liquid surface by line by line application we use the exact solution for the radiative flux to positive direction at distance x within a non-scattering plane layer

$$\dot{q}_{ex}^+ = \int_0^\infty \dot{q}_{\lambda,ex}^+(\tau) d\lambda \quad (10)$$

$$\dot{q}_{\lambda,ex}^+ = E_{b,\lambda}(T_\infty)2E_3(\tau) + E_{b,\lambda}(T(x))2 \int_0^\infty E_2(\tau') d\tau'$$

where $\tau = \kappa x$ is the optical thickness, T_∞ and $T(x)$ are the temperatures of the external source (flame) and liquid, and $E_n(\tau)$ are the exponential integral functions of order n .

- Optimize to find a value for absorption coefficient κ that minimizes some error metric between the predicted flux \dot{q}^+ from solution of Eq. (2) and the flux calculated from Eq. (8).

Two choices need to be made in this process:

- Choice of optimization metric: Do we want to reproduce the heat source distribution \dot{q}''' accurately (Eq. (10)) or do we want to match the flux \dot{q}^+ at

certain distance from the surface (Eq. (9)). The latter choice will lead to correct amount of energy being deposited in the liquid layer

- The path length L at which the flux \dot{q}^+ is matched or over which the heat source distribution \dot{q}''' is matched.

These choices lead to either

$$\text{Method 1: } \kappa = \arg \min \left[\left| \frac{\dot{q}_{\text{ex}}^+(L)}{\dot{q}_{\text{ex}}^+(0)} - \frac{\dot{q}^+(L)}{\dot{q}^+(0)} \right| \right] \quad (11)$$

or

$$\text{Method 2: } \kappa = \arg \min \left[\int_0^L \left(\frac{\dot{q}^+(x)}{\dot{q}^+(0)} - \frac{I(x)}{I(0)} \right)^2 dx \right]. \quad (12)$$

For methanol and ethanol absorption coefficient spectra is available, but the assumption of blackbody radiation is not applicable for low-sooting fuels. The absorption coefficient for ethanol is calculated with the help of measured emission spectrum of ethanol flame data of Suo-Anttila et al. (2007). The absorption coefficient for methanol is based on the absorption coefficient of ethanol.

Figure 1a) Shows the absorption coefficient spectrum of heptane, with blackbody radiation intensity overlaid. It is clear that the blackbody radiation misses the highest peaks of the spectrum. Figure 1b) shows decay of incident radiation for various liquid fuels as predicted by Eq. (10). Finally, Figure 1c) compares predictions of the two-flux model with Eq. (10) for absorption coefficient determined by Eq. (9) and Eq. (8).

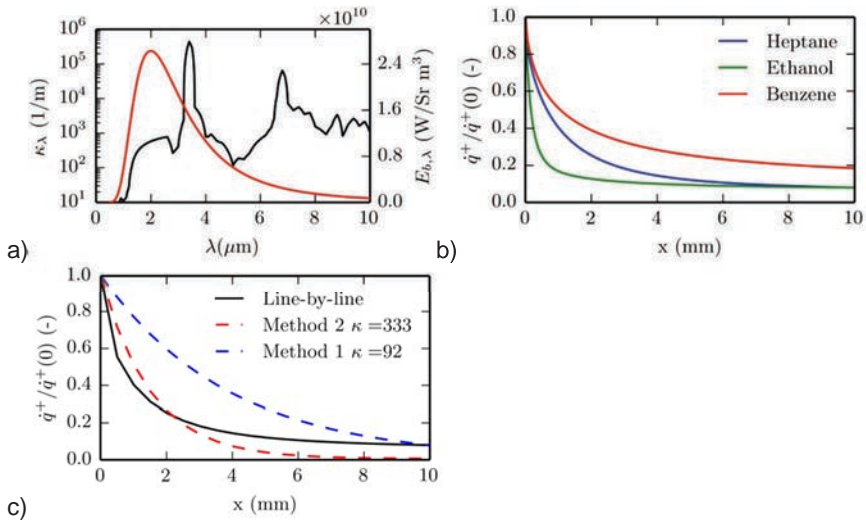


Figure 1. a) black line: Absorption coefficient spectrum of liquid heptane. Red line: blackbody emissive power at temperature 1450 K b) Attenuation of radiation for selected liquids. Predictions from Eq. (8). c) Comparisons of the absorption coefficients determined by the two methods for heptane and path length of 10mm.

Table 2. Effective absorption coefficients determined by Methods 1 and 2.

Path length (mm)	Method 1					Method 2				
	1	5	10	15	50	1	5	10	15	50
Benzene	342	139	86	62	21	396	212	162	144	132
Water	1205	340	190	136	49	1393	1336	1345	1345	1345
Ethanol	1044	303	168	116	35	1236	1134	1140	1140	1141
Heptane	458	216	130	92	31	512	355	335	333	333
Toluene	456	158	90	63	21	537	289	227	211	207

In depth convection

There are several possible sources of motion within fuel. One source is uneven burning rate of fuel. This will cause a fuel to flow towards regions of high burning rates. Second source are the hot walls of the pool where heat transferred through the pool walls creates natural convection currents. Third source is the in-depth radiation absorption. During pool combustion, the pool surface is cooled by evaporation. The heat to the surface is provided by conduction and convection from both the liquid phase and gas phase. Therefore the liquid side convection can have an important effect on the heat balance on the liquid surface.

Accurately modeling all these phenomena would require solving the full Navier Stokes equations for the liquid phase together with heat transfer modeling for the pool walls. Such approach is too time-consuming for practical work and too complex for use in engineering calculations. Instead, a simplified model is sought. Our goal is to model the overall effective heat transfer through the whole fuel layer.

Since Eq. 1 does not explicitly contain convective heat transfer within the pool, the easiest way to include the effect of convection is to increase the thermal conductivity λ . Values for effective thermal conductivity could be sought in terms of Nusselt number correlations. Nusselt number is calculated from a correlation for internally heated horizontal plane layer with isothermal top boundary and thermally insulated bottom boundary (Kulacki,1977)

$$Nu = \frac{\lambda_{eff}}{\lambda} = 0.338Ra_i^{0.227} . \quad (13)$$

The internal Rayleigh number is calculated from (Tasaka, 2005)

$$Ra_i = \frac{g\chi\dot{q}L}{\lambda\nu\alpha} \frac{\eta^3}{Q(\eta)} \left[1 - \left(1 + \frac{1}{\eta} \right) \exp\left(-\frac{1}{\eta}\right) \right] \quad (14)$$

where g is gravitational acceleration, χ is the coefficient of thermal expansion of liquid, \dot{q} is the volumetric heat source and L is the height of the fluid layer. In the denominator ν is the kinematic viscosity and α is the thermal diffusivity. $Q(\eta)$ is a normalization constant and $\eta=1/k$ is the length scale associated with the source distribution.

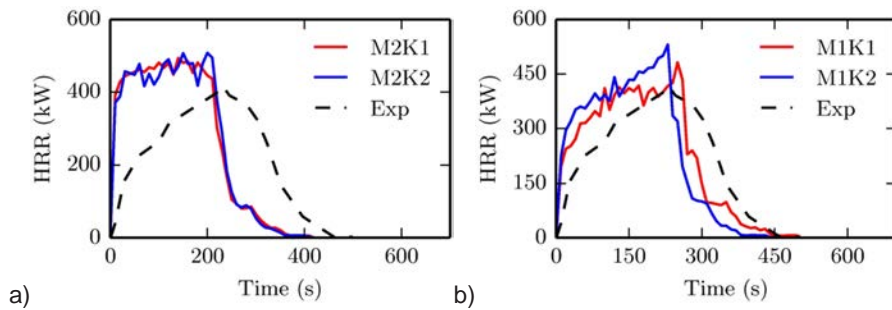


Figure 2. Heat Release Rates of Ethanol pool fires with different absorption coefficients and thermal conductivities. Experimental data from (Thomas, 2007). a) Models with absorption coefficient determined by Method 1. b) Models with absorption coefficient determined by Method 2.

Results

In this section we compare results from simulations with experimental data and empirical correlations. First, we focus on the effect of the absorption coefficient and thermal conductivity. After this we compare burning rate predictions with multiple empirical correlations and conduct sensitivity studies.

Two models, named K1 and K2, for thermal conductivity and two models, named M1 and M2, for the absorption coefficient are considered. In model K1 the thermal conductivity is equal to the literary value of liquid conductivity. In model K2 the thermal conductivity is defined by Eq. (13). Absorption coefficient is calculated from Eq. (12) in model M2 and from Eq. (11) in model M1.

First we test the predicted burning rates of FDS against the large ethanol pool fire case from Victoria University (Thomas,2007). In these tests, ethanol was burned under a hood in $0.81 \times 0.70 \times 0.05 \text{ m}^3$ fuel trays constructed from steel. The computational model of the fires consists of a $0.81 \times 0.70 \text{ m}^2$ surface depicting the pool and 5 cm lip around the pool. In the test under consideration there is 5 liters of ethanol in the pool. This translates to 9 mm thickness for the liquid layer. Table 4 lists the values used in these simulations.

Table 4 Absorption coefficients and thermal conductivities for Ethanol pool fire simulations. The first two models emphasize the heat transfer through the whole liquid layer. While the two latter models attempt to recreate the correct distribution of heat source within the liquid.

Table 5 Parameters for the ethanol simulation cases

Model	κ	λ
M1K1	160	0.17
M1K2	160	0.89
M2K1	1140	0.17
M2K2	1140	0.89

Figure 1 shows the effect of various modeling assumptions on the burning rate of a ethanol pool fire. In all cases the heat release rate rises too quickly. This is caused by the modeling of mass transfer coefficient in Eq. (7). Peak HRR is also over predicted in all cases. Figure 1a) and b) shows that the thermal conductivity from Eq. (13) has a small effect while the difference between the two absorption coefficients is more pronounced. Enhanced thermal conductivity has a larger effect when value of the absorption coefficient is lower. Decreasing the absorption coefficient (Figure 1b) leads to slower increase in burning rate which matches the rate in the experimental result. The slow decay of the fire is not correctly predicted.

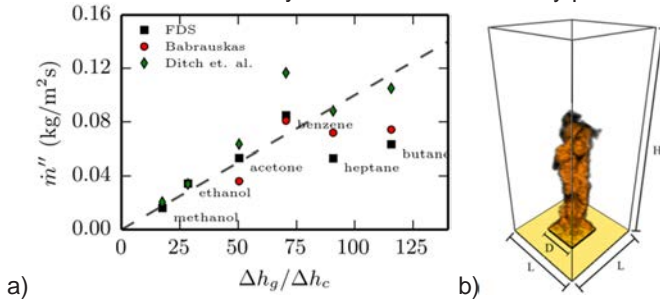


Figure 3. a) Burning rates of 1m² pool fires b) Illustration of the computational model of pool fire

To expand our selection of fuels and pool sizes. A series of large pool fires is simulated. These simulations consider large 1m x 1m rectangular pools. A 5 cm discretization interval is used for the mesh and the size of the computational domain is 1.6 m x 1.6 m x 4.8 m. There is a 5 cm lip on the pools. Computational domain is illustrated in Figure 1b.

We make use of empirical correlations to validate the results. The maximum burning rates of liquid pool fires are well correlated with

$$\dot{m} = 1 \times 10^{-3} \frac{\Delta h_c}{\Delta h_g}; \quad \Delta h_g = \Delta h_v + \int_{T_0}^{T_b} c_p dT. \quad (15)$$

The predicted burning rates are compared with experimental correlations. A well-known correlation by Babrauskas gives the mass burning rate per unit area as a function of pool diameter

$$\dot{m}'' = \dot{m}''_{\infty} [1 - \exp[-k\beta D]]. \quad (16)$$

An empirical correlation for the heat flux incident on pool surface given by (Ditch, 2014)

$$\dot{q}'' = \dot{m}'' \Delta h_g = 12.5 + 68.3 Y_s^{\frac{1}{4}} \left\{ 1 - \exp \left(- \left[\frac{4}{3} \Delta h_g D \right]^{\frac{3}{2}} \right) \right\}. \quad (17)$$

Figure 2 shows a comparison of FDS predicted burning rates and those predicted by Eqs. (13) and (14). In most cases the burning rates predicted by FDS are lower than those predicted by Eq. (14).

Largest differences in mass loss rate between simulation predictions and Eq. (15) are seen for heptane and butane. For butane, using correct value for the absorption coefficient could result in better predictions. There is considerable scatter in the literature for mass burning rates of heptane. Several reasons for the scatter in burning rates have been proposed. These reasons include varying lip heights, fuel level control and pan shape. The predictions for butane have largest scatter of all fuels considered here. Due to its low boiling point, butane is likely to be boiling in any experiments. The evaporation model considered here does not include boiling and thus is likely to lack some essential physics for predicting butane pool fires.

For benzene Eq. 16 predicts a very high mass loss rate. This is due to the very high soot yield of benzene. Ditch et al. (2014) noted that there is very little data for large benzene fires but for a 6 m pool fire the value $0.09 \text{ kg/m}^2\text{s}$ has been reported. This value agrees well with the predictions of FDS and Eq. (15).

Conclusions

This paper considered modeling of liquid pool fires and the effect of in-depth heat transfer in the liquid phase on predicted burning rates. Effective radiative absorption coefficients based on spectrally resolved data were used when available. Effect of in-depth convective heat transfer was modeled by an effective thermal conductivity in the one-dimensional conduction equation.

Grid refinement studies showed that the maximum burning rates can be predicted accurately when the gas phase equations are solved on a fine enough grid. The most important parameters in predicting the burning rate are related to the gas phase combustion. In-depth heat transfer in the form of in-depth radiation absorption and enhanced heat transfer in the liquid due to convective motions may be important in predicting the detailed dynamics of the fire.

All pool fires considered in this paper were in open atmosphere or in large rooms. Better models for the internal heat transfer and validation of burning rate predictions in confined situations are future research topics. However, the results indicate that the prediction of pool fire burning rates is mostly an issue of predicting the heat flux to the pool surface. Effects of the compartment walls and oxygen levels are then included through the heat flux predictions. Therefore, using this model in compartment fire calculations seems justified. This is an important result from the perspective of NPP fire analyses, since fires in NPPs are likely to occur in compartments.

References

- Chen B., Lu S, Li C., Kang Q, and Lecoustre V , 2011. Initial fuel temperature effects on burning rate of pool fire. *Journal of Hazardous Materials*, 188(13):369–374.
- Ditch B., de Ris J., Blanchat T., Chaos M., Bill R., and Dorofeev S. 2013. Pool fires an empirical correlation. *Combustion and Flame*, 160(12):2964 – 2974.
- Hayasaka H., 1997. Unsteady burning rates of small pool fires. In 5th Symposium on Fire Safety Science, pages 499–510,.
- Haynes, W (Ed.). 2015. *CRC Handbook of Chemistry and Physics*, 95th ed., CRC Press/Taylor and Francis, Boca Raton, Florida, (Internet Version 2015).
- Kulacki, F. and Emara, A. 1977. Steady and transient thermal convection in a fluid layer with uniform volumetric energy sources. *Journal of Fluid Mechanics*, 83(02), 375-395.
- Linstrom, P and Mallard, W (Eds). 2014. *NIST Chemistry WebBook*, NIST Standard Reference Database Number 69.
- McGrattan, K., Hostikka, S., McDermott, R., Floyd, J., Weinschenk, C., Overholt, K. 2013. *Fire Dynamics Simulator Technical Reference Guide Volume 1: Mathematical model*. National Institute of Standard and Technology. NIST Special Publication 1018, Sixth Edition
- Suo-Anttila, J. M., Blanchat, T. K., Ricks, A. J., and Brown, A. L. 2009. Characterization of thermal radiation spectra in 2m pool fires. *Proceedings of the Combustion Institute*, 32(2), 2567-2574.
- Tasaka, Y., Takeda, Y. 2005. Effects of heat source distribution on natural convection induced by internal heating. *International journal of heat and mass transfer*, 48(6), 1164-1174.
- Tewarson, A. 2008. Generation of Heat and Gaseous, Liquid, and Solid Products in Fires. In *SFPE Handbook of Fire Protection Engineering*, 4th ed. 3-1 – 3-59.
- Thomas, I. R., Moinuddin, K. A., and Bennetts, I. D. 2007. The effect of fuel quantity and location on small enclosure fires. *Journal of Fire Protection Engineering*, 17(2), 85-102.
- Vali, A., Nobes, D. S., & Kostiuk, L. W. 2014. Transport phenomena within the liquid phase of a laboratory-scale circular methanol pool fire. *Combustion and Flame*, 161(4), 1076-1084.

42. PRA development and application (PRADA)

42.1 PRADA summary report

Ilkka Karanta¹, Markus Porthin¹, Antti Toppila²

¹VTT Technical Research Centre of Finland Ltd
P.O. Box 1000, FI-02044 Espoo, Finland

²Aalto University, Systems Analysis Laboratory
P.O. Box 11100, FI-00076 Aalto, Finland

Abstract

The aim of the PRADA project was to develop tools and use of probabilistic risk assessment (PRA). The project consisted of four tasks. In the human reliability analysis task, VTT participated in the international EXAM-HRA project. On level 2 PSA, a passive safety device called autocatalytic hydrogen recombiner was analysed, and a pilot study of simulating a passive containment cooling system (PCCS) using MELCOR was conducted. Also on level 2, the integrated deterministic and probabilistic safety analysis (IDPSA) methodology was applied to ex-vessel steam explosions in a BWR; initially the deterministic accident progression simulations were conducted with MELCOR, but later pressure loads to container structure were analysed more accurately with a specialized fuel-coolant interaction code called MC3D. A literature survey was conducted on ex-vessel debris coolability, and two scenarios (pressurized and gravity-driven melt ejection) were analysed. On level 3 PSA, VTT participated in a Nordic project, creating a pilot to assess what the radiological consequences to the general population of some large cities in the Fukushima prefecture might have been, if the Fukushima Daiichi nuclear accident had happened in weather conditions prevailing typically in that part of Japan in March, and not the particular conditions of March 2011; the results indicate that the insignificant radiological consequences (no expected cancer deaths in the general public) predicted by UNSCEAR are to be expected.

Introduction

The aim of the PRADA (PRA Development and Application) project was to develop tools and use of probabilistic risk analysis (PRA). A central challenge in PRA is to extensively identify and assess quantitatively processes, events, factors and phenomena related to nuclear safety. Due to the complexity of the systems analysed, PRA involves multidisciplinary approaches and handling different kinds of uncertainties, with widely varying empirical data.

PRADA was divided into four independent and mutually complementary tasks: human reliability analysis (HRA), passive systems reliability, dynamic PSA (including level 2 PSA, and the analysis of prevention and emergency projects), level 3 PSA, and the handling of imprecise probabilities in reliability analysis. Handling of imprecise probabilities was carried out by Aalto University, and all the other tasks by VTT.

Main objectives

General goals of the PRADA project were to:

- Improve and develop methods for risk-informed decision making to support strategic and operative plant management
- Improve and develop PRA methods in terms of uncertainties and critical areas
- Develop PRA knowledge and expertise in Finland
- Foster international co-operation and import the best practices of the field into Finland

Human reliability analysis

In PRADA, the main activity in the human reliability analysis (HRA) area has been to participate in the Nordic, German and Swiss collaboration project EXAM-HRA (2009 – 2015), which assesses HRA applications in existing probabilistic safety analysis (PSA) studies (Bladh et al., 2014). The overall project objective is to provide guidance for a state of the art HRA for purposes of PSA, to ensure that plant specific properties are properly taken into consideration in the analysis. This shall also provide means to identify areas for plant improvement based on HRA and PSA results.

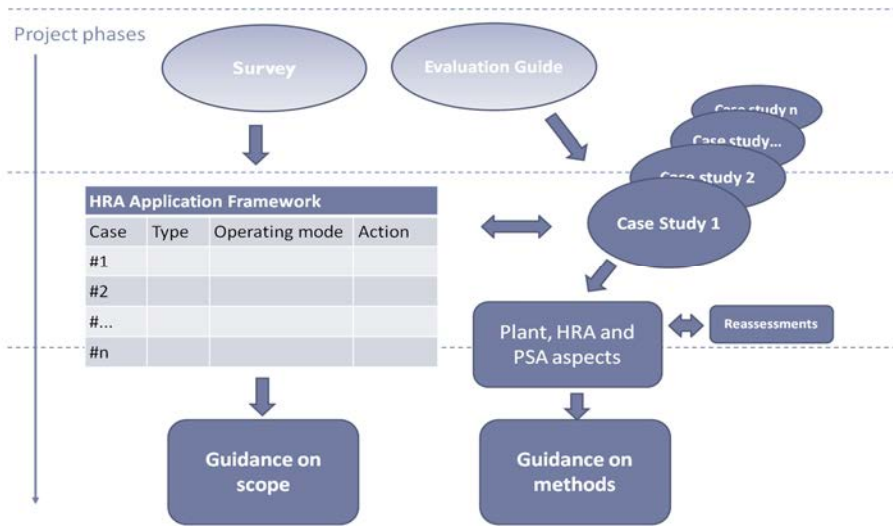


Figure 1. Overview of the EXAM-HRA project.

The project was performed in several consecutive phases, as shown in Figure 1. In the first phase, a framework for identifying discrepancies in existing HRA applications was developed. This includes a survey and screening process for operator actions in existing PSA studies as well as an evaluation guide on how to perform the case studies.

The survey provides an overview of performed HRA applications, including app. 420 operator actions from six PSA studies, and constitutes basis for the selection of scenarios and actions for assessment in case studies in the following phases. The case studies resulted in observations that allow for improvements of both plant features as well as the HRA itself. Additional assessments were performed on a number of operator actions in order to generate more comprehensive observations regarding both the plant features and HRA applications.

The gained insights from the survey and case studies are concluded in two guidance documents, which form the main results of the project:

- HRA application guide (EXAM HRA project report, 2015b)
- A practical guide to HRA (EXAM HRA project report, 2015a)

The HRA application guide provides guidance of the scope of human failure events to include in HRA applications in a plant specific PSA level 1 or 2 in order to improve the consistency of in-depth HRA and human error probability assessment. Accordingly, the guide is the result of performed survey and case studies in the EXAM-HRA project and presents an overview of operator actions represented by human failure events which are recommended to be covered in an HRA. The application guide can be used as a tool for identification of relevant human actions. By following the guide,

means are provided to get an understanding of how the human failure event scope has been defined and how analysed operator actions have been chosen.

The practical guide to HRA is intended to support a PSA practitioner in performing an HRA in form of a report easy to read with clear recommendations. The guide presents an overview of HRA methods and a summary of international guidance documents concerning the HRA process available in literature. Furthermore, it provides guidance on how to perform different tasks of the HRA process, based on the conclusions from the survey and case studies. In the guide, the HRA process is divided in tasks and attributes as shown in Table 1. Guidance on each item in the table is given in form of:

- Considerations, problem definition stemming from the assessments made of existing applications
- Recommendations based on the evaluations, formulated with the objective to reduce variability of HRA studies
- Examples, providing supporting observations from case studies made of existing applications

Table 1. The tasks and attributes of the HRA process.

HFE Definition			Quantification	V&V
Selection	Data collection	Qualitative analysis		
Identification	Plant organization / management	Task analysis	Methodology	Reasonableness
			PSF calculation	
Screening	Task specific information		PSF Assessment	Dependencies
		Uncertainties		
Errors of Commission	Task context	Recoveries		Adequacy
		Minimum believable results		
		Actions without procedures		
			HRA for hazards	
Documentation				
HRA Team				

There were also other activities performed within HRA. The Enhanced Bayesian THERP is a human reliability analysis method developed initially from similar methods used at Olkiluoto and Forsmark probabilistic risk assessment methods. In PRADA, the method was developed further, based on experience and insights

gained from the International HRA Empirical Study and EXAM-HRA. The connection of the performance shaping factors to probability, and the use of time correlation curve were further developed.

A literature review on challenges of HRA in the digitalization of nuclear power plant control rooms was written. It turned out that literature on the topic is scarce.

Level 2 probabilistic safety analysis

Passive safety systems do not need any external input such as mechanical or electrical power to operate. Instead, they rely on natural laws, internally stored energy or material properties. Assessing the reliability of passive systems is challenging due to their reliance on physical principles, which complicates modelling. Significant amounts of uncertainty related to passive systems, both of epistemic and aleatory kind, pose further difficulties. The measures which determine failure states of passive systems are typically continuous – e.g. a percentage value of nominal performance – and therefore the choice of failure criteria is an ambiguous task. In passive systems reliability analysis, a diploma thesis was completed on the use of passive autocatalytic hydrogen recombiners (PAR) to prevent hydrogen explosions in a severe accident. In it, a simplified Failure Modes and Effects Analysis (FMEA) was conducted, and a general framework of combining PAR reliability analysis with containment event tree modelling was developed. The main result of the analyses was that in the computational experiments, PARs didn't work effectively in preventing hydrogen explosions, at least in the positions that were tried; the main reasons for this inefficiency seem to be that the PAR starts slowly, giving the hydrogen time to explode, and that it isn't efficient if not placed properly. When properly placed, research by others strongly indicates that PARs prevent hydrogen explosions.

A pilot study of simulating another passive safety system, a passive containment cooling system (PCCS), using MELCOR was conducted (Männistö and Karanta 2012). The PCCS proved to not function as expected in the case study. The original intention was to use the MELCOR simulation results to also obtain a quantitative reliability assessment for the PCCS. Since the safety function was not fulfilled, this was not possible (or in other words, the reliability would be zero). In the context of passive systems reliability framework some useful insights were gained, however. The purpose of the PCCS was to control containment temperature and pressure in a severe accident. Applied to the Olkiluoto plant model we can find suitable candidates for failure criteria. In the MELCOR analysis the containment pressure limit is also controlled by the rupture disks, and this gives the upper limit for the pressure in the scenario. It follows that the containment pressure limit can be used as a basis for a failure criterion. MELCOR analysis results also revealed that the following three variables have the greatest impact on the heat transfer capability of the PCCS: drywell to wetwell differential pressure, noncondensable gas mole fraction, pressure in the drywell. Each of these variables was shown to have a quantified effect on the performance. Drywell to wetwell differential pressure was noticed to be essential for the functioning of the PCCS system at all. According to the MELCOR simulations, a

pressure difference of 10 kPa is required for any heat transfer. However, due to this reason the PCCS does not fulfil the safety function for which it is designed.

VTT also participated in the Nordic Deterministic-Probabilistic Safety Analysis Methodology (DPSA) project in cooperation with Kungliga Tekniska Högskolan and Lloyd's Register. The project handled Integrated Deterministic and Probabilistic Safety Analysis (IDPSA), which is a framework referring to the variety of different approaches and tools developed for combined probabilistic and deterministic analysis during the last decades. Two workshops were arranged (Adolfsson et al. 2011 and Adolfsson et al. 2012).

Steam explosions were studied in the IDPSA framework, with two case studies concerning the Olkiluoto nuclear power plant units 1 and 2. In the first case study (Silvonen 2013), deterministic accident progression simulations were performed with MELCOR and the knowledge obtained from them was then implemented into a probabilistic containment event tree model of the plant (Figure 2) constructed with SPSA. Ex-vessel steam explosions and source term were modeled more rigorously than many other parts of the model. Analysis results were expressed mainly in terms of radionuclide releases to the environment, but instead of accurate numerical values the successful illustration of methodological approach was of higher importance. During the work, it was noticed that use of a specialized analysis tool to model fuel coolant interactions (FCI) would be important in order to introduce even more detailed and plant-specific approach, but this time literature and expert judgment had to be relied upon.

In the second steam explosion case study (Silvonen 2014a), the first case study was supplemented by providing more detailed analysis on ex-vessel steam explosion loads posed to containment structure of a BWR reactor. The analyses were conducted with MC3D code, which is a multidimensional numerical tool devoted to analysis of FCI phenomena. Results can be reflected to steam explosion modeling implemented in a level 2 PRA model developed last year, and the analysis can thus be regarded to be an application of IDPSA methodology. Focus of this study is on safety considerations and complex physics and mathematical modelling are given less (if any) attention.

The analysis cases were studied for two different vessel failure modes and by using two fragmentation models. The first case was a single large central hole in the reactor pressure vessel lower head, and the second melt ejection mode is a result from multiple simultaneous failures of vessel penetrations, representing instrumentation and control rod guide tube failures. Limited sensitivity analyses were performed for fragmentation model parameters and for explosion triggering time.

Core damage sequence PDS	Containment leak-tightness ISOL	RCS depressurization DEPR	ECCS recovery ECCS	Very early containment failure VEF	Vessel failure VF	Early containment failure EF	Late containment failure LF	Consequence
	ISOL_OK	DEPR_OK	REC	NO_VEF	NO_VF	NO_EF	NO_LF	#1
					VF	NO_EF	NO_LF	#2
							LF	#3
						EF	NO_LF	#4
				VEF	NO_VF	NO_EF	NO_LF	#5
					VF	NO_EF	NO_LF	#6
			NO_REC	NO_VEF	VF	NO_EF	NO_LF	#7
							LF	#8
						EF	NO_LF	#9
				VEF	VF	NO_EF	NO_LF	#10
		NO_DEPR	REC	NO_VEF	NO_VF	NO_EF	NO_LF	#11
					VF	NO_EF	NO_LF	#12
							LF	#13
						EF	NO_LF	#14
				VEF	NO_VF	NO_EF	NO_LF	#15
					VF	NO_EF	NO_LF	#16
			NO_REC	NO_VEF	VF	NO_EF	NO_LF	#17
							LF	#18
						EF	NO_LF	#19
				VEF	VF	NO_EF	NO_LF	#20
	NO_ISOL	DEPR_OK	NO_REC	NO_VEF	VF			#21

Figure 2. The containment event tree developed for the first steam explosion case study. The upwards branches represent successes in safety functions whereas downwards branches result in unwanted consequences.

Results showed generally quite large pressures and impulses in comparison with e.g. results obtained in OECD's SERENA program (OECD 2006), and for multiple melt jets the pressure loads were even higher than for single jet case. Throughout the analyses there were difficulties to trigger explosions and to compare different cases thus became more complicated. Although it is difficult to validate results and more detailed modelling would be necessary in order to draw more credible conclusions, this study produced useful information e.g. from IDPSA perspective and also enhanced modeling capabilities at VTT.

Also a literature study (Silvonen 2014b) on ex-vessel debris bed coolability from safety analysis perspective was conducted, especially regarding level 2 probabilistic risk assessment (PRA). The goal is to explore practical and risk-informed ways to deal with debris coolability issues in plant scale risk considerations. Anal-

yses exploit deterministic accident progression simulations which are performed using MELCOR, and thus this study builds upon IDPSA (integrated deterministic and probabilistic safety assessment) framework. The literature study covered the most important debris bed parameters that can affect debris coolability. Also mechanisms that provide cooling were briefly presented. Empirical research on debris coolability has been performed at VTT and also elsewhere. Analytical capabilities play a crucial role in coolability assessment, and some codes developed for that purpose were introduced in short.

Prevention and emergency operations modelling

Prevention and emergency (P&E) operations are fast response operations for preventing adverse events from disturbing a system's operations or damaging its equipment or structures, for responding to and mitigating the consequences of adverse events, and for recovering from such events (Karanta, 2014). They are operations that involve more than one actor, more than one task to be completed, precedence relations between tasks, usually limited resources and a finite amount of time for completion.

Within nuclear safety, the main goals of prevention and emergency operations are to prevent production breaks and damage to utility, minimize damage, protect personnel and prevent a release of radioactive substances. Some examples of such operations are recovery from a loss of coolant accident (LOCA), evacuation of personnel, and fire extinguishing.

There are four major kinds of risks involved with prevention and emergency operations:

- Cost risk, or the risk that the cost of an operation exceeds some prespecified limit
- End product quality risk, or the risk that the end product of the operation (e.g. repaired dam, reactor after a recovery from LOCA) does not meet its specifications
- Schedule risk, or the risk that the operation (or parts of it) take more time than is allowed
- Safety risk, or the risk that the during the course of the operation the safety of some people (e.g. operation workers) is compromised

(Karanta 2014) proposed that modelling P&E operations as projects would incorporate several advantages: foremost, the scientific results of decades of project management research would be available to bear on the analysis. In that report, activity networks were chosen as the representation formalism for P&E operations, and a small case study – blocking oil from entering the cooling water system of Fortum's Loviisa nuclear power plant – was presented.

Two case studies on the modelling and analysis of prevention and emergency operations were conducted. The first case (Karanta 2014) concerned the construction of an oil dam from booms to prevent leaked oil from reaching the feedwater system of a nuclear power plant. It turned out that activity networks are a suitable

model class for describing an operation when the activities to be conducted are fixed in advance. The second case (Karanta 2015) handled the clearing of roads leading to Hästholmen from fallen trees after a heavy storm. The problem was modelled as an activity network.

Level 3 probabilistic safety analysis

In level 3 PSA, a proposed interface between levels 2 and 3 has been defined (Karanta 2013). Also an initial requirements specification for a new PSA level 3 code has been written.

The main effort on level 3, however, has gone to Nordic cooperation project Addressing off-site consequence criteria using Level 3 PSA (L3PSA). The project has received NKS/NPSAG funding, and has been conducted in cooperation with the Swedish companies Scandpower (now Lloyd's Register Consulting), Risk Pilot and ES-Konsult. In the project, a questionnaire study has been conducted on the uses and needs in level 3 PSA, appropriate risk metrics have been defined for level 3, regulations, guides and standards followed, and pilot applications developed.

VTT's main contribution in L3PSA has been to develop a level 3 PSA pilot application (Rossi et al. 2014, Karanta et al. 2015). The pilot studies the Fukushima nuclear accident from an alternative history point of view. The number of deaths in the general public resulting from the radioactive release has been estimated to be 0 by UNSCEAR. The pilot tries to answer the question: was the low number of current and future casualties the result of good luck, or was it to be expected. The probabilistic parts of the situation (weather, evacuation and shielding success probability) were handled in an event tree, constructed in the SPSA code. The deterministic parts (atmospheric dispersion, dose calculations) were handled in VTT's ARANO code. The results obtained indicate that the result is typical of what one might expect, given the weather conditions in that part of Japan in general in March, and the efficiency of the evacuation operation in the Fukushima prefecture in March 2011. The constructed model indicates that with probability 0.957, there would have been no cancer deaths in the largest towns close to the site, and the expected number of cancer deaths would have been 16. All in all, the number of cancer death would have remained low with a very high probability, as indicated by the Farmer's curve (Figure 3). Also a sensitivity and uncertainty analysis was carried out.

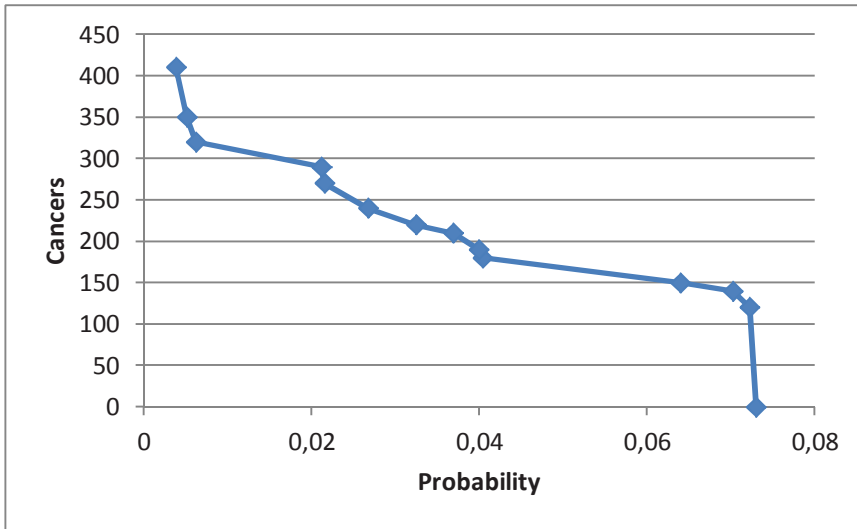


Figure 3. Farmer's curve for the probability of exceeding the given number of cancer deaths obtained in the pilot.

Imprecise probabilities in PRA

In probabilistic risk analysis (PRA), the safety of a system is analysed with respect to random events such as component failures, earth quakes, and fires. This random nature of the events can be captured using probabilities and the uncertainty whether an event with a given probability is realized or not is called *aleatory uncertainty* (Apostolakis 1991).

The numerical values of the probabilities are uncertain because of rounding/truncating errors, model bias, statistical estimation error and expert assessment uncertainty. This uncertainty about our knowledge of the probabilities is called *epistemic uncertainty* (Apostolakis 1991). Epistemic uncertainty can have a significant impact on the recommendations of a PRA model. Therefore it is important to quantify how reliable the PRA models are with respect to epistemic uncertainty.

This project has developed methods for analysing the impact of epistemic uncertainty in the context of fault tree analysis, which is a widely used PRA method in nuclear safety. We consider models where the alternatives are evaluated with regard to a numerical measure computed using the events' probabilities, such as the reliability of the system. We model epistemic uncertainty about the evaluations using interval-valued probabilities, where the lower and upper bounds of the interval correspond to plausible lower and upper bounds of the probabilities, respectively.

Decision recommendations are derived by using the concept of dominance: an alternative A is dominated if there exists another alternative B that is at least as good as A for all probabilities within the intervals and strictly better for some probabilities

within the intervals. Because dominated alternatives are inferior to the alternatives that dominated them, it is recommended to select a non-dominated alternative.

In Toppila, A. & Salo (2012, 2013), we present a computational framework for prioritizing events using risk importance measures when epistemic uncertainty about model parameters is expressed using interval-valued probabilities (see also Jussila 2013). Risk importance measures are widely used for identifying the parts of a system that are the most significant sources of risk. An example of a risk importance measure is the Birnbaum risk importance measure of a component C, which can be interpreted as the increase in reliability when C is changed from totally unreliable to fully reliable, keeping other components' reliabilities fixed.

Figure 1 provides illustrative results for the residual heat removal system of a nuclear power plant which has 31 basic events and 147 minimal cut sets. The diagram on the left presents an example of the results when analyzing the Fussell-Vesely measures of the components of a residual heat removal system. In this panel, a directed arc indicates a dominance relation. For instance, the arc from 1 to 6 indicates that component 1 dominates component 6 with respect to the Fussell-Vesely measure under the given probability intervals. The non-dominated set consists of components 1-5, which the model recommends to be considered for improvement.

In Toppila & Salo (2015a), we present a portfolio optimization model for resource allocation to risk reduction activities under interval-valued probabilities (see also Losoi, 2013). We used the non-dominated portfolios to derive recommendations about which actions are more cost-effective than others in improving system reliability. Figure 4 (right) shows for portfolios of actions are cost-efficient for improving the reliability of the example residual heat removal system when 1) each failure probability is within an interval whose width is half of the 90% estimated confidence interval and 2) each failure probability can be set to zero through an action for a cost of one unit (green = cost-efficient, red = not cost-efficient, grey = analyze further using other metrics such as importance measures).

The exact computation of non-dominated portfolios belongs to a class of challenging optimization problems. We have improved the computational capability by building a novel method based on total order interactions. For instance, the problem for the residual heat removal system took initially 30 hours to solve; but, after several algorithmic improvements, this problem has now become tractable and can be solved in about 2.5 hours. Even though this method is based on a simplification of the reliability function, it still generates a sufficient number of non-dominated solutions for deriving meaningful implications for decision making (see Table 1). The computational methods still have potential for improvement which is ongoing research in the Aalto University (Toppila & Salo 2015b).

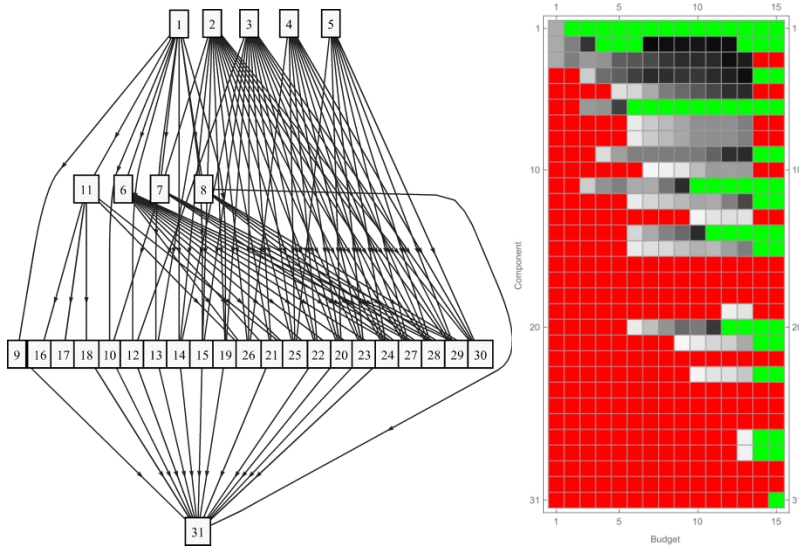


Figure 4. A dominance graph (left) and a core index matrix (right) of a residual heat removal system.

Table 2. Share of the non-dominated set that could be computed using the improved algorithm.

Budget	1	2	3	4	5	6	7	8	9	10	11	12	13	14	15
Share of ND set (%)	100	100	100	100	100	42	75	85	72	74	39	25	67	0	0

References

- Adolfsson, Y., Holmberg, J.-E., Hultqvist, G., Kudinov, P., Männistö, I. (eds). Proceedings of the Deterministic/probabilistic safety analysis workshop October 2011, VTT Research Report VTT-R-07266-11, 2011, Espoo.
- Adolfsson, Y., Holmberg, J.-E., Karanta, I., Kudinov, P. (eds). Proceedings of the Deterministic/probabilistic safety analysis workshop November 2012, VTT Research Report VTT-R-08589-12, 2012, Espoo.
- Apostolakis, G 1990. The concept of probability in safety assessment of technological systems. *Science* 250(4986), 1359-1364.
- Bladh, K., Frohm, J., Iseland, T., Karlsson, A., Becker, G., Tunturivuori, L., Porthin, M., Olsson, A., Böhm, J., Johanson, G., Jonsson, S. 2014. Evaluation of Existing Applications and Guidance on Methods for HRA – EXAM-HRA - Phase 3a Summary Report. NKS-R report number NKS-305.
- EXAM HRA project report, 2015a. A practical guide to HRA. Report under preparation.
- EXAM HRA project report, 2015b. HRA application guide. Report under preparation.
- Jussila, T. 2013. Yhteisviat ja intervallitodennäköisyydet vikapuuanalyysissä. Aalto university, Bachelor's Thesis.
- Karanta, I. 2013. Level 3 PSA from a software architecture point of view. VTT Research Report VTT-R-01071-13, 2013, Espoo.
- Karanta, I. Modelling of prevention and emergency operations for probabilistic risk analysis. VTT Research Report VTT-R-01743-14, 2014, Espoo.
- Karanta, I. Clearing of roads to Hästholmen after a storm – a case study in emergency operations modelling. VTT-R-05654-14, 2015, Espoo.
- Karanta, I., Tyrväinen, T., Rossi, J. Applying IDPSA in PSA level 3 – a pilot study. VTT Research Report VTT-R-05661-14, 2014, Espoo.
- Losoi, M. 2013. Optimal Risk Reduction Portfolios in Fault Tree Analysis. Aalto university, Bachelor's Thesis.
- Männistö, I., Karanta, I.. Passive Systems Reliability – Application of MELCOR Simulations for PCCS Case Study. Proceedings of the 11th International Probabilistic Safety Assessment and Management Conference & The Annual European Safety and Reliability Conference 2012 (PSAM11 ESREL 12), Helsinki, Finland, 25–29 June 2012, Volume 4, Curran Associates Inc. 2012, ISBN 978-1-62276-436-5, 2778-2785.

- OECD Nuclear Energy Agency, "OECD research programme on fuel-coolant interaction, Steam Explosion Resolution for Nuclear Applications - SERENA - Final Report," Paris, 2006.
- Rossi, J., Karanta, I., Silvonen, T. A plan for a pilot study of level 3 PSA using IDPSA. VTT Research Report VTT-R-00559-14, 2014, Espoo.
- Silvonen, T. Steam explosion case study using IDPSA methodology. VTT Research Report VTT-R-05974-13, 2013, Espoo.
- Silvonen, T. MC3D simulations of ex-vessel steam explosions in IDPSA framework. VTT-R-02944-14, 2014a, Espoo.
- Silvonen, T. Treatment of ex-vessel debris coolability in IDPSA context. VTT-R-02943-14, 2014b, Espoo.
- Toppila, A. & Salo, A. 2012. Prioritizing Failure Events in Fault Tree Analysis Using Interval-valued Probability Estimates. Proceedings of the International Conference on Probabilistic Safety Assessment and Management & Annual European Safety and Reliability Conference, 25-29 June 2012, Helsinki, Finland.
- Toppila, A. & Salo, A. 2013. A computational framework for prioritization of events in fault tree analysis under interval-valued probabilities. IEEE Transactions on Reliability 62(3), 583-595.
- Toppila, A. & Salo, A. 2015a. Selection of risk reduction portfolios under interval-valued probabilities. Manuscript, Aalto University.
- Toppila, A. & Salo, A. 2015b. Computation of non-dominated portfolios using binary decision diagrams. Working paper, Aalto University.

43. FinPSA knowledge transfer (FINPSA-TRANSFER)

43.1 FINPSA-TRANSFER summary report

Teemu Mätäsniemi¹, Tero Tyrväinen², Kim Björkman² & Ilkka Niemelä³

¹VTT Technical Research Centre of Finland Ltd
Tekniikankatu 1, P.O. Box 1300, FI-33101 Tampere

²VTT Technical Research Centre of Finland Ltd
Vuorimiehentie 3, P.O. Box 1000, FI-02044 VTT

³STUK - Radiation and Nuclear Safety Authority
P.O. Box 14, FI-00881 Helsinki

Abstract

This paper represents achievements of FinPSA knowledge transfer (2012-2014) project which focussed to development and maintenance of probabilistic risk analysis (PRA) tools and knowledge transfer to new experts. Level 1 and 2 PRA tools and their integration are concerned. The paper considers also the business value of tools and how to improve it by re-implementation, documentation, verification and validation.

Introduction

Probabilistic risk analyses (PRA) are carried out for nuclear power plants (NPP) in order to provide systematic plant analyses, to give confidence that a design complies with safety objectives and to demonstrate that a balanced design has been achieved. Complex plant design and physical phenomena explain also many challenges in the analyses and tool support. This paper represents achievements of FinPSA knowledge transfer (2012-2014) project which focussed to development and maintenance of PRA tools and knowledge transfer from STUK - Radiation and Nuclear Safety Authority Finland to new experts of VTT Technical Research Centre of

Finland. In addition, the project demonstrated practices and skills in the development of software products critical to safety.

The paper starts with a short background and objective descriptions. These familiarize a reader with the tools and their initial situation. Also, tool specific objectives are stated. The following chapters progress according to PRA analysis phases from core damage analysis (level 1) via plant damage states (interface trees) to containment event tree analysis (level 2). The report concentrates on software tool support in these phases. In addition, references contain a quite comprehensive list of project reports for further readings.

Background and objectives

FinPSA and SPSA are software tools originally developed by the Finnish Radiation and Nuclear Safety Authority (STUK). SPSA supported both level 1 and 2 analyses. Its implementation was completed in early 1993. Development of FinPSA was started in 2000 and the software was launched to customers in 2005. At the beginning of FinPSA knowledge transfer project, FinPSA tool supported only level 1 analysis.

Since the application area of FinPSA and SPSA is to support PRA for nuclear power plants, a long lifetime is an essential feature of the software. This fact emphasises the role of software processes and their contributions to the qualities of the software. FinPSA and SPSA were in different positions in this context as illustrated by grey ellipses in the following figure.

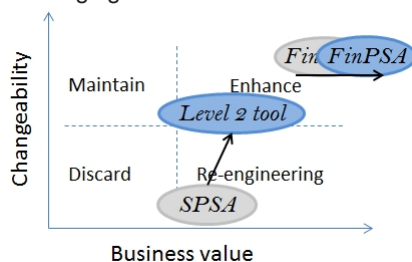


Figure 1. Decision matrix (Jacobson and Lindström 1991), what to do with FinPSA and SPSA.

FinPSA had been developed and maintained with the newest software development tools and it was one of the most powerful PRA tool in the market. In addition, its implementation utilized several design patterns and algorithms which are already tested in the predecessor (SPSA) software. The user interface of FinPSA was user friendly, it provided clear modelling concepts to an analyst and it had numerous new capabilities compared to SPSA. So, the maintenance of the software was quite easy and it had a high business value. Thus, it was realistic to assign FinPSA to enhance category and to continue its development and maintenance.

On the other hand, SPSA had been developed with old technologies which do not operate in the newest operating systems. In addition, restructuring of the code with a newer compiler was not realistic originating from the lack of documentation. However, SPSA had very attractive modelling environment which allows modelling of causal dependencies and time-dependencies of complex phenomena and interactions needed in the level 2 analysis. So, SPSA was assigned between re-engineering and discard categories as shown in the Figure 1.

Before the project, FinPSA and SPSA had been developed with little resources for documentation. Thus, the traceability and validation of requirements had only been partly implemented or forgotten totally. In consequence, it was challenging to prove the quality of FinPSA to unfamiliar audience, to prove the correctness of analysis results and to show that the software satisfies requirements stated by international standards. Objective for level 1 tool (FinPSA) was set to overcome these restrictions. In the first project year it was also realized that a new prototype of level 2 tool had to be developed as an updated version of SPSA. The lack of maintainability and other limitations of SPSA promote this decision. Thus, the objective for level 2 tool was to support existing models and much higher tool changeability as illustrated by a blue ellipse in Figure 1.

Level 1

A level 1 model in FinPSA consists of event trees, fault trees, hazard map, I&C model and reliability data of the components of the model. The objective of the level 1 analysis is to calculate the core damage frequency of a nuclear power plant. In the analysis, minimal cut sets, which are minimal combinations of basic events that cause the core damage, are generated. The core damage frequency is calculated based on minimal cut sets and the probabilities of basic events. FinPSA level 1 models can also be applied to the risk analysis of other complex systems in the similar manner.

The features of level 1 include possibilities to rank basic events using risk importance measures and perform uncertainty analysis, sensitivity analysis and time-dependent calculation. FinPSA contains features to model also asymmetric common cause failures. The results of FinPSA level 1 are traceable so that the origin of each minimal cut set is known and can be illustrated in a fault tree.

FinPSA level 1 support was already well established before the project. However, even if SPSA and later FinPSA had been used for 20 years with no error reports from users, the development practises were not adequate. The work of the project concentrated therefore on ensuring good maintenance and proving the quality of the tool. The work was started by writing a requirements specification based on international guidelines and user requirements (Niemelä and Björkman 2013). The work also included detailed documentation of the units, architecture and algorithms of the software (Niemelä and Mätäsniemi 2013a/b/c & 2014). In addition, software testing was carefully planned, executed and documented (Tyrväinen 2014b/c) and a quality

assurance plan was written (Tyrväinen 2014a). The transfer of the knowledge on the level 1 software code was supported by internal training sessions and meetings.

During 2012 end user experiences from using FinPSA were collected. End user requirements were documented, analysed, classified, and prioritized. FinPSA level 1 requirements specification (Niemelä and Björkman 2013) was prepared. The goal was to demonstrate that FinPSA conforms to related international standards and to link FinPSA specific requirements to framework represented in the standards. For level 1 requirements specification, about 280 requirements were specified. Of the requirements about 60 originated from end user requirements. FinPSA seems to fulfil all of the requirements obtained from IAEA SSG-3 standard except that verification and validation has not reached full coverage of properties yet.

Already in the early phase, it was understood that the testing of the level 1 software has to be planned and performed carefully because of its importance to nuclear safety and its complexity. A verification and validation plan (Tyrväinen 2014b) with over fifty properties was prepared based on the requirements specification (Niemelä and Björkman 2013). All tests were prioritised and the correctness of minimal cut sets and quantification results were identified to be the most important properties for testing. Tests were performed and a verification and validation results document (Tyrväinen 2014c) was written for the properties related to generation of minimal cut sets and PRA modelling. The result of the whole process was an established practise to document, prioritise and perform tests. Many test runs were also automated using script files launched outside the software and a plan was written for automatic checking of test results (Tyrväinen 2015). In general, the testing activities supported the knowledge transfer excellently because the functionalities of the software had to be studied in detail.

A quality assurance study of safety related software was started by a literature survey (Tyrväinen and Mätäsniemi 2013b) in which both PRA standards and software quality assurance standards were examined. PRA standards address computer codes only briefly. A moderate set of general guidelines could be constructed by putting findings from different sources together. Based on the literature study, a quality assurance plan was written for FinPSA (Tyrväinen 2014a). The plan includes the roles of the employees, development and maintenance practices, configuration management plan and references to the other relevant product documentation.

The development of the software code included improvements in the heuristic of minimal cut set search algorithm, the calculation of the total frequency and the manipulation of attributes of selected accident sequences. In addition, many deficiencies were fixed during the project.

Interface trees

For the integration of level 1 and level 2 the interface trees are used. In SPSA level 1 binning rules were used for the integration. Binning rules mapped event tree sequence minimal cut sets (MCS) to plant damage state (PDS) MCSs (In SPSA there

is also another set of binning rules, which are used to classify end states of level 2 sequences into release categories).

Figure 2 illustrates the concept of integrating PRA levels 1 and 2. Interface trees are used to link event tree sequences to plant damage states. These trees incorporate, for example, containment systems or other systems that do not directly affect the occurrence of core damage (i.e. systems which do not contribute to the success criteria for preventing core damage) into the PRA.

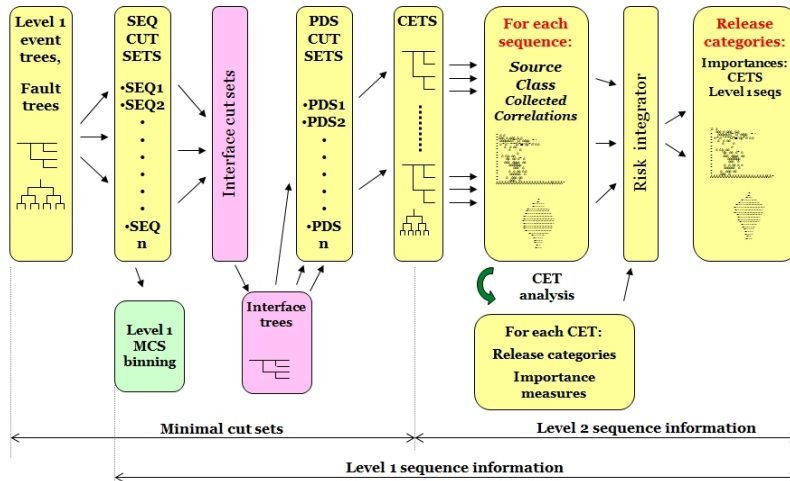


Figure 2. Concept of FinPSA for PRA level 1 and 2 integration

For each interface tree sequence a PDS can be specified similarly to specifying consequences for event tree sequences. Interface tree sequence minimal cut sets can be combined to form PDS minimal cut sets.

At the beginning of the project, FinPSA allowed to create graphical interface trees, to set interface trees for event tree sequences and to mismatch the MCSs of the event tree sequences for which a specific interface tree is defined. These combined MCSs function as the initial conditions (corresponds to the initial event of event trees) for interface trees. Also, the interface trees documentation related to design, implementation and testing was very limited or non-existing. For that reason, software requirements specifications for level 1 [(Niemelä 2013) and level 2 (Björkman 2013a) were developed. The level 1 and 2 interface was included in the level 1 specification. The level 2 work brought also out additional requirements for the interface trees.

FinPSA interface tree implementation is based on the presented idea (Figure 2), the collected requirements and the event tree implementation. In 2013, the basic interface tree functionality was implemented and included in FinPSA releases as a default. The functionalities cover editing of interface trees and computation of MCSs for interface tree sequences and their combination into PDS MCSs. Each PDS MCSs can be traced back to the interface tree and event tree sequence, and visual-

ized in the automatically generated sequence fault tree. FinPSA enables also the creation of a PDS matrix. A PDS matrix illustrates the contribution of each event tree to the total frequency of each PDS. The interface tree design and implementation have been described in (Björkman 2013b). To keep high quality, the verification and validation of interface trees were performed (Tyrväinen 2014d, Tyrväinen 2014e) and FinPSA manual was updated.

One of the main achievements of interface tree development was education of new FinPSA developers. The work provided valuable information on the architecture of FinPSA code, as well as on used data structures and algorithms both on general and implementation level. Additionally, the general knowhow on software development was enhanced.

Level 2

The level 2 probabilistic risk analysis is carried out in order to identify the accident sequences that lead to challenges to the containment and releases of radioactive material to the environment. Possible severe accident progressions are modelled by using containment event trees (CETs) to analyse ways of releases and to estimate frequency, magnitude and other relevant characteristics of the release of radioactive material. The analysis is based on plant damage states which categorize level 1 accident sequences based on accident timelines and loads on the containment. The objective of the level 2 analysis is to define accident progression, fission product evolution, retention and transport through each of the major barriers to the environment after the core damage. Amount and isotopic composition of radioactive material releases are calculated. Radionuclide releases are expressed as source terms and finally their amounts are grouped to release categories.

An example CET is represented in Figure 3. A CET is a graphical tree which represents the progression of an accident sequence. The contents of the tree have been divided to columns and rows. The columns are called headings or sections and each column represents a question related to severe accident management.

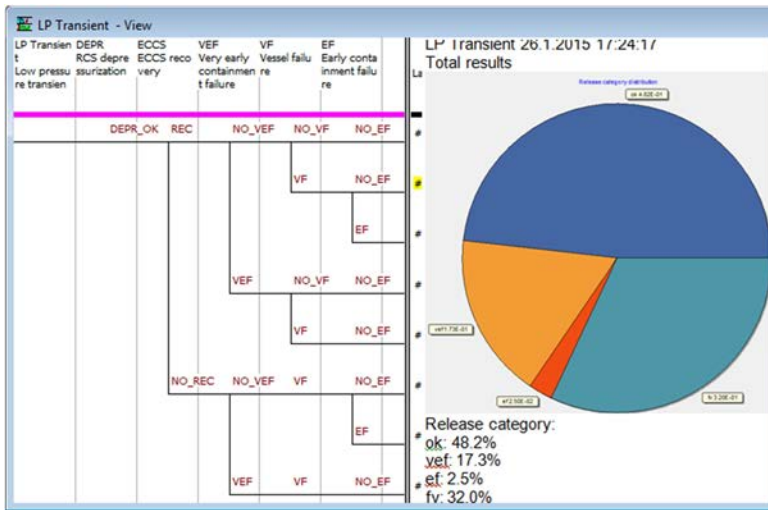


Figure 3. Example containment event tree

There can be several different answers (max. 8) to a question of a CET column. The conditional probabilities of the answers are calculated using functions which are written by user in the tool's own modelling language. The probabilities can depend on the earlier evolution of the accident because variable values from previous CET columns can be used in the calculation. User defined functions are also used to model state and structural changes in control volumes and barriers (parametric model).

The project work for this phase concentrated on re-implementation of the level 2 tool and its co-operation with level 1 tool (FinPSA). The requirements specification was prepared (Björkman 2013a) based on IAEA SSG-4 (2010) and end user requirements. In addition, a couple of quality attributes were selected: traceability, openness, teamwork, efficiency and maintainability. The software shall be able to trace and explain all logical results and their uncertainties (traceability). Openness ensures data import and export possibilities. Several users should be able to maintain a model at the same time (teamwork). Efficient algorithms with multicore or distributed computing environment should be applied. This makes it possible to solve large models. Finally, the tool is implemented and programmed in such way that it can be used for a long time and created models shall be transferable to possible new tools (maintainability). That is essential for guaranteeing the long lifetime of PRA models related to the life span of a NPP.

The level 2 tool architecture was designed according to the stated requirements (Mätäsnämi et al. 2014a). The architecture was seen as an information refining process in which software modules or functional units utilize some information and produce other information. The architecture is presented in the Figure 4.

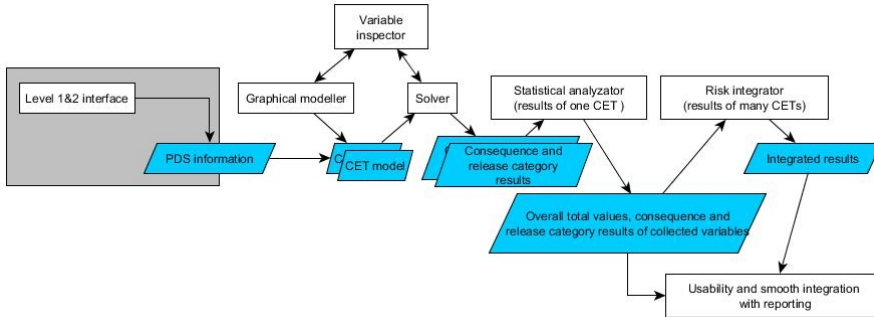


Figure 4. Level 2 architecture

Information blocks (parallelograms) between the modules establish dependencies between them. The purpose of the graphical modeller is to enable editing of the containment event trees. A solver works as a calculation engine which resolves CET execution model and simulates results. Based on simulation results, the statistical analyzator performs statistical analyses which include statistics for frequency and variables and their correlations in each sequence and release category as well as over all sequences. Risk integrator, variables inspector and error recovery have not been implemented yet. Development of these issues is needed before level 2 tool is ready for full-scope plant level analysis. Architecture design was continued by detailed design (Mätäsniemi et al. 2014b), implementation and verification and validation (Tyrväinen et al. 2014f, 2014g).

On these days, level 2 tool is in prototype phase. The tool calculates correct results for the existing Olkiluoto 1 & 2 (NPPs) model. In addition, a preliminary user guide was prepared and an end user training session was organized. The tool was implemented modularly with modern technologies and its maintainability and changeability are much better than earlier. Finally, level 2 functionality was integrated with level 1 tool (FinPSA).

Acknowledgement

We would like to show our gratitude to SARIF2014 - The Finnish Research Programme on Nuclear Power Plant Safety 2011 – 2014 and especially Nuclear Waste Management Fund, TVO, ENSI and Fortum for giving us a good possibility to organize FinPSA knowledge transfer project and to educate new PRA tool experts. In addition, FinPSA end user group members had an important role in guiding of the work.

Espoo 29.1.2015

Authors

References

- Jacobson, I. and Lindström, F. 1991. Re-engineering of old systems to an object-oriented architecture. In: ACM SIGPLAN, Proceeding OOPSLA '91 Conference proceedings on Object-oriented programming systems, languages, and applications. pp 340 – 350. New York, USA. ISBN 0-201-55417-8
- Björkman, K. 2013a. FinPSA – Software requirements – Level 2 documentation. Version 1.0. 18 p. Espoo: VTT Technical Research Centre of Finland. VTT Research Report VTT-R-00364-13. Limited Distribution.
- Björkman, K. 2013b. FinPSA – Software design – Interface trees and level 2 demonstration. 12 p. Espoo: VTT Technical Research Centre of Finland. VTT Research Report VTT-R-07014-13. Limited Distribution.
- IAEA SSG-3. 2010. Development and application of level 1 probabilistic safety assessment for nuclear power plants: specific safety guide. In: IAEA safety standards series. Vienna. International Atomic Energy Agency. ISBN 978–92–0–114509–3
- IAEA SSG-4. 2010. Development and application of level 2 probabilistic safety assessment for nuclear power plants : specific safety guide. In: IAEA safety standards series. Vienna. International Atomic Energy Agency. ISBN 978–92–0–102210–3
- Mätäsniemi T., Tyrväinen, T., Silvonen, T., Björkman, K. 2014a. FinPSA – Software design – level 2 architecture. 25 p. Espoo. VTT Technical Research Centre of Finland, VTT Research Report VTT-R-00604-14.
- Mätäsniemi, T., Tyrväinen, T., Björkman, K., Silvonen, T. 2014b. FinPSA – Software design – Level 2 detailed design. 56 p. Espoo. VTT Technical Research Centre of Finland. VTT Research Report VTT-R-04887-14.
- Niemelä, I. & Björkman, K. 2013. FinPSA – Software requirements – Level 1 documentation. Version 1.0. 52 p. Espoo: VTT Technical Research Centre of Finland. VTT Research Report VTT-R-00447-13. Limited Distribution.
- Niemelä, I. & Mätäsniemi T. 2013a. FinPSA – Software design – Architecture documentation. Version 1.0. 32 p. Espoo: VTT Technical Research Centre of Finland. VTT interim report. Limited Distribution.
- Niemelä, I. & Mätäsniemi T. 2013b. FinPSA – Software design – Main unit documentation. Version 1.0. 198 p. Espoo: VTT Technical Research Centre of Finland. VTT Research Report VTT-R-00353-13. Limited Distribution.

- Niemelä, I. & Mätäsniemi T. 2013c. FinPSA – Software design – Supporting unit documentation. Version 1.0. 98 p. Espoo: VTT Technical Research Centre of Finland. VTT Research Report VTT-R-00351-13. Limited Distribution.
- Niemelä, I. & Mätäsniemi T. 2014. FinPSA – Software design – Level 1 complex algorithms. Version 1.0. 49 p. Espoo: VTT Technical Research Centre of Finland. VTT Research Report VTT-R-00583-14. Limited Distribution.
- Tyrväinen, T. and Mätäsniemi, T. 2013b. Quality assurance of a safety analysis software. Version 1.0. 16 p. Espoo: VTT Technical Research Centre of Finland. VTT Research Report VTT-R-00241-13.
- Tyrväinen T., 2014a. FinPSA – Quality assurance – Quality assurance plan. 11 p. Espoo: VTT Technical Research Centre of Finland. VTT Research Report VTT-R-00393-14.
- Tyrväinen T., 2014b. FinPSA – Software testing – Verification and validation plan. Version 1.2. 298 p. Espoo: VTT Technical Research Centre of Finland. VTT Research Report VTT-R-04125-14.
- Tyrväinen T. 2014c. FinPSA – Software testing – Verification and validation results. 99 p. Espoo: VTT Technical Research Centre of Finland. VTT Research Report VTT-R-06927-13.
- Tyrväinen T. 2014d. FinPSA – Software testing – Verification and validation plan for interface trees. Version 1.2. 43 p. Espoo: VTT Technical Research Centre of Finland. VTT Research Report VTT-R-04127-14.
- Tyrväinen T. 2014e. FinPSA – Software testing – Verification and validation results for interface trees. 26 p. Espoo: VTT Technical Research Centre of Finland. VTT Research Report VTT-R-02430-14.
- Tyrväinen, T., Mätäsniemi, T. 2014f. FinPSA – Software testing – Verification and validation plan for level 2. 56 p. Espoo. VTT Technical Research Centre of Finland. VTT Research Report VTT-R-06210-14.
- Tyrväinen, T., Mätäsniemi, T. 2014g. FinPSA – Software testing – Verification and validation results for level 2. 38 p. Espoo. VTT Technical Research Centre of Finland, VTT Research Report VTT-R-06211-14.
- Tyrväinen T. 2015. FinPSA – Software testing – Plan for level 1 run result comparison. 30 p. Espoo: VTT Technical Research Centre of Finland. VTT Research Report VTT-R-04113-14.

44. Enhancement of Lappeenranta instrumentation of nuclear safety experiments (ELAINE)

44.1 ELAINE summary report

Arto Ylönen, Heikki Purhonen, Lauri Pyy, Vesa Riikonen, Antti Räsänen,
Joonas Telkkä

Lappeenranta University of Technology
P.O. Box 20, FI-53851 Lappeenranta

Abstract

The main goal of the project was to increase the quality and quantity of the measured data generated by the Nuclear Safety Research Unit at Lappeenranta University of Technology (LUT) in order to meet the requirements imposed by today's Computational Fluid Dynamics (CFD) modelling.

One of the main challenges in experimental research is “extracting” the studied physical quantities from the test arrangement for the use of the analysts as numerical data. In nuclear safety research this data is mostly used for the validation purposes. Quality of the data depends on the capabilities of the data gathering chain. The needs for the quality (and quantity) of test data has changed dramatically in the last few years, mainly due to more extensive use of CFD computation. The focus is now on 3D quantities instead of series of single point measurements, i.e. velocity and scalar fields, etc. Therefore, three major measurement techniques, High-Speed Cameras (HSC), Particle Image Velocimetry (PIV) and Wire-Mesh Sensors (WMS), were acquired to LUT in 2011-2014.

Another challenge is how to store and distribute this research data to the end users of the results, and hence the database software (EDS) was developed in the project to accommodate the needs of storing and distribution of the experimental data.

Introduction

High quality validation data is needed for the development of computational tools for flow dynamical studies. The phrase “CFD grade data” is commonly used for the data of such quality (high spatial or temporal resolution or both) that can be directly used for the qualitative and/or quantitative comparisons between the experiment and the model predictions [1]. The improvement of the computational tools will eventually reduce the number of expensive experimental campaigns as the tools would be good and accurate enough to study various flow problems without any experimental support. The capability to capture flows in better resolution than with traditional measurement techniques enables us to observe previously unseen phenomena and to explain physically the flow behaviour. Figure 1 illustrates the path from the experimental set-up to CFD-grade data. The selection of applicable measurement techniques depends on the phenomena in question.

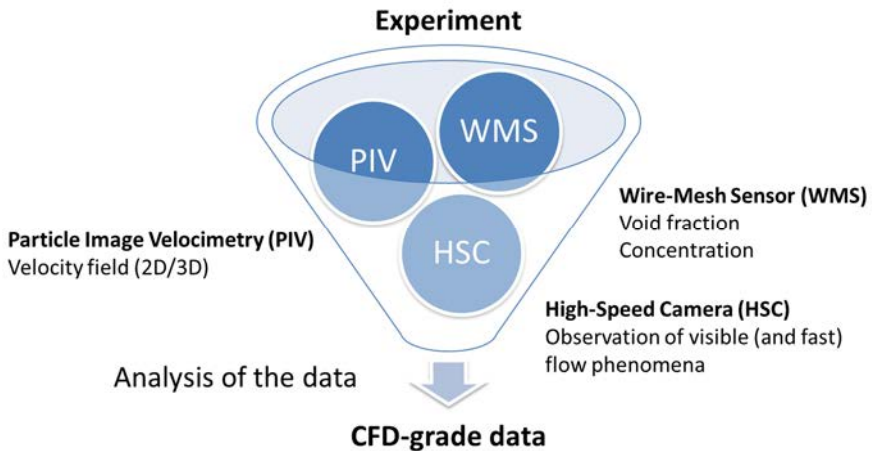


Figure 1. From experiment to CFD grade data.

Above mentioned reasons have motivated to upgrade existing research infrastructure to meet modern standards in the quality of the experimental data. Recently, three major measurement techniques, High-Speed Cameras (HSC), Particle Image Velocimetry (PIV) and Wire-Mesh Sensors (WMS), were acquired to LUT to better support the modelling efforts and to increase the knowledge of the physics behind different flow phenomena. First two methods are optical measurement techniques that rely on the optical access to observe the flow. Last method is based on the measurement of electrical properties (conductance or capacitance) of the fluid using a measurement grid that is placed in a flow channel.

Main objectives

The ELAINE research project had several objectives in 2011–2014.

- Acquisitions of the three major measurement systems and to apply these techniques for the thermal-hydraulic experiments conducted in Lappeenranta
 - Particle Image Velocimetry (PIV), 2011
 - Wire-Mesh Sensor (WMS) hardware, 2012
 - High-Speed Camera (HSC) system, 2013
- Building up know-how and expertise related to the advanced measurement techniques
- Acquisition and installation of the main circulation pumps to the PWR PACTEL test facility
- Development of new Electronic Data Storage (EDS) software for the distribution and storage of experimental data
- Maintenance tasks of the existing Lappeenranta nuclear safety research infrastructure (sensor/hardware upgrades, sensor calibration and testing, legally required facility inspections)

Particle Image Velocimetry (PIV)

Within the ELAINE project a PIV system was acquired from LaVision Ltd. in 2011. The arrangement was designed to enable Stereo-PIV measurements inside the PPOOLEX suppression pool test facility. The preliminary measurements in the PPOOLEX facility were conducted in the end of 2011. The initial goal was to measure velocity fields near the outlet of a blowdown pipe with a stable steam interface.

The experimental work continued with single-phase measurements to further test out the arrangement and the system. The initial measurements with steam release to the water pool were conducted in the beginning of 2013 and the need for phase-separation was observed as the reflections from the steam bubble were too severe. Even with the phase-separation using special camera filters the optical nature caused by the condensing steam and the bubble itself is found too challenging for PIV use [2]. The fluctuations caused by the chugging steam do not allow time-averaging of the velocity fields and hence the results obtained so far have been instantaneous velocity fields when the raw particle image quality has been high enough. Some examples of these velocity fields are presented in Figure 2.

More detailed description of the conducted experimental activities and conclusions can be found in the special article “Experiences and conducted experimental work with PIV in the ELAINE project”.

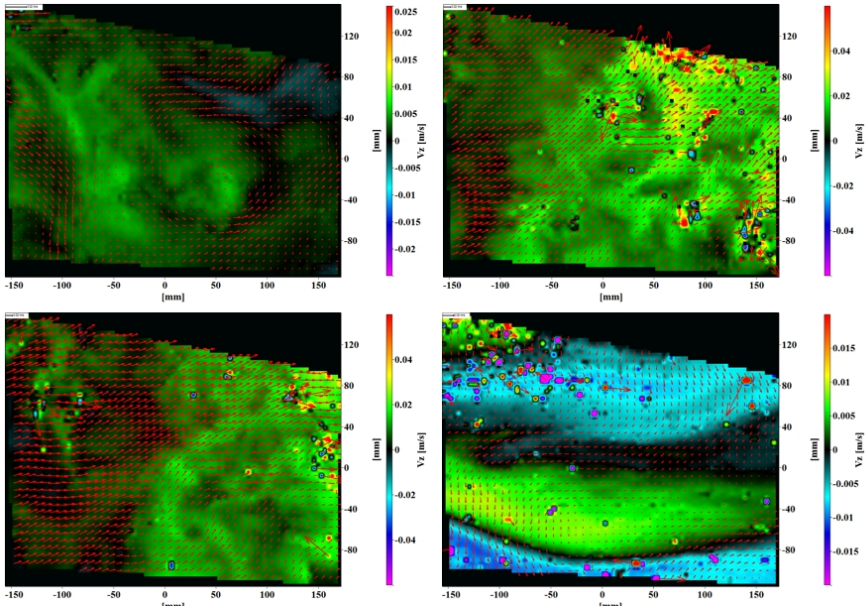


Figure 2. Examples of instantaneous velocity fields (the PPOOLEX test facility).

High-Speed Camera (HSC) system

In 2013, the system of three modern High-Speed Cameras (HSC) was acquired to LUT. In 2014, the HSC system was mainly used in the PPOOLEX experiments to observe the rapid behaviour of collapsing steam bubbles.

In the ELAINE project, the image recognition algorithms have been developed with MATLAB to analyse the HSC footage from the three cameras. The use of three different viewing angles improves the accuracy of bubble size analysis as it reduces the number of required assumptions for the shape of the bubble. Figure 3 shows example images from the HSC footage that has been run through the image recognition routines. The recognized steam-water interface is illustrated with the red continuous line. The differences between the line and the interface show that there is still room for the improvement as some small bubbles disturb the detection of major interface. These challenges may be tackled with the improvement of numerical interface detection methods and lighting conditions for the HSCs.

As described in the introduction, the high-speed imaging can be applied for the observation of visible (and fast) flow phenomena that cannot be captured using the normal video cameras that have typically very low frame rates.

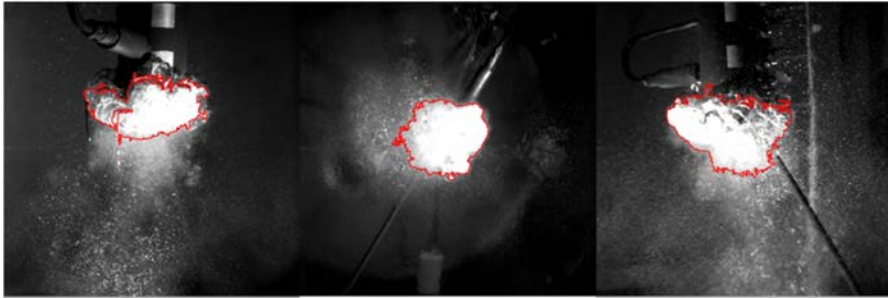


Figure 3. Example of image recognition used for HSC footage from three cameras (the PPOOLEX test facility).

Wire-Mesh Sensor (WMS) technique

The WMS technique is the state-of-the-art method for measuring single- and two-phase flows. The Wire-Mesh Sensor (WMS) measurement technique is based on the measurement of electrical properties (conductance or capacitance) of the fluid. The measurement system is made out of two parts: data acquisition and sensor units. The data acquisition system was purchased from Helmholtz-Zentrum Dresden-Rossendorf (HZDR) in 2012. The system (WMS200) can be used to measure up to 128×128 sensor at 1250 Hz. Transmitter and receiver boxes are connected to the sensor to perform a measurement. The sensor can be constructed from a grid of wires that are connected to standard Printed Circuit Boards (PCB). A small gap is left between the transmitter and receiver wires to allow the measurement of electrical properties of fluid or fluid mixture at those locations. The raw measurement values are converted to the values of mixing (dimensionless mixing scalar) or gas content (void fraction) depending on the type of the experiment. Figure 4 shows the wire grid of a 32×32 WMS and how it is installed to the HIPE test facility.

A new test facility was designed to support all experimental activities related to the advanced measurement techniques. The test facility is also the first one with Wire-Mesh Sensors in LUT and Finland. The facility has a transparent test section (Acrylic pipe with an inside diameter of 50 mm), whose alignment can be changed arbitrarily between vertical and horizontal (Figure 5), hence it is called as HIPE (=Horizontal and Inclined Pipe flow Experiments).

The WMS technique was actively used in 2014 as more than 800 two-phase flow measurements were conducted. The different two-phase flows were measured at various inclinations of the pipe to form a test matrix (vertical, horizontal and 8 angles in-between). Some numerical methods were tested to detect the type of the flow such as clustering of the experiments according to some selected parameters. These experiments also showed some clear limits for the applicability of the measurement method as with some low liquid flow rates air bubbles were slowed down drastically by the WMS. This is a known issue in WMS measurements and it is not visible anymore after a certain liquid velocity that is unique for the sensor design

(sensor resolution and thickness of the wires). Figure 6 shows two example frames from the void fraction measurements performed in LUT. In addition, a new type of WMS was designed and manufactured to study the axial development of two-phase flow in a pipe. The sensor will be tested in the HIPE test facility early 2015 [3].

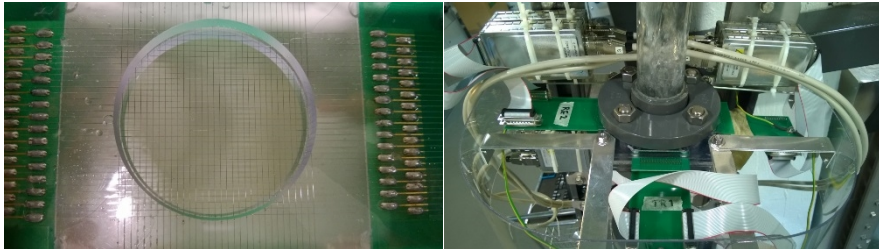


Figure 4. The 32 × 32 WMS of the HIPE test facility (left), overview of the sensor installation (right).

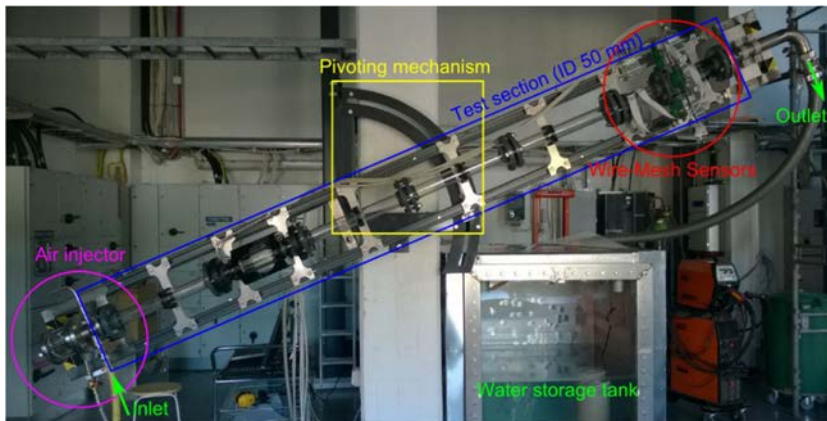


Figure 5. The HIPE test facility during two-phase flow experiments in an inclined pipe.

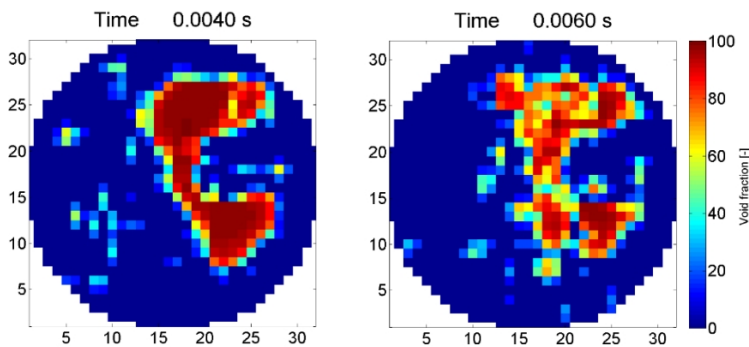


Figure 6. Example frames from the WMS void fraction measurements (Air-Water experiments in the HIPE test facility), 32 × 32 WMS.

Data storage and distributing system development (EDS)

The last link in the chain of experimental research is storing the results in archives in an efficient and convenient manner as well as distributing the results in a controlled way. The STRESA database, developed in an EU project mainly by JRC Ispra, was used at LUT for this purpose. However, the support of STRESA has been suspended and the software used in the database was no longer compatible with the operating systems currently in use at LUT. This is why a new replacing software with similar functions as in STRESA was developed in the project. The new data storage and distributing system (EDS) enables the distribution of the experimental data across the research partners in a fluent and secure way.

Figure 7. Layout of the main page of LUT Experiment Data Storage (EDS).

Overview of test facility maintenance and upgrade activities

The main circulation pumps for PWR PACTEL were introduced in 2012 plans to expand the applicability and to ease the use of the facility, especially in the preparatory phase of the tests. Purchase of the PWR PACTEL main circulation pumps and assorted equipment, such as power feeds, drives, safety automation and mounting pedestals was completed in 2012. Preparation for the installation of the pumps and the assorted equipment to the PWR PACTEL facility was also carried out in 2012. Installation of the pumps was realised in spring/summer 2013 after the delivery of

the pumps in early 2013. The facility maintenance related activities include the inspections of horizontal and vertical steam generators (PACTEL and PWR PACTEL) and checking of temperature, pressure and differential pressure sensors in PWR PACTEL. Several new thermocouples were installed to the secondary side of vertical steam generators. In addition, some hardware was purchased to remove non-condensable gases from the water of the test facility. This system was firstly applied for the PPOOLEX test facility.



Figure 8. New main circulation pump of the PWR PACTEL test facility.

International co-operation

International co-operation was launched with University of Michigan (U-M, U.S.) and Paul Scherrer Institut (PSI, Switzerland) to exchange experiences and know-how on the use of advanced measurement techniques. A research visit was arranged to PSI (spring 2014) on the horizontal mixing experiments of gases using PIV and Laser-Induced Fluorescence (LIF) techniques (HOMER test facility). Also issues related to the PIV measurements in containment experiments (PANDA and PPOOLEX) were discussed during the visit. A research visit to U-M was realized in late autumn 2014 when two researchers from LUT helped with single-phase PIV measurement of jet flow (water tank set-up). The duration of both visits was two weeks. Most valuable outcomes of the research visits are in the networking with measurement technique experts and in the exchange of ideas.

Applications

Outcomes of the ELAINE project are related to the enhancement of measurement capabilities and in the maintaining and upgrading of the existing research infrastructure. Major investments were carried out to update available measurement hardware to the 21st century and to support the development of computational tools in Finland. The project enables the study of many nuclear safety related issues with a new level of detail and many scientific outcomes can be expected in the future. The project also produced the software for the data storage and distribution (EDS) that enables fluent and secure distribution of experimental data across the research partners.

Conclusions

In the ELAINE project several measurement technique and infrastructure related activities were carried out. The acquisitions of measurement systems enable new quality and quantity of data from the thermal-hydraulic experiments conducted in Lappeenranta. The project has enabled building up know-how and expertise related to the advanced measurement techniques and their use in the nuclear safety research. The development of the new software enables fluent storage and distribution of the experimental data. In addition, series of maintenance and upgrade activities of the existing infrastructure have been essential to secure their availability for the thermal-hydraulic experiments.

Acknowledgements

The authors wish to acknowledge the financial support from the Academy of Finland (NUCPRI project), Lappeenranta University of Technology (LUT) and Teollisuuden Voima Oyj (TVO).

References

1. Prasser, H.-M., 2008. Novel experimental measuring techniques required to provide data for CFD validation. *Nuclear Engineering and Design*. 238, 744-770.
2. Ylönen, A., Pyy, L. & Telkkä, J., 2013. ELAINE 1/2013 Report on the status of new measuring systems. LUT. 14 p.
3. Ylönen, A., Pyy, L. & Telkkä, J., 2014. ELAINE 1/2014 Report on the status of new measuring systems. LUT. 14 p.

44.2 Experiences and conducted experimental work with PIV in the ELAINE project

Lauri Pyy, Joonas Telkkä
Lappeenranta University of Technology
P.O. Box 20, FI-53851 Lappeenranta

Abstract

Particle Image Velocimetry (PIV) is an optical measuring technique to obtain velocity information of a flow in interest. With PIV it is possible to achieve two or three dimensional velocity fields from a measurement area instead of a single point in a flow. Depending on the PIV system specifications it is possible to achieve velocity information with high temporal or spatial resolution. Measured flow can be either in liquid or gaseous form. PIV is nowadays widely applied to flow field studies.

The main focus of the PIV measurements has been to apply the measurement system to the PPOOLEX test facility and further, to two-phase flow velocity measurements. The implementation of the PIV system was carried out as a master's thesis work. The experimental work started with single-phase measurements and has continued to two-phase measurements with steam blowdown to water. The main focus has been in measuring the velocity fields of water phase by utilizing phase-separation.

In addition to the experimental work conducted at LUT, a trip to a PIV training course and two research visits were organized. The training course in Göttingen, Germany, emphasized on the general use of the LaVision equipment and the DaVis8 software. During the research visit to Paul Scherrer Institut (PSI), Switzerland, both PIV and LIF, Laser Induced Fluorescence, measurements were performed in a test facility that models turbulent mixing of gases in a horizontal, rectangular channel. The research visit to University of Michigan, U.S., focused on single-phase PIV measurements in an open pool test facility.

Introduction

Particle Image Velocimetry (PIV) measuring system was acquired for Laboratory of Nuclear Engineering as a part of the advanced flow measurement systems to obtain validation data for the development of computational tools for flow dynamics. So far PIV has been utilized in the PPOOLEX facility for measuring single- and two-phase flows within the facility.

Measurement system

The acquired PIV system consists of a dual-cavity laser head, two cameras and a system computer with a DaVis analysing software by LaVision. The use of two cameras enables measurement of three dimensional velocity fields from a measurement plane, also known as stereo-PIV.

The system was purchased in 2011 from LaVisionUK Ltd. The system setup is presented in Figure 1.

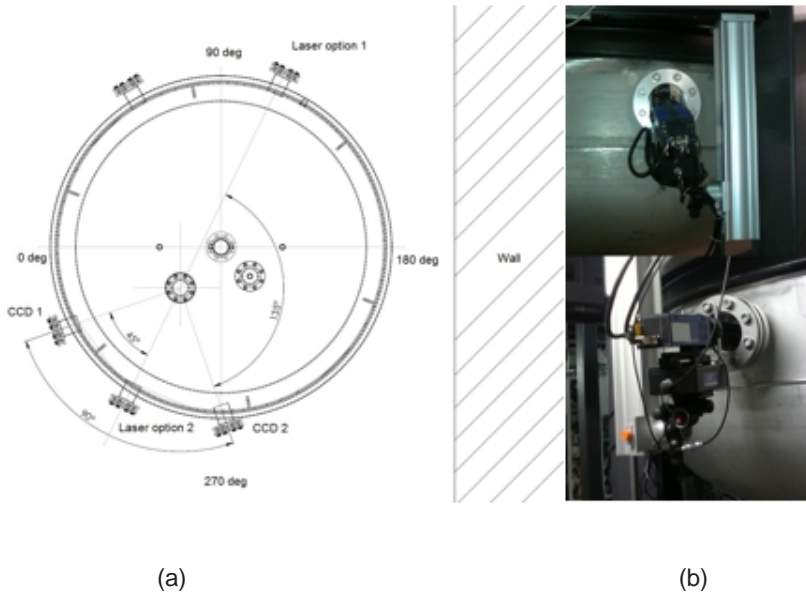


Figure 1. (a) The PIV setup for PPOOLEX and (b) camera placement in front of the observation windows to visualize the optical access inside the PPOOLEX test facility.

The setup was designed for stereo-PIV use utilizing two cameras and a laser. So far there has not been any need to use the observation window called "Laser option 2". Planar-PIV (one camera perpendicular to the laser sheet) can be executed by using CCD 1 and CCD 2 windows, but a need for planar-PIV has not been met yet. System specifications for the laser unit and the cameras are presented in Table 1.

Table 1. The main specifications for the laser unit and the cameras

Attribute	Performance value
Laser	
Beam diameter	6.35 mm
Pulse wavelength	532 nm
Pulse energy @ 532 nm	180 mJ
Maximum repetition rate	15 Hz
Cameras	
Size of the CCD chip	2048 × 2048 pixels
Pixel size	7.4 × 7.4 μm^2
Maximum frame rate	14 Hz

The acquired system is a slow speed system and the emphasis is in producing velocity information with a high spatial resolution instead of a high temporal resolution. The light sheet is produced with an optical arrangement consisting of two spherical lenses and one cylindrical divergence lens. The divergence lens can be changed according to need. The system has three divergence lenses with focal lengths of -10 mm, -20 mm and -50 mm. The working distance for the sheet is from 300 mm up to 2000 mm.

Experimental evolution

The experimental main focus has been in applying the PIV system for PPOOLEX and further, for two-phase flow velocity measurements with steam and water. Master's thesis work "Utilization of Particle Image Velocimetry in PPOOLEX condensation experiments" was carried out in the beginning of the project, and it focused on implementing PIV measurements in the PPOOLEX facility.

The experimental work started with single-phase measurements. A stable steam interface in the outlet of the blowdown pipe of PPOOLEX was created. The measurement of the velocities of the ambient water phase was carried out. It was found that the steam interface creates fluctuations in the vicinity of the blowdown pipe outlet. As there was no stable flow pattern, time-averaging was impossible. The setup for the cameras and the laser was found feasible for future studies. The implementation was successfully carried out.

The following experiments were named DCC0 and DCC00. This time water was injected through the blowdown pipe to further investigate the PIV setup. It was found that when measuring single-phase flow, the setup works well and there are little to

none optical distortions. The working distance for cameras is relatively long because the outer diameter of PPOOLEX is 2.4 meters. The seeding was typical glass hollow spheres with an average diameter of 10 μm .

The first experiment with steam release to the water pool was called DCC01. Blow-downs with different steam mass flows were measured and quickly it was seen that the reflections from the steam bubbles oversaturate the particle images. The reflections were at the level that was considered to be harmful to the camera chips. After this result the focus was put to separate water and steam phases. For the phase separation fluorescent particles and long-pass filters were acquired and the PIV system updated. The fluorescent particles were Rhodamine B doped PMMA particles with an average diameter of 20 μm .

The first experiment utilizing phase-separation was called DCC02. The experiment focused on the velocity measurement of the water-phase as the reflections from the steam bubbles were to be cut-out with the new filters. One major question was also the illumination power of the laser and whether the fluorescent light from the particles would be adequate. In DCC02 it was found that the laser can provide enough illuminating power, and the seeding was visible to cameras with the new long-pass filters on. A major setback was in the form of bubble reflections. Even with the long-pass filters the steam bubble, when being large enough in size, reflected the light strongly to the cameras. To avoid the reflections it was decided to use a shorter blowdown pipe, and thus measuring the velocity fields beneath the steam release.

In between the next experiment in PPOOLEX, a novel particle feeding system was built. The new system allowed the injection of the tracer particles directly to the blowdown pipe if there is a need for single-phase measurements in the future. Also testing of the endoscope for the PIV camera was conducted. The endoscope is operational with the long-pass filter if phase separation is required.

With the shorter pipe the measurement of the water phase was possible. The measurement plane was approximately 300 mm below the exit of the blowdown pipe. The experiment series utilizing the shorter blowdown pipe was called MIX-07, a thermal stratification and mixing experiment. It was found that the water phase was almost static during the experiment.

The previous long-pass filters were not able to handle the reflections from the surface of the steam bubbles. It was decided to acquire different, red band-pass, filters to further investigate the steam release and the ambient water phase. The preliminary testing implied that the new red band-pass filters drastically cut down the reflections. It was also observed that the laser power is adequate to light the fluorescent tracer particles. In DCC06 and DCC07, direct contact condensation experiments, the new filters were tested for the first time. The filter performance was good but it was found out that the condensing steam and the bubbles itself create an extremely challenging optical environment. Whenever steam is present in the measurement plane or between the plane and the camera, the raw image quality is poor as well as

the corresponding vector image. In addition, whenever the steam release does not penetrate the measurement plane the water phase is stable or fluctuating which does not allow time-averaging of the vector fields. The only way to present the results are single time step velocity fields if the optical quality of the raw particle image is adequate enough. To avoid the steam release to penetrate the measurement plane, an additional experiment called DCC08 was conducted. The measurement plane was moved to the front of the blowdown pipe (on the laser side) and the cameras were moved to the upper observation windows that were in prior used for the video cameras. This setup was found infeasible as the steam release blocked completely the view for camera 2. The upper observation windows also did not allow the cameras to be in a 90 degree angle or even to have similar angles towards the measurement plane as they are not designed specifically for the PIV use.

Examples of raw images in different stages of PIV measurements are presented in Figure 2.

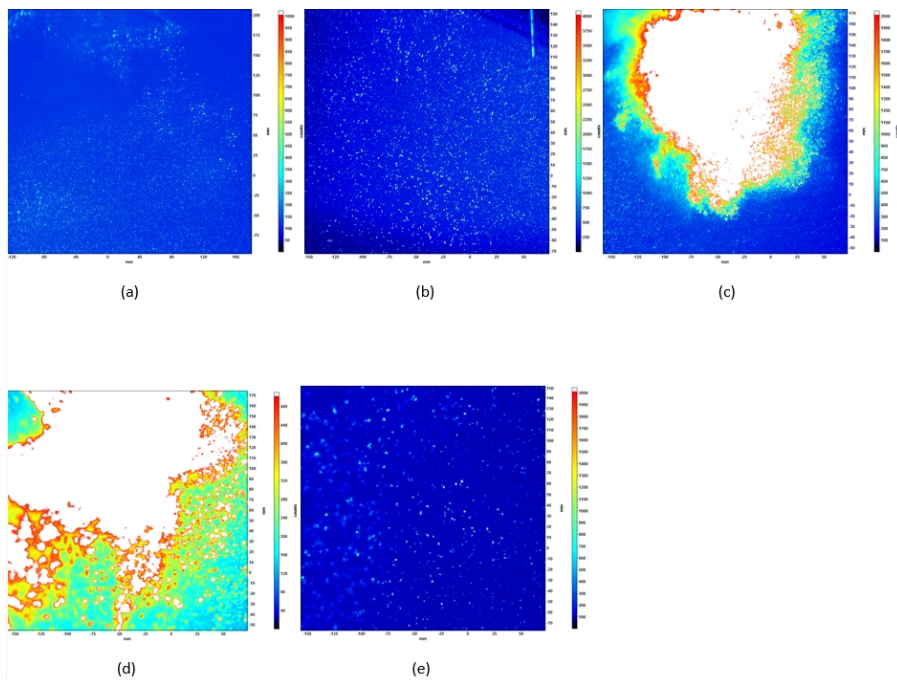


Figure 2. Examples of raw particle images in (a) with steam interface in the outlet of the blowdown pipe, (b) in a single-phase (water-water) measurement, (c) with steam release to the measurement plane (no phase-separation), (d) with steam release to the measurement plane (phase-separation with orange long-pass filters) and (e) steam release to the measurement plane (phase-separation with red band-pass filters).

As it can be seen in Figure 2 the raw particle images in (c) and in (d) are extreme examples with a major steam release. The recording media is saturated with the light from the laser leaving little or no area with visible tracer particles. In example (e) the steam release is at the same level but the filter performs better with the reflection. In example (e) other optical distortion forms are better visible in the form of blurred tracer particles behind the steam bubble. It can be concluded that with the knowledge gained so far from the two-phase flow experiments, the optical conditions whenever a steam release is present in the measurement plane, are too challenging to produce good quality raw images. The first two examples (a) and (b) are possible to measure although there are other problems for PIV use for example in form of fluctuating water-phase. Two examples of processed velocity fields are presented in Figure 3.

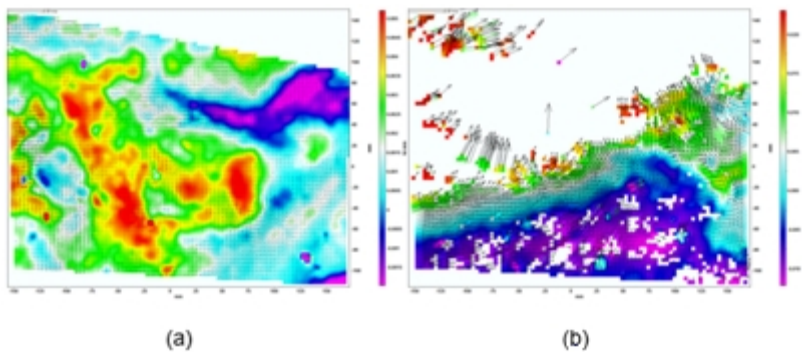


Figure 3. (a) An example of a velocity field without optical disturbance and (b) an example with steam release to the water phase.

As it can be seen in Figure 3, the PIV algorithm needs optically adequate data to be able to perform. The example (b) is a result when vector analysing is performed in a situation similar to one in Figure 2, example (e). There are missing vectors where the software cannot perform cross correlation on the basis of the raw particle images. This is the case when the steam is present in the measurement plane. With the full freedom with placing of the cameras and the laser the steam disturbance could be avoided but this is unfortunately not the case in the PPOOLEX experiments.

Research visits and training

During the ELAINE project Lauri Pyy and Joonas Telkkä attended to The DaVis PIV Seminar in Göttingen, Germany in 2012. Moreover, two research visits were organized in 2014, first to Paul Scherrer Institut (PSI, Switzerland) and next to University of Michigan (U-M, U.S.).

The DaVis PIV Seminar, Göttingen, Germany

The three-day DaVis PIV Seminar was held on 27th - 29th of November, 2012 at the LaVision GmbH facilities in Göttingen, Germany. The aim of the participation was to improve skills on using different PIV measurement systems, as well as to learn to use the DaVis8 software. The three-day seminar was divided into lectures and hands-on workshops.

The first day lectures included basic knowledge of PIV, and the basics of the DaVis8 software were also introduced. PIV measurement hardware was also presented during the first day. The second day lectures covered the optimization of recording parameters. Result evaluation of PIV recordings was also discussed. Further, vector post-processing with the DaVis8 software was displayed. During the third day lectures advanced PIV setups were introduced. For example stereo-PIV, micro-PIV, tomographic PIV and time-resolved PIV techniques were presented. Tool dialogs for the vector post-processing with the DaVis8 software were also introduced.

There were altogether five laboratory sessions during the seminar. The first session, a two-dimensional planar PIV measurement, was comprised of focusing the cameras, optimizing the seeding density and practicing the usage of contrast and scaling. The second lab session was a stereo-PIV measurement that included practicing the usage of a Scheimpflug adapter, calibration and stereo self-calibration. The third measurement session concerned time-resolved PIV. The last two workshops were software sessions, during which the use of the DaVis8 software was practiced under a guidance.

Research visit to Paul Scherrer Institut, Switzerland

Research visit to Paul Scherrer Institut (PSI) in Villigen, Switzerland, took place in March 2014 and it included activities with both PIV and LIF (Laser Induced Fluorescence) measurement systems. Measurements were conducted with the HOMER test facility, where turbulent mixing of two gases in a horizontal, rectangular channel is currently being studied. Lauri Pyy and Joonas Telkkä attended to the research visit. The host of the visit was Dr. Domenico Paladino, and the measurements were performed with local doctoral student Benedikt Krohn.

The test facility has two parallel channels which unite to one, larger channel. In the first experiment pressurized air was directed to the channel using the same particle density for both channels. In the second experiment the lower channel included more tracer particles in order to have a difference of the particle density between the two channels. The aim of this experiment was to investigate whether the accuracy of the measurement weakens as the particle density changes. Also the turbulent mixing zone between the two flows was visualized clearly with different densities.

The tracer particle size was changed to the next experiments compared to the previous ones. In the third experiment a high particle density with a homogeneous distri-

bution was used. To the fourth experiment the particle densities were changed by lowering the density of the upper channel. In the fifth experiment the particle density was homogeneous again, but with a lower particle density.

Two LIF measurements were conducted in PSI during the visit. The aim of these experiments was to achieve a LIF signal, which had not succeeded earlier with the HOMER facility, and to get familiar with the LIF measurement principles. The LIF measurements were performed with a 266 nm ultraviolet laser light and one camera. Toluene was used as a tracer in the LIF experiments, and nitrogen was directed to upper and lower channels. Toluene was directed to the lower channel, and a concentration profile was achieved as a result. Hence, the LIF measurements can be considered successful.

Research visit to University of Michigan, U.S.

The purpose of the Research visit to University of Michigan (U-M) in Ann Arbor was to get familiar with the experimental thermal hydraulic research at Nuclear Engineering and Radiological Sciences Department, emphasis being on the PIV measurements. The two-week visit took place in November 2014, and the participants were Lauri Pyy and Joonas Telkkä. The host of the visit was an associate professor of the department, Dr. Annalisa Manera. The measurements were conducted with Dr. Victor Petrov and Dr. Thien Duy Nguyen.

The PIV measurement system that was used during the visit is a high-speed system. The maximum frequency of the double-cavity laser was 10 kHz, and the maximum frequency of the Phantom CMOS cameras was 800 Hz with a full resolution. The test facility that was used is a cubic, transparent tank, which has three inlets/outlets on one side and three inlets/outlets at the bottom. The purpose of the PIV measurements was to investigate water flow dynamics close to the water inlets and inside the tank, as well as to study stratification phenomena in the tank.

During the first week three single-phase 2D PIV measurements were conducted. In the first experiment the field of view was comprised of adjacent views of the two cameras, with a slight overlap. The tracer particles used in this experiment were hollow glass spheres with an average diameter of 10 μm . The aim of the experiment was to combine the two adjacent raw images into one single, larger vector image, and this was done successfully.

The purpose of the second experiment was to study the effect of the camera angle on the resulting vector images. Both cameras had the same field of view. One camera was directed perpendicularly to the measurement area, while the other one had an approximately 10° angle. When observing the results, it was noticed that a slight camera angle doesn't affect much the resulting vector images.

In the third experiment the effect of the measurement frequency to the results was studied. It was noticed that with the selected water flow the optimal measurement

frequency was approximately 350 Hz. On the last day of the first week Mr. Richard Prevost from LaVision came to give guidance to LIF measurements. He went through a procedure to perform an LIF measurement with a LaVision PIV system without an actual LIF package.

The purpose of the experiments during the second week was still to study the working parameters of the PIV measurement system and the functioning of the DaVis PIV algorithm. In the experiments the effect of the frequency on the results was studied. The frequency difference was achieved by means of “downsampling”, i.e. dropping a certain part of the raw images out of the calculation.

In overall, the research visit to University of Michigan was a success. New ways to exploit DaVis program in 2D PIV measurements were learned, and it was clearly seen that PIV is a good flow measurement technique, as long as the measurement setup and the test conditions are straightforward enough.

Summary and conclusions

So far the experiments conducted in the PPOOLEX facility have been challenging in many aspects. Firstly, there are strict limitations set by the test facility itself. The observation windows for the cameras are fixed and small in size due to the structural restrictions as the PPOOLEX is a pressure vessel. The laser power has been found to be adequate but for the cameras the viewing angles are problematic. Whenever cameras are tilted out of their “sweet spot” there are distortions on the outer regions of the measurement plane which Scheimpflug adjustment cannot compensate.

The phase separation is possible with the new red band-pass filters. The filtering capabilities are found to be adequate even for the steam and air bubbles. This was not the case with the initial orange long-pass filters. Phase separation, even when working, does not exclude the optical distortion problems that are created by condensation and the bubble itself. The bubble acts as a lens and the tracer particles behind are magnified and blurred. Stereo-PIV measurement enables three component velocity field from a measurement plane to be examined. But any bubbles or other optical distortions between the measurement plane and the camera create problems that cannot be overcome. An optical measurement system needs optically robust data to be applied successfully.

The fluctuating water phase also creates another problem for time-averaging of the results. There is no clear stream from the outlet of the blowdown pipe except in the single-phase case when water is injected from the blowdown pipe. Up till the end of 2014 there have been difficulties to evaluate the uncertainties of single velocity fields. The newest version of the DaVis analysing software enables to create uncertainty maps for different velocity components. The norm before this was to produce artificial particle images with certain attributes and compare them to the ones obtained from the experiment. This method can be applied in a simple experimental matrix where the conditions can be fully controlled.

The PIV system in use is a slow speed system and it is capable of providing velocity information with a high spatial resolution, which can be thought of being the system's advantage when compared to other measurement systems. And as being an optical measurement system the only factor that influences the measurable flow are the tiny tracer particles.

The overall know-how for PIV was developed with the two separate research visits and one PIV training course by LaVision. The PIV training course emphasized on the general use of the DaVis software, and there were both theoretical and practical studies done. During the research visit to PSI the focus was on PIV and LIF measurements in a test facility that models turbulent mixing of gases in a horizontal, rectangular channel. The optical arrangement was simple and the results were easy to obtain. During the latest research visit to University of Michigan single-phase PIV experiments were performed in an open pool test facility. Once again, with a simple optical arrangement the results were easy to obtain. During the visit there was also an opportunity to execute LIF measurements, this time in a water phase. In addition to the development of the practical know-how, important contacts with internationally respected university and institute were tied and a possibility for the future co-operation and the exchange of ideas.

So far the challenges when applying PIV in the PPOOLEX facility have been too great in the case of two-phase flow. The optical conditions and the limitations set by the facility itself have been found to be extremely challenging for PIV. In general PIV is a good and widely applied method for flow measurements, but as an optical measurement system, PIV needs optically robust data to succeed. Experiments done in the simpler facilities in PSI and U-M have been successful. In the future PIV will be applied in the HIPE test facility which should guarantee better optical access and test conditions. In general it can be said that the experimental matrix should be kept as simple as possible to achieve good quality results. When applying this principle the PIV system should be able to produce velocity information with a high spatial resolution.

References

1. Pyy, L., 2011. Utilization of Particle Image Velocimetry in PPOOLEX Condensation Experiments. LUT. 94 p.
2. Ylönen, A., Pyy, L. & Telkkä, J., 2013. ELAINE 1/2013 Report on the status of new measuring systems. LUT. 14 p.
3. Ylönen, A., Pyy, L. & Telkkä, J., 2014. ELAINE 1/2014 Report on the status of new measuring systems. LUT. 14 p.

45. Renewal of hot cell infrastructure (REHOT)

45.1 REHOT summary report

Wade Karlsen

VTT Technical Research Centre of Finland Ltd
P.O. Box 1000, FI-02044 Espoo

Abstract

The primary objective of the four year REHOT project was to plan and execute the hot-cell portion of the radioactive materials research and testing infrastructure renewal as a part of the new VTT Centre for Nuclear Safety. This included the planning and making of critical equipment investments for the hot-cell facility, training of the technical personnel that will be staffing the facility, as well planning the technical construction of the hot laboratory portion of the new facility concurrent with the engineering design of the Centre for Nuclear Safety. Central to this were the shielding cells themselves, to be constructed of suitable materials and equipped with appropriated manipulators and devices to provide protection against human radiation exposure in line with the ALARA principle. These are being designed utilizing an external engineering design consultant, which requires collecting information about and describing procedures to be employed in conducting specific tests and processes within the cells remotely with the assistance of manipulators, jigs, tools and other in-cell devices.

Introduction

VTT has been hosting the Finnish national hot laboratory infrastructure since the first nuclear power plants were constructed in Finland in the 1970's. Historically the principle radioactive materials handling has been for the testing of reactor pressure vessel steels, but over time the activities have broadened to outgrow both the capacity and capabilities of the existing facilities. As such, a decision was made in 2011 to build a whole new facility, with the additional goal of gathering most of the VTT Nu-

clear Safety research personnel currently scattered around the Otaniemi campus, into a single, compact facility called the VTT Centre for Nuclear Safety (CNS). The facility would house new radiological laboratories and contemporary hot cells.

The VTT CNS and its hot cell facility is a national infrastructure hosted by VTT, and is considered an important element in fulfilling the national requirements for independent competencies for domestic nuclear power generation. The REHOT project is an integral part of the overall infrastructure renewal process surrounding the VTT CNS. As shown in the schematic of Figure 1, the overall process involves not only the construction and equipping of the new CNS facilities, but also moving from the existing facilities at Otakaari 3 (OK3), to the new facilities, the decommissioning of the OK3 facilities, and ramping up operations in the new facilities. The REHOT project focuses on the implementation of the new radioactive materials research infrastructure in particular.

The design of the VTT CNS in its current rendition has been on-going since 2012. The process was initiated in 2008 with preliminary assessment of the needs and options as a part of the SAFIR2010 AKTUS project. The facility is to be owned by the Finnish State real-estate company Senaattikiinteistöt, with VTT renting the building from them as the end user. As such, the facility design process involves close cooperation between VTT researchers (the end users) and the design team employed by Senaattikiinteistöt. Regulation and oversight by the authorities involves the local municipal government, building department and emergency services, as well as Radiation and Nuclear Safety Authority, Finland-STUK.

Description of the VTT Centre for Nuclear Safety

The location of the new VTT CNS is Kivimiehentie 3 in Otaniemi. The location and position is shown in Figure 2. Since in some cases shipment of radioactive materials involves large trucks, the location also enables driving and turning access for large tractor and trailer combinations. As visible in the site layout (Figure 2), the

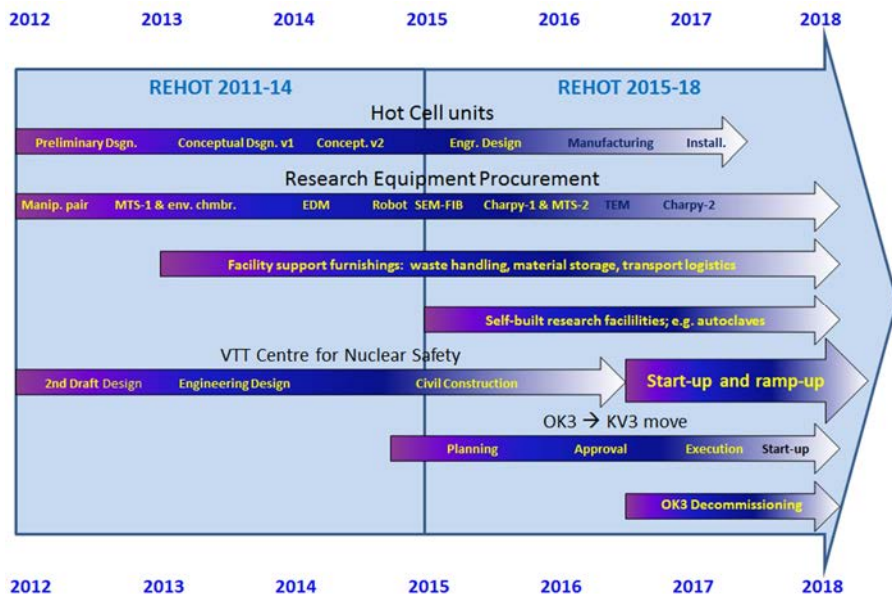


Figure 1: Schematic of processes involved in the infrastructure renewal over the 2012 through 2018 period.

facility includes an office wing and a laboratory wing. The office wing is 3,300 m² and includes a ground-level conference centre, above which are three floors of modern, flexible office space for 150 people. It features an architecturally striking, angular facade on the Kivimiehentie street side, intended to produce the distinct, yet complementary appearance shown in Figure 2. The office wing is planned to serve nuclear sector researchers in areas such as computerized fluid dynamics, process modelling (APROS), fusion plasma computations, severe accidents, core-computations, nuclear waste-management and safety assessments, as well as the staff working in the laboratory wing. The laboratory wing is a more conventional, rectangular wing and includes a basement level and two floors of laboratory space. The laboratory activities include research involving radiochemistry, nuclear waste management, dosimetry, failure analysis as well as mechanical and microstructural characterisation of structural materials. Shipping radioactive materials into and out of the facilities occurs through a gated courtyard and covered loading dock at the basement level, at the rear of the building. A separate report describing the VTT CNS was made in 2013.



Figure 2: Site of the VTT Centre for Nuclear Safety in Otaniemi, Kivimiehentie 3 (left), and Architect's rendition of the facade of the office wing of the building. (SARC Arkkitehtitoimisto).

Progress in REHOT

Over the course of the SAFIR2014 program, the renewal of the hot cell infrastructure made great strides forward. Based on the assessment of needs conducted in the AKTUS project, a draft facility design was made as in collaboration between VTT and A-Insinöörit, the engineering company employed by Senaattikiinteistöt. This was subsequently turned into an engineering design during 2012 and over the 2013 period the floor plans of the facility were subjected to some further modifications, and then the detailed design process was carried out to generate the detailed layouts of furnishings and building systems on a room-by-room basis. At this point a

risk assessment of the activities in the building was also carried out, and a separate report made. In 2013 the draft plans of the laboratory facility and the activities it is foreseen to contain, as well as the practices that will be employed, were presented to STUK's radioactive handling facilities evaluators for review. A preliminary, non-binding assessment was received with some specific recommendations for improvement, which were subsequently implemented into the design. The ground breaking for the CNS began immediately in 2014, and by the end of the year it had taken on its final external shape with most of the concrete works completed, as shown in the collage of photos in Figure 3. At the same time the detailed designs of the facility systems were reviewed, modified and concluded. The expected time of completion of the building is the end of 2016.



Figure 3: Progress on construction of THE VTT Centre for Nuclear safety in 2014, CW from upper left, January, June, September and December.

With regards to the hot cells themselves, the REHOT project first gathered information regarding all of the various activities that are to be carried out in the A-laboratory and the hot-cell facilities. The facilities must enable a wide variety of research-related activities proper, as well as provide the supporting handling, storage and maintenance infrastructure. Many of the preparation, test and characterization activities must take place inside the shielded cells. The REHOT project chapter in the Safir Interim Report (2013) summarized those activities, but a number of separate reports were also made on specific topics, including mechanical testing, microscopy and materials characterization, and waste handling. A significant milestone in 2013 was the execution of a hot-cell conceptual design and preliminary cost estimate, which was made on a contract with Merrick & Company. A reassessment of the design was then carried out by VTT and utilized to develop a more evolved de-

sign specification. The design specification formed the core document for the tendering process for the engineering design and fabrication of the hot cell facilities. The tendering process was then carried out in 2014, and the contract was awarded to Isotope Technologies Dresden GmbH (ITD).

Description of hot cells

The planned hot cell facility is aimed at the mechanical testing and microstructural characterization of beta- and gamma-emitting materials used in nuclear power plant structures. In addition to providing shielding around the equipment used with the radioactive materials, there is also a need for reception and orderly temporary storage of radioactive specimens, cutting and machining of irradiated materials for test or metallographic specimen preparation, as well as collection, temporary storage, and internal transport of radioactive wastes generated in the laboratory.

The contract with ITD includes a suite of six hot cells on the main floor (referred to as cells 1.1 through 1.6), located above a two-station utility cell in the basement (referred to as cell 3.1), as well as a shielded glove-box (referred to as cell 2.1). The cells will be for housing the equipment and devices used in conjunction with the radioactive material. The current portfolio of equipment foreseen to be installed in the cells is listed in Table 1, together with proposed cell locations, equipment main purpose, and its dimensions. It is expected that a small impact tester and one mechanical test station and their auxiliary equipment will be integrated into cell 1.4 as a part of the contract, but the rest of the equipment integration will be carried out by VTT. As shown schematically in Figure 4, the main floor hot cells are arranged in two rows with a closed access space between the rows from which the interiors of individual cells can be accessed. A shielded, enclosed facility (referred to as cell 1.7) connects the two upstairs cell rows, and features a lift to transport test specimens from the basement cell 3.1 to the connection cell 1.7. The primary purpose of cell 1.7 is to transport specimens between the basement and the two upstairs cell rows in a shielded manner, as illustrated in the schematic of Figure 5. The design and fabrication of this transport system is included in the contract, as are three facility transfer casks that are matched to the transport ports in the cells as an alternative transportation route within the facility (e.g. to cell 2.1).

The engineering design of the new hot cells with ITD will take about one year, and then fabrication, pre-assembly, and on-site installation will be carried out over the two subsequent years. According to the schedule proposed by ITD, commissioning of the hot cells can be expected in the first half of 2017.

Table 1. Summary of hot cell equipment arrangement

Floor	Main floor hot cell		Equipment	
Main	1.1	Machining	Electric discharge machine Drilling machine	GF CUT200 TBD
	1.2	Machining	Electron beam welder	CVE 2010
	1.3	Metallography	Cutting Hot moulding Cold moulding	Struers Minitom Struers CitoPress Struers CitoVac
	1.4	Mechanical testing	Universal testing machine Environment chamber Impact tester Tempering unit	MTS 370.10 MTS 651.10E-04 Zwick HIT25 TZE unit
	1.5	Mechanical testing	Universal testing machine HT furnace	MTS 810.10 Maytec HTO-08
	1.6	Measurements	Hardness Specimen dimensions, Fracture surface documentation	Duramin A300 TBD TBD
	1.7	Specimen transfer	Elevator	TBD
Main	Shielded glove box		Equipment	
	2.1	Metallography	Grinding Polishing Etching (chem. / electrochem.) Washing Drying Blanking, Thinning Optical microscope Stereo microscope	Struers TegraForce Struers TegraPol Struers TegraDoser Magnet stirrer Ultrasound washer Hot air blower Puncher 1/3 mm Struers Tenupol TBD TBD
Basement	Utility cell		Equipment	
	3.1	Reception / Documentation Cask / Capsule opening Machining	3-axis linear milling machine Cutting band saw Rotation device Machine tables Storage cell Documentation equipments	Mirage MRY1500 TBD TBD TBD TBD TBD

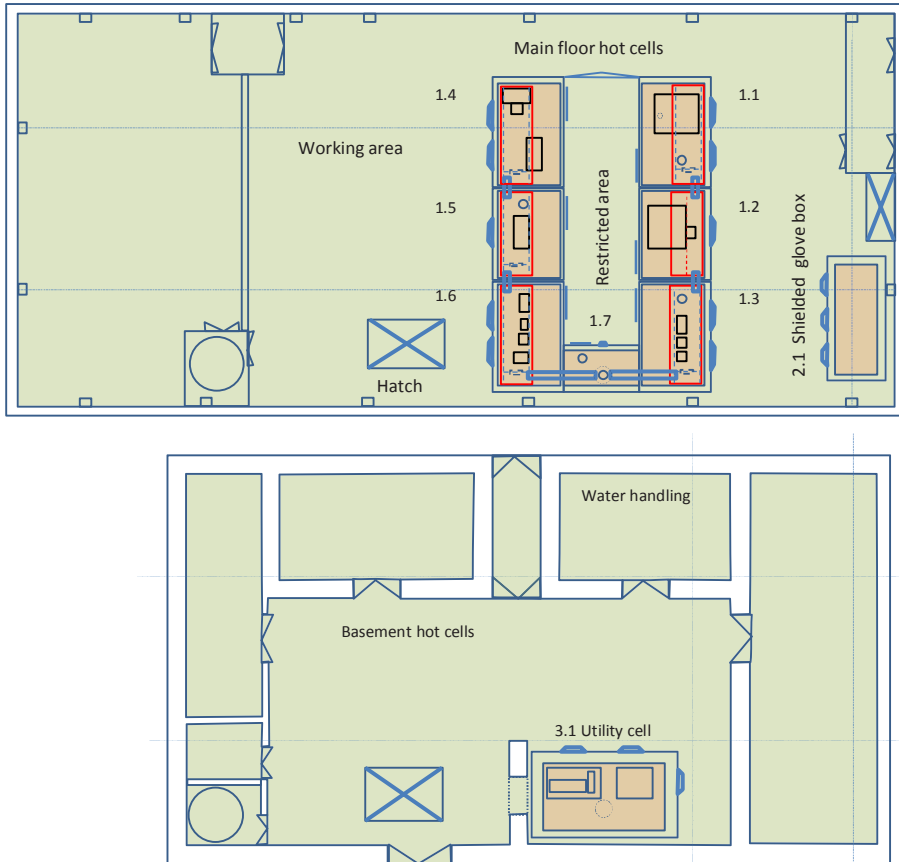


Figure 4. Proposed layout of hot cells on main floor (upper) and in the basement (lower). Features to note are the hatch which enables lifting heavy objects from the basement to the main floor with the 10t bridge crane in the main floor high-bay, the connection between cells 3.1 and 1.7, and the connection requirement between cell 1.1 and the water handling room in the basement.

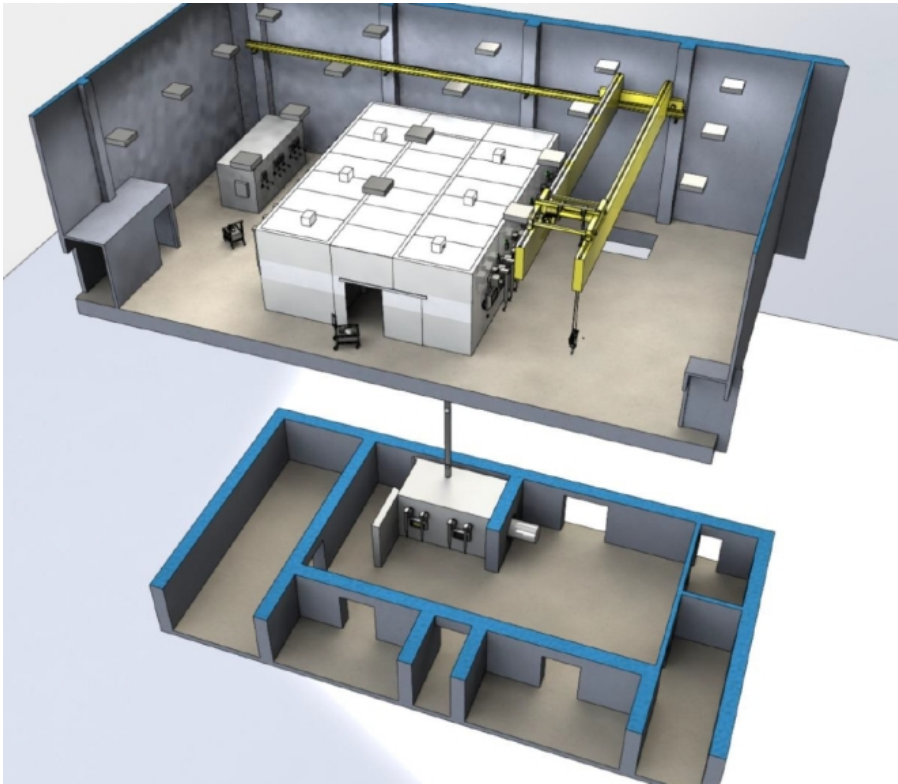


Figure 5: A model of the proposed hot cell facilities in the context of the building. Features to note are the hatch which enables lifting heavy objects from the basement to the main floor with the 10t bridge crane in the main floor high-bay, the connection between cells 3.1 and 1.7, and the connection requirement between cell 1.1 and the water handling room in the basement.

References

- Aho-Mantila, I., Ehrnstén, U., Jäppinen, T., Karlsen, W., Lappalainen, P., Lydman, J., Lyytikäinen, T., Mattila, M., Paasila, P., Toivonen, A., Tähtinen, S., Valo, M. Renewal of hot-cell infrastructure (REHOT) in SAFIR2014. The Finnish Research Programme on Nuclear Power Plant Safety 2011-2014. Interim Report, Simola, Kaisa (ed.), VTT TECHNOLOGY 80, Copyright © VTT 2013, p.433
- Aho-Mantila, I., Ehrnstén, U., Karlsen, W., Lappalainen, P., Lydman, J., Lyytikäinen, T., Mattila, M., Paasila, M., Toivonen, A., Tähtinen, S., Valo, M., Veivo, J. Hot Cell toiminnankuvaus. VTT Report VTT-R-00737-13, 38p.
- Karlsen, W. Equipment procurement and installation schedule. VTT Report VTT-R-00996-13, 14p.
- Karlsen, W. Hot-cell equipment investment financing. VTT-R-01379-13, 9p.
- Aho-Mantila, I., Ehrnstén, U., Jäppinen, T., Karlsen, W., Lappalainen, P., Lydman, J., Lyytikäinen, T., Mattila, M., Paasila, M., Toivonen, A., Tähtinen, S., Veivo, J. Hot Cell activities and design considerations. VTT Report VTT-R-05328-13. 56 p.
- Kuusela P. and Karanta, I. Ydinturvallisuustalon säteilyriskien kartoitus. VTT Report VTT-R-06289-13. 98 p. CONFIDENTIAL.
- Karlsen, W. Hot Cell Conceptual Design for VTT by Merrick & Company. VTT Report VTT-R-06084-13. 103 p.
- Ehrnstén, U., Autio, J-M., Karlsen, W. Hot cell microscopy activities and design considerations. VTT Report VTT-R-00629-14. 18 p.
- Tähtinen, S. REHOT - Mechanical testing. VTT Report VTT-R-00552-14. 31 p.
- Aho-Mantila, I., Lappalainen, P., Lydman J., Paasila, M. Ydinturvallisuustalon hot cell -laboratorion jätteenkäsittelysuunnitelma, luonnos. VTT Report VTT-R-00580-14. 19 p.
- Karlsen, W. VTT Centre for Nuclear Safety- 2013 Progress Report. VTT Report VTT-R-00967-14. 24 p.
- Tähtinen, S., Karlsen, W. Engineering design and manufacturing of radioactive materials testing hot cells. VTT Report VTT-R-03470-14. 27 p.
- Tähtinen, S., Kekki, T., Toivonen, A. Arvio kuumakammion säteilysuojauksesta VTT Report VTT-R-02244-14. 20 p.

45.2 Mechanical testing of radioactive materials in a hot cell environment

Seppo Tähtinen, Wade Karlsen

VTT Technical Research Centre of Finland Ltd
P.O. Box 1000, FI-02044 Espoo

Abstract

Specimen preparation, mechanical testing and dimensional measurements are principle technical activities foreseen to be carried out in the main floor hot cells. The first priority in defining those activities and equipment arises from the execution of the pressure vessel steel irradiation surveillance programs emphasizing mechanical testing capability to determine material strength and toughness properties. The second priority, although almost equally important, is the ability to prepare sub-size test specimens and reconstituted specimens to increase usage and number of data points obtained from the limited amount of active material available. The third priority arises from the need to carry out failure analysis on reactor internals, emphasizing the ability to handle and to prepare test specimens for mechanical tests and metallographic analysis from highly active material blocks. The fourth priority, and future focus area, is material research on various irradiated materials in relation to material test reactors and future development of nuclear power reactors as part of international research programs. One important aspect is also the ability to work with miniaturized test specimens. The following mechanical testing equipment have been identified and are described in this report: impact testers with 300 J and 50 J hammers, universal testing machine with environmental chamber and furnace, measuring stations for dimensions and fracture surfaces, and supplementary equipment like electric discharge machine and electron beam welder.

Introduction

Handling of irradiated materials for mechanical testing requires proper shielding against direct irradiation, primarily gamma and beta radiation, and potential contamination. In order to follow the radiation safety regulations and ALARA principles on minimising personal dose of radiation workers, the use of hot cells is preferable. The present hot cell layout on the main floor area of the VTT Centre for Nuclear Safety (CNS) consists of three adjacent hot cells in two rows, with space between the cell rows. This rear area allows for manned entry to the cells via a shield door in the back of each cell. Adjacent hot cell are connected to each other by through-wall access ports managed by manipulators. This relatively simple and proven hot cell layout allows, in the first hand, an efficient radiation safety design, because most of the material transfer and handling occurs inside and between the hot cells by manipulators. This is mainly managed by two design features considered essential:

firstly, a shielded elevator between the transport cask opening cell in the basement and the hot cell line(s) on the main floor, and second, the co-location of the electro-discharge machine (EDM) on the main floor over the liquid waste handling room in the basement. These functional connections between the main floor and basement operations essentially determine the location of certain equipment and also the location of the complete hot cell block on the main floor area.

In the present state of planning, the technical activities shown in Table 1 are designed to be carried out in the main floor hot cells, e.g., specimen preparation, mechanical testing, and dimensional measurements. The first priority in defining those activities and the equipment needs arises from the need to carry out pressure vessel steel irradiation surveillance programs, emphasizing mechanical testing capability like impact tester and universal testing machine to determine impact, tensile and fracture toughness properties. The second priority, although almost equally important, is the ability to prepare test specimens utilizing the reconstitution technique by applying electric discharge machine, and electron beam welding. The third priority arises from the need to carry out failure analysis on reactor internals, emphasizing the ability to prepare test specimens for mechanical tests and metallographic analysis from highly activated material blocks using the electric discharge machine or other machining equipment. The fourth priority, and future focus area, includes material research on various irradiated materials in relation to material test reactors and future development of nuclear power reactors as part of international research programs. An important aspect related particularly to reconstitution technique and irradiations in material test reactors is the ability to work with sub-sized test specimens.

Hot cell components

The main components comprising the bulk of the cost of a hot cell unit are the shielding material, the shielding window, and the manipulators.

The functional requirements for the shield walls of the hot cells are to provide adequate shielding against gamma and beta radiation emission from neutron activated

Table 1. Present plan for main floor hot cell activities and typical equipment involved in mechanical testing.

Activity	Objective	Typical output	Equipment
Specimen preparation	<ul style="list-style-type: none"> • Direct specimen manufacturing from large blocks • Specimen manufacturing for reconstitution tests • Specimen preparation for metallography 	<ul style="list-style-type: none"> • Tensile specimens • Impact specimens • Fracture toughness specimens • Optical metallography billets • Electron microscopy billets 	<ul style="list-style-type: none"> • Electric discharge machine • Electron beam welder • Drill • Diamond saw • Hot / cold moulder
Mechanical testing	<ul style="list-style-type: none"> • Tensile test • Impact test • Fracture toughness test 	<ul style="list-style-type: none"> • Tensile load versus elongation (σ, ϵ) • Impact load versus de- 	<ul style="list-style-type: none"> • 2 x Instrumented impact hammers, 300J and 50J with

	<ul style="list-style-type: none"> • Fatigue test • Creep test • Hardness 	<ul style="list-style-type: none"> • flexion (P, t) • Impact energy versus temperature (E, T) • Load versus load line displacement and crack opening (P, δ, COD) • Creep strain versus time (ϵ_d, ϵ_a, t) • Precrack length (a_0) • Load/elongation versus no. of cycles (σ/ϵ, c) • Vickers hardness number (HV) 	<ul style="list-style-type: none"> • tempering units • 2 x Universal test machines, 100 kN with environmental chambers and furnace • Hardness tester • Bellows driven biaxial creep tester
Dimensional measurements	<ul style="list-style-type: none"> • Test specimen dimensions before and after mechanical testing • Fracture surface characterization 	<ul style="list-style-type: none"> • Length, width, height • Diameter • Notch angle • Notch tip radius • Notch position • Lateral expansion • Ductile fracture area • Initial and final crack length 	<ul style="list-style-type: none"> • Digital extensimeters • Stereomicroscope with digital camera • Diameter measurement, e.g. laser

materials, and to provide adequate structural strength with foreseen penetrations of the hot cell walls. Generally the higher the atomic number of the shield material, the better shielding properties the wall material will have. The main radiation of importance for nuclear power plant structural materials is gamma radiation from ^{60}Co . The attenuation of ^{60}Co gamma in lead is roughly 1.7 or 5 times that of steel or concrete, respectively. From the raw material cost point of view, lead is about 2 to 3 times more expensive than steel, while concrete is even cheaper.

The main purpose of the radiation shielding window is to provide adequate viewing with sufficient shielding properties. Shielding is most commonly provided by doping the glass by lead oxide, but also other dopants can be used in order to optimise shielding properties. Normally the lead glass density varies from 3.3 to 5.2 g cm⁻³, which provides 1/2 or 1/3 less gamma radiation shielding as compared to a solid lead wall with a density of 11.3 g cm⁻³.

A remote manipulator is a device which, through electronic, hydraulic or mechanical linkage, allows a hand-like mechanism to be controlled by a human operator. One of the most important features of the manipulator is the slave arm coverage, which determines the working space of the manipulator. All the operations designed to be done in the hot cells have to be located inside the manipulator coverage space. There are two major types of master slave manipulators, e.g., articulated (shoulder, elbow, wrist) and telescopic (no elbow) type of manipulators. Telescopic manipulators can also be motorised so that horizontal movement, telescopic extension, and gripping are electrically controlled. The major difference between articulated and telescopic manipulators is the slave arm coverage space, which is larger in the case of telescopic manipulators. It is also noteworthy that mechanical manipulators have a direct force/load response to the master arm user, whereas motorised telescopic manipulators lack some degree of this feedback.

Test equipment installed in the hot cells require air-tight access ports in the cell containment to enable hands-on access for instrument calibration, tool changes, etc. which can be carried out when there are no unshielded radioactive sources present inside the cell. Likewise, for operation of the equipment at the cell working face, instrumentation design requires several penetrations for various power and instrumentation cables and tubes, to provide a connection between test equipment and data acquisition, and control units. Basically, hot cell cable feed-through should be more-or-less leak tight in order to prevent contamination and to maintain pressure difference for ventilation purposes. If the hot cell structure consists of a stainless steel inner liner, then there are two possible locations for cable feed-throughs, e.g., sealed cable connectors in the inner liner wall and/or sealed cable feed-through in the lead shield wall. The advantage of the manipulator-operated cable connector wall inside the hot cell is the easy replacement of equipment and instruments without requiring manual access inside the cell.

VTT manipulator test station

As a part of the REHOT project, VTT purchased a pair of model A201 mechanical articulated master slave manipulators from Wälischmiller Engineering GmbH, and installed them in a test station. The test station allows exploration of the key installation parameters, and enables testing of the remote operation of various equipment or mock ups or cell interior furnishing. The manipulator test station with a tensile testing mock-up and an example of a simple hexagon wrench tool are shown in Figure 1.

Impact Testing

The basic requirements for an impact tester are capabilities to carry out conventional and instrumented impact tests and dynamic fracture mechanic tests in the temperature range from about -100°C to about 300°C, according to requirements set by relevant testing standards and accredited testing laboratory procedures. The

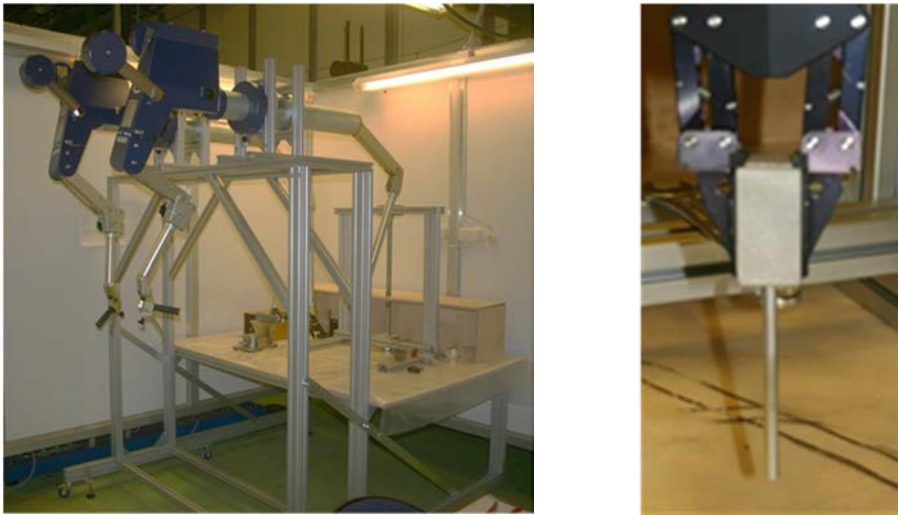


Figure 1: VTT manipulator test station with tensile testing mock-up (left), and an example of a hexagonal wrench modified for holding in a manipulator grip.

most commonly used test specimens are Charpy-V specimens with dimensions of 10x10x55 mm and sub-size Charpy-V specimens down to dimensions of 3x4x27 mm. Basically, the specimen size requirements means that there is a need for two impact hammers, e.g., one with a maximum energy of 300 J and other with maximum energy of about 50 J. Relevant impact testing standards and procedures expected to all be implemented in the new facilities include:

ISO EN 148-1:2006(E): Metallic materials-Charpy pendulum impact test-Part 1: Test method.

ISO EN 148-2:1998(E): Metallic materials-Charpy pendulum impact test-Part 2: Verification of test machines.

ISO EN 148-3:1998(E): Metallic materials-Charpy pendulum impact test-Part 3: Preparation and characterization of Charpy V reference test pieces for verification of test machines.

ASTM E 23-07a: Standard Test Methods for Notched Bar Impact Testing of Metallic Materials.

ISO EN 14556:2000(E): Steel-Charpy V-notch pendulum impact test- Instrumented test method.

T259-HC/CH-V-1b: Instrumented Charpy-V impact test

A characteristic feature of the pendulum impact hammer is that the basic instrument is mechanically stiff and firmly anchored to the floor. The stiffness requirement for the foundation is that its weight is at least more than 40 times the mass of the largest pendulum expected to be utilised in the experiments.

In practice, two main devices are of interest: a large, floor-mounted, *instrumented* pendulum impact tester, or a small, table mounted impact tester. Zwick GmbH & Co offers good candidates in both types; the Zwick RKP 450 model with 300 J pendulum

arm and head, and the Zwick HIT50 model. Zwick can also supply a tempering and automated feeding unit, model TZE, covering the temperature range from -180°C to 300°C by using liquid nitrogen for cooling and resistance heaters for heating. In semi-automatic mode the specimen handling inside the tempering unit is performed by two manually operated pneumatic slides, and specimen alignment at the specimen support and the start of the test are done automatically.

In practice the big impact tester can be installed only in one position, e.g., hammer swing is parallel to the front wall of the hot cell, but the smaller hammer can also be installed with the swing perpendicular to the front wall. The test specimens are transported in and out of the hot cell manually by manipulators through the transport ports between the adjacent hot cells. Test specimens are loaded into the tempering magazine by manipulators, and also the tested specimen halves are picked up by manipulators. The tempering magazine can be loaded also in a separate hot cell connected with dimensional measurements of the test specimens. Management of broken specimen halves is expected to be one of the most demanding operation against which the manipulator coverage needs be designed. Various kinds of safety hoods and conveyor systems can also be designed to limit the space available to collect and manage the broken specimen halves. Operation of the tempering unit and the impact tester is carried out outside the hot cell by the operator. Figure 2 shows different hot cell installations and approximate space allocations for hammer, tempering unit and manipulators. It is noted that most of the space allocation is needed in front of the impact tester.



Figure 2: Examples of different hot cell installations showing space requirements for hammer, tempering unit and manipulators.

Typical data collected during the impact test is time, load, angular position of pendulum after impact, and specimen temperature. After the impact test, the specimen halves are collected, the fracture surfaces are documented, and lateral expansion is measured. Both documentation and measuring actions need specific rigs located either in the same or in another hot cell.

Calibration of the impact tester is carried out according to standard procedure ISO 148-2:1998. The standard procedure describes two methods of verification, and the verification equipment shall have a certified traceability to the International Unit System.

- 1) Direct method: static in nature, involving measurement of the critical parts of the machine to ensure that it meets the standard requirements. Method shall be used when a machine is being installed or prepared, or if the indirect method gives an incorrect result.
- 2) Indirect method: dynamic in nature, using reference test pieces to verify points on the measuring scale.

Verification or calibration of the impact tester involves the inspection of the complete machine, e.g., foundation, machine framework, pendulum including the hammer and striker, anvil, together with supports and indicating equipment. The indirect method is less demanding when compared to the amount of measurements, but it is carried out more frequently, at least every 12 months.

One of the major challenges when installing the impact tester in the hot cells, is to verify that there is sufficient free space and access ports available to carry out the direct verification measurements. However, it is noted that complete direct verification procedure is required only when the impact tester is installed for the first time, or after some major modifications.

Universal testing machine

The first priority for the universal testing machine (UTM) is the capability to carry out tensile and fracture toughness tests in the temperature range from -100°C to about 350°C according to requirements set by relevant testing standards and accredited testing laboratory procedures. The most commonly used tensile test specimens are flat, miniature specimens with dimensions of $1 \times 2 \times 20$ mm, or larger cylindrical specimens 4-6 mm in diameter. Fracture toughness specimens are either three-point-bend specimen with dimensions of $10/5 \times 10 \times 55$ mm down to $3 \times 4 \times 27$ mm or C(T) specimens with varying specimen width from 25.4 mm down to 4 mm.

Fracture toughness specimens are pre-cracked, and therefore a technical ability for fatigue pre-cracking is also needed. Fatigue pre-cracking is performed at ambient temperature, and while not as fast, standard UTMs can be employed. To increase throughput, a dedicated pre-cracking machine could be justified.

The second priority for the universal testing machine is the capability to carry out various other types of mechanical tests, e.g., high/low cycle fatigue, fatigue crack growth, constant load, thermal creep, shear punch tests etc. using various types of test specimens.

Due to the relatively large variety of different tests and test specimen geometries, two separate universal testing machines is the minimum foreseen for hot cell testing. Due to requirements for fatigue precracking and low/high cycle fatigue testing, at least one of the testing machines should be a servo-hydraulic machine, which is most suitable for the alternating loading mode requirements.

Several standardized testing practices are foreseen to be deployed in the hot cell:

Tensile testing

ISO EN 6892-1:2009: Metallic materials. Tensile testing. Part 1: Method of test at room temperature

ISO EN 6892-2:2011: Metallic materials. Tensile testing. Part 2: Method of test at elevated temperature

ASTM E8/8M-11: Standard Test Methods for Tension Testing of Metallic Materials

ASTM E21-09: Standard Test Methods for Elevated Temperature Tension Tests of Metallic Materials

Fracture mechanic testing and prefatigue

ASTM E1921-08: Standard Test Method for Determination of Reference Temperature, T_0 , for ferritic Steels in the Transition Range

ASTM E1820-08: Standard Test Method for Measurement of Fracture Toughness

ESIS P2-92: Procedure for Determining the Fracture Behaviour of Materials

Calibration

ISO EN 7500-1:2004: Metallic materials-Verification of static uniaxial testing machines-Part 1: Tension/compression testing machines-Verification and calibration of the force measuring system

ISO 9513: Metallic materials-Calibration of extensometers used in uniaxial testing

The requirements for testing temperatures from sub-zero to elevated temperatures mean that an environmental chamber (both sub-zero and elevated temperatures in the same furnace) or separate low and high temperature furnaces are an integral part of universal testing machines. Furnace design and construction is closely-related to the strain measurement method to be employed, and the furnace design should also allow easy specimen and tool handling.

In principle, there is two possible ways to install a universal testing machine in a hot cell. The open installation allows all the equipment (e.g., testing machine, environmental chamber and measuring instruments) to be in the same hot cell space available for remote operation with manipulators. The advantage of open installation is relatively easy remote manoeuvring and available open space for instrument installation. Closed installation utilises an internal liner which separates the actual testing machine from the active materials handling area. In closed installation, only the environmental chamber and specimen gripping tools and are visible for remote manoeuvring with manipulators. The obvious advantages are abilities to limit the space for manipulator operations, and also for potential contamination. However, it is also noted that closed installation reduces the versatility of the universal testing machines. Both alternatives are illustrated in Figure 3.

Readiness to carry out a relatively large variety of different mechanical tests using relatively large variety of different specimen geometries is one of the most challenging targets for remotely-operated mechanical testing. In addition to strain measurement methods presently applied, also non-contact laser methods and extensometers with long ceramic contact rods should be evaluated for strain measurement at ele-

vated temperatures. An alternative design option, however, is to minimise the number of different specimen mounting and gripping tools, together with the number of different strain measuring instruments. It is noted that all different sizes of compact tension (C(T)) specimens need different gripping tools and specific instruments particularly crack mouth opening displacement (CMOD) probes. On the other hand, single edge bend (SE(B)) specimens with different width but similar length can be tested with same tools and instruments. Also different tensile test specimens needs different tools and instruments.

Accredited testing procedures require frequent calibration of measuring instruments, e.g., load transducer, specimen deflection transducer, CMOD gauge and specimen temperature thermocouple. The load transducer, specimen deflection transducer and thermocouple are permanently assembled, e.g., not reinstalled after individual test, and they are calibrated every twelve months or when reinstalled. Calibration requires manual access and installation of calibration device in the test machine. The CMOD gauge needs to be assembled during every test and therefore calibration or verification measurement against calibrated device is required before every testing campaign.

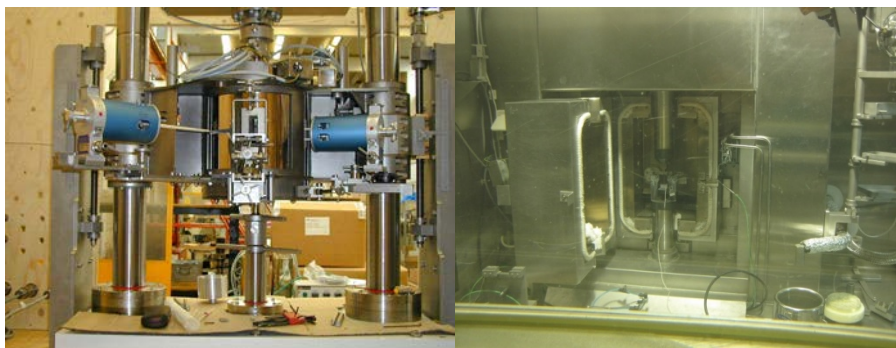


Figure 3: Universal testing machine installed in hot cell (left) open installation with testing machine, furnace and measuring instruments in the same space and (right) closed installation, where internal lining separates testing machine body from active material handling space.

Dimensional measurements

The basic requirements set for dimensional measurements in the hot cell are the capability to measure dimensions of the test specimens before and after the mechanical tests to the required level of accuracy. In addition, fracture surfaces also need to be characterised and documented.

The above indicated standard procedures specify the required dimensions and tolerances for impact, tensile and fracture toughness test specimens. They include not only precise specimen geometry, but quantification of side grooves, surface roughness and notch radii. Standard procedures do not specify the exact measuring method, but the applied method should be able to verify the required tolerances.

The main dimensions like width and thickness shall be measured within 0,05 mm or 0,5% accuracy. For fracture toughness specimens the apparent crack length measurement accuracy shall be 0,025 mm. The dimensional measurements are carried out using specific rigs located either in a separate hot cell or in the same cell where the actual testing is performed.

One of the main challenges of dimensional measurements is to minimise the amount of measuring stations, and to design a multipurpose station which meets most of the measuring needs. In addition to dimensional measurements, fracture surface characterisation, e.g., crack extension, ductile fracture area, need to be documented. Also the dimensions of the Charpy V-notch and side grooves of fracture toughness specimens shall be measured. The measuring devices can be mechanical, optical and/or laser based devices.

Supplementary equipment

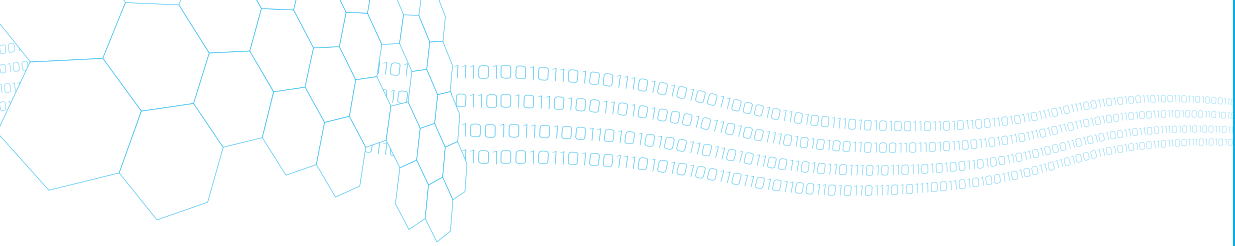
The first priority for the supplementary equipment is to increase the productivity of the surveillance programmes by increasing the number of data points from irradiated material, enabled by utilising miniaturised specimens, and specimens reconstituted from the already tested specimen pieces. For this purpose the electric discharge machine (EDM) is used to e.g. cut full size Charpy-V specimens into either four 5x5x27 mm or six 3x4x27 mm new test specimens, or just to cut material inserts for reconstituted specimens. The electron beam welder (EBW) is used to weld together the active insert and unirradiated material sections in order to produce a new full-size test specimen. The final machining or cutting of the new test specimen is carried out by EDM. The second priority for the supplementary equipment is that the EDM has the capability to produce test specimens directly from almost any shape of active material block, with a minimum amount of mechanical machining. The details of deploying such equipment in a hot cell is beyond the scope of this paper.

Summary and conclusions

The most challenging issue for mechanical testing capability in a hot cell environment is the modification of standard laboratory equipment and measuring instruments for remote controlled operations. It seems that engineering knowledge and practical experience on such modification work exists at least for impact testers and universal testing machines, but it is often carried out as in-house work by the research institutes. It is evident that equipment installation issues have to be taken into account in the early stages of hot cell design and manufacturing.

Mechanic testing equipment like impact tester and universal testing machine can be installed in the hot cell by utilising internal steel liner which is used to limit the space allocated for active material handling. Additionally, the liner serves as a contamination barrier providing glove box type access ports for manual operations and for waste disposal from the active material testing space.

Title	SAFIR2014 – The Finnish Research Programme on Nuclear Power Plant Safety 2011–2014 Final Report
Author(s)	Jari Hämäläinen & Vesa Suolonen (eds.)
Abstract	<p>The Finnish Nuclear Power Plant Safety Research Programme 2011–2014, SAFIR2014, was a 4-year national technical and scientific research programme on the safety of nuclear power plants. The programme was funded by the Finnish State Nuclear Waste Management Fund (VYR), as well as other key organisations operating in the area of nuclear energy. The programme provided the necessary conditions for maintaining knowledge needed for ensuring the continuance of safe use of nuclear power, for developing new know-how and for participation in international co-operation. Major part of Finnish public research on nuclear power plant safety during the years 2011–2014 was carried out in the SAFIR2014 programme.</p> <p>The SAFIR2014 Steering Group, responsible of the strategic alignments of the programme, consisted of representatives of the Radiation and Nuclear Safety Authority (STUK), Ministry of Employment and the Economy (MEE), Technical Research Centre of Finland Ltd (VTT), Teollisuuden Voima Oyj (TVO), Fortum, Fennovoima Oy, Lappeenranta University of Technology (LUT), Aalto University (Aalto), Finnish Funding Agency for Technology and Innovation (Tekes), Finnish Institute of Occupational Health (FIOH) and the Swedish Radiation Safety Authority (SSM).</p> <p>The research programme was divided into nine areas: Man, organisation and society, Automation and control room, Fuel research and reactor analysis, Thermal hydraulics, Severe accidents, Structural safety of reactor circuits, Construction safety, Probabilistic risk analysis (PRA), and Development of research infrastructure. A reference group was assigned to each of these areas to respond for the scientific guidance and to supervise the projects in the area.</p> <p>Research projects of the programme were chosen on the basis of annual call for proposals. The annual volume of the SAFIR2014-programme in 2011–2014 was approximately 10 M€ and 70 person years. Main funding organisations were the Finnish State Nuclear Waste Management Fund (VYR) with over 5 M€ and VTT with nearly 3 M€ annually. In 2014 research was carried out in 45 projects.</p> <p>The research in the programme was carried out by VTT Technical Research Centre of Finland Ltd, Lappeenranta University of Technology, Aalto University, University of Jyväskylä, Finnish Meteorological Institute, Finnish Institute of Occupational Health, and Finnish Software Measurement Association FISMA. A few subcontractors also contributed to the work in some projects.</p> <p>This report gives a summary of the technical results of the SAFIR2014 programme from the entire programme with emphasis on the results achieved during the years 2013–2014. The results obtained during the years 2011–2012 have been reported in detail in the Interim Seminar Report.</p>
ISBN, ISSN	ISBN 978-951-38-8226-6 (Soft back ed.) ISBN 978-951-38-8227-3 (URL: http://www.vtt.fi/publications/index.jsp) ISSN-L 2242-1211 ISSN 2242-1211 (Print) ISSN 2242-122X (Online)
Date	March 2015
Language	English
Pages	722 p.
Name of the project	The Finnish Nuclear Power Plant Safety Research Programme 2011-2014, SAFIR2014
Commissioned by	MEE
Keywords	nuclear safety, safety management, nuclear power plants, human factors, safety culture, automation systems, control room, nuclear fuels, reactor physics, core transient analysis, thermal hydraulics, modelling, severe accidents, structural safety, construction safety, risk assessment, research infrastructure
Publisher	VTT Technical Research Centre of Finland Ltd P.O. Box 1000, FI-02044 VTT, Finland, Tel. 020 722 111



SAFIR2014 – The Finnish Research Programme on Nuclear Power Plant Safety 2011–2014

Final Report

The Finnish Nuclear Power Plant Safety Research Programme 2011–2014, SAFIR2014, was a 4-year national technical and scientific research programme on the safety of nuclear power plants. The programme was funded by the Finnish State Nuclear Waste Management Fund (VYR), as well as other key organisations operating in the area of nuclear energy.

The programme was divided into nine research areas: Man, organisation and society, Automation and control room, Fuel research and reactor analysis, Thermal hydraulics, Severe accidents, Structural safety of reactor circuits, Construction safety, Probabilistic risk analysis (PRA), and the Development of research infrastructure.

The annual volume of the SAFIR2014-programme in 2011–2014 was approximately 10 M€ and 70 person years with 45 projects.

The research in the programme was carried out by VTT Technical Research Centre of Finland Ltd, Lappeenranta University of Technology, Aalto University, University of Jyväskylä, Finnish Meteorological Institute, Finnish Institute of Occupational Health, and Finnish Software Measurement Association FISMA.

This report gives a summary of the research results of the SAFIR2014 programme with an emphasis on the results achieved during the years 2013–2014.

ISBN 978-951-38-8226-6 (Soft back ed.)
ISBN 978-951-38-8227-3 (URL: <http://www.vtt.fi/publications/index.jsp>)
ISSN-L 2242-1211
ISSN 2242-1211 (Print)
ISSN 2242-122X (Online)

